Characterization of the membrane-bound full-length complex between cytochrome b_5 and cytochrome P450 2B4

by

Stéphanie Valérie Le Clair

A dissertation submitted in partial fulfillment
of the requirements for the degree of
Doctor of Philosophy
(Chemistry)
in the University of Michigan
2013

Doctoral Committee:

Professor Ayyalusamy Ramamoorthy, Chair
Professor Michael Morris
Professor Kristina Håkansson
Assistant Professor Akira Ono

© Stéphanie Valérie Le Clair 2013

DEDICATION

To the Ramslab family

ACKNOWLEDGEMENTS

I would like to thank John, Sylvia and all other invaluable staff at C.H. – they saved my life in more ways than one. Thank you to Shani, Denise, Gustavo and Kevin for being essential parts of both my support system and my life – I would not have made it through graduate school without them. I would also like to thank Myron Campbell for believing me and taking my situation seriously.

Importantly, I would like to thank Rams – he has really supported me throughout this graduate school journey. I am forever grateful to him for his kindness and support, and for giving me the room to grow as a scientist and a person. He has been the greatest sponsor for which I could have ever asked. Like any relationships, there were ups and downs, but through it all, I always knew that Rams had good intentions and wanted what was best for me. Thank you, Rams.

I would like to thank the Rams Lab members – I consider all of them family. They were all such wonderful coworkers and made graduate school so much fun (we have pictures to prove it!). Special thanks to Neil for being so dedicated to teaching all of us the theory behind NMR. Thank you to Kevin for always listening, exploring U of M buildings and for pulling me through both the fun and hard times of graduate school. Thank you to Kazu for all the laughs and for paying me visits when we both stayed late in the lab. Thank you to Ron for being an older brother to me and continuing to support me even after leaving the lab. Thank you to Ron also for starting all the Rams lab traditions (the last supper, the birthday tradition and recess) and for creating a new kind of atmosphere in the lab. Thank you to both Ron and Pieter for all the inside jokes and for being a continuous source of laughter (the videos still make me laugh). Thank you to Vivek for always being willing to teach me about structure determination. Thank you to Shivani for teaching me how to prepare NMR samples, run NMR experiments and run HADDOCK simulations. Thank you to Meng for reminding me why I love science, for making research fun again and for keeping me company on late nights when I was working on my thesis in the office. Thank you to Nicole for the dance party and all the silliness. Thank you to the entire Cytochrome Team for stimulating scientific discussions both in group meetings and every day. Thank you to each member of the Rams lab – I always knew that I could talk to each one of them about any research obstacle I encountered. Thank you to my parents who allowed me to obtain an excellent undergraduate education. Thank you to all my professors at St. Mary’s who made me love science and who are great mentors and friends, even to this day. Thank you to SAPAC, OSCR and the Dean of Students Advisory Board for giving additional opportunities to grow as a person. Thank you to the SAPAC and OSCR staff for being so caring, encouraging and always being willing to meet with me and field any of my questions.

TABLE OF CONTENTS

DEDICATION..ii

ACKNOWLEDGMENTS..iii

LIST OF TABLES...xi

LIST OF FIGURES..xiv

LIST OF APPENDICES..xx

LIST OF ABBREVIATIONS...xxi

CHAPTER 1 - Introduction: Biological background.. 1

1.1 Cytochrome b_5 (cyt b_5) 1

1.1.1 Cyt b_5 background 1

1.1.2 Cyt b_5 significance 4

1.1.3 Cyt b_5 and its promiscuous association with numerous redox partners 5

1.1.4 Rabbit cyt b_5 7

1.2 Cytochrome P450 (cyt P450) 11

1.2.1 Background and significance 11

1.2.2 Structure and membrane topology of rabbit cyt P450 2B4 13

1.3 The role of cyt b_5 in cyt P450 reactions 20

1.4 Redox partner association theories 31

1.5 Isotropic bicelles as a model membrane 33

1.5.1 DMPC/DHPC isotropic bicelles 35

1.6 Goals of this research and dissertation layout 39

1.7 References 40

CHAPTER 2 - Experimental methods for studying protein-protein complexes 78

2.1 Site-directed mutagenesis and double mutant cycle analysis 78

2.2 ^{1}H-^{15}N-TROSY-HSQC spectra for the study of large proteins 81

2.3 NMR chemical shift perturbation analysis 83

2.4 NMR differential line broadening analysis 85

2.5 High Ambiguity Driven biomolecular DOCKing (HADDOCK) 86

2.5.1 Ambiguous Interaction Restraints (AIRs) 87

2.5.2. Unambiguous restraints 88

2.6 References 89

CHAPTER 3 - Structure and dynamics of full-length cytochrome b_5 96

3.1 Summary 96

3.2 Introduction 97

3.3 Materials and methods 99

3.3.1 Materials 99

3.3.2 Protein production and purification 100

3.3.3 Solution NMR spectroscopy 101

3.3.3.1 Sequence specific assignment and structural determination 101

3.3.3.2 Backbone ^{15}N relaxation measurements 102

3.3.4 TENSOR2 analysis 104

3.3.5 Structure determination of the cyt b_5 soluble domain 104

3.3.6 Solid-state NMR spectroscopy 105

3.3.7 Docking of heme into the cyt b_5 NMR structure 106

3.4 Results 107

3.4.1 Sequence specific assignment of cyt b_5 107

3.4.2 Three-dimensional tertiary structure calculation of the soluble domain of full-length cyt b_5 116

3.4.3 Backbone relaxation measurements 127

3.4.4 The structure of the soluble domain of cyt b_5 is unaffected by its membrane environment 131

3.4.5 Establishing the topology and structure of the transmembrane domain of full-length cyt b_5 in bicelles 136

3.5 Discussion 137
3.6 Conclusion 143
3.7 Contributions 144
3.8 References 145

CHAPTER 4 - Using NMR, mutagenesis and HADDOCK to determine the interface between cytochrome b_5 and cytochrome P450 2B4 154
4.1 Summary 154
4.2 Introduction 155
4.3 Materials and methods 159
4.3.1 Materials 159
4.3.2 Expression and purification of wild-type rabbit cyt P450 2B4, rat cyt P450 reductase (CPR) and rabbit cyt b_5 160
4.3.3 Generation of mutants of cyt P450 2B4 and cyt b_5 460
4.3.4 Solution NMR of the cyt b_5-cyt P450 complex 161
4.3.5 Determination of cyt P450 2B4 activity in solution and bicelles 162
4.3.5.1 Methoxyflurane 162
4.3.5.2 Benzphetamine 163
4.3.6 Determination of cyt b_5-cyt P450 equilibrium dissociation constant (K_d) in the presence of a substrate/ligand 164
4.3.7 Cyt b_5-cyt P450 complex HADDOCK structure calculation 164
4.3.7.1 Structure of cyt b_5 and cyt P450 2B4 used for docking simulations 165
4.3.7.2 Generating the ligand topology files and parameter files 166
4.3.7.3 Modifying the pdb files for HADDOCK 167
4.3.7.4 Instructions for running HADDOCK 167
4.3.7.5 Histidine protonation states 168
4.3.7.6 Solvent accessibility calculation for this chapter 169
4.3.7.7 Unambiguous restraints for the hemes and 4-CPI 169
4.3.7.8 Ambiguous restraints 171
4.3.7.9 Unambiguous restraints 173

4.3.7.10 Summary of restraints used in the manuscript[61] 174
4.3.7.11 Analysis of HADDOCK structures 175
4.4 Results 176
4.4.1 Single site-directed mutagenesis of cyt b_5 176
4.4.2 Single site-directed mutagenesis of cyt P450 178
4.4.3 Double mutant cycle analysis 179
4.4.4 Cyt P450 2B4 and cyt b_5 are well-folded and active under NMR conditions 183
4.4.5 Observation via NMR of complex formation between ^{15}N-labeled cyt b_5 with substrate-free or substrate-bound cyt P450 185
4.4.6 HADDOCK results for the various runs performed 186
4.4.6.1 Only unambiguous restraints considered 188
4.4.6.2 Only the ambiguous restraints considered 198
4.4.7 Final HADDOCK generated structures 204
4.5 Discussion 211
4.5.1 Identification of the binding epitope for cyt P450 2B4 on cyt b_5 by NMR 211
4.5.2 Mutagenesis identifies the “hot spots” of the cyt b_5-cyt P450 complex 215
4.5.3 Analysis of the cyt b_5-cyt P450 predicted interaction interface 217
4.5.4 Electron transfer pathway between cyt b_5 and cyt P450 221
4.6 Conclusion 222
4.7 Contributions 223
4.8 References 224

CHAPTER 5 - Anatomy of the cytochrome b_5 interface in its stereospecific and encounter complexes with cytochrome P450 233
5.1 Summary 233
5.2 Introduction 234
5.3 Materials and methods 237
5.3.1 Materials 237
5.3.2 NMR sample preparation and experiments 237
5.3.3 NMR data analysis 238

5.3.4 Calculation of solvent accessibility of cyt b_5 residues 240

5.3.5 Circular dichroism experiments of cyt P450 2B4.. 241

5.4 Results.. 242

5.4.1 NaCl does not affect the structures of cyt b_5 and cyt P450 2B4................... 242

5.4.2 Interaction between cyt b_5 and substrate-free cyt P450 246

5.4.3 Interaction between cyt b_5 and substrate-bound cyt P450 249

5.4.4 The effect of increasing ionic strength 254

5.5 Discussion... 255

5.5.1 Characterizing the cyt b_5-cyt P450 2B4 complex.. 255

5.5.2 The interface between cyt b_5 and substrate-free cyt P450 2B4.................... 256

5.5.3 Encounter complexes between cyt b_5 and substrate-bound cyt P450 258

5.5.4 Stereospecific complexes between cyt b_5 and substrate-bound cyt P450 ... 260

5.6 Conclusion.. 264

5.7 Contributions 267

5.8 References 267

CHAPTER 6 - The role of the cytochrome b_5 linker region in complex formation with cytochrome P450 2B4 274

6.1 Summary 274

6.2 Introduction 275

6.3 Materials and methods... 277

6.3.1 Materials 277

6.3.2 Solution NMR... 278

6.3.2.1 Structure determination of mutant cyt b_5.. 278

6.3.2.2 Backbone ^{15}N relaxation measurements of mutant cyt b_5.................... 279

6.3.2.3 NaCl titration on mutant cyt b_5-cyt P450 complex samples.................. 280

6.4 Results.. 282

6.4.1 Sequence specific assignment of the soluble domain of full-length *m*-cyt b_5 282

6.4.2 Structure of the soluble domain of full-length *m*-cyt b_5............................... 283

6.4.3 Backbone relaxation measurements of mutant cyt b_5 in DPC micelles 302

6.4.3.1 Statistical analysis of R_1, R_2 and R_2/R_1 and steady-state NOE parameters of mutant cyt b_5 302

6.4.3.2 Comparison of the relaxation measurements of mutant and wild-type cyt b_5 304

6.4.4 NaCl titration experiments 304

6.4.4.1 Interaction between *m*-cyt b_5 and substrate-free cyt P450 304

6.4.4.2 Interaction between *m*-cyt b_5 and substrate-bound cyt P450 308

6.5 Discussion 313

6.5.1 The structure of mutant cyt b_5 is very similar to wild-type cyt b_5 313

6.5.2 Shortening of the linker does not affect internal dynamics of cyt b_5 but causes the soluble domain to diffuse through solution differently 314

6.5.3 The effect of the length of the linker on the complex formation between cyt b_5 and cyt P450 315

6.6 Conclusion 318

6.8 References 319

CHAPTER 7 - Conclusions and future directions 324

7.1 Conclusions 324

7.2 Future directions 328

7.3 References 330

APPENDICES 332

LIST OF TABLES

Table 1.1 Cursory summary of cyt b_5 residues proposed to be at the interface with redox partners other than cyt P450. 8

Table 1.2 Summary of cyt b_5 residues proposed to be at the interface with various cyts P450. 25

Table 1.3 Summary of cyt P450 residues proposed to be at the interface with cyt b_5 28

Table 3.1 List of restraints used for incorporating the heme (type B) into the NMR structure of cyt b_5 using HADDOCK 2.1[63,64]. 107

Table 3.2 NMR and refinement statistics for the cyt b_5 NMR structure. 119

Table 3.3 Hydrogen-bond restraints used for the determination of the NMR structure of cyt b_5. 120

Table 3.4 β-turns present in full-length cyt b_5 structure solved by NMR. 124

Table 4.1 Sequences of oligonucleotide primers used to mutate cyt b_5 cDNA.............161

Table 4.2 Restraints between 4-CPI and cyt P450 2B4. 169

Table 4.3 Restraints between cyt P450 and its heme. 170

Table 4.4 Restraints between cyt b_5 and its heme. 170

Table 4.5 Table of Ambiguous Interaction Restraints (AIRs) used in the manuscript.[61] 172

Table 4.6 Semi-flexible segments that were set explicitly based on restraints in Table 4.5. 172

Table 4.7 Solvent accessible heme atoms in cyt b_5. 172

Table 4.8 List of all unambiguous restraints which were assessed. 174

Table 4.9 List of ambiguous and unambiguous restraints used in the manuscript[61]..... 175

Table 4.10 Final list of semi-flexible segments used in the publication.[61] 175

Table 4.11 Determination of the K_d and methoxyflurane (MF) metabolism of cyt b_5-cyt P450 complexes between mutants of cyt b_5 and wild-type cyt P450. 177

Table 4.12: Determination of the K_d and MF metabolism of cyt b_5-cyt P450 complexes between mutants of cyt P450 and wild-type cyt b_5. 179

Table 4.13 Double mutant cycle analysis of mutants of cyt P450 and cyt b_5. A comparison of the difference in free energy of binding values ($\Delta\Delta G$) between mutant and wild-type proteins to determine the residues interacting at the cyt b_5-cyt P450 interface. 181

Table 4.14 $\Delta\Delta G_{int}$ ranges obtained (calculated based on K_d measurement errors) for the double mutant cycle analysis. 182

Table 4.15 A comparison of the metabolism of methoxyflurane and benzphetamine by cyt P450 2B4 in solution and bicelles in the presence and absence of cyt b_5. 185

Table 4.16 Violations of unambiguous restraints for the HADDOCK simulation with only restraints #1-4 in Table 4.8. This simulation did not include any ambiguous restraints. 189

Table 4.17 Four clusters of complex structures for the HADDOCK simulation with only restraints #1-4 in Table 4.8. This simulation did not include any ambiguous restraints. 189

Table 4.18 Hydrogen bonds and salt bridges at the complex interface of cluster I for the HADDOCK simulation with only restraints #1-4 in Table 4.8. 191

Table 4.19 Violations of unambiguous restraints for the HADDOCK simulation with only restraints #1-3 in Table 4.8. 193

Table 4.20 Eight clusters of complex structures obtained for the HADDOCK simulation with only restraints #1-3 in Table 4.8. 193

Table 4.21 Hydrogen bonds and salt bridge contacts in cluster I for the HADDOCK simulation with only restraints #1-3 in Table 4.8. 195

Table 4.22 Hydrogen bonds and salt bridge contacts in cluster II for the HADDOCK simulation with only restraints #1-3 in Table 4.8. 195

Table 4.23 Violations of ambiguous restraints for the HADDOCK simulation with only the ambiguous restraints in Table 4.5. 199

Table 4.24 Six clusters of complex structures for the HADDOCK simulation with only the ambiguous restraints in Table 4.5.. 199

Table 4.25 Hydrogen bonds and salt bridges in cluster I for the HADDOCK simulation with only the ambiguous restraints in Table 4.5. 201

Table 4.26 Eleven clusters of complex structures for the HADDOCK simulation in which semi-flexible segments were those listed in Table 4.6. Only the ambiguous restraints in Table 4.5 were used for this simulation. 202

Table 4.27 Energy statistics for the two lowest energy clusters of the HADDOCK complex between cyt b_5 and cyt P450. 206

Table 4.28 Non-covalent interactions in HADDOCK-generated cluster I and II 210

Table 5.1 Residues for which only incomplete (or no) intensity information could be obtained in the given experiments.. 240

Table 5.2 Cyt b_5 residues that experience extensive line broadening in the presence of substrate-free cyt P450, at different ionic strengths. 247

Table 5.3 Cyt b_5 resonances present in the spectrum for the complex between cyt b_5 and substrate-bound cyt P450... 250

Table 5.4 Cyt b_5 residues that experience extensive line broadening in the presence of BHT-bound cyt P450, at different ionic strengths. 250

Table 6.1 Differences in the cross-peaks observed in the ^{15}N-HSQC-NOESY spectrum of mutant cyt b_5 and wild-type cyt b_5 for β-sheet structures... 294

Table 6.2 Differences in the cross-peaks observed in the ^{15}N-HSQC-NOESY spectrum of mutant cyt b_5 and wild-type cyt b_5 for α-helical structures.. 294

Table 6.3 NMR structural statistics for mutant cyt b_5. 298

Table 6.4 Mutant cyt b_5 residues that experienced extensive line broadening in complex with BHT-bound cyt P450 over the range of 0-100 mM NaCl. 311

LIST OF FIGURES

Figure 1.1 Sequence of rabbit cyt b_5 2

Figure 1.2 Domains of microsomal cyt b_5 2

Figure 1.3 Electrostatic potential surface for the soluble domain of rabbit cyt b_5 3

Figure 1.4 Cyt P450 2B4 structural domains. 14

Figure 1.5 Electrostatic potential surface for the proximal side (where the heme is closest to the surface) of the soluble domain of cyt P450 2B4 15

Figure 1.6 Heme showing through the proximal surface of cyt P450 2B4 18

Figure 1.8 Cyt P450 2B4 orientation in the membrane based on atomic force microscopy.[236] 19

Figure 1.9 Important segments for membrane binding of mammalian cyts P450, proposed by Williams *et al.*[230] 19

Figure 1.10 Important segments of cyt P450 2B4 for membrane binding proposed by Zhao *et al.*[197] 20

Figure 1.11 Sequence alignment of cyt P450 2B4 with several other cyts P450 that interact with cyt b_5 23

Figure 1.12 Dynamic docking model between redox partners. 32

Figure 1.13 Model of isotropic bicelles.[365] 34

Figure 1.14 Structures of lipids used in bicelles (DMPC and DHPC) 37

Figure 1.15 Size of q = 0.25 DMPC/DHPC (5% (w/v) and above) isotropic bicelles, and cyt b_5 and cyt P450 2B4, *to scale* 38

Figure 2.1 Diagram of a double mutant cycle 38

Figure 3.1 Heme type B molecule. 111

Figure 3.2 ^1H-^1H planes extracted from a 3D ^{15}N-NOESY-HSQC recorded on fully protonated U-^{13}C, ^{15}N-cyt b_5 in DPC micelles. 112

Figure 3.3 ^{1}H-^{15}N-TROSY-HSQC spectrum of full-length cyt b_5 in 150 mM DPC micelles. 113

Figure 3.4 Schematic representation of the sequential and medium range NOE connectivities involving NH, Hα and Hβ protons 114

Figure 3.5 Hα-NH and NH-NH NOE connectivities observed in the ^{15}N-HSQC-NOESY spectrum for helical segments of cyt b_5 115

Figure 3.6 NOE connectivities observed within the β-strands of cyt b_5 116

Figure 3.7 Proposed hydrogen bonds within the β-sheets of cyt b_5. 117

Figure 3.8 Overlay of the thirty lowest energy cyt b_5 structures generated from CYANA 2.1 based on the NMR restraints in Table 3.2 122

Figure 3.9 Overlay of the five lowest energy structures obtained from docking the heme (type B) molecule into the NMR structure of cyt b_5, using HADDOCK[63,64] 123

Figure 3.10 Ramachandran plot for the NMR structure of full-length cyt b_5 (M1-D134) in DPC micelles, produced by CYANA 2.1.[58] 123

Figure 3.11 Sequence and secondary structure of the soluble domain of full-length rabbit cyt b_5, incorporated in DPC micelles, solved by solution NMR and generated by CYANA 2.1. 124

Figure 3.12 Simplified schematic diagram of the cyt b_5 structure showing the different secondary structure elements and how they are connected 125

Figure 3.13 All β-strands present in the structure of wild-type cyt b_5, showing the likely hydrogen bonds. 126

Figure 3.14 Sequence and structure comparison of our NMR structure of cyt b_5 with other NMR structures of cyt b_5 127

Figure 3.15 ^{15}N-R_1, -R_2, R_2/R_1 and ^{15}N-{^{1}H }-NOE relaxation parameters obtained for full-length cyt b_5 at 900 MHz in DPC micelles. 133

Figure 3.16 ^{1}H-^{15}N-TROSY-HSQC spectra of U-^{15}N-cyt b_5 in 45 mM DPC micelles and 10% (w/v) DMPC/DHPC isotropic bicelles q = 0.25 overlaid on top. 134

Figure 3.17 The central region of the ^{1}H-^{15}N-TROSY-HSQC spectra of U-^{15}N-cyt b_5 in 45 mM DPC micelles and 10% (w/v) DMPC/DHPC isotropic bicelles $q = 0.25$ overlaid on top. 135

Figure 3.18 The central region of the ^{1}H-^{15}N-TROSY-HSQC spectra of two samples of cyt b_5 in DPC micelles: ^{15}N-cyt b_5 and ^{13}C,^{15}N-cyt b_5 overlaid on top. 136

Figure 3.19 The transmembrane domain of cyt b_5 is visible under magic angle spinning NMR. ^{1}H-^{15}N HMQC spectrum recorded on a selectively ^{15}N-alanine labeled sample of cyt b_5 incorporated in DPC micelles 139

Figure 3.20 High-resolution NMR structure of rabbit microsomal cyt b_5. 140

Figure 4.1 CYANA labeling scheme of histidine atoms. 168

Figure 4.2 Labeling scheme of heme (type B) molecule from cyt b_5, with the passive atoms for HADDOCK labeled. 173

Figure 4.3 Mutagenesis of cyt b_5 residues. 177

Figure 4.4: Cyt P450 2B4 hot spots for cyt b_5 determined by mutagenesis 180

Figure 4.5 Cyt P450 is reconstituted in a functional form in DMPC/DHPC bicelles. 184

Figure 4.6 Mapping the effect of cyt P450 binding to cyt b_5 using NMR 187

Figure 4.7 A closer look at how the four (#1-4 in Table 4.8) unambiguous restraints hold cyt b_5 in place in cluster I. 190

Figure 4.8 Center of mass representation of the different clusters obtained for the HADDOCK simulation with only restraints #1-4 in Table 4.8. 190

Figure 4.9 Complex structures (clusters I and II) obtained for the HADDOCK simulation with only restraints #1-4 in Table 4.8 191

Figure 4.10 Lowest energy structure from cluster I and cluster II for the HADDOCK simulation with only restraints #1-3 in Table 4.8. 194

Figure 4.11 Center of mass representation of the different clusters obtained for the HADDOCK simulation with only restraints #1-3 in Table 4.8. 194

Figure 4.12 Complex structures (clusters I and II) obtained for the HADDOCK simulation with only the ambiguous restraints in Table 4.5. 200

Figure 4.13 Center of mass representation of the different clusters for the HADDOCK simulation with only the ambiguous restraints in Table 4.5. 200

Figure 4.14 Center of mass representation of the different clusters for the HADDOCK simulation in which semi-flexible segments were those listed in Table 4.6. 203

Figure 4.15 Cluster V for the HADDOCK simulation in which semi-flexible segments were those listed in Table 4.6. 204

Figure 4.16 Center of mass representation of the HADDOCK docking solution for the cyt b_5-cyt P450 complex. 205

Figure 4.17 The two final clusters of cyt b_5-cyt P450 complex structures obtained from HADDOCK. 206

Figure 4.18 Structure of the full-length membrane-bound cyt b_5-cyt P450 complex and electron pathway prediction.. 207

Figure 4.19 Interacting surfaces of cyt b_5 and cyt P450 2B4 208

Figure 4.20 Residues at the binding interface of the membrane-bound cyt b_5-cyt P450 complex.. 209

Figure 5.1. Cleft opening on the top of cyt b_5 as determined by MD simulations in Storch *et al.*[29]... 240

Figure 5.2. The secondary structure of cyt P450 is not affected upon addition of NaCl. 243

Figure 5.3. The overall structure of cyt b_5 is not affected by the presence of NaCl....... 244

Figure 5.4. Addition of BHT affects neither intensities nor chemical shifts of cyt b_5 backbone NH nuclei. 245

Figure 5.5 Effect of NaCl on the relative intensities of selected cyt b_5 residues in the presence of substrate-free cyt P450.. 247

Figure 5.6 Residues playing a role in the formation of the stereospecific and encounter complexes between cyt b_5 and substrate-free cyt P450.. 248

Figure 5.7. ^1H-^{15}N-TROSY-HSQC spectrum of cyt b_5 with substrate-bound cyt P450 (1:1) in isotropic bicelles. 251

Figure 5.8 Residues on all sides of cyt b_5 are involved in encounter complexes between cyt b_5 and cyt P450. 252

Figure 5.9 Effect of NaCl on the relative intensities of selected cyt b_5 residues in the presence of substrate-bound cyt P450........ 253

Figure 5.10 Residues playing a role in the stereospecific complex formation between cyt b_5 and substrate-bound cyt P450. 253

Figure 5.11 Cluster I of the data-driven simulated cyt b_5-cyt P450 structure (obtained in Chapter 4) is in agreement with the findings that only the lower cleft of cyt b_5 interacts with cyt P450 (from this Chapter)........ 262

Figure 5.12. Electrostatic potential surface for the proximal side (where the heme is closest to the surface) of the soluble domain of cyt P450 2B4.. 265

Figure 5.13 Summary of cyt b_5 residues involved in the association with cytP450 266

Figure 6.1 Comparison of ^1H-^{15}N-TROSY-HSQC spectra of wild-type cyt b_5 and mutant cyt b_5, each incorporated in DPC micelles........ 285

Figure 6.2 Comparison of the central region of the ^1H-^{15}N-TROSY-HSQC spectra of wild-type cyt b_5 and mutant cyt b_5, each incorporated in DPC micelles. 286

Figure 6.3 Comparison of sections of the ^1H-^{15}N-TROSY-HSQC spectra of wild-type cyt b_5 and mutant cyt b_5 287

Figure 6.4 Comparison of ^1H-^{15}N-TROSY-HSQC spectra of wild-type cyt b_5 and mutant cyt b_5, each incorporated in DMPC/DHPC isotropic bicelles (*q* ratio of 0.25)........ 288

Figure 6.5 Comparison of the central region of the ^1H-^{15}N-TROSY-HSQC spectra of wild-type cyt b_5 and mutant cyt b_5, each incorporated in DMPC/DHPC isotropic bicelles (*q* ratio of 0.25). 289

Figure 6.6 Labeled ^1H-^{15}N-TROSY-HSQC spectrum of *m*-cyt b_5 (E97-D104) in DPC micelles. 290

Figure 6.7 A closer look at the crowded region of the ^1H-^{15}N-TROSY-HSQC spectrum in Figure 6.6. 291

Figure 6.8 Comparison of Hα-NH and NH-NHNOE connectivities for all helices (α1-α5 and 3_{10}) in mutant cyt b_5 and wild-type cyt b_5, based on ^{15}N-HSQC-NOESY. 295

Figure 6.9 NOE connectivities comparison, within the β-strands, between mutant cyt b_5 and wild-type cyt b_5 based on ^{15}N-HSQC-NOESY. 296

Figure 6.10 NOE connectivity plot for mutant cyt b_5 incorporated in DPC micelles. 297

Figure 6.11 Ramachandran plot for the backbone structure of mutant cyt b_5. 298

Figure 6.12 Low energy structures of *m*-cyt b_5 calculated by CYANA2.1 from 856 NOE restraints and 112 dihedral angles (Table 6.3). 299

Figure 6.13 Secondary structure and sequence of the soluble domain of *m*-cyt b_5 (E97-D104), incorporated in DPC micelles, generated from CYANA. 300

Figure 6.14 Comparison of secondary structure elements for wild-type cyt b_5 and mutant cyt b_5 (E97-D104) based on the CYANA-generated structures 301

Figure 6.15 ^{15}N-R_1, -R_2 and ^{1}H{^{15}N}-NOE relaxation parameters obtained for mutant cyt b_5 at 900 MHz in DPC micelles. 305

Figure 6.16 Effect of NaCl on the relative intensities of selected *m*-cyt b_5 residues in the presence of substrate-free cyt P450. 307

Figure 6.17 Residues playing a role in the complex formation between *m*-cyt b_5 and substrate-free cyt P450. 308

Figure 6.18 ^{1}H-^{15}N-TROSY-HSQC spectrum of *m*-cyt b_5 with substrate-bound cyt P450 (1:1) in bicelles. 309

Figure 6.19 Effect of NaCl on the relative intensities of selected *m*-cyt b_5 residues in the presence of substrate-bound cyt P450. 310

Figure 6.20 Residues playing a role in the complex formation between *m*-cyt b_5 and substrate-bound cyt P450. 312

Figure 6.21 CO assay UV-Vis spectrum showing that cyt P450 is in its active conformation (blue) under the NMR conditions 313

LIST OF APPENDICES

Appendix A - Instructions for running HADDOCK on the cyt b_5-cyt P450 complex........ 334
Appendix B - Histidine protonation states........ 341
    Instructions for generating the pqr files to assess protonation........ 341
    Generating electrostatic potential surfaces........ 343
    References........ 343
Appendix C - Solvent accessibility of cyt b_5 residues........ 345
Appendix D - Preparing isotropic bicelles........ 351

LIST OF ABBREVIATIONS

1-CPI	1-(4-chlorophenyl) imidazole
AIR	ambiguous interaction restraints
APBS	Adaptive Poisson-Boltzmann Solver
BHT	3,5-di-*tert*-butyl-4-hydroxytoluene
CCP4	collaborative computational project number 4
CPMG	Carr-Purcell-Meiboom-Gill
CPR	cytochrome P450 reductase
CSPs	chemical shift perturbations
cyt c	cytochrome c
cyt b_5	cytochrome b_5
cyts b_5	cytochromes b_5
cyt P450	cytochrome P450
cyts P450	cytochromes P450
DHPC	1,2-dihexanoyl-*sn*-glycero-3-phosphocholine
DLPC	1,2-dilauroyl-*sn*-glycero-3-phosphocholine
DMPC	1,2-dimyristoyl-*sn*-glycero-3-phosphocholine
DOSY	diffusion-ordered spectroscopy
DPC	dodecylphosphocholine
DSS	2,2-dimethyl-2-silapentane-5-sulfonate
EDC	1-ethyl-3-(3-dimethylaminopropyl)carbodiimide
ER	endoplasmic reticulum
ET	electron transfer
HADDOCK	high ambiguity driven biomolecular docking
HARLEM	hamiltonians to research large molecules
HIMSELF	heteronuclear isotropic mixing leading to spin exchange via the local field
HSQC	heteronuclear single quantum coherence
HMQC	heteronuclear multiple quantum correlation
INEPT	insensitive nuclei enhanced by polarization transfer
LB	lysogeny broth
MD	molecular dynamics
MF	methoxyflurane
NMR	nuclear magnetic resonance
TROSY	transverse relaxation optimized spectroscopy
NOE	nuclear overhauser effect
NOESY	nuclear overhauser enhancement spectroscopy

PC	phosphocholine
PISA	polarity index slant angle (chapter 3)
PISA	protein interfaces, surfaces and assemblies (chapter 4)
PIWIMz	polarization inversion by windowless isotropic mixing
PRE	paramagnetic relaxation enhancement
SLF	separated local field
SDS PAGE	sodium dodecyl sulfate polyacrylamide gel electrophoresis
SOFAST	band-selective optimized-flip-angle short-transient
SSDM	single site-directed mutagenesis
TOCSY	total correlation spectroscopy
TROSY	transverse relaxation optimized spectroscopy
U-	uniformly labeled
WIM	windowless mixing

CHAPTER 1

Introduction: Biological background

1.1 Cytochrome b_5 (cyt b_5)

1.1.1 Cyt b_5 background

Cytochrome b_5 (cyt b_5) is a 15.4 kDa hemoprotein that plays a key role in a number of electron transfer reactions. It was first discovered in the endoplasmic reticulum (ER) of liver tissue in 1952 by Strittmatter *et al.*[1] In mammals, it is a ubiquitous protein found in three locations:[2–4] the outer mitochondrial membrane, the ER membrane and erythrocytes. The membrane-anchored form of cyt b_5 that sits on the cytoplasmic side of the ER membrane[5] is commonly referred to as microsomal cyt b_5 and contains three separate domains: an N-terminal, cytosolic, heme-containing domain (≈70 amino acid residues), a linker region (≈15 residues), and a C-terminal, hydrophobic, membrane-binding domain (≈40 residues) (Figures 1.1 and 1.2).[6] The soluble version of the protein (located in erythrocytes) merely consists of the hydrophilic heme-containing domain of microsomal cyt b_5, and is often referred to as truncated cyt b_5.[2,6–9] Cyt b_5 is an acidic protein with around 20% of its residues as glutamates or aspartates (Figure 1.1), especially around the heme-edge (Figure 1.2).[10] Only high-resolution structures of the soluble domain of truncated cyt b_5 have been solved by Nuclear Magnetic Resonance (NMR) and X-ray crystallography (both wild-type[11–27] and mutants[28–35] of different species); the cyt b_5 sequences in these structures often have deletions at the beginning of the N-terminus and truncation either in or after the linker region. No structure of the soluble domain, and linker region, of the full-length protein is currently known. As for the membrane domain, which spans the ER membrane,[36] circular dichroism and Fourier Transform Infrared experiments have indicated that it is at least 50% helical,[37–39] and recent solid-state NMR experiments have shown that it is a single-pass transmembrane α-helix[40].

```
1                 10                  20                  30                  40
M A A Q S D K D V K Y Y T L E E I K K H N H S K S T W L I L H H K V Y D L T K F

41                50                  60                  70                  80
L E E H P G G E E V L R E Q A G G D A T E N F E D V G H S T D A R E L S K T F I

81                90                 100                 110                 120
I G E L H P D D R S K L S K P M E T L I T T V D S N S S W W T N W V I P A I S A
                  |---------- linker ---------|

121               130
L I V A L M Y R L Y M A D D
```

Figure 1.1 Sequence of rabbit cyt b$_5$. Residues in blue and red are positively and negatively charged, respectively. In green are the histidines that coordinate the heme Fe(III). The linker residues are labeled according to Clarke *et al*.[6]

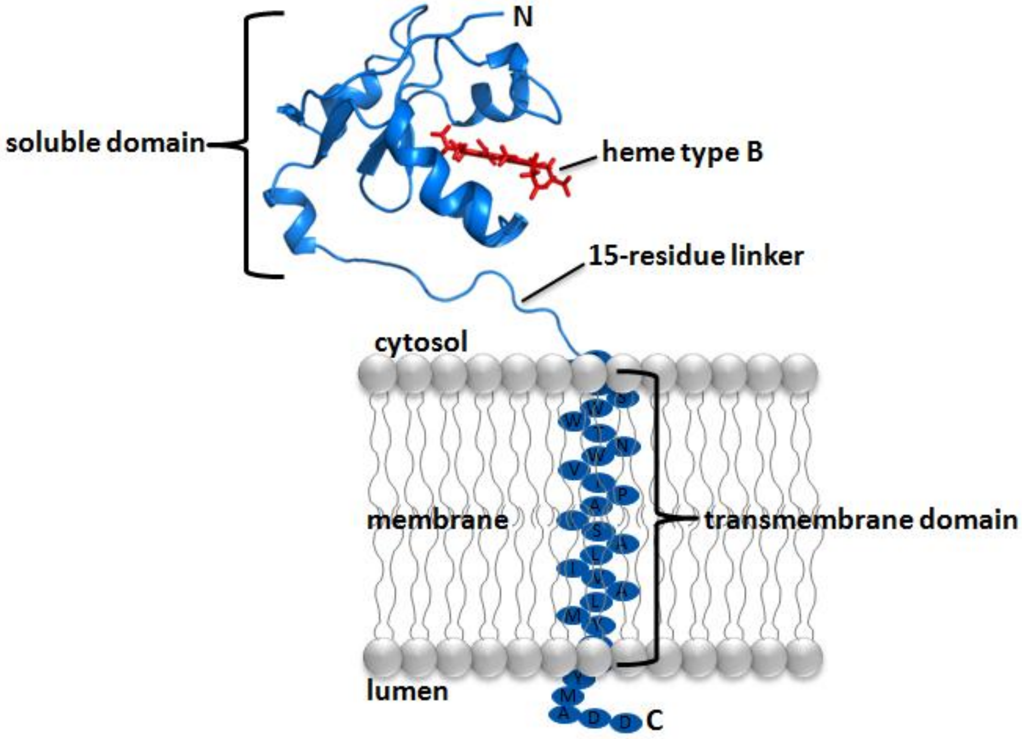

Figure 1.2 Domains of microsomal cyt b$_5$. The solution NMR structure of the soluble domain of cyt b$_5$ (Chapter 3) was used to create this figure.

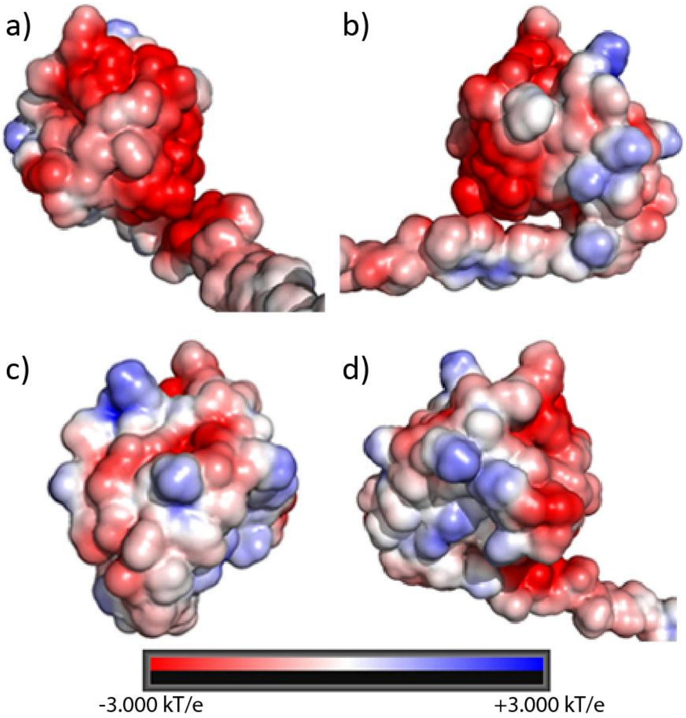

Figure 1.3 Electrostatic potential surface for the soluble domain of rabbit cyt b_5 calculated using the PDB2PQR[41,42] server and PyMOL[43] with the APBS plugin 2.1.[44] Panel a) is the proximal side of cyt b_5 where the heme is solvent exposed, and b) through d) are successive counter-clockwise 90° from the orientation in a). The cyt b_5 structure used for the generation of this figure is the NMR-derived structure presented in Chapter 3.

Cyt b_5 is found in mammals, invertebrates and plants. Comparisons of cyt b_5 sequences can be found in numerous publications.[3,6,25] The sequence of rabbit cyt b_5 (studied in this thesis) is extremely similar to other vertebrates and only mildly similar to non-vertebrates (Figure 1.1).[6] The heme-domain of cyt b_5 is the most strongly conserved region, with rabbit cyt b_5 sharing 74-95% sequence homology with other vertebrates, but only 40-59% with the cytochromes b_5 (cyts b_5) of plants and invertebrates.[6] In this domain, the most strongly conserved residues are H44 and H68, which are ligated axially to the heme Fe(III). Both the linker length and sequence of microsomal cyts b_5 are conserved to a high degree (60-80%) in vertebrates, with K94 being the most conserved residue.[6] The membrane-binding domain is also strongly conserved among vertebrates (78-96%), but not among non-vertebrates.[6]

1.1.2 Cyt b_5 significance

Cyt b_5 is involved in a number of physiologically vital functions. The truncated isoform of cyt b_5 is involved in reducing methemoglobin to hemoglobin in erythrocytes.[45,46] Membrane-bound cyts b_5 are involved in the fatty acid desaturation system;[2,9,47–49] possibly aid in fatty acid elongation;[50–52] carry out a key role in the biosynthesis of cholesterol;[2,3] and participate in the hydroxylation of N-acetyl-neuraminic acid.[53] Cyt b_5 is also a part of the microsomal oxidation and hydroxylation systems in which it interacts with a variety of cytochromes P450.[2,3,54–57]

Because of its various roles, deficiencies and mutations of cyt b_5 have been associated with different abnormalities and health conditions. In 1986, the first case of congenital methemoglobinemia (type IV)[58] due to a deficiency of truncated cyt b_5 was discovered.[59,60] Methemoglobinemia is a blood disorder characterized by abnormally high amounts of methemoglobin (the oxidized form of hemoglobin) in the bloodstream, which results in lower amounts of oxygen being delivered to tissues.[61] The patient’s erythrocyte cyt b_5 levels were only ~25% of the normal level. In the same case, the patient was also diagnosed as a pseudohermaphrodite male because of the cyt b_5 deficiency.[60,62] It was hypothesized that the decreased amount of cyt b_5 resulted in low levels of androgen synthesis (specifically testosterone), which caused the pseudohermaphrodism.[62] In 2010 and 2012, two additional studies of cyt b_5 genetic mutations (W27X and H44L, respectively) reported patients with ambiguous genetalia and concluded that this was a result of low or absent 17,20-lyase activity (termed isolated 17,20-lyase deficiency).[63,64]

Since the content of cyt b_5 has been shown to decrease with aging,[65] some have hypothesized that cyt b_5 might be implicated in Alzheimer's disease. Cyt b_5 participates in a reaction that ensures the functioning of the lipid-radical cycles; it transports an electron from the outer membrane to peroxyl radical ($LOO^{\cdot}$), which is found in the inner membrane. Without this reduction, adenine nucleotide transporter cannot be activated, and lipid peroxidation is induced. The increase in the rate of lipid peroxidation causes the formation of ageing aldehydes (e.g. malonic dialdehyde and methylglyoxal). Alzheimer's disease, and other age-related diseases, have been associated with elevated levels of aldehydes.[66,67]

Cyt b_5 has also been determined to be a major reductant of indoleamine 2,3-dioxygenase (IDO) in humans.[68,69] IDO is an enzyme that catalyzes the beginning of the metabolism of *L*-tryptophan. To this regard, deficiencies and/or mutations of cyt b_5 are indirectly involved in cancer (where IDO is overexpressed and blocks activation of T lymphocytes),[70–72] neurodegenerative diseases,[73] depression,[74] and cataracts.[75]

1.1.3 Cyt b_5 and its promiscuous association with numerous redox partners

Cyt b_5 interacts with both electron acceptor proteins and electron donor proteins.[7,76,77] As discussed in the previous section, the truncated isoform of cyt b_5 reduces methemoglobin;[45,46] it can also donate an electron to metmyoglobin.[78] The membrane-bound form of cyt b_5 can accept electrons from NADH-cyt b_5 reductase[76,77,79–81] and NADPH-cytochrome P450 reductase,[82,83] and can transfer electrons to numerous proteins such as cytochromes P450 (cyts P450),[84–92] indoleamine 2,3-dioxygenase,[68,69] stearyl coenzyme A desaturase[48,49,82,93] and other fatty acid desaturase enzymes[2]. For an extensive list of all the known redox partners of cyt b_5, please refer to an excellent review article by Schenkman *et al.*[3] Cyt b_5 amino acid residues implicated in some of these interactions are shown in Tables 1.1 and 1.2. While the hydrophobic segment of microsomal cyt b_5 has been shown not to be needed for electron transfer between cyt b_5 and its reductase,[94] it has been proved necessary for successful complex formation with stearyl-CoA desaturase[39,49,82] and NADPH-cytochrome P450 reductase[82,83,95].

As mentioned, cyt b_5 forms complexes with a variety of cyts P450 (more details in Section 1.3).[84–92] Cyt b_5 regulates the activity of cyt P45017α, which is a key enzyme in the biosynthesis of glucocorticoids and sex hormones.[96] The mitochondrial cyt P450scc cholesterol side-chain cleavage reaction is stimulated by cyt b_5.[89,90] Cyt b_5 also participates in the catalytic activity of cyt P450 3A4 (e.g. 6β-hydroxylation of testosterone).[56,57,97–99] The C-terminal hydrophobic domain of cyt b_5 is required for interaction with all cyts P450, including cyt P450 2B4.[2,7,84,87,100,101] Truncated cyt b_5 is only capable of donating an electron to the soluble bacterial protein cyt $P450_{cam}$.[102]

Extensive work has been done on the complex between cytochrome *c* (cyt *c*) and cyt b_5, which can interact with each other in their truncated forms.[30,31,95,103–127] Cyt b_5 can reduce cyt *c*, and may be a physiological partner of cyt b_5 in the initiation of cell apoptosis.[128] A cursory list of cyt b_5 residues involved in complex formation with cyt *c* are provided in Table 1.1.

1.1.4 Rabbit cyt b_5

Rabbit cyt b_5 was used in the work presented in this thesis for two key reasons. (a) NMR studies require high concentrations of isotopically labeled protein. The Waskell lab has successfully established the protocol for the over-expression and subsequent purification of full-length rabbit cyt b_5 in *Escherichia coli*,[129] as well as the conditions for the expression of the ^{15}N-labeled protein[40]. Our lab has effectively applied solid-state NMR to the purified labeled protein.[40,130,131] Similar ^{15}N-labeled protein expression and purification procedures have also been applied to a mutant of cyt b_5 (used in Chapter 6), which has also been used for solid-state NMR method development in our lab.[132,133] (b) As discussed in Section 1.1.1, the entire sequence of full-length rabbit cyt b_5 is highly homologous to that of other vertebrates.[6] The structure of full-length rabbit cyt b_5 and the residue-specific details of its interactions with cyt P450 2B4, presented in this thesis, should thus be applicable to other mammalian cyts b_5.

Table 1.1 Cursory summary of cyt b_5 residues proposed to be at the interface with redox partners other than cyt P450.

Cyt b_5	Redox partner	Experimental Technique	Interface residues and notes	Non-interface residues	Reference
bovine liver	NADH-cyt b_5 reductase	modification of lysyl residues by acetylated or trinitrophenylation		lysyl residues	134
bovine	tuna heart cyt *c*	least squares fitting model	Carboxyl groups of E53, E49, D65, as well as the most exposed heme propionates [+5]*		135
bovine	NADH-cyt b_5 reductase	modification of carboxyl group with methylamine (or glycine ethyl ester – residues not identified)	E48, E49, E53 [+1], propionate of heme, and a fifth unidentified side chain carboxyl group		79
bovine liver	methemoglobin subunits	computer graphics-generated model	E49, E48, E53, D65 and heme propionates [+5]		136
bovine heart	metmyoglobin from bovine heart & yellowfin tuna	^{1}H NMR	largest CSPs[1] for heme 6-propionate methylene group		78
bovine liver	cyt *c*	DME[1] substituted heme	an ensemble of protein-protein complexes exist in solution as a precursor to efficient electron-transfer geometry		112
rabbit cyt b_5	NADPH-cyt P450 reductase	EDC[2] cross-linking		charge-pairing interactions	95 and 137
rat	horse heart cyt *c*	SSDM[3], high-pressure technique and UV-Vis binding assay	D65(N), E53(Q), E49(Q), heme propionates (DME) [+5]		110
bovine liver	horse heart cyt *c*	EDC[2] cross-linking		did not find residues 59-77 to be important but they say their technique was inadequate	111

Cyt b_5	Redox partner	Experimental Technique	Interface residues and notes	Non-interface residues	Reference
bovine liver	NADH-cyt b_5 reductase	EDC[2] cross-linking	heme propionates, E53 and/or E61, E48 and/or E49 [+1]		80
rat liver	horse heart cyt *c*	ΔG	E49(Q), E53(Q), D65(N), heme propionates (DME) [+5]	Q13 (K18 in our b_5) E42(Q), E48(Q), E61(Q), D71(S)	138
bovine	cyt *c*	$Cr(en)_3^{3+}$ solvent paramagnetic effect	G47 and E48, with heme being partly accessible [+5]	H31, A59, T60, H85	139
bovine	yeast iso-1-ferricytochrome *c*	Brownian dynamics method simulated diffusional docking	E53, E61, D65 & heme [+5] E49, E53, D65 & heme (two clusters of complexes) ionic strength dependence		140
bovine	cyt *c*	mutation and UV-Vis assays	E49A, E61A [+5] double mutant E49A/E61A must be ionic strength dependent		122
bovine	pig liver NADH-cyt b_5 reductase	FRODO computer docking	E49, D71 and propionates [+5]		81
bovine	horse heart cyt *c*	mutation & cycle voltammetry	E49, E61 or both [+5]		120
human erythrocyte	human erythrocyte NADH-cyt b_5 reductase	activity assays	E42, E43, D58, E64 [+1]	removal of one or all: E48, E49, E53, E61, D65, heme propionates	76
human erythrocyte	human erythrocyte NADH-cyt b_5 reductase	mutation & UV-Vis binding assays	E43(A), D71(A) [+1]	E42(A), E64(A), E74(A)	77
bovine liver	horse heart cyt *c*	electron transfer rate, and binding assay	E49, E61 and both		114
bovine	ferrous cyt *c*		Y11, H20, N22(H22), S23, K24, S25, W27, H31, E42, G56 and T60 [+5]		126

Cyt b_5	Redox partner	Experimental Technique	Interface residues and notes	Non-interface residues	Reference
bovine	ferric cyt *c*		much smaller CSPs than for ferrous cytc, with the largest shifts for G56, H31, A59 and I81 [+5]		126
bovine	horse cyt *c*	titration in NMR using CSPs[4] comparison between a quadruple mutant of cyt b_5 and wild-type	Quadruple mutant E49(A), E53(A), E61(A) and D65(A) [+5]		30
oxidized bovine	horse heart cyt *c*	NMR & various combinations of mutants (double & triple)	E45(removal), E53(removal), E61(A), D65(A) [+5]		124
bovine liver	horse heart cyt *c*	UV-Vis binding assay, Stopped flow kinetics	F35(Y) actually increases the ET[5] rate but binding constant is the same	F35(L) – no effect on binding or ET[5] rate; disproves aromatic channel theory F35(Y) – no effect on binding	127
bovine	horse heart cyt *c*	• CSP[4] • NMR relaxation rates • NMR cross saturation	• L14, H20, I29, H44, G46, E49, A59, E61, V66, H68, S69, A72 [+5] • E43, A59, V66, G67, H68 [+5] • G47, E48, L51, E64, D65, G82 [+5]		103
bovine liver	horse heart cyt *c*	SSDM[3], double & triple mutants of cyt b_5, UV-Vis binding assay, stop flow kinetics, Brownian Dynamics simulation	E44(A), E56(A), E44/E56(A), E44/E48(A) E48/E56A), E48A/D60A, E44/E48/E56(A), E44/E56/D60(A), E48/E56/D60(A), E44/E48/E56/D60(A) – all these weaken binding but ET is still possible V45(H/E) lower binding & scattered docking geometries[+5]	P40(V), F58(Y/W), V61(H/E) F35(Y/L) does not affect binding or ET	107

[1] DME: dimethyl ester; [2] EDC: 1-ethyl-3-(3-dimethylaminopropyl)carboiimide; [3]SSDM: single site-directed mutagenesis; [4]CSPs: chemical shift perturbations; and [5]ET: electron transfer

*the number in the [] bracket indicates the number added to align the cyt b_5 sequence (the sequences are highly homologous and thus only the sequence numbering needs to be shifted).

The parentheses () contain the identity of the amino acid to which the residue was mutated.

1.2 Cytochrome P450 (cyt P450)

1.2.1 Background and significance

Cytochrome P450 (cyt P450) is a protein found in organisms from all biological kingdoms, including plants, fungi, bacteria, insects and animals.[141,142] In mammals, all cyts P450 are membrane-bound, with most of them localized in the endoplasmic reticulum and some in the mitochondrion.[143] Humans possess 57 membrane-bound cyts P450, which are found in all tissues of the body and in all cell types.[144,145] Cyts P450 metabolize a wide array of endogenous (steroids, retinoids, fatty acids, etc.) and exogenous compounds (drugs, environmental toxins, plant products, etc).[146] One of the most studied reactions in which cyts P450 are involved is the regio- and stereospecific oxidation of non-activated hydrocarbons,[147] which follow this reaction stoichiometry: $NADPH + H^+ + R + O_2 \rightarrow NADP^+ + H_2O + RO$, where R is the substrate and RO is the product. In performing this reaction, cyts P450 are able to convert hydrophobic compounds intro hydrophilic products that can be excreted from the body via urine. Cyts P450 are responsible for the Phase I oxidative metabolism of xenobiotics in which a C-H bond is converted to a C-OH bond.[143,148–150] Depending on how the compound is converted to a hydrophilic molecule, cyts P450 can convert an inactive compound into a pharmacologically active one (pro-drug), or convert an inert compound into a toxic one. Metabolism performed by cyts P450 therefore regulates the therapeutic effectiveness and side effects of drugs. By understanding the variations in human cyts P450 (on an individual level), and thereby being able to predict whether a drug will be pharmacologically active or toxic, it is hoped that doctors will be able to better personalize drugs to patients in the future.[150–152]

Although a large focus of the research on cyts P450 has centered on their involvement in the metabolism of drugs, cyts P450 are also involved in other physiological pathways, including cholesterol metabolism, bile-acid biosynthesis and metabolism, as well as vitamin D_3 synthesis and metabolism.[143,153] Several important functions have been ascribed to cyts P450 present in the brain,[154] including the regulation of compounds that can cross the blood-brain barrier,[155] and the biosynthesis of dopamine and 5-hydroxytryptamine.[156,157]

Cyts P450 also heavily influence the development and/or treatment of certain health conditions.[153] Cyts P450 have been linked to the pathogenesis and progression of cardiovascular diseases.[158] Cyt P450 1B1 has been shown to be overexpressed in numerous human cancers, including breast, colon, lung, skin and brain cancers.[159,160] Mutations in cyt P450 1B1 can also cause primary congenital glaucoma.[161] Cyts P450 are also involved in inflammatory disorders, pulmonary hypertension and coronary artery disease.[153,162,163] A specific cyt P450 isoform is the target for the treatment of prostate cancer.[164,165] Tamoxifen, an important pro-drug against breast cancer, is metabolized to its active form by cyts P450.[166–168]

Hydroxylating inactive C-H compounds via traditional organic chemistry pathways is a very challenging task. Utilizing cyts P450 to do this in synthetic systems has therefore been highly sought out, with many review articles dedicated to the research done towards this feat.[147,169–172] An example of this application of cyts P450 was the engineering of yeast to produce the precursor of an antimalarial drug.[173]

Many additional review articles and books have been dedicated to various aspects of cyts P450.[141,144,146,147,150,151,174–188]

1.2.2 Structure and membrane topology of rabbit cyt P450 2B4

Rabbit cyt P450 2B4 (studied in this thesis) was the first mammalian cyt P450 isolated from microsomal membranes.[189] The structure of cyt P450 2B4,[190–199] its binding to substrates,[200–205] stabilization of its O_2 intermediate[206,207] and its peculiar interaction with cyt b_5[6,200,201,205,208–213] have been studied extensively; these findings can be extrapolated to other mammalian microsomal cyts P450, particularly cyt P450 2B6.[199,214] Similarly to rabbit cyt b_5, the Waskell lab has established a protocol for the overexpression and purification of full-length cyt P450 2B4;[215] this allowed us to perform studies of the complex between isotopically-labeled full-length cyt b_5 and unlabeled full-length cyt P450 at high concentrations suitable for NMR (Chapters 4-6). Expression of recombinant human cyt P450 (e.g. cyt P450 3A4) yields significantly lower quantities of protein, which currently make it unsuitable for NMR studies. Human cyts P450 are also typically less stable than the rabbit proteins; e.g. human cyt P450 3A4 loses its heme and can form dimers via its surface disulfide bridges.

Cyt P450 2B4 is a 55.7 kDa protein found on the cytoplasmic side of the ER membrane of rabbit hepatocytes.[216] The structure of microsomal cyts P450 consists of a large, heme-containing soluble domain (≈53 kDa) and a transmembrane anchor (Figure 1.3). In cyt P450 2B4, the heme (type B) is axially coordinated to residue C436. Cyt P450

2B4 is a highly charged protein with a depression on its proximal surface, where the heme comes closest to the surface (Figure 1.4 and Figure 1.5). The N-terminus, which caps the end of the transmembrane domain, is known to face the luminal side of the ER membrane.[217–220] The structure of truncated cyt P450 2B4 has been solved in the presence of various ligands[190–197,199] and in one open conformation[198]. The structure of the transmembrane domain, however, is unknown, though it is estimated to be a single α-helix, based on the thickness of the non-polar region of the ER membrane (30-40 Å) and the dimensions of a typical helix.[221]

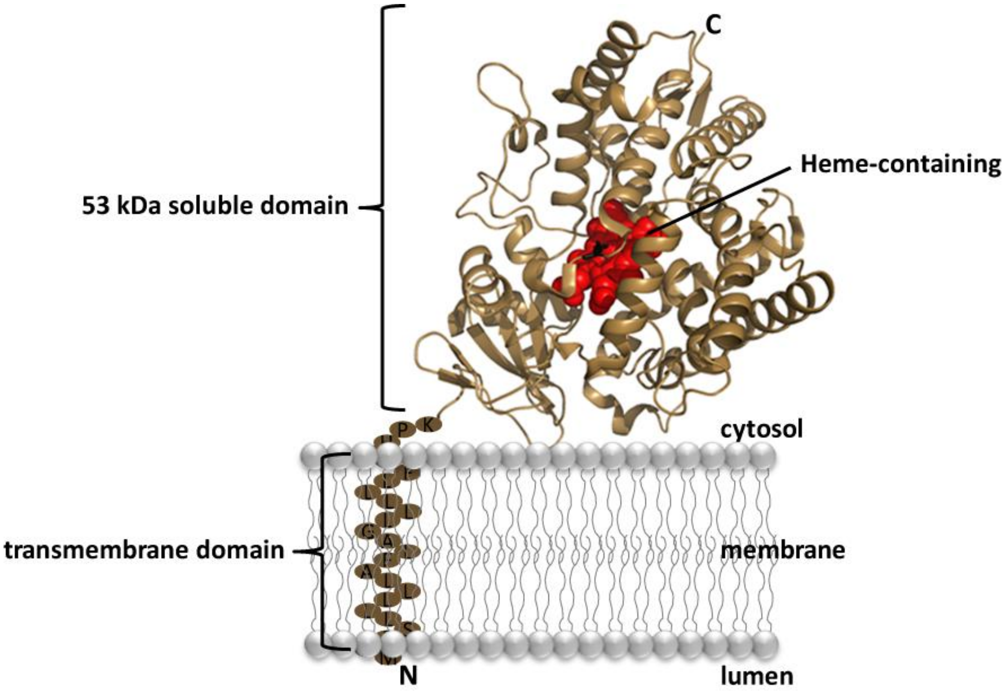
C
Heme-containing
53 kDa soluble domain
K
P
cytosol
L
L
L
G
A
A
L
L
L
S
transmembrane domain
membrane
N
lumen

Figure 1.4 Cyt P450 2B4 structural domains.

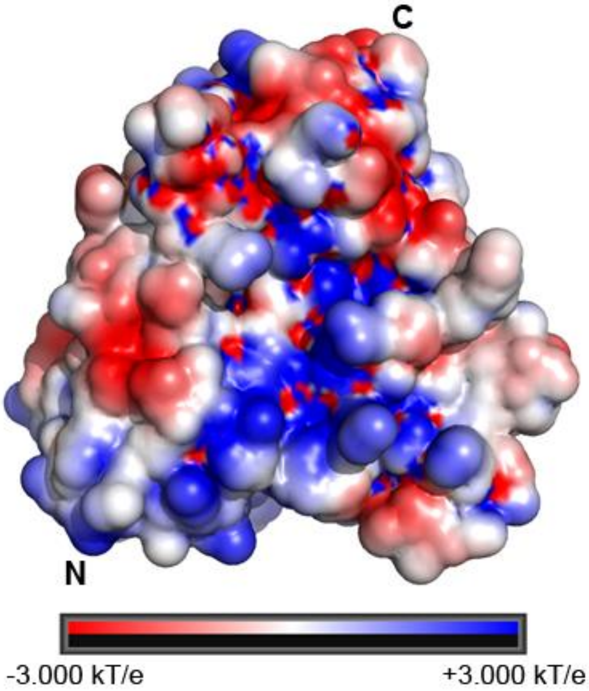

Figure 1.5 Electrostatic potential surface for the proximal side (where the heme is closest to the surface) of the soluble domain of cyt P450 2B4 calculated using the PDB2PQR[41,42] server and PyMOL[43] with the APBS plugin 2.1.[44]

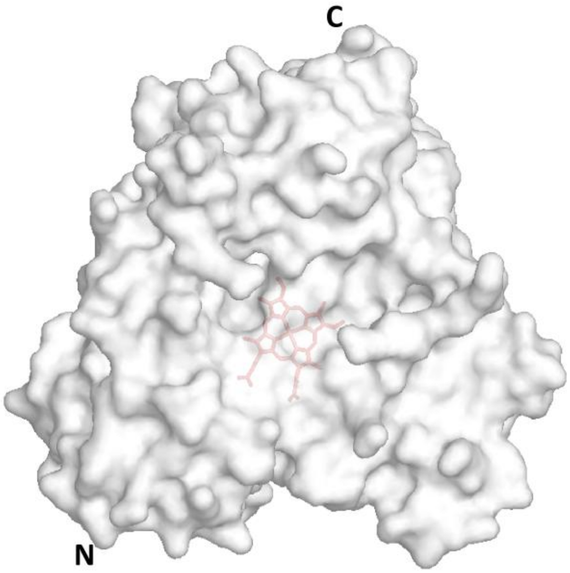

Figure 1.6 Heme showing through the proximal surface of cyt P450 2B4. This surface representation of cyt P450 was prepare with PyMOL[43] and the PDB structure 1SUO[191].

The sequence and secondary structure elements for truncated cyt P450 2B4, pdb structure 1SUO,[191] can be found in Figure 1.6. Five "plastic regions" (PR), which undergo conformational changes upon ligand binding, have been identified for cyt P450 2B4: PR1 (residues 39-57), PR2 (residues 101-140), PR3 (residues 177-188), PR4 (residues 203-298), and PR5 (residues 474-480).[197]

Eukaryotic truncated cyts P450 have been shown to bind to the membrane even in the absence of their N-terminal transmembrane domain.[221] Truncated cyt P450 1A1 (lacking residues 2-30) was found to still be membrane-bound, even at 800 mM NaCl, which indicates that other regions of cyt P450 interact hydrophobically with the membrane.[222] The truncated forms of cyt P450 2E1 and cyt P450c17 were also found to bind tightly to the bacterial membrane and the interactions were shown, as well, to be unperturbed by high ionic strengths or alkaline pH.[223,224] The ability of truncated cyt P450 to bind to membranes has been shown for a variety of other microsomal cyts P450,[224–228] including cyt P450 2B4.[226] Previous papers have reported that cyt P450 2B4 is not deeply imbedded[229] but does have additional segments binding to the membrane (~500 $Å^2$) since a single transmembrane helix would only account for a surface area of 120-250 $Å^2$.[230]

Apart from their hydrophobic N-terminus region, microsomal cyts P450 are postulated to interact with the membrane via the loop before helix A, the B'/C loop and residues between F and G helices (Figure 1.8).[230] These additional membrane interactions allow for the catalytic active center to be more rigidly held in a specific orientation above the bilayer. Additionally, the burial of a large portion of cyt P450 inside the membrane allows for the entrance of the substrate access channel to be inside the bilayer, where the hydrophobic substrates are more soluble.[199,230–232] This orientation places both the heme and the proximal surface of cyt P450 (where the heme comes closest to the surface) perpendicular to the membrane surface, in an orientation which leads to optimal contact with its redox partners.[221,233–236] This orientation also allows the electrostatic dipole of cyt P450 to be parallel to the membrane surface. For cyt P450 2C5, the hydrophobic surface was found to include six residues before helix A, ten residues after helix A, residues corresponding to $\beta_{2\text{-}2}$ in other cyt P450 structures, and the C-terminal end of the region between the F- and G-helix.[237] For cyt P450 19, it is believed that the segments that could be buried in the membrane include parts of β1 and β2 sheets, the B’ helix, and the F-G loop.[238] For cyt P450 2B4, Zhao *et al.* have proposed that the hydrophobic surface binding the membrane consists of residues 30-45 before helix A, $\beta_{1\text{-}1}$-$\beta_{1\text{-}2}$ loop, residues 101-116 before helix C, helix F’ and flanking residues (Figure 1.9).[197] The B’/C loop and F/G region contain five phenylalanines (108, 212, 220 and 223) which are known to have a tendency to penetrate the hydrophobic regions of membranes.[236] Above the proposed membrane-submerged regions, there are basic residues that would interact favorably with the lipid headgroups. This model proposed by Zhao *et al.* also agrees with previous atomic force microscopic measurements which indicated that cyt P450 sits about 35 ± 5 Å above the phospholipid-water boundary (Figure 1.8).[236]

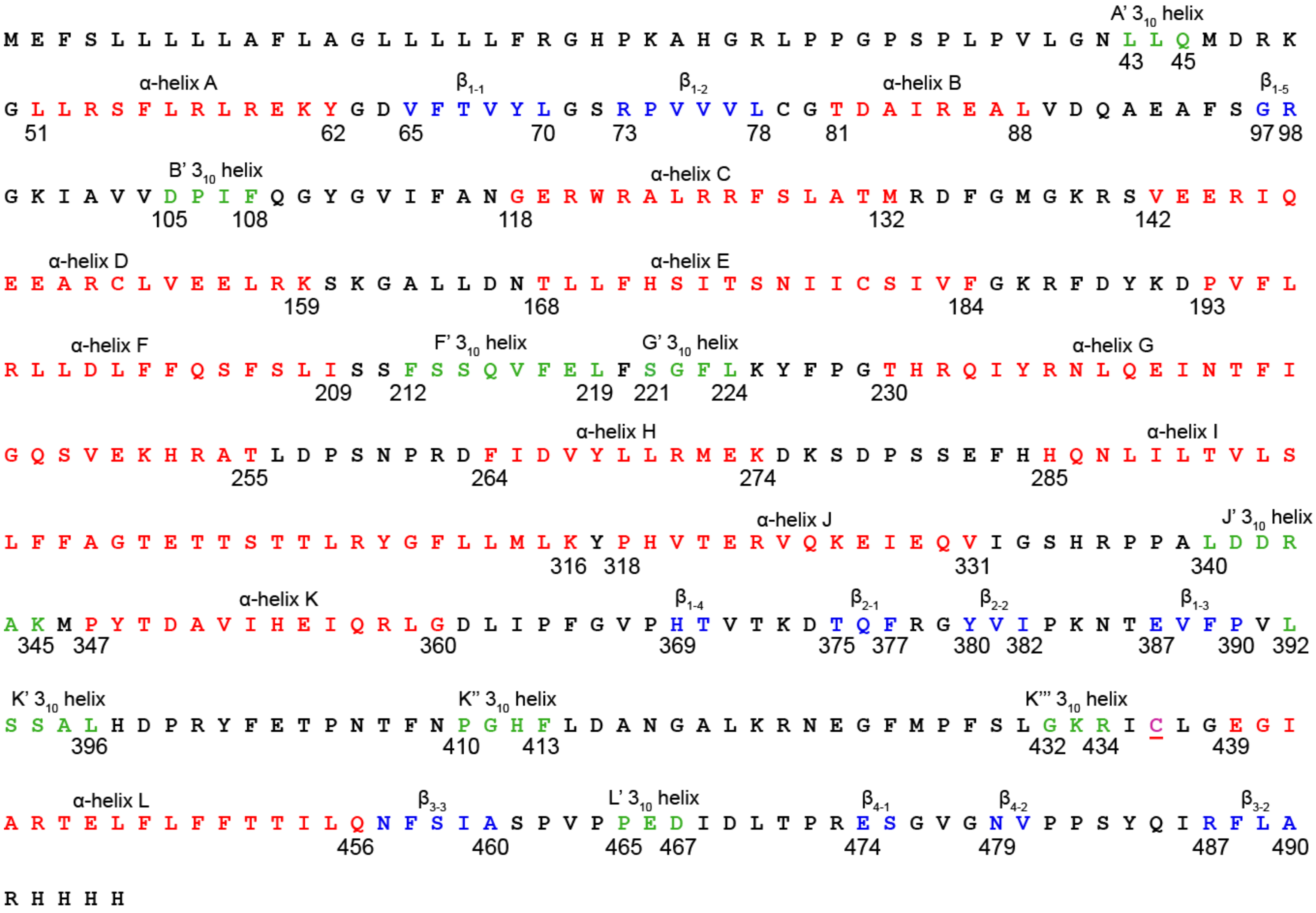
A' 3₁₀ helix
M E F S L L L L L A F L A G L L L L L F R G H P K A H G R L P P G P S P L P V L G N L L Q M D R K
43 45
α-helix A
β1-1
β1-2
α-helix B
β1-5
G L L R S F L R L R E K Y G D V F T V Y L G S R P V V V L C G T D A I R E A L V D Q A E A F S G R
51 62 65 70 73 78 81 88 97 98
B' 3₁₀ helix
α-helix C
G K I A V V D P I F Q G Y G V I F A N G E R W R A L R R F S L A T M R D F G M G K R S V E E R I Q
105 108 118 132 142
α-helix D
α-helix E
E E A R C L V E E L R K S K G A L L D N T L L F H S I T S N I I C S I V F G K R F D Y K D P V F L
159 168 184 193
α-helix F
F' 3₁₀ helix
G' 3₁₀ helix
α-helix G
R L L D L F F Q S F S L I S S F S S Q V F E L F S G F L K Y F P G T H R Q I Y R N L Q E I N T F I
209 212 219 221 224 230
α-helix H
α-helix I
G Q S V E K H R A T L D P S N P R D F I D V Y L L R M E K D K S D P S S E F H H Q N L I L T V L S
255 264 274 285
α-helix J
J' 3₁₀ helix
L F F A G T E T T S T T L R Y G F L L M L K Y P H V T E R V Q K E I E Q V I G S H R P P A L D D R
316 318 331 340
α-helix K
β1-4
β2-1
β2-2
β1-3
A K M P Y T D A V I H E I Q R L G D L I P F G V P H T V T K D T Q F R G Y V I P K N T E V F P V L
345 347 360 369 375 377 380 382 387 390 392
K' 3₁₀ helix
K'' 3₁₀ helix
K''' 3₁₀ helix
S S A L H D P R Y F E T P N T F N P G H F L D A N G A L K R N E G F M P F S L G K R I C L G E G I
396 410 413 432 434 439
α-helix L
β3-3
L' 3₁₀ helix
β4-1
β4-2
β3-2
A R T E L F L F F T T I L Q N F S I A S P V P P E D I D L T P R E S G V G N V P P S Y Q I R F L A
456 460 465 467 474 479 487 490
R H H H H

Figure 1.7 Sequence and secondary structure elements of cyt P450 2B4 (based on structure with PDB code 1SUO[191]).

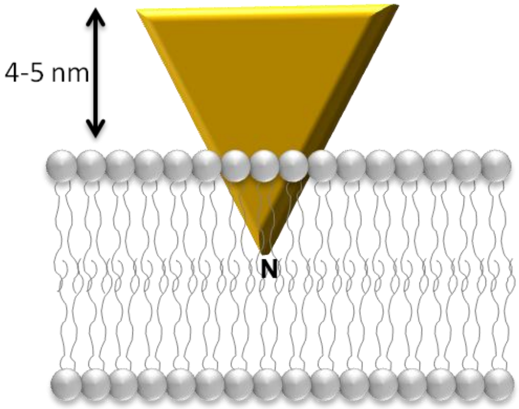

Figure 1.8 Cyt P450 2B4 orientation in the membrane based on atomic force microscopy.[236]

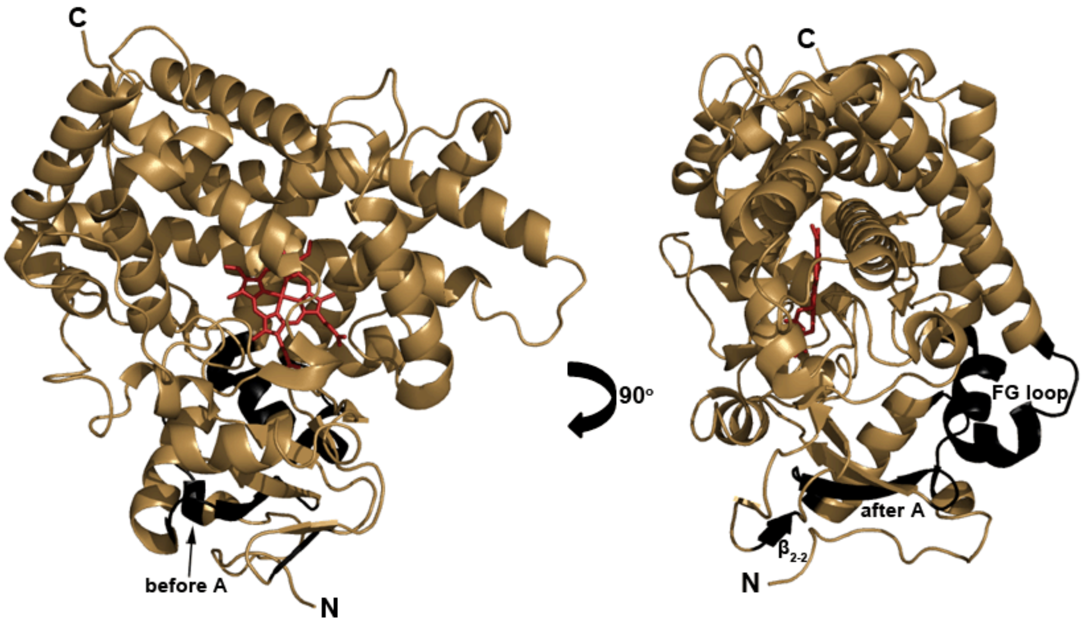
C
before A
N
90°
C
FG loop
after A
β_{2-2}
N

Figure 1.9 Important segments (black) for membrane binding of mammalian cyts P450, proposed by Williams *et al.*[230] **PDB structure 1SUO**[191] **of cyt P450 2B4 was used for this figure.**

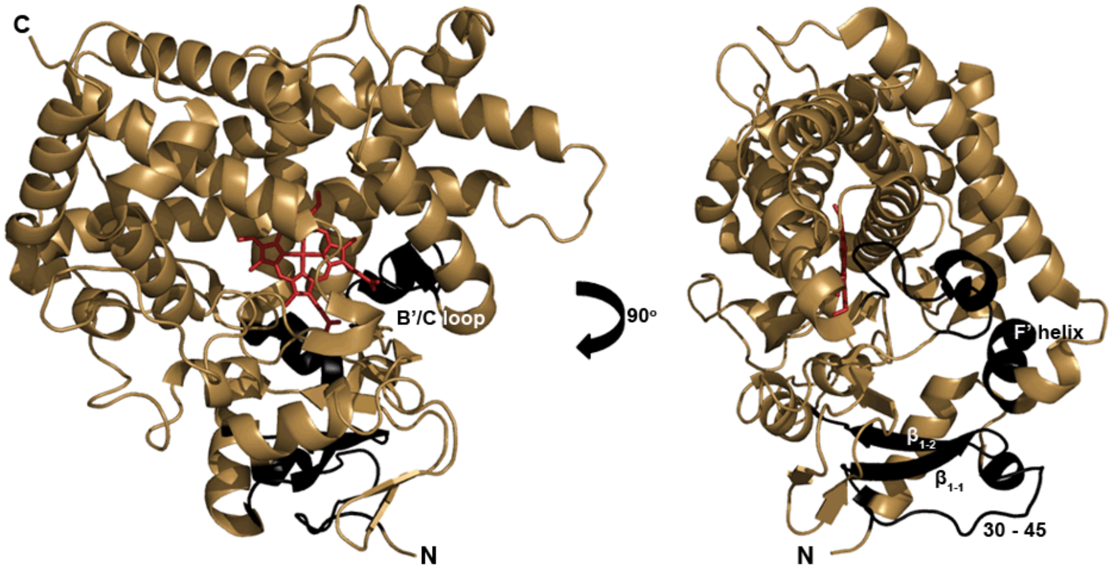

Figure 1.10 Important segments (black) of cyt P450 2B4 for membrane binding proposed by Zhao *et al.*[197] PDB structure 1SUO was used for this figure.[191]

1.3 The role of cyt b_5 in cyt P450 reactions

As mentioned in Section 1.1.3, cyt b_5 interacts with many isoforms of cyt P450. Hildebrandt and Estabrook were the first to suggest that cyt b_5 participates in cyt P450 reactions.[54] This turned out to be a controversial finding, with Jansson and Schenkman publishing a direct rebuttal of their paper, using the exact same title but swapping out "for" with "against" in "Evidence for the participation of cytochrome b_5 in the hepatic microsomal mixed-function oxidase reaction."[239] Subsequently, a series of studies on *in vitro* systems were published to prove the involvement of cyt b_5 in cyt P450 reactions.[240–244] Over 30 years later, it was finally unequivocally established that cyt b_5 did have a function in cyt P450 reactions *in vivo*.[245,246]

Two electrons are required for the cycle in which cyt P450 catalyzes the insertion of “activated” molecular oxygen into a substrate (see Section 1.2.1). Cyt P450 obtains both electrons from its redox partners: cyt P450 reductase and cyt b_5.[247] Whereas cyt P450 reductase can donate both electrons to cyt P450, cyt b_5 can only donate the second electron due to its high redox potential compared to ferric cyt P450.[151,209] A lot of attention has been drawn to the variable role that cyt b_5 plays in cyt P450 reactions: cyt b_5 has been shown to stimulate, inhibit or have no effect on cyt P450-catalyzed reactions, depending on the following variables: the specific isoform of cyt P450, the substrate of the reaction and the sample conditions.[3,212,248,249] This can be partially explained by the observation that cyt b_5 and cyt P450 reductase share overlapping but non-identical binding sites on the proximal side of cyt P450 2B4 (Figure 1.4 and Figure 1.5).[211] At low concentrations, cyt b_5 can accelerate cyt P450 metabolism by up to 100-fold faster, which allows less time for side product formation than in the presence of cyt P450 reductase.[208,247] At higher concentrations, however, cyt b_5 competes with cyt P450 reductase and inhibits reductase from binding to cyt P450, thereby inhibiting both the delivery of the first electron and its catalytic activity.[209] At a cyt b_5 concentration where the inhibitory and stimulatory effects are equal, cyt b_5 will appear to have no effect on the activity of cyt P450.[247] There is currently no consensus on the mechanism by which cyt b_5 interacts with cyt P450. Three hypotheses exist: either cyt b_5 transfers an electron to cyt P450, or cyt b_5 causes an allosteric effect on cyt P450, or both of these mechanisms happen simultaneously.[3,57,97,250,251]

Numerous studies have addressed the residues at the interface between different isoforms of cyt b_5 and cyt P450 using cross-linking, mutagenesis, mass spectrometry and computer modeling, among other techniques. See Table 1.2 for a list of cyt b_5 residues proposed to interact (or not) with cyt P450, and Table 1.3 for cyt P450 residues that have been implicated to be at the interface with cyt b_5. Figure 1.10 is provided as a reference for how the residues of various cyt P450 isoforms were translated into the corresponding cyt P450 2B4 residues (studied in this thesis).

Figure 1.11 Sequence alignment of cyt P450 2B4 with several other cyts P450 that interact with cyt b_5. Sequences were obtained from UniProt[252] and the sequence alignment was completed using ClustalW2.[253,254]

```
                                               1       10        20        30        40        50         60        70
                                                        |         |         |         |         |          |         |
P00178|RABBIT P450 2B4   ----------------------MEFSLLLLLAFLAGLLLLLFRGHPKAHGRLPPGPSPLPVLGNLLQMDRKG-LLRSFLRLREKYGDVFTVYLGSRPVVV
P00176|RAT P450 2B1      ----------------------MEPTILLLLALLVGFLLLLVRGHPKSRGNFPPGPRPLPLLGNLLQLDRGG-LLNSFMQLREKYGDVFTVHLGPRPVVM
P20852|MOUSE P450 2A5    -------------------MLTSGLLLVAAVAFLSVLVLMSVWKQRKLSGKLPPGPTPLPFIGNFLQLNTEQ-MYNSLMKISQRYGPVFTIYLGPRRIVV
P08683|RAT P450 2C11     -----------------------MDPVLVLVLTLSSLLLLSLWRQSFGRGKLPPGPTPLPIIGNTLQIYMKD-IGQSIKKFSKVYGPIFTLYLGMKPFVV
P10632|HUMAN P450 2C8    -----------------------MEPFVVLVLCLSFMLLFSLWRQSCRRRKLPPGPTPLPIIGNMLQIDVKD-ICKSFTNFSKVYGPVFTVYFGMNPIVV
P05181|HUMAN P450 2E1    --------------------MSALGVTVALLVWAAFLLLVSMWRQVHSSWNLPPGPFPLPIIGNLFQLELKN-IPKSFTRLAQRFGPVFTLYVGSQRMVV
P05185|BOVINE P450 17A1  -------------------------MWLLLAVFLLTLAYLFWPKTKHSGAKYPRSLPSLPLVGSLPFLPRRGQQHKNFFKLQEKYGPIYSFRLGSKTTVM
P05093|HUMAN P450 17A1   -------------------------MWELVALLLLTLAYLFWPKRRCPGAKYPKSLLSLPLVGSLPFLPRHGHMHNNFFKLQKKYGPIYSVRMGTKTTVI
Q29RV2|BOVINE P450 3A4   ---------------MELIPSFSMETWVLLATSLVLLYIYGTYSYGLFKKLGIPGPRPVPYFG--STMAYHKGIPEFDNQCFKKYGKMWGFYEGRQPMLA
P00189|BOVINE P450 11A1  MLARGLPLRSALVKACPPILSTVGEGWGHHRVGTGEGAGISTKTPRPYSEIPSPGDNGWLNLYHFWREKGSQRIHFRHIENFQKYGPIYREKLGNLESVY
P00183|PSEU PUT P450cam  ----------------------------------------MTTETIQSNANLAPLPPHVPEHLVFDFDMYNPSNLSAGVQEAWAVLQESNVPDLVWTRCN
                          80        90          100       110         120       130       140       150       160
                           |         |            |         |           |         |         |         |         |
P00178|RABBIT P450 2B4   LCGTDAIREALVDQA---EAFSGRGKIAVVDPIFQGYGVIFAN--GERWRALRRFSLATMRDFGMGKRSVEERIQEEARCLVEELRKSKGA---LLDNTL
P00176|RAT P450 2B1      LCGTDTIKEALVGQA---EDFSGRGTIAVIEPIFKEYGVIFAN--GERWKALRRFSLATMRDFGMGKRSVEERIQEEAQCLVEELRKSQGA---PLDPTF
P20852|MOUSE P450 2A5    LCGQEAVKEALVDQA---EEFSGRGEQATFDWLFKGYGVVFSS--GERAKQLRRFSIATLRDFGVGKRGIEERIQEEAGFLIDSFRKTNGA---FIDPTF
P08683|RAT P450 2C11     LHGYEAVKEALVDLG---EEFSGRGSFPVSERVNKGLGVIFSN--GMQWKEIRRFSIMTLRTFGMGKRTIEDRIQEEAQCLVEELRKSKGA---PFDPTF
P10632|HUMAN P450 2C8    FHGYEAVKEALIDNG---EEFSGRGNSPISQRITKGLGIISSN--GKRWKEIRRFSLTTLRNFGMGKRSIEDRVQEEAHCLVEELRKTKAS---PCDPTF
P05181|HUMAN P450 2E1    MHGYKAVKEALLDYK---DEFSGRGDLPAFHAHRD-RGIIFNN--GPTWKDIRRFSLTTLRNYGMGKQGNESRIQREAHFLLEALRKTQGQ---PFDPTF
P05185|BOVINE P450 17A1  IGHHQLAREVLLKKG---KEFSGRPKVATLDILSDNQKGIAFADHGAHWQLHRKLALNAFALFKDGNLKLEKIINQEANVLCDFLATQHGE---AIDLSE
P05093|HUMAN P450 17A1   VGHHQLAKEVLIKKG---KDFSGRPQMATLDIASNNRKGIAFADSGAHWQLHRRLAMATFALFKDGDQKLEKIICQEISTLCDMLATHNGQ---SIDISF
Q29RV2|BOVINE P450 3A4   ITDPDIIKTVLVKEC---YSVFTNRRIFGPMGIMKYAISLAWD---EQWKRIRTLLSPAFTSGKLKEMFPIIGQYGDMLVRNLRKEAEKGN---PVNMKD
P00189|BOVINE P450 11A1  IIHPEDVAHLFKFEGSYPERYDIPPWLAYHRYYQKPIGVLFKKSGTWKKDRVVLNTEVMAPEAIKNFIPLLNPVSQDFVSLLHKRIKQQGSGKFVGDIKE
P00183|PSEU PUT P450cam  GGHWIATRGQLIREAYEDYRHFSSECPFIPREAGEAYDFIPTS---MDPPEQRQFRALANQVVGMPVVDKLENRIQELACSLIESLRPQGQ--------C
                       170       180       190       200       210       220       230       240       250       260
                         |         |         |         |         |         |         |         |         |         |
P00178|RABBIT P450 2B4   LFHSITSNIICSIVFGKRFDYKDPVFLRLLDLFFQSFSLISSFSSQVFELFPGFLKHFPGTHRQIYRNLQEINTFIGQSVEKHRATLDPSNPRDFIDVYL
P00176|RAT P450 2B1      LFQCITANIICSIVFGERFDYTDRQFLRLLELFYRTFSLLSSFSSQVFEFFSGFLKYFPGAHRQISKNLQEILDYIGHIVEKHRATLDPSAPRDFIDTYL
P20852|MOUSE P450 2A5    YLSRTVSNVISSIVFGDRFDYEDKEFLSLLRMMLGSFQFTATSMGQLYEMFSSVMKHLPGPQQQAFKELQGLEDFITKKVEHNQRTLDPNSPRDFIDSFL
P08683|RAT P450 2C11     ILGCAPCNVICSIIFQNRFDYKDPTFLNLMHRFNENFRLFSSPWLQVCNTFPAIIDYFPGSHNQVLKNFFYIKNYVLEKVKEHQESLDKDNPRDFIDCFL
P10632|HUMAN P450 2C8    ILGCAPCNVICSVVFQKRFDYKDQNFLTLMKRFNENFRILNSPWIQVCNNFPLLIDCFPGTHNKVLKNVALTRSYIREKVKEHQASLDVNNPRDFIDCFL
P05181|HUMAN P450 2E1    LIGCAPCNVIADILFRKHFDYNDEKFLRLMYLFNENFHLLSTPWLQLYNNFPSFLHYLPGSHRKVIKNVAEVKEYVSERVKEHHQSLDPNCPRDLTDCLL
P05185|BOVINE P450 17A1  PLSLAVTNIISFICFNFSFKNEDPALKAIQNVNDGILEVLS--KEVLLDIFPVLKIFPSKAMEKMKGCVQTRNELLNEILEKCQENFSSDSITNLLHILI
P05093|HUMAN P450 17A1   PVFVAVTNVISLICFNTSYKNGDPELNVIQNYNEGIIDNLS--KDSLVDLVPWLKIFPNKTLEKLKSHVKIRNDLLNKILENYKEKFRSDSITNMLDTLM
Q29RV2|BOVINE P450 3A4   MFGAYSMDVITGTAFGVNIDSLNNPHDPFVEHSKNLLRFRPFDPFILSIILFPFLNPVFEILN-ITLFPKSTVDFFTKSVKKIKESRLTDKQMNRVDLLQ
P00189|BOVINE P450 11A1  DLFHFAFESITNVMFGERLGMLEETVNPEAQKFIDAVYKMFHTSVPLLNVPPELYRLFR---TKTWRDHVAAWDTIFNKAEKYTEIFYQDLRRKTEFRNY
P00183|PSEU PUT P450cam  NFTEDYAEPFPIRIFMLLAGLPEEDIPHLKYLTDQMTRPDGS--------------------MTFAEAKEALYDYLIPIIEQRRQKPGTDAISIVANGQV
```

```
                       270             280       290       300       310       320       330       340       350       360
                         |               |         |         |         |         |         |         |         |         |
P00178|RABBIT P450 2B4   LRMEKDKSD------PSSEFHHQNLILTVLSLFFAGTETTSTTLRYGFLLMLKYPHVTERVQKEIEQVIGSHRPPALDDRAKMPYTDAVIHEIQRLGDLI
P00176|RAT P450 2B1      LRMEKEKSN------HHTEFHHENLMISLLSLFFAGTETSSTTLRYGFLLMLKYPHVAEKVQKEIDQVIGSHRLPTLDDRSKMPYTDAVIHEIQRFSDLV
P20852|MOUSE P450 2A5    IRMLEEKKN------PNTEFYMKNLVLTTLNLFFAGTETVSTTLRYGFLLLMKHPDIEAKVHEEIDRVIGRNRQPKYEDRMKMPYTEAVIHEIQRFADMI
P08683|RAT P450 2C11     NKMEQEKHN------PQSEFTLESLVATVTDMFGAGTETTSTTLRYGLLLLLKHVDVTAKVQEEIERVIGRNRSPCMKDRSQMPYTDAVVHEIQRYIDLV
P10632|HUMAN P450 2C8    IKMEQEKDN------QKSEFNIENLVGTVADLFVAGTETTSTTLRYGLLLLLKHPEVTAKVQEEIDHVIGRHRSPCMQDRSHMPYTDAVVHEIQRYSDLV
P05181|HUMAN P450 2E1    VEMEKEKHS------AERLYTMDGITVTVADLFFAGTETTSTTLRYGLLILMKYPEIEEKLHEEIDRVIGPSRIPAIKDRQEMPYMDAVVHEIQRFITLV
P05185|BOVINE P450 17A1  QAKVNADNNNAGPDQDSKLLSNRHMLATIGDIFGAGVETTTSVIKWIVAYLLHHPSLKKRIQDDIDQIIGFNRTPTISDRNRLVLLEATIREVLRIRPVA
P05093|HUMAN P450 17A1   QAKMNSDNGNAGPDQDSELLSDNHILTTIGDIFGAGVETTTSVVKWTLAFLLHNPQVKKKLYEEIDQNVGFSRTPTISDRNRLLLLEATIREVLRLRPVA
Q29RV2|BOVINE P450 3A4   LMINSQNSKE---IDNHKALSDIELVAQSTIFIFGGYETTSSTLSFIIYELTTHPHVQQKVQEEIDATFPNKAPPTYDALVQMEYLDMVVNETLRMFPIA
P00189|BOVINE P450 11A1  PGILYCLLK-------SEKMLLEDVKANITEMLAGGVNTTSMTLQWHLYEMARSLNVQEMLREEVLNARRQAEGDISKMLQMVPLLKASIKETLRLHPIS
P00183|PSEU PUT P450cam  NGR---------------PITSDEAKRMCGLLLVGGLDTVVNFLSFSMEFLAKSPEHRQELIERPERIP--------------------AACEELLRRFS
                             370       380       390       400       410       420         430       440       450       460
                               |         |         |         |         |         |           |         |         |         |
P00178|RABBIT P450 2B4   PFGVPHTVTKDTQFRGYVIPKNTEVFPVLSSALHDPRYFETPNTFNPGHFLDANGALKRNE--GFMPFSLGKRICLGEGIARTELFLFFTTILQNFSIAS
P00176|RAT P450 2B1      PIGVPHRVTKDTMFRGYLLPKNTEVYPILSSALHDPQYFDHPDSFNPEHFLDANGALKKSE--AFMPFSTGKRICLGEGIARNELFLFFTTILQNFSVSS
P20852|MOUSE P450 2A5    PMGLARRVTKDTKFRDFLLPKGTEVFPMLGSVLKDPKFFSNPKDFNPKHFLDDKGQFKKND--AFVPFSIGKRYCFGEGLARMELFLFLTNIMQNFHFKS
P08683|RAT P450 2C11     PTNLPHLVTRDIKFRNYFIPKGTNVIVSLSSILHDDKEFPNPEKFDPGHFLDERGNFKKSD--YFMPFSAGKRICAGEALARTELFLFFTTILQNFNLKS
P10632|HUMAN P450 2C8    PTGVPHAVTTDTKFRNYLIPKGTTIMALLTSVLHDDKEFPNPNIFDPGHFLDKNGNFKKSD--YFMPFSAGKRICAGEGLARMELFLFLTTILQNFNLKS
P05181|HUMAN P450 2E1    PSNLPHEATRDTIFRGYLIPKGTVVVPTLDSVLYDNQEFPDPEKFKPEHFLNENGKFKYSD--YFKPFSTGKRVCAGEGLARMELFLLLCAILQHFNLKP
P05185|BOVINE P450 17A1  PTLIPHKAVIDSSIGDLTIDKGTDVVVNLWALHHSEKEWQHPDLFMPERFLDPTGTQLISPSLSYLPFGAGPRSCVGEMLARQELFLFMSRLLQRFNLEI
P05093|HUMAN P450 17A1   PMLIPHKANVDSSIGEFAVDKGTEVIINLWALHHNEKEWHQPDQFMPERFLNPAGTQLISPSVSYLPFGAGPRSCIGEILARQELFLIMAWLLQRFDLEV
Q29RV2|BOVINE P450 3A4   GR-LERVCKKDVEIHGVTIPKGTTVLVPLFVLHNNPELWPEPEEFRPERFSKNNKDSINPY--VYLPFGTGPRNCLGMRFAIMNIKLALVRILQNFSFKP
P00189|BOVINE P450 11A1  VT-LQRYPESDLVLQDYLIPAKTLVQVAIYAMGRDPAFFSSPDKFDPTRWLSKDKDLIHFR---NLGFGWGVRQCVGRRIAELEMTLFLIHILENFKVEM
P00183|PSEU PUT P450cam  LVADGRILTSDYEFHGVQLKKGDQILLPQMLSGLDERENACPMHVDFSRQKVS-----------HTTFGHGSHLCLGQHLARREIIVTLKEWLTRIPDFS
                               470       480       490
                                 |         |         |
P00178|RABBIT P450 2B4   PVPPEDIDLTPRESGVGNVPPSYQIRFLAR------------
P00176|RAT P450 2B1      HLAPKDIDLTPKESGIGKIPPTYQICFSAR------------
P20852|MOUSE P450 2A5    TQAPQDIDVSPRLVGFATIPPTYTMSFLSR------------
P08683|RAT P450 2C11     LVDVKDIDTTPAISGFGHLPPFYEACFIPVQRADSLSSHL--
P10632|HUMAN P450 2C8    VDDLKNLNTTAVTKGIVSLPPSYQICFIPV------------
P05181|HUMAN P450 2E1    LVDPKDIDLSPIHIGFGCIPPRYKLCVIPRS-----------
P05185|BOVINE P450 17A1  PDDGKLPSLEGHASLVLQIKPFKVKIEVRQAWKEAQAEGSTP
P05093|HUMAN P450 17A1   PDDGQLPSLEGIPKVVFLIDSFKVKIKVRQAWREAQAEGST-
Q29RV2|BOVINE P450 3A4   CKETQIPLKLYTQGLTQPEQPVILKVVPRGLGPQVEPDFL--
P00189|BOVINE P450 11A1  QHIG-DVDTIFNLILTPDKPIFLVFRPFNQDPPQA-------
P00183|PSEU PUT P450cam  IAPGAQIQHKSGIVSGVQALPLVWDPATTKAV----------
```

Table 1.2 Summary of cyt b_5 residues proposed to be at the interface with various cyts P450.

Cyt b_5	**Cyt P450**	**Experimental Technique**	**Cyt b_5 interface residues**	**Non-interface residues**	**Other findings**	**Reference**
rat	cyt P450 2B4	modification of carboxyl groups, binding affinity and ET[3]	carboxyl groups			92
rat	cyt P450 RLM5	• K_d ↓ when heme propionates underwent esterification • ↓ demethylase activity	heme propionates		also looked at ionic strength – caused binding to decrease	255
rat	cyt P450 2B4	EDC[1] cross-linking	carboxyl groups			256
rat	cyt P450 2B4	hydrostatic pressure dissociation			~ 2 ion pairs to cyt P450 truncated cyt b_5 also interacts with cyt P450 in 1:1 complex	257
rat liver	cyt P450$_{cam}$	computer modeling	E49(C), E53, D65 & heme propionate [+5]		ion pairs to cyt P450: 1) E49-*L414*, E53-*R85*, D65-*S128*, heme propionate-*R443* 2) E49-*S128*, E53-*R443*, D65-*L414*, heme propionate-*R85*	258
rat liver	cyt P450$_{cam}$	reexamination of the model proposed by Stayton *et al.*[258]	D65 [+5]		ion pair to cyt P450: D65-*R125*	259
rabbit	cyt P450 2B4	nitration of tyrosine groups in the presence of cyt P450	Y130 and Y35 [+1]	Y12	Y130 controls docking of cyt b_5 Y35 functionally important for ET[3] Y11 inaccessible to nitration even with cyt b_5 alone	260
various	cyt P450 2B4	molecular modeling and docking	E48, E49, V50, E53, E61, E64, D65, V66, Q69, heme [+5]		ion pairs to cyt P450: E48-N417, E49-R422, V50-V89&I423, E53-R85, E61-K433, E64-R126, D65-R122, V66-L129, heme-R133, heme-R443	261
rat	bovine mitochondrial cyt P450scc	• SSDM[2] • No changes in binding • Saw ↓ in activity • All 3 mutants disturb structure	E42(K)	E48(K), D65(A)	truncated cyt b_5 did not stimulate or bind cyt P450	7

Cyt b$_5$	**Cyt P450**	**Experimental Technique**	**Cyt b$_5$ interface residues**	**Non-interface residues**	**Other findings**	**Reference**
rat	bovine cyt P45017α	• SSDM^2 • Saw ↓ in activity • All 3 mutants disturb structure	E42(K), E48(K)	D65(A)	truncated cyt b$_5$ did not stimulate cyt P450 activity	7
rat	recombinant cyt P450 3A4	• SSDM^2 • Saw ↓ in activity • All 3 mutants disturb structure	E42(K), E48(K)	D65(A)	truncated cyt b$_5$ did not stimulate cyt P450 activity	7
bovine	homology model of cyt P450 2E1	docking by "O" and the Molecular Operating Environment	E48, E49, E53, D58, E61, D65 [+5] and S23, P45, G46, V50, S93 [+5]		• ion pairs to cyt P450: E61-*K433*, D58-*M427*, E48-*D341*, E49-*R343*, E53-*K421*, E53-*R343*, E53-*R443*, D65-*R125*, D65-*K433* • H-bonds to cyt P450: S23-*K345*, V50-*D134, S93-E424, S93-R85* (x2), P45-*R133*, G46-*D134*	262
human	cyt P450 2E1	EDC^1 cross-linking	D58, E61 [+5]		ion pairs to cyt P450: *E61-K433, D56-M427*	262
human	human cyt P450c17	• SSDM^2 and double mutant • activity assay in yeast microsome and HEK-293 cells	E48(G), E49(G), E48(G)/E49(G) and possibly R52(G)	K33(G), K39(G), E53(G), Q54(G), E61(G), R73(G)	D36(G), E42(G), D58(G), D65(G), E74(G) were grouped into a third class of mutations	263
rabbit	cyt P450 2B4	double mutant cycle analysis	D65(A), V66(A)		ion pairs to cyt P450: D65, V66 in contact with R122, R126 and K433	247
human	human cyt P450 2E1	• SSDM^2 and double mutant • Activity assays in DLPC^4, control yeast microsomal lipids and yeast microsomes	D58(G), D65(G)	K33(G), D36(G), K39(G), E42(G), E48(G), E49(G), R52(G), E53(G), G54(G), E61(G), R73(G), E74(G)	The effect of some of these mutations is highly dependent on the reconstitution system	264
human	human cyt P450c17	• SSDM^2 and double mutant • Activity assays in DLPC^4, control yeast microsomal lipids and yeast microsomes	E48(G), E49(G), E48(G)/E49(G)		D36(G) and D58(G) are required under some conditions (lipids)	264

Cyt b_5	**Cyt P450**	**Experimental Technique**	**Cyt b_5 interface residues**	**Non-interface residues**	**Other findings**	**Reference**
human	human cyt P450 2C19	• SSDM[2] and double mutant • Activity assays in DLPC[4], control yeast microsomal lipids and yeast microsomes	D58(G), D65(G) and D58(G)/D65(G)		D36(G) might be important depending on the lipids	264
human	human cyt P450 3A4	EDC[1] cross-linking	E61 and E42 or E48		ion pairs to cyt P450: • E61-*R122*|K127 and E61-K96 (equivalent to *D90* in our sequence, so no corresponding ion pair) • E42-K421 or E48-K421 (K421 is equivalent to *D415* in our sequence , so no corresponding ion pair)	265
human homology model of bovine holo cyt b_5 and rat apo cyt b_5	human cyt P450 3A4	ZDOCK based on cross-linking results (previous row)	the α2−loop−α3 and α4−loop−α5 segments, with additionally one heme propionate group for holo cyt b_5			265

[1] EDC: 1-ethyl-3-(3-dimethylaminopropyl)carbodiimide; [2]SSDM: single site-directed mutagenesis; [3]ET: electron transfer; and [4]DLPC: 1,2-dilauroyl-*sn*-glycero-3-phosphocholine.

The number in the [] bracket indicates the number added to align the cyt b_5 sequence (the sequences are highly homologous and thus only the sequence numbering needs to be shifted).

The parenthesis () contains the identity of the amino acid to which the residue was mutated.

The number in italics is the corresponding cyt P450 2B4 residue based on the sequence alignment in Figure 1.10. On the right of the | symbol is the residue of the cyt P450 isoform studied; e.g. K127 in cyt P450 3A4 translates to R122 in cyt P450 2B4, and it would listed as *R122*|K127.

Ion pairs are listed as cyt b_5 residue - cyt P450 residue.

Table 1.3 Summary of cyt P450 residues proposed to be at the interface with cyt b$_5$. See a more thorough list of residues mutated/tested in a review paper by Hlavica *et al.*[266]

Cyt b$_5$	**Cyt P450**	**Experimental Technique**	**Cyt P450 interface residues**	**Non-interface residues**	**Other findings**	**Reference**
rat	cyt P450 2B4	EDC[1] cross-linking	amino groups			256
rat liver	cyt P450$_{cam}$	computer modeling	*L414*|K344, *R85*|R72, *S128*|R112, *R443*|R364		ion pairs: 1) *L414*-E49*, R85*-E53*, S128*-D65*, R443*-heme propionate 2) *S128*-E49*, R443*-E53, *L414*-D65*, R85*-heme propionate	258
rat	mouse cyt P450coh		*R126*|R129 variable role for *F206*|F209			55
rat liver	cyt P450$_{cam}$	reexamination of the model proposed by Stayton *et al.*[258]	*R125*|R109		*R125*-D65	259
rat	cyt P450 2B1	ELISA[2] and SSDM[3]	cyt P450 residues *116-134*|116-134 *R122*|K122(E) and *R126*|R125(E)			259
rabbit	cyt P450 2B4	derivatization of histidines, UV-Vis and enzyme assays	histidines			267
bovine	cyt P450 2B4	geometric fit algorithm for protein docking	1. D47-L51, F171, Y190, K191, L199, F203, F206, E301, R308, L470-S475, N479 (distal) 2. K100, I101, V104, D105, F108, Q109, V113, I114 (face ⊥ to heme) 3. M132-D134, K139, R140, R271, K274, K276, H354, K421-N423, F426-F429, K433-I435, L437, E439, G440, R443, T444, F447 (proximal surface)			268

Cyt b$_5$	Cyt P450	Experimental Technique	Cyt P450 interface residues	Non-interface residues	Other findings	Reference
rabbit	cyt P450 2B4	SSDM^3, binding & activity assays	R122, R126, R133, F135, M137, K139, K433	Y190, H226, K276, K421, R422, R443, Y484		211
various	cyt P450 2B4 (some based on homology models)		N417, R422, V89, I423, R85, K433, R126, R122, L129, Q91, R133, R443		N417-E48, R422-E49, V89&I423-V50, R85-E53, K433-E61, R126-E64, R122-D65, L129-V66, R133-heme, R443-heme	269
human	cyt P450c17	SSDM^3 & activity assays	*R343*|R347			270
human	cyt P450 2E1	activity assays and binding assay	*M427*|K428(A), *K433*|K434(A) and double mutant (the two residues act synergistically)			262
bovine	homology model of cyt P450 2E1	docking by "O" and the Molecular Operating Environment	*K433*|K434, *M427*|K428, *D341*|K342, *R343*|R344, *R443*|R444, *R125*|R126, *K421*|K422		ion pairs to cyt b$_5$: *K433*-E61, *M427*-D58, *D341*-E48, *R343*-E49, *K421*-E53, *R343*-E53, *R443*-E53, *R125*-D65, *K433*-D65	262
human	human cyt P450 2E1	EDC^1 cross-linking	*M427*|K428, *K433*|K434		ion pairs to cyt b$_5$: *K433*-E61, *M427*-D56	262
rat	cyt P450$_{cam}$	NMR CSPs^4 in ^{1}H-^{15}N HSQC^5 spectrum	C-helix residues near *R85*|R72 in the B helix and near *L414*|K344 (neither of those residues is assigned) many more (see reference)	L-helix is not involved (includes *R443*|R364)		271
rabbit	cyt P450 2B4	double mutant cycle	R122, R126 and K433		ion pairs to cyt b$_5$: R122, R126 and K433 in contact with D65, V66	247
rat	human cyt P450 2C8	SSDM^3 and double mutant	*R140*|R139(K), *R400*|K399(R) double mutant has higher activity than wild-type			272

Cyt b_5	**Cyt P450**	**Experimental Technique**	**Cyt P450 interface residues**	**Non-interface residues**	**Other findings**	**Reference**
human	human cyt P450 3A4	EDC[1] cross-linking	*R122*|K127 and K96 (corresponds to *D90*) K421 (corresponds to *D415*)		ion pairs: E61-*R122*|K127 and E61-K96 (equivalent to D90 in our sequence, so cannot be a possible pair) E42-K421 or E48-K421 (K421 is equivalent to D415 in our sequence , so no corresponding ion pair)	265
human homology model of bovine holo cyt b_5 and rat apo cyt b_5	human cyt P450 3A4	ZDOCK based on cross-linking results	• for holo cyt b_5: helix B, the B−B′ loop, the C−D loop, helices D, J′, and K, the K″−L meander region, the β-bulge, and helix L • for apo cyt b_5: helix B, the B−B′loop, helix C, the C−D loop, helix D, the K″−L meander region, and the β-bulge • for both holo and apo cyt b_5: B-B′ loop and helix C of cyt P450 interact with α4 and α5 of cyt b_5			265

[1] EDC: 1-ethyl-3-(3-dimethylaminopropyl)carbodiimide; [2]ELISA: enzyme-linked immunosorbent assay; [3]SSDM: single site-directed mutagenesis; [4]CSPs: chemical shift perturbations; and [5]HSQC: heteronuclear single quantum coherence.

The number in italics is the corresponding cyt P450 2B4 residue based on the sequence alignment in Figure 1.10. On the right of the | symbol is the residue of the cyt P450 isoform studied; e.g. K127 in cyt P450 3A4 translates to R122 in cyt P450 2B4, and it would listed as *R122*|K127.

The parentheses () contain the identity of the amino acid to which the residue was mutated.

Ion pairs are listed as cyt P450 residue - cyt b_5 residue.

1.4 Redox partner association theories

Electron transfer complexes have two requirements. First, they must be able to achieve high turnover of electrons; this means that they need to associate and dissociate quickly with one another. For this reason, they will appear to have low affinity (K_d in the μM-mM range),[273] a high k_{off} (> 1000 s^{-1}) and a complex lifetime in the milliseconds.[274] Similarly, the k_{on} will approach the diffusion limit, in order to facilitate the high turnover.[274] Second, redox proteins generally have more than one binding partner that share similar binding sites. For this to be true, they must lose some specificity to each binding partner to allow for the ability to associate promiscuously with the other partners. However, because the electron transfer rate decreases exponentially with distance between the redox centers,[275] for large proteins some specificity is required to bring the redox partners close enough for electron transfer[274] (with a distance between the redox cofactors edges of less than 14 Å[275]).

Proteins diffuse through solution, or the membrane, according to Brownian motion, experiencing constant collisions with water, lipids and other nearby molecules.[276] When they collide with another protein, the proteins form a transient complex in which rotational and translational motions are allowed. This macrocollision leads to numerous microcollisions in which the proteins scan each other's surfaces, finding favorable orientations.[277] For redox partners especially, these macrocollisions are enhanced by the presence of long-range electrostatic attraction.[274,278,279] This additional interaction allows for the pre-orientation of the two redox centers[280] and lengthens the lifetime of the transient complex, thereby increasing the probability of finding a productive microcollision in which electron transfer can occur.[281] This transient complex has been referred to as an “encounter complex”[274,278,282–284] and the entire process as dynamic docking (Figure 1.11).[107,112,285–290] In 1991, McLendon proposed the “velcro” model[291] to describe the various orientations that proteins can adopt during the encounter complex; this idea is widely accepted.[273,278,292–294] Out of the multiple orientations the proteins take on with respect to each other, perhaps one or more orientation(s) can result in a “productive complex” or “stereospecific complex” in which the two redox centers are close enough to allow for electron transfer (Figure 1.11). The encounter complex is largely driven by long-range electrostatic interactions; and at this stage, the two proteins are still solvated and interact via van der Waals[276] and hydrogen bonding contacts[295] with the solvent (as opposed to their protein partner). The productive/stereospecific complex, on the other end, is formed via close-range interactions, such as hydrogen bonding, salt bridges and hydrophobic contacts, in order to steer the two redox center into each other’s electron transfer range.[274,278,296,297]

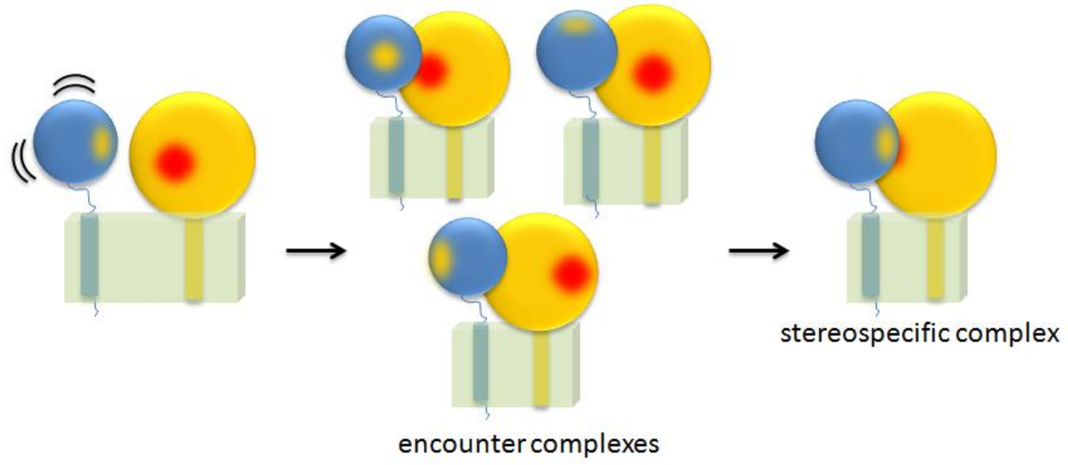

Figure 1.12 Dynamic docking model between redox partners. This figure was adapted from the figure presented by Suh *et al.*[298]

Experimental proof of these theories has come in a number of ways. For plastocyanin and cytochrome f, cross-linking at low ionic strengths has shown the presence of multiple orientations *other* than the productive complex.[299] Using paramagnetic relaxation enhancement (PRE), various research groups have been able to visualize the formation of both the encounter complexes and stereospecific complexes formed between redox partners.[119,283,300–307] For example, cyt *c* has been shown to sample about half of the surface of adrenodoxin.[308] It is notable that in some cases, the two proteins may never progress past the encounter complex, such as for cyt *c* and adrenodoxin; however, even in those very dynamic complexes, electron transfer can still occur.[274,308]

1.5 Isotropic bicelles as a model membrane

To mimic the membrane environment, organic solvent mixtures,[309] detergent micelles,[310–313] lipid vesicles and bicelles have been used over the years.[314–319] Although detergent micelles have proven excellent for structure determination via solution NMR,[320,321] micelles can introduce artifacts in the structures of proteins and peptides due to their high curvature[322–327] or cause inhibition of protein activity[328,329] or denature the protein; furthermore, micelles do not mimic the bilayer environment well.[318] Lipid vesicles, on the other hand, are not amenable to high-resolution solution NMR due to their large size and slow tumbling, on the NMR timescale, which leads to line broadening (they are suitable for solid-state NMR, however). Due to these difficulties with other membrane mimetics, bicelles have stepped in to fill the gap. Initially introduced as a "mixed micelle" between lipid and detergent in 1981,[330] bicelles are now generally composed of two types of lipids: long-chain lipids and shorter chain lipids (since Gabriel *et al.* in 1984).[331] Though the morphology of bicelles can changed with concentration, *q* ratio (the molar ratio of the long chain to short chain lipids), and temperature,[332] bicelles with a concentration above 5% (w/v), and a *q* ratio below 1 have a well-established morphology and size,[333–337] which fit the original theoretical model for ideal bicelles.[338] These isotropic bicelles adopt a discoid shape that consists of a unilamellar bilayer of the long-chain lipids, with the edges capped with a rim of the short-chain lipids (Figure 1.12).[339–341] Their small size allows for isotropic tumbling in solution (hence the name), which is needed for solution NMR. They are also suitable for circular dichroism[342–345] and x-ray crystallography.[346–348] Several review papers have been dedicated to their application for membrane protein reconstitution.[349–356] High-resolution structures of membrane proteins, incorporated in isotropic bicelles, have been successfully determined via NMR.[333,350] At higher *q* ratios ($q \geq 2.5$), bicelles align in the magnetic field, allowing for static solid-state experiments (see a recent review by Dürr *et al*.[354] for an overview of the morphologies possible).[332,338,357–362] The proteins' functional forms are generally retained when incorporated in a bicelle environment.[363,364]

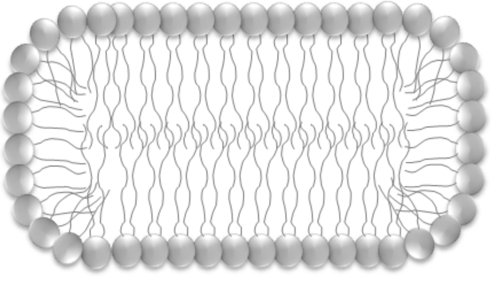

Figure 1.13 Model of isotropic bicelles.[365]

One of the key advantages of isotropic bicelles is that they are arranged in a single, planar bilayer composed of lipids and therefore are better able mimic the physiological bilayer environment. It is also possible to modulate the lipid composition of bicelles to make them more analogous to cell membranes. For example, cholesterol,[366–369] different chain length lipids,[370,371] unsaturated lipids,[366,370] charged lipids,[372–375] spingomyelin[376] and gangliosides[343] have been used successfully incorporated in bicelles.

1.5.1 DMPC/DHPC isotropic bicelles

The most common type of bicelles consists of a combination of DMPC (14-carbon acyl chain) and DHPC (6-carbon acyl chain) lipids (Figure 1.13).[334,336,337,365,377–381] DMPC/DHPC isotropic bicelles serve as a good bilayer system for NMR structural studies because the lipid dynamics within those isotropic bicelles are the same as those within unilamellar vesicles of DMPC.[378] DMPC/DHPC bicelles were used in this thesis for several additional reasons: 1) phosphatidylcholine is the most common headgroup on the cytoplasmic side of the ER membrane and 2) 14-carbon acyl chain.

1) The lipid headgroup composition of the ER membrane is 55% phosphatidylcholine (PC), 20-25% phosphatidylethanolamine (PE), 5-10% phosphatidylserine (PS), 5-10% phosphatidylinositol (PI) and 4-7% sphingomyelin.[382–388] These lipids are however distributed asymmetrically among the cytoplasmic and luminal sides of the ER membrane: 39-56% PC lipids, 84-92% PE lipids, 82-97% PS lipids, 16-23% PI lipids and 13-15% sphingomyelin are found on the cytoplasmic side (the endpoints of

the ranges are based on two isolated measurements, and the sphingomyelin measurement was noted to be unreliable).[389] Using the average composition of each lipid headgroup (55% PC, 23% PE, 8% PS, 8% PI and 6% sphingomyelin), the lipid headgroup composition of the cytoplasmic side can thus be calculated as 42-51% PC, 35-41% PE, 12-13% PS, 2-3% PI and 1-2% sphingomyelin. PC lipids should therefore be a good initial model of the ER membrane since this PC headgroup consists of ~50% of the lipids.

2) It is important to use acyl chains that mimic the thickness of the ER bilayer (50-80 Å thick based on electron microscopy[382,390–392]). An analysis of the fatty acid chain lengths revealed that most lipids were either 16 or 18 acyl chains long. Unfortunately, longer acyl chains may not be amenable to solution NMR experiments and DMPC has previously been shown to be a good model membrane for cyt P450.[393]

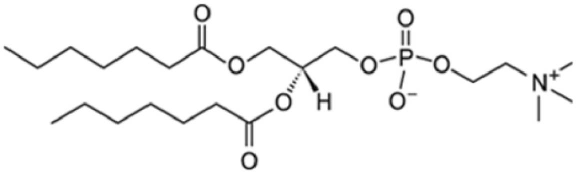

1,2-diheptanoyl-*sn*-glycero-3-phosphocholine (DHPC)

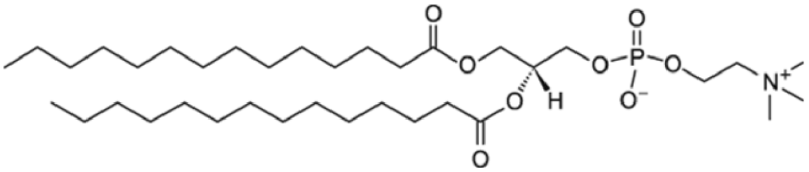

1,2-dimyristoyl-*sn*-glycero-3-phosphocholine (DMPC)

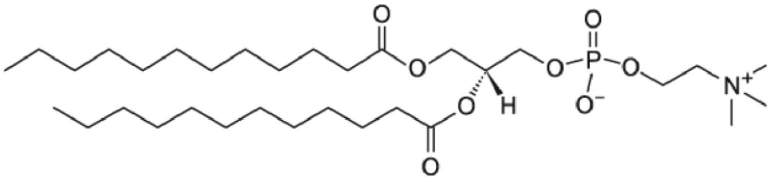

1,2-dilauroyl-*sn*-glycero-3-phosphocholine (DLPC)

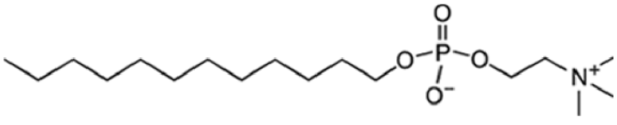

dodecylphosphocholine (DPC)

Figure 1.14 Structures of lipids used in bicelles (DMPC and DHPC). For reference, the structures of DLPC (12-carbon acyl chain lipid, used in activity assays) and DPC (12-carbon acyl chain detergent, used in Chapter 3) are also presented.

The size of a DMPC/DHPC bicelle with a *q* ratio of 0.25 is shown in Figure 1.14. Comparatively, for isotropic bicelles with a *q* ratio of 0.5, the diameter has been estimated to be 122 Å with a height of 61 Å [365], or a diameter of 96-97 Å with a thickness of 40 Å.[335] Hydrated bilayer thickness of a DMPC vesicle has been determined to be 62.6 Å previously.[394] Bicelle diameters were found to range from 42 ± 6 to 86 ± 8 Å, in small angle neutron scattering experiments, for *q* ratios of 0.2 to 0.5, with a bilayer depth of 42 ± 4 Å.[336]

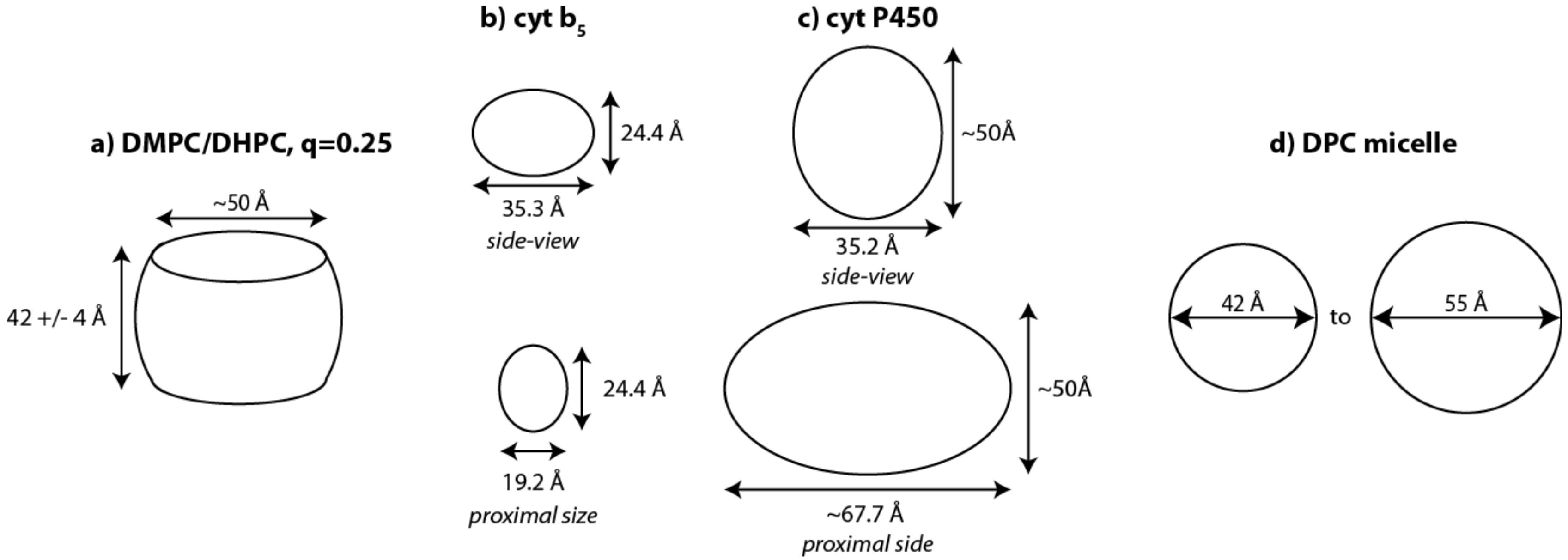
b) cyt b5
c) cyt P450
a) DMPC/DHPC, q=0.25
d) DPC micelle
~50 Å
42 +/- 4 Å
24.4 Å
35.3 Å
side-view
24.4 Å
19.2 Å
proximal size
~50Å
35.2 Å
side-view
~50Å
~67.7 Å
proximal side
42 Å
to
55 Å

Figure 1.15 Size of *q* = 0.25 DMPC/DHPC (5% (w/v) and above) isotropic bicelles, and cyt b_5 and cyt P450 2B4, *to scale.* a) Isotropic bicelle size is based on the formula in Luchette *et al.*[336] which originated from Vold *et al.*[338] A thickness of 40 Å was estimated from Wu *et al.*[335] and Loudet-Courreges *et al.*[395] The phosphate-to-phosphate thickness of DMPC has also been estimated to be 34 Å.[396] The dimensions for the proteins in a) and b), were obtained from space-filling models in PyMOL for the NMR structure of cyt b_5 (Chapter 3) and cyt P450 2B4 structure of PDB code 1SUO. d) DPC micelle size is shown for comparison;[397–402] however, it should be noted that the micelle size adapts to the protein and that the hydrophobic dimensions are not well-defined.[318]

1.6 Goals of this research and dissertation layout

Although a lot of structural information has been published on cyt b_5,[11–27] all studies have been performed on truncated cyt b_5. As mentioned in Section 1.1.3, truncated cyt b_5 does not interact with microsomal cyts P450.[2,7,84,87] Similarly, while mutagenesis and cross-linking has been used to characterize the interface between cyts b_5 and cyts P450, very little of this work has been done in bilayers, with most of it being performed in DLPC micelles or no membrane environment. The goal of the work presented in this thesis is to characterize the complex formation between cyt b_5 and cyt P450 2B4 in a membrane environment, in the absence of any protein modifications, using NMR. Because it is difficult to crystallize membrane proteins and X-ray crystallography only provides a static picture of proteins and complexes, NMR was used to study the structure and dynamics of cyt b_5 and its ability to form complexes in a membrane mimetic. NMR techniques, mutagenesis and docking methods for the studies performed in this thesis can be found in Chapter 2.

In Chapter 3, we present the structure of full-length cyt b_5 in a membrane mimetic, and the completed sequence specific resonance assignment. The dynamics of the cyt b_5 residues, as well as the overall tumbling of the soluble domain, are characterized in Chapter 3. This structure is then used in Chapter 4 to begin the characterization of the complex between full-length cyt b_5 and full-length cyt P450 2B4 in the absence of a cyt P450 substrate. Mutagenesis and NMR results are combined to present a model of the complex between cyt b_5 and cyt P450 using a data-driven docking algorithm. In Chapter 5, we specifically assign the cyt b_5 residues interacting in the encounter complexes versus those interacting in the productive/stereospecific complexes with cyt P450 by utilizing a new NMR approach. In Chapter 6, we characterize the role of the cyt b_5 linker in complex formation with cyt P450 to understand why the linker needs to be a certain length for the complex to be functional. Throughout this dissertation, we also glean more insights into the dynamic nature of electron transfer complexes.

1.7 References

(1) Strittmatter, C.; Ball, E. A hemochromogen component of liver microsomes. *Proc. Nal. Acad. Sci.* **1952**, *38*, 19–25.

(2) Vergères, G.; Waskell, L. Cytochrome b_5, its functions, structure and membrane topology. *Biochimie* **1995**, *77*, 604–620.

(3) Schenkman, J. B.; Jansson, I. The many roles of cytochrome b_5. *Pharmacol. Ther.* **2003**, *97*, 139–152.

(4) Oshino, N. Cytochrome b_5 and its physiological significance. *Pharmacol. Ther. Part A* **1978**, *2*, 477–515.

(5) Ito, A.; Sato, R. Proteolytic microdissection of smooth-surfaced vesicles of liver microsomes. *J. Cell Biol.* **1969**, *40*, 179–189.

(6) Clarke, T. A.; Im, S.-C.; Bidwai, A.; Waskell, L. The role of the length and sequence of the linker domain of cytochrome b_5 in stimulating cytochrome P450 2B4 catalysis. *J. Biol. Chem.y* **2004**, *279*, 36809–36818.

(7) Chudaev, M. V; Gilep, A. A.; Usanov, S. A. Site-directed mutagenesis of cytochrome b_5 for studies of its interaction with cytochrome P450. *Biochemistry (Mosc)* **2001**, *66*, 667–681.

(8) Hanlon, M. R.; Begum, R. R.; Newbold, R. J.; Whitford, D.; Wallace, B. A. In vitro membrane-inserted conformation of the cytochrome b_5 tail. *Biochem. J.* **2000**, *352*, 117–124.

(9) Ozols, J. The role of microsomal cytochrome b_5 in the metabolism of ethanol, drugs and the desaturation of fatty acids. *Ann. Clin. Res.* **1976**, *8 Suppl 17*, 182–192.

(10) Schenkman, J. B.; Jansson, I.; Davis, G.; Tamburini, P. P.; Lu, Z.; Zhang, Z.; Rusling, J. F. Protein-Protein Interactions in the P450 Monooxygenase System. In *Molecular and applied aspects of oxidative drug metabolizing enzymes*; Arinç, E.; Schenkman, J. B.; Hodgson, E., Eds.; Springer: New York, 1999; pp. 21–39.

(11) Arnesano, F.; Banci, L.; Bertini, I.; Felli, I. C. The solution structure of oxidized rat microsomal cytochrome b_5. *Biochemistry* **1998**, *37*, 173–184.

(12) Arnesano, F.; Banci, L.; Bertini, I.; Felli, I. C.; Koulougliotis, D. Solution structure of the B form of oxidized rat microsomal cytochrome b_5 and backbone dynamics via ^{15}N rotating-frame NMR-relaxation measurements. Biological implications. *Eur. J. Biochem.* **1999**, *260*, 347–354.

(13) Arnesano, F.; Banci, L.; Bertini, I.; Koulougliotis, D. Solution structure of oxidized rat microsomal cytochrome b_5 in the presence of 2 M guanidinium chloride: monitoring the early steps in protein unfolding. *Biochemistry* **1998**, *37*, 17082–17092.

(14) Banci, L.; Bertini, I.; Rosato, A.; Scacchieri, S. Solution structure of oxidized microsomal rabbit cytochrome b_5. Factors determining the heterogeneous binding of the heme. *Eur. J. Biochem.* **2000**, *267*, 755–766.

(15) Bhattacharya, S.; Falzone, C. J.; Lecomte, J. T. Backbone dynamics of apocytochrome b_5 in its native, partially folded state. *Biochemistry* **1999**, *38*, 2577–2589.

(16) Dangi, B.; Blankman, J. I.; Miller, C. J.; Volkman, B. F.; Guiles, R. D. Contribution of backbone dynamics to entropy changes occurring on oxidation of cytochrome b_5. Can redox linked changes in hydrogen bond networks modulate reduction potentials? *J. Phys. Chem. B* **1998**, *102*, 8201–8208.

(17) Durley, R. C. E.; Mathews, F. S. Refinement and structural analysis of bovine cytochrome b_5 at 1.5 angstrom resolution. *Acta Crystallogr. D-Biol. Crystallogr.* **1996**, *52*, 65–76.

(18) Falzone, C. J.; Wang, Y.; Vu, B. C.; Scott, N. L.; Bhattacharya, S.; Lecomte, J. T. Structural and dynamic perturbations induced by heme binding in cytochrome b_5. *Biochemistry* **2001**, *40*, 4879–4891.

(19) Falzone, C. J.; Mayer, M. R.; Whiteman, E. L.; Moore, C. D.; Lecomte, J. T. Design challenges for hemoproteins: the solution structure of apocytochrome b_5. *Biochemistry* **1996**, *35*, 6519–6526.

(20) Guiles, R. D.; Basus, V. J.; Kuntz, I. D.; Waskell, L. Sequence-specific ^{1}H and ^{15}N resonance assignments for both equilibrium forms of the soluble heme binding domain of rat ferrocytochrome b_5. *Biochemistry* **1992**, *31*, 11365–11375.

(21) Guiles, R. D.; Altman, J.; Kuntz, I. D.; Waskell, L.; Lipka, J. J. Structural studies of cytochrome b_5: complete sequence-specific resonance assignments for the trypsin-solubilized microsomal ferrocytochrome b_5 obtained from pig and calf. *Biochemistry* **1990**, *29*, 1276–1289.

(22) Mathews, F. S.; Levine, M.; Argos, P. The structure of calf liver cytochrome b_5 at 2.8 A resolution. *Nat. New Biol.* **1971**, *233*, 15–16.

(23) Muskett, F. W.; Kelly, G. P.; Whitford, D. The solution structure of bovine ferricytochrome b_5 determined using heteronuclear NMR methods. *J. Mol. Biol.* **1996**, *258*, 172–189.

(24) Parthasarathy, S.; Altuve, A.; Terzyan, S.; Zhang, X.; Kuczera, K.; Rivera, M.; Benson, D. R. Accommodating a nonconservative internal mutation by water-mediated hydrogen bonding between β-sheet strands: a comparison of human and rat type B (mitochondrial) cytochrome b_5. *Biochemistry* **2011**, *50*, 5544–5554.

(25) Wang, L.; Cowley, A. B.; Terzyan, S.; Zhang, X.; Benson, D. R. Comparison of cytochromes b_5 from insects and vertebrates. *Proteins* **2007**, *67*, 293–304.

(26) Wu, J.; Gan, J. H.; Xia, Z. X.; Wang, Y. H.; Wang, W. H.; Xue, L. L.; Xie, Y.; Huang, Z. X. Crystal structure of recombinant trypsin-solubilized fragment of cytochrome b_5 and the structural comparison with Val61His mutant. *Proteins* **2000**, *40*, 249–257.

(27) Yokota, T.; Nakajima, Y.; Yamakura, F.; Sugio, S.; Hashimoto, M.; Takamiya, S. Unique structure of Ascaris suum b_5-type cytochrome: an additional alpha-helix and positively charged residues on the surface domain interact with redox partners. *Biochem. J.* **2006**, *394*, 437–447.

(28) Zhang, Q.; Cao, C.; Wang, Z.-Q.; Wang, Y.-H.; Wu, H.; Huang, Z.-X. The comparative study on the solution structures of the oxidized bovine microsomal cytochrome b_5 and mutant V45H. *Protein Sci.* **2004**, *13*, 2161–2169.

(29) Yao, P.; Wu, J.; Wang, Y.-H.; Sun, B.-Y.; Xia, Z.-X.; Huang, Z.-X. X-ray crystallography, CD and kinetic studies revealed the essence of the abnormal behaviors of the cytochrome b_5 Phe35-->Tyr mutant. *Eur. J. Biochem.* **2002**, *269*, 4287–4296.

(30) Wu, Y.; Wang, Y.; Qian, C.; Lu, J.; Li, E.; Wang, W.; Xie, Y.; Wang, J.; Zhu, D.; Huang, Z.; Tang, W. Solution structure of cytochrome b_5 mutant (E44/48/56A/D60A) and its interaction with cytochrome c. *Eur. J. Biochem.* **2001**, *268*, 1620–1630.

(31) Wang, Z.-Q.; Wu, J.; Wang, Y.-H.; Qian, W.; Xie, Y.; Xia, Z.-X.; Huang, Z.-X. Proline-40 is essential to maintaining cytochrome b_5' s stability and its electron transfer with cytochrome c. *Chin. J. Chem.* **2010**, *20*, 1212–1224.

(32) Shan, L.; Lu, J. X.; Gan, J. H.; Wang, Y. H.; Huang, Z. X.; Xia, Z. X. Structure of the F58W mutant of cytochrome b_5: the mutation leads to multiple conformations and weakens stacking interactions. *Acta Crystallogr. Sect. D: Biol. Crystallogr.* **2005**, *61*, 180–189.

(33) Gan, J. H.; Wu, J.; Wang, Z. Q.; Wang, Y. H.; Huang, Z. X.; Xia, Z. X. Structures of V45E and V45Y mutants and structure comparison of a variety of cytochrome b_5 mutants. *Acta Crystallogr. Sect. D: Biol. Crystallogr.* **2002**, *58*, 1298–1306.

(34) Cao, C.; Zhang, Q.; Xue, L.-L.; Ma, J.; Wang, Y.-H.; Wu, H.; Huang, Z.-X. The solution structure of the oxidized bovine microsomal cytochrome b_5 mutant V61H. *Biochem. Biophys. Res. Commun.* **2003**, *307*, 600–609.

(35) Banci, L.; Bertini, I.; Branchini, B.; Hajieva, P.; Spyroulias, G.; Turano, P. Dimethyl propionate ester heme-containing cytochrome b_5: structure and stability. *J. Biol. Inorg. Chem.* **2001**, *6*, 490–503.

(36) Kuroda, R.; Kinoshita, J.; Honsho, M.; Mitoma, J.; Ito, A. In situ topology of cytochrome b_5 in the endoplasmic reticulum membrane. *J. Biochem.* **1996**, *120*, 828–833.

(37) Holloway, P. W.; Buchheit, C. Topography of the membrane-binding domain of cytochrome b_5 in lipids by Fourier-transform infrared spectroscopy. *Biochemistry* **1990**, *29*, 9631–9637.

(38) Holloway, P. W.; Mantsch, H. H. Structure of cytochrome b_5 in solution by Fourier-transform infrared spectroscopy. *Biochemistry* **1989**, *28*, 931–935.

(39) Dailey, H. A.; Strittmatter, P. Structural and functional properties of the membrane binding segment of cytochrome b_5. *J. Biol. Chem.* **1978**, *253*, 8203–8209.

(40) Dürr, U. H.; Yamamoto, K.; Im, S.-C.; Waskell, L.; Ramamoorthy, A. Solid-state NMR reveals structural and dynamical properties of a membrane-anchored electron-carrier protein, cytochrome b_5. *J. Am. Chem. Soc.* **2007**, *129*, 6670–6671.

(41) Dolinsky, T. J.; Nielsen, J. E.; McCammon, J. A.; Baker, N. A. PDB2PQR: an automated pipeline for the setup of Poisson-Boltzmann electrostatics calculations. *Nucleic Acids Res.* **2004**, *32*, W665–W667.

(42) Dolinsky, T. J.; Czodrowski, P.; Li, H.; Nielsen, J. E.; Jensen, J. H.; Klebe, G.; Baker, N. A. PDB2PQR: expanding and upgrading automated preparation of biomolecular structures for molecular simulations. *Nucleic Acids Res.* **2007**, *35*, W522–W525.

(43) DeLano, W. L. The PyMOL Molecular Graphics System, Version 1.5.0.4 Schrödinger, LLC **2010**.

(44) Baker, N. A.; Sept, D.; Joseph, S.; Holst, M. J.; McCammon, J. A. Electrostatics of nanosystems: Application to microtubules and the ribosome. *Proc. Natl. Acad. Sci. U.S.A.* **2001**, *98*, 10037–10041.

(45) Abe, K.; Sugita, Y. Properties of cytochrome b_5 and methemoglobin reduction in human erythrocytes. *Eur. J. Biochem.* **1979**, *101*, 423–428.

(46) Hultquist, D. E.; Passon, P. G. Catalysis of methaemoglobin reduction by erythrocyte cytochrome b_5 and cytochrome b_5 reductase. *Nat. New Biol.* **1971**, *229*, 252–254.

(47) Napier, J. A.; Sayanova, O.; Stobart, A. K.; Shewry, P. R. A new class of cytochrome b_5 fusion proteins. *Biochem. J.* **1997**, *328 (Pt 2)*, 717–718.

(48) Oshino, N.; Imai, Y.; Sato, R. A function of cytochrome b_5 in fatty acid desaturation by rat liver microsomes. *J. Biochem.* **1971**, *69*, 155–167.

(49) Strittmatter, P.; Spatz, L.; Corcoran, D.; Rogers, M. J.; Setlow, B.; Redline, R. Purification and properties of rat liver microsomal stearyl coenzyme A desaturase. *Proc. Natl. Acad. Sci. U.S.A.* **1974**, *71*, 4565–4569.

(50) Keyes, S. R.; Alfano, J. A.; Jansson, I.; Cinti, D. L. Rat liver microsomal elongation of fatty acids. Possible involvement of cytochrome b_5. *J. Biol. Chem.* **1979**, *254*, 7778–7784.

(51) Demirkapi, N.; Carreau, J. P.; Ghesquier, D. Evidence against cytochrome b_5 involvement in liver microsomal fatty acid elongation. *Biochim. Biophys. Acta* **1991**, *1082*, 49–56.

(52) Cinti, D. L.; Cook, L.; Nagi, M. N.; Suneja, S. K. The fatty acid chain elongation system of mammalian endoplasmic reticulum. *Prog. Lipid Res.* **1992**, *31*, 1–51.

(53) Takematsu, H.; Kawano, T.; Koyama, S.; Kozutsumi, Y.; Suzuki, A.; Kawasaki, T. Reaction mechanism underlying CMP-N-acetylneuraminic acid hydroxylation in mouse liver: formation of a ternary complex of cytochrome b_5, CMP-N-acetylneuraminic acid, and a hydroxylation enzyme. *J. Biochem.* **1994**, *115*, 381–386.

(54) Hildebrandt, A.; Estabrook, R. W. Evidence for the participation of cytochrome b_5 in hepatic microsomal mixed-function oxidation reactions. *Arch. Biochem. Biophys.* **1971**, *143*, 66–79.

(55) Juvonen, R. O.; Iwasaki, M.; Negishi, M. Roles of residues 129 and 209 in the alteration by cytochrome b_5 of hydroxylase activities in mouse 2A P450S. *Biochemistry* **1992**, *31*, 11519–11523.

(56) Yamazaki, H.; Nakano, M.; Imai, Y.; Ueng, Y. F.; Guengerich, F. P.; Shimada, T. Roles of cytochrome b_5 in the oxidation of testosterone and nifedipine by recombinant cytochrome P450 3A4 and by human liver microsomes. *Arch. Biochem. Biophys.* **1996**, *325*, 174–182.

(57) Perret, A.; Pompon, D. Electron shuttle between membrane-bound cytochrome P450 3A4 and b_5 rules uncoupling mechanisms. *Biochemistry* **1998**, *37*, 11412–11424.

(58) Mansouri, A.; Lurie, A. A. Concise review: methemoglobinemia. *Am. J. Hemat.* **1993**, *42*, 7–12.

(59) Hegesh, E.; Hegesh, J.; Kaftory, A. Congenital methemoglobinemia with a deficiency of cytochrome b_5. *New Engl. J. Med.* **1986**, *314*, 757–761.

(60) Beauvais, P. Les méthémoglobinémies héréditaires. *Archives de Pédiatrie* **2000**, *7*, 513–518.

(61) Percy, M. J.; McFerran, N. V; Lappin, T. R. J. Disorders of oxidised haemoglobin. *Blood Rev.* **2005**, *19*, 61–68.

(62) Giordano, S. J.; Kaftory, A.; Steggles, A. W. A splicing mutation in the cytochrome b_5 gene from a patient with congenital methemoglobinemia and pseudohermaphrodism. *Hum. Genet.* **1994**, *93*, 568–570.

(63) Kok, R. C.; Timmerman, M. A.; Wolffenbuttel, K. P.; Drop, S. L. S.; De Jong, F. H. Isolated 17,20-lyase deficiency due to the cytochrome b_5 mutation W27X. *J. Clin. Endocrin. Metab.* **2010**, *95*, 994–999.

(64) Idkowiak, J.; Randell, T.; Dhir, V.; Patel, P.; Shackleton, C. H. L.; Taylor, N. F.; Krone, N.; Arlt, W. A missense mutation in the human cytochrome b_5 gene causes 46,XY disorder of sex development due to true isolated 17,20 lyase deficiency. *J. Clin. Endocrin. Metab.* **2012**, *97*, E465–E475.

(65) Plewka, A.; Kamiński, M.; Plewka, D. Ontogenesis of hepatocyte respiration processes in relation to rat liver cytochrome P450-dependent monooxygenase system. *Mech. Ageing Dev.* **1998**, *105*, 197–207.

(66) Dmitriev, L. F. Shortage of lipid-radical cycles in membranes as a possible prime cause of energetic failure in aging and Alzheimer disease. *Neurochem. Res.* **2007**, *32*, 1278–1291.

(67) Dmitriev, L. F.; Titov, V. N. Lipid peroxidation in relation to ageing and the role of endogenous aldehydes in diabetes and other age-related diseases. *Ageing Res. Rev.* **2010**, *9*, 200–210.

(68) Maghzal, G. J.; Thomas, S. R.; Hunt, N. H.; Stocker, R. Cytochrome b_5, not superoxide anion radical, is a major reductant of indoleamine 2,3-dioxygenase in human cells. *J. Biol. Chem.* **2008**, *283*, 12014–12025.

(69) Vottero, E.; Mitchell, D. A.; Page, M. J.; MacGillivray, R. T. A.; Sadowski, I. J.; Roberge, M.; Mauk, A. G. Cytochrome b_5 is a major reductant in vivo of human indoleamine 2,3-dioxygenase expressed in yeast. *FEBS Lett.* **2006**, *580*, 2265–2268.

(70) Muller, A. J.; DuHadaway, J. B.; Donover, P. S.; Sutanto-Ward, E.; Prendergast, G. C. Inhibition of indoleamine 2,3-dioxygenase, an immunoregulatory target of the cancer suppression gene Bin1, potentiates cancer chemotherapy. *Nat. Med.* **2005**, *11*, 312–319.

(71) Munn, D. H.; Shafizadeh, E.; Attwood, J. T.; Bondarev, I.; Pashine, A.; Mellor, A. L. Inhibition of T cell proliferation by macrophage tryptophan catabolism. *J. Exp. Med.* **1999**, *189*, 1363–1372.

(72) Grohmann, U.; Fallarino, F.; Puccetti, P. Tolerance, DCs and tryptophan: much ado about IDO. *Trends Immunol.* **2003**, *24*, 242–248.

(73) Widner, B.; Leblhuber, F.; Walli, J.; Tilz, G. P.; Demel, U.; Fuchs, D. Degradation of tryptophan in neurodegenerative disorders. *Adv. Exp. Med. Biol.* **1999**, *467*, 133–138.

(74) Wichers, M. C.; Maes, M. The role of indoleamine 2,3-dioxygenase (IDO) in the pathophysiology of interferon-alpha-induced depression. *J. Psych. Neurosci.* **2004**, *29*, 11–17.

(75) Takikawa, O.; Truscott, R. J. W.; Fukao, M.; Miwa, S. Age-related nuclear cataract and indoleamine 2,3-dioxygenase-initiated tryptophan metabolism in the human lens. *Adv. Exp. Med. Biol.* **2003**, *527*, 277–285.

(76) Shirabe, K.; Nagai, T.; Yubisui, T.; Takeshita, M. Electrostatic interaction between NADH-cytochrome b_5 reductase and cytochrome b_5 studied by site-directed mutagenesis. *Biochim. Biophys. Acta* **1998**, *1384*, 16–22.

(77) Kawano, M.; Shirabe, K.; Nagai, T.; Takeshita, M. Role of carboxyl residues surrounding heme of human cytochrome b_5 in the electrostatic interaction with NADH-cytochrome b_5 reductase. *Biochem. Biophys. Res. Commun.* **1998**, *245*, 666–669.

(78) Livingston, D. J.; McLachlan, S. J.; La Mar, G. N.; Brown, W. D. Myoglobin: cytochrome b_5 interactions and the kinetic mechanism of metmyoglobin reductase. *J. Biol. Chem.* **1985**, *260*, 15699–15707.

(79) Dailey, H. A.; Strittmatter, P. Modification and identification of cytochrome b_5 carboxyl groups involved in protein-protein interaction with cytochrome b_5 reductase. *J. Biol. Chem.* **1979**, *254*, 5388–5396.

(80) Strittmatter, P.; Hackett, C. S.; Korza, G.; Ozols, J. Characterization of the covalent cross-links of the active-sites of amidinated cytochrome-b_5 and NADH-cytochrome-b_5 reductase. *J. Biol. Chem.* **1990**, *265*, 21709–21713.

(81) Nishida, H.; Miki, K. Electrostatic properties deduced from refined structures of NADH-cytochrome b_5 reductase and the other flavin-dependent reductases: pyridine nucleotide-binding and interaction with an electron-transfer partner. *Proteins* **1996**, *26*, 32–41.

(82) Dailey, H. A.; Strittmatter, P. Characterization of the interaction of amphipathic cytochrome b_5 with stearyl coenzyme A desaturase and NADPH:cytochrome P-450 reductase. *J. Biol. Chem.* **1980**, *255*, 5184–5189.

(83) Enoch, H. G.; Strittmatter, P. Cytochrome b_5 reduction by NADPH-cytochrome P-450 reductase. *J. Biol. Chem.* **1979**, *254*, 8976–8981.

(84) Chiang, J. Y. Interaction of purified microsomal cytochrome P-450 with cytochrome b_5. *Arch. Biochem. Biophys.* **1981**, *211*, 662–673.

(85) Miki, N.; Sugiyama, T.; Yamano, T. Purification and characterization of cytochrome P-450 with high affinity for cytochrome b_5. *J. Biochem.* **1980**, *88*, 307–310.

(86) Usanov, S. A.; Bendzko, P.; Pfeil, W.; Jänig, G. R.; Ruckpaul, K. The role of the hydrophobic fragment of cytochrome b_5 in the interaction with cytochrome P-450. *Bioorg. Khim.* **1983**, *9*, 450–461.

(87) Bendzko, P.; Usanov, S. A.; Pfeil, W.; Ruckpaul, K. Role of the hydrophobic tail of cytochrome b_5 in the interaction with cytochrome P-450 LM2. *Acta Biol. Med. Ger.* **1982**, *41*, K1–K8.

(88) Omata, Y.; Robinson, R. C.; Gelboin, H. V; Pincus, M. R.; Friedman, F. K. Specificity of the cytochrome P-450 interaction with cytochrome b_5. *FEBS Lett.* **1994**, *346*, 241–245.

(89) Usanov, S. A.; Chashchin, V. L. Interaction of cytochrome P-450scc with cytochrome b_5. *FEBS Lett.* **1991**, *278*, 279–282.

(90) Usanov, S. A.; Chashchin, V. L.; Akhrem, A. A. Interaction of cholesterol hydroxylating cytochrome P-450 with cytochrome b_5. *Biochemistry (Moscow)* **1989**, *54*, 472–486.

(91) Honkakoski, P.; Linnala-Kankkunen, A.; Usanov, S. A.; Lang, M. A. Highly homologous cytochromes P-450 and b_5: a model to study protein-protein interactions in a reconstituted monooxygenase system. *Biochim. Biophys. Acta* **1992**, *1122*, 6–14.

(92) Tamburini, P. P.; White, R. E.; Schenkman, J. B. Chemical characterization of protein-protein interactions between cytochrome P-450 and cytochrome b_5. *J. Biol. Chem.* **1985**, *260*, 4007–4015.

(93) Holloway, P. W.; Katz, J. T. A requirement for cytochrome b_5 in microsomal stearyl coenzyme A desaturation. *Biochemistry* **1972**, *11*, 3689–3696.

(94) Spatz, L.; Strittmatter, P. A form of cytochrome b_5 that contains an additional hydrophobic sequence of 40 amino acid residues. *Proc. Natl. Acad. Sci. U.S.A.* **1971**, *68*, 1042–1046.

(95) Nisimoto, Y.; Otsuka-Murakami, H. Cytochrome b_5, cytochrome c, and cytochrome P-450 interactions with NADPH-cytochrome P-450 reductase in phospholipid vesicles. *Biochemistry* **1988**, *27*, 5869–5876.

(96) Kominami, S.; Ogawa, N.; Morimune, R.; De-Ying, H.; Takemori, S. The role of cytochrome b_5 in adrenal microsomal steroidogenesis. *J. Steroid Biochem. Mol. Biol.* **1992**, *42*, 57–64.

(97) Yamazaki, H.; Johnson, W. W.; Ueng, Y. F.; Shimada, T.; Guengerich, F. P. Lack of electron transfer from cytochrome b_5 in stimulation of catalytic activities of cytochrome P450 3A4. Characterization of a reconstituted cytochrome P450 3A4/NADPH-cytochrome P450 reductase system and studies with apo-cytochrome b_5. *J. Biol. Chem.* **1996**, *271*, 27438–27444.

(98) Peyronneau, M. A.; Renaud, J. P.; Truan, G.; Urban, P.; Pompon, D.; Mansuy, D. Optimization of yeast-expressed human liver cytochrome P450 3A4 catalytic activities by coexpressing NADPH-cytochrome P450 reductase and cytochrome b_5. *Eur. J. Biochem.* **1992**, *207*, 109–116.

(99) Voice, M. W.; Zhang, Y.; Wolf, C. R.; Burchell, B.; Friedberg, T. Effects of human cytochrome b_5 on CYP3A4 activity and stability in vivo. *Arch. Biochem. Biophys.* **1999**, *366*, 116–124.

(100) Kossor, D. C.; Kominami, S.; Takemori, S.; Colby, H. D. Destruction of testicular cytochrome P-450 by 7 alpha-thiospironolactone is catalyzed by the 17 alpha-hydroxylase. *J. Steroid Biochem. Mol. Biol.* **1992**, *42*, 421–424.

(101) Katagiri, M.; Kagawa, N.; Waterman, M. R. The role of cytochrome b_5 in the biosynthesis of androgens by human P450c17. *Arch. Biochem. Biophys.* **1995**, *317*, 343–347.

(102) Stayton, P. S.; Fisher, M. T.; Sligar, S. G. Determination of cytochrome b_5 association reactions. Characterization of metmyoglobin and cytochrome P-450cam binding to genetically engineered cytochrome b_5. *J. Biol. Chem.* **1988**, *263*, 13544–13548.

(103) Shao, W.; Im, S.-C.; Zuiderweg, E. R.; Waskell, L. Mapping the binding interface of the cytochrome b_5-cytochrome c complex by nuclear magnetic resonance. *Biochemistry* **2003**, *42*, 14774–14784.

(104) Rodríguez-Marañón, M. J.; Qiu, F.; Stark, R. E.; White, S. P.; Zhang, X.; Foundling, S. I.; Rodríguez, V.; Schilling, C. L.; Bunce, R. A.; Rivera, M. 13C NMR spectroscopic and X-ray crystallographic study of the role played by mitochondrial cytochrome b_5 heme propionates in the electrostatic binding to cytochrome c. *Biochemistry* **1996**, *35*, 16378–16390.

(105) Seetharaman, R.; White, S. P.; Rivera, M. Electrochemical measurement of second-order electron transfer rate constants for the reaction between cytochrome b_5 and cytochrome c. *Biochemistry* **1996**, *35*, 12455–45463.

(106) Stonehuerner, J.; Williams, J. B.; Millett, F. Interaction between cytochrome c and cytochrome b_5. *Biochemistry* **1979**, *18*, 5422–5427.

(107) Ren, Y.; Wang, W.-H.; Wang, Y.-H.; Case, M.; Qian, W.; McLendon, G.; Huang, Z.-X. Mapping the electron transfer interface between cytochrome b_5 and cytochrome c. *Biochemistry* **2004**, *43*, 3527–3536.

(108) Eley, C. G.; Moore, G. R. ^{1}H-N.M.R. investigation of the interaction between cytochrome c and cytochrome b_5. *Biochem. J.* **1983**, *215*, 11–21.

(109) Meyer, T. E.; Rivera, M.; Walker, F. A.; Mauk, M. R.; Mauk, A. G.; Cusanovich, M. A.; Tollin, G. Laser flash photolysis studies of electron transfer to the cytochrome b_5-cytochrome c complex. *Biochemistry* **1993**, *32*, 622–627.

(110) Rodgers, K. K.; Pochapsky, T. C.; Sligar, S. G. Probing the mechanisms of macromolecular recognition: the cytochrome b_5-cytochrome c complex. *Science* **1988**, *240*, 1657–1659.

(111) Mauk, M. R.; Mauk, A. G. Crosslinking of cytochrome c and cytochrome b_5 with a water-soluble carbodiimide. Reaction conditions, product analysis and critique of the technique. *Eur. J. Biochem.* **1989**, *186*, 473–486.

(112) Mauk, M. R.; Mauk, A. G.; Weber, P. C.; Matthew, J. B. Electrostatic analysis of the interaction of cytochrome c with native and dimethyl ester heme substituted cytochrome b_5. *Biochemistry* **1986**, *25*, 7085–7091.

(113) Durham, B.; Fairris, J. L.; McLean, M.; Millett, F.; Scott, J. R.; Sligar, S. G.; Willie, A. Electron transfer from cytochrome b_5 to cytochrome c. *J. Bioenerg. Biomembr.* **1995**, *27*, 331–340.

(114) Sun, Y. L.; Wang, Y. H.; Yan, M. M.; Sun, B. Y.; Xie, Y.; Huang, Z. X.; Jiang, S. K.; Wu, H. M. Structure, interaction and electron transfer between cytochrome b_5, its E44A and/or E56A mutants and cytochrome c. *J. Mol. Biol.* **1999**, *285*, 347–359.

(115) Ng, S.; Smith, M. B.; Smith, H. T.; Millett, F. Effect of modification of individual cytochrome c lysines on the reaction with cytochrome b_5. *Biochemistry* **1977**, *16*, 4975–4978.

(116) Mauk, A. G.; Mauk, M. R.; Moore, G. R.; Northrup, S. H. Experimental and theoretical analysis of the interaction between cytochrome c and cytochrome b_5. *J. Bioenerg. Biomembr.* **1995**, *27*, 311–330.

(117) Mauk, M. R.; Reid, L. S.; Mauk, A. G. Spectrophotometric analysis of the interaction between cytochrome b_5 and cytochrome c. *Biochemistry* **1982**, *21*, 1843–1846.

(118) Hartshorn, R. T.; Mauk, A. G.; Mauk, M. R.; Moore, G. R. NMR study of the interaction between cytochrome b_5 and cytochrome c. Observation of a ternary complex formed by the two proteins and $[Cr(en)_3]^{3+}$. *FEBS Lett.* **1987**, *213*, 391–395.

(119) Volkov, A. N.; Ferrari, D.; Worrall, J. A. R.; Bonvin, A. M. J. J.; Ubbink, M. The orientations of cytochrome c in the highly dynamic complex with cytochrome b_5 visualized by NMR and docking using HADDOCK. *Protein Sci.* **2005**, *14*, 799–811.

(120) Qian, W.; Sun, Y. L.; Wang, Y. H.; Zhuang, J. H.; Xie, Y.; Huang, Z. X. The influence of mutation at Glu44 and Glu56 of cytochrome b_5 on the protein's stabilization and interaction between cytochrome c and cytochrome b_5. *Biochemistry* **1998**, *37*, 14137–14150.

(121) Miura, R.; Sugiyama, T.; Akasaka, K.; Yamano, T. An NMR study on the interaction between cytochrome b_5 and cytochrome c. *Biochem. Int* **1980**, *1*, 532–538.

(122) Sun, Y. L.; Xie, Y.; Wang, Y. H.; Xiao, G. T.; Huang, Z. X. The influence of Glu44 and Glu56 of cytochrome b_5 on the protein structure and interaction with cytochrome c. *Protein Eng.* **1996**, *9*, 555–558.

(123) Deep, S.; Im, S.-C.; Zuiderweg, E. R.; Waskell, L. Characterization and calculation of a cytochrome c-cytochrome b_5 complex using NMR data. *Biochemistry* **2005**, *44*, 10654–10668.

(124) Qian, C.; Yao, Y.; Ye, K.; Wang, J.; Tang, W.; Wang, Y.; Wang, W.; Lu, J.; Xie, Y.; Huang, Z. Effects of charged amino-acid mutation on the solution structure of cytochrome b_5 and binding between cytochrome b_5 and cytochrome c. *Protein Sci.* **2001**, *10*, 2451–2459.

(125) Burch, A. M.; Rigby, S. E.; Funk, W. D.; MacGillivray, R. T.; Mauk, M. R.; Mauk, A. G.; Moore, G. R. NMR characterization of surface interactions in the cytochrome b_5-cytochrome c complex. *Science* **1990**, *247*, 831–833.

(126) Hom, K.; Ma, Q. F.; Wolfe, G.; Zhang, H.; Storch, E. M.; Daggett, V.; Basus, V. J.; Waskell, L. NMR studies of the association of cytochrome b_5 with cytochrome c. *Biochemistry* **2000**, *39*, 14025–14039.

(127) Yao, P.; Wang, Y.-H.; Sun, B.-Y.; Xie, Y.; Hirota, S.; Yamauchi, O.; Huang, Z.-X. Kinetic studies on the oxidation of cytochrome b_5 Phe35 mutants with cytochrome c, plastocyanin and inorganic complexes. *J. Biol. Inorg. Chem.* **2002**, *7*, 375–383.

(128) Davydov, D. R. Microsomal monooxygenase in apoptosis: another target for cytochrome c signaling? *Trends Biochem. Sci.* **2001**, *26*, 155–160.

(129) Mulrooney, S. B.; Waskell, L. High-level expression in Escherichia coli and purification of the membrane-bound form of cytochrome b_5. *Protein Expression Purif.* **2000**, *19*, 173–178.

(130) Dürr, U. H.; Waskell, L.; Ramamoorthy, A. The cytochromes P450 and b_5 and their reductases--promising targets for structural studies by advanced solid-state NMR spectroscopy. *Biochim Biophys Acta* **2007**, *1768*, 3235–3259.

(131) Xu, J.; Durr, U. H.; Im, S.-C.; Gan, Z.; Waskell, L.; Ramamoorthy, A. Bicelle-enabled structural studies on a membrane-associated cytochrome b_5 by solid-state MAS NMR spectroscopy. *Angew. Chem. Int. Ed. Engl.* **2008**, *47*, 7864–7867.

(132) Soong, R.; Smith, P. E.; Xu, J.; Yamamoto, K.; Im, S. C.; Waskell, L.; Ramamoorthy, A. Proton-evolved local-field solid-state NMR studies of cytochrome b_5 embedded in bicelles, revealing both structural and dynamical information. *J. Am. Chem. Soc.* **2010**, *132*, 5779–5788.

(133) Xu, J.; Soong, R.; Im, S.-C. C.; Waskell, L.; Ramamoorthy, A. INEPT-based separated-local-field NMR spectroscopy: a unique approach to elucidate side-chain dynamics of membrane-associated proteins. *J. Am. Chem. Soc.* **2010**, *132*, 9944–9947.

(134) Ozols, J.; Strittmatter, P. The reactivity of the lysyl residues of cytochrome b_5. *J. Biol. Chem.* **1966**, *241*, 4793–4797.

(135) Salemme, F. R. An hypothetical structure for an intermolecular electron transfer complex of cytochromes c and b_5. *J. Mol. Biol.* **1976**, *102*, 563–568.

(136) Poulos, T. L.; Mauk, A. G. Models for the complexes formed between cytochrome b_5 and the subunits of methemoglobin. *J. Biol. Chem.* **1983**, *258*, 7369–7373.

(137) Nisimoto, Y.; Lambeth, J. D. NADPH-cytochrome P-450 reductase-cytochrome b_5 interactions: crosslinking of the phospholipid vesicle-associated proteins by a water-soluble carbodiimide. *Arch. Biochem. Biophys.* **1985**, *241*, 386–396.

(138) Rodgers, K. K.; Sligar, S. G. Mapping electrostatic interactions in macromolecular associations. *J. Mol. Biol.* **1991**, *221*, 1453–1460.

(139) Whitford, D. The identification of cation-binding domains on the surface of microsomal cytochrome b_5 using ^{1}H-NMR paramagnetic difference spectroscopy. *Eur. J. Biochem.* **1992**, *203*, 211–223.

(140) Northrup, S. H.; Thomasson, K. A.; Miller, C. M.; Barker, P. D.; Eltis, L. D.; Guillemette, J. G.; Inglis, S. C.; Mauk, A. G. Effects of charged amino acid mutations on the bimolecular kinetics of reduction of yeast iso-1-ferricytochrome c by bovine ferrocytochrome b_5. *Biochemistry* **1993**, *32*, 6613–6623.

(141) Nelson, D. R. Progress in tracing the evolutionary paths of cytochrome P450. *Biochim. Biophys. Acta - Proteins and Proteomics* **2011**, *1814*, 14–18.

(142) Nelson, D. R. The cytochrome p450 homepage. *Hum. Genomics* **2009**, *4*, 59–65.

(143) Guengerich, F. P. Cytochromes P450, drugs, and diseases. *Mol. Interv.* **2003**, *3*, 194–204.

(144) Guengerich, F. P.; Wu, Z. L.; Bartleson, C. J. Function of human cytochrome P450s: characterization of the orphans. *Biochem. Biophys. Res. Commun.* **2005**, *338*, 465–469.

(145) Nelson, D. R. Comparison of P450s from human and fugu: 420 million years of vertebrate P450 evolution. *Arch. Biochem. Biophys.* **2003**, *409*, 18–24.

(146) Nelson, D. R.; Koymans, L.; Kamataki, T.; Stegeman, J. J.; Feyereisen, R.; Waxman, D. J.; Waterman, M. R.; Gotoh, O.; Coon, M. J.; Estabrook, R. W.; Gunsalus, I. C.; Nebert, D. W. P450 superfamily: update on new sequences, gene mapping, accession numbers and nomenclature. *Pharmacogenetics* **1996**, *6*, 1–42.

(147) Ortiz de Montellano, P. R. Hydrocarbon hydroxylation by cytochrome P450 enzymes. *Chem. Rev.* **2010**, *110*, 932–948.

(148) Chu, V.; Einolf, H. J.; Evers, R.; Kumar, G.; Moore, D.; Ripp, S.; Silva, J.; Sinha, V.; Sinz, M.; Skerjanec, A. In vitro and in vivo induction of cytochrome p450: a survey of the current practices and recommendations: a pharmaceutical research and manufacturers of america perspective. *Drug Metab. Dispos.* **2009**, *37*, 1339–1354.

(149) Lubet, R. A.; Mayer, R. T.; Cameron, J. W.; Nims, R. W.; Burke, M. D.; Wolff, T.; Guengerich, F. P. Dealkylation of pentoxyresorufin: a rapid and sensitive assay for measuring induction of cytochrome(s) P-450 by phenobarbital and other xenobiotics in the rat. *Arch. Biochem. Biophys.* **1985**, *238*, 43–48.

(150) Wang, J.-F.; Zhang, C.-C.; Chou, K.-C.; Wei, D.-Q. Structure of cytochrome p450s and personalized drug. *Curr. Med. Chem.* **2009**, *16*, 232–244.

(151) Guengerich, F. P. Cytochrome P450s and other enzymes in drug metabolism and toxicity. *AAPS J.* **2006**, *8*, E101–E111.

(152) Schwaiblmair, M.; Behr, W.; Foerg, W.; Berghaus, T. Cytochrome P450 polymorphisms and drug-induced interstitial lung disease. *Expert Opin. Drug Metab. Toxicol.* **2011**, *7*, 1547–1560.

(153) Nebert, D. W.; Russell, D. W. Clinical importance of the cytochromes P450. *Lancet* **2002**, *360*, 1155–1162.

(154) Ferguson, C. S.; Tyndale, R. F. Cytochrome P450 enzymes in the brain : emerging evidence of biological significance. *Trends Pharmacol. Sci.* **2011**, *32*, 708–714.

(155) Meyer, R. P.; Gehlhaus, M.; Knoth, R.; Volk, B. Expression and function of cytochrome P450 in brain drug metabolism. *Curr. Drug Metab.* **2007**, *8*, 297–306.

(156) Bromek, E.; Haduch, A.; Gołembiowska, K.; Daniel, W. A. Cytochrome P450 mediates dopamine formation in the brain in vivo. *J. Neurochem.* **2011**, *118*, 806–815.

(157) Yu, A.-M.; Idle, J. R.; Byrd, L. G.; Krausz, K. W.; Küpfer, A.; Gonzalez, F. J. Regeneration of serotonin from 5-methoxytryptamine by polymorphic human CYP2D6. *Pharmacogenetics* **2003**, *13*, 173–81.

(158) Fleming, I. Cytochrome P450-dependent eicosanoid production and crosstalk. *Curr. Opin. Lipidol.* **2011**, *22*, 403–409.

(159) Murray, G. I.; Taylor, M. C.; Mcfadyen, M. C. E.; Mckay, A.; Greenlee, F.; Burke, M. D.; Melvin, W. T. Tumor-specific expression of cytochrome P450 CYP1B1 tumor-specific. *Cancer Res.* **1997**, *57*, 3026–3031.

(160) Chun, Y.; Kim, S. Discovery of cytochrome P450 1B1 inhibitors as new promising. *Med. Res. Rev.* **2003**, *23*, 657–668.

(161) Stoilov, I.; Akarsu, a N.; Sarfarazi, M. Identification of three different truncating mutations in cytochrome P4501B1 (CYP1B1) as the principal cause of primary congenital glaucoma (Buphthalmos) in families linked to the GLC3A locus on chromosome 2p21. *Hum. Mol. Genet.* **1997**, *6*, 641–647.

(162) Hennan, J. K.; Huang, J.; Barrett, T. D.; Driscoll, E. M.; Willens, D. E.; Park, A. M.; Crofford, L. J.; Lucchesi, B. R. Effects of selective cyclooxygenase-2 inhibition on vascular responses and thrombosis in canine coronary arteries. *Circulation* **2001**, *104*, 820–825.

(163) Tuder, R. M.; Cool, C. D.; Yeager, M.; Taraseviciene-Stewart, L.; Bull, T. M.; Voelkel, N. F. The Pathobiology of Pulmonary Hypertension: Endothelium. *Clin. Chest Med.* **2001**, *22*, 405–418.

(164) O'Donnell, A.; Judson, I.; Dowsett, M.; Raynaud, F.; Dearnaley, D.; Mason, M.; Harland, S.; Robbins, A.; Halbert, G.; Nutley, B.; Jarman, M. Hormonal impact of the 17alpha-hydroxylase/C(17,20)-lyase inhibitor abiraterone acetate (CB7630) in patients with prostate cancer. *Br. J. Cancer* **2004**, *90*, 2317–2325.

(165) Chen, T. C.; Sakaki, T.; Yamamoto, K.; Kittaka, A. The roles of cytochrome P450 enzymes in prostate cancer development and treatment. *Anticancer Res.* **2012**, *32*, 291–298.

(166) Singh, M. S.; Francis, P. A.; Michael, M. Tamoxifen, cytochrome P450 genes and breast cancer clinical outcomes. *The Breast (Edinburgh, Scotland)* **2011**, *20*, 111–118.

(167) Rae, J. M.; Sikora, M. J.; Henry, N. L.; Li, L.; Kim, S.; Oesterreich, S.; Skaar, T. C.; Nguyen, A. T.; Desta, Z.; Storniolo, A. M.; Flockhart, D. A.; Hayes, D. F.; Stearns, V. Cytochrome P450 2D6 activity predicts discontinuation of tamoxifen therapy in breast cancer patients. *Pharmacogenomics J.* **2009**, *9*, 258–264.

(168) Orlando, L.; Schiavone, P.; Fedele, P.; Calvani, N.; Nacci, A.; Rizzo, P.; Marino, A.; D'Amico, M.; Sponziello, F.; Mazzoni, E.; Cinefra, M.; Fazio, N.; Maiello, E.; Silvestris, N.; Colucci, G.; Cinieri, S. Molecularly targeted endocrine therapies for breast cancer. *Cancer Treat. Rev.* **2010**, *36 Suppl 3*, S67–S71.

(169) Fasan, R. Tuning P450 Enzymes as Oxidation Catalysts. *ACS Catalysis* **2012**, *2*, 647–666.

(170) Chefson, A.; Auclair, K. Progress towards the easier use of P450 enzymes. *Mol. Biosyst.* **2006**, *2*, 462–469.

(171) Jung, S. T.; Lauchli, R.; Arnold, F. H. Cytochrome P450: taming a wild type enzyme. *Curr. Opin. Biotechnol.* **2011**, 1–9.

(172) Urlacher, V. B.; Girhard, M. Cytochrome P450 monooxygenases : an update on perspectives for synthetic application. *Trends in Biotechnol.* **2012**, *30*, 26–36.

(173) Ro, D. K.; Paradise, E. M.; Ouellet, M.; Fisher, K. J.; Newman, K. L.; Ndungu, J. M.; Ho, K. A.; Eachus, R. A.; Ham, T. S.; Kirby, J.; Chang, M. C.; Withers, S. T.; Shiba, Y.; Sarpong, R.; Keasling, J. D. Production of the antimalarial drug precursor artemisinic acid in engineered yeast. *Nature* **2006**, *440*, 940–943.

(174) Nelson, D. R. Cytochrome P450 and the individuality of species. *Arch. Biochem. Biophys.* **1999**, *369*, 1–10.

(175) *Cytochrome P450: Structure, Mechanism, and Biochemistry*; Ortiz de Montellano, P. R., Ed.; Second.; Springer US: Boston, MA, 2005.

(176) Danielson, P. B. The cytochrome P450 superfamily: biochemistry, evolution and drug metabolism in humans. *Curr. Drug Metab.* **2002**, *3*, 561–597.

(177) Ingelman-Sundberg, M. Bioactivation or inactivation of toxic compounds? *Trends Pharmacol. Sci.* **1980**, *1*, 176–179.

(178) Isin, E. M.; Guengerich, F. P. Substrate binding to cytochromes P450. *Anal. Bioanal. Chem.* **2008**, *392*, 1019–1030.

(179) Luthra, A.; Denisov, I. G.; Sligar, S. G. Spectroscopic features of cytochrome P450 reaction intermediates. *Arch. Biochem. Biophys.* **2011**, *507*, 26–35.

(180) Pochapsky, T. C.; Kazanis, S.; Dang, M. Conformational plasticity and structure/function relationships in cytochromes P450. *Antioxid. Redox Signal.* **2010**, *13*, 1273–1296.

(181) Porter, T. D.; Coon, M. J. Cytochrome P-450. Multiplicity of isoforms, substrates, and catalytic and regulatory mechanisms. *J. Biol. Chem.* **1991**, *266*, 13469–13472.

(182) Poulos, T. L. Cytochrome P450 flexibility. *Proc. Natl. Acad. Sci. U.S.A.* **2003**, *100*, 13121–13122.

(183) Reed, J. R.; Backes, W. L. Formation of P450 · P450 complexes and their effect on P450 function. *Pharmacol. Ther.* **2012**, *133*, 299–310.

(184) Shaik, S.; Cohen, S.; Wang, Y.; Chen, H.; Kumar, D.; Thiel, W. P450 enzymes: their structure, reactivity, and selectivity-modeled by QM/MM calculations. *Chem. Rev.* **2010**, *110*, 949–1017.

(185) Shakunthala, N. New cytochrome P450 mechanisms: implications for understanding molecular basis for drug toxicity at the level of the cytochrome. *Expert Opin. Drug Metab. Toxicol.* **2010**, *6*, 1–15.

(186) Guengerich, F. P. Common and uncommon cytochrome P450 reactions related to metabolism and chemical toxicity. *Chemical Res. Toxicol.* **2001**, *14*, 611–650.

(187) Lamb, D. C.; Waterman, M. R.; Kelly, S. L.; Guengerich, F. P. Cytochromes P450 and drug discovery. *Curr. Opin. Biotechnol.* **2007**, *18*, 504–512.

(188) Guengerich, F. P. Mechanisms of cytochrome P450 substrate oxidation: MiniReview. *J. Biochem. Mol. Toxicol.* **2007**, *21*, 163–168.

(189) Lu, A. Y.; Coon, M. J. Role of hemoprotein P-450 in fatty acid omega-hydroxylation in a soluble enzyme system from liver microsomes. *J. Biol. Chem.* **1968**, *243*, 1331–1332.

(190) Gay, S. C.; Sun, L.; Maekawa, K.; Halpert, J. R.; Stout, C. D. Crystal structures of cytochrome P450 2B4 in complex with the inhibitor 1-biphenyl-4-methyl-1H-imidazole: ligand-induced structural response through alpha-helical repositioning. *Biochemistry* **2009**, *48*, 4762–4771.

(191) Scott, E. E.; White, M. A.; He, Y. A.; Johnson, E. F.; Stout, C. D.; Halpert, J. R. Structure of mammalian cytochrome P450 2B4 complexed with 4-(4-chlorophenyl)imidazole at 1.9-A resolution: Insight into the range of P450 conformations and the coordination of redox partner binding. *J. Biol. Chem.* **2004**, *279*, 27294–27301.

(192) Gay, S. C.; Zhang, H.; Wilderman, P. R.; Roberts, A. G.; Liu, T.; Li, S.; Lin, H.; Zhang, Q.; Woods, V. L.; Stout, C. D.; Hollenberg, P. F.; Halpert, J. R. Structural analysis of mammalian cytochrome P450 2B4 covalently bound to the mechanism-based inactivator tert-butylphenylacetylene: Insight into partial enzymatic activity. *Biochemistry* **2011**, *50*, 4903–4911.

(193) Gay, S. C.; Roberts, A. G.; Maekawa, K.; Talakad, J. C.; Hong, W.-X.; Zhang, Q.; Stout, C. D.; Halpert, J. R. Structures of cytochrome P450 2B4 complexed with the antiplatelet drugs ticlopidine and clopidogrel. *Biochemistry* **2010**, *49*, 8709–8720.

(194) Zhao, Y.; Sun, L.; Muralidhara, B. K.; Kumar, S.; White, M. a; Stout, C. D.; Halpert, J. R. Structural and thermodynamic consequences of 1-(4-chlorophenyl)imidazole binding to cytochrome P450 2B4. *Biochemistry* **2007**, *46*, 11559–11567.

(195) Wilderman, P. R.; Shah, M. B.; Liu, T.; Li, S.; Hsu, S.; Roberts, A. G.; Goodlett, D. R.; Zhang, Q.; Woods, V. L.; Stout, C. D.; Halpert, J. R. Plasticity of cytochrome P450 2B4 as investigated by hydrogen-deuterium exchange mass spectrometry and X-ray crystallography. *J. Biol. Chem.* **2010**, *285*, 38602–38611.

(196) Wilderman, P. R.; Gay, S. C.; Jang, H.-H.; Zhang, Q.; Stout, C. D.; Halpert, J. R. Investigation by site-directed mutagenesis of the role of cytochrome P450 2B4 non-active-site residues in protein-ligand interactions based on crystal structures of the ligand-bound enzyme. *FEBS J.* **2012**, *279*, 1607–1620.

(197) Zhao, Y.; White, M. A.; Muralidhara, B. K.; Sun, L.; Halpert, J. R.; Stout, C. D. Structure of microsomal cytochrome P450 2B4 complexed with the antifungal drug bifonazole: Insight into P450 conformational plasticity and membrane interaction. *J. Biol. Chem.* **2006**, *281*, 5973–5981.

(198) Scott, E. E.; He, Y. A.; Wester, M. R.; White, M. A.; Chin, C. C.; Halpert, J. R.; Johnson, E. F.; Stout, C. D. An open conformation of mammalian cytochrome P4502B4 at 1.6-angstrom resolution. *Proc. Natl. Acad. Sci. U.S.A.* **2003**, *100*, 13196–13201.

(199) Shah, M. B.; Wilderman, P. R.; Pascual, J.; Zhang, Q.; Stout, C. D.; Halpert, J. R. Conformational adaptation of human cytochrome P450 2B6 and rabbit cytochrome P450 2B4 revealed upon binding multiple amlodipine molecules. *Biochemistry* **2012**, *51*, 7225–7238.

(200) Gruenke, L. D.; Konopka, K.; Cadieu, M.; Waskell, L. The stoichiometry of the cytochrome P-450-catalyzed metabolism of methoxyflurane and benzphetamine in the presence and absence of cytochrome b_5. *J. Biol. Chem.* **1995**, *270*, 24707–24718.

(201) Waskell, L. A.; Vigne, J. L.; Vergeres, G. Site of action of substrates requiring cytochrome b_5 for oxidation by cytochrome P450. *Methods in Enzymology* **1991**, *206*, 523–9.

(202) Harris, D. L.; Park, J.-Y.; Gruenke, L.; Waskell, L. Theoretical study of the ligand-CYP2B4 complexes: effect of structure on binding free energies and heme spin state. *Proteins* **2004**, *55*, 895–914.

(203) Muralidhara, B. K.; Halpert, J. R. Thermodynamics of ligand binding to P450 2B4 and P450eryF studied by isothermal titration calorimetry. *Drug Metab. Rev.* **2007**, *39*, 539–556.

(204) Sheng, X.; Zhang, H.; Im, S.-C.; Horner, J. H.; Waskell, L.; Hollenberg, P. F.; Newcomb, M. Kinetics of Oxidation of Benzphetamine by Compounds I of Cytochrome P450 2B4 and Its Mutants. *J. Am. Chem. Soc.* **2009**, *131*, 2971–2976.

(205) Mak, P. J.; Im, S.-C.; Zhang, H.; Waskell, L. A.; Kincaid, J. R. Resonance Raman studies of cytochrome P450 2B4 in its interactions with substrates and redox partners. *Biochemistry* **2008**, *47*, 3950–3963.

(206) Perera, R.; Sono, M.; Kinloch, R.; Zhang, H.; Tarasev, M.; Im, S.-C.; Waskell, L.; Dawson, J. H. Stabilization and spectroscopic characterization of the dioxygen complex of wild-type cytochrome P4502B4 (CYP2B4) and its distal side E301Q, T302A and proximal side F429H mutants at subzero temperatures. *Biochim. Biophys. Acta* **2011**, *1814*, 69–75.

(207) Davydov, R.; Razeghifard, R.; Im, S.-C.; Waskell, L.; Hoffman, B. M. Characterization of the microsomal cytochrome P450 2B4 O2 activation intermediates by cryoreduction and electron paramagnetic resonance. *Biochemistry* **2008**, *47*, 9661–9666.

(208) Zhang, H.; Im, S.-C.; Waskell, L. Cytochrome b_5 increases the rate of product formation by cytochrome P450 2B4 and competes with cytochrome P450 reductase for a binding site on cytochrome P450 2B4. *J. Biol. Chem.* **2007**, *282*, 29766–29776.

(209) Zhang, H.; Hamdane, D.; Im, S.-C.; Waskell, L. Cytochrome b_5 inhibits electron transfer from NADPH-cytochrome P450 reductase to ferric cytochrome P450 2B4. *J. Biol. Chem.* **2008**, *283*, 5217–5225.

(210) Mulrooney, S. B.; Meinhardt, D. R.; Waskell, L. The alpha-helical membrane spanning domain of cytochrome b_5 interacts with cytochrome P450 via nonspecific interactions. *Biochim. Biophys. Acta* **2004**, *1674*, 319–326.

(211) Bridges, A.; Gruenke, L.; Chang, Y. T.; Vakser, I. A.; Loew, G.; Waskell, L. Identification of the binding site on cytochrome P450 2B4 for cytochrome b_5 and cytochrome P450 reductase. *J. Biol. Chem.* **1998**, *273*, 17036–17049.

(212) Zhang, H.; Myshkin, E.; Waskell, L. Role of cytochrome b_5 in catalysis by cytochrome P450 2B4. *Biochem. Biophys. Res. Commun.* **2005**, *338*, 499–506.

(213) Canova-Davis, E.; Chiang, J. Y. L.; Waskell, L. Obligatory role of cytochrome-b_5 in the microsomal metabolism of methoxyflurane. *Biochem. Pharmacol.* **1985**, *34*, 1907–1912.

(214) Guengerich, F. P. Human Cytochrome P450 Enzymes. In *Cytochrome P450: Structure, Mechanism, and Biochemistry*; Ortiz de Montellano, P. R., Ed.; Springer US: Boston, MA, 2005; pp. 377–530.

(215) Saribas, A. S.; Gruenke, L.; Waskell, L. Overexpression and purification of the membrane-bound cytochrome P450 2B4. *Protein Expr. Purif.* **2001**, *21*, 303–309.

(216) De Lemos-Chiarandini, C.; Frey, A. B.; Sabatini, D. D.; Kreibich, G. Determination of the membrane topology of the phenobarbital-inducible rat liver cytochrome P-450 isoenzyme PB-4 using site-specific antibodies. *J. Cell Biol.* **1987**, *104*, 209–219.

(217) Thomas, P. E.; Lu, A. Y.; West, S. B.; Ryan, D.; Miwa, G. T.; Levin, W. Accessibility of cytochrome P450 in microsomal membranes: inhibition of metabolism by antibodies to cytochrome P450. *Mol. Pharmacol.* **1977**, *13*, 819–831.

(218) Matsuura, S.; Fujii-Kuriyama, Y.; Tashiro, Y. Immunoelectron microscope localization of cytochrome P-450 on microsomes and other membrane structures of rat hepatocytes. *J. Cell Biol.* **1978**, *78*, 503–519.

(219) Matsuura, S.; Fujii-Kuriyama, Y.; Tashiro, Y. Quantitative immunoelectron-microscopic analyses of the distribution of cytochrome P-450 molecules on rat liver microsomes. *J. Cell Sci.* **1979**, *36*, 413–435.

(220) Nilsson, O. S.; DePierre, J. W.; Dallner, G. Investigation of the transverse topology of the microsomal membrane using combinations of proteases and the non-penetrating reagent diazobenzene sulfonate. *Biochim. Biophys. Acta* **1978**, *511*, 93–104.

(221) Von Wachenfeldt, C.; Johnson, E. F. Structures of Eukaryotic Cytochrome P450 Enzymes. In *Cytochrome P450: Structure, Mechanism, and Biochemistry*; Ortiz, P. R., Ed.; Plenum Press: New York, 1995; pp. 183–223.

(222) Ohta, Y.; Sakaki, T.; Yabusaki, Y.; Ohkawa, H.; Kawato, S. Rotation and membrane topology of genetically expressed methylcholanthrene-inducible cytochrome P-450IA1 lacking the N-terminal hydrophobic segment in yeast microsomes. *J. Biol. Chem.* **1994**, *269*, 15597–15600.

(223) Larson, J. R.; Coon, M. J.; Porter, T. D. Purification and properties of a shortened form of cytochrome P-450 2E1: deletion of the NH2-terminal membrane-insertion signal peptide does not alter the catalytic activities. *Proc. Natl. Acad. Sci. U.S.A.* **1991**, *88*, 9141–9145.

(224) Sagara, Y.; Barnes, H. J.; Waterman, M. R. Expression in Escherichia coli of functional cytochrome P450c17 lacking its hydrophobic amino-terminal signal anchor. *Arch. Biochem. Biophys.* **1993**, *304*, 272–278.

(225) Li, Y. C.; Chiang, J. Y. The expression of a catalytically active cholesterol 7 alpha-hydroxylase cytochrome P450 in Escherichia coli. *J. Biol. Chem.* **1991**, *266*, 19186–19191.

(226) Pernecky, S. J.; Larson, J. R.; Philpot, R. M.; Coon, M. J. Expression of truncated forms of liver microsomal P450 cytochromes 2B4 and 2E1 in Escherichia coli: influence of NH2-terminal region on localization in cytosol and membranes. *Proc. Natl. Acad. Sci. U.S.A* **1993**, *90*, 2651–2655.

(227) Kempf, A. C.; Zanger, U. M.; Meyer, U. A. Truncated human P450 2D6: expression in Escherichia coli, Ni(2+)-chelate affinity purification, and characterization of solubility and aggregation. *Arch. Biochem. Biophys.* **1995**, *321*, 277–288.

(228) Dong, M. S.; Bell, L. C.; Guo, Z.; Phillips, D. R.; Blair, I. A.; Guengerich, F. P. Identification of retained N-formylmethionine in bacterial recombinant mammalian cytochrome P450 proteins with the N-terminal sequence MALLLAVFL...: roles of residues 3-5 in retention and membrane topology. *Biochemistry* **1996**, *35*, 10031–10040.

(229) Shank-Retzlaff, M. L.; Raner, G. M.; Coon, M. J.; Sligar, S. G. Membrane topology of cytochrome P450 2B4 in Langmuir-Blodgett monolayers. *Arch. Biochem. Biophys.* **1998**, *359*, 82–88.

(230) Williams, P. A.; Cosme, J.; Sridhar, V.; Johnson, E. F.; McRee, D. E. Mammalian microsomal cytochrome P450 monooxygenase: structural adaptations for membrane binding and functional diversity. *Mol. Cell* **2000**, *5*, 121–131.

(231) Berka, K.; Hendrychová, T.; Anzenbacher, P.; Otyepka, M. Membrane position of ibuprofen agrees with suggested access path entrance to cytochrome P450 2C9 active site. *J. Phys. Chem. A* **2011**, *115*, 11248–11255.

(232) Wade, R. C.; Winn, P. J.; Schlichting, I.; Sudarko A survey of active site access channels in cytochromes P450. *J. Inorg. Biochem.* **2004**, *98*, 1175–1182.

(233) Etter, H. U.; Richter, C.; Ohta, Y.; Winterhalter, K. H.; Sasabe, H.; Kawato, S. Rotation and interaction with epoxide hydrase of cytochrome P-450 in proteoliposomes. *J. Biol. Chem.* **1991**, *266*, 18600–18605.

(234) Gut, J.; Richter, C.; Cherry, R. J.; Winterhalter, K. H.; Kawato, S. Rotation of cytochrome P-450. Complex formation of cytochrome P-450 with NADPH-cytochrome P-450 reductase in liposomes demonstrated by combining protein rotation with antibody-induced cross-linking. *J. Biol. Chem.* **1983**, *258*, 8588–8594.

(235) Kawato, S.; Gut, J.; Cherry, R. J.; Winterhalter, K. H.; Richter, C. Rotation of cytochrome P-450. I. Investigations of protein-protein interactions of cytochrome P-450 in phospholipid vesicles and liver microsomes. *J. Biol. Chem.* **1982**, *257*, 7023–7029.

(236) Bayburt, T. H.; Sligar, S. G. Single-molecule height measurements on microsomal cytochrome P450 in nanometer-scale phospholipid bilayer disks. *Proc. Natl. Acad. Sci. U.S.A.* **2002**, *99*, 6725–6730.

(237) Williams, P. A.; Cosme, J.; Sridhar, V.; Johnson, E. F.; McRee, D. E. Microsomal cytochrome P450 2C5: comparison to microbial P450s and unique features. *J. Inorg. Biochem.* **2000**, *81*, 183–190.

(238) Graham-Lorence, S.; Amarneh, B.; White, R. E.; Peterson, J. A.; Simpson, E. R. A three-dimensional model of aromatase cytochrome P450. *Protein Sci.* **1995**, *4*, 1065–1080.

(239) Jansson, I.; Schenkman, J. B. Evidence against participation of cytochrome b_5 in the hepatic microsomal mixed-function oxidase reaction. *Mol. Pharmacol.* **1973**, *9*, 840–845.

(240) Correia, M. A.; Mannering, G. J. Reduced diphosphopyridine nucleotide synergism of the reduced triphosphopyridine nucleotide-dependent mixed-function oxidase system of hepatic microsomes. II. Role of the type I drug-binding site of cytochrome P-450. *Mol. Pharmacol.* **1973**, *9*, 470–485.

(241) Sasame, H. A.; Mitchell, J. R.; Thorgeirsson, S.; Gillette, J. R. Relationship between NADH and NADPH oxidation during drug metabolism. *Drug Metab. Dispos.* **1973**, *1*, 150–155.

(242) Mannering, G. J.; Kuwahara, S.; Omura, T. Immunochemical evidence for the participation of cytochrome b_5 in the NADH synergism of the NADPH-dependent mono-oxidase system of hepatic microsomes. *Biochem. Biophys. Res. Commun.* **1974**, *57*, 476–481.

(243) Jansson, I.; Schenkman, J. B. Studies on three microsomal electron transfer enzyme systems. Specificity of electron flow pathways. *Arch. Biochem. Biophys.* **1977**, *178*, 89–107.

(244) Noshiro, M.; Harada, N.; Omura, T. Immunochemical study on the participation of cytochrome b_5 in drug oxidation reactions of mouse liver microsomes. *Biochem. Biophys. Res. Commun.* **1979**, *91*, 207–213.

(245) Finn, R. D.; McLaughlin, L. A.; Ronseaux, S.; Rosewell, I.; Houston, J. B.; Henderson, C. J.; Wolf, C. R. Defining the in vivo role for cytochrome b_5 in cytochrome P450 function through the conditional hepatic deletion of microsomal cytochrome b_5. *J. Biol. Chem.* **2008**, *283*, 31385–31393.

(246) McLaughlin, L. A.; Ronseaux, S.; Finn, R. D.; Henderson, C. J.; Roland Wolf, C. Deletion of microsomal cytochrome b_5 profoundly affects hepatic and extrahepatic drug metabolism. *Mol. Pharmacol.* **2010**, *78*, 269–278.

(247) Im, S.-C.; Waskell, L. The interaction of microsomal cytochrome P450 2B4 with its redox partners, cytochrome P450 reductase and cytochrome b_5. *Arch. Biochem. Biophys.* **2011**, *507*, 144–153.

(248) Schenkman, J. B.; Jansson, I. Interactions between cytochrome P450 and cytochrome b_5. *Drug Metabolism Reviews* **1999**, *31*, 351–364.

(249) Porter, T. D. The roles of cytochrome b_5 in cytochrome P450 reactions. *J. Biochem. Mol. Toxicol.* **2002**, *16*, 311–316.

(250) Yamazaki, H.; Shimada, T.; Martin, M. V; Guengerich, F. P. Stimulation of cytochrome P450 reactions by apo-cytochrome b_5: Evidence against transfer of heme from cytochrome P450 3A4 to apo-cytochrome b_5 or heme oxygenase. *J. Biol. Chem.* **2001**, *276*, 30885–30891.

(251) Murataliev, M. B.; Guzov, V. M.; Walker, F. A.; Feyereisen, R. P450 reductase and cytochrome b_5 interactions with cytochrome P450: effects on house fly CYP6A1 catalysis. *Insect Biochem. Mol. Biol.* **2008**, *38*, 1008–1015.

(252) Consortium, T. U. Reorganizing the protein space at the Universal Protein Resource (UniProt). *Nucleic Acids Res.* **2012**, *40*, D71–D75.

(253) Larkin, M. A.; Blackshields, G.; Brown, N. P.; Chenna, R.; McGettigan, P. A.; McWilliam, H.; Valentin, F.; Wallace, I. M.; Wilm, A.; Lopez, R.; Thompson, J. D.; Gibson, T. J.; Higgins, D. G. Clustal W and Clustal X version 2.0. *Bioinformatics (Oxford, England)* **2007**, *23*, 2947–2948.

(254) Goujon, M.; McWilliam, H.; Li, W.; Valentin, F.; Squizzato, S.; Paern, J.; Lopez, R. A new bioinformatics analysis tools framework at EMBL-EBI. *Nucleic Acids Res.* **2010**, *38*, W695–W699.

(255) Tamburini, P. P.; Schenkman, J. B. Mechanism of interaction between cytochromes P-450 RLM5 and b_5: evidence for an electrostatic mechanism involving cytochrome b_5 heme propionate groups. *Arch. Biochem. Biophys.* **1986**, *245*, 512–522.

(256) Tamburini, P. P.; MacFarquhar, S.; Schenkman, J. B. Evidence of binary complex formations between cytochrome P-450, cytochrome b_5, and NADPH-cytochrome P-450 reductase of hepatic microsomes. *Biochem. Biophys. Res. Commun.* **1986**, *134*, 519–526.

(257) Fisher, M. T.; White, R. E.; Sligar, S. G. Pressure dissociation of a protein-protein electron-transfer complex. *J. Am. Chem. Soc.* **1986**, *108*, 6835–6837.

(258) Stayton, P. S.; Poulos, T. L.; Sligar, S. G. Putidaredoxin competitively inhibits cytochrome b_5-cytochrome P-450cam association: a proposed molecular model for a cytochrome P-450cam electron-transfer complex. *Biochemistry* **1989**, *28*, 8201–8205.

(259) Omata, Y.; Sakamoto, H.; Robinson, R. C.; Pincus, M. R.; Friedman, F. K. Interaction between cytochrome P450 2B1 and cytochrome b_5: inhibition by synthetic peptides indicates a role for P450 residues Lys-122 and Arg-125. *Biochem. Biophys. Res. Commun.* **1994**, *201*, 1090–1095.

(260) Hlavica, P.; Kellermann, J.; Golly, I.; Lehnerer, M. Chemical modification of Tyr34 and Tyr129 in rabbit liver microsomal cytochrome b_5 affects interaction with cytochrome P-450 2B4. *Eur. J. Biochem.* **1994**, *224*, 1039–1046.

(261) Lewis, D. F.; Lake, B. G.; Dickins, M.; Eddershaw, P. J.; Tarbit, M. H.; Goldfarb, P. S. Molecular modelling of CYP2B6, the human CYP2B isoform, by homology with the substrate-bound CYP102 crystal structure: evaluation of CYP2B6 substrate characteristics, the cytochrome b_5 binding site and comparisons with CYP2B1 and CYP2B4. *Xenobiotica* **1999**, *29*, 361–393.

(262) Gao, Q.; Doneanu, C. E.; Shaffer, S. A.; Adman, E. T.; Goodlett, D. R.; Nelson, S. D. Identification of the interactions between cytochrome P450 2E1 and cytochrome b_5 by mass spectrometry and site-directed mutagenesis. *J. Biol. Chem.* **2006**, *281*, 20404–20417.

(263) Naffin-Olivos, J. L.; Auchus, R. J. Human cytochrome b_5 requires residues E48 and E49 to stimulate the 17,20-lyase activity of cytochrome P450c17. *Biochemistry* **2006**, *45*, 755–762.

(264) Peng, H.-M.; Auchus, R. J. The action of cytochrome b_5 on CYP2E1 and CYP2C19 activities requires anionic residues D58 and D65. *Biochemistry* **2012**.

(265) Zhao, C.; Gao, Q.; Roberts, A. G.; Shaffer, S. A.; Doneanu, C. E.; Xue, S.; Goodlett, D. R.; Nelson, S. D.; Atkins, W. M. Cross-linking mass spectrometry and mutagenesis confirm the functional importance of surface interactions between CYP3A4 and holo/apo cytochrome b_5. *Biochemistry* **2012**, *51*, 9488–9500.

(266) Hlavica, P.; Schulze, J.; Lewis, D. F. V Functional interaction of cytochrome P450 with its redox partners: a critical assessment and update of the topology of predicted contact regions. *J. Inorg. Biochem.* **2003**, *96*, 279–297.

(267) Hlavica, P.; Lehnerer, M.; Eulitz, M. Histidine residues in rabbit liver microsomal cytochrome P-450 2B4 control electron transfer from NADPH-cytochrome P-450 reductase and cytochrome b_5. *Biochem. J.* **1996**, *318*, 857–862.

(268) Chang, Y. T.; Stiffelman, O. B.; Vakser, I. A.; Loew, G. H.; Bridges, A.; Waskell, L. Construction of a 3D model of cytochrome P450 2B4. *Protein Eng.* **1997**, *10*, 119–129.

(269) Lewis, D. F.; Lake, B. G. Molecular modelling of mammalian CYP2B isoforms and their interaction with substrates, inhibitors and redox partners. *Xenobiotica* **1997**, *27*, 443–478.

(270) Geller, D. H.; Auchus, R. J.; Miller, W. L. P450c17 mutations R347H and R358Q selectively disrupt 17,20-lyase activity by disrupting interactions with P450 oxidoreductase and cytochrome b_5. *Mol. Endocrinol.* **1999**, *13*, 167–175.

(271) Rui, L.; Pochapsky, S. S.; Pochapsky, T. C. Comparison of the complexes formed by cytochrome P450cam with cytochrome b_5 and putidaredoxin, two effectors of camphor hydroxylase activity. *Biochemistry* **2006**, *45*, 3887–3897.

(272) Kaspera, R.; Naraharisetti, S. B.; Evangelista, E. A.; Marciante, K. D.; Psaty, B. M.; Totah, R. a Drug metabolism by CYP2C8.3 is determined by substrate dependent interactions with cytochrome P450 reductase and cytochrome b_5. *Biochem. Pharmacol.* **2011**, *82*, 681–691.

(273) Crowley, P. B.; Ubbink, M. Close encounters of the transient kind: protein interactions in the photosynthetic redox chain investigated by NMR spectroscopy. *Acc. Chem. Res.* **2003**, *36*, 723–730.

(274) Bashir, Q.; Scanu, S.; Ubbink, M. Dynamics in electron transfer protein complexes. *FEBS J.* **2011**, *278*, 1391–1400.

(275) Page, C. C.; Moser, C. C.; Dutton, P. L. Mechanism for electron transfer within and between proteins. *Curr. Opin. Chem. Biol.* **2003**, *7*, 551–556.

(276) Berg, O. G.; Von Hippel, P. H. Diffusion-controlled macromolecular interactions. *Ann. Rev. Biophys. Biophys. Chem.* **1985**, *14*, 131–160.

(277) Northrup, S. H.; Luton, J. a; Boles, J. O.; Reynolds, J. C. Brownian dynamics simulation of protein association. *J. Comput.-Aided Mol. Des.* **1988**, *1*, 291–311.

(278) Ubbink, M. The courtship of proteins: understanding the encounter complex. *FEBS Lett.* **2009**, *583*, 1060–1066.

(279) Bendall, D. S. Interprotein electron transfer. In *Protein Electron Transfer*; Bendall, D. S., Ed.; BIOS Scientific Publishers Ltd: Oxford, 1996; pp. 43–64.

(280) Hoefling, M.; Gottschalk, K. E. Barnase-Barstar: From first encounter to final complex. *J. Struct. Biol.* **2010**, *171*, 52–63.

(281) Janin, J. The kinetics of protein-protein recognition. *Proteins* **1997**, *28*, 153–161.

(282) Rosokha, S. V; Kochi, J. K. Fresh look at electron-transfer mechanisms via the donor/acceptor bindings in the critical encounter complex. *Acc. Chem. Res.* **2008**, *41*, 641–653.

(283) Volkov, A. N.; Ubbink, M.; Van Nuland, N. a J. Mapping the encounter state of a transient protein complex by PRE NMR spectroscopy. *J. Biomol. NMR* **2010**, *48*, 225–236.

(284) Prudêncio, M.; Ubbink, M. Transient complexes of redox proteins: structural and dynamic details from NMR studies. *J. Mol. Recogn.* **2004**, *17*, 524–539.

(285) Root, D. D.; Stewart, S.; Xu, J. Dynamic docking of myosin and actin observed with resonance energy transfer. *Biochemistry* **2002**, *41*, 1786–1794.

(286) Yue, H.; Waldeck, D. H.; Petrović, J.; Clark, R. A. The effect of ionic strength on the electron-transfer rate of surface immobilized cytochrome c. *J. Phys. Chem. B* **2006**, *110*, 5062–5072.

(287) Lim, A. R.; Sishta, B. P.; Mauk, A. G. Contribution of the heme propionate groups to the electron transfer and electrostatic properties of myoglobin. *J. Inorg. Biochem.* **2006**, *100*, 2017–2023.

(288) Zhang, X.-F.; Xie, L.; Liu, Y.; Xiang, J.-F.; Li, L.; Tang, Y.-L. Molecular interaction and energy transfer between human serum albumin and bioactive component Aloe dihydrocoumarin. *J. Mol. Struct.* **2008**, *888*, 145–151.

(289) Lasey, R. C.; Liu, L.; Zang, L.; Ogawa, M. Y. Peptide-protein interactions: photoinduced electron-transfer within the preformed and encounter complexes of a designed metallopeptide and cytochrome c. *Biochemistry* **2003**, *42*, 3904–3910.

(290) Wheeler, K. E.; Nocek, J. M.; Cull, D. A.; Yatsunyk, L. A.; Rosenzweig, A. C.; Hoffman, B. M. Dynamic docking of cytochrome b_5 with myoglobin and alpha-hemoglobin: heme-neutralization "squares" and the binding of electron-transfer-reactive configurations. *J. Am. Chem. Soc.* **2007**, *129*, 3906–3917.

(291) Mclendon, G. Control of biological electron transport via molecular recognition and binding: The "velcro" model. In *Structure & Bonding, Volume 75: Long-Range Electron Transfer in Biology*; Clarke, M. J.; Goodenough, J. B.; Ibers, J. A.; Jorgensen, C. K.; Mingos, D. M. P.; Neilands, J. B.; Palmer, G. A.; Reinen, D.; Sadler, P. J.; Weiss, R.; Williams, R. J. P., Eds.; Springer-Verlag: Berlin, 1991; pp. 159–174.

(292) Ubbink, M.; Ejdebäck, M.; Karlsson, B. G.; Bendall, D. S. The structure of the complex of plastocyanin and cytochrome f, determined by paramagnetic NMR and restrained rigid-body molecular dynamics. *Structure (London, England : 1993)* **1998**, *6*, 323–335.

(293) Miyashita, O.; Okamura, M. Y.; Onuchic, J. N. Interprotein electron transfer from cytochrome c2 to photosynthetic reaction center: tunneling across an aqueous interface. *Proc. Natl. Acad. Sci. U.S.A.* **2005**, *102*, 3558–3563.

(294) Crowley, P. B.; Carrondo, M. A. The architecture of the binding site in redox protein complexes: implications for fast dissociation. *Proteins Struct. Funct. Bioinf.* **2004**, *55*, 603–612.

(295) Dill, K. A. Dominant forces in protein folding. *Biochemistry* **1990**, *29*, 7133–7155.

(296) Schlarb-Ridley, B. G.; Bendall, D. S.; Howe, C. J. Relation between interface properties and kinetics of electron transfer in the interaction of cytochrome f and plastocyanin from plants and the cyanobacterium Phormidium laminosum. *Biochemistry* **2003**, *42*, 4057–4063.

(297) Camacho, C. J.; Kimura, S. R.; DeLisi, C.; Vajda, S. Kinetics of desolvation-mediated protein-protein binding. *Biophys. J.* **2000**, *78*, 1094–1105.

(298) Suh, J.-Y.; Tang, C.; Clore, G. M. Role of electrostatic interactions in transient encounter complexes in protein-protein association investigated by paramagnetic relaxation enhancement. *J. Am. Chem. Soc.* **2007**, *129*, 12954–12955.

(299) Qin, L.; Kostić, N. M. Importance of protein rearrangement in the electron-transfer reaction between the physiological partners cytochrome f and plastocyanin. *Biochemistry* **1993**, *32*, 6073–6080.

(300) Tang, C.; Iwahara, J.; Clore, G. M. Visualization of transient encounter complexes in protein-protein association. *Nature* **2006**, *444*, 383–386.

(301) Iwahara, J.; Clore, G. M. Detecting transient intermediates in macromolecular binding by paramagnetic NMR. *Nature* **2006**, *440*, 1227–1230.

(302) Fawzi, N. L.; Doucleff, M.; Suh, J.-Y.; Clore, G. M. Mechanistic details of a protein-protein association pathway revealed by paramagnetic relaxation enhancement titration measurements. *Proc. Natl. Acad. Sci. U.S.A.* **2010**, *107*, 1379–1384.

(303) Clore, G. M.; Tang, C.; Iwahara, J. Elucidating transient macromolecular interactions using paramagnetic relaxation enhancement. *Curr. Opin. Struct. Biol.* **2007**, *17*, 603–616.

(304) Yu, D.; Volkov, A. N.; Tang, C. Characterizing dynamic protein-protein interactions using differentially scaled paramagnetic relaxation enhancement. *J. Am. Chem. Soc.* **2009**, *131*, 17291–17297.

(305) Volkov, A. N.; Worrall, J. A.; Holtzmann, E.; Ubbink, M. Solution structure and dynamics of the complex between cytochrome c and cytochrome c peroxidase determined by paramagnetic NMR. *Proc. Natl. Acad. Sci. U.S.A* **2006**, *103*, 18945–18950.

(306) Bashir, Q.; Volkov, A. N.; Ullmann, G. M.; Ubbink, M. Visualization of the encounter ensemble of the transient electron transfer complex of cytochrome c and cytochrome c peroxidase. *J. Am. Chem. Soc.* **2010**, *132*, 241–247.

(307) Xu, X.; Keizers, P. H. J.; Reinle, W.; Hannemann, F.; Bernhardt, R.; Ubbink, M. Intermolecular dynamics studied by paramagnetic tagging. *J. Biomol. NMR* **2009**, *43*, 247–254.

(308) Xu, X.; Reinle, W.; Hannemann, F.; Konarev, P. V; Svergun, D. I.; Bernhardt, R.; Ubbink, M. Dynamics in a pure encounter complex of two proteins studied by solution scattering and paramagnetic NMR spectroscopy. *J. Am. Chem. Soc.* **2008**, *130*, 6395–6403.

(309) Montserret, R.; Saint, N.; Vanbelle, C.; Salvay, A. G.; Simorre, J.-P.; Ebel, C.; Sapay, N.; Renisio, J.-G.; Böckmann, A.; Steinmann, E.; Pietschmann, T.; Dubuisson, J.; Chipot, C.; Penin, F. NMR structure and ion channel activity of the p7 protein from hepatitis C virus. *J. Biol. Chem.* **2010**, *285*, 31446–31461.

(310) Sanders, C. R.; Hoffmann, A. K.; Grayn, D. N.; Keyes, M. H.; Ellis, C. D. French swimwear for membrane proteins. *ChemBioChem* **2004**, *5*, 423–426.

(311) Beswick, V.; Guerois, R.; Cordier-Ochsenbein, F.; Coïc, Y. M.; Tam, H.-D.; Tostain, J.; Noël, J.-P.; Sanson, A.; Neumann, J.-M. Dodecylphosphocholine micelles as a membrane-like environment: new results from NMR relaxation and paramagnetic relaxation enhancement analysis. *Eur. Biophys. J.* **1999**, *28*, 48–58.

(312) Vinogradova, O.; Sonnichsen, F.; Sanders, C. R. On choosing a detergent for solution NMR studies of membrane proteins. *J. Biomol. NMR* **1998**, *11*, 381–386.

(313) Howell, S. C.; Mesleh, M. F.; Opella, S. J. NMR structure determination of a membrane protein with two transmembrane helices in micelles: MerF of the bacterial mercury detoxification system. *Biochemistry* **2005**, *44*, 5196–5206.

(314) Kang, C.; Li, Q. Solution NMR study of integral membrane proteins. *Curr. Opin. Chem. Biol.* **2011**, *15*, 560–569.

(315) Xu, Y.; Yushmanov, V. E.; Tang, P. NMR studies of drug interaction with membranes and membrane-associated proteins. *Biosci. Rep.* **2002**, *22*, 175–196.

(316) Warschawski, D. E.; Arnold, A. a; Beaugrand, M.; Gravel, A.; Chartrand, E.; Marcotte, I. Choosing membrane mimetics for NMR structural studies of transmembrane proteins. *Biochim. Biophys. Acta* **2011**, *1808*, 1957–1974.

(317) Marassi, F. M.; Opella, S. J. NMR structural studies of membrane proteins. *Curr. Opin. Struct. Biol.* **1998**, *8*, 640–648.

(318) Cross, T. A.; Sharma, M.; Yi, M.; Zhou, H.-X. Influence of solubilizing environments on membrane protein structures. *Trends in Biochem. Sci.* **2011**, *36*, 117–125.

(319) Bordag, N.; Keller, S. Alpha-helical transmembrane peptides: a “divide and conquer” approach to membrane proteins. *Chem. Phys. Lipids* **2010**, *163*, 1–26.

(320) Hong, M.; Zhang, Y.; Hu, F. Membrane protein structure and dynamics from NMR spectroscopy. *Ann. Rev. Phys. Chem.* **2012**, *63*, 1–24.

(321) Kakalis, L. T.; Kumosinski, T. F.; Farrell, H. M. A multinuclear, high-resolution NMR study of bovine casein micelles and submicelles. *Biophys. Chem.* **1990**, *38*, 87–98.

(322) Okada, A.; Wakamatsu, K.; Miyazawa, T.; Higashijima, T. Vesicle-bound conformation of melittin: transferred nuclear Overhauser enhancement analysis in the presence of perdeuterated phosphatidylcholine vesicles. *Biochemistry* **1994**, *33*, 9438–9446.

(323) Choi, J.-S.; Braymer, J. J.; Nanga, R. P. R.; Ramamoorthy, A.; Lim, M. H. Design of small molecules that target metal-A{beta} species and regulate metal-induced A{beta} aggregation and neurotoxicity. *Proc. Natl. Acad. Sci. U.S.A.* **2010**, *107*, 21990–21995.

(324) Nanga, R. P. R.; Brender, J. R.; Xu, J.; Veglia, G.; Ramamoorthy, A. Structures of rat and human islet amyloid polypeptide IAPP(1-19) in micelles by NMR spectroscopy. *Biochemistry* **2008**, *47*, 12689–12697.

(325) Chou, J. J.; Kaufman, J. D.; Stahl, S. J.; Wingfield, P. T.; Bax, A. Micelle-induced curvature in a water-insoluble HIV-1 Env peptide revealed by NMR dipolar coupling measurement in stretched polyacrylamide gel. *J. Am. Chem. Soc.* **2002**, *124*, 2450–2451.

(326) Matthews, E. E.; Zoonens, M.; Engelman, D. M. Dynamic helix interactions in transmembrane signaling. *Cell* **2006**, *127*, 447–450.

(327) Matsuzaki, K.; Sugishita, K.; Ishibe, N.; Ueha, M.; Nakata, S.; Miyajima, K.; Epand, R. M. Relationship of membrane curvature to the formation of pores by magainin 2. *Biochemistry* **1998**, *37*, 11856–11863.

(328) Kessi, J.; Poirée, J. C.; Wehrli, E.; Bachofen, R.; Semenza, G.; Hauser, H. Short-chain phosphatidylcholines as superior detergents in solubilizing membrane proteins and preserving biological activity. *Biochemistry* **1994**, *33*, 10825–10836.

(329) Poget, S. F.; Girvin, M. E. Solution NMR of membrane proteins in bilayer mimics: small is beautiful, but sometimes bigger is better. *Biochim. Biophys. Acta* **2007**, *1768*, 3098–3106.

(330) Müller, K. Structural dimorphism of bile salt/lecithin mixed micelles. A possible regulatory mechanism for cholesterol solubility in bile? X-ray structure analysis. *Biochemistry* **1981**, *20*, 404–414.

(331) Gabriel, N. E.; Roberts, M. F. Spontaneous formation of stable unilamellar vesicles. *Biochemistry* **1984**, *23*, 4011–4015.

(332) Sanders, C. R.; Hare, B. J.; Howard, K. P.; Prestegard, J. H. Magnetically-oriented phospholipid micelles as a tool for the study of membrane-associated molecules. *Prog. Nucl. Magn. Reson. Spectr.* **1994**, *26*, 421–444.

(333) Glover, K. J.; Whiles, J. A.; Wu, G.; Yu, N.; Deems, R.; Struppe, J. O.; Stark, R. E.; Komives, E. A.; Vold, R. R. Structural evaluation of phospholipid bicelles for solution-state studies of membrane-associated biomolecules. *Biophys. J.* **2001**, *81*, 2163–2171.

(334) Van Dam, L.; Karlsson, G.; Edwards, K. Direct observation and characterization of DMPC/DHPC aggregates under conditions relevant for biological solution NMR. *Biochim. Biophys. Acta* **2004**, *1664*, 241–256.

(335) Wu, H.; Su, K.; Guan, X.; Sublette, M. E.; Stark, R. E. Assessing the size, stability, and utility of isotropically tumbling bicelle systems for structural biology. *Biochim. Biophys. Acta* **2010**, *1798*, 482–488.

(336) Luchette, P. a; Vetman, T. N.; Prosser, R. S.; Hancock, R. E.; Nieh, M. P.; Glinka, C. J.; Krueger, S.; Katsaras, J. Morphology of fast-tumbling bicelles: a small angle neutron scattering and NMR study. *Biochim. Biophys. Acta* **2001**, *1513*, 83–94.

(337) Triba, M. N.; Warschawski, D. E.; Devaux, P. F. Reinvestigation by phosphorus NMR of lipid distribution in bicelles. *Biophys. J.* **2005**, *88*, 1887–901.

(338) Vold, R. R.; Prosser, R. S. Magnetically oriented phospholipid bilayered micelles for structural studies of polypeptides. Does the ideal bicelle exist? *J. Magn. Reson. Series B* **1996**, *113*, 267–271.

(339) Sanders 2nd, C. R.; Prestegard, J. H. Magnetically orientable phospholipid bilayers containing small amounts of a bile salt analogue, CHAPSO. *Biophys. J.* **1990**, *58*, 447–460.

(340) Sanders, II, C. R.; Schwonek, J. P. Characterization of magnetically orientable bilayers in mixtures of dihexanoylphosphatidylcholine and dimyristoylphosphatidylcholine by solid-state NMR. *Biochemistry* **1992**, *31*, 8898–905.

(341) Sanders, C. R.; Schaff, J. E.; Prestegard, J. H. Orientational behavior of phosphatidylcholine bilayers in the presence of aromatic amphiphiles and a magnetic field. *Biophys. J.* **1993**, *64*, 1069–1080.

(342) Loudet, C.; Khemtémourian, L.; Aussenac, F.; Gineste, S.; Achard, M.-F.; Dufourc, E. J. Bicelle membranes and their use for hydrophobic peptide studies by circular dichroism and solid state NMR. *Biochim. Biophys. Acta* **2005**, *1724*, 315–323.

(343) Gayen, A.; Goswami, S. K.; Mukhopadhyay, C. NMR evidence of GM1-induced conformational change of Substance P using isotropic bicelles. *Biochim. Biophys. Acta - Biomembranes* **2011**, *1808*, 127–139.

(344) Bertelsen, K.; Vad, B.; Nielsen, E. H.; Hansen, S. K.; Skrydstrup, T.; Otzen, D. E.; Vosegaard, T.; Nielsen, N. C. Long-term-stable ether-lipid vs conventional ester-lipid bicelles in oriented solid-state NMR: altered structural information in studies of antimicrobial peptides. *J. Phys. Chem. B* **2011**, *115*, 1767–1774.

(345) Hu, W.; Webb, L. J. Direct measurement of the membrane dipole field in bicelles using vibrational stark effect spectroscopy. *J. Phys. Chem. Lett.* **2011**, *2*, 1925–1930.

(346) Faham, S.; Bowie, J. U. Bicelle crystallization: a new method for crystallizing membrane proteins yields a monomeric bacteriorhodopsin structure. *J. Mol. Biol.* **2002**, *316*, 1–6.

(347) Faham, S.; Boulting, G. L.; Massey, E. A.; Yohannan, S.; Yang, D.; Bowie, J. U. Crystallization of bacteriorhodopsin from bicelle formulations at room temperature. *Protein Sci.* **2005**, *14*, 836–840.

(348) Faham, S.; Ujwal, R.; Abramson, J.; Bowie, J. U. CHAPTER 5 Practical Aspects of Membrane Proteins Crystallization in Bicelles. *Curr. Top. Membr.* **2009**, *63*, 109–125.

(349) Sanders, C. R.; Prosser, R. S. Bicelles: a model membrane system for all seasons? *Structure* **1998**, *6*, 1227–1234.

(350) Vold, R. R.; Prosser, R. S.; Deese, A. J. Isotropic solutions of phospholipid bicelles: a new membrane mimetic for high-resolution NMR studies of polypeptides. *J. Biomol. NMR* **1997**, *9*, 329–335.

(351) Whiles, J. A.; Deems, R.; Vold, R. R.; Dennis, E. A. Bicelles in structure–function studies of membrane-associated proteins. *Bioorg. Chem.* **2002**, *30*, 431–442.

(352) Marcotte, I.; Auger, M. Bicelles as model membranes for solid- and solution-state NMR studies of membrane peptides and proteins. *Concepts Magn. Reson. Part A* **2005**, *24A*, 17–37.

(353) Diller, A.; Loudet, C.; Aussenac, F.; Raffard, G.; Fournier, S.; Laguerre, M.; Grélard, A.; Opella, S. J.; Marassi, F. M.; Dufourc, E. J. Bicelles: A natural "molecular goniometer" for structural, dynamical and topological studies of molecules in membranes. *Biochimie* **2009**, *91*, 744–751.

(354) Dürr, U. H. N.; Gildenberg, M.; Ramamoorthy, A. The magic of bicelles lights up membrane protein structure. *Chem. Rev.* **2012**, *112*, 6054-6074.

(355) Prosser, R. S.; Evanics, F.; Kitevski, J. L.; Al-Abdul-Wahid, M. S. Current applications of bicelles in NMR studies of membrane-associated amphiphiles and proteins. *Biochemistry* **2006**, *45*, 8453–8465.

(356) Dürr, U. H. N.; Soong, R.; Ramamoorthy, A. When the detergent meets bilayer: Birth and coming of age of lipid bicelles. *Prog. NMR Spec.* **2012**.

(357) De Angelis, A. A.; Jones, D. H.; Grant, C. V; Park, S. H.; Mesleh, M. F.; Opella, S. J. NMR experiments on aligned samples of membrane proteins. In *Methods in Enzymology,* Elsevier Academic Press Inc: San Diego, 2005; Vol. 394, pp. 350–382.

(358) De Angelis, A. A.; Opella, S. J. Bicelle samples for solid-state NMR of membrane proteins. *Nat. Protoc.* **2007**, *2*, 2332–2338.

(359) De Angelis, A. A.; Nevzorov, A. A.; Park, S. H.; Howell, S. C.; Mrse, A. A.; Opella, S. J. High-resolution NMR spectroscopy of membrane proteins in aligned bicelles. *J. Am. Chem. Soc.* **2004**, *126*, 15340–15341.

(360) Park, S. H.; Prytulla, S.; De Angelis, A. A.; Brown, J. M.; Kiefer, H.; Opella, S. J. High-resolution NMR spectroscopy of a GPCR in aligned bicelles. *J. Am. Chem. Soc.* **2006**, *128*, 7402–7403.

(361) De Angelis, A. A.; Howell, S. C.; Nevzorov, A. A.; Opella, S. J. Structure determination of a membrane protein with two trans-membrane helices in aligned phospholipid bicelles by solid-state NMR spectroscopy. *J. Am. Chem. Soc.* **2006**, *128*, 12256–12267.

(362) Triba, M. N.; Zoonens, M.; Popot, J. L.; Devaux, P. F.; Warschawski, D. E. Reconstitution and alignment by a magnetic field of a beta-barrel membrane protein in bicelles. *Eur. Biophys. J. Biophys. Lett.* **2006**, *35*, 268–275.

(363) Czerski, L.; Sanders, C. R. Functionality of a membrane protein in bicelles. *Anal. Biochem.* **2000**, *284*, 327–333.

(364) Poget, S. F.; Cahill, S. M.; Girvin, M. E. Isotropic bicelles stabilize the functional form of a small multidrug-resistance pump for NMR structural studies. *J. Am. Chem. Soc.* **2007**, *129*, 2432–2433.

(365) Andersson, A.; Mäler, L. Size and shape of fast-tumbling bicelles as determined by translational diffusion. *Langmuir* **2006**, *22*, 2447–2449.

(366) Cho, H. S.; Dominick, J. L.; Spence, M. M. Lipid domains in bicelles containing unsaturated lipids and cholesterol. *J. Phys. Chem. B* **2010**, *114*, 9238–9245.

(367) Ghimire, H.; Inbaraj, J. J.; Lorigan, G. A. A comparative study of the effect of cholesterol on bicelle model membranes using X-band and Q-band EPR spectroscopy. *Chem. Phys. Lipids* **2009**, *160*, 98–104.

(368) Minto, R. E.; Adhikari, P. R.; Lorigan, G. a A 2H solid-state NMR spectroscopic investigation of biomimetic bicelles containing cholesterol and polyunsaturated phosphatidylcholine. *Chem. Phys. Lipids* **2004**, *132*, 55–64.

(369) Sasaki, H.; Fukuzawa, S.; Kikuchi, J.; Yokoyama, S.; Hirota, H.; Tachibana, K. Cholesterol doping induced enhanced stability of bicelles. *Langmuir* **2003**, *19*, 9841–9844.

(370) Triba, M. N.; Devaux, P. F.; Warschawski, D. E. Effects of lipid chain length and unsaturation on bicelles stability. A phosphorus NMR study. *Biophys. J.* **2006**, *91*, 1357–1367.

(371) Shapiro, R. A.; Brindley, A. J.; Martin, R. W. Thermal stabilization of DMPC/DHPC bicelles by addition of cholesterol sulfate. *J. Am. Chem. Soc.* **2010**, *132*, 11406–11407.

(372) Struppe, J.; Whiles, J. A.; Vold, R. R. Acidic phospholipid bicelles: a versatile model membrane system. *Biophy. J.* **2000**, *78*, 281–289.

(373) Baek, S.-B.; Lim, S.-C.; Lee, H.-J.; Lee, H.-C.; Kim, C. An NMR study on the conformation of substance P in acidic bicelles. *Bull. Korean Chem. Soc.* **2011**, *32*, 3702–3706.

(374) Bárány-Wallje, E.; Andersson, A.; Gräslund, A.; Mäler, L. Dynamics of transportan in bicelles is surface charge dependent. *J. Biomol. NMR* **2006**, *35*, 137–147.

(375) Ellena, J. F.; Burnitz, M. C.; Cafiso, D. S. Location of the myristoylated alanine-rich C-kinase substrate (MARCKS) effector domain in negatively charged phospholipid bicelles. *Biophys. J.* **2003**, *85*, 2442–2448.

(376) Yamaguchi, T.; Suzuki, T.; Yasuda, T.; Oishi, T.; Matsumori, N.; Murata, M. NMR-based conformational analysis of sphingomyelin in bicelles. *Bioorg. Med. Chem.* **2012**, *20*, 270–278.

(377) Sternin, E.; Nizza, D.; Gawrisch, K. Temperature dependence of DMPC/DHPC mixing in a bicellar solution and its structural implications. *Langmuir* **2001**, *17*, 2610–2616.

(378) Andersson, A.; Mäler, L. Magnetic resonance investigations of lipid motion in isotropic bicelles. *Langmuir* **2005**, *21*, 7702–7709.

(379) Son, W. S.; Park, S. H.; Nothnagel, H. J.; Lu, G. J.; Wang, Y.; Zhang, H.; Cook, G. a; Howell, S. C.; Opella, S. J. "q-Titration" of long-chain and short-chain lipids differentiates between structured and mobile residues of membrane proteins studied in bicelles by solution NMR spectroscopy. *J. Magn. Reson.* **2012**, *214*, 111–118.

(380) Dvinskikh, S.; Dürr, U.; Yamamoto, K.; Ramamoorthy, A. A high-resolution solid-state NMR approach for the structural studies of bicelles. *J. Am. Chem. Soc.* **2006**, *128*, 6326–6327.

(381) Lee, D.; Walter, K. F.; Bruckner, A. K.; Hilty, C.; Becker, S.; Griesinger, C. Bilayer in small bicelles revealed by lipid-protein interactions using NMR spectroscopy. *J. Am. Chem. Soc.* **2008**, *130*, 13822–13823.

(382) Depierre, J. W.; Dallner, G. Structural aspects of the membrane of the endoplasmic reticulum. *Biochim. Biophys. Acta* **1975**, *415*, 411–472.

(383) Glaumann, H.; Dallner, G. Lipid composition and turnover of rough and smooth microsomal membranes in rat liver. *J. Lipid Res.* **1968**, *9*, 720–729.

(384) Dallner, G.; Ernster, L. Subfractionation and composition of microsomal membranes: a review. *J. Histochem. Cytochem.* **1968**, *16*, 611–632.

(385) Manganiello, V.; Phillips, A. The relationship between ribosomes and the endoplasmic reticulum during protein synthesis. *J. Biol. Chem.* **1965**, *240*, 3951–3959.

(386) Morin, F.; Tay, S.; Simpkins, H. A comparative study of the molecular structures of the plasma membranes and the smooth and the rough endoplasmic-reticulum membranes from rat liver. *Biochem. J.* **1972**, *129*, 781–788.

(387) Davison, S. C.; Wills, E. D. Phospholipid synthesis in rat liver endoplasmic reticulum after the administration of phenobarbitone and 20-methylcholanthrene. *Biochem. J.* **1974**, *142*, 19–26.

(388) Lee, T. C.; Snyder, F. Phospholipid metabolism in rat liver endoplasmic reticulum. Structural analyses, turnover studies and enzymic activities. *Biochim. Biophys. Acta* **1973**, *291*, 71–82.

(389) Nilsson, O.; Dallner, G. Distribution of constitutive enzymes and phospholipids in microsomal membranes of rat liver. *FEBS Lett.* **1975**, *58*, 190–193.

(390) Wibo, M. Electron microscope examination of subcellular fractions: III. Quantitative analysis of the microsomal fraction isolated from rat liver. *J. Cell Biol.* **1971**, *51*, 52–71.

(391) Yamamoto, T. On the thickness of the unit membrane. *J. Cell Biol.* **1963**, *17*, 413–421.

(392) Sjöstrand, F. S. A comparison of plasma membrane, cytomembranes, and mitochondrial membrane elements with respect to ultrastructural features. *J. Ultrastruct. Res.* **1963**, *9*, 561–580.

(393) Praporski, S.; Ng, S. M.; Nguyen, A. D.; Corbin, C. J.; Mechler, A.; Zheng, J.; Conley, A. J.; Martin, L. L. Organization of cytochrome P450 enzymes involved in sex steroid synthesis: PROTEIN-PROTEIN INTERACTIONS IN LIPID MEMBRANES. *J. Biol. Chem.* **2009**, *284*, 33224–33232.

(394) Kucerka, N.; Liu, Y.; Chu, N.; Petrache, H. I.; Tristram-Nagle, S.; Nagle, J. F. Structure of fully hydrated fluid phase DMPC and DLPC lipid bilayers using X-ray scattering from oriented multilamellar arrays and from unilamellar vesicles. *Biophys. J.* **2005**, *88*, 2626–2637.

(395) Loudet-Courreges, C.; Nallet, F.; Dufourc, E. J.; Oda, R. Unprecedented observation of days-long remnant orientation of phospholipid bicelles: a small-angle X-ray scattering and theoretical study. *Langmuir* **2011**, *27*, 9122–9130.

(396) Lewis, B. A.; Engelman, D. M. Lipid bilayer thickness varies linearly with acyl chain length in fluid phosphatidylcholine vesicles. *J. Mol. Biol.* **1983**, *166*, 211–217.

(397) Lauterwein, J.; Bösch, C.; Brown, L. R.; Wüthrich, K.; Bosch, C.; Withrich, K. Physicochemical studies of the protein-lipid interactions in melittin-containing micelles. *Biochim. Biophys. Acta* **1979**, *556*, 244–264.

(398) Kallick, D. A.; Tessmer, M. R.; Watts, C. R.; Li, C. Y. The use of dodecylphosphocholine micelles in solution NMR. *J. Magn. Reson. B* **1995**, *109*, 60–65.

(399) Gao, X.; Wong, T. C. Studies of the binding and structure of adrenocorticotropin peptides in membrane mimics by NMR spectroscopy and pulsed-field gradient diffusion. *Biophys. J.* **1998**, *74*, 1871–1888.

(400) Wymore, T.; Gao, X. F.; Wong, T. C. Molecular dynamics simulation of the structure and dynamics of a dodecylphosphocholine micelle in aqueous solution. *J. Mol. Struct.* **1999**, *485-486*, 195–210.

(401) Yao, H.; Stuart, R. A.; Cai, S.; Sem, D. S. Structural characterization of the transmembrane domain from subunit e of yeast F1Fo-ATP synthase: a helical GXXXG motif located just under the micelle surface. *Biochemistry* **2008**, *47*, 1910–1917.

(402) Göbl, C.; Dulle, M.; Hohlweg, W.; Grossauer, J.; Falsone, S. F.; Glatter, O.; Zangger, K. Influence of phosphocholine alkyl chain length on peptide-micelle interactions and micellar size and shape. *J. Phys. Chem. B* **2010**, *114*, 4717–4724.

CHAPTER 2

Experimental methods for studying protein-protein complexes

2.1 Site-directed mutagenesis and double mutant cycle analysis

To determine residues involved in hot spots at protein-protein complex interfaces, it is common to perform alanine scans of residues on the surface of each protein partner.[1–3] Mutation to alanine eliminates all interactions that could be coming from the amino acid’s side chain, beyond the β-carbon atom. This mutation thereby allows for probing the importance of the side chain of the original residue. Mutation to alanine also minimizes the formation of new interactions between the mutated amino acid and nearby residues. Residues that increase the binding free energy of a complex by more than 2 kcal/mol are typically considered to be in the binding hot spots and constitute less than 5% of interface residues.[4,5]

In a double mutant cycle analysis, two residues, which are believed to be interacting with one another, are mutated separately and then simultaneously in order to give rise to a cycle (Figure 2.1).[3,6–10] The method was first introduced in 1984 by Carter *et al.*[11] By calculating the Gibbs free energy of the single mutants versus the double mutants, it is possible to establish whether two amino acids are interacting with one another. There are several conventions when looking at papers on double mutant cycle analysis; I will be presenting the equations applicable to the research presented in this thesis. For a system with protein-1 and protein-2 interacting, the basis of the experiments is as follows:

- Measure K_d between wild-type protein-1 and wild-type protein-2. Calculate ΔG_{00} and $\Delta\Delta G_{00}$.
- Mutate one residue on protein-1 and measure K_d to wild-type protein-2. Calculate ΔG_{10} and $\Delta\Delta G_{10}$.
- Mutate one residue on protein-2 and measure K_d to wild-type protein-1. Calculate ΔG_{01} and $\Delta\Delta G_{01}$.
- Measure K_d between the protein-1 mutant and protein-2 mutant. Calculate ΔG_{11} and $\Delta\Delta G_{11}$.

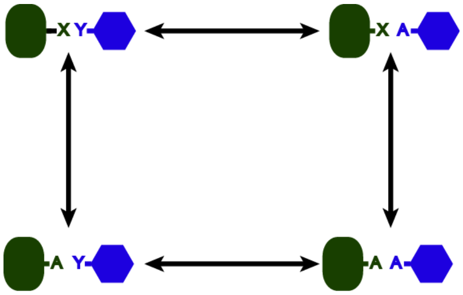

Figure 2.1 Diagram of a double mutant cycle. The blue hexagon and green oval represent the two proteins under study. X and Y are the original amino acids which interact with each other. Both X and Y are mutated to alanine separately and the additivity of the two single mutants is compared to the double mutant.

The equations needed to perform a double mutant analysis follow basic thermodynamics (note that the convention in the studies done by the Waskell lab uses Equation 2.1 in which there is no negative sign in front of RT). The following equations are utilized to obtain the $\Delta(\Delta)G$ values needed for comparisons:

$\Delta G = RT\ln(K_d)$ **Equation 2.1**

$\Delta\Delta G = \Delta G_{mutant} - \Delta G_{wild\text{-}type}$ **Equation 2.2**

$\Delta\Delta G_{int} = \Delta\Delta G_{01} + \Delta\Delta G_{10} - \Delta\Delta G_{11}$ *(Cohavi 2009)* **Equation 2.3**

where $\Delta\Delta G$ is the difference in free energy of binding between a complex containing a single mutant protein and a complex with two wild-type proteins (it is the free energy cost/advantage of the single mutation); $\Delta\Delta G_{int}$ is the $\Delta\Delta G$ of interaction between the two mutant proteins; $\Delta\Delta G_{01}$ is the $\Delta\Delta G$ of interaction between wild-type protein-1 and mutant protein-2; $\Delta\Delta G_{10}$ is the $\Delta\Delta G$ of interaction between mutant protein-1 and wild-type protein-2; $\Delta\Delta G_{11}$ is the $\Delta\Delta G$ of interaction between mutant protein-1 and mutant protein-2; T = 298 K; and R = 1.987 cal/K·mol.

According to the convention presented here, when $\Delta\Delta G > 0$ the mutation reduces specificity, whereas when $\Delta\Delta G < 0$ the mutation enhances specificity, and when $\Delta\Delta G = 0$ the mutation causes no effect.[12] A positive $\Delta\Delta G_{int}$ value indicates that the double mutant is more unstable than the sum of the single mutants and that the residues therefore interact cooperatively in the wild-type complex. A negative $\Delta\Delta G_{int}$ implies that the double mutant is more stable (and has favorable interactions) compared to the wild-type case; in this case, the double mutant actually enhances the binding between the two proteins. A value of zero for $\Delta\Delta G_{int}$ indicates that there is no coupling between the perturbations and that they behave independently (i.e. the effect of the single mutations is additive and equals that of the double mutant).[3,13] The magnitude of the positive $\Delta\Delta G_{int}$ value indicates the type and strength of non-covalent interactions between the two residues. The coupling energy decreases with increase in the inter-residue distance.[12] The $\Delta\Delta G_{int}$ values can be indicative of the following types of interactions:[14]

- $\Delta\Delta G_{int} \leq 0.5$ kcal/mol : Electrostatic interactions
- $\Delta\Delta G_{int} \approx 1$ kcal/mol : Aromatic-aromatic interactions
- $\Delta\Delta G_{int} \approx 1\text{-}5$ kcal/mol : Surface and buried salt-bridges

In order to determine what value of $\Delta\Delta G_{int}$ is significant, it is important to know what the experimental error (2σ) is.[12,15] In previous experiments, the experimental error has been estimated to be 0.35 kcal/mol,[11,12] 0.3 kcal/mol[13] or 0.41-0.53 kcal/mol[15]. The following thresholds of $\Delta\Delta G_{int}$ have been considered significant: 0.60 kcal/mol,[16] 0.3 kcal/mol,[15] and 0.2 kcal/mol.[17]

2.2 ^{1}H-^{15}N-TROSY-HSQC spectra for the study of large proteins

The simplest NMR experiment consists of running a one dimensional ^{1}H-NMR spectrum. Protons (^{1}Hs) are magnetically active and have a natural abundance of 100%. This type of experiment is typically well suited for small molecules for which databases have been built, e.g. the SDBS database.[18] The chemical shift (in ppm) of each resonance (the NMR term for "peak") is indicative of its chemical environment; i.e. the identity of its neighboring atoms. For a protein, which contains on the order of thousands of protons, the 1D ^{1}H-NMR spectrum is very crowded and the individual resonances cannot be resolved. For this reason, two- and three-dimensional NMR experiments are frequently used for proteins; a particularly common 2D experiment is the Heteronuclear Single Quantum Coherence (HSQC) experiment. These HSQC experiments typically correlate the following pairs of nuclei: ^{13}C and ^{1}H, or ^{15}N and ^{1}H. ^{1}H-^{15}N-HSQC spectra are typically used because the resonances are much more dispersed than in ^{1}H-^{13}C-HSQC spectra. Neither ^{13}C nor ^{15}N have high natural abundances (with 1.1% and 0.37%, respectively), but overexpressing proteins that are uniformly labeled with ^{13}C or ^{15}N nuclei, or both nuclei simultaneously, is possible through the use of labeled expression media; it is not always straightforward, though, especially for membrane proteins. In a ^{1}H-^{15}N-HSQC spectrum, one dimension contains the chemical shifts of the ^{1}H nuclei while the other dimension contains the chemical shifts of the ^{15}N nuclei. Each resonance in the spectrum comes from the correlation between two bonded ^{1}H and ^{15}N nuclei. Since a protein is composed of amino acids, the majority of the resonances come from backbone NH atoms, although side chains from tryptophans, asparagines and glutamine also appear. The backbone NH chemical shifts are a function of the identity of the side-chain, as well as a function of the secondary structure in which the particular amino acid is involved. With the use of a ^{1}H-^{15}N-HSQC spectrum, each amino acid can be monitored (via both its chemical shift: Section 2.3, or its intensity: Section 2.4) as a function of any titrant. The larger the protein, the more resonances will be present in the spectrum; therefore, the use of higher magnetic field NMR spectrometers (800-900 MHz) is common in order to increase both sensitivity and spectral dispersion.

Additional barriers arise when studying large protein molecules (> 25 kDa). As mentioned, higher magnetic fields do improve the resolution and dispersion of crowded NMR spectra of proteins.[19] However, with larger proteins, the observed nuclei are surrounded by a sea of proton nuclei (proton bath) which aids the observed nuclei's relaxation and leads to considerable signal broadening. It is therefore typically necessary to deuterate the proteins in order to increase the sensitivity.[20–22] Due to the slow tumbling (high correlation time) of large molecules, the T_2 (transverse) relaxation mechanisms of protein nuclei are also enhanced, which leads to less signal being detected by the NMR receiver. Therefore, in conjunction with deuteration and high magnetic fields, it is also usually necessary to employ a common technique called Transverse Relaxation Optimized Spectroscopy (TROSY),[21,23,24] first introduced by Pervushin *et al.*[25] TROSY aids in reducing the transverse relaxation rates for large molecules through the use of constructive interference between dipolar coupling and chemical shift anisotropy, such that satisfactory line-widths and sensitivity can be achieved. A helpful review article on TROSY was written by Fernández *et al.*[24] and the theory behind TROSY is very thoroughly (and clearly!) explained by Keeler in his book[26].

2.3 NMR chemical shift perturbation analysis

As mentioned in the previous section, $^{1}H,^{15}N$ HSQC NMR spectra are often used to study ^{15}N-labeled proteins. In these spectra, each ^{15}NH groups of the protein gives rise to one resonance/peak; the position and intensity of each ^{15}NH resonance is dependent on its dynamics and chemical environment (see previous section). With this information, it is possible to monitor the chemical environment of each backbone ^{15}NH of a ^{15}N-labeled protein upon addition of an unlabeled protein. Residues, which are at the interface with the unlabeled protein, should experience changes in their ^{15}NH chemical shift environment upon addition of the unlabeled protein and the resonance(s) chemical shifts/intensities of the interfacial residues will typically be modulated by the interacting protein. This method has been documented in many excellent review articles.[27–29] The technique in which chemical shift changes are monitored to identify interfacial residues is referred to as chemical shift perturbations, and has been used to characterize the binding interface of other cytochrome complexes, including cyt b_5-cyt c.[30,31] If the bound and unbound forms of the ^{15}N-labeled protein are in fast exchange, the resonance will be at the average chemical shift of the two forms. If the two proteins are in slow exchange, the two populations will show different resonances in the HSQC spectrum, and depending on the stoichiometries of the two proteins, there will be more/less of the unbound form and more/less of the bound form of the labeled protein (i.e. as more of the unlabeled protein is added, there will be more bound form); some kinetic line broadening can also occur. Intermediate exchange can lead to resonances being poorly defined and kinetic line broadening; if the resonances broaden enough, they can disappear from the spectrum, at which case the interaction interface becomes identified by the progressive disappearance of peaks.

Chemical shift perturbations can be calculated in the ^{1}H dimension and in the ^{15}N dimension. However, it is common to report the weighted average chemical shift perturbations of the backbone amide ^{15}NH resonances:[31]

$$\Delta\delta = \sqrt{\left((\omega_{HN}\Delta\ {}^{1}HN)^2 + \left(\omega_N\Delta^{15}N\right)^2\right)} \qquad \textbf{Equation 2.4}$$

where $\Delta\delta$ represents the average (NH) chemical shift perturbation and ω denotes the weight factor of the nucleus with ω_{HN} = 1 and ω_N = 0.154.[32]

In cases of allosteric regulation, large changes in chemical shifts will be observed, indicative of conformational changes upon addition of the unlabeled protein; chemical shift perturbations will not aid in mapping the interface in these cases.[33,34]

2.4 NMR differential line broadening analysis

Broadening of resonances in an NMR spectrum can come from various sources: intermediate or slow exchange between different conformations, or an increase in relaxation (either transverse or longitudinal relaxation). In rapidly exchanging bound/unbound systems, differences in intensity will arise from both faster relaxation in the bound state and differences in the chemical shift between the free and bound states.[35] When looking at a protein-protein complex, the chemical exchange would be between the free and bound (to its partner) states of the labeled protein. As mentioned in the previous section, when the chemical exchange is at a slow to intermediate regime, line broadening can occur.[36–38] Overall spectral broadening can occur due to T_2 relaxation enhancement because of an increase in the transverse relaxation rate due to a longer correlation time for the complex (from its larger size) compared to the free labeled protein. Even in cases where only the free labeled protein is visible in the spectrum (and the bound, complexed form is invisible), it has been shown that the binding interface on small proteins contacting larger proteins can be identified by looking at differential line broadening observed from the NMR signal in the free state.[39,40] This occurs when the rate of complex formation is fast and the protein comes off fast enough to affect the intensity of the free state.[41] The proximity of adjacent nuclei, in the complex, could also enhance the transverse relaxation rate (R_2) through dipolar coupling.[42,43] Residues that continue to have sharp resonances in the bound state still retain a lot of mobility even in the complex, meaning that there are no strong, direct interactions between those residues and the binding partner.[44,45] Isolating the specific contributions to line broadening is still challenging; however, differential line broadening can often be attributed to interfacial residues, despite knowing the origin of the broadening. Whether due to the chemical exchange or relaxation enhancement, residues that broaden can generally be found at the interface, or are somehow affected upon complex formation (which also provides valuable information).[38,44–48] Extensive discussions of differential line broadening contributions can be found in several excellent papers.[49,50]

2.5 High Ambiguity Driven biomolecular DOCKing (HADDOCK)

HADDOCK[51,52] is a data-driven docking method that has been proven to be highly effective in predicting protein-protein complex structures.[31,53–59] Various types of information on the protein-protein interface can be inputted as restraints, including data from mutagenesis, mass spectrometry, and various NMR parameters (chemical shift perturbation, paramagnetic relaxation enhancement, residual dipolar couplings, etc.).[60] The three stages of the HADDOCK docking process are briefly described below, with the number of structures defined for our docking experiments (in Chapter 4) at each stage:[51,61]

1. Randomization of orientations and rigid body energy minimization.
    i. The two proteins, positioned at a certain distance from each other in space, are randomly rotated around their respective center of masses.
    ii. Rigid body docking and energy minimization (translations and rotations are allowed).
    iii. 2000 complex conformations are calculated by the end of this stage.

2. The best 500 solutions are then submitted to semi-rigid simulated annealing in torsion angle space (the restraints are taken into account at this stage, which restricts how much the amino acids are allowed to move).
    i. Considered as rigid bodies, the respective orientations of the proteins are optimized at a high temperature.
    ii. The side chains at the interface are allowed to move.
    iii. Both side chains and backbone atoms at the interface are allowed to move (some conformational rearrangements).
    iv. The resulting structures are subjected to energy minimization.
3. The best 150 structures are selected for final refinement in Cartesian space with explicit solvent (using a 8 Å shell of TIP3P water molecules). The lowest 50 structures are subsequently submitted for analysis.

2.5.1 Ambiguous Interaction Restraints (AIRs)

To set AIRs, active and passive residues on each protein need to be defined. Active residues are residues that have been experimentally identified as being likely at the interface between the two proteins and that are solvent accessible (as defined by another program such as NACCESS[62]). Passive residues are solvent-accessible residues flanking the active residues (these are defined based on the known structure of the protein); an example of how to pick passive residues can be found on the HADDOCK website.[63] AIRs are defined as ambiguous intermolecular distance with a maximum value of 2 Å between any atoms of an active residue of protein A with any atoms of either active or passive residues of protein B.[51,64] Each active residue has a single AIR restraint that is defined between that residue and all active and passive residues on the other protein. Typically, if a residue comes within 3-4 Å of an active or passive residue of the partner protein, the AIR restraint is satisfied. The 3 Å limit is a compromise between hydrogen-hydrogen, and heavy atom-heavy atom minimum van der Waals distances.[51] Generating AIR restraints is fairly simply and consists of inputting a string of numbers listing all residue defined as active and passive residues on each protein partner (specifying the segment ID for each protein), and selecting an upper distance limit for AIRs (the default is set at 2 Å) at: HADDOCK main webpage[61] → Project setup → Generate AIR restraint file.

Previous publications have used double mutant cycle analysis as ambiguous restraints in HADDOCK by using experimentally identified residues as active residues on each protein, with the interacting residues restrained to a range of 3-7 Å for heavy atoms and a range of 2-5 Å for hydrogens, with a maximum effective distance of 2 Å.[65] It is also common to use AIRs based on chemical shift perturbation data.[53,56,58,65–67]

2.5.2. Unambiguous restraints

In HADDOCK, it is also possible to define strict atom-atom inter- and intra-molecular distances as unambiguous restraints during the docking simulation. These distances are defined based on experimental data and are given a range of distances. The format is:

assign <atom selection><target distance><lower error value><upper error value>[68]

An example would be:

assign (resid 66 and name NH and segid A) (resid 433 and name NH and segid B) 6.0 4.0 2.0 which would be translated to mean: Set the distance between the NH atoms of residue 66 in Protein A to be within 6 Å (with a range of 2.0-8.0 Å) from the NH atoms of residue 433 in Protein B. Additional CNS syntax that can be used to select specific atoms can be found at two websites.[68,69] Unambiguous restraints are much stricter restraints than AIRs as they define the distance between two specific residues or atoms. A previous publication used double mutant cycle analysis results as unambiguous restraints, with a range of 3-7 Å for all side-chain heavy atoms.[17]

2.6 References

(1) Lau, F. T.; Fersht, A. R. Conversion of allosteric inhibition to activation in phosphofructokinase by protein engineering. *Nature* **1987**, *326*, 811–812.

(2) Cunningham, B. C.; Wells, J. A. High-resolution epitope mapping of hGH-receptor interactions by alanine-scanning mutagenesis. *Science* **1989**, *244*, 1081–1085.

(3) Di Cera, E. Site-specific thermodynamics: understanding cooperativity in molecular recognition. *Chem. Rev.* **1998**, *98*, 1563–1592.

(4) Ofran, Y.; Rost, B. Protein-protein interaction hotspots carved into sequences. *PLoS Comput. Biol.* **2007**, *3*, e119.

(5) Bogan, A. A.; Thorn, K. S. Anatomy of hot spots in protein interfaces. *J. Mol. Biol.* **1998**, *280*, 1–9.

(6) Horovitz, A. Double-mutant cycles: a powerful tool for analyzing protein structure and function. *Fold. Des.* **1996**, *1*, R121–R126.

(7) Wells, J. A. Additivity of mutational effects in proteins. *Biochemistry* **1990**, *29*, 8509–8517.

(8) Mildvan, A. S.; Weber, D. J.; Kuliopulos, A. Quantitative interpretations of double mutations of enzymes. *Arch. Biochem. Biophys.* **1992**, *294*, 327–340.

(9) LiCata, V. J.; Ackers, G. K. Long-range, small magnitude nonadditivity of mutational effects in proteins. *Biochemistry* **1995**, *34*, 3133–3139.

(10) Di Cera, E. *Thermodynamic Theory of Site-Specific Binding Processes in Biological Macromolecules*; Cambridge University Press: Cambridge, United Kingdom, 1995.

(11) Carter, P. J.; Winter, G.; Wilkinson, A. J.; Fersht, A. R. The use of double mutants to detect structural changes in the active site of the tyrosyl-tRNA synthetase (Bacillus stearothermophilus). *Cell* **1984**, *38*, 835–840.

(12) Schreiber, G.; Fersht, A. R. Energetics of protein-protein interactions: analysis of the barnase-barstar interface by single mutations and double mutant cycles. *J. Mol. Biol.* **1995**, *248*, 478–486.

(13) Frisch, C.; Schreiber, G.; Johnson, C. M.; Fersht, A. R. Thermodynamics of the interaction of barnase and barstar: changes in free energy versus changes in enthalpy on mutation. *J. Mol. Biol.* **1997**, *267*, 696–706.

(14) Horovitz, A. Double-mutant cycles: a powerful tool for analyzing protein structure and function. *Fold. Des.* **1996**, *1*, R121–R126.

(15) Harel, M.; Cohen, M.; Schreiber, G. On the dynamic nature of the transition state for protein-protein association as determined by double-mutant cycle analysis and simulation. *J. Mol. Biol.* **2007**, *371*, 180–196.

(16) Roisman, L. C.; Piehler, J.; Trosset, J. Y.; Scheraga, H. A.; Schreiber, G. Structure of the interferon-receptor complex determined by distance constraints from double-mutant cycles and flexible docking. *Proc. Natl. Acad. Sci. U.S.A.* **2001**, *98*, 13231–13236.

(17) Cohavi, O.; Tobi, D.; Schreiber, G. Docking of antizyme to ornithine decarboxylase and antizyme inhibitor using experimental mutant and double-mutant cycle data. *J. Mol. Biol.* **2009**, *390*, 503–515.

(18) SDBSWeb : http://riodb01.ibase.aist.go.jp/sdbs/ (National Institute of Advanced Industrial Science and Technology).

(19) Griswold, I. J.; Dahlquist, F. W. Bigger is better: megadalton protein NMR in solution. *Nat. Struct. Biol.* **2002**, *9*, 567–568.

(20) Ulmer, T. S.; Campbell, I. D.; Boyd, J. Amide proton relaxation measurements employing a highly deuterated protein. *J. Magn. Reson.* **2004**, *166*, 190–201.

(21) Clore, G. M.; Gronenborn, A. M. NMR structure determination of proteins and protein complexes larger than 20 kDa. *Curr. Opin. Chem. Biol.* **1998**, *2*, 564–570.

(22) Ohki, S.; Kainosho, M. Stable isotope labeling methods for protein NMR spectroscopy. *Prog. Nucl. Magn. Reson. Spectrosc.* **2008**, *53*, 208–226.

(23) Riek, R.; Pervushin, K.; Wüthrich, K. TROSY and CRINEPT: NMR with large molecular and supramolecular structures in solution. *Trends Biochem. Sci.* **2000**, *25*, 462–468.

(24) Fernández, C.; Wider, G. TROSY in NMR studies of the structure and function of large biological macromolecules. *Curr. Opin. Struct. Biol.* **2003**, *13*, 570–580.

(25) Pervushin, K.; Riek, R.; Wider, G.; Wuthrich, K. Attenuated T_2 relaxation by mutual cancellation of dipole-dipole coupling and chemical shift anisotropy indicates an avenue to NMR structures of very large biological macromolecules in solution. *Proc. Natl. Acad. Sci. U.S.A.* **1997**, *94*, 12366–12371.

(26) Keeler, J. *Understanding NMR Spectroscopy*; 2nd ed.; John Wiley & Sons: Chichester, UK, 2010.

(27) Pellecchia, M.; Montgomery, D. L.; Stevens, S. Y.; Vander Kooi, C. W.; Feng, H. P.; Gierasch, L. M.; Zuiderweg, E. R. Structural insights into substrate binding by the molecular chaperone DnaK. *Nat. Struct. Biol.* **2000**, *7*, 298–303.

(28) Stevens, S. Y.; Sanker, S.; Kent, C.; Zuiderweg, E. R. Delineation of the allosteric mechanism of a cytidylyltransferase exhibiting negative cooperativity. *Nat. Struct. Biol.* **2001**, *8*, 947–952.

(29) Zuiderweg, E. R. P. Mapping protein-protein interactions in solution by NMR spectroscopy. *Biochemistry* **2002**, *41*, 1–7.

(30) Shao, W.; Im, S.-C.; Zuiderweg, E. R.; Waskell, L. Mapping the binding interface of the cytochrome b_5-cytochrome c complex by nuclear magnetic resonance. *Biochemistry* **2003**, *42*, 14774–14784.

(31) Deep, S.; Im, S.-C.; Zuiderweg, E. R.; Waskell, L. Characterization and calculation of a cytochrome c-cytochrome b_5 complex using NMR data. *Biochemistry* **2005**, *44*, 10654–10668.

(32) Evenas, J.; Tugarinov, V.; Skrynnikov, N. R.; Goto, N. K.; Muhandiram, R.; Kay, L. E. Ligand-induced structural changes to maltodextrin-binding protein as studied by solution NMR spectroscopy. *J. Mol. Biol.* **2001**, *309*, 961–974.

(33) Van Nuland, N. A.; Kroon, G. J.; Dijkstra, K.; Wolters, G. K.; Scheek, R. M.; Robillard, G. T. The NMR determination of the IIA(mtl) binding site on HPr of the Escherichia coli phosphoenol pyruvate-dependent phosphotransferase system. *FEBS Lett.* **1993**, *315*, 11–15.

(34) Chen, Y.; Reizer, J.; Saier Jr., M. H.; Fairbrother, W. J.; Wright, P. E. Mapping of the binding interfaces of the proteins of the bacterial phosphotransferase system, HPr and IIAglc. *Biochemistry* **1993**, *32*, 32–37.

(35) Fejzo, J.; Lepre, C. A.; Peng, J. W.; Su, M. S.; Thomson, J. A.; Moore, J. M. Dynamic NMR studies of ligand-receptor interactions: design and analysis of a rapidly exchanging complex of FKBP-12/FK506 with a 24 kDa calcineurin fragment. *Protein Sci.* **1996**, *5*, 1917–1921.

(36) Gronenborn, A.; Birdsall, B.; Hyde, E. I.; Roberts, G. C. K.; Feeney, J.; Burgen, A. S. V. Direct observation by NMR of two coexisting conformations of an enzyme–ligand complex in solution. *Nature* **1981**, *290*, 273–274.

(37) Gronenborn, A.; Birdsall, B.; Hyde, E.; Roberts, G.; Feeney, J.; Burgen, A. ^{1}H and ^{31}P NMR characterization of two conformations of the trimethoprim-NADP+-dihydrofolate reductase complex. *Mol. Pharmacol.* **1981**, *20*, 145–153.

(38) Günther, U.; Mittag, T.; Schaffhausen, B. Probing Src homology 2 domain ligand interactions by differential line broadening. *Biochemistry* **2002**, *41*, 11658–11669.

(39) Sette, M.; Van Tilborg, P.; Spurio, R.; Kaptein, R.; Paci, M.; Gualerzi, C. O.; Boelens, R. The structure of the translational initiation factor IF1 from E. coli contains an oligomer-binding motif. *EMBO J.* **1997**, *16*, 1436–1443.

(40) Matsuo, H.; Walters, K. J.; Teruya, K.; Tanaka, T.; Gassner, G. T.; Lippard, S. J.; Kyogoku, Y.; Wagner, G. Identification by NMR spectroscopy of residues at contact surfaces in large, slowly exchanging macromolecular complexes. *J. Am. Chem. Soc.* **1999**, *121*, 9903–9904.

(41) Ni, F.; Zhu, Y.; Scheraga, H. A. Thrombin-bound structures of designed analogs of human fibrinopeptide A determined by quantitative transferred NOE spectroscopy: a new structural basis for thrombin specificity. *J. Mol. Biol.* **1995**, *252*, 656–671.

(42) Balaram, P.; Bothner-By, A. A.; Dadok, J. Negative nuclear Overhuaser effects as probes of macromolecular structure. *J. Am. Chem. Soc.* **1972**, *94*, 4015–4017.

(43) Balaram, P.; Bothner-By, A. A.; Breslow, E. Localization of tyrosine at the binding site of neurophysin II by negative nuclear Overhouser effects. *J. Am. Chem. Soc.* **1972**, *94*, 4017–4018.

(44) Panchal, S. C.; Kaiser, D. a; Torres, E.; Pollard, T. D.; Rosen, M. K. A conserved amphipathic helix in WASP/Scar proteins is essential for activation of Arp2/3 complex. *Nat. Struct. Biol.* **2003**, *10*, 591–598.

(45) Schneider, M. L.; Post, C. B. Solution structure of a band 3 peptide inhibitor bound to aldolase: a proposed mechanism for regulating binding by tyrosine phosphorylation. *Biochemistry* **1995**, *34*, 16574–16584.

(46) Shi, J.; Wei, Z.; Song, J. Dissection study on the severe acute respiratory syndrome 3C-like protease reveals the critical role of the extra domain in dimerization of the enzyme: defining the extra domain as a new target for design of highly specific protease inhibitors. *J. Biol. Chem.* **2004**, *279*, 24765–24773.

(47) Tolkatchev, D.; Ng, A.; Zhu, B.; Ni, F. Identification of a thrombin-binding region in the sixth epidermal growth factor-like repeat of human thrombomodulin. *Biochemistry* **2000**, *39*, 10365–10372.

(48) Walters, K. J.; Gassner, G. T.; Lippard, S. J.; Wagner, G. Structure of the soluble methane monooxygenase regulatory protein B. *Proc. Natl. Acad. Sci. U.S.A* **1999**, *96*, 7877–7882.

(49) Ni, F. Two-Dimensional Transferred Nuclear-Overhauser Effects with Incomplete Averaging of Free- and Bound-Ligand Resonances. *J. Magn. Reson., Ser. B* **1995**, *106*, 147–155.

(50) Ni, F. Recent developments in transferred NOE methods. *Prog. Nucl. Magn. Reson. Spectrosc.* **1994**, *26*, 517–606.

(51) Dominguez, C.; Boelens, R.; Bonvin, A. M. HADDOCK: a protein-protein docking approach based on biochemical or biophysical information. *J. Am. Chem. Soc.* **2003**, *125*, 1731–1737.

(52) De Vries, S. J.; Van Dijk, A. D.; Krzeminski, M.; Van Dijk, M.; Thureau, A.; Hsu, V.; Wassenaar, T.; Bonvin, A. M. HADDOCK versus HADDOCK: new features and performance of HADDOCK2.0 on the CAPRI targets. *Proteins* **2007**, *69*, 726–733.

(53) Beck, M. R.; Otey, C. A.; Campbell, S. L. Structural characterization of the interactions between palladin and α-actinin. *J. Mol. Biol.* **2011**, *413*, 712–725.

(54) Xu, X.; Schürmann, P.; Chung, J.-S.; Hass, M. a S.; Kim, S.-K.; Hirasawa, M.; Tripathy, J. N.; Knaff, D. B.; Ubbink, M. Ternary protein complex of ferredoxin, ferredoxin:thioredoxin reductase, and thioredoxin studied by paramagnetic NMR spectroscopy. *J. Am. Chem. Soc.* **2009**, *131*, 17576–17582.

(55) Luna, R. E.; Arthanari, H.; Hiraishi, H.; Nanda, J.; Martin-Marcos, P.; Markus, M. a; Akabayov, B.; Milbradt, A. G.; Luna, L. E.; Seo, H.-C.; Hyberts, S. G.; Fahmy, A.; Reibarkh, M.; Miles, D.; Hagner, P. R.; O'Day, E. M.; Yi, T.; Marintchev, A.; Hinnebusch, A. G.; Lorsch, J. R.; Asano, K.; Wagner, G. The C-terminal domain of eukaryotic initiation factor 5 promotes start codon recognition by its dynamic interplay with eIF1 and eIF2β. *Cell Rep.* **2012**, *1*, 689–702.

(56) Jensen, G. a; Andersen, O. M.; Bonvin, A. M. J. J.; Bjerrum-Bohr, I.; Etzerodt, M.; Thøgersen, H. C.; O'Shea, C.; Poulsen, F. M.; Kragelund, B. B. Binding site structure of one LRP-RAP complex: implications for a common ligand-receptor binding motif. *J. Mol. Biol.* **2006**, *362*, 700–716.

(57) Huang, H.; Vogel, H. J. Structural basis for the activation of platelet integrin αIIbβ3 by calcium- and integrin-binding protein 1. *J. Am. Chem. Soc.* **2012**, *134*, 3864–3872.

(58) Volkov, A. N.; Bashir, Q.; Worrall, J. A. R.; Ubbink, M. Binding hot spot in the weak protein complex of physiological redox partners yeast cytochrome C and cytochrome C peroxidase. *J. Mol. Biol.* **2009**, *385*, 1003–1013.

(59) van Dijk, A. D. J.; Ciofi-baffoni, S.; Banci, L.; Bertini, I.; Boelens, R.; Bonvin, A. M. J. J. Modeling protein-protein complexes involved in the cytochrome c oxidase copper-delivery pathway. *J. Proteome Res.* **2007**, 1530–1539.

(60) Van Dijk, A. D. J.; Boelens, R.; Bonvin, A. M. J. J. Data-driven docking for the study of biomolecular complexes. *FEBS J.* **2005**, *272*, 293–312.

(61) Bonvin, A. High Ambiguity Driven biomolecular DOCKing based on biochemical and/or biophysical information. http://www.nmr.chem.uu.nl/haddock/.

(62) Hubbard, S. J.; Thornton, J. M. NACCESS **1993**.

(63) Bonvin, A. Use of NMR chemical shift perturbation data: 3. Defining passive residues http://www.nmr.chem.uu.nl/haddock/generate_air_help.html#CSP.

(64) De Vries, S. J.; Van Dijk, M.; Bonvin, A. M. J. J. The HADDOCK web server for data-driven biomolecular docking. *Nat. Protoc.* **2010**, *5*, 883–897.

(65) Quadt-Akabayov, S. R.; Chill, J. H.; Levy, R.; Kessler, N.; Anglister, J. Determination of the human type I interferon receptor binding site on human interferon-α2 by cross saturation and an NMR-based model of the complex. *Protein Sci.* **2006**, *15*, 2656–2668.

(66) Volkov, A. N.; Ferrari, D.; Worrall, J. A. R.; Bonvin, A. M. J. J.; Ubbink, M. The orientations of cytochrome c in the highly dynamic complex with cytochrome b_5 visualized by NMR and docking using HADDOCK. *Protein Sci.* **2005**, *14*, 799–811.

(67) Gao, G.; Prutzman, K. C.; King, M. L.; Scheswohl, D. M.; DeRose, E. F.; London, R. E.; Schaller, M. D.; Campbell, S. L. NMR solution structure of the focal adhesion targeting domain of focal adhesion kinase in complex with a paxillin LD peptide: evidence for a two-site binding model. *J. Biol. Chem.* **2004**, *279*, 8441–8451.

(68) CNS - atom selection http://cns-online.org/v1.21/syntax_manual/html/atom-selection.html.

(69) Selecting atoms in CNS http://cns- online.org/v1.21/ tutorial/language/ atom_sele_basic/ text.html.

CHAPTER 3

Structure and dynamics of full-length cytochrome b_5

3.1 Summary

In this chapter, we report the first solution NMR studies performed on full-length cytochrome b_5 incorporated in two different membrane mimetics. Only the soluble domain of full-length cyt b_5 is visible in the solution NMR experiments due to the fast tumbling of the soluble domain relative to the entire cyt b_5/micelle complex or cyt b_5/isotropic bicelle complex. The resonances of 88.5% of the backbone and side chain atoms of the soluble domain have been assigned and the labeled ^{1}H-^{15}N-TROSY-HSQC spectrum is presented; this spectrum will serve as the basis of all experiments performed on the cyt b_5-cyt P450 complex in the following chapters. The structure of the soluble domain of full-length cyt b_5, incorporated in DPC micelles, is reported with a backbone RMSD of 0.32 ± 0.10 Å. The linker of full-length cyt b_5 is conclusively established to be unstructured. The cyt b_5 structure, with the heme molecule (type B) docked with HADDOCK, is shown. Analysis of ^{15}N relaxation measurements emphasizes the high flexibility of the N-terminal and linker residues. The diffusion tensor components of the soluble domain of full-length cyt b_5, and its effective correlation time, are described as determined by TENSOR2. We also find that the structure

Adapted into a manuscript entitled "NMR structure of full-length mammalian cytochrome b_5" by Ahuja S., Vivekanandan S., Popovych N., Le Clair S., Huang R., Jahr N., Soong R., Xu J., Yamamoto K., Nanga R. P., Im S.-C., Waskell L. and Ramamoorthy A. This study was supported by NIH (GM084018 and GM095640 to A. R. and GM35533 to L. W.).

of the soluble domain appears to be very similar in DPC micelles and DMPC/DHPC isotropic bicelles. The solid-state NMR structure of the α-helical transmembrane domain of full-length cyt b_5 is also reported, along with its average orientation, in DMPC/DHPC lipid bicelles. While the full-length cyt b_5 structure only differs slightly from the previously published truncated cyt b_5 structure, its relaxation parameters are drastically different.

3.2 Introduction

Cytochromes b_5 (cyts b_5) are ubiquitous electron-transport proteins found in plants, mammals, invertebrates, fungi and prokaryotic organisms.[1,2] In mammals, cyts b_5 exist as membrane-anchored proteins found in either the endoplasmic reticulum (ER) or the outer mitochondrial membrane, and as a soluble protein found in erythrocytes.[1] The isoform of cytochrome b_5 (cyt b_5), which sits on the cytoplasmic side of the ER membrane[3] (referred to as microsomal cyt b_5) is a predominantly acidic, 15 kDa (≈134 amino acids) membrane protein which contains three separate domains: a large, N-terminal, cytosolic, heme-containing domain (≈89 amino acids), a 15-residue linker region, and a C-terminal hydrophobic membrane-binding domain (≈20 residues). The sequences of all three domains of microsomal cyt b_5 are highly conserved across mammals.[2] The soluble version of the protein (found in erythrocytes) merely consists of the hydrophilic heme-containing domain of microsomal cyt b_5.[4] Cyt b_5 contains a type B heme, which is located in the hydrophobic core of the soluble cytosolic domain, with the highly conserved H68 and H44 coordinating the heme iron as the 5th and 6th ligands.[5] As discussed in Chapter 1, microsomal cyts b_5 participate in a number of key reactions, including fatty acid desaturation,[4,6–9] the biosynthesis of cholesterol[1,4] and sex hormones,[10] and the hydroxylation of N-acetyl-neuraminic acid[11]. In these various roles, cyt b_5 interacts with both electron acceptor and electron donor proteins, such as NADH cyt b_5 reductase, various cytochromes P450 (cyts P450),[1,4,12–15] stearyl-CoA desaturase[9,16,17] and indoleamine dioxygenase[18,19].

High-resolution structures of truncated, microsomal, wild-type cyts b_5 have been solved by solution NMR and X-ray crystallography.[20–24] However, neither the structures nor the dynamics of full-length cyts b_5 (containing the transmembrane domain) are currently available. Additionally, while the interaction of cyt b_5 with various membranes has been studied fairly extensively,[25–27] the structure of cyt b_5, when incorporated in a membrane environment, is lacking. Circular dichroism and Fourier Transform Infrared experiments have indicated that the transmembrane (TM) domain is at least 50% helical[16,28,29] and recent solid-state NMR results from our lab have shown that the TM domain is a single-pass transmembrane helix.[30] The membrane-binding domain of cyt b_5 is highly conserved (78-96% sequence similarity among vertebrates)[1] and has been shown to be important for proper insertion of cyt b_5 into the ER membrane[31,32] and the outer membrane of the mitochondria[33]. An important role for the TM domain has also been shown in the interactions of cyt b_5 with its redox partners: truncated cyt b_5 is incapable of interacting with any microsomal cyts P450[4,34–36] and is only capable of electron transfer to soluble oxidative enzyme (e.g. cytochrome c and metmyoglobin). Furthermore, a poly-leucine mutant of cyt b_5 (where the putative TM domain was replaced by 22 consecutive leucines) had a significantly reduced ability to bind to both cyt P450 and NADH cyt b_5 reductase.[37]

The TM domain of cyt b_5 is connected to the cytosolic domain by a flexible linker region that is important for orienting the catalytic domain of cyt b_5 in a position that is favorable for interaction with its redox partners.[2] It has been shown recently that the length of the linker region is important for the interaction between cyt b_5 and cyt P450, and a minimum of 7 residues is required for a productive interaction. However, the exact sequence of the linker region is not critical.[2]

In order to fully understand the role of the transmembrane domain and the linker region in the interaction of membrane-bound cyt b_5 with its redox partners, it is important to first determine the full-length structure of cyt b_5. In this chapter, we present the first full-length tertiary structure of cyt b_5, in a membrane mimetic, solved using a combination of solution and solid-state NMR spectroscopy. Relaxation NMR measurements on the full-length cyt b_5 are also reported to characterize and assess the dynamics of the protein's soluble domain and linker region.

3.3 Materials and methods

3.3.1 Materials

1,2-dihexanoyl-*sn*-glycero-3-phosphocholine (DHPC) and 1,2-dimyristoyl-*sn*-glycero-3-phosphocholine (DMPC) were purchased from Avanti Polar Lipids (Alabaster, AL). C41 cells were purchased from Lucigen (Middleton, MI). U-^{13}C, ^{15}N and ^{2}H CELTONE rich medium, ^{15}N-CELTONE rich media, ^{13}C, ^{15}N-CELTONE rich media, ^{2}H-dodecylphosphocholine (DPC), ^{13}C-glucose, ^{15}N-ammonium sulfate, 2,2-dimethyl-2-

silapentane-5-sulfonate (DSS) and D_2O were purchased from Cambridge Isotope Laboratories (Andover, MA). Resins and buffer components were purchased from Sigma-Aldrich. Glycerol for NMR experiments was purchased from Sigma-Aldrich and Roche Applied Science. The NMR samples were placed into 5 mm symmetrical D_2O-matched Shigemi NMR microtubes (Shigemi, Inc, Alison Park, PA).

3.3.2 Protein production and purification

Wild-type rabbit, full-length cyt b_5 was overexpressed and purified using the protocols described previoulsy.[38,39] Uniformly labeled ^{15}N-cyt b_5, U-^{15}N, ^{13}C-cyt b_5 and U-^{15}N, ^{13}C, ^{2}H-cyt b_5 were expressed using Celtone-N, Celtone-CN and Celtone-DCN complete media, respectively, with additional supplements listed in Dürr *et al*.[30] Prior to expressing U-^{15}N, ^{13}C, ^{2}H-cyt b_5, C41 cells containing pLW01-cyt b_5 plasmid were adapted to grow in 100% Lysogeny Broth (LB) medium by gradually increasing the D_2O concentration in the LB medium from 10, 30, 60, 80 to 100% D_2O. After each successive cycle, an LB culture was inoculated with three colonies that had been grown on a plate containing a lower amount of D_2O. The liquid culture with the higher amount of D_2O was incubated for up to ~8 hours at 37 °C with shaking at 250 rpm. A volume of 50 µL of the resulting culture was plated on an LB agar plate containing 0.24 mM carbenicillin and the higher D_2O concentration. This process was repeated until the cells were able to grow on LB plates containing 100% D_2O. The protocols for the expression of U-^{15}N, ^{13}C, ^{2}H-cyt b_5, ^{15}N, ^{13}C-cyt b_5 and ^{15}N-cyt b_5 were identical; however, the cells were harvested at a different time. For U-^{15}N-cyt b_5 and U-^{15}N, ^{13}C-cyt b_5, the cells were harvested after 20 hours of incubation at 35 °C with shaking at 200 rpm, while for U-^{15}N, ^{13}C, ^{2}H-cyt b_5, cells were harvested after 48 hours. Purification of cyt b_5 was performed as described elsewhere.[38,39] Each purified protein exhibited a single band on an SDS PAGE gel.

3.3.3 Solution NMR Spectroscopy

All solution NMR experiments were performed at 298 K on a Bruker 900 MHz NMR spectrometer equipped with a 5 mm triple-resonance TXI cryo-probe. Samples for NMR were prepared using an appropriate amount of protein (0.1 mM - 0.5 mM) in 100 mM potassium phosphate buffer at pH 7.4 and 5% (w/v) glycerol (referred to as NMR buffer) incorporated into either deuterated dodecylphosphocholine (DPC-D38, 45 mM or 150 mM) micelles or lipid isotropic bicelles composed of 1,2-dimyristoyl-*sn*-glycero-3-phosphocholine (DMPC) and 1,2-dihexanoyl-*sn*-glycero-3-phosphocholine (DHPC) lipids. Protein NMR samples in isotropic bicelles were prepared using a 10% (w/v) mixture of DMPC and DHPC lipids in 1:4 molar ratio (as described previously[30] and in Appendix D).

3.3.3.1 Sequence specific assignment and structural determination

3D-TROSY versions of HNCA and HNCACB spectra of U-^{15}N, ^{13}C-enriched cyt b_5 were recorded with spectral widths of 15290 Hz (^{1}H), 3571 Hz (^{15}N) and 8048 Hz (^{13}C). 3D-TROSY versions of the HN(CA)CO and HNCO experiments were recorded with spectral widths of 15290 Hz (^{1}H), 3571 Hz (^{15}N) and 5681 Hz (^{13}C). No visible protein aggregation or degradation was evident and periodic ^{1}H-^{15}N-TROSY-HSQC experiments were conducted to verify that line-width broadening or chemical shift changes associated with aggregation did not occur.

Sequence specific assignment of ^{1}HN, ^{15}N, ^{13}Cα, ^{13}Cβ and ^{13}CO backbone resonances was achieved using a set of TROSY-based 3D HNCO, HN(CA)CO, HNCA, HN(CO)CA and HNCACB experiments.[40,41] Intra-residue, inter-residue and sequential nuclear overhauser effect (NOE) restraints were obtained from 3D ^{15}N-HSQC-NOESY and ^{13}C-HSQC-NOESY spectra on fully-protonated U-^{15}N, ^{13}C-labeled cyt b$_5$ in DPC-D38 micelles; these experiments were conducted at optimal mixing times of 80 ms and 100 ms, respectively. A 3D ^{15}N-HSQC-TOCSY spectrum was also collected to assist in the assignment of inter-residue NOEs. The 3D TOCSY and NOESY spectra were recorded with spectral widths of 15290 Hz, 3571 Hz and 4200 Hz for ^{1}H, ^{15}N and aliphatic protons, respectively. All aromatic side chain protons and carbon atoms were assigned using ^{1}H-^{1}H-NOESY and 3D-NOESY. All 3D experiments made use of pulsed-field gradients for coherence selection and artifact suppression, and utilized gradient sensitivity enhancement schemes. Quadrature detection in the indirectly detected dimensions was achieved using either the States/TPPI (time proportional phase incrementation) or the echo/antiecho method. The ^{1}H chemical shifts were referenced to 2,2-dimethyl-2-silapentane-5-sulfonate (DSS) at 0.0 ppm and the ^{13}C and ^{15}N chemical shifts were referenced indirectly.[42] All NMR spectra were processed using either NMRPipe[43] or TopSpin 2.0 (Bruker). Sequential and NOE assignments were made using Sparky[44].

3.3.3.2 Backbone ^{15}N relaxation measurements

The ^{15}N longitudinal relaxation rate (R_1), ^{15}N transverse relaxation rate (R_2) and ^{15}N-{^{1}H} steady-state nuclear overhauser effect (NOE) were measured on a sample containing 0.2 mM U-^{15}N, ^{13}C, ^{2}H-labeled cyt b$_5$ in NMR buffer with 45 mM DPC. The ^{15}N longitudinal and transverse relaxation time constants, T_1 and T_2, respectively, were determined by collecting a time series of ^{15}N-HSQC spectra with sensitivity enhancement. For T_1 measurements, the spectra were collected with relaxation delays of 5, 40, 80, 130, 210, 330, 470, 630, 800, 1000 and 1400 ms (duplicate points for 40 and 130 ms). T_2 measurements were achieved by Carr-Purcell-Meiboom-Gill (CPMG) spin echo experiments[45] with relaxation delays of 7.2, 14.4, 28.8, 43.2, 72, 100.8, 115.2 and 158.4 (with duplicate points for 14.4 and 43.2 ms). In the CPMG pulse train, the delays between the 180 degree pulses were set to 0.9 ms. For both T_1 and T_2 measurements, a recycle delay of 1 s was used and 2048 x 256 complex data points were collected with 24 scans and 16 dummy scans, and duplicate points for two relaxation delays were recorded for estimation of errors. 2D ^{15}N-{^{1}H} steady-state NOE experiments[46,47] with water flip-back pulse for water suppression[48] were recorded with and without pre-saturation of the amide protons; the proton saturation period and recycle delay were 3 s and 4 s, respectively, and 2048 x 256 complex data points were collected with 20 scans and 16 dummy scans. All the spectra were processed using NMRPipe[43] and peak heights were determined using Sparky[44]. T_1 and T_2 values were calculated by fitting the peak heights as a function of relaxation delays in Sparky[44]. The NOE values were calculated with NOE= $I_{saturated}/I_{unsaturated}$, where $I_{saturated}$ and $I_{unsaturated}$ are the peak heights for each residue with and without pre-saturation, respectively; the error was calculated in the same manner as Bailey *et al.*[49]

3.3.4 TENSOR2 analysis

Relaxation data were analyzed using the Lipari-Szabo model-free analysis[50,51] in TENSOR2[52]. The chemical shift anisotropy tensor angle from the N-H bond vector was set at 18° according to the work done by Pandey *et al.* on full-length rabbit cyt b_5 in DPC micelles.[53] The value of τ_c (for the isotropic model) and diffusion tensor (for the anisotropic model) were calculated based on the relaxation parameters of residues within secondary structure elements[54] of the soluble domain (K10-R89), which had NOE > 0.65 and an R_2/R_1 value within 1.5 standard deviations from the mean.[55] The errors for the diffusion tensor components and the isotropic correlation time were obtained from 1000 Monte Carlo simulations.

3.3.5 Structure determination of the cyt b_5 soluble domain

Initial restraints for the backbone torsion angles ϕ and ψ were obtained from chemical shifts using TALOS[56], provided as part of the NMRPipe[43] package, and NOE patterns. The upper bound for all NOE distance restraints was initially set to 5 Å and adjusted for non-stereospecific assignment of methylene and methyl protons using the method described originally for DYANA.[57] The structure calculations were performed with CYANA 2.1[58], which uses simulated annealing in combination with molecular dynamics in torsion angle space. Chemical shift tolerances of 0.02, 0.3 and 0.45 ppm were used for ^1H, ^{13}C and ^{15}N, respectively. For initial structure calculations, only unambiguous peak assignments, obtained from 3D NOESY, were used. More than 90% of the peaks were assigned manually and the remaining peaks were assigned using

CYANA 2.1[58]. Using these assignments and TALOS-derived torsion angle restraints, an initial ensemble of NMR structures was generated. Initial violated restraints were identified and eliminated in subsequent rounds of structure calculations until a consistent set of restraints was obtained with no violations greater than 0.2 Å in the ensemble. Assignments of ambiguous NOE cross-peaks were then made by applying a structure-aided filtering strategy in repeated rounds of structure calculations. Starting *ab initio*, 100 conformers were calculated in 10,000 annealing steps each. PyMOL[59] was used to visualize the resulting ensemble of energy-minimized conformers.

3.3.6 Solid-State NMR Spectroscopy

Magnetically-aligned DMPC/DHPC bicelles, with a molar ratio of DMPC to DHPC of 3.5:1 and a weight percentage of lipid of 30% (w/v), containing U-^{15}N-cyt b_5 were prepared as described elsewhere[30]. A two-dimensional Separated Local Field (SLF) NMR experiment using the HIMSELF[60] (heteronuclear isotropic mixing leading to spin exchange via the local field) pulse sequence was obtained at 310 K using a ramped-cross-polarization contact time of 0.8 ms, 2 s recycle delay and 32 t_1 increments on a Bruker 900 MHz NMR spectrometer. Radio frequency field strengths of 50 and 35 kHz were used for the WIM (windowless mixing)[61] sequence during t_1 and SPINAL-64[62] decoupling during acquisition, respectively.

3.3.7 Docking of heme into the cyt b_5 NMR structure

HADDOCK 2.1 (High Ambiguity Driven biomolecular DOCKing)[63,64] was used to incorporate the heme molecule into the NMR structure of cyt b_5 presented in this paper. For the docking, the two molecules used were the heme molecule (type B) and the twenty NMR-derived low-energy structures of cyt b_5 (Section 3.4.2 and Figure 3.8). Unambiguous restraints (Table 3.1) were compiled based on distances (between the heme and certain cyt b_5 residues) measured from the available NMR structure of cyt b_5 (PDB code 1DO9)[20]. During the docking steps, only residues adjacent to H44 and H68 (which coordinate the heme Fe(III)) were set as semi-flexible (43-46 and 66-70, respectively). The protonation state for histidines 44 and 68 was set to singly protonated at HD1 to account for the coordination to the Fe(III). As a first step, rigid body energy minimization was used to dock 2000 structures. The second step included the semi-rigid simulated annealing and the best 500 structures were selected for refinement. The best 200 structures were then selected for final refinement with explicit solvent in an 8.0 Å shell of TIP3P water molecules. The 50 lowest energy structures were then subjected to a detailed analysis.

Table 3.1 List of restraints used for incorporating the heme (type B) into the NMR structure of cyt b_5 using HADDOCK 2.1[63,64].

Cyt b_5 residue, atom	Heme atom	Distance (Å)	Lower distance margin (Å)	Upper distance margin (Å)
L28, HD1#	HAB	5.0	1.8	5.0
L28, HD2#	HBC2	5.0	1.8	5.0
L28, HD2#	HMC1	5.0	1.8	5.0
L30, HE	Fe(III)	5.0	1.8	5.0
H44, NE2	Fe(III)	2.2	2.2	2.2
H68, NE2	Fe(III)	2.2	2.2	2.2
L30, HD1#	HMC1	5.0	1.8	5.0
L30, HD2#	HMC1	5.0	1.8	5.0
L30, HD1#	HBB2	5.0	1.8	5.0
H44, HD2	HB	5.0	3.0	5.0
H44, HE1	HD	5.0	3.0	5.0
H68, HD2	HB	5.0	3.0	5.0
H68, HE1	HD	5.0	3.0	5.0
H44, HD2	HMB2	5.0	3.0	5.0
H44, HD2	HMA2	5.0	3.0	5.0
H44, HE1	HAC	5.0	3.0	5.0
H44, HE1	HMD1	5.0	3.0	5.0
H68, HD2	HMB1	5.0	3.0	5.0
H68, HD2	HMA3	5.0	3.0	5.0
H68, HE1	HMC3	5.0	3.0	5.0

3.4 Results

3.4.1 Sequence specific assignment of cyt b_5

Isotopically labeled, full-length, wild-type, oxidized, microsomal rabbit cyt b_5 was reconstituted in detergent (DPC) micelles. Standard TROSY-based multidimensional solution NMR experiments and isotopic labeling schemes, including perdeuteration, were employed to assist in resonance assignment and structure determination. Figure 3.3 and Figure 3.20b present well-resolved ^{1}H-^{15}N-TROSY-HSQC spectra of uniformly ^{13}C, ^{15}N, ^{2}H-labeled full-length cyt b_5 incorporated in DPC micelles at 25 °C. The ^{1}H-^{15}N-

TROSY-HSQC spectra exhibited well-resolved and dispersed NH correlations of cyt b_5 residues, suggesting that the protein was well folded and monomeric under our sample conditions.

Using standard three-dimensional solution NMR experiments, NMR resonance assignment was achieved for 88.5% of the backbone and side chain atoms of residues from the soluble domain of full-length cyt b_5. Unambiguous backbone assignments for non-proline residues included the following ranges of residues in the soluble domain K7-H22, K24-I29, H31-H32, V34-H44, E48-H85, D87-R89, L92-S93, M96-L99, T101-D104 and N106. Unambiguous assignment was also obtained for the backbone of the C-terminal residues Y127, D133 and D134. Ambiguous assignment was obtained for residues A124, M126 and R128. Accordingly, residues that did not have backbone assignment were thus the proline residues (P45, P86, P95 and P116), the N-terminus (M1-D6), soluble domain residues S23, L30, K33, G46, and G47, linker residues S90, K91, K94, I100, the transmembrane domain residues S105, S107-V123 and C-terminal residues L125, L129, Y130, M131 and A132. A fully assigned ^{1}H-^{15}N-TROSY-HSQC can be found in Figure 3.3. Full chemical shift assignments of ^{1}H, ^{13}C and ^{15}N atoms has been deposited into the Biological Magnetic Resonance Bank (code 18919).

An inspection of the ^{1}H-^{15}N-TROSY-HSQC of cyt b_5 reveals two or more NMR resonances for many residues. These additional NMR resonances are a result of the two isomers (major and minor) of cyt b_5 that differ by a 180° rotation of the heme plane about the axis that cuts through the *meso*-carbon atoms α and γ (Figure 3.1).[65,66] During the expression of cyt b_5, heme (type B) is added to apo-cyt b_5 and inserts in the two different heme orientations; at this stage, the two isomers are in relatively equal in populations[67] but interconversion (in the direction leading to a higher population of the more stable conformer) takes place until they reach equilibrium.[68] Steric interactions of the 2-vinyl group of the heme in the minor conformer causes the heme to protrude out of the binding pocket by around 1 Å (compared to the major isomer) for rat cyt b_5, and the minor isomer of rabbit cyt b_5 likely experiences an even larger displacement because of higher steric demands in the back of the heme pocket by L28 (instead of the valine residue present in rat cyt b_5);[20,69] see Figure 3.12 to see the location of L28. This displacement of the heme makes the S69 amide unable to hydrogen bond with one of the heme propionates.[69] Similarly, the displacement of the heme also substantially disrupts the hydrophobic aromatic overlap between the heme system and residues F40 and F63.[69] The absence of these interactions in the minor isomer contributes to its thermodynamic instability compared to the major isomer. The ratio of the populations of the two isomers can be calculated by determining the peak intensity ratio (here in the ^{1}H-^{15}N-TROSY-HSQC spectrum) for identical residues in the two isomeric forms. The major/minor isomer ratio in our study for full-length rabbit cyt b_5 in 45 mM DPC was determined to be about 6.6:1 which is similar to 5:1 ratio previously obtained for truncated rabbit cyt b_5[20] and nearly identical to the isomer ratio of 6.5:1 for truncated bovine cyt $b_{5.}$[70] The ratios depend on the cyt b_5 species and has been reported to be as high as 1.5:1 for rat cyt b_5,[71] despite the sequence similarity between rat and rabbit cyt b_5, see Figure 3.14. Interestingly, the major/minor isomer ratio differed when cyt b_5 was in 45 mM (Figure 3.20b) or 150 mM (Figure 3.3) DPC micelles, with less minor isomer in the presence of 150 mM DPC. Although backbone assignments were done for the resonance peaks of both the major and minor isomers, all structure analyses were performed for the major isomer of ferric cyt b_5.

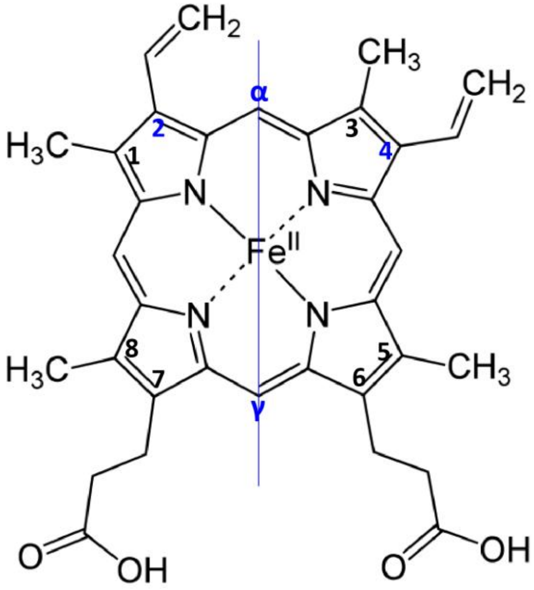

Figure 3.1 Heme type B molecule. This figures shows positions 2 and 4 to which the vinyl groups are attached, as well as the α-γ *meso*-axis (through the *meso*-carbons labeled α and γ).[66]

NMR resonance assignments of the major isomer of cyt b_5 in DPC micelles revealed that the ^{1}H-^{15}N-TROSY-HSQC spectrum is dominated by resonances from the soluble heme-containing domain and the flexible linker of cyt b_5 (Figure 3.3). The absence of amide resonances for residues M1-D6, S23 and K33 is likely due to high solvent exchange rates. Residues from the transmembrane (TM) domain of cyt b_5 could not be identified in the ^{1}H-^{15}N-TROSY-HSQC spectrum. To identify the cause of the lack of transmembrane domain resonances in solution NMR, and to determine the structure and membrane topology of the TM domain, solid-state NMR was utilized (Section 3.4.5). It is important to note here that the full-length form of cyt b_5 incorporated in a membrane mimetic (DPC micelles or lipid bicelles) was used for all solution as well as solid-state NMR measurements.

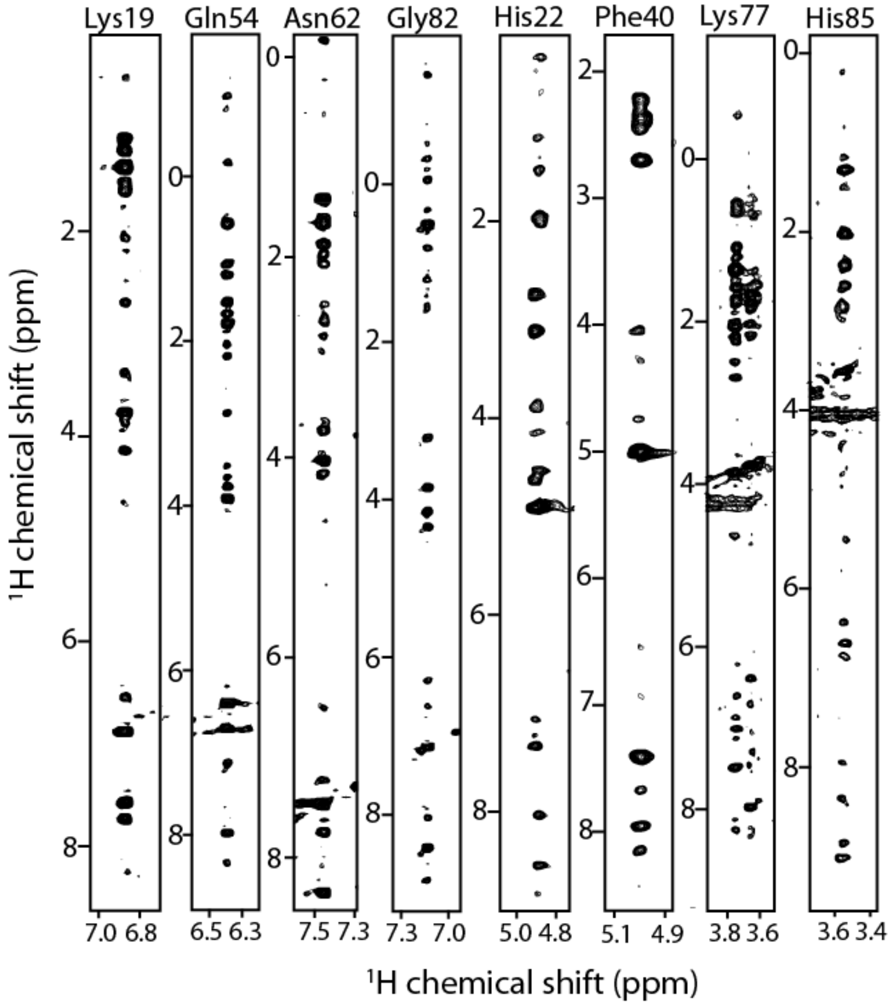

Figure 3.2 **^{1}H-^{1}H planes extracted from a 3D ^{15}N-NOESY-HSQC recorded on fully protonated U-^{13}C, ^{15}N-cyt b_5 in DPC micelles.**

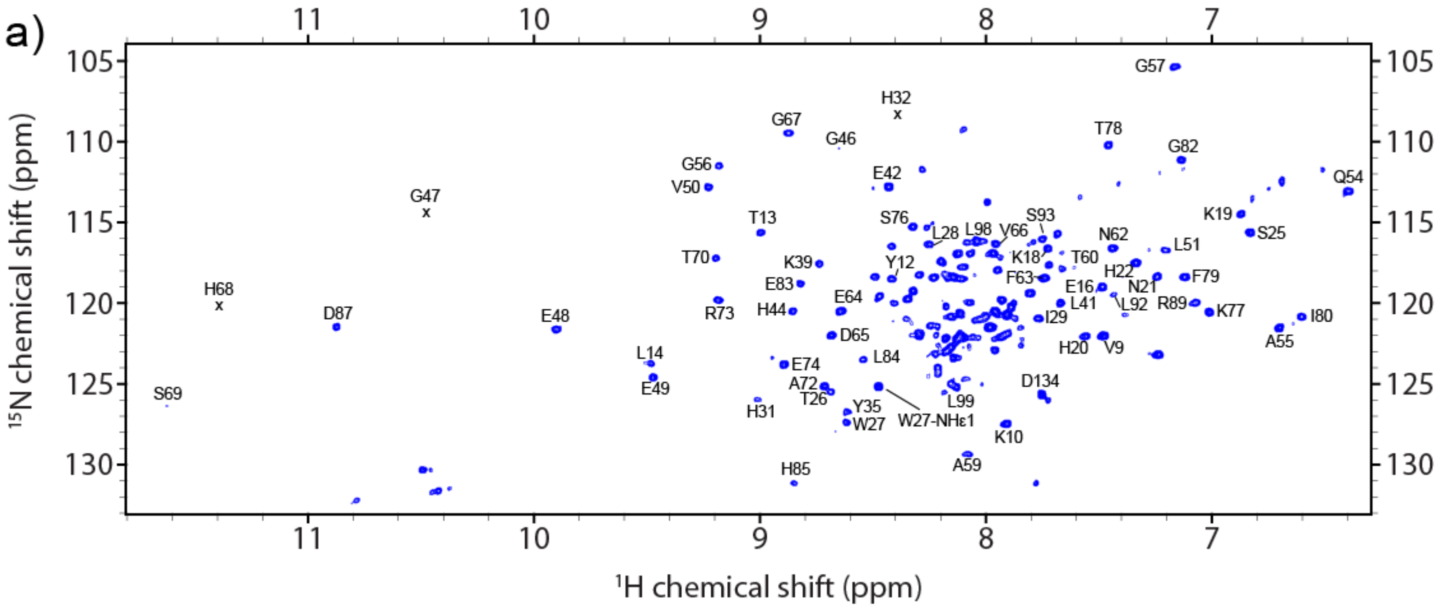

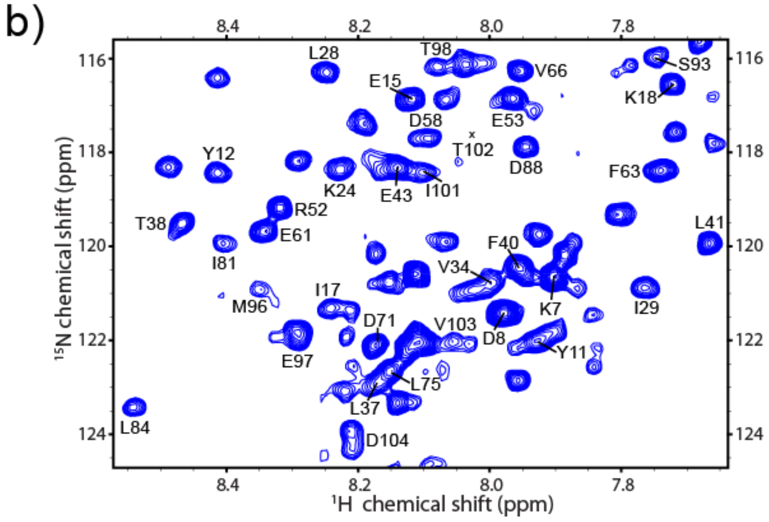

Figure 3.3 ^{1}H-^{15}N-TROSY-HSQC spectrum of full-length cyt b$_5$ in 150 mM DPC micelles. The cross-peaks are labeled with all of the residue specific assignment of cyt b$_5$. Unlabeled peaks are either side chain resonances (Asn, Gln) or represent the lower populated isomer with the 180° rotated heme. (a) Full HSQC spectrum and (b) a zoomed in look at the crowded region. A concentration of 150 mM DPC micelles was used to make this figure because the spectrum is less crowded than in 45 mM DPC due to a lower population of the minor isomer in 150 mM DPC.

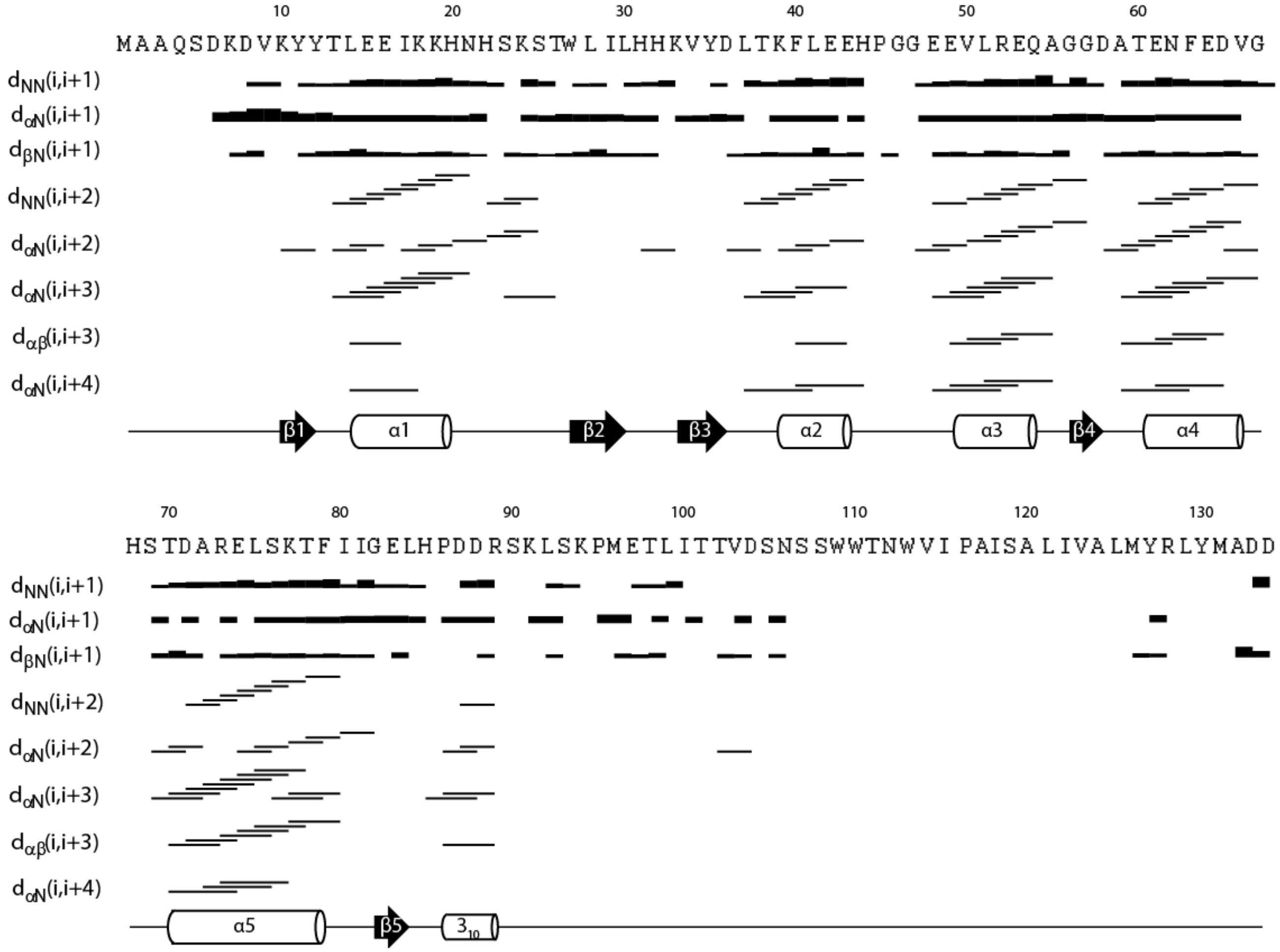

Figure 3.4 Schematic representation of the sequential and medium range NOE connectivities involving NH, Hα and Hβ protons. The secondary structure of cyt b_5 is shown for comparison. The secondary structure was obtained based on the CYANA 2.1-generated structure (Figure 3.8) as defined by the NMR restraints (Table 3.2). The thickness of the bar indicates the NOE intensities.

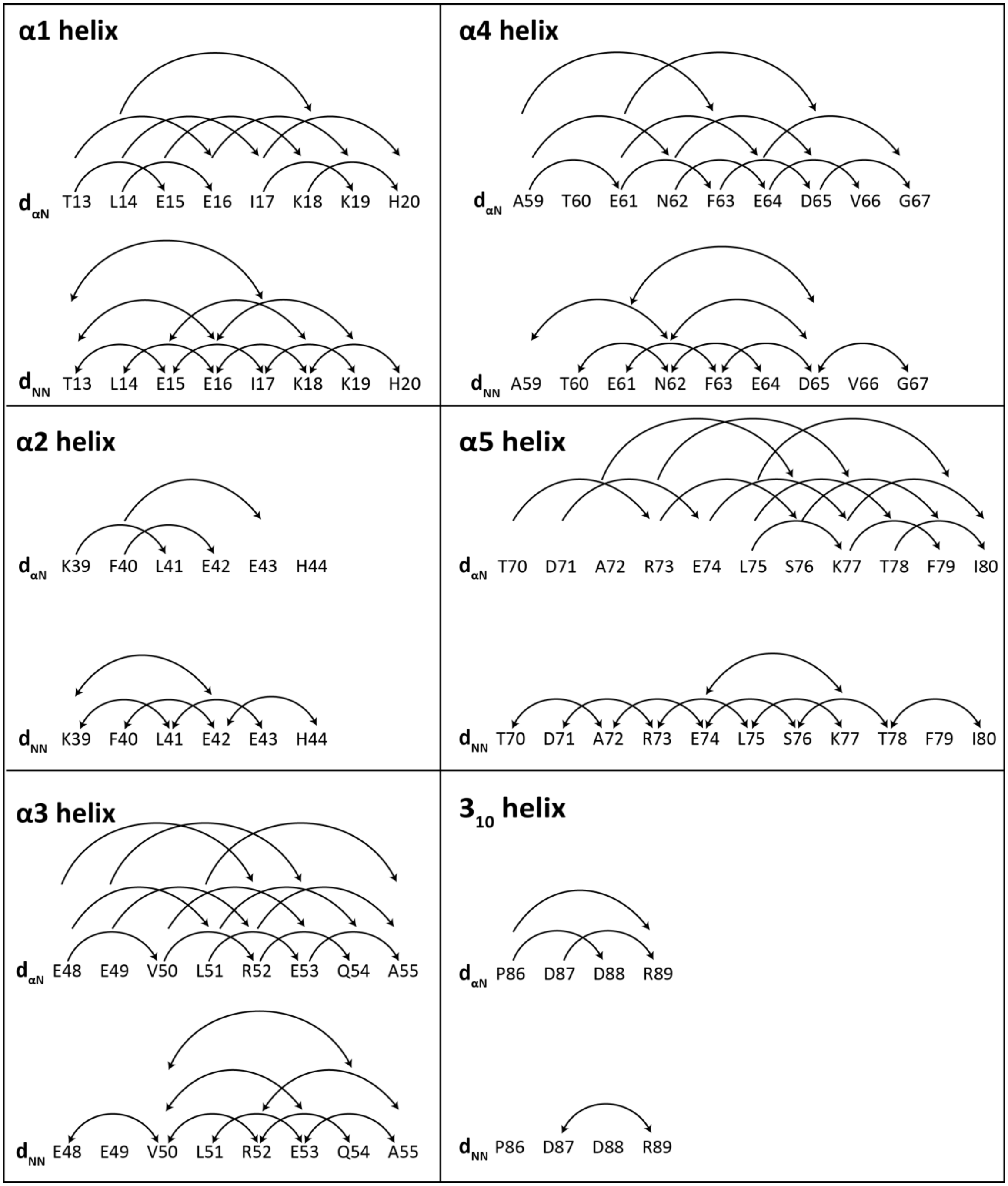
α1 helix
dαN T13 L14 E15 E16 I17 K18 K19 H20
dNN T13 L14 E15 E16 I17 K18 K19 H20
α4 helix
dαN A59 T60 E61 N62 F63 E64 D65 V66 G67
dNN A59 T60 E61 N62 F63 E64 D65 V66 G67
α2 helix
dαN K39 F40 L41 E42 E43 H44
dNN K39 F40 L41 E42 E43 H44
α5 helix
dαN T70 D71 A72 R73 E74 L75 S76 K77 T78 F79 I80
dNN T70 D71 A72 R73 E74 L75 S76 K77 T78 F79 I80
α3 helix
dαN E48 E49 V50 L51 R52 E53 Q54 A55
dNN E48 E49 V50 L51 R52 E53 Q54 A55
3₁₀ helix
dαN P86 D87 D88 R89
dNN P86 D87 D88 R89

Figure 3.5 Hα-NH and NH-NH NOE connectivities observed in the ^{15}N-HSQC-NOESY spectrum for helical segments of cyt b_5. The connectivities ($d_{\alpha N}$ for Hα-NH and d_{NN} for NH-NH) are shown for α-helices 1-5 and the 3_{10} helix. These segments were chosen based on the final structure generated from CYANA 2.1 via NMR restraints (Figure 3.8).

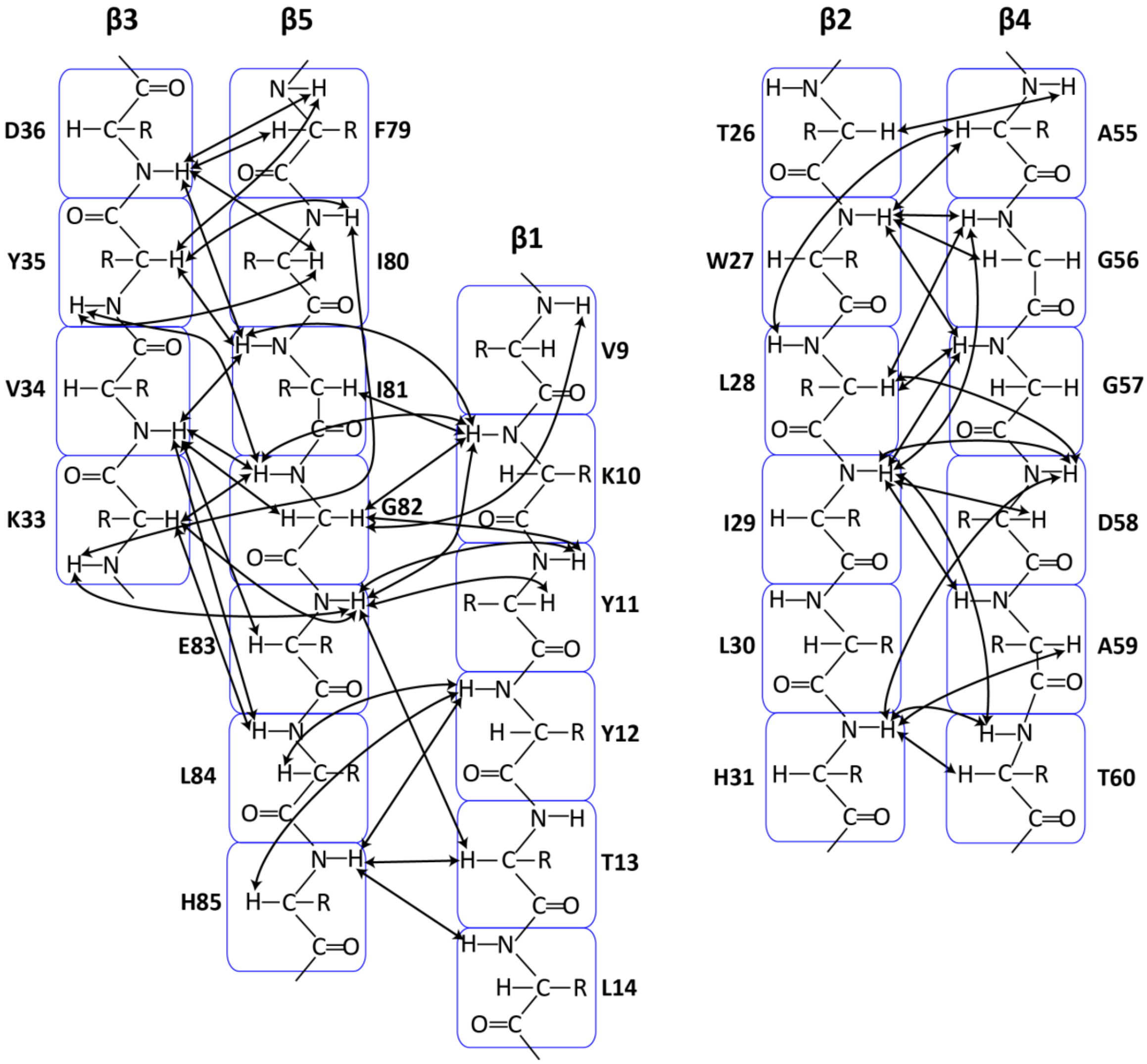
β3
β5
β1
β2
β4
D36
Y35
V34
K33
F79
I80
I81
G82
E83
L84
H85
V9
K10
Y11
Y12
T13
L14
T26
W27
L28
I29
L30
H31
A55
G56
G57
D58
A59
T60

Figure 3.6 NOE connectivities observed within the β-strands of cyt b_5. This analysis was initially done simply by looking at the ^{15}N-HSQC-NOESY cross-peaks, and was then modified to reflect the orientation of atoms in the β-strands as observed in the CYANA 2.1 generated structure (obtained from NMR restraints) in Figures 3.13. It can be seen that the β-sheets are not ideal β-sheets (as shown in textbooks). For example, I81, G56 and A59 are twisted/distorted. The β-sheet system on the left is a mirror image of the one presented in Figure 3.12.

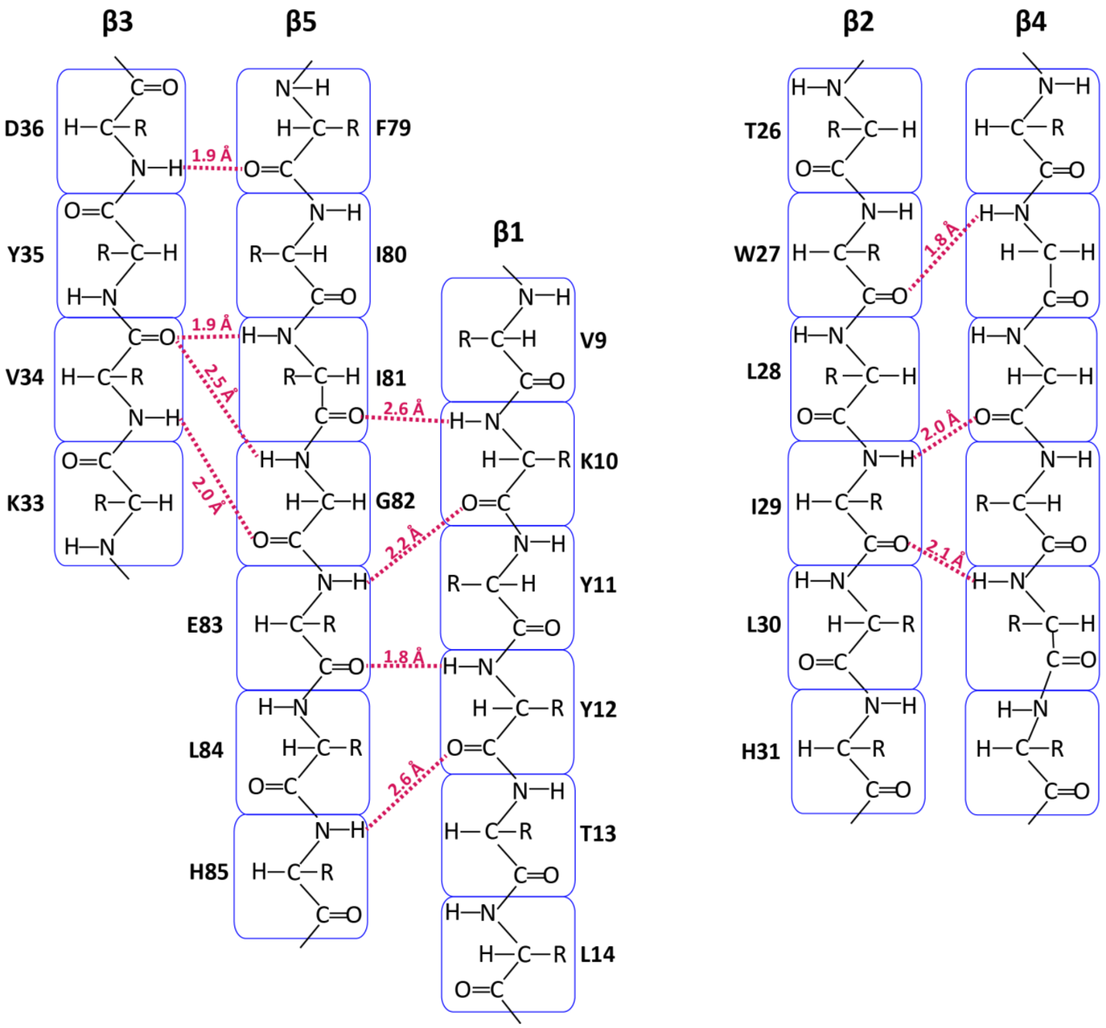
β3
β5
β1
β2
β4
D36
Y35
V34
K33
F79
I80
I81
G82
E83
L84
H85
V9
K10
Y11
Y12
T13
L14
T26
W27
L28
I29
L30
H31
A55
G56
G57
D58
A59
T60
1.9 Å
1.9 Å
2.5 Å
2.0 Å
2.6 Å
2.2 Å
1.8 Å
2.6 Å
1.8 Å
2.0 Å
2.1 Å

Figure 3.7 Proposed hydrogen bonds within the β-sheets of cyt b_5. This figure was generated following Figure 3.6. The hydrogen bonds are predicted based on the orientation of and distances between the NH and CO atoms. The distances between the atoms were calculated using PyMOL[59]. All of these hydrogen bonds were input as restraints in CYANA 2.1 except for K10-NH to I81-CO and Y12-CO to H85-NH.

3.4.2 Three-dimensional tertiary structure calculation of the soluble domain of full-length cyt b_5

A high-resolution solution structure of the major isomer of ferric cyt b_5 (15 kDa) in DPC micelles was calculated using a total of 1787 NOE restraints (Table 3.2). Strips from the ^{15}N-NOESY-HSQC can be found in Figure 3.2; the majority of cross-peaks were well resolved. Schematic representations of the NOE connectivities within the different secondary structure elements can be found in Figure 3.4, Figure 3.5 and Figure 3.6. Distances derived from NOE restraints in conjunction with 39 hydrogen bonds (Table 3.3) and 112 (ϕ and ψ) dihedral angles were inputted for structure determination into CYANA 2.1[58]. Thirty minimum energy conformers (Figure 3.8) with a backbone and heavy atoms RMSD values of 0.32 ± 0.10 Å and 0.82 ± 0.10 Å, respectively, were selected from 100 structures calculated in 10,000 annealing steps. Distance restraints used for structural calculations and Ramachandran statistics can be found in Table 3.2. HADDOCK 2.1[63,64] was used to dock the heme molecule (type B) into the twenty NMR-derived lowest-energy structures of cyt b_5 (see Methods Section 3.3.7). Fifty low energy structures were obtained with no restraint violations. The five lowest energy HADDOCK-generated structures are presented in Figure 3.9. The 23 lowest energy NMR-derived structures of the soluble domain of full-length cyt b_5, containing the heme docked by HADDOCK, were deposited in the Protein Data Bank (code 2M33) and the Biological Magnetic Resonance Bank (code 18919).

The sequence and NMR-derived secondary structure of the soluble domain of full-length cyt b_5 can be found in Figure 3.11. The structure of the heme domain of cyt b_5 contains five α-helices, five β-strands and one 3_{10} helix. The N-terminus is unstructured, with residues M1-D6 not observable by NMR (see Section 3.4.1) and residues K7-V9 as random coil. The first β-sheet is observed for residues K10-Y12 with an α-helix (α1, L14-H20) following shortly after. The proximal heme binding portion of cyt b_5 consists of two helices in the lower cleft, labeled as α4 (T60-V66) and α5 (T70-F79), two helices in the upper cleft, labeled as α2 (K39-E43) and α3 (E49-Q54), and three β-strands at the back of the pocket, labeled as β3 (K33-D36), β2 (W27-L30) and β4 (G56-D58) (these structures can best be seen in Figure 3.8a and can be seen in the labeled schematic in Figure 3.12). At the end of the structured soluble domain lie a β-strand (β5, G82-L84) and a 3_{10} helix (P86-R89). The linker region (S90-D104) was found to be completely random coil.

The five β-strands combine to form two rather complex β-sheet systems. One of the β-sheet systems involves β1 and β3 being hydrogen bonded on either side of β5 (forming a β5 sandwich); β1/β5 form a parallel β-sheet and β3/β5 form an anti-parallel β-sheet. This can be seen schematically in Figure 3.6 and Figure 3.12 and from the actual strands in the NMR structure as presented in Figure 3.13a. The other parallel β-sheet formed between β4 and β2 is more conventional and can be visualized in Figure 3.13b, as well as schematically in Figure 3.6 and Figure 3.12. All three of the β-sheets in cyt b_5 are, however, distorted/twisted with atom orientations differing from the "ideal" β-sheet hydrogen bonding network (as presented in textbooks); this can be seen in Figure 3.13 and schematically in Figure 3.6.

A loop of six residues is present between α1 and β2 (referred to as the α1-β2 loop). Four β-turns were identified, according to their ϕ and ψ angles, between β2-β3, β3-α2, α2-α3 and α3-β4 (a list of the residues and the types of turns in which they are involved are listed in Table 3.4). It is interesting to note that there are several areas in which only 1-3 residues are present between two secondary structure elements, such as T13, G47-E48, A59, G67-S69, I80-I81 and H85. Based on these structural assignments, H44, which coordinates the heme from the upper cleft of cyt b_5, is found in a type VIa β-turn and H68, which coordinates the heme from the lower cleft of cyt b_5 is found in a loop region.

Table 3.2 NMR and refinement statistics for the cyt b_5 NMR structure.

NMR distance and dihedral constraints	
Distance constraints	
Total NOE	1787
Intra-residue	377
Inter-residue	
Sequential ($\|i-j\| = 1$)	513
Medium-range ($\|i-j\| < 4$)	412
Long-range ($\|i-j\| > 5$)	485
Hydrogen bonds[1]	39
Total dihedral angle restraints	
ϕ	56
ψ	56
Structure statistics	
Violations	
Distance constraints (Å)	0.2
Dihedral angle constraints (º)	0
Max. dihedral angle violation (º)	0
Max. distance constraint violation (Å)	0.18
Ramachandran plot	
Most favored (%)	71.70
Allowed (%)	25.90
Generously (%)	2.30
Disallowed (%)	0.00
Average RMSD (K7-R89) (Å)	
Heavy	0.82 ± 0.10
Backbone	0.32 ± 0.10

[1] Hydrogen bond restraints can be found in Table 3.3.

Table 3.3 Hydrogen-bond restraints used for the determination of the NMR structure of cyt b_5.

Residue # and atom	Residue # and atom
12 N-H	83 C=O
29 C=O	59 N-H
29 N-H	57 C=O
41 C=O	44 N-H
17 N-H	13 C=O
69 C=O	72 N-H
16 N-H	13 C=O
69 C=O	73 N-H
70 C=O	74 N-H
19 N-H	16 C=O
56 N-H	27 C=O
76 C=O	79 N-H
30 N-H	33 C=O
71 C=O	75 N-H
35 N-H	28 C=O
72 C=O	76 N-H
34 N-H	82 C=O
89 N-H	86 C=O
40 C=O	44 N-H
66 N-H	63 C=O
81 N-H	34 C=O
82 C=O	34 N-H
54 N-H	51 C=O
55 N-H	52 C=O
51 N-H	48 C=O
53 N-H	49 C=O
62 N-H	59 C=O
66 N-H	63 C=O
67 N-H	63 C=O
63 N-H	59 C=O
57 N-H	54 C=O
52 N-H	48 C=O
78 N-H	75 C=O
36 N-H	79 C=O
83 N-H	10 C=O
90 N-H	86 C=O
92 N-H	87 C=O
43 N-H	40 C=O
77 N-H	74 C=O

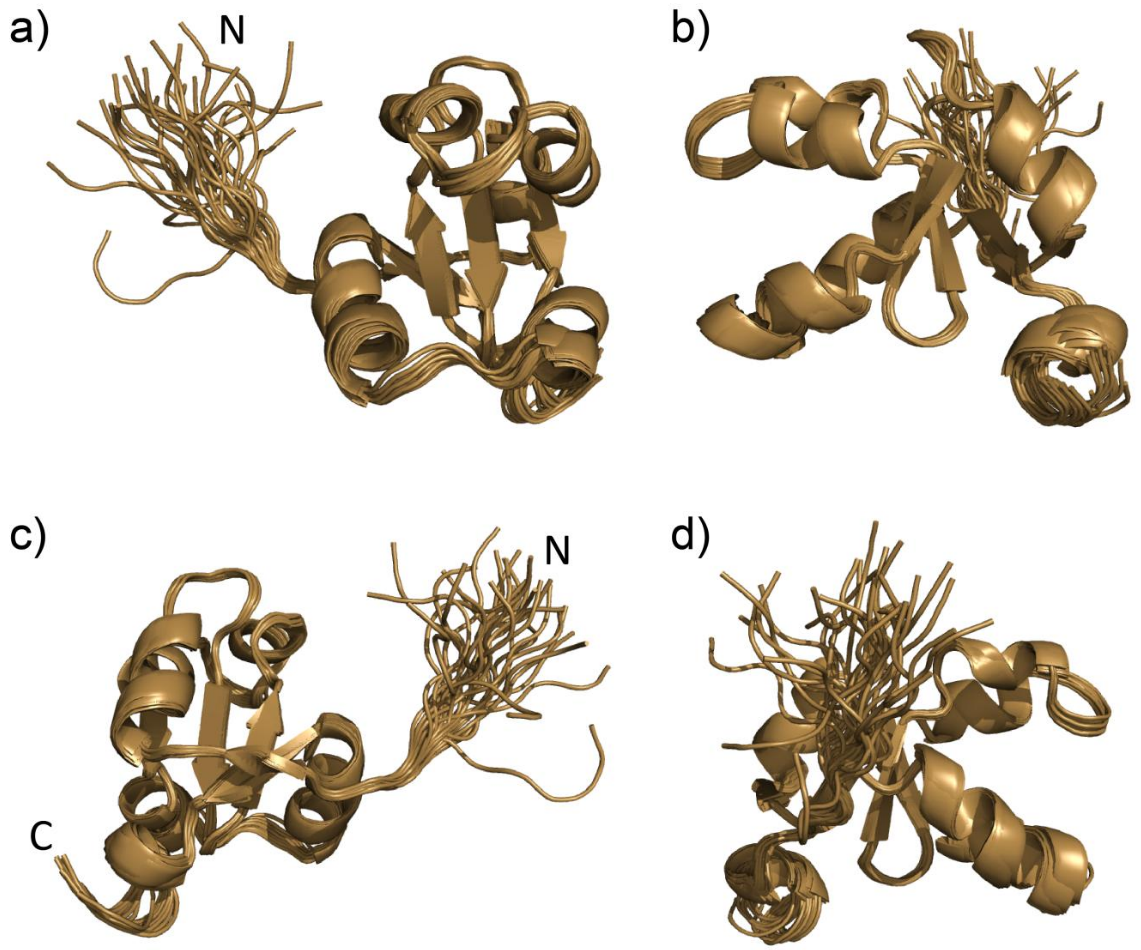

Figure 3.8 Overlay of the thirty lowest energy cyt b_5 structures generated from CYANA 2.1 based on the NMR restraints in Table 3.2. The backbone RMSD (K7-R89) is 0.32 ± 0.10 Å. Only residues from the N-terminus and the structured soluble domain are shown. Because the linker had no restraints and was completely unstructured, the RMSD of the linker region is very high and was therefore omitted from the figure.

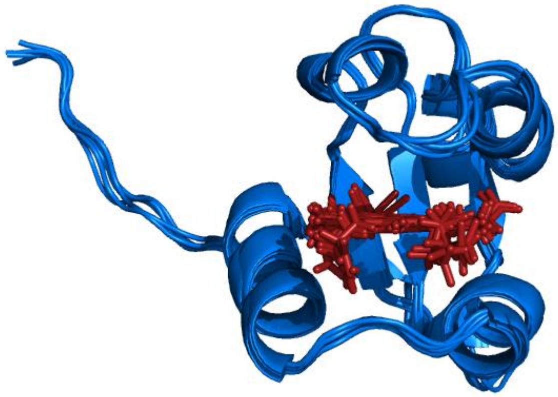

Figure 3.9 Overlay of the five lowest energy structures obtained from docking the heme (type B) molecule into the NMR structure of cyt b_5, using HADDOCK[63,64]. The restraints can be found in Table 3.1. No violations were obtained in these HADDOCK simulations. The 23 lowest energy structures were deposited into the Protein Data Bank with code 2M33.

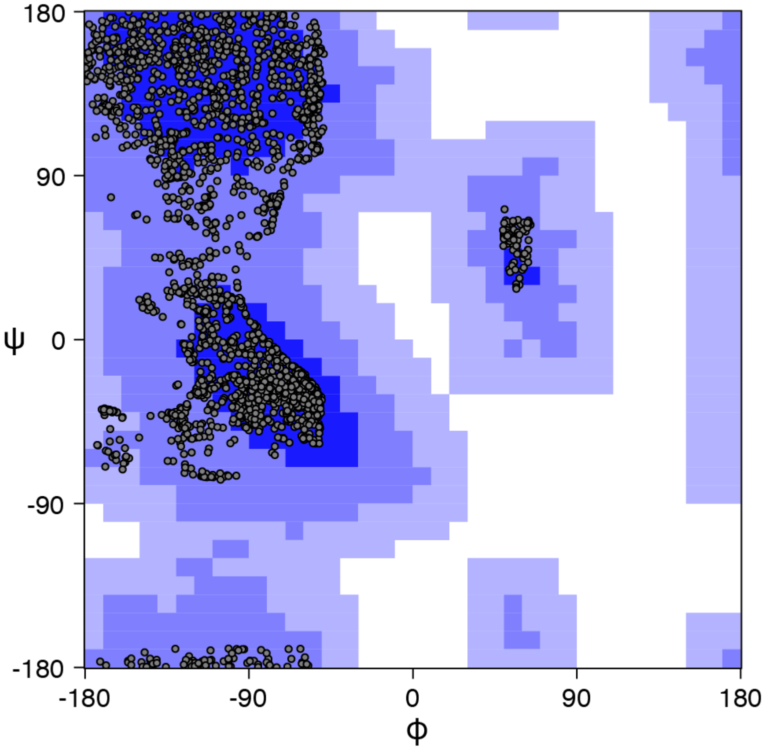

Figure 3.10 Ramachandran plot for the NMR structure of full-length cyt b_5 (M1-D134) in DPC micelles, produced by CYANA 2.1.[58]

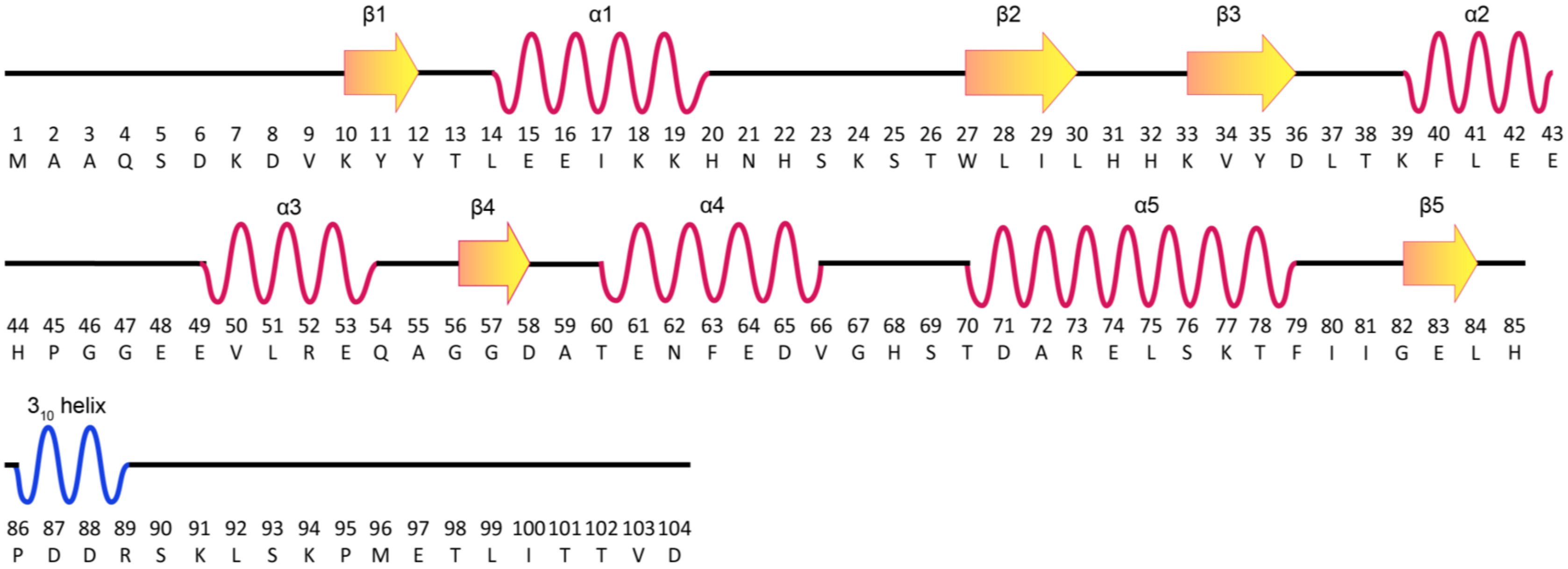
β1
α1
β2
β3
α2
1 2 3 4 5 6 7 8 9 10 11 12 13 14 15 16 17 18 19 20 21 22 23 24 25 26 27 28 29 30 31 32 33 34 35 36 37 38 39 40 41 42 43
M A A Q S D K D V K Y Y T L E E I K K H N H S K S T W L I L H H K V Y D L T K F L E E
α3
β4
α4
α5
β5
44 45 46 47 48 49 50 51 52 53 54 55 56 57 58 59 60 61 62 63 64 65 66 67 68 69 70 71 72 73 74 75 76 77 78 79 80 81 82 83 84 85
H P G G E E V L R E Q A G G D A T E N F E D V G H S T D A R E L S K T F I I G E L H
3₁₀ helix
86 87 88 89 90 91 92 93 94 95 96 97 98 99 100 101 102 103 104
P D D R S K L S K P M E T L I T T V D

Figure 3.11 Sequence and secondary structure of the soluble domain of full-length rabbit cyt b$_5$, incorporated in DPC micelles, solved by solution NMR and generated by CYANA 2.1. The secondary structure boundaries were defined by MOLMOL[72] and the observed presence/absence of NOEs.

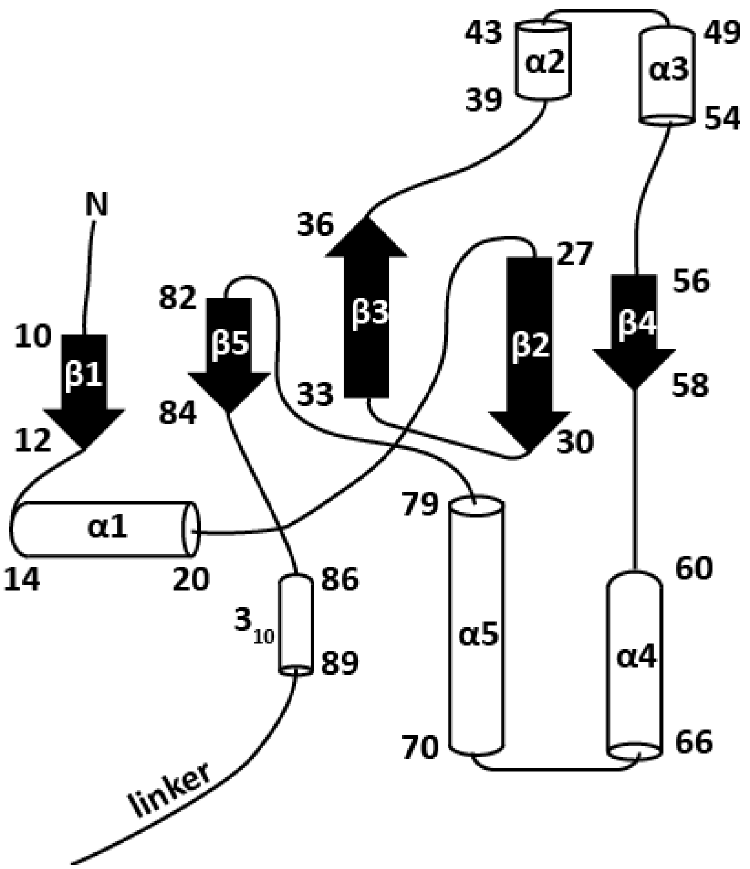
43
α2
39
49
α3
54
N
36
27
β3
β2
56
β4
82
β5
10
β1
33
58
84
12
30
79
α1
14
20
86
3_{10}
89
60
α5
α4
70
66
linker

Figure 3.12 Simplified schematic diagram of the cyt b$_5$ structure showing the different secondary structure elements and how they are connected. Residues K39-Q54 serve as the upper cleft and residues T60-F79 serve as the lower cleft; the heme is coordinated by H44 and H68. The β-strands K33-D36, W27-L30 and G56-D58 serve as the back of the heme binding pocket. All secondary structure elements on the left of the diagram are either in the posterior of the cyt b$_5$ structure or the bottom of cyt b$_5$ (residue L84 to linker).

Table 3.4 β-turns present in full-length cyt b$_5$ structure solved by NMR.

Residues	β-turn type
I29-H32	Type II
L37-F40	Type I
E43-G46	Type VIa
Q54-G57	Type II

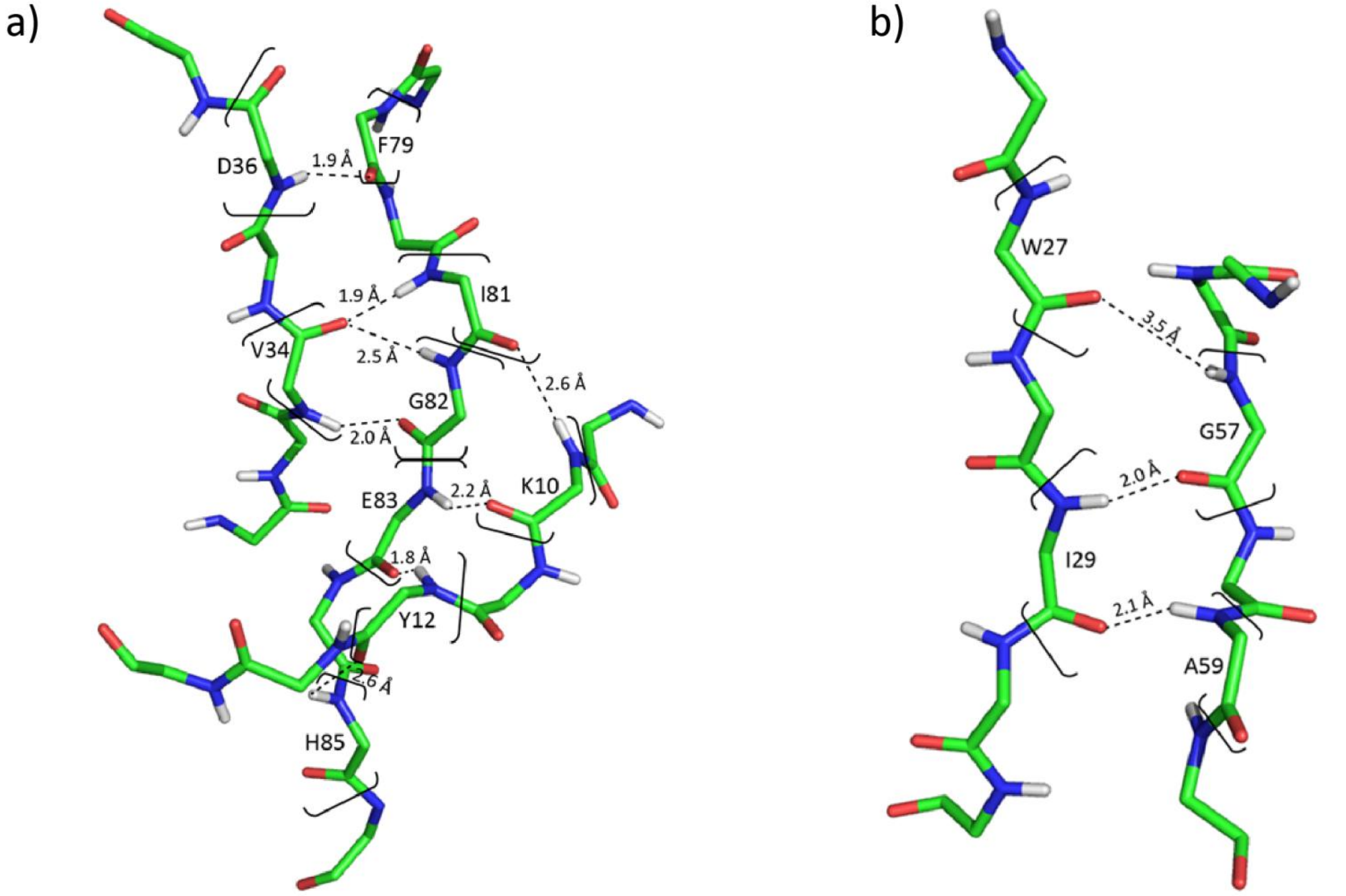
a)
D36
1.9 Å
F79
1.9 Å
I81
V34
2.5 Å
G82
2.6 Å
2.0 Å
E83
2.2 Å
K10
1.8 Å
Y12
2.6 Å
H85
b)
W27
3.5 Å
G57
2.0 Å
I29
2.1 Å
A59

Figure 3.13 All β-strands present in the structure of wild-type cyt b_5, showing the likely hydrogen bonds. In red: oxygen, blue: nitrogen, green: carbon and white: hydrogen. This figure was generated with PyMOL[59].

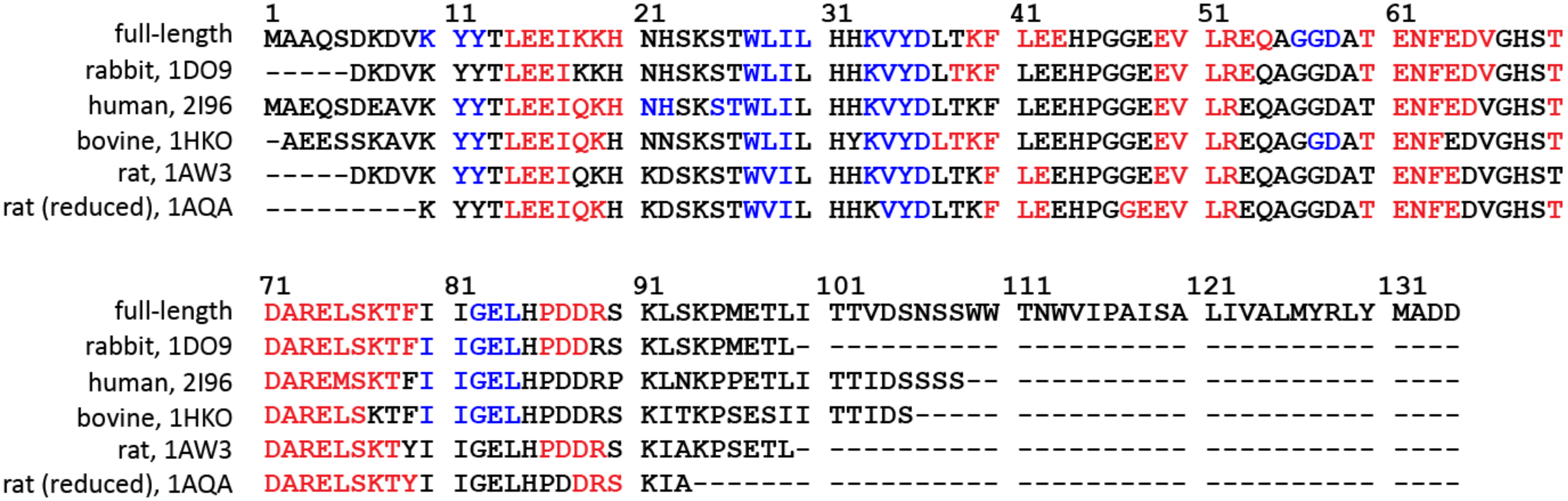

```
                      1          11         21         31         41         51         61
         full-length  MAAQSDKDVK YYTLEEIKKH NHSKSTWLIL HHKVYDLTKF LEEHPGGEEV LREQAGGDAT ENFEDVGHST
       rabbit, 1DO9   -----DKDVK YYTLEEIKKH NHSKSTWLIL HHKVYDLTKF LEEHPGGEEV LREQAGGDAT ENFEDVGHST
        human, 2I96   MAEQSDEAVK YYTLEEIQKH NHSKSTWLIL HHKVYDLTKF LEEHPGGEEV LREQAGGDAT ENFEDVGHST
       bovine, 1HKO   -AEESSKAVK YYTLEEIQKH NNSKSTWLIL HYKVYDLTKF LEEHPGGEEV LREQAGGDAT ENFEDVGHST
          rat, 1AW3   -----DKDVK YYTLEEIQKH KDSKSTWVIL HHKVYDLTKF LEEHPGGEEV LREQAGGDAT ENFEDVGHST
rat (reduced), 1AQA   ---------K YYTLEEIQKH KDSKSTWVIL HHKVYDLTKF LEEHPGGEEV LREQAGGDAT ENFEDVGHST

                      71         81         91         101        111        121        131
         full-length  DARELSKTFI IGELHPDDRS KLSKPMETLI TTVDSNSSWW TNWVIPAISA LIVALMYRLY MADD
       rabbit, 1DO9   DARELSKTFI IGELHPDDRS KLSKPMETL- ---------- ---------- ---------- ----
        human, 2I96   DAREMSKTFI IGELHPDDRP KLNKPPETLI TTIDSSSS-- ---------- ---------- ----
       bovine, 1HKO   DARELSKTFI IGELHPDDRS KITKPSESII TTIDS----- ---------- ---------- ----
          rat, 1AW3   DARELSKTYI IGELHPDDRS KIAKPSETL- ---------- ---------- ---------- ----
rat (reduced), 1AQA   DARELSKTYI IGELHPDDRS KIA------- ---------- ---------- ---------- ----
```

Figure 3.14 Sequence and structure comparison of our NMR structure of cyt b_5 with other NMR structures of cyt b_5. Wild-type, ferric cyt b_5 (unless otherwise noted) from the following species: rabbit (1DO9)[20]**,** human (2I96)[21], bovine (1HKO)[22], rat (1AW3)[23] and rat (reduced) (1AQA)[24]. Secondary structure elements are color coded, with red for α-helices and blue for β-sheets. The sequence alignment was performed by Sequence Annotated by Structure (SAS)[73] and then trimmed down to cover fewer PDB structures (some of the PDB structures were superseded by more recent structures and were therefore removed).

3.4.3 Backbone relaxation measurements

The R_1, R_2 and ^{15}N-{^{1}H} NOE values were measured for full-length ^{13}C, ^{15}N, ^{2}H-labeled cyt b_5 in DPC micelles at 900 MHz (Figure 3.15). In the following analyses, a deviation greater than one standard deviation from the mean (for the entire range of the measurement ± its respective fitting error) was deemed significant. Residues with a fitting error greater than 15% were omitted from all analyses. The average R_1 value for all observed cyt b_5 residues (K7-D104) in DPC micelles was 1.06 ± 0.35 s^{-1}. This value is much smaller than the average R_1 values obtained for truncated rat (both reduced and oxidized), bovine and human cyt b_5 of 1.9 ± 0.1, 1.92 ± 0.07 and 1.87 ± 0.25 s^{-1}, respectively.[21,74,75] Since the cyt b_5 under study here was full-length, the dynamics of the N-terminus and linker regions, in addition to the soluble domain, could be monitored. N-terminal residues K7-D8 and the assigned linker residues (L92, S93, M96-L99 and T101-D104) had significantly higher R_1 values (averages of 1.96 ± 0.07 s^{-1} and 1.74 ± 0.09 s^{-1}, respectively) than all other residues in cyt b_5. Residue E49 also appeared to have a large R_1 value (1.54 s^{-1}) but the accuracy of this measurement was low (error of 25%). If we consider only the compact soluble domain (K10-R89), the average R_1 value for cyt b_5 residues was 0.925 ± 0.157 s^{-1}; this value is more than half the value obtained for truncated human cyt b_5 (1.87 ± 0.24 s^{-1})[21]. Within this subset, a few residues had R_1 values significantly larger than others (> 1.082 s^{-1} for their entire error range): H22 (1.28 s^{-1}), K24 (1.25 s^{-1}), D71 (1.21 s^{-1}) and L84 (1.26 s^{-1}); these residues are located in loops and at/near the end of a secondary structure element and all these residues (except for L84) were shown to be dynamic via molecular dynamics (MD) simulations.[76] Within the same subset, residues with R_1 values significantly lower (< 0.768 s^{-1} for their entire error range) were identified as L28 (0.710 s^{-1}), E42 (0.724 s^{-1}), E43 (0.684 s^{-1}), A55 (0.712 s^{-1}) and V66 (0.732 s^{-1}); these residues are in secondary structure elements, except for A55 which is a one-residue gap between secondary structure elements and therefore cannot experience high mobility. It should be noted that A55 was hypothesized to be dynamic from MD simulations but is shown here to less dynamic based on R_1 measurements.[76]

The average R_2 value for all observed cyt b_5 residues (K7-D104) in DPC micelles was 23.0 ± 4.0 s^{-1}. This value is more than double the value obtained for truncated ferrous rat cyt b_5 (~8 s^{-1}),[69] truncated ferric bovine cyt b_5 (9.44 ± 0.93 s^{-1})[74] and truncated human cyt b_5 (7.4 ± 1.7 s^{-1})[21]. The R_2 values were significantly lower for K7-V9 (average of 12.3 ± 2.2 s^{-1}) and linker residues S93, E97-L99 and T102-D104 (average of 16.2 ± 0.5 s^{-1}). If we consider only the compact soluble domain (K10-R89), the average R_2 value was still around the same magnitude, at 24.2 ± 2.7 s^{-1}. Within this subset, K10 (19.8 s^{-1}), E42 (19.3 s^{-1}), E43 (19.6 s^{-1}), H44 (19.8 s^{-1}) and G67 (20.1 s^{-1}) had significantly lower R_2 values (< 21.5 s^{-1} for their entire error range). Within this same subset, D87 (33.4 s^{-1}) and D88 (30.3 s^{-1}) had significantly higher (> 26.9 s^{-1} for their entire error range) R_2 values.

The paramagnetic Fe(III) is expected to have a negligible effect on the ^{15}N relaxation rates of any residue farther than 7.0 Å from the Fe(III) of cyt b_5.[75,77,78] Based on our NMR structure of cyt b_5, the only backbone amide nitrogen that is within 7.0 Å from the Fe(III) is for residue S69, which is 6.98 Å away. Despite the proximity of the S69 amide nitrogen, its relaxation parameters are not different from nearby residues, although its R_2 and NOE values have relatively large errors (Figure 3.15). Other residues that have backbone amide nitrogens that are close to 7.0 Å are H44 (7.44 Å), G46 (7.67 Å), H68 (7.21 Å) and A72 (7.34 Å). None of these amide nitrogens exhibited a behavior that differed from other nearby residues and both of their rates and NOE values were close to the average values. It should be noted that the relaxation measurements of H68 could not be completed because of the large error in the peak height measurements of its resonance.

The average R_2/R_1 value was 23.6 ± 7.1 for all observed cyt b_5 residues (K7-D104) in DPC micelles. The average R_2/R_1 value for bovine cyt b_5 was 5.9 ± 0.9,[77] which is about one quarter less than what we obtained for full-length cyt b_5 incorporated in a membrane. N-terminal residues K7-K10 and linker residues L92-S93, M96-L99 and T101-D104 had R_2/R_1 values significantly lower than other residues (averages of 8.1 ± 4.2 and 10.2 ± 1.2, respectively), and none had R_2/R_1 values that were significantly higher. The N-terminus and linker residues therefore experience fast time scale motions.[79,80] Within the structured soluble domain (K10-R89), the average R_2/R_1 value was elevated at 26.5 ± 3.3. Within this subset, K10 (19.4), G67 (20.2), D71 (20.1) and L84 (19.8) had significantly lower R_2/R_1 values (their entire error range was < 23.1) because they had R_2 values on the lower end; and no residues had significantly higher R_2/R_1 values.

The average steady-state NOE value for all observed cyt b_5 residues (K7-D104) in DPC micelles was 0.80 ± 0.20. This value is similar to the one obtained for truncated bovine[74] and human[21] cyt b_5 (within the error ranges) and is typical for natively folded proteins.[46] N-terminal residues K7-K10 and linker residues S93, M96-L99 and T101-D104 had significantly lower NOE values, with averages of 0.47 ± 0.06 and 0.38 ± 0.07, respectively. The remainder of the residues (Y11-R89 and L92) had an average NOE value of 0.87 ± 0.11; this overlaps with the value for truncated human cyt b_5 of 0.75 ± 0.05.[21] Within this subset, H31 (0.70), E42 (0.69), E43 (0.60), L51 (0.65), R73 (0.61) and L75 (0.72) had significantly lower NOE values (< 0.77 for their entire error range). The N-terminal and linker residues, as well as H31, E42-R43, L51, R73 and L75 therefore have large amplitude fast internal motions. Residues L51, R73 and L75 agree with residues highlighted as dynamic by MD simulations.[76] We can highlight the additional residues H31 and E42-E43 as also having large amplitude fast internal motions.

With the TENSOR2[52] analysis, the best fit (lowest χ^2_{exp}) was obtained for the fully anisotropic rotational model ($\chi^2_{(5\%)} = 67.32$ and $\chi^2_{exp} = 61.72$). This is consistent with what was found for the TENSOR2 analysis of truncated ferrous rat cyt b_5.[69] After the Monte Carlo simulations, the axially symmetric model was accepted even at the 90% confidence level ($\chi^2_{(10\%)}$ of 63.70). The principal components of the anisotropic rotational diffusion tensor were $D_x = (1.431 \pm 0.057) \times 10^7\ s^{-1}$, $D_y = (1.477 \pm 0.054) \times 10^7\ s^{-1}$ and $D_z = (1.716 \pm 0.083) \times 10^7\ s^{-1}$. This indicates that the diffusion of cyt b_5 is best described by the prolate axially symmetric (in which D_x and D_y have similar values).[81] The diffusion tensor can also be written as $D_{\perp} = (1.452 \pm 0.044) \times 10^7\ s^{-1}$ and $D_{//} = (1.726 \pm 0.081) \times 10^7\ s^{-1}$. From the three anisotropic tensor values, $\tau_{c,eff}$ was calculated to be 10.8 ns (see formula in Eisenmann *et al.*[81]). This value is twice as large as the ones obtained for truncated rat and bovine cyt b_5, which had τ_c values of 5.0 and 4.6 ns, respectively,[74,75] and for a high concentration of truncated bovine cyt b_5 (6.7 ns).[77] As a reference, the isotropic model yields a τ_c of 10.74 ± 0.09 ns ($\chi^2_{exp} = 69.88$ and $\chi^2_{(5\%)} = 73.22$).

3.4.4 The structure of the soluble domain of cyt b_5 is unaffected by its membrane environment

The ^{1}H-^{15}N-TROSY-HSQC spectrum was also obtained for full-length cyt b_5 in 10% (w/v) DMPC/DHPC isotropic bicelles with a *q* ratio of 0.25. The majority of the spectrum was nearly identical to the one obtained in DPC micelles (Figure 3.16). The largest chemical shift changes were observed for the tryptophan side chains (NH) resonances of W109, W110 and W113 (unassigned in the spectrum, Figure 3.16). The other resonances which experienced chemical shift changes are labeled in Figure 3.17. Many of these residues are located either at the C-terminus (D133 and D134), linker residues (L92, K94, E97 and L99), and some are resonances from the minor cyt b_5 isomer (L28*, D58*, Y12* and likely more that were not conclusively assigned). Chemical shift differences were also seen for residues K18, I29, D58, A59, D65, L84, H85 and D87, which are in the structured soluble domain, but the chemical shifts of these residues appear to vary based on the sample (see Figure 3.18) and should not be interpreted to mean that these residues are affected by the membrane mimetic environment differences. Four additional residues, L14, T60, E61 and R89, also experienced shifts (Figure 3.17), but these residues were also seen as shifting between different samples of cyt b_5 in DPC micelles (data not shown).

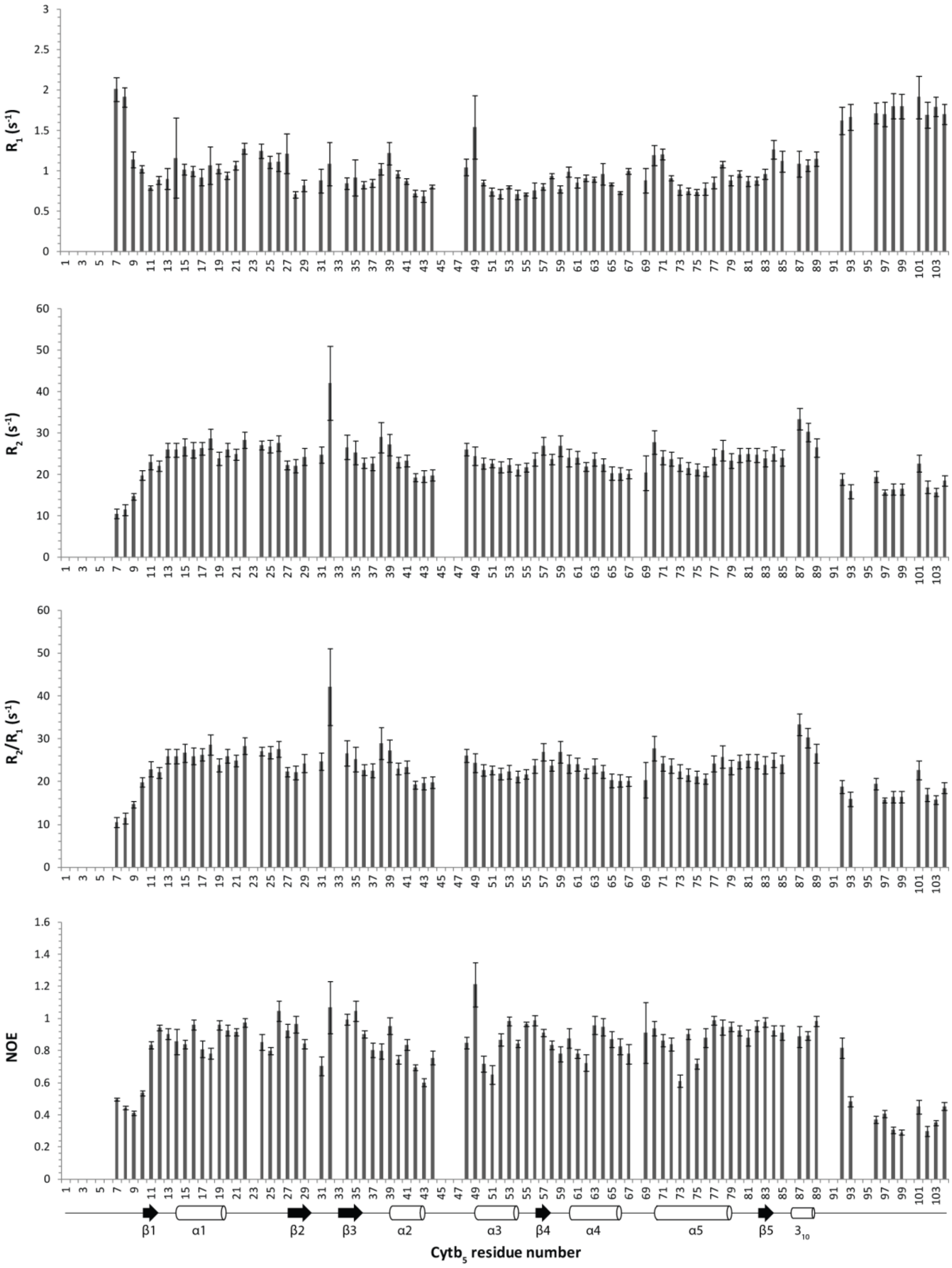

Figure 3.15 ^{15}N-R_1, -R_2, R_2/R_1 and ^{15}N-{^{1}H }-NOE relaxation parameters obtained for full-length cyt b$_5$ at 900 MHz in DPC micelles. The relaxation parameters are plotted versus residue number for R_1 (^{15}N$_x$), R_2 (^{15}N$_{x,y}$), R_2/R_1 and NOE in 45 mM DPC micelles.

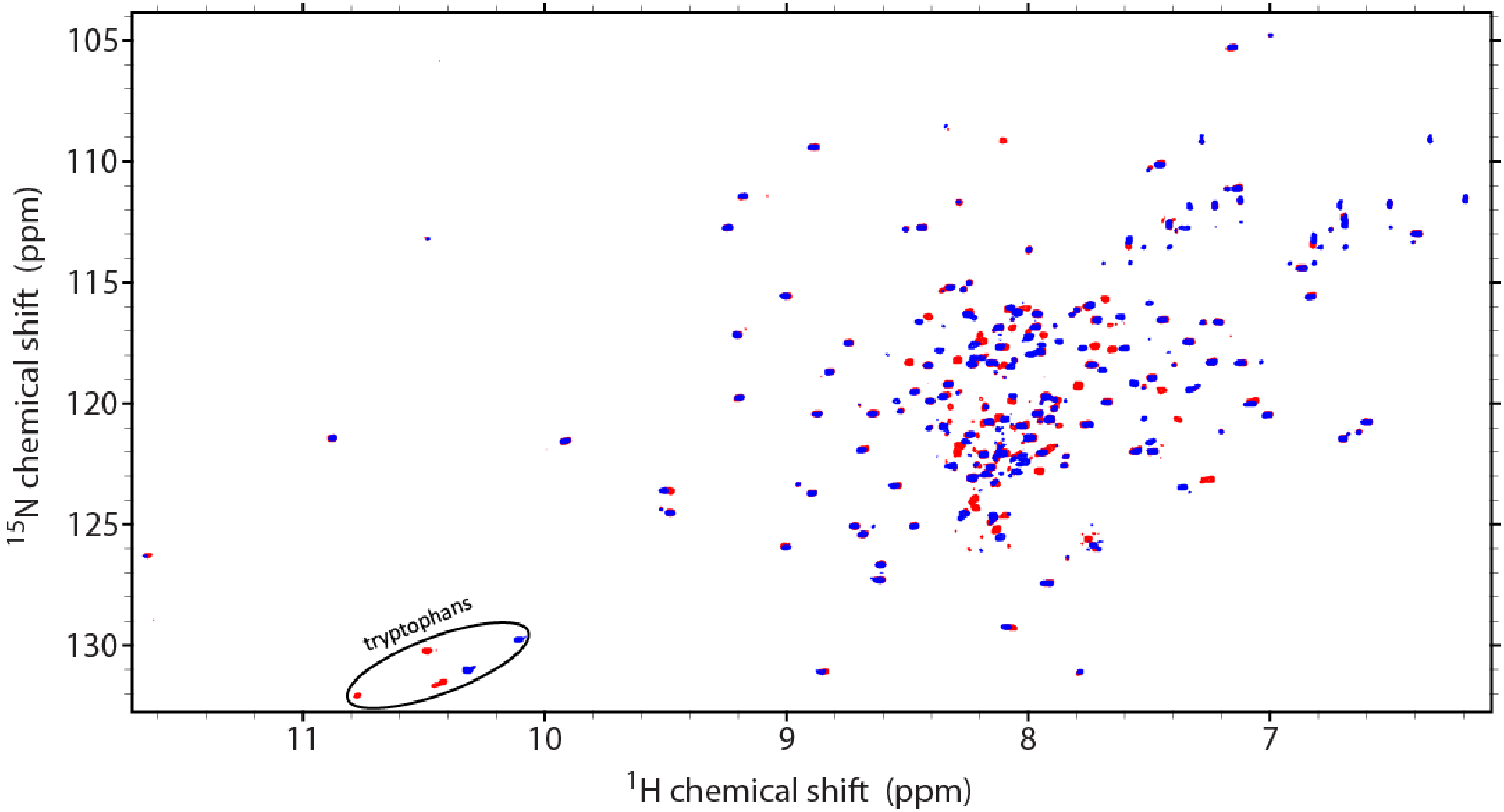

Figure 3.16 ^{1}H-^{15}N-TROSY-HSQC spectra of U-^{15}N-cyt b$_5$ in 45 mM DPC micelles (red) and 10% (w/v) DMPC/DHPC isotropic bicelles *q* = 0.25 (blue) overlaid on top. Nearly all residues exhibit the same chemical shift in both dimensions, indicating that the secondary and tertiary structures of cyt b$_5$ are similar in both membrane mimetics. Residues which appear to experience a different chemical environment are labeled in Figure 3.17.

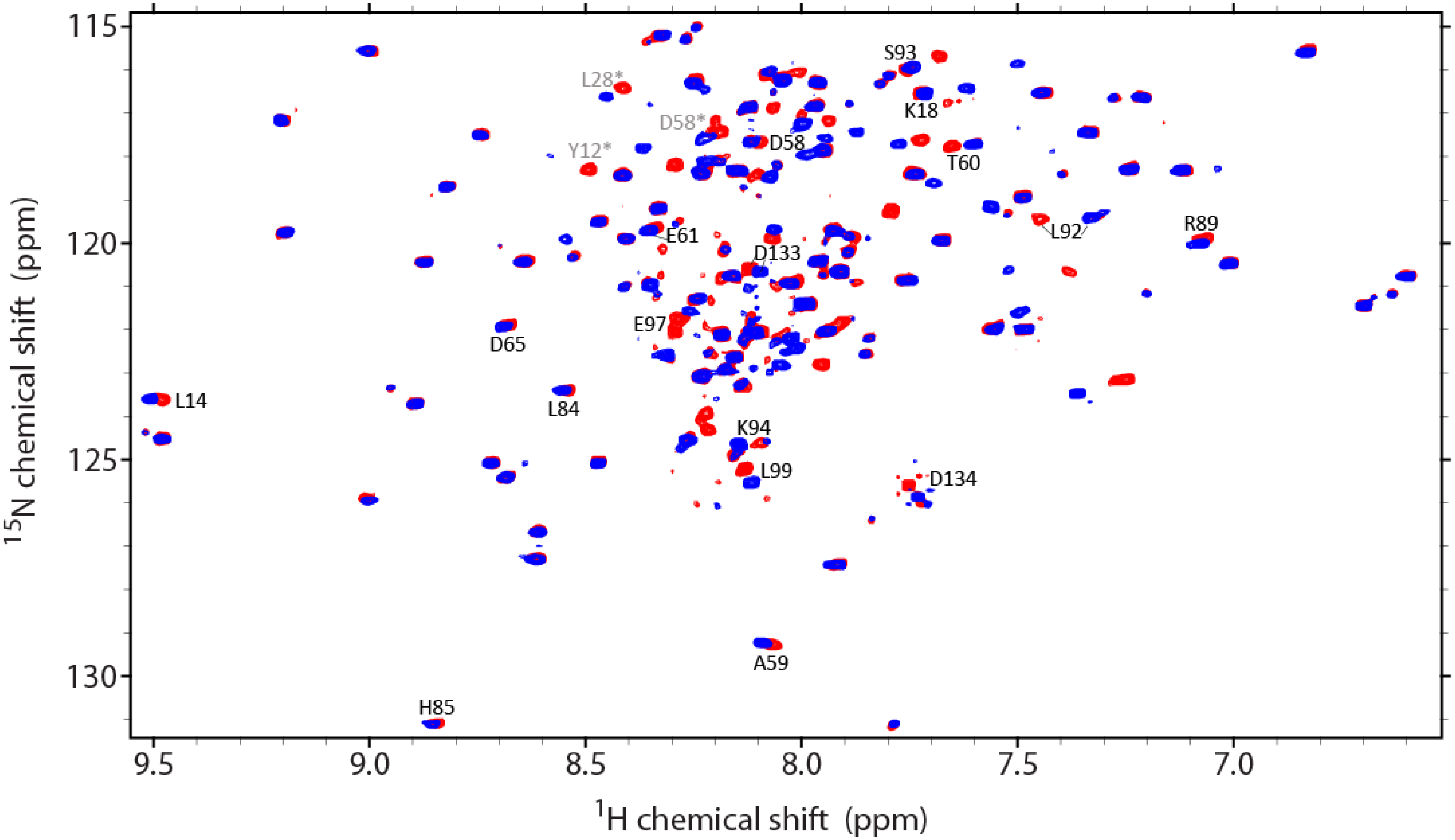

Figure 3.17 The central region of the ^{1}H-^{15}N-TROSY-HSQC spectra of U-^{15}N-cyt b_5 in 45 mM DPC micelles (red) and 10% (w/v) DMPC/DHPC isotropic bicelles *q* = 0.25 (blue) overlaid on top. The residues which experience a shift are labeled when assignment was unambiguous (Section 3.4.1). Most of the shifted residues are either at the C-terminus, the linker region (or residues adjacent to the linker), or second conformer peaks. The remaining labeled residues were also observed to shift in other spectra and their perturbations are likely not caused by the membrane mimetic.

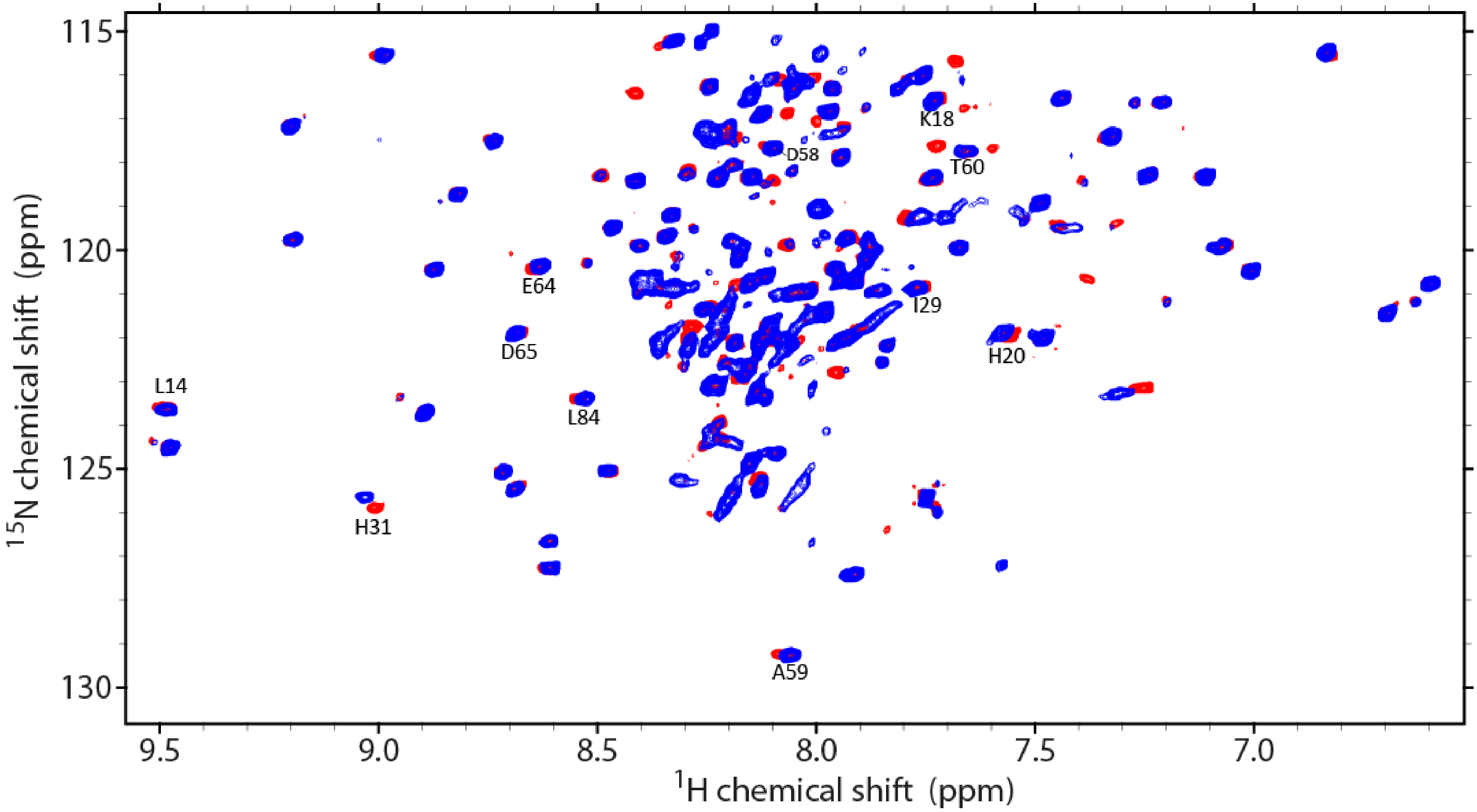

Figure 3.18 The central region of the ^{1}H-^{15}N-TROSY-HSQC spectra of two samples of cyt b_5 in DPC micelles: ^{15}N-cyt b_5 (red) and ^{13}C,^{15}N-cyt b_5 (blue) overlaid on top. This comparison shows that some of the resonances shift based on the sample conditions. H85 and D87 (not shown) are also shifted in the same way as the previous figure (Figure 3.17) and Figure 6.4 in Chapter 6, respectively.

3.4.5 Establishing the topology and structure of the transmembrane domain of full-length cyt b_5 in bicelles

As mentioned in Section 3.4.1, the resonances for residues in the TM domain of cyt b_5, reconstituted in isotropic bicelles (DMPC/DHPC) or DPC micelles, were not identified in the ^{1}H-^{15}N-TROSY-HSQC solution NMR spectra. While sequential NOE assignment could not be carried out for the residues in the transmembrane domain, ambiguous NOE assignments, without secondary structural information, were made possible for the Hα and side chain protons of residues L121 to D134 in solution NMR. A ^{1}H-^{15}N-HMQC spectrum recorded under magic angle spinning on a selectively ^{15}N-alanine labeled sample of cyt b_5 incorporated in DPC micelles displayed broad resonances for the backbone amide-NHs of the four alanines present in the TM domain of cyt b_5, along with narrow resonances observed for the alanines in the soluble domain (Figure 3.19). These data suggest that the restricted motion of the TM domain of cyt b_5 incorporated in a DPC micelle, or isotropic bicelle, causes significant broadening of the transmembrane domain resonances due to fast spin-spin relaxation. Therefore, to obtain the structure of the TM domain of cyt b_5, we employed an alternate technique of static solid-state NMR spectroscopy on uniformly ^{15}N-labeled full-length cyt b_5 incorporated in bicelles[82] composed of DMPC and DHPC lipids in a 3.5:1 molar ratio, which were magnetically-aligned in the external magnetic field.

A two-dimensional SLF NMR experiment using the HIMSELF[30] pulse sequence, which is based on the PIWIMz (polarization inversion by windowless isotropic mixing) pulse scheme, was performed on magnetically-aligned bicelles containing cyt b_5 (Figure

3.20c). The resultant 2D SLF spectrum correlates ^{15}N chemical shifts with ^{1}H-^{15}N dipolar couplings. The two-dimensional spectrum in Figure 3.20c exhibits a distinct circular PISA (polarity index slant angle)-wheel pattern of resonances between 60-100 ppm, which is indicative of an α-helical conformation and was assigned to the TM anchor of cyt b_5 based on our previous work.[30,83]

The resonances in the SLF spectrum of a membrane protein depend on the orientational constraints with respect to the external magnetic field rather than interactions between the individual residues. Therefore, it is possible to derive valuable structural constraints from the observed resonance pattern despite the lack of complete resonance assignment for the PISA wheel. The observed PISA wheel was empirically fitted[84] to determine the average tilt angle of the TM α-helix with respect to the bilayer normal. The resonance pattern was consistent with an average tilt of 15 ± 3°, in agreement with our previously published work.[30] The value of the overall order parameter of the TM domain was estimated to be 0.86. Additionally, a “structure fitting algorithm” developed by Opella and coworkers[85] was used in combination with the solid-state SLF NMR data to determine the backbone structure of the TM anchor as presented in Figure 3.20a.

3.5 Discussion

Compared to the previously published structure of rabbit cyt b_5, in which residues M1-S5 (in our sequence) and L99-D134 were truncated (PDB code 1DO9),[20] our solution NMR structure of the soluble domain of full-length rabbit cyt b_5 incorporated in DPC micelles has some key structural differences (see Figure 3.14).

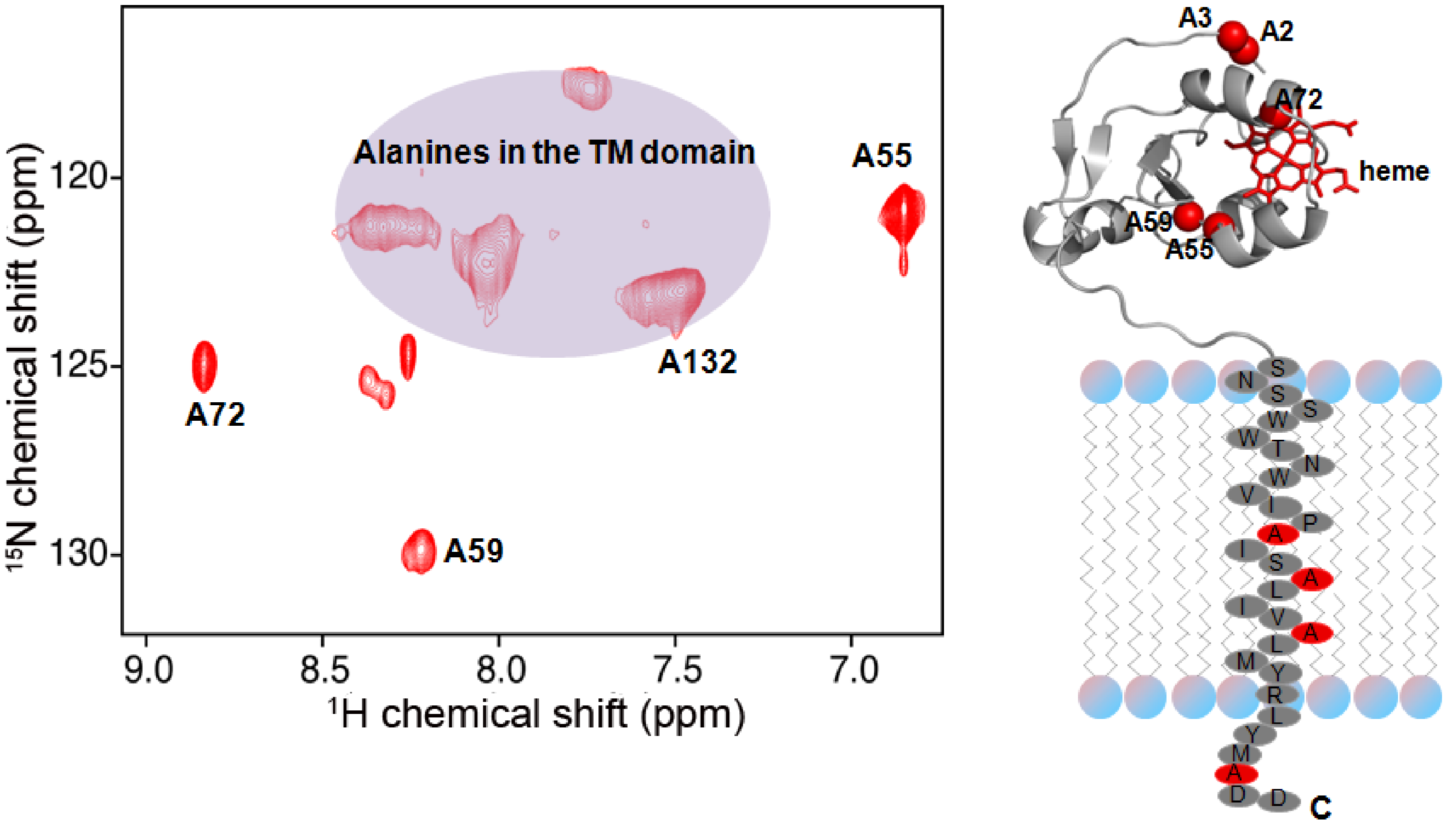

Figure 3.19 The transmembrane domain of cyt b$_5$ is visible under magic angle spinning NMR. ^{1}H-^{15}N HMQC spectrum recorded on a selectively ^{15}N-alanine labeled sample of cyt b$_5$ incorporated in DPC micelles. This spectrum was obtained from a 600 MHz Varian solid-state NMR spectrometer under a 2.5 kHz spinning speed of the sample at 37 °C using a double-resonance magic angle spinning nanoprobe.

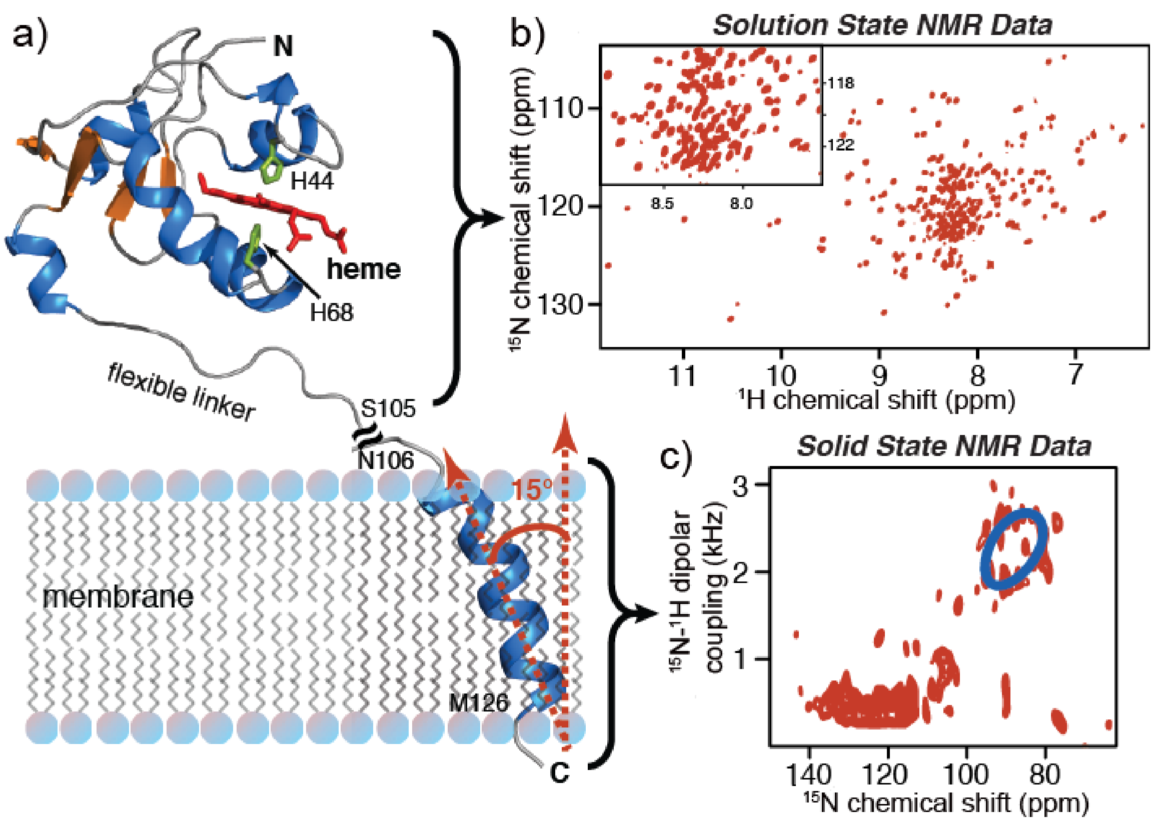
a)
N
H44
heme
H68
flexible linker
S105
N106
15°
membrane
M126
C
b)
Solution State NMR Data
110
120
130
^{15}N chemical shift (ppm)
118
122
8.5
8.0
11
10
9
8
7
^{1}H chemical shift (ppm)
c)
Solid State NMR Data
3
2
1
^{15}N-^{1}H dipolar coupling (kHz)
140
120
100
80
^{15}N chemical shift (ppm)

Figure 3.20 High-resolution NMR structure of rabbit microsomal cyt b$_5$. (a) NMR structure of full-length cyt b$_5$ obtained from a combined solution and solid-state NMR approach. The soluble heme domain structure (residues M1-S105) of full-length cyt b$_5$ was solved in DPC micelles by solution NMR, with a backbone RMSD of 0.32 Å. The transmembrane domain structure (residues N106-M126) of full-length cyt b$_5$ was determined in aligned DMPC/DHPC bicelles using solid-state NMR spectroscopy. The structures of the soluble domain and TM domain were combined to make this figure. (b) A ^{1}H-^{15}N-TROSY-HSQC spectrum of uniformly ^{15}N, ^{13}C and ^{2}H-labeled cyt b$_5$ in micelles exhibiting well-resolved peaks. (c) 2D HIMSELF spectrum of uniformly ^{15}N-labeled cyt b$_5$ reconstituted in aligned DMPC/DHPC bicelles. The blue ring presents the best-fit for the helical wheel pattern of resonances from the α-helical transmembrane domain of cyt b$_5$.

One of the differences is the presence of β1 (K10-Y12) in our structure, which is absent in 1DO9[20]; this is likely due to their truncation of residues M1-S5 which possibly causes residues D6-Y12 have more mobility, hence their lack of structure. This β1-strand is, however, found in other species (Figure 3.14), but typically does not include residue K10.[21–23] The length of α1 also varies depending on the species; in our structure, it encompasses L14-H20, which is identical to the human cyt b_5 structure[21] but three residues longer than the previous rabbit cyt b_5 structure[22]. While residues W27-I29 are generally involved in a β-strand[20–24] (labeled β2 in our case), our structure is the only one that also includes residue L30. The β3-strand (K33-D36) is identical in all structures.[20–24] Residues K39-E43 form the helix α2 in our structure, which is twice as long as the helix observed in the previous rabbit cyt b_5 structure;[20] the rat structures do, however, include L41-E42 in this helix.[23,24] The third α-helix (α3) covers E49-Q54 in our structure, which is one residue longer than the previous rabbit cyt b_5 structure.[20] Helices α4 and α5 in our structure were identical to those found in the previous rabbit cyt b_5 structure[20] and encompasses residues T60-V66 and T70-F79, respectively; their lengths vary for other species.[21–24] The β4-strand (G56-D58) is absent in most of the other cyt b_5 structures[20,21,23,24] except for bovine cyt b_5 for which it only includes G57-D58.[22] The β5-strand, which encompasses G82-L84 in our structure, appears to be longer in other structures[20–22] and absent in the rat cyt b_5 structures[23,24]. The 3_{10} helix (P86-R89) is one residue shorter in the previous rabbit structure[20] but is absent in bovine[22] and human[21] cyt b_5.

The linker region (S90-D104), which connects the cytosolic heme domain to the α-helical transmembrane anchor, was previously characterized as random coil for truncated microsomal rabbit cyt b_5;[20] however, the sequence was truncated at linker residue L99. An extended unstructured conformation of the linker was also observed for the NMR structures of cyt b_5 for which the sequences were truncated following the linker region (and therefore contained the entire linker).[21,22] We show here that for full-length cyt b_5, incorporated in DPC micelles, the linker region was also found to be random coil. Neither intra- nor inter-residue NOEs were observed for most of the linker residues (S90-D104) due to the rapid solvent exchange at those amide positions. A cyt b_5 linker region of at least 6-8 amino acids has been shown to be necessary to enable formation of a functional complex between cyt b_5 and its full-length redox partner cyt P450.[2] The extended form of the cyt b_5 linker region, presented in this chapter, likely provides the flexibility and orientational freedom necessary for efficient complex formation with its redox partners.[2]

The dynamics of full-length cyt b_5 were observed to be vastly different than for previously characterized truncated cyts b_5. For full-length cyt b_5, the rates for R_1 were much smaller and those for R_2 were much larger than all previously reported values for truncated cyt b_5.[69,74,75,77,78] Statistical analyses of the R_1, R_2, R_2/R_1 and NOE values were performed and the dynamics of different regions of cyt b_5 were established. The unstructured N-terminal and linker region residues were seen as having increased mobility, on a fast time scale, compared to the rest of the soluble domain of cyt b_5 (high R_1, low R_2 and low NOE).[86] This high mobility of the cyt b_5 linker region must also contribute to the ability of cyt b_5 to interact successfully with its redox partners. Low R_2 values, as observed for the N-terminus, are typical for the ends of a protein, even for unfolded proteins.[87] Within the structured soluble domain, higher dynamics were seen for the α1-β2 loop (H22 and K24), which is involved in the cleft opening, on top of cyt b_5, proposed by MD simulations (Figure 5.1).[76] Residue D71 was also shown to have high internal motions (large R_1), which agrees with MD simulations.[76] Additionally, L84 was found to have fast time scale motions (large R_1), which had not been identified in previous studies; this residue is found at the end of the β5-strand. R_1 measurements also indicated that the motion was found to be most restricted for the short one-residue link between α3 and β4, in addition to backbone nitrogens in secondary structures. Interestingly, the 3_{10} helix right before the linker region was shown to be flexible on the ms-μs time scale (high R_2). The only disagreement with the previous MD simulations[76] was for residue A55, which was not seen as dynamic on any time scale for full-length cyt b_5 and in fact experienced less motions than the remainder of the soluble domain of cyt b_5 (low R_1). The paramagnetic Fe(III) center did not have a discernible effect on the relaxation rates of any observable cyt b_5 residues.

For molecules of the size of cyt b_5 (15 kDa), ^{15}N-{^{1}H} steady-state NOE is more sensitive to internal dynamics than R_1 and R_2 by a factor of 5 and 30, respectively.[46] By analyzing the heteronuclear NOE data, additional residues of the soluble domain of full-length cyt b_5 (compared to the R_1 and R_2 analysis) were identified as having large amplitude fast internal motions: the β2-β3 loop (H31), helices α2 (E42-E43), α3 (L51) and α5 (R73 and L75). The latter two regions agree with previous studies showing higher mobility of those regions in truncated rat cyt b_5[75] and via MD simulations[76]. The dynamic nature of helix α2 (found here) is congruent with previous studies that have referred to this helix as "poorly defined" for bovine cyt b_5.[22] Interestingly, H31 was found to be highly dynamic despite its location in the short gap between β2 and β3.

The soluble domain of cyt b_5 was found to have a prolate axially symmetric diffusion tensor, and the effective correlation time (with a value of 10.8 ns) was double the values obtained for truncated variants.[74,75] The increase in correlation time is likely, in part, caused by the hydrodynamic drag coming from the linker,[88] which affects the reorientation of the soluble domain.

3.6 Conclusion

Here we have presented the first full-length structure of rabbit cyt b_5 incorporated in a membrane mimetic (DPC micelles or lipid bicelles) obtained using a combination of solution and solid-state NMR spectroscopy. The heme domain and linker region structures were established using solution NMR, and the transmembrane domain structure and topology was determined using solid-state NMR; full-length cyt b_5 was used for all NMR measurements. The structure of the soluble domain of full-length rabbit cyt b_5, incorporated in DPC micelles, was found to be similar but not identical to the previously reported structure of truncated rabbit cyt b_5. Our NMR structure has additional β-strands (β1 and β4), longer (α1, β2, α2 and α3) and shorter (β5 and 3_{10} helix) segments for some of the secondary structure elements and only three identical segments (β3, α4 and α5). The N-terminus and linker residues were found to be unstructured and very flexible via relaxation measurements. Only few loop residues (in the β2-β3 and α1-β2 loops) were defined as flexible; all others were as rigid as the structured regions. The dynamics of full-length cyt b_5, highlighted by the relaxation measurements, were observed to be vastly different than for previously characterized truncated cyt b_5, which lack the interaction with the membrane mimetic. The overall tumbling of the soluble domain of full-length cyt b_5 was found to be anisotropic and its correlation time was found to be much larger than for truncated cyt b_5. These differences in the relaxation parameters and tumbling of cyt b_5 could be responsible for the inability of truncated cyt b_5 to form a functional complex with cyt P450. The overall structure of the soluble domain of cyt b_5 does not appear to be affected by the membrane mimetic, likely because the long flexible linker keeps the soluble domain distant from the membrane. Solid-state SLF NMR data, in combination with a "structure fitting algorithm" was used to determine the α-helical structure of the transmembrane domain of cyt b_5. The detailed knowledge of the microsomal full-length cyt b_5 structure will prove essential in understanding the interaction of cyt b_5 with its redox partners (e.g. NADH cyt b_5 reductase and cyt P450). This NMR structure of full-length microsomal ferric cyt b_5 was used in all of the following chapters.

3.7 Contributions

Le Clair prepared all figures except for the solid-state data and NOE strip plots; wrote the entire chapter; analyzed all the NOE connectivities to make the figures; verified the end points of each secondary structure element; performed the HADDOCK simulations prior to the final run; statistically analyzed all relaxation data (R_1, R_2, R_2/R_1 and NOE); performed the TENSOR2 analysis; did all comparisons between the cyt b_5

spectrum in DPC micelles versus DMPC/DHPC isotropic bicelles (and further analysis of all cyt b_5 samples in DPC micelles to check for peak shifting). Ahuja ran all solution NMR experiments. Ahuja and Vivekanandan solved the structure of the soluble domain of cytochrome b_5. Popovych performed the final HADDOCK simulation. Soong, Xu, Yamamoto and Nanga solved the structure of the TM domain. Huang analyzed the relaxation data and performed initial TENSOR2 analyses. Im expressed all cyt b_5 proteins.

3.8 References

(1) Schenkman, J. B.; Jansson, I. The many roles of cytochrome b_5. *Pharmacol. Ther.* **2003**, *97*, 139–152.

(2) Clarke, T. A.; Im, S.-C.; Bidwai, A.; Waskell, L. The role of the length and sequence of the linker domain of cytochrome b_5 in stimulating cytochrome P450 2B4 catalysis. *J. Biol. Chem.* **2004**, *279*, 36809–36818.

(3) Ito, A.; Sato, R. Proteolytic microdissection of smooth-surfaced vesicles of liver microsomes. *J. Cell Biol.* **1969**, *40*, 179–189.

(4) Vergères, G.; Waskell, L. Cytochrome b_5, its functions, structure and membrane topology. *Biochimie* **1995**, *77*, 604–620.

(5) Lederer, F. The cytochrome b_5-fold : An adaptable module. *Biochimie* **1994**, *76*, 674–692.

(6) Ozols, J. The role of microsomal cytochrome b_5 in the metabolism of ethanol, drugs and the desaturation of fatty acids. *Ann. Clin. Res.* **1976**, *8 Suppl 17*, 182–192.

(7) Napier, J. A; Sayanova, O.; Stobart, A. K.; Shewry, P. R. A new class of cytochrome b_5 fusion proteins. *Biochem. J.* **1997**, *328 (Pt 2)*, 717–718.

(8) Oshino, N.; Imai, Y.; Sato, R. A function of cytochrome b_5 in fatty acid desaturation by rat liver microsomes. *J. Biochem.* **1971**, *69*, 155–167.

(9) Strittmatter, P.; Spatz, L.; Corcoran, D.; Rogers, M. J.; Setlow, B.; Redline, R. Purification and properties of rat liver microsomal stearyl coenzyme A desaturase. *Proc. Natl. Acad. Sci. U.S.A.* **1974**, *71*, 4565–4569.

(10) Kominami, S.; Ogawa, N.; Morimune, R.; De-Ying, H.; Takemori, S. The role of cytochrome b_5 in adrenal microsomal steroidogenesis. *J. Steroid Biochem. Mol. Biol.* **1992**, *42*, 57–64.

(11) Takematsu, H.; Kawano, T.; Koyama, S.; Kozutsumi, Y.; Suzuki, A.; Kawasaki, T. Reaction mechanism underlying CMP-N-acetylneuraminic acid hydroxylation in mouse liver: formation of a ternary complex of cytochrome b_5, CMP-N-acetylneuraminic acid, and a hydroxylation enzyme. *J. Biochem.* **1994**, *115*, 381–386.

(12) Hildebrandt, A.; Estabrook, R. W. Evidence for the participation of cytochrome b_5 in hepatic microsomal mixed-function oxidation reactions. *Arch. Biochem. Biophys.* **1971**, *143*, 66–79.

(13) Juvonen, R. O.; Iwasaki, M.; Negishi, M. Roles of residues 129 and 209 in the alteration by cytochrome b_5 of hydroxylase activities in mouse 2A P450S. *Biochemistry* **1992**, *31*, 11519–11523.

(14) Yamazaki, H.; Nakano, M.; Imai, Y.; Ueng, Y. F.; Guengerich, F. P.; Shimada, T. Roles of cytochrome b_5 in the oxidation of testosterone and nifedipine by recombinant cytochrome P450 3A4 and by human liver microsomes. *Arch. Biochem. Biophys.* **1996**, *325*, 174–182.

(15) Perret, A.; Pompon, D. Electron shuttle between membrane-bound cytochrome P450 3A4 and b_5 rules uncoupling mechanisms. *Biochemistry* **1998**, *37*, 11412–11424.

(16) Dailey, H. A.; Strittmatter, P. Structural and functional properties of the membrane binding segment of cytochrome b_5. *J. Biol. Chem.* **1978**, *253*, 8203–8209.

(17) Dailey, H. A.; Strittmatter, P. Characterization of the interaction of amphipathic cytochrome b_5 with stearyl coenzyme A desaturase and NADPH:cytochrome P-450 reductase. *J. Biol. Chem.* **1980**, *255*, 5184–5189.

(18) Maghzal, G. J.; Thomas, S. R.; Hunt, N. H.; Stocker, R. Cytochrome b_5, not superoxide anion radical, is a major reductant of indoleamine 2,3-dioxygenase in human cells. *J. Biol. Chem.* **2008**, *283*, 12014–12025.

(19) Vottero, E.; Mitchell, D. A.; Page, M. J.; MacGillivray, R. T. A.; Sadowski, I. J.; Roberge, M.; Mauk, A. G. Cytochrome b_5 is a major reductant in vivo of human indoleamine 2,3-dioxygenase expressed in yeast. *FEBS Lett.* **2006**, *580*, 2265–2268.

(20) Banci, L.; Bertini, I.; Rosato, A.; Scacchieri, S. Solution structure of oxidized microsomal rabbit cytochrome b_5. Factors determining the heterogeneous binding of the heme. *Eur. J. Biochem.* **2000**, *267*, 755–766.

(21) Nunez, M.; Guittet, E.; Pompon, D.; Van Heijenoort, C.; Truan, G. NMR structure note: oxidized microsomal human cytochrome b_5. *J. Biomol. NMR* **2010**, *47*, 289–295.

(22) Muskett, F. W.; Kelly, G. P.; Whitford, D. The solution structure of bovine ferricytochrome b_5 determined using heteronuclear NMR methods. *J. Mol. Biol.* **1996**, *258*, 172–189.

(23) Arnesano, F.; Banci, L.; Bertini, I.; Felli, I. C. The solution structure of oxidized rat microsomal cytochrome b_5. *Biochemistry* **1998**, *37*, 173–184.

(24) Banci, L.; Bertini, I.; Ferroni, F.; Rosato, A. Solution structure of reduced microsomal rat cytochrome b_5. *Eur. J. Biochem.* **1997**, *249*, 270–279.

(25) Başaran, N.; Doebler, R. W.; Goldston, H.; Holloway, P. W. Effect of lipid unsaturation on the binding of native and a mutant form of cytochrome b_5 to membranes. *Biochemistry* **1999**, *38*, 15245–15252.

(26) Greenhut, S. F.; Taylor, K. M.; Roseman, M. A Tight insertion of cytochrome b_5 into large unilamellar vesicles. *Biochim. Biophys. Acta* **1993**, *1149*, 1–9.

(27) Chester, D. W.; Skita, V.; Young, H. S.; Mavromoustakos, T.; Strittmatter, P. Bilayer structure and physical dynamics of the cytochrome b_5 dimyristoylphosphatidylcholine interaction. *Biophys. J.* **1992**, *61*, 1224–1243.

(28) Holloway, P. W.; Buchheit, C. Topography of the membrane-binding domain of cytochrome b_5 in lipids by Fourier-transform infrared spectroscopy. *Biochemistry* **1990**, *29*, 9631–9637.

(29) Holloway, P. W.; Mantsch, H. H. Structure of cytochrome b_5 in solution by Fourier-transform infrared spectroscopy. *Biochemistry* **1989**, *28*, 931–935.

(30) Durr, U. H.; Yamamoto, K.; Im, S.-C.; Waskell, L.; Ramamoorthy, A. Solid-state NMR reveals structural and dynamical properties of a membrane-anchored electron-carrier protein, cytochrome b_5. *J. Am. Chem. Soc.* **2007**, *129*, 6670–6671.

(31) Pedrazzini, E.; Villa, A.; Borgese, N. A mutant cytochrome b_5 with a lengthened membrane anchor escapes from the endoplasmic reticulum and reaches the plasma membrane. *Proc. Natl. Acad. Sci. U.S.A.* **1996**, *93*, 4207–4212.

(32) Mitoma, J.; Ito, A. The carboxy-terminal 10 amino acid residues of cytochrome b_5 are necessary for its targeting to the endoplasmic reticulum. *EMBO J.* **1992**, *11*, 4197–4203.

(33) De Silvestris, M.; D'Arrigo, A.; Borgese, N. The targeting information of the mitochondrial outer membrane isoform of cytochrome b_5 is contained within the carboxyl-terminal region. *FEBS Lett.* **1995**, *370*, 69–74.

(34) Chudaev, M. V; Gilep, A. A.; Usanov, S. A. Site-directed mutagenesis of cytochrome b_5 for studies of its interaction with cytochrome P450. *Biochemistry (Mosc)* **2001**, *66*, 667–681.

(35) Chiang, J. Y. Interaction of purified microsomal cytochrome P-450 with cytochrome b_5. *Arch. Biochem. Biophys.* **1981**, *211*, 662–673.

(36) Bendzko, P.; Usanov, S. A.; Pfeil, W.; Ruckpaul, K. Role of the hydrophobic tail of cytochrome b_5 in the interaction with cytochrome P-450 LM2. *Acta Biol. Med. Ger.* **1982**, *41*, K1–K8.

(37) Vergères, G.; Waskell, L. Expression of cytochrome-b_5 in yeast and characterization of mutants of the membrane-anchoring domain. *J. Biol. Chem.* **1992**, *267*, 12583–12591.

(38) Mulrooney, S. B.; Waskell, L. High-level expression in Escherichia coli and purification of the membrane-bound form of cytochrome b_5. *Protein Expression Purif.* **2000**, *19*, 173–178.

(39) Bridges, A.; Gruenke, L.; Chang, Y. T.; Vakser, I. A.; Loew, G.; Waskell, L. Identification of the binding site on cytochrome P450 2B4 for cytochrome b_5 and cytochrome P450 reductase. *J. Biol. Chem.* **1998**, *273*, 17036–17049.

(40) Salzmann, M.; Wider, G.; Pervushin, K.; Wuthrich, K. Improved sensitivity and coherence selection for [^{15}N,^{1}H]-TROSY elements in triple resonance experiments. *J. Biomol. NMR* **1999**, *15*, 181–184.

(41) Kay, L. E.; Ikura, M.; Tschudin, R.; Bax, A. 3-Dimensional triple-resonance NMR-spectroscopy of isotopically enriched proteins. *J. Magn. Reson.* **1990**, *89*, 496–514.

(42) Harris, R. K.; Becker, E. D.; Cabral de Menezes, S. M.; Goodfellow, R.; Granger, P. NMR nomenclature: nuclear spin properties and conventions for chemical shifts. IUPAC recommendations 2001. *Magn. Reson. Chem.* **2002**, *40*, 489–505.

(43) Delaglio, F.; Grzesiek, S.; Vuister, G. W.; Zhu, G.; Pfeifer, J.; Bax, A. NMRPipe - a multidimensional spectral processing system based on unix pipes. *J. Biomol. NMR* **1995**, *6*, 277–293.

(44) Kneller, D. G.; Kuntz, I. D. UCSF Sparky - an NMR display, annotation and assignment tool. *J. Cell. Biochem.* **1993**, 254.

(45) Palmer III, A. G.; Skelton, N. J.; Chazin, W. J.; Wright, P. E.; Rance, M. Suppression of the effects of cross-correlation between dipolar and anisotropic chemical shift relaxation mechanisms in the measurement of spin-spin relaxation rates. *Mol. Phys.* **1992**, *75*, 699–711.

(46) Kay, L. E.; Torchia, D. A.; Bax, A. Backbone dynamics of proteins as studied by ^{15}N inverse detected heteronuclear NMR spectroscopy: application to staphylococcal nuclease. *Biochemistry* **1989**, *28*, 8972–8979.

(47) Farrow, N. A.; Zhang, O.; Forman-Kay, J. D.; Kay, L. E. Comparison of the backbone dynamics of a folded and an unfolded SH3 domain existing in equilibrium in aqueous buffer. *Biochemistry* **1995**, *34*, 868–878.

(48) Grzesiek, S.; Bax, A. The importance of not saturating water in protein NMR. Application to sensitivity enhancement and NOE measurements. *J. Am. Chem. Soc.* **1993**, *115*, 12593–12594.

(49) Bailey, L. K.; Campbell, L. J.; Evetts, K. A.; Littlefield, K.; Rajendra, E.; Nietlispach, D.; Owen, D.; Mott, H. R. The structure of binder of Arl2 (BART) reveals a novel G protein binding domain: implications for function. *J. Biol. Chem.* **2009**, *284*, 992–999.

(50) Lipari, G.; Szabo, A. Model-free approach to the interpretation of nuclear magnetic resonance relaxation in macromolecules. 1. Theory and range of validity. *J. Am. Chem. Soc.* **1982**, *104*, 4546–4559.

(51) Lipari, G.; Szabo, A. Model-free approach to the interpretation of nuclear magnetic resonance relaxation in macromolecules. 2. Analysis of experimental results. *J. Am. Chem. Soc.* **1982**, *104*, 4559–4570.

(52) Dosset, P.; Hus, J. C.; Blackledge, M.; Marion, D. Efficient analysis of macromolecular rotational diffusion from heteronuclear relaxation data. *J. Biomol. NMR* **2000**, *16*, 23–28.

(53) Pandey, M. K.; Vivekanandan, S.; Ahuja, S.; Pichumani, K.; Im, S.-C.; Waskell, L.; Ramamoorthy, A. Determination of ^{15}N chemical shift anisotropy from a

membrane-bound protein by NMR spectroscopy. *J. Phys. Chem. B* **2012**, *116*, 7181–7189.

(54) Sibille, N.; Favier, A.; Azuaga, A. I.; Ganshaw, G.; Bott, R.; Bonvin, A. M. J. J.; Boelens, R.; Van Nuland, N. A. J. Comparative NMR study on the impact of point mutations on protein stability of Pseudomonas mendocina lipase. *Protein Sci.* **2006**, *15*, 1915–1927.

(55) Sharpe, T.; Jonsson, A. L.; Rutherford, T. J.; Daggett, V.; Fersht, A. R. The role of the turn in beta-hairpin formation during WW domain folding. *Protein Sci.* **2007**, *16*, 2233–2239.

(56) Cornilescu, G.; Delaglio, F.; Bax, A. Protein backbone angle restraints from searching a database for chemical shift and sequence homology. *J. Biomol. NMR* **1999**, *13*, 289–302.

(57) Güntert, P.; Mumenthaler, C.; Wüthrich, K. Torsion angle dynamics for NMR structure calculation with the new program DYANA. *J. Mol. Biol.* **1997**, *273*, 283–298.

(58) Güntert, P. Automated NMR structure calculation with CYANA. *Methods Mol. Biol.* **2004**, *278*, 353–378.

(59) DeLano, W. L. The PyMOL Molecular Graphics System, Version 1.5.0.4 Schrödinger, LLC **2010**.

(60) Dvinskikh, S. V; Yamamoto, K.; Ramamoorthy, A. Heteronuclear isotropic mixing separated local field NMR spectroscopy. *J. Chem. Phys.* **2006**, *125*, 34507.

(61) Caravatti, P.; Braunschweiler, L.; Ernst, R. R. Heteronuclear correlation spectroscopy in rotating solids. *Chem. Phys. Lett.* **1983**, *100*, 305–310.

(62) Fung, B. M.; Khitrin, A. K.; Ermolaev, K. An improved broadband decoupling sequence for liquid crystals and solids. *J. Magn. Reson.* **2000**, *142*, 97–101.

(63) De Vries, S. J.; Van Dijk, M.; Bonvin, A. M. J. J. The HADDOCK web server for data-driven biomolecular docking. *Nat. Protoc.* **2010**, *5*, 883–897.

(64) De Vries, S. J.; Van Dijk, A. D.; Krzeminski, M.; Van Dijk, M.; Thureau, A.; Hsu, V.; Wassenaar, T.; Bonvin, A. M. HADDOCK versus HADDOCK: new features and performance of HADDOCK2.0 on the CAPRI targets. *Proteins* **2007**, *69*, 726–733.

(65) La Mar, G. N.; Burns, P. D.; Jackson, J. T.; Smith, K. M.; Langry, K. C.; Strittmatter, P. Proton magnetic resonance determination of the relative heme orientations in

disordered native and reconstituted ferricytochrome b_5. Assignment of heme resonances by deuterium labeling. *J. Biol. Chem.* **1981**, *256*, 6075–6079.

(66) Keller, R. M.; Wüthrich, K. Structural study of the heme crevice in cytochrome b_5 based on individual assignments of the ^{1}H-NMR lines of the heme group and selected amino acid residues. *Biochim. Biophys. Acta* **1980**, *621*, 204–217.

(67) Keller, R.; Groudinsky, O.; Wüthrich, K. Contact-shifted resonances in the ^{1}H NMR spectra of cytochrome b_5 Resonance identification and spin density distribution in the heme group. *Biochim. Biophys. Acta* **1976**, *427*, 497–511.

(68) McLachlan, S. J.; La Mar, G. N.; Burns, P. D.; Smith, K. M.; Langry, K. C. ^{1}H-NMR assignments and the dynamics of interconversion of the isomeric forms of cytochrome b_5 in solution. *Biochim. Biophys. Acta* **1986**, *874*, 274–284.

(69) Dangi, B.; Sarma, S.; Yan, C.; Banville, D. L.; Guiles, R. D. The origin of differences in the physical properties of the equilibrium forms of cytochrome b_5 revealed through high-resolution NMR structures and backbone dynamic analyses. *Biochemistry* **1998**, *37*, 8289–8302.

(70) Zhang, Q.; Cao, C.; Wang, Z.-Q.; Wang, Y.-H.; Wu, H.; Huang, Z.-X. The comparative study on the solution structures of the oxidized bovine microsomal cytochrome b_5 and mutant V45H. *Protein Sci.* **2004**, *13*, 2161–2169.

(71) Lee, K. B.; La Mar, G. N.; Kehres, L. A.; Fujinari, E. M.; Smith, K. M.; Pochapsky, T. C.; Sligar, S. G. ^{1}H NMR study of the influence of hydrophobic contacts on protein-prosthetic group recognition in bovine and rat ferricytochrome b_5. *Biochemistry* **1990**, *29*, 9623–9631.

(72) Koradi, R.; Billeter, M.; Wüthrich, K. MOLMOL: a program for display and analysis of macromolecular structures. *J. Mol. Graphics* **1996**, *14*, 51–55.

(73) Milburn, D.; Laskowski, R. A; Thornton, J. M. Sequences annotated by structure: a tool to facilitate the use of structural information in sequence analysis. *Protein Eng.* **1998**, *11*, 855–859.

(74) Kelly, G. P.; Muskett, F. W.; Whitford, D. Analysis of backbone dynamics in cytochrome b_5 using ^{15}N-NMR relaxation measurements. *Eur. J. Biochem.* **1997**, *245*, 349–354.

(75) Banci, L.; Bertini, I.; Cavazza, C.; Felli, I. C.; Koulougliotis, D. Probing the backbone dynamics of oxidized and reduced rat microsomal cytochrome b_5 via ^{15}N rotating

frame NMR relaxation measurements: biological implications. *Biochemistry* **1998**, *37*, 12320–12330.

(76) Storch, E. M.; Daggett, V. Molecular dynamics simulation of cytochrome b_5: implications for protein-protein recognition. *Biochemistry* **1995**, *34*, 9682–9693.

(77) Worrall, J. A. R.; Liu, Y.; Crowley, P. B.; Nocek, J. M.; Hoffman, B. M.; Ubbink, M. Myoglobin and cytochrome b_5: a nuclear magnetic resonance study of a highly dynamic protein complex. *Biochemistry* **2002**, *41*, 11721–11730.

(78) Dangi, B.; Blankman, J. I.; Miller, C. J.; Volkman, B. F.; Guiles, R. D. Contribution of backbone dynamics to entropy changes occurring on oxidation of cytochrome b_5. Can redox linked changes in hydrogen bond networks modulate reduction potentials? *J. Phys. Chem. B* **1998**, *102*, 8201–8208.

(79) Habazettl, J.; Myers, L. C.; Yuan, F.; Verdine, G. L.; Wagner, G. Backbone dynamics, amide hydrogen exchange, and resonance assignments of the DNA methylphosphotriester repair domain of Escherichia coli Ada using NMR. *Biochemistry* **1996**, *35*, 9335–9348.

(80) d'Auvergne, E. J.; Gooley, P. R. Set theory formulation of the model-free problem and the diffusion seeded model-free paradigm. *Mol. Biosyst.* **2007**, *3*, 483–494.

(81) Eisenmann, A.; Schwarz, S.; Prasch, S.; Schweimer, K.; Rösch, P. The *E. coli* NusA carboxy-terminal domains are structurally similar and show specific RNAP- and λN interaction. *Protein Sci.* **2005**, *14*, 2018–2029.

(82) Sanders, C. R.; Hare, B. J.; Howard, K. P.; Prestegard, J. H. Magnetically-oriented phospholipid micelles as a tool for the study of membrane-associated molecules. *Prog. Nucl. Magn. Reson. Spectrosc.* **1994**, *26*, 421–444.

(83) Soong, R.; Smith, P. E.; Xu, J.; Yamamoto, K.; Im, S. C.; Waskell, L.; Ramamoorthy, A. Proton-evolved local-field solid-state NMR studies of cytochrome b_5 embedded in bicelles, revealing both structural and dynamical information. *J. Am. Chem. Soc.* **2010**, *132*, 5779–5788.

(84) Denny, J. K.; Wang, J.; Cross, T. A.; Quine, J. R. PISEMA powder patterns and PISA wheels. *J. Magn. Reson.* **2001**, *152*, 217–226.

(85) Nevzorov, A. A.; Opella, S. J. Structural fitting of PISEMA spectra of aligned proteins. *J. Magn. Reson.* **2003**, *160*, 33–39.

(86) Calligari, P. A.; Salgado, G. F.; Pelupessy, P.; Lopes, P.; Ouazzani, J.; Bodenhausen, G.; Abergel, D. Insights into internal dynamics of 6-phosphogluconolactonase

from Trypanosoma brucei studied by nuclear magnetic resonance and molecular dynamics. *Proteins* **2012**, *80*, 1196–1210.

(87) Schwalbe, H.; Fiebig, K. M.; Buck, M.; Jones, J. A.; Grimshaw, S. B.; Spencer, A.; Glaser, S. J.; Smith, L. J.; Dobson, C. M. Structural and dynamical properties of a denatured protein. Heteronuclear 3D NMR experiments and theoretical simulations of lysozyme in 8 M urea. *Biochemistry* **1997**, *36*, 8977–8991.

(88) Walsh, J. D.; Meier, K.; Ishima, R.; Gronenborn, A. M. NMR studies on domain diffusion and alignment in modular GB1 repeats. *Biophys. J.* **2010**, *99*, 2636–2646.

CHAPTER 4

Using NMR, mutagenesis and HADDOCK to determine the interface between cytochrome b_5 and cytochrome P450 2B4

4.1 Summary

In this chapter, differential line broadening of the cyt b_5 NMR resonances was used to characterize the interaction epitope for cyt P450 2B4. Single site-directed mutagenesis and double mutant cycle analyses were performed to identify the binding hot spots on cyt b_5 and with which residues on cyt P450 they interacted. The combination of these data was then used to generate complex structures with HADDOCK. Different settings and parameters were tested with HADDOCK and are reported in this chapter, and we show that unambiguous restraints (here from the double mutant cycle analysis) are needed in order for the HADDOCK structures to converge into possible orientations of cyt b_5 and cyt P450. Two final low energy complex structures were proposed and we present a detailed analysis of the interfacial residues, as well as the kinds of interactions in which they are involved. The electron transfer pathway between the two proteins, predicted by HARLEM, is also shown.

Adapted from the manuscript entitled "A structural model of the membrane-bound cytochrome P450-cytochrome b_5 complex from NMR and mutagenesis data" by Ahuja S., Jahr N., Im S.-C., Vivekanandan S., Popovych N., Xu J., Soong R., Le Clair S. V., Nanga R. P., Yamamoto K., Bridges A., Waskell L. and Ramamoorthy A. This study was supported by NIH (GM084018 and GM095640 to A. R. and GM35533 to L. W.) and a VA Merit grant (to L. W.).

4.2 Introduction

Cytochromes P450 (cyts P450) are a ubiquitous superfamily of mixed-function oxygenases, which are found in all kingdoms of life but are especially abundant in eukaryotes. Humans possess 57 different membrane-bound cyts P450.[1] They are found in all tissues of the body and are responsible for influencing a dazzling array of biochemical and physiological processes, including embryonic development, blood coagulation, and the metabolism of carcinogens, environmental toxins, over 50% of drugs in use, vitamin D and other exogenous and endogenous compounds.[2,3]

Cyt P450 easily catalyzes the insertion of one atom of "activated" molecular oxygen into a substrate, using two protons from water and two electrons from NAD(P)H. Electrons destined for cyt P450 are first delivered to its redox partners, cyt P450 reductase (CPR) and cyt b_5, which then transfer electrons to cyt P450.[4] CPR is capable of transferring both electrons to cyt P450; however, cyt b_5 is capable of donating only the second electron due to its high redox potential as compared to ferric cyt P450.[5–8] The influence of cyt b_5 on the activity of cyt P450 has been shown to depend on the cyt P450 isozyme and the substrate involved. While cyt b_5 can enhance some catalytic reactions of cyt P450, it has no effect or even inhibits other reactions.[4,6,8–11] At low concentrations, cyt b_5 enhances the rate of catalysis by up to 100-fold, whereas at high concentrations it inhibits catalysis by competing with CPR in binding to cyt P450 and preventing the transfer of the first electron.[4,5,12] Cyt b_5 and CPR are both negatively charged proteins, which are known to have overlapping binding sites on cyt P450.[13]

When the stimulatory and inhibitory effects of cyt b_5 are equal, cyt b_5 will appear to have no effect on the catalytic activity of cyt P450.

To obtain an in-depth understanding of the molecular basis of the effects of cyt b_5 on cyt P450 activity, it is necessary to determine the structure of the complex between the full-length forms of cyt b_5 and cyt P450. Only the full-length, membrane-binding form of microsomal cyt b_5 influences the enzymatic activity of cyt P450.[14,15] Currently, all reported X-ray and NMR structural data pertain to truncated forms of cyt P450 and cyt b_5, in which their membrane anchors have been removed.[16–19] The one exception is aromatase (CYP19); however, no electron density was observed for the N-terminal residues that are supposed to constitute the transmembrane region of the protein.[20]

Despite recent advances in NMR methodology and isotopic labeling schemes, the structure determination of large membrane-bound protein-protein (~70 kDa) complexes remains a monumental task. The large size of the complex, in a membrane mimetic, presents considerable challenges in terms of sample stability, spectral sensitivity and resolution. To identify residues at protein-protein interfaces, the most widely utilized techniques include single site-directed mutagenesis of each protein partner (Section 2.1) and chemical shift perturbations monitoring with NMR (Section 2.3).[21,22] Single site-directed mutagenesis and subsequent measurements of binding constants have been used to successfully identify hot spot residues at the complex interface for decades.[23,24] Although not as routinely used, double mutant cycle analysis can additionally be employed to home in on the identity of residues (from each protein partner) interacting cooperatively with one another at the interface (see Section 2.1 for more information).[25–30] To determine the interface in the absence of mutagenesis, and in a physiological environment, NMR chemical shift perturbations analysis is routinely used (Section 2.3). However, this type of analysis requires that the complex be relatively long-lived on the NMR time scale. In the case of redox complexes, it is known that their lifetimes are short-lived and that many complexes are formed in solution at any given time (Section 1.4). During NMR experiments, redox protein residues therefore display a chemical shift that is the average of the free protein and all bound forms (in which the redox partners adopt various orientations with respect to one another); this leads to averaging of the chemical shifts and the observation of very little perturbations.[31–33] Although not as easily understood, differential line broadening can then step in to fill the gap because it relies on the relaxation parameters of the residues, which cannot be averaged out. In fact, even when the bound state is invisible to NMR, the binding interface can still be identified by looking at differential line broadening observed from the NMR signal arising from the unbound protein,[34,35] when the rate of complex formation is fast and the protein comes off fast enough to affect the intensity of the free state.[36] For a more thorough discussion on relaxation and differential line broadening, refer to Section 2.4. In this chapter, to study the complex interface between cyt b_5 and cyt P450 2B4, we applied a variety of these experimental techniques: single site-directed mutagenesis of cyt b_5, double mutant cycle analysis between cyt b_5 and cyt P450 2B4, and differential line broadening observed for cyt b_5 residues upon interaction with cyt P450 2B4.

When experimental results cannot provide a detailed structure of the interface (i.e. all residues interacting, the kind of non-covalent interactions and the orientation of the proteins/residues), various docking methods can be utilized to generate a structure of the protein complex.[37–39] High Ambiguity Driven biomolecular DOCKing (HADDOCK)[40–43] stands out among the pack because of its ability to incorporate a variety of restraints obtained experimentally, with a particular emphasis on NMR data and mutagenesis (see Section 2.5). HADDOCK has proven to be highly effective in predicting protein-protein complex structures[44–46] and has even been applied to a few cytochrome complexes.[47–49] In this chapter, two different types of experimental restraints were incorporated during docking via HADDOCK: unambiguous restraints and ambiguous restraints. The unambiguous restraints define two residues/atoms (from opposing protein partners) as being a certain distance from one another (Section 2.5.2); in this chapter, we defined the interacting residues as those obtained from the double mutant cycle analysis. Ambiguous restraints were then used to define which residues were at/near the interface (Section 2.5.1); for this purpose, we defined the active residues as the solvent accessible residues that are believed to be at the interface (based on NMR differential line broadening for cyt b_5 and single site-directed mutagenesis for cyt P450) and passive residues as solvent accessible, neighboring residues of the active residues. Since we would like to eventually apply this similar type of methodology to other redox complexes, it was also important to determine how much importance/weight each type of restraint held in the complex structure generation (i.e. which were necessary/superfluous). For example, do we need double mutant cycle analysis or are ambiguous restraints sufficient to obtain a complex structure that is likely productive (as gauged by the orientation of cyt b_5 relative to the membrane, and the intermolecular heme distance between cyt b_5 and cyt P450)?

In this chapter, single site-directed mutagenesis, double mutant cycle analysis, and NMR differential line broadening were used to calculate the structure of the complex , using HADDOCK, between microsomal rabbit cyt P450 2B4 (56 kDa) and rabbit cyt b_5 (15 kDa) in their full-length forms. The extensive structural knowledge of the cyt b_5-cyt P450 complex provided here will prove to be essential in unraveling the molecular mechanism by which cyt b_5 regulates the rate of catalysis of cyt P450.[4]

4.3 Materials and methods

4.3.1 Materials

The QuikChange II XL site-directed mutagenesis kit was purchased from Stratagene. L-3-dilauroylphosphatidylcholine (DLPC) was purchased from Doosan Serdary Research Laboratories (Toronto, Canada) and methoxyflurane was obtained from Abbott Laboratories (Abbott Park, IL). 1,2-dihexanoyl-*sn*-glycero-3-phosphocholine (DHPC) and 1,2-dimyristoyl-*sn*-glycero-3-phosphocholine (DMPC) were purchased from Avanti Polar Lipids (Alabaster, AL). C41 cells were purchased from Lucigen (Middleton, MI). ^{15}N CELTONE rich media, ^{2}H-dodecylphosphocholine (DPC), ^{13}C-glucose, ^{15}N-ammonium sulfate and D_2O were purchased from Cambridge Isotope Laboratories (Andover, MA). Resins, buffer components, benzphetamine and 3,5-di-*tert*-butyl-4-hydroxytoluene (BHT) were purchased from Sigma-Aldrich. Glycerol for NMR experiments was purchased from Sigma-Aldrich and Roche Applied Science. 1-(4-

chlorophenyl)imidazole (1-CPI) was purchased from Oakwood Product, Inc (West Columbia, SC).

4.3.2 Expression and purification of wild-type rabbit cyt P450 2B4, rat cyt P450 reductase (CPR) and rabbit cyt b_5

The cyt P450 2B4 and cyt b_5 cDNA in pLW01 and cyt P450-reductase (CPR) cDNA in pSC-CPR plasmids were expressed in *E. coli* C41 cells and purified as described previously.[13,50,51] U-^{15}N cyt b_5 was expressed as described in Chapter 3. Purification of cyt b_5, cyt P450 and CPR was performed as described elsewhere.[13,51] Each purified protein exhibited a single band on an SDS PAGE gel. Cyt P450 concentration was quantified by the method of Omura and Sato.[52]

4.3.3 Generation of mutants of cyt P450 2B4 and cyt b_5

Mutagenesis was performed using a QuikChange II XL site-directed mutagenesis kit (Stratagene) according to the manufacturer's instructions. The oligonucleotides used to generate the cyt b_5 mutants are shown in Table 4.1 and those for the cyt P450 2B4 mutants can be found in Bridges *et al.*[13] All oligonucleotides were synthesized by Integrated DNA Technologies. Following mutagenesis, the sequence of the entire mutated gene was determined at the University of Michigan DNA Sequence Core Facility to confirm the mutation.

Table 4.1 Sequences of oligonucleotide primers used to mutate cyt b_5 cDNA.

P45A	5’-CTGGAGGAGCACgccGGAGGGGAGGAA
G46A	5’-GGAGGAGCACCCTgccGGGGAGGAAGTC
E49A	5’-GGAGGGGAGgccGTCCTGAGGGAACAAGC
V50A	5’-GGAGGGGAGGAAgccCTGAGGGAACAAGC
E53A	5’-AGTCCTGAGGgccCAAGCTGGGGGCGA
Q54A	5’-AGTCCTGAGGGAAgccGCTGGGGGCGATGC
N62A	5’-GGCGATGCCACTGAAgccTTTGAGGACGTC
D65A	5’-GAAAACTTTGAGgccGTCGGGCACTC
V66A	5’-CTTTGAGGACgccGGGCACTCGAC
D71A	5’-CGGGCACTCGACAgccGCCAGAGAGCTG
L75A	5’-CAGATGCCAGAGAGgccTCCAAGACCTTC

*The bases that were added to introduce the indicated mutation are shown in lowercase letters.

**Sequences of oligonucleotide primers used to mutate cyt P450 cDNA have been published previously.[13]

4.3.4 Solution NMR of the cyt b_5-cyt P450 complex

All solution NMR experiments were performed at 298 K on a Bruker 900 MHz NMR spectrometer equipped with a 5 mm triple-resonance TXI cryo-probe. NMR spectra were processed with Topspin 2.1 (Bruker) and analyzed in Sparky[53]. Complex samples contained a 1:1 molar complex of 0.1 mM isotopically ^{15}N-labeled cyt b_5 and unlabeled cyt P450 2B4 in NMR buffer in 10% (w/v) isotropic bicelles with a composition of DMPC and DHPC lipids in a 1:4 molar ratio (*q* ratio of DMPC/DHPC = 0.25). Isotropic bicelles were added to the preformed complex just before transferring to a Shigemi tube. Isotropic bicelles were prepared as outlined previously[54] and in Appendix D. For experiments in the presence of the substrate and inhibitor (BHT and 1-CPI), the small molecule was added to a final concentration of 0.2 mM to the preformed (and concentrated) cyt b_5-cyt P450 sample (1:2 molar ratio for cyt P450:substrate) before the addition of isotropic bicelles. In order to assess the formation of the cyt b_5-cyt P450 complex in the presence of BHT, three cyt P450 titration points were performed in the sample. All titration points were carried out by adding aliquots of an unlabeled cyt P450 stock solution to a final concentration of 0.03 mM, 0.06 mM and 0.10 mM cyt P450, to a sample containing 0.1 mM ^{15}N-labeled cyt b_5 in isotropic bicelles. To demonstrate that an active form of the complex was being studied, SDS gels were run before and after NMR experiments, and CO assays (Figure 4.5) and activity assays were performed (Table 4.15).

4.3.5 Determination of cyt P450 2B4 activity in solution and bicelles

4.3.5.1 Methoxyflurane

The metabolism of the anesthetic compound methoxyflurane ($C_3H_4Cl_2F_2O$) by cyt P450 2B4 was measured in a reconstituted aqueous system with and without cyt b_5.[14] The activity of cyt P450 was also measured in bicelles in the presence and absence of cyt b_5. The activity was quantified by recording the amount of fluoride ions produced. The components were mixed together in the following sequence: cyt P450 2B4, CPR and DLPC. The mixture was then incubated for 5 minutes at room temperature, and either cyt b_5 or buffer was added to the mixture, which was then incubated for an additional 1 hour at room temperature. Following the 1 hour incubation, 50 mM potassium phosphate buffer of pH 7.4 saturated with methoxyflurane (1 µL/mL), glucose-6-phosphate and glucose-6-phosphate dehydrogenase were added, and the solution was further incubated at 37 °C for 5 min. NADPH was added to start the reaction. The final volume of the reaction mixture was 500 µL and it contained 50 mM potassium phosphate buffer, 1 µM cyt P450 2B4, 1 µM CPR, 120 µM DLPC, 1 µL/mL methoxyflurane, 300 μM NADPH, 5 mM glucose-6-phosphate, 1 U/mL glucose-6-phosphate dehydrogenase and cyt b_5 (0 or 1 μM). The resulting reaction mixture was incubated at 37 °C with shaking at 150 rpm for 30 min and then quenched by heating at 70 °C for 2 min. The fluoride ion concentration of the solution was quantified using a fluoride ion electrode (Thermo Scientific). The assay for the metabolism of methoxyflurane in the presence of bicelles was conducted as described above except that the cyt P450-CPR-cyt b_5 complex was added to DMPC/DHPC (3.5/1) bicelles at 4 °C. Bicelles were prepared and pre-cooled as previously described.[54] The mixture was incubated at 4 °C for 30 min. The potassium phosphate buffer saturated with methoxyflurane and the NADPH generating system were added. The final concentration of DMPC was 110 mM. The result of the methoxyflurane assay is presented in Table 4.11, Table 4.12 and Table 4.15.

4.3.5.2 Benzphetamine

The metabolism of benzphetamine was measured by determining the amount of formaldehyde produced by the N-demethylation of benzphetamine using Nash's reagent as described previously.[13] The final concentration of the reactants in the mixture was 50 mM potassium phosphate buffer (pH 7.4), 0.2 μM cyt P450 2B4, 0.2 μM CPR, 24 μM DLPC, 1 mM benzphetamine, 300 μM NADPH, 0 or 50 mM DMPC/DHPC bicelles and cyt b_5 (0 or 0.2 μM). The results of the benzphetamine assays are presented in Table 4.15.

4.3.6 Determination of cyt b_5-cyt P450 equilibrium dissociation constant (K_d) in the presence of a substrate/ligand

The K_d of the binding between ferric cyt P450 2B4 and ferric cyt b_5 was determined as previously described[13] by measuring the type I spectral change (a decrease at 420 nm and an increase at 385 nm in absorption) occurring when cyt b_5 is added to an aqueous solution of cyt P450 2B4, in the presence of the substrate such as methoxyflurane or BHT. The K_d could not be calculated in either micelles or bicelles due to an absence of type I spectral change in the presence of a membrane mimetic. The K_d was used to calculate the free energy of binding, ΔG, using Equation 2.1 in Chapter 2. The K_d for the complex formation of all possible pairs of wild-type and mutants combinations of cyt P450 2B4 and cyt b_5 was determined as described previously[13] and are presented in Table 4.11, Table 4.12, and Table 4.13.

4.3.7 Cyt b_5-cyt P450 complex HADDOCK structure calculation

HADDOCK involves rigid-body docking, followed by molecular dynamics simulations that allow selected amino acid side chains, as well as parts of the backbone, to move freely, in order to improve the complementarity and electrostatic interactions at the interface. The HADDOCK 2.1[40,41] algorithm was used in all the simulations performed in this chapter. In all simulations, rigid-body energy minimization was done for 2000 structures of the complex. The second step included semi-rigid simulated annealing from which the best 500 structures were selected for refinement. The best 150 structures were further refined with explicit solvent in an 8.0 Å shell of TIP3P water molecules. The 50 lowest energy structures were selected for the final analysis and grouped into clusters based on the backbone RMSD.

4.3.7.1 Structure of cyt b_5 and cyt P450 2B4 used for docking simulations

For the HADDOCK calculations, the NMR structure of full-length cyt b_5 (Chapter 3). This structure consists of a structured soluble domain from residues K7 to R89, and an unstructured linker from residue S90 to D104. A high-resolution structure of the transmembrane domain of cyt b_5 was not obtained, but the unstructured tail was left in some of the docking simulation in order to make the clustering of the different complex structures easier. No interactions were seen between the transmembrane domain of cyt b_5 and cyt P450 2B4.

The structure used for cyt P450 2B4 has PDB code 1SUO[55]. This structure contains the ligand 4-(4-chlorophenyl)imidazole (4-CPI); this was done to account for any structural changes that occur to cyt P450 upon binding substrate (cyt P450 is believed to go from an open form to a closed form when bound to a ligand). Overall, the many different crystal structure of cyt P450 2B4 bound to different ligands are similar; minimal changes are observed on the proximal side of cyt P450 (where the heme is closest to the surface). While there are some structural changes based on the ligand, the changes are primarily on the distal side and are likely due to surface binding of the ligand or may be attributed to crystal contacts. The structure of 1SUO contains no excess ligand on the proximal surface, and the ligand is only found inside the binding pocket.

4.3.7.2 Generating the ligand topology files and parameter files

The PRODRG2[56] server (http://davapc1.bioch.dundee.ac.uk/prodrg/) was used to generate both the ligand topology and parameter files. The following steps were taken:

- Go to the tab "Run PRODRG."
- Get a token by submitting your email address.
- Input the PDB coordinates or whatever input you have for your molecule
- Will generate two text files: _ _ _- _ _ _ _param.txt (red: ligand code; blue: pdb code) _ _ _- _ _ _ _top.txt
- The "param.txt" file is the parameter file and the "top.txt" file is the topology file.
- Go inside the topology file and look at how it refers to the ligand, i.e. Residue _ _ _, the three-letter code the server has given for the heteroatom. In our case, it referred to the ligand as CPH in the topology file and not CPZ (which is what was used in the pdb file for P450). Go into the protein pdb file and change the ligand name in your pdb files according to the nomenclature used in these topology files. It's easier to edit the pdb file than the ligand files because they are less complicated.
- Remove the following from ligand.param: NBONds <BR> TOLERANCE=0.5 NBXMOD=5 WMIN=1.5 <BR> REPEL=1.0 REXPONENT=4 IREXPONENT=1 RCONST=16.0 <BR> CTONNB=5.5 CTOFNB=6.0 CUTNB=7.0 <BR> END – this is done so that electrostatic interactions are taken into account in the energy minimization.
- ligand.param can include information on the ligand and the heme, so if it contains information on the heme, make sure to copy and paste the information from the param.txt file you just generated and input it into the ligand.param file you already have with the heme. The ligand part usually starts with "evaluate (…)" and with "eval" in the front of every line. Replace this part with the generated ligand file until "set message=on echo=on end."

4.3.7.3 Modifying the pdb files for HADDOCK

The PDB file obtained from the Protein Data Bank needs to be modified prior to running HADDOCK. The following need to be done to the PDB file:

- Remove everything prior to “`ATOM      1`”.
- Keep only one protein monomer (if have A, B, C, etc, keep only monomer A).
- Delete lines for water molecules (HOH).
- Delete lines with connections (CONNECT).
- Remove TER lines, which just separate sections in the PDB.
- Remove all A’s (which just indicate the monomer identity). Replace all “_A_” with “___” (read: “spaceAspace” and “spacespacespace”).
- *Don’t delete* HETATM (heteroatoms).
- Replace all “HETATM” (atoms of the ligand) with “ATOM__” [HADDOCK doesn’t recognize HETATM] [need two spaces to account for the right number of characters].
- Replace “FE” to “FE+3” [HADDOCK recognizes only the metals with the charge].
- Replace “HEM” with “HEB” for heme B (HEM is for heme C).
- Replace “CYS 436” (represents cysteine with H still attached to S) with “CYF 436” (represents cysteine without H attached to S) – cysteine is coordinated to the Fe with the H removed.
- Change the ligand name depending on your ligand topology file code, if it’s different. For all the runs, the ligand was kept inside the PDB to maintain the integrity of the crystal structure.
- Keep “END” at the end.

4.3.7.4 Instructions for running HADDOCK

A manual and HADDOCK tutorials can be found on their very informative website (http://www.nmr.chem.uu.nl/haddock/). However, the presence of 4-CPI, the cyt b_5 heme and the cyt P450 heme warrant additional instructions, which can be found in Appendix A.

4.3.7.5 Histidine protonation states

In HADDOCK, the default protonation state of the histidine is set as doubly protonated (both HD1 and HE2, see Figure 4.1). To set manually the protonation states of the histidines, it is necessary to determine whether HD1 or HE2 is protonated, both are de-protonated or both are de-protonated. The protonation state of all histidines at pH 7.4 was determined by generating the PQR file via the PDB2PQR server[57,58] at pH 7.4 (Appendix B). For cyt b_5, none of the histidines were doubly protonated, with the following histidines being singly protonated at HD1: 20, 22, 44, 68 and 85; and the following singly protonated at HE2: 31 and 32. For cyt P450 2B4 (using the PDB structure 1SUO), residue 252 was determined to be doubly protonated and therefore left at the default setting. The other histidines had the following singly protonation states, with HD1 for 284, 285, 354, 369, 397 and 492, and HE2 for 172, 231,319, 335 and 412. The following residues need to be entered in the "histidine patches" section of the *run.cns* file. In total, 11 residues have HD1 set as singly protonated, and 7 residues have HE2 set as singly protonated.

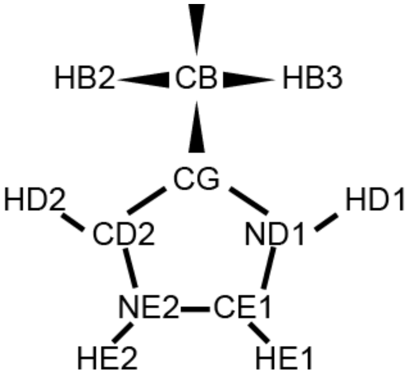

Figure 4.1 CYANA labeling scheme of histidine atoms.

4.3.7.6 Solvent accessibility calculation for this chapter

The solvent accessibility of cyt P450 and cyt b_5 were determined by Accelrys Software Inc.[59] and ASAView[60], respectively. Residues which had solvent accessibility greater than 40% were considered solvent accessible.

4.3.7.7 Unambiguous restraints for the hemes and 4-CPI

To prevent unwanted results, a set of unambiguous restraints was used to keep the non-protein molecules in place during the docking simulation. Restraints for the ligand 4-CPI (present in the 1SUO structure) can be found in Table 4.2; 4-CPI is labeled as residue #600 in the PDB text. The restraints to hold the hemes of both cyt P450 2B4 and cyt b_5 can be found in Table 4.3 and Table 4.4, respectively; the heme is labeled as residue #500 in the PDB files.

Table 4.2 Restraints between 4-CPI and cyt P450 2B4.

Residue#-AtomName #1	Residue#-AtomName #2	Distance (Å)	Lower distance margin (Å)	Upper distance margin (Å)
600 N1	500 "FE+3"	2.30	0.0	0.0
600 C5	500 NB	3.10	0.0	0.0
600 C5	500 NC	3.60	0.0	0.0
600 N1	500 NC	3.10	0.0	0.0
600 N1	500 NA	2.80	0.0	0.0
600 C2	500 ND	3.30	0.0	0.0
600 N1	436 SG	4.39	0.0	0.0

Table 4.3 Restraints between cyt P450 and its heme.

Residue#-AtomName #1	Residue#-AtomName #2	Distance (Å)	Lower distance margin (Å)	Upper distance margin (Å)
436–SG	500–"FE+3"	2.3	0.5	0.0
500–"FE+3"	436–SG	2.3	0.5	0.0
500–"FE+3"	500–NA	2.06	0.0	0.0
500–"FE+3"	500–NB	2.05	0.0	0.0
500–"FE+3"	500–NC	2.07	0.0	0.0
500–"FE+3"	500–ND	2.05	0.0	0.0
500–O2A	369–NE2	3.13	0.0	0.0
500– O2D	98–NH2	3.24	0.0	0.0
500– CBC	295–O	4.00	0.0	0.0
500–CBC	295–CB	4.69	0.0	0.0
500–C3C	298–CB	4.36	0.0	0.0
500–C2C	298–CB	5.14	0.0	0.0
500–CMB	302–CG2	4.98	0.0	0.0
500–CMB	302–CB	4.50	0.0	0.0
500–CMB	302–OG1	4.64	0.0	0.0
500–C2B	302–OG1	3.69	0.0	0.0
500–C3B	302–OG1	3.07	0.0	0.0
500–CAB	302–OG1	3.30	0.0	0.0

Table 4.4 Restraints between cyt b_5 and its heme.

Residue#-AtomName #1	Residue#-AtomName #2	Distance (Å)	Lower distance margin (Å)	Upper distance margin (Å)
500–HAB	28–HD1#	5.0	3.2	0.0
500–HBC2	28–HD2#	5.0	3.2	0.0
500–HMC1	28–HD2#	5.0	3.2	0.0
500–"FE+3"	30–HE	5.0	3.2	0.0
500–"FE+3"	44–NE2	2.3	0.5	0.0
500–"FE+3"	68–NE2	2.3	0.5	0.0
500–HMC1	30–HD1#	5.0	3.2	0.0
500–HMC1	30–HD2#	5.0	3.2	0.0
500–HBB2	30–HD1#	5.0	3.2	0.0
500–HB	44–HD2	5.0	2.0	0.0
500–HD	44–HE1	5.0	2.0	0.0
500–HB	68–HD2	5.0	2.0	0.0
500–HD	68–HE1	5.0	2.0	0.0
500–HMB2	44–HD2	5.0	2.0	0.0
500–HMA2	44–HD2	5.0	2.0	0.0
500-HAC	44–HE1	5.0	2.0	0.0

500-HMD1	44–HE1	5.0	2.0	0.0
500-HMB1	68–HD2	5.0	2.0	0.0
500-HMA3	68–HD2	5.0	2.0	0.0
500-HMC3	68–HE1	5.0	2.0	0.0

4.3.7.8 Ambiguous restraints

Ambiguous restraints for cyt b_5 (Table 4.5) were determined based on the findings of the NMR differential line broadening (Section 4.4.5 and Figure 4.6). On the side of cyt P450 2B4, active residues (Table 4.5) were determined from the site-directed mutagenesis analysis done by Bridges *et al*. and Table 4.12.[13] For cyt b_5, neighboring residues to the active residues were chosen as passive residues (Table 4.5). For cyt P450, passive residues were assigned to the entire proximal surface, where the heme comes closest to the surface (Table 4.5). This was done for two reasons: cyt P450 has been reported to interact with its redox partners via this proximal surface and the mutagenesis results only probed a very small portion of this surface (Figure 4.4). All residues used as active or passive were assessed to be solvent accessible (Section 4.3.7.6).

Different settings for the semi-flexible segments were tested: the automatic setting from HADDOCK (which takes the residues at the interface of the complexes and allows them to be semi-flexible), and setting the semi-flexible segments explicitly by taking the active and passive residues, as well as +/- 2 residues on each side of those residues (Table 4.6). Unless otherwise noted, the runs were performed with the semi-flexible segments set as automatic.

Table 4.5 Table of Ambiguous Interaction Restraints (AIRs) used in the manuscript.[61]

cyt b_5

Active residues	39 48 49 65 66 70 71 73 74 [7 residues]
Passive residues	43 44 45 46 47 50 61 62 64 67 69 77 [12 residues]

cyt P450

Active residues	122 126 133 135 137 139 433 [7 residues]
Passive residues	28 29 30 62 64 82 86 90 93 118 119 129 130 134 136 138 140 141 142 143 144 257 258 259 260 273 274 276 277 278 279 280 284 322 323 326 329 330 331 334 335 336 341 344 345 348 372 373 374 376 378 379 384 385 399 400 403 404 410 411 415 416 417 420 421 422 424 432 435 436 440 442 [72 residues]

Table 4.6 Semi-flexible segments that were set explicitly based on restraints in Table 4.5.

cyt b_5	37-52, 59-79 [2 segments]
cyt P450	26-32 60-66 80-95 116-146 255-262 271-286 320-350 370-387 397-406 408-426 430-444 [11 segments]

Unfortunately, the software was unable to calculate the solvent accessibility of the heme atoms of cyt b_5. We know, however, that the proximal side of the heme (labeled in Figure 4.2) of cyt b_5 is solvent exposed. Based on the cyt b_5 NMR structure as viewed in PyMOL,[62] a number of heme atoms were deemed to be solvent accessible and labeled as passive atoms in some of the HADDOCK runs (Table 4.7 and Figure 4.2):

Table 4.7 Solvent accessible heme atoms in cyt b_5.

Location in cyt b_5	**Accessible heme atoms**
Near residues 70-73	CMA, HMA1, HMA2, HMA3, CAA, HAA1, HAA2, CBA, HBA1, HBA2, CGA, O1A and O2A
Near residues 60-66	CMD, HMD1, HMD2, HMD3, CAD, HAD1, HAD2, CBD, HBD1, HBD2, CGD, O1D and O2D

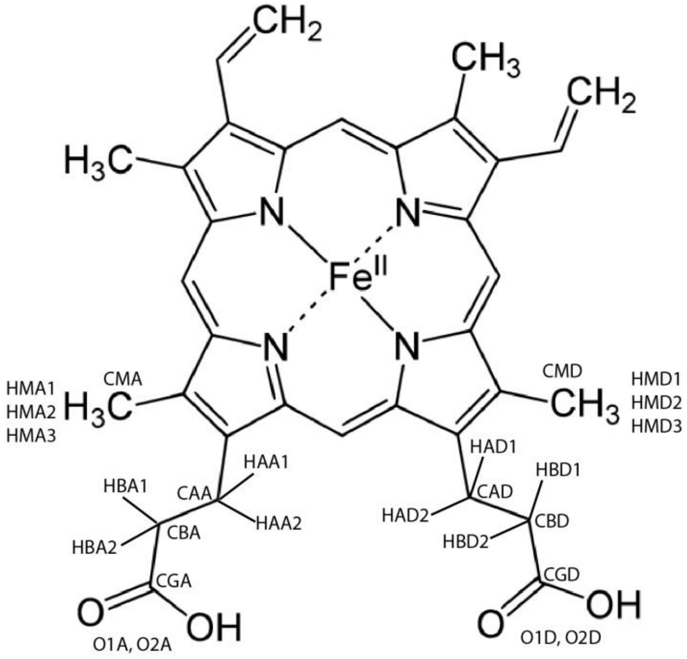
CH2
CH3
CH2
H3C
N
N
Fe^II
N
N
HMA1
HMA2
HMA3
CMA
H3C
CMD
CH3
HMD1
HMD2
HMD3
HAA1
HBA1
CAA
HAA2
HBA2
CBA
CGA
O
OH
O1A, O2A
HAD1
HBD1
CAD
HAD2
CBD
HBD2
CGD
O
OH
O1D, O2D

Figure 4.2 Labeling scheme of heme (type B) molecule from cyt b_5, with the passive atoms for HADDOCK labeled.

4.3.7.9 Unambiguous restraints

Unambiguous restraints were set based on the double mutant cycle analysis (Section 4.4.3). A distance range between NH atoms was chosen of 2 to 8 Å based on the range of intermolecular interactions (and to account for the fact that some residues do not interact with the NH and instead interact with the side chain). Different unambiguous restraints were used based on different thresholds for $\Delta\Delta G_{int}$ used (Table 4.13 and Table 4.14). See Section 4.3.7.10 for an explanation of why the final four restraints were chosen.

Table 4.8 List of all unambiguous restraints which were assessed.

#	Cyt b_5	Cyt P450	Distance (Å)	Lower distance margin (Å)	Upper distance margin (Å)
1	D65-NH	K433-NH	6.0	-4.0	+2.0
2	V66-NH	K433-NH	6.0	-4.0	+2.0
3	D65-NH	R122-NH	6.0	-4.0	+2.0
4	V66-NH	R122-NH	6.0	-4.0	+2.0
5	V66-NH	K139-NH	6.0	-4.0	+2.0
6	D65-NH	F135-NH	6.0	-4.0	+2.0

4.3.7.10 Summary of restraints used in the manuscript[61]

In the manuscript,[61] HADDOCK was used to dock cyt b_5 and cyt P450 based on four unambiguous restraints (#1-4 in Table 4.8) derived from the double mutant cycle analysis, and ambiguous restraints derived from NMR and site-directed mutagenesis experiments (Table 4.9). Unambiguous restraints #1-4 were used because #1-3 had $\Delta\Delta G_{int}$ > 1 kcal/mol (Table 4.13); restraint #4 was added because of the proximity of V66 to D65 and to hold the two proteins in a specific orientation.

Unambiguous restraints were not used between cyt b_5 residues V66 and D65 with cyt P450 residues K139 and F135 for additional reasons: the error range for these additional $\Delta\Delta G_{int}$ values was larger than others (see Table 4.13 and Table 4.14) and therefore the measurement may not be as reliable, and these two residues are found in the flexible CD loop of cyt P450 (Figure 1.6 in Chapter 1). We hypothesize that the mutation of both of these residues induces a structural perturbation in the flexible C-helix, which in turn destabilizes the interaction between cyt P450 and cyt b_5. The mutation of K139 to alanine has been shown to disrupt a hydrogen-bond network between the K139 amino group and P261 and N260 in the GH loop,[55] suggesting an allosteric interaction between the C-helix and the G-H loop.

Table 4.9 List of ambiguous and unambiguous restraints used in the manuscript[61]. Active and passive residues were defined for cyt b_5 based on differential line broadening and solvent accessibility > 40% in ASAView.[60] Active and passive residues were defined for cyt P450 based on site-directed mutagenesis and solvent accessibility > 40% in Accelrys Software Inc.[59] Unambiguous restraints were defined based on the double mutant cycle analysis with distances defined in Table 4.8.

	cyt b_5	**cyt P450**
Unambiguous restraints	D65-R122, V66-R122, D65-K433, V66-K433	
Ambiguous restraints, Active	K39, E48, E49, T70, D71, R73, E74	R122, R126, R133, F135, M137, K139, K433
Ambiguous restraints, Passive	E43, H44, P45, G46, G47, V50, E61, N62, E64, G67, S69, K77	79 residues with > 40% solvent accessibility on the proximal side of cyt P450 where the heme is closest to the surface

Table 4.10 Final list of semi-flexible segments used in the publication.[61]

cyt b_5	40-42, 46-59, 60-66, and 70-79 [4 segments]
cyt P450	118-144, 339-346, 414-433, and 439-446 [4 segments]

4.3.7.11 Analysis of HADDOCK structures

The fifty complex structures for each HADDOCK simulation were grouped into different clusters based on their orientation of cyt b_5 relative to cyt P450. This analysis could be performed relatively easily based on the orientation of the C-terminal tail of cyt b_5. The RMSD value (~ 1 Å or less) was calculated for each structure within each cluster by aligning each structure to a reference structure using the *align* command in PyMOL.[62] All structures were then aligned to the lowest energy structure, and the center of mass was calculated for one structure from each cluster and for all cyt b_5

orientations that did not fit within a cluster. The center of mass was calculated only for the soluble domain (residue 1 through 89) of the cyt b_5 structure, using the *center_of_mass.py* script from the PyMOL wiki webpage.

To determine the hydrogen bonds and the salt bridges at the interface of the lowest energy structure of the selected cluster, the PDB of that complex structure was uploaded onto the online interactive tool PDBePISA (Protein Interfaces, Surfaces and Assemblies)[63,64] and an analysis was performed. CCP4[65] was used to establish the van der Waals contacts at the interface in the final complex structure. The violations were determined from the HADDOCK-generated file *ana_dist_viol_all.lis*.

4.4 Results

4.4.1 Single site-directed mutagenesis of cyt b_5

The following mutants behave similarly to wild-type cyt b_5: P45A, G46A, E53A, Q54A and L75A (data not shown). Additionally, E42A, E43A, V50A, N62A and D71A mutants of cyt b_5 also behaved similarly to wild-type cyt b_5 (Table 4.11 and Figure 4.3). These residues are believed not to be at the interface of the cyt b_5-cyt P450 complex and do not to play a role in the enhancement of cyt P450 metabolism.

Out of the remaining mutants, the E49A mutant had a slight increase in K_d (from 0.022 to 0.032 μM) and a very modest decrease in methoxyflurane (MF) metabolism (from 1.35 to 1.17 nmol F^- formed/min/nmol cyt P450) (Table 4.11 and Figure 4.3). However, mutation of V66 and D65 to alanines caused the K_d to drastically increase (15- and 7-fold, respectively) and the MF metabolism to decrease by 84% and 43%, respectively, compared to wild-type cyt b_5 (Table 4.11 and Figure 4.3). This clearly indicates that V66 and D65 are essential for the interaction between cyt b_5 and cyt P450.

Table 4.11 Determination of the K_d and methoxyflurane (MF) metabolism of cyt b_5-cyt P450 complexes between mutants of cyt b_5 and wild-type cyt P450.

cyt b_5 mutants	K_d cyt b_5-cyt P450 complex (μM $\pm$ S.D.)	MF metabolism (nmol F^- formed /min/nmol P450 $\pm$ S.D.)	Ratio of activity ± cyt b_5
no cyt b_5 (control)		0.19 ± 0.2	
wild-type	0.022 ± 0.003	1.35 ± 0.02	7.1
E42A	0.012 ± 0.002	1.10 ± 0.1	5.8
E43A	0.015 ± 0.003	1.41 ± 0.2	7.4
E49A	0.032 ± 0.004	1.17 ± 0.2	6.2
V50A	0.016 ± 0.001	1.08 ± 0.2	5.7
N62A	0.010 ± 0.004	0.92 ± 0.1	4.8
D65A	0.332 ± 0.033	0.22 ± 0.02	1.1
V66A	0.152 ± 0.019	0.77 ± 0.1	4.1
D71A	0.017 ± 0.008	1.66 ± 0.2	8.7

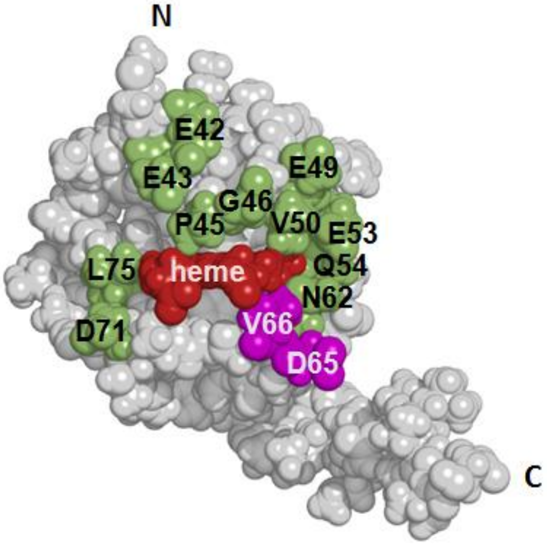

Figure 4.3 Mutagenesis of cyt b_5 residues. Mutational results highlighting the residues important for both binding to cyt P450 and MF metabolism are in magenta and those that are inconsequential in both respects are in green. This view is the proximal side of cyt b_5.

4.4.2 Single site-directed mutagenesis of cyt P450

The following mutants of cyt P450 2B4 were previously shown to affect neither the ability of cyt P450 to bind to cyt b_5 nor its ability to metabolize methoxyflurane: F115A, Y190A, K276A, H335A, K421A and Y484A (Table 4.12 and Figure 4.4).[13] The same is true for H226A, which was shown by Bridges *et al.*[13] and has since been repeated as shown in Table 4.12 and Figure 4.4. Although cyt P450 mutants R422A and R443A showed no change in binding to cyt b_5, they showed a decrease in methoxyflurane metabolism by 50% and 59%, respectively; these residues appear to play a significant role in the interaction between cyt P450 reductase and cyt P450.[13]

As shown in Table 4.12, the following mutations of cyt P450 affect both its binding to cyt b_5 (K_d increase of 10-fold or more) and MF metabolism (decrease by up to 95%): R122A, R126A, R133A, F135A, M137A, K139A and K433A (Figure 4.4). This work was first done by Bridges *et al.*[13] and repeated recently[61] (Table 4.12).

In summary, based on the site-directed mutagenesis work done by Bridges *et al.*[13] and Table 4.12, R122 (C α-helix), R126 (C α-helix), R133 (C-D loop), F135 (C-D loop), M137 (C-D loop), K139 (C-D loop) and K433 (K''' 3_{10} helix) were identified as being important in the interactions of cyt P450 2B4 with cyt b_5 (Figure 4.4). K433 has also been implicated to be in the binding site for cyt P450 reductase.[66–68] These results can be used as ambiguous restraints for the HADDOCK simulation (Section 4.3.7.8).

Table 4.12: Determination of the K_d and MF metabolism of cyt b$_5$-cyt P450 complexes between mutants of cyt P450 and wild-type cyt b$_5$.

cyt P450 mutants	K_d cyt b$_5$-cyt P450 complex (μM ± S.D.)	MF metabolism (nmol F$^-$ formed /min/nmol P450 ± S.D.)	Ratio of activity ± cyt b$_5$
wild-type	0.022 ± 0.003	1.32 ± 0.02	8.3
R122A	0.221 ± 0.06	0.54 ± 0.03	3.4
R126A	0.453 ± 0.06	0.19 ± 0.1	1.2
R133A	1.502 ± 0.18	0.06 ± 0.1	0.29
F135A	0.205 ± 0.05	0.43 ± 0.1	2.7
M137A	0.379 ± 0.07	0.33 ± 0.2	1.7
K139A	0.611 ± 0.13	0.12 ± 0.2	0.75
K433A	0.458 ± 0.04	0.05 ± 0.01	0.31
H226A	0.032 ± 0.009	1.37 ± 0.3	8.5

4.4.3 Double mutant cycle analysis

The results from the double mutant cycle analysis can be found in Table 4.13. When using a high threshold of 0.5 kcal/mol for the $\Delta\Delta G_{int}$, the following residues' side chains can be highlighted as significant in the interactions between cyt b$_5$ and cyt P450: R122-D65, K139-V66, K433-D65 and K433-V66.[61] The K_d value for the K139-V66 double mutant, however, has a larger error (K_d = 1.400 ± 0.180) than the other K_d values (σ of 0.010-0.071), and its value may not be reliable (Section 4.3.7.10). However, a simulation was done with K139-V66 (restraint #5 in Table 4.8) and a description of the results can be found in Section 4.4.6.1 (see the last paragraph of this section).

The error of the $\Delta\Delta G_{int}$ measurement is typically in the range of 0.3-0.53 kcal/mol (Section 2.1). If we lower the threshold to 0.35 kcal/mol (a threshold of 0.3 kcal/mol has been used recently[69]), we can now include R122-V66 ($\Delta\Delta G_{int}$ = 0.37 kcal/mol), F135-D65 ($\Delta\Delta G_{int}$ = 0.46 kcal/mol), K139-D65 ($\Delta\Delta G_{int}$ = 0.38 kcal/mol).

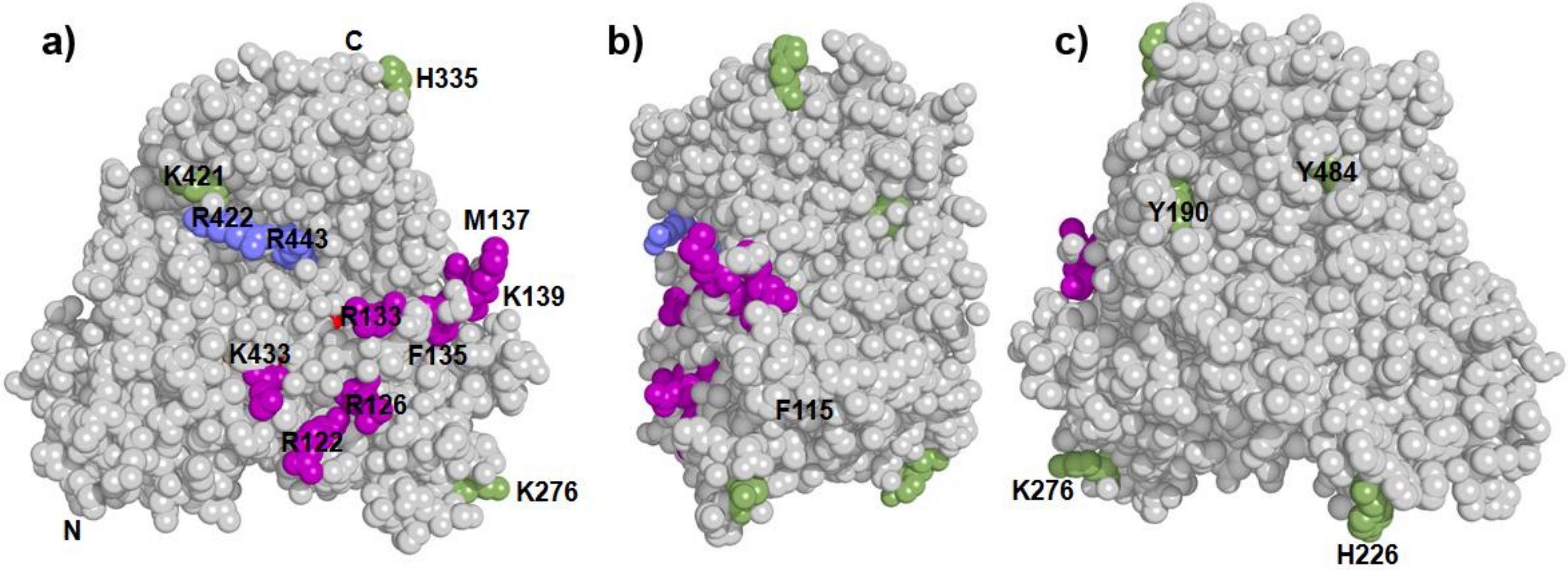
a)
C
H335
K421
R422
R443
M137
K139
R133
F135
K433
R126
R122
K276
N
b)
F115
c)
Y484
Y190
K276
H226

Figure 4.4: Cyt P450 2B4 hot spots for cyt b_5 determined by mutagenesis. Cyt P450 mutational results highlighting the residues important for both binding to cyt b_5 and for MF metabolism in magenta. In blue are the residues that, when mutated to alanine, showed no change in the K_d value to cyt b_5 but showed a decrease in MF metabolism (important for cyt P450 reductase interaction). The residues that are inconsequential in both binding to cyt b_5 and MF metabolism are colored in green. Panel a) shows the proximal side of cyt P450 where the heme comes closest to the surface, and panels b) and c) show a) rotated by 90° and 180° counterclockwise, respectively. Structure is of PDB code 1SUO.[55]

However, similarly to K139-V66 (mentioned above), the measurement for F135-D65 also has a large error (σ of 0.110). Additionally, as mentioned in Section 4.3.7.10, these two residues (F135 and K139) are located on the unstructured CD loop (Figure 1.6) and assigning distance constraints on a flexible portion of the protein may not be appropriate. A simulation was done with both restraint #5 (previous paragraph) and restraint #6 (D65-F135) in Table 4.8 (see last paragraph of this section for explanation), the results are discussed in Section 4.4.6.1.

Table 4.13 Double mutant cycle analysis of mutants of cyt P450 and cyt b$_5$. A comparison of the difference in free energy of binding values (*ΔΔG*) between mutant and wild-type proteins to determine the residues interacting at the cyt b$_5$-cyt P450 interface.

Cyt P450	**Cyt b$_5$**	***K$_d$* (μM) cyt b$_5$-cyt P450**	**Free energy of binding (kcal/mol) *ΔG*^{a} cyt b$_5$-cyt P450**	**Difference in free energy of binding (kcal/mol)**	
				***ΔΔG*^{b} of mutant-wild-type**	***ΔΔG*^{c} interaction of double mutants**
wild-type	WT	0.022 ± 0.003	-10.43		
R122A	WT	0.221 ± 0.010	-9.07	1.36	
wild-type	D65A	0.332 ± 0.032	-8.82	1.61	
R122A	**D65A**	0.558 ± 0.065	-8.52	1.91	**1.06**
wild-type	V66A	0.152 ± 0.019	-9.29	1.14	
R122A	**V66A**	0.814 ± 0.033	-8.29	2.14	**0.37**
R126A	WT	0.454 ± 0.042	-8.64	1.79	
wild-type	D65A	0.332 ± 0.042	-8.82	1.61	
R126A	D65A	18.33 ± 1.500	-6.45	3.98	-0.58
wild-type	V66A	0.152 ± 0.010	-9.29	1.14	
R126A	V66A	5.149 ± 0.930	-7.20	3.23	-0.30
F135A	WT	0.205 ± 0.021	-9.11	1.32	
wild-type	D65A	0.332 ± 0.042	-8.82	1.61	
F135A	D65A	1.420 ± 0.110	-7.96	2.47	0.46
wild-type	V66A	0.152 ± 0.010	-9.29	1.14	
F135A	V66A	0.959 ± 0.130	-8.20	2.23	0.23

Cyt P450	Cyt b_5	K_d (μM) cyt b_5-cyt P450	Free energy of binding (kcal/mol) ΔG^a cyt b_5-cyt P450	Difference in free energy of binding (kcal/mol)	
				$\Delta\Delta G^b$ of mutant-wild-type	$\Delta\Delta G^c$ interaction of double mutants
M137A	WT	0.379 ± 0.040	-8.75	1.68	
wild-type	D65A	0.332 ± 0.012	-8.82	1.61	
M137A	D65A	3.951 ± 0.440	-7.36	3.07	0.22
wild-type	V66A	0.152 ± 0.010	-9.29	1.14	
M137A	V66A	1.583 ± 0.142	-7.90	2.53	0.30
K139A	WT	0.611 ± 0.050	-8.46	1.97	
wild-type	D65A	0.332 ± 0.012	-8.82	1.61	
K139A	D65A	4.831 ± 0.042	-7.24	3.19	0.38
wild-type	V66A	0.152 ± 0.010	-9.29	1.14	
K139A	V66A	1.400 ± 0.18	-7.97	2.46	0.65
K433A	WT	0.458 ± 0.053	-8.63	1.80	
wild-type	D65A	0.332 ± 0.012	-8.82	1.61	
K433A	**D65A**	0.869± 0.071	-8.26	2.17	**1.23**
wild-type	V66A	0.152 ± 0.010	-9.29	1.14	
K433A	**V66A**	0.487 ± 0.052	-8.60	1.83	**1.11**

*All K_d values were measured in the presence of methoxyflurane. See Section 2.1. WT stands for wild-type.

Based on the errors in the K_d values, the ranges of every $\Delta G_{binding}$, $\Delta\Delta G_{mut\text{-}wt}$ and $\Delta\Delta G_{int}$ were calculated. Below are the largest ranges of $\Delta\Delta G_{int}$ that are possible based on the errors in every K_d measurement.

Table 4.14 $\Delta\Delta G_{int}$ ranges obtained (calculated based on K_d measurement errors) for the double mutant cycle analysis.

Double mutant	$\Delta\Delta G_{int}$ range
R122-D65	0.97 – 1.16
R122-V66	0.25 – 0.49
R126-D65	-0.65 – -0.52
R126-V66	-0.32 – -0.24
F135-D65	0.40 – 0.52
F135-V66	0.17 – 0.30
M137-D65	0.13 – 0.32

Double mutant	**$\Delta\Delta G_{int}$ range**
M137-V66	0.21 – 0.39
K139-D65	0.22 – 0.55
K139-V66	0.58 – 0.74
K433-D65	1.13 – 1.34
K433-V66	1.04 – 1.18

If we look at the data and use a threshold such that the entire error range is above the threshold (Table 4.14), we obtain slightly different results than when using only the absolute values in Table 4.13. When using a high threshold of 0.50 kcal/mol, the following double mutants can be deemed as interacting in the cyt b_5-cyt P450 complex: R122-D65, K139-V66, K433-D65 and K433-V66. If using a lower threshold of 0.35 kcal/mol, the following double mutants are deemed as interacting in the wild-type complex: R122-D65, *F135-D65*, K139-V66, K433-D65 and K433-V66 (in italics is the additional one when lowering the threshold from 0.50 to 0.35 kcal/mol). Because of these results (based on the entire error ranges), restraints #5 and restraints #5 and #6 conjunctly (Table 4.8) were also tested with HADDOCK. See Section 4.4.6.1 for an explanation of the docking results with these unambiguous restraints included. In the end, however, only the bolded interactions in Table 4.13 were used as unambiguous restraints (Table 4.9).

4.4.4 Cyt P450 2B4 and cyt b_5 are well-folded and active under NMR conditions

CO assays performed on cyt P450 2B4 in isotropic bicelles (q = 0.25) revealed the characteristic 450 nm peak, which is indicative that the active site of cyt P450 is well-folded and that cyt P450 is not denatured in the presence of bicelles (Figure 4.5).

Similarly, activity assays done using DMPC/DHPC bicelles revealed that cyt P450 2B4 is still active in isotropic bicelles and that cyt b_5 is able to stimulate cyt P450 metabolism under these conditions (Table 4.15). It can be seen that the activity is reduced in bicelles when compared to assays done in solution with minimal DLPC. This has three possible causes: 1) the substrate partitions into the membrane and cannot reach cyt P450, 2) the product partitions into the membrane and cannot be detected by the fluoride ion electron and 3) some cyt P450 might not be active in the bicelle sample.

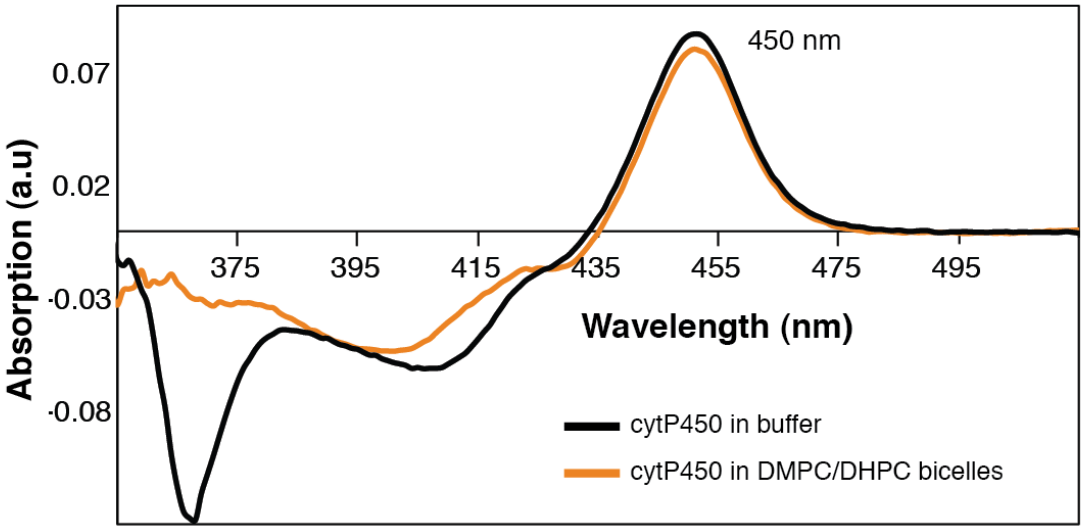

Figure 4.5 Cyt P450 is reconstituted in a functional form in DMPC/DHPC bicelles. The carbon monoxide (CO) difference spectra of cyt P450 2B4 were measured to determine the percentage of the functional form of cyt P450. We monitored the absorption increase at 450 nm as a result of the formation of the ferrous-cyt P450 bound to CO in both solution and bicelles. A few grains of dithionite were added to the sample containing 1 µM cyt P450 in 100 mM potassium phosphate, pH 7.4, and 5% (w/v) glycerol (with and without 2.0% (w/v) DMPC/DHPC isotropic bicelles, *q* = 0.25). The sample was mixed and incubated at room temperature for 5 min. The baseline spectrum of the reaction mixture was recorded from 600 nm to 300 nm. Subsequently, CO gas was bubbled gently through the dithionite-reduced solution for a few seconds and the reduced-CO difference spectrum was recorded at 25 °C.

Table 4.15 A comparison of the metabolism of methoxyflurane and benzphetamine by cyt P450 2B4 in solution and bicelles in the presence and absence of cyt b$_5$.

[cyt P450] (μM)	Bicelles [DMPC/DHPC] (mM)	nmoles F$^-$/min/nmol cyt P450 2B4 or nmoles CH$_2$O/min/nmol cyt P450 2B4			Relative activity in bicelles
		-cyt b$_5$	+cyt b$_5$	+cyt b$_5$/-cyt b$_5$	
Methoxyflurane metabolism					
1	-	0.19 ± 0.02	1.35 ± 0.04	7.1	100
1	-	0.22 ± 0.03	0.97 ± 0.02	4.4	72
1	-	0.15 ± 0.04	0.63 ± 0.12	4.4	47
1	59.0/16.76	0.10 ± 0.02	0.45 ± 0.04	4.5	33
Benzphetamine metabolism					
0.2	-	46 ± 2	52 ± 2	1.1	100
0.2	-	30 ± 4	43 ± 5	1.4	83
0.2	36.88/10.47	33 ± 3	37 ± 5	1.1	71

4.4.5 Observation via NMR of complex formation between ^{15}N-labeled cyt b$_5$ with substrate-free or substrate-bound cyt P450

As mentioned in Chapter 2 and the introduction of this chapter, it is possible to establish the residues at the interface based on either chemical shift perturbations or changes in intensity. Overall line broadening (due to an increase in size and decrease in T_2 upon complex formation) was observed for cyt b$_5$ in complex with both substrate-free and substrate-bound cyt P450. In the complex between cyt b$_5$ and substrate-free cyt P450 (Figure 4.6, yellow), a closer inspection of the spectrum revealed differential line broadening for some residues and a detailed analysis was performed. A threshold of > 20% decrease in intensity was considered significant line broadening, with the following residues being identified: I17, S23, K24, Y35, L37, K39, F40, H44, H48, E49, F63, D65, V66, T70, D71, A72, R73, E74, L75, S76, F79, I81 and D88 (orange in Figure 4.6b). While the linker region is colored orange in Figure 4.6b, measurement of the intensities for the linker region residues was not reliable due to the presence of 3-4 conformers/peaks for each residue. For the following residues, the % intensity change is actually above 100% (because of the normalization procedure): 9-10, 21-22, 25 and 54. The error is therefore ~27%. The threshold of 20% is therefore not as reliable as it should be but it is what was used for the manuscript.[61] The next chapters will focus on a more thorough and definite method for determining the interface between the two proteins. However, for the HADDOCK simulations, the residues listed above, which were determined to be solvent accessible based on ASAView,[60] were used as active residues (see Table 4.9).

Upon addition of substrate-bound cyt P450, extensive line broadening was observed that encompassed residues on all sides of cyt b_5 (Figure 4.6c). The broadening was seen progressively as more cyt P450 was titrated into the NMR sample (Figure 4.6, histograms A-C). Due to the drastic reduction in peak intensities, even with the addition of the smallest amount of cyt P450, further analysis was not pursued in the manuscript[61] and this chapter. Chapter 5 will discuss the cyt b_5 interface in more details, both in the presence and absence of BHT.

4.4.6 HADDOCK results for the various runs performed

In this section, for all HADDOCK-generated cyt b_5-cyt P450 structures, the orientation of cyt P450 2B4 was set according to numerous publications listing that cyts P450 are attached to the membrane by the N-terminus signal anchor and that additional portions of cyt P450 are also buried below the membrane surface.[70,71] A discussion on the membrane topology of cyts P450 can be found in Section 1.2.2.

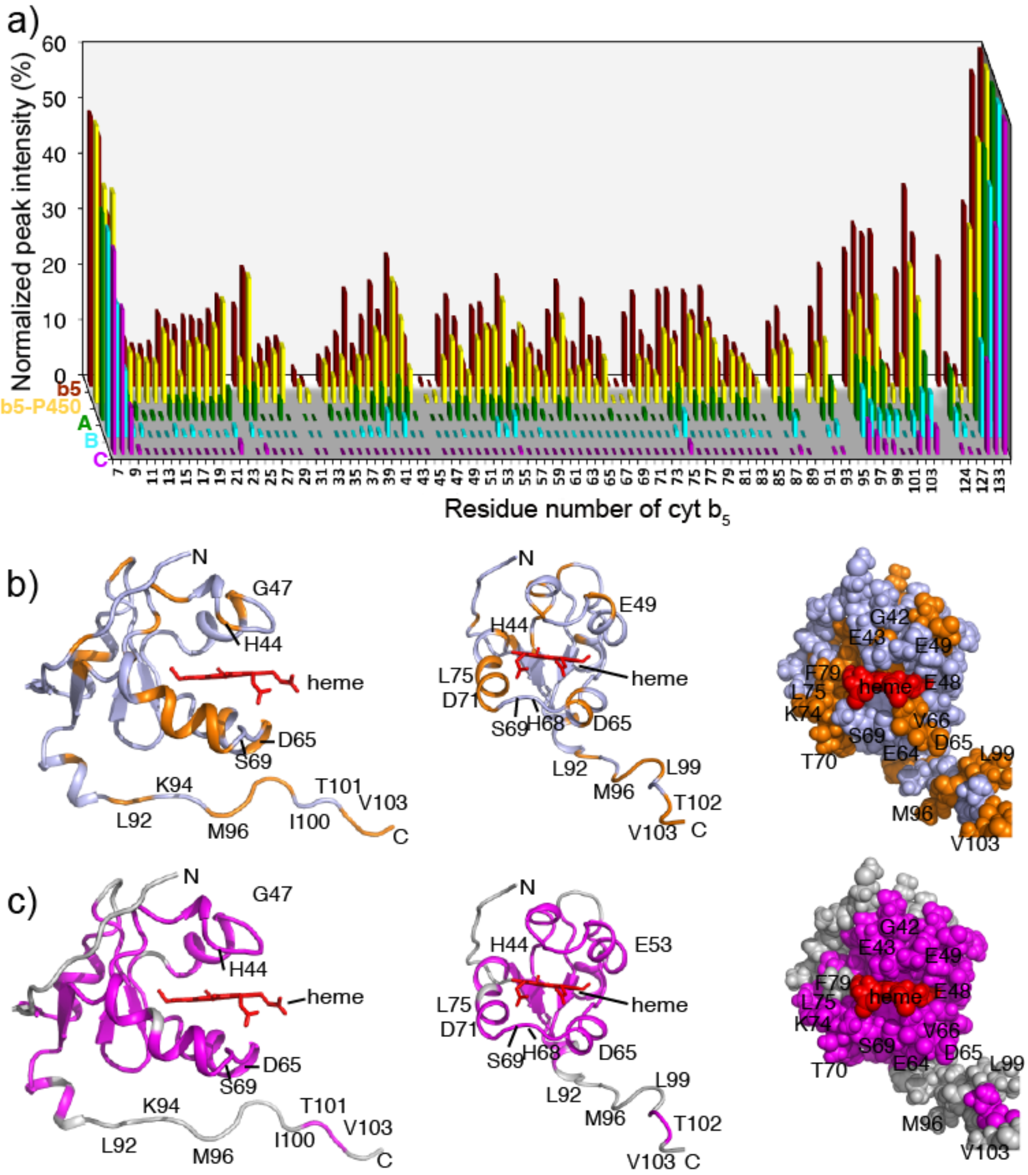

Figure 4.6 Mapping the effect of cyt P450 binding to cyt b_5 using NMR. (a) A histogram representing the differential line broadening NMR data for the cyt b_5-cyt P450 complex. The amide peak intensities for free cyt b_5 (red) and for cyt b_5 residues in a 1:1 equimolar complex with substrate-free cyt P450 (yellow) are presented. Green, cyan and magenta highlight the extensive peak broadening observed for cyt b_5 residues upon addition of the increasing amounts of unlabeled cyt P450 bound to BHT (A=1:0.3, B=1:0.6 and C=1:1 molar ratios between cyt b_5 and cyt P450). All peak intensities were normalized to the C-terminal residue, D134, in the unbound cyt b_5 spectrum to account for the change in intensity upon complex formation. (b) and (c) present two different views of cyt b_5 rotated by 90° with respect to each other and a space filling representation of the second view. (b) Cyt b_5 residues exhibiting extensive line broadening upon complex formation with an equimolar amount of substrate/ligand-free cyt P450 are colored orange onto the NMR structure of cyt b_5. (c) Cyt b_5 residues whose resonances are broadened beyond detection upon complex formation with an equimolar amount of cyt P450 bound to BHT are represented in magenta.

4.4.6.1 Only unambiguous restraints considered

As mentioned in Section 4.4.3, different combinations of restraints were tested to assess the weight of each restraint in Table 4.9. To test whether the ambiguous restraints influenced the docking results, complex structures were calculated with only the unambiguous restraints (#1-4 in Table 4.8). Complex structures obtained could be clustered into four groups/clusters of structures (Table 4.17) based on the orientation of cyt b_5 with respect to cyt P450 (see Section 4.3.7.11). The two lowest energy clusters, with 13 and 10 structures, respectively, were labeled as clusters I and II (Table 4.17). All four of the unambiguous restraints were violated, with only the restraint for V66-R122 being violated in less than 40% of the structures (Table 4.16). All structures had a cyt b_5 center of mass in a location that could be considered productive based on the orientation of cyt b_5 with respect to cyt P450 (Figure 4.8). This can further be seen by looking at the location of the cyt b_5 soluble domain in clusters I and II in Figure 4.9 and remembering that the linker is unstructured and flexible (Chapter 3). Both clusters I and II might also be productive orientations since the shortest heme-edge to heme-edge distance was 10.3 and 13.9 Å for clusters I and II, respectively, which is within the 14 Å limit needed for electron transfer.[72] Figure 4.7 shows how the unambiguous restraints hold cyt b_5 relative to cyt P450. Upon analysis of the interface of cluster I, nine hydrogen bonds (H-bonds) and ten salt bridges were found (Table 4.18). While there was some overlap in the types of non-covalent interactions found at the interface between Table 4.18 and Table 4.28 (the final interface analysis in the HADDOCK structure published), such as hydrogen bonds for N62-E93, E64-R126 and D65-R122, and salt bridges for N64-

R126 and D65-R122, the complex generated here had more interactions for cyt b_5 D71, and the cyt b_5 heme, with cyt P450. While these complex structures, particularly clusters I and II, are possible productive orientations for the cyt b_5-cyt P450 complex, the violations were far too many in order for these simulation results to ever be considered for publication. Additionally, their populations were each only one fifth of the fifty structures. Adding ambiguous restraints appears to be necessary in order to ameliorate the docking, minimize the violations and converge to a smaller number of solutions.

Table 4.16 Violations of unambiguous restraints for the HADDOCK simulation with only restraints #1-4 in Table 4.8. This simulation did not include any ambiguous restraints.

Cyt b_5	Cyt P450	Restraint range (Å)	R_{avg} (Å)	# of structures
V66-NH	K433-NH	2.0-8.0	12.740	26
D65-NH	K433-NH	2.0-8.0	11.982	42
D65-NH	R122-NH	2.0-8.0	10.602	20
V66-NH	R122-NH	2.0-8.0	10.530	13

Table 4.17 Four clusters of complex structures for the HADDOCK simulation with only restraints #1-4 in Table 4.8. This simulation did not include any ambiguous restraints.

Cluster #	# of structures	# of structures in the lowest 10 energy structures	Average RMSD (Å)
I	13	5 (50%)	0.516
II	10	2 (20%)	0.456
III	6	2 (20%)	0.412
IV	7	0	0.403
none	14	1	

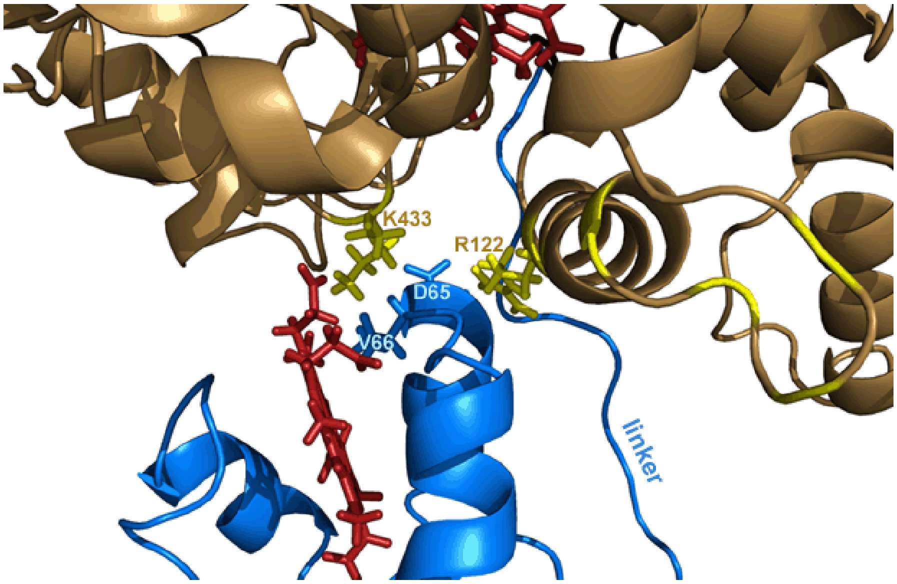
K433
R122
D65
V66
linker

Figure 4.7 A closer look at how the four (#1-4 in Table 4.8) unambiguous restraints hold cyt b_5 in place in cluster I. The side chains of the labeled amino acids are shown as sticks.

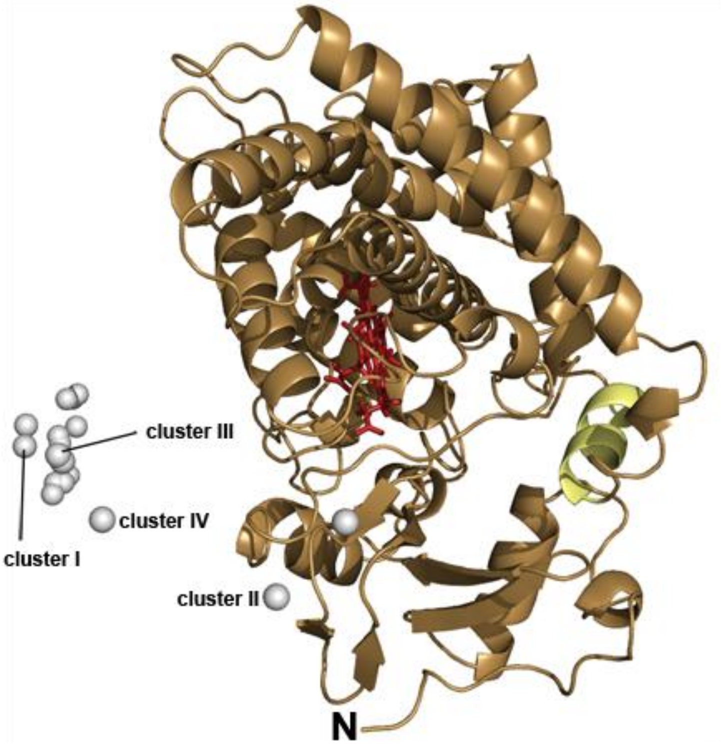
cluster III
cluster IV
cluster I
cluster II
N

Figure 4.8 Center of mass representation of the different clusters obtained for the HADDOCK simulation with only restraints #1-4 in Table 4.8. Each white sphere is a cyt b_5 center of mass (calculated from only the soluble domain) of the different orientations of cyt b_5 relative to cyt P450 (brown).

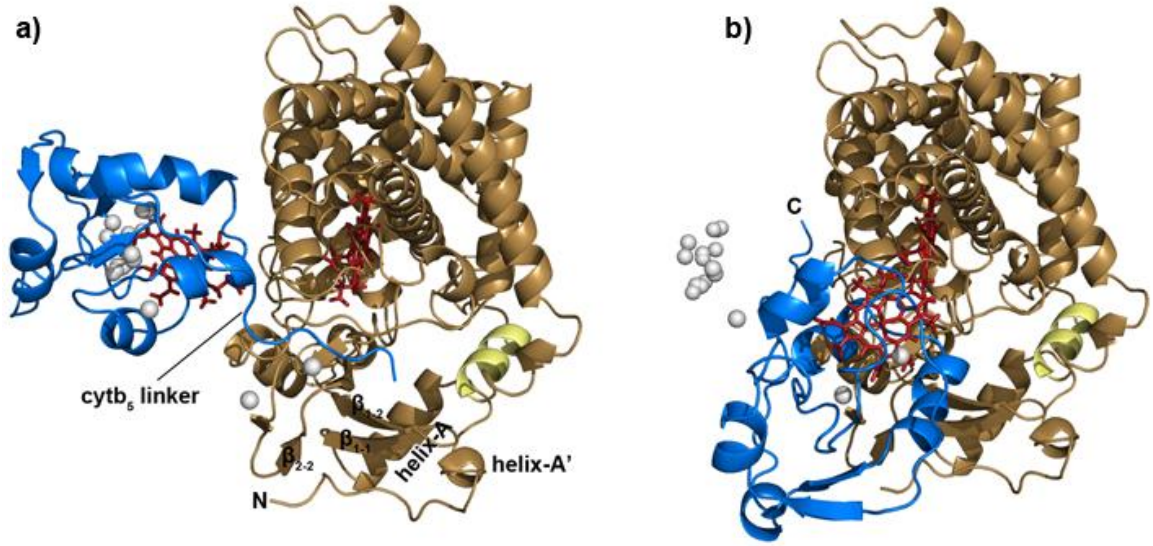

Figure 4.9 Complex structures (clusters I and II) obtained for the HADDOCK simulation with only restraints #1-4 in Table 4.8. Cyt b_5 is in blue, and cyt P450 is in brown with the F' 3_{10} helix in yellow. a) Lowest energy structure from cluster I. The N-terminus of cyt b_5 is facing directly into the plane of the paper and its linker is coming out of the side facing the viewer. b) Lowest energy structure from cluster II. Cyt b_5 is rotated by 180°, with the C-terminus pointing into the plane of the paper and the N-terminus on the side facing the viewer, with cyt b_5 shifted downwards compared to cluster I. The white dots are the center of masses of cyt b_5 from other complex structures generated (see Figure 4.8). The orientation of cyt P450 will be identical to this figure in all the following figures.

Table 4.18 Hydrogen bonds and salt bridges at the complex interface of cluster I for the HADDOCK simulation with only restraints #1-4 in Table 4.8.

Cyt b_5 residue [atom]	Interatom distance (Å)	Cyt P450 residue [atom]	Type of interaction
N62 [HD22]	1.68	E93 [OE1]	H-bond
E64 [OE1]	1.56	R126 [HH12]	H-bond
E64 [OE2]	1.62	R126 [HH22]	H-bond
D65 [OD2]	1.72	R122 [HH11]	H-bond
D71 [OD1]	1.68	R133 [HH12]	H-bond
D71 [OD2]	1.61	R133 [HH22]	H-bond
Heme [O1D]	3.81	K433[N]	H-bond
Heme [O2D]	3.62	K433[N]	H-bond
Heme [O1D]	1.66	K433 [HZ3]	H-bond
E64 [OE1]	3.56	R126 [NH2]	salt bridge
E64 [OE1]	2.61	R126 [NH1]	salt bridge
E64 [OE2]	2.65	R126 [NH2]	salt bridge
E64 [OE2]	3.31	R126 [NH1]	salt bridge

Cyt b_5 residue [atom]	Interatom distance (Å)	Cyt P450 residue [atom]	Type of interaction
D65 [OD2]	2.66	R122 [NH1]	salt bridge
D65 [OD2]	3.91	R122 [NE]	salt bridge
D71 [OD1]	2.72	R133 [NH1]	salt bridge
D71 [OD1]	3.61	R133 [NH2]	salt bridge
D71 [OD2]	3.37	R133 [NH1]	salt bridge
D71 [OD2]	2.66	R133 [NH2]	salt bridge

Because restraint #4 in Table 4.8 had a very small positive $\Delta\Delta G_{int}$ (0.37 kcal/mol), a HADDOCK calculation was also performed with only the three unambiguous restraints that had $\Delta\Delta G_{int}$ > 1.0 kcal/mol (restraints #1-3 in Table 4.8). Complex structures generated from this run could be clustered into eight groups of structures with similar populations (Table 4.20). The two lowest energy clusters were labeled as clusters I and II, which consisted of ten and seven structures, respectively (Table 4.20). All three of the unambiguous restraints were violated in $\geq$ 36% of the structures (Table 4.19). However, all structures had a cyt b_5 center of mass in a location that could be considered possible based on the location of the soluble domain of cyt b_5 with respect to cyt P450 (Figure 4.11), including clusters I and II (Figure 4.10). However, when calculating the heme-edge to heme-edge distance, as seen in Figure 4.10, the values were 16.5 and 11.5 Å for clusters I and II, respectively. Upon analysis of the interface of cluster I, fifteen hydrogen bonds and four salt bridges were found (Table 4.21), but many interactions took place between residues of cyt P450 that have not been experimentally studied yet (e.g. A92 and E93) and there was no overlap with the non-covalent interactions found in Table 4.28. Cluster I can also be disregarded since its heme-edge to heme-edge distance is beyond 14 Å.[72] Upon analysis of the interface of cluster II, eleven hydrogen bonds and ten salt bridges were found (Table 4.22); similarly to cluster I, there was no overlap with the non-covalent interactions found in Table 4.28; however, in cluster II, R422 was found at the interface, which is not possible since it is known that mutation of R422 does not affect cyt b_5-cyt P450 binding (Table 4.12 and elsewhere[13]).

Table 4.19 Violations of unambiguous restraints for the HADDOCK simulation with only restraints #1-3 in Table 4.8.

Cyt b_5	Cyt P450	Restraint range (Å)	R_{avg} (Å)	# of structures
V66	K433	2.0-8.0	10.627	18
D65	K433	2.0-8.0	10.521	18
D65	R122	2.0-8.0	12.873	45

Table 4.20 Eight clusters of complex structures obtained for the HADDOCK simulation with only restraints #1-3 in Table 4.8.

Cluster #	# of structures	# of structures in the lowest 10 energy structures	Average RMSD (Å)
I	10	2 (20%)	0.644
II	7	2 (20%)	0.599
III	6	2 (20%)	0.675
IV	4	2 (20%)	0.700
V	8	1 (10%)	0.561
VI	5	0	0.883
VII	3	0	0.497
VIII	4	0	0.626
none	3	1 (10%)	

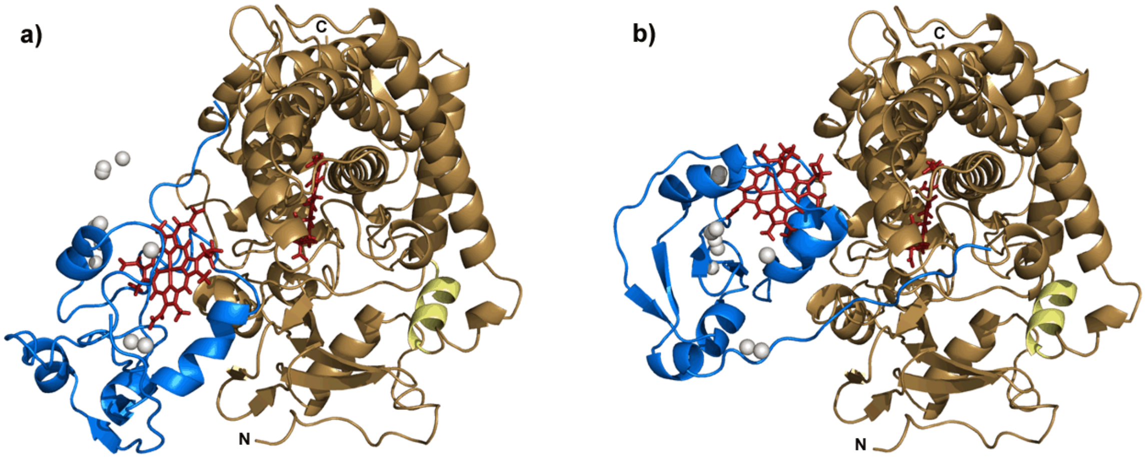

Figure 4.10 Lowest energy structure from a) cluster I and b) cluster II for the HADDOCK simulation with only restraints #1-3 in Table 4.8. Cyt b_5 is in blue, and cyt P450 is in brown. Each white sphere is a cyt b_5 center of mass (calculated from only the soluble domain) of the other orientations of cyt b_5 relative to cyt P450 (brown).

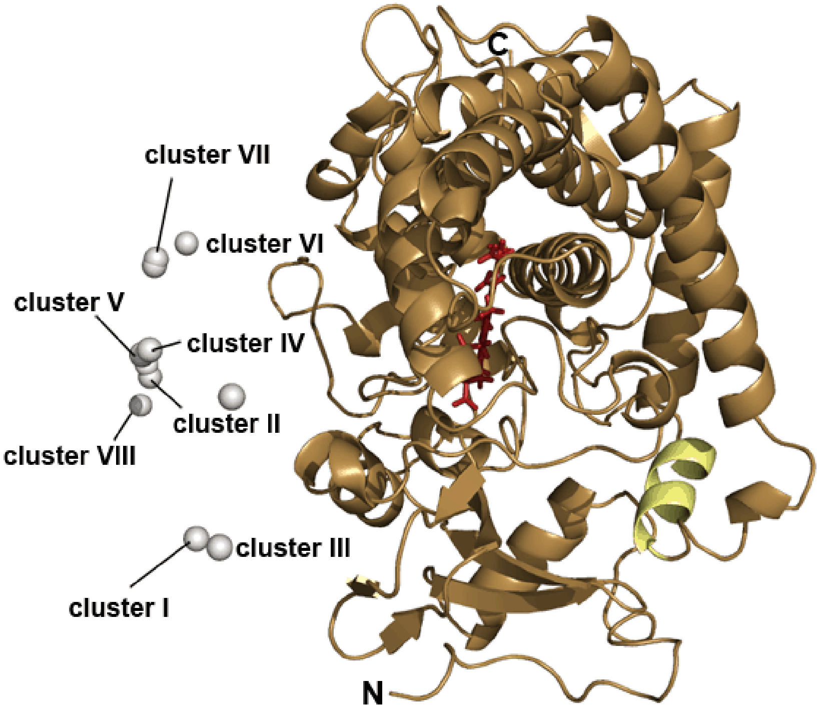
C
cluster VII
cluster VI
cluster V
cluster IV
cluster II
cluster VIII
cluster III
cluster I
N

Figure 4.11 Center of mass representation of the different clusters obtained for the HADDOCK simulation with only restraints #1-3 in Table 4.8. Each white sphere is a cyt b_5 center of mass (calculated from only the soluble domain) of the different orientations of cyt b_5 relative to cyt P450 (brown).

Table 4.21 Hydrogen bonds and salt bridge contacts in cluster I for the HADDOCK simulation with only restraints #1-3 in Table 4.8.

Cyt b_5 residue [atom]	Interatom distance (Å)	Cyt P450 residue [atom]	Type of interaction
H68 [N]	3.25	E93 [OE1]	H-bond
R73 [HH12]	2.38	E93 [OE2]	H-bond
R73 [HH11]	2.28	T372 [OG1]	H-bond
R73 [HH22]	1.87	E93 [OE2]	H-bond
E64 [OE1]	3.27	A92 [N]	H-bond
E64 [OE1]	2.79	E93 [N]	H-bond
E64 [OE2]	3.00	E93 [N]	H-bond
E64 [OE2]	1.58	K433 [HZ1]	H-bond
E64 [O]	1.86	K433 [HZ2]	H-bond
V66 [O]	1.78	R126 [HH21]	H-bond
G67 [O]	1.92	R122 [HE]	H-bond
R73 [O]	1.90	N373 [HZ1]	H-bond
E74 [OE1]	1.70	N384 [HZ2]	H-bond
Heme [O2D]	1.69	R126 [HH12]	H-bond
Heme [O2D]	2.41	R126 [HH22]	H-bond
R73 [NH1]	3.14	E93 [OE2]	salt-bridge
R73 [NH2]	2.78	E93 [OE2]	salt-bridge
R73 [NH2]	3.43	E93 [OE1]	salt-bridge
E64 [OE2]	2.62	K433 [NZ]	salt-bridge

Table 4.22 Hydrogen bonds and salt bridge contacts in cluster II for the HADDOCK simulation with only restraints #1-3 in Table 4.8.

Cyt b_5 residue [atom]	Interatom distance (Å)	Cyt P450 residue [atom]	Type of interaction
K18 [HZ1]	1.70	D90 [OD1]	H-bond
R52 [HH21]	2.10	E424 [OE1]	H-bond
E48 [OE1]	1.62	R422 [HH12]	H-bond
E48 [OE2]	1.84	R422 [HH22]	H-bond
E53 [OE1]	3.14	K433 [N]	H-bond
E61 [OE1]	3.14	E93 [N]	H-bond
E61 [OE1]	1.64	K433 [HZ1]	H-bond
E64 [O]	2.13	R122 [HH21]	H-bond
V66 [O]	1.72	R126 [HE]	H-bond
G67 [O]	2.05	R126 [HH21]	H-bond
Heme [O2D]	1.72	R126 [HH22]	H-bond
K18 [NZ]	3.46	D90 [OD2]	salt-bridge
K18 [NZ]	2.75	D90 [OD1]	salt-bridge
R52 [NH2]	2.81	E424 [OE1]	salt-bridge
E48 [OE1]	2.64	R422 [NH1]	salt-bridge
E48 [OE1]	3.14	R422 [NH2]	salt-bridge

Cyt b_5 residue [atom]	**Interatom distance (Å)**	**Cyt P450 residue [atom]**	**Type of interaction**
E48 [OE2]	3.74	R422 [NH1]	salt-bridge
E48 [OE2]	2.83	R422 [NH2]	salt-bridge
E53 [OE1]	3.98	K433 [NZ]	salt-bridge
E53 [OE2]	3.42	K433 [NZ]	salt-bridge
E61 [OE1]	2.66	K433 [NZ]	salt-bridge

In both of the runs previously discussed in this section, most of the cyt b_5 orientations were in a position that could be considered possible, with the center of mass of cyt b_5 being located near the N-terminus of cyt P450 (which would not lead to electron transfer but is physiologically possible depending on how much of cyt P450 2B4 is buried under the membrane), or directly at the center of the proximal side of cyt P450 (where the heme comes closest to the surface), with only the latter orientation allowing for electron transfer. The lower cleft of cyt b_5 is held in the concavity between cyt P450 K433 and R122, with the first four unambiguous restraints in Table 4.8. Figure 4.7 shows how the side chains of cyt b_5 V66 and D65 are oriented with respect to the cyt P450 side chains of K433 and R122.

By comparing the two runs (four restraints versus three restraints), it is possible to see that the fourth restraint between V66 and R122, which has the lowest $\Delta\Delta G_{int}$, makes a very large impact on the clustering of the resulting complex structures. In the run with four restraints, there were four main populations of structures composed of 13, 10, 6 and 7 structures each. Cluster I contained half of the 10 lowest energy structures and the remainder were half in cluster II and the other half in cluster III. With removal of the fourth restraint (having only restraints #1-3 in Table 4.8), there were now five clusters (with 10, 7, 6, 4 and 8 structures) with relatively equal populations of the lowest 10 energy structures (1 or 2). The fourth restraint therefore restricts the interactions enough that the simulation is able to converge into fewer solutions. If we look at the specifics of the interactions between the two runs, it can be seen that the salt bridges and hydrogen bonds between the two proteins' soluble domains in their respective cluster I are also different. Interactions between cyt b_5 residues N62, E64, D65, D71 and heme propionates and cyt P450 residues E93, R122, R126, R133 and K433 were seen for the run with restraints #1-4; and interactions between cyt b_5 residues E64, V66, G67, H68, R73, E74 and heme propionates and cyt P450 residues A92, E93, R122, R126, T372, N373, N384 and K433 were seen for the run with only restraints #1-3. More residues are involved in these types of interactions in the run with three restraints because the unambiguous restraints are not holding the two proteins as specifically together.

Other runs were also performed in which restraint #4 (Table 4.8) was removed and other restraints were included which had higher experimental $\Delta\Delta G_{int}$. One such run was performed with restraint #5, and another run was performed with restraints #5 and #6 (Table 4.8). In both cases, the docking simulations did not converge. For the run with restraint #5, nine clusters were obtained (the 10 lowest energy structures were spread out among the clusters), and for the run with restraints #5 and #6, seven clusters were obtained (half of the lowest energy structures lied in one cluster and the remainder were spread out among clusters). For the reasons listed in Section 4.3.7.10 and the fact that the complex structures were spread over too many different clusters, an analysis of the hydrogen bonds and salt bridges, using PISA, was not done for these two runs.

4.4.6.2 Only the ambiguous restraints considered

Complex structures obtained with only ambiguous restraints (found in Table 4.5) could be clustered into six groups of structures (Table 4.24). The two lowest energy clusters, labeled as clusters I and II, had 7 and 10 structures, respectively. As is typical for ambiguous restraints in HADDOCK, a long list of violations were generated (Table 4.23); this is because violations are listed for every atom of every passive and active residue on cyt b_5 to every atom of every passive and active residue on cyt P450. By looking at the generated complex structures, it could be seen that the majority of the cyt b_5 orientations were near the C-terminus of cyt P450 (Figures 4.12 and 4.13). These orientations are not physiologically relevant as the N-terminus of cyt P450 is anchored to the membrane and the distance between the membrane and the top of cyt P450 2B4 has been estimated to be around 30-50 Å.[70,71] Furthermore, the distance calculated from the cyt b_5 heme edge to the cyt P450 heme edge is too large to allow for electron transfer between the two redox centers,[72,73] e.g. for cluster I the distance was 15.7 Å. Only three structures (out of the fifty) had cyt b_5 orientations which might be physiologically plausible because of their orientation relative to cyt P450.

Table 4.23 Violations of ambiguous restraints for the HADDOCK simulation with only the ambiguous restraints in Table 4.5.

Cyt P450	Cyt b_5	R_{avg} (Å)	# of structures
433	all residues	5.146	39
all residues	49	4.972	36
all residues	48	4.590	32
137	all residues	4.453	9
122	all residues	4.441	48
all residues	6	4.129	21
all residues	71	4.000	8
135	all residues	3.819	15
139	all residues	3.788	33
133	all residues	3.719	17
126	all residues	3.644	18
all residues	74	3.576	12
all residues	39	3.388	39
all residues	70	3.342	24
all residues	73	3.241	32

Table 4.24 Six clusters of complex structures for the HADDOCK simulation with only the ambiguous restraints in Table 4.5.

Cluster #	# of structures	# of structures in the lowest 10 energy structures	Average RMSD (Å)
I	7	3 (30%)	0.494
II	10	2 (20%)	0.526
III	9	2 (20%)	0.458
IV	6	1 (10%)	0.466
V	4	0	0.491
VI	2	0	0.489
none	12	2 (20%)	

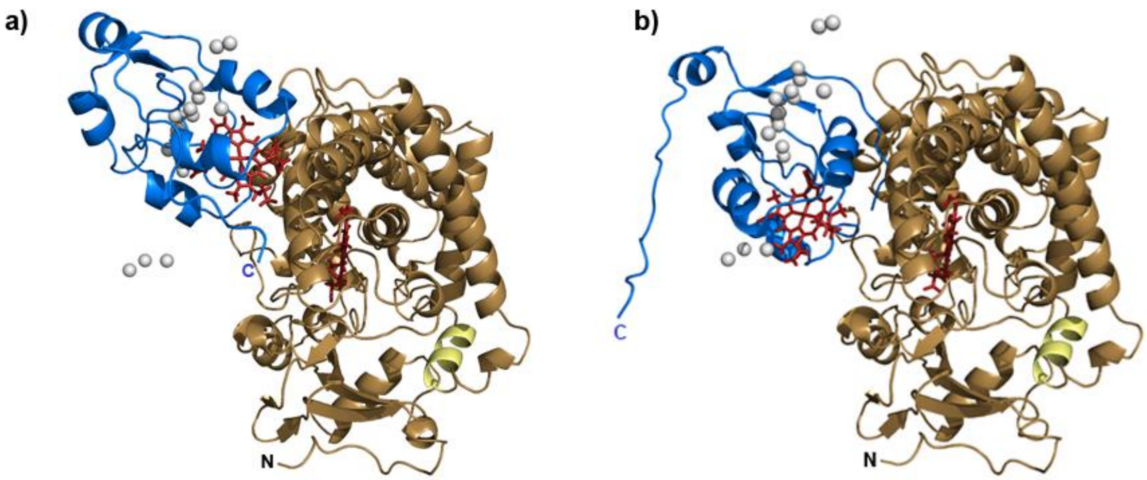

Figure 4.12 Complex structures (clusters I and II) obtained for the HADDOCK simulation with only the ambiguous restraints in Table 4.5. Cyt b_5 is in blue and cyt P450 is in brown with the F' 3_{10} helix in yellow. a) Lowest energy structure from cluster I. b) Lowest energy structure from cluster II. Each white sphere is a cyt b_5 center of mass (calculated from only the soluble domain) of the other orientations of cyt b_5 relative to cyt P450 (brown).

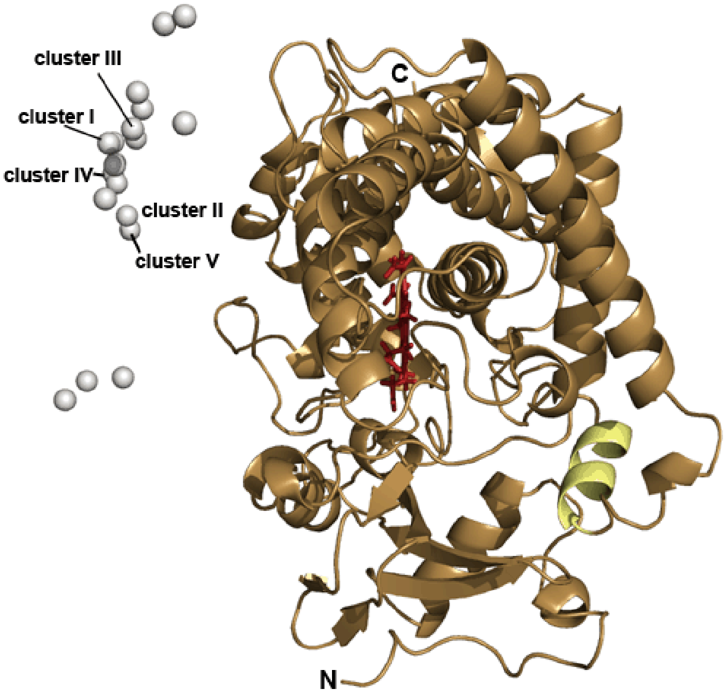

Figure 4.13 Center of mass representation of the different clusters for the HADDOCK simulation with only the ambiguous restraints in Table 4.5. Each white sphere is a cyt b_5 center of mass (calculated from only the soluble domain) of the different orientations of cyt b_5 relative to cyt P450 (brown).

Table 4.25 Hydrogen bonds and salt bridges in cluster I for the HADDOCK simulation with only the ambiguous restraints in Table 4.5.

Cyt b_5 residue [atom]	Interatom distance (Å)	Cyt P450 residue [atom]	Type of interaction
E42 [O]	1.83	R133[HH11]	H-bond
D71 [OD1]	1.61	K139[HZ1]	H-bond
D71 [OD2]	1.79	N260[HD22]	H-bond
Heme [O1D]	1.60	R126 [HH21]	H-bond
Heme [O2D]	1.70	R271 [HH12]	H-bond
D71 [OD1]	2.59	K139 [NZ]	Salt bridge
D71 [OD2]	3.43	K139 [NZ]	Salt bridge

Two settings for the semi-flexible segments were also tested: a setting where HADDOCK selected the residues at the interface automatically during the run and allowed them to be semi-flexible (discussed above) and a second setting where the semi-flexible segments were selected based on the range of active and passive residues (see Section 4.3.7.8). When setting the semi-flexible segments explicitly, as shown in Table 4.6, the number of clusters dramatically increased from six (Table 4.23) to eleven (Table 4.26). The center of mass orientations of cyt b_5 were similar for this run (Figure 4.14) as for the run with the semi-flexible segments set automatically (Figure 4.13). Cluster V of this run appeared to be a plausible solution but the heme-edge to heme-edge distance was longer than 14 Å (Figure 4.15). Since we do not have complete information on the entire proximal surface of cyt P450, it seems more logical to use the automatic settings where HADDOCK decides which segments to set as semi-flexible based on the complex structures it generates prior to stage 2 of the docking process. However, because we wanted to perform rigid body docking and not allow the structures of either cyt b_5 or cyt P450 to change too much during docking, the semi-flexible segments were set as listed in Table 4.10 – this set of residues is less than when setting all semi-flexible segments explicitly as done in Table 4.6 and restricts the amount of motions that the residues can undergo during simulated annealing.

Table 4.26 Eleven clusters of complex structures for the HADDOCK simulation in which semi-flexible segments were those listed in Table 4.6. Only the ambiguous restraints in Table 4.5 were used for this simulation.

Cluster #	# of structures	# of structures in the lowest 10 energy structures	Average RMSD (Å)
I	6	3 (30%)	1.084
II	4	1 (10%)	0.917
III	4	1 (10%)	0.967
IV	2	1 (10%)	1.072
V	3	1 (10%)	0.912
VI	3	1 (10%)	1.017
VII	2	1 (10%)	0.927
VIII	5	0	1.088
IX	2	0	0.944
X	2	0	0.990
XI	2	0	0.847
none	14	1 (10%)	

A simulation was also done in which the heme propionate atoms were added to the list of passive residues of cyt b_5 (Table 4.7). This was done based on previous studies that have shown that the propionates are involved in interactions with cyt P450,[74–76] and the fact that the atoms are proximal to residues identified via NMR differential line broadening. The solutions to the runs in which the heme atoms were considered passive residues had more clusters and more structures that did not fit within clusters (data not shown). Despite these results, the more restraints are given to the protein-protein docking, the more accurate the simulation results. Additionally, the contribution of the cyt b_5 heme passive atoms may differ in the presence of the unambiguous restraints.

However, this was considered after the submission of the manuscript so the heme atoms are not included in Table 4.9. It should be noted that the cyt b_5 heme atoms are found at the interface of our final cyt b_5-cyt P450 complexes (Table 4.28).

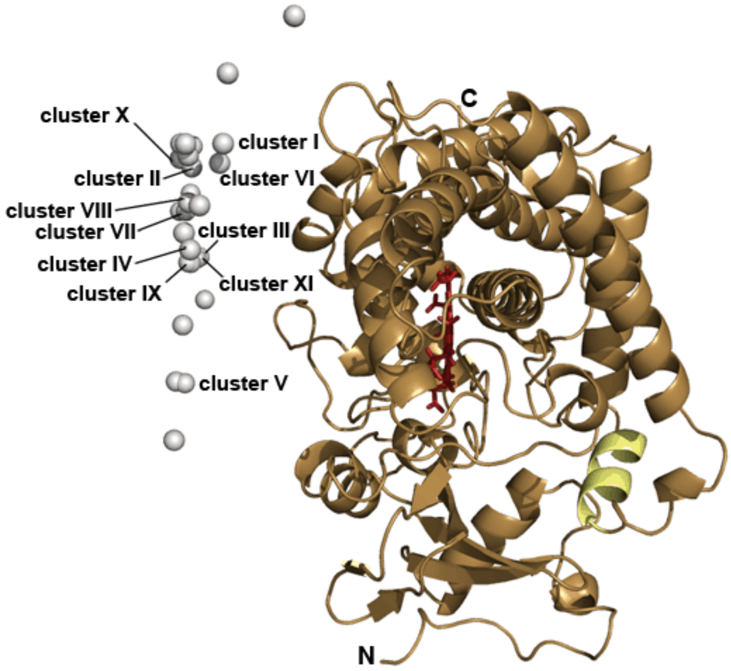
cluster X
cluster I
cluster II
cluster VI
cluster VIII
cluster VII
cluster III
cluster IV
cluster XI
cluster IX
cluster V
C
N

Figure 4.14 Center of mass representation of the different clusters for the HADDOCK simulation in which semi-flexible segments were those listed in Table 4.6. Only the ambiguous restraints in Table 4.5 were used for this simulation. Each white spheres represents a cyt b_5 center of mass (calculated from only the soluble domain) of the different orientations of cyt b_5 relative to cyt P450 (brown).

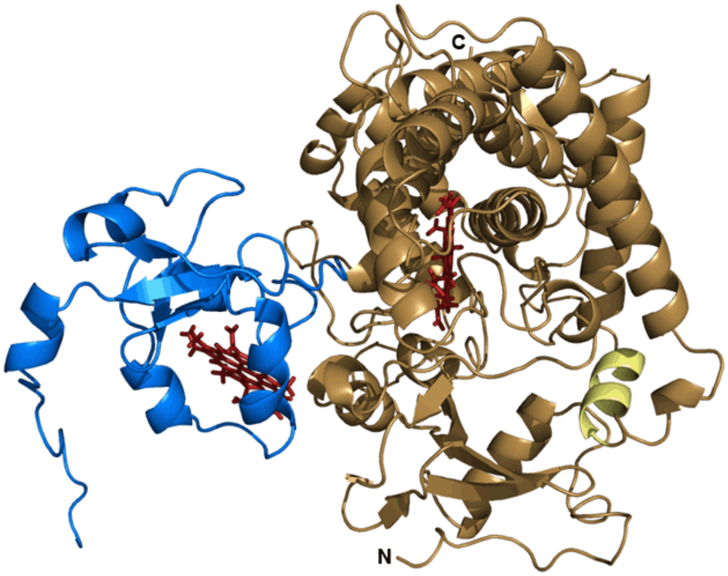

Figure 4.15 Cluster V for the HADDOCK simulation in which semi-flexible segments were those listed in Table 4.6. The complex of this structure was shown because the center of mass of cyt b_5 appears to be in a productive location according to Figure 4.14. Upon closer inspection, however, the heme-edge to heme-edge distance was determined to be 16.1 Å, which would not allow for electron transfer.[72]

4.4.7 Final HADDOCK generated structures

With the final parameters chosen (Section 4.3.7.10), the HADDOCK simulation resulted in two low energy clusters with populations of 21 and 14 structures for clusters I and II, respectively (Figure 4.17). The energy statistics of clusters I and II can be found in Table 4.27. The differences between clusters I and II can be seen by looking at the interaction interfaces highlighted in Figure 4.19. Cluster II (Figure 4.19c) involves the interaction of both the upper and lower cleft of cyt b_5, whereas cluster I (Figure 4.19b) involves the interaction of only the lower cleft of cyt b_5. The center of mass representation of the other, less populated clusters can be found in Figure 4.16.

The heme-edge to heme-edge distance was 9.0 and 7.4 Å for clusters I and II, respectively, which is within the 14 Å limit.[72] The Fe to Fe distance between cyt b_5 and cyt P450 was 20.9 and 19.3 Å for clusters I and II, respectively. The shortest electron transfer pathway was predicted using HARLEM[77] for both clusters and is shown in Figure 4.18b. The residues at the interface of the cyt b_5-cyt P450 complex for both clusters I and II are labeled and listed in Figure 4.20 and Table 4.28, respectively.

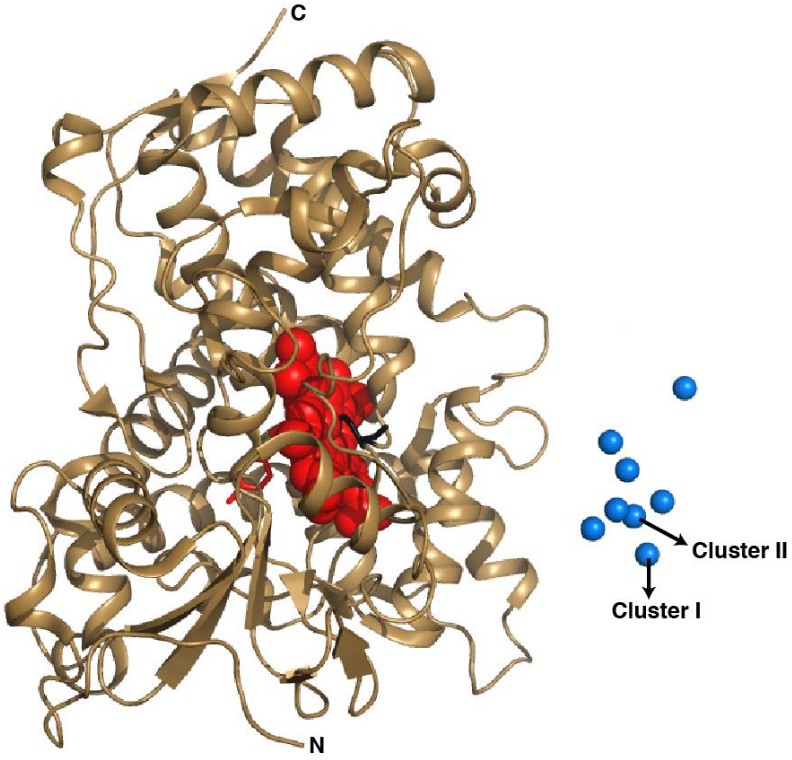

Figure 4.16 Center of mass representation of the HADDOCK docking solution for the cyt b_5-cyt P450 complex.

The final 50 lowest energy complex orientations generated from HADDOCK were clustered based on the RMSD from a reference structure. 35 out of the 50 final structures were clustered into two main subpopulations (I and II). However, the remaining 15 structures were further clustered into smaller groups based on RMSD from the reference structure. The figure above presents the center of mass of cyt b_5, presented in blue spheres, superimposed on the cartoon representation of cyt P450. The center of mass was calculated for one structure from each of the clusters representing the different complex orientations.

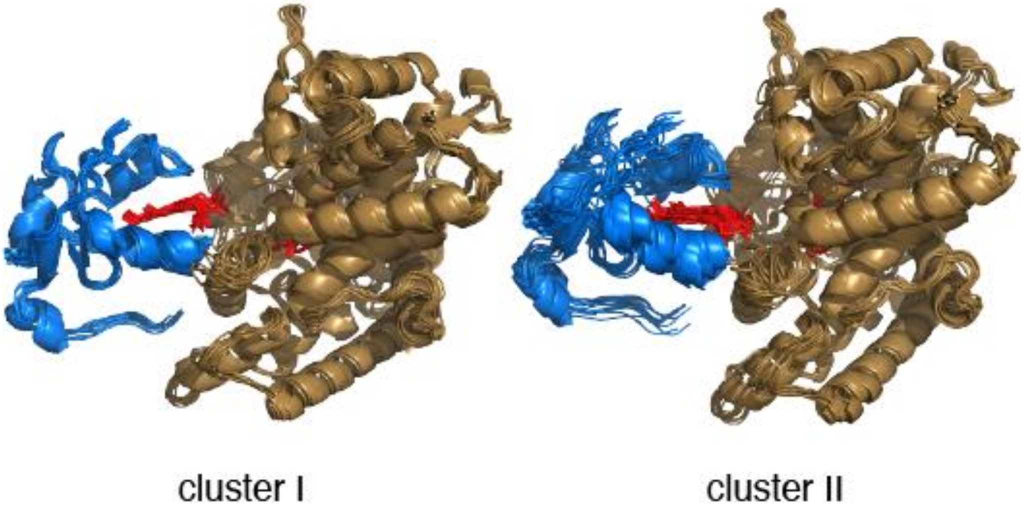

Figure 4.17 The two final clusters of cyt b_5-cyt P450 complex structures obtained from HADDOCK. An overlay of the 10 lowest energy structures from the two main subpopulations (clusters I and II) of docked structures for the cyt b_5-cyt P450 complex generated from HADDOCK.[61]

Table 4.27 Energy statistics for the two lowest energy clusters of the HADDOCK complex between cyt b_5 and cyt P450.

Parameters	Cluster I	Cluster II
Number of structures from the 50 lowest energy docked solutions	21	14
Backbone RMSD (as compared to the reference structure, Å)	0.81 ± 0.29	2.67 ± 0.42
Total energy (kcal/mol)	-435.8 ± 38.0	-470.7 ± 49.7
van der Waals energy (kcal/mol)	-43.8 ± 8.0	-29.5 ± 7.2
Electrostatic energy (kcal/mol)	-392.0 ± 37.2	-441.2 ± 53.7
Desolvation energy (kcal/mol)	33.9 ± 3.0	35.8 ± 3.6
Interface surface area (Å^2)	937.0 ± 88.0	903.1 ± 77.7

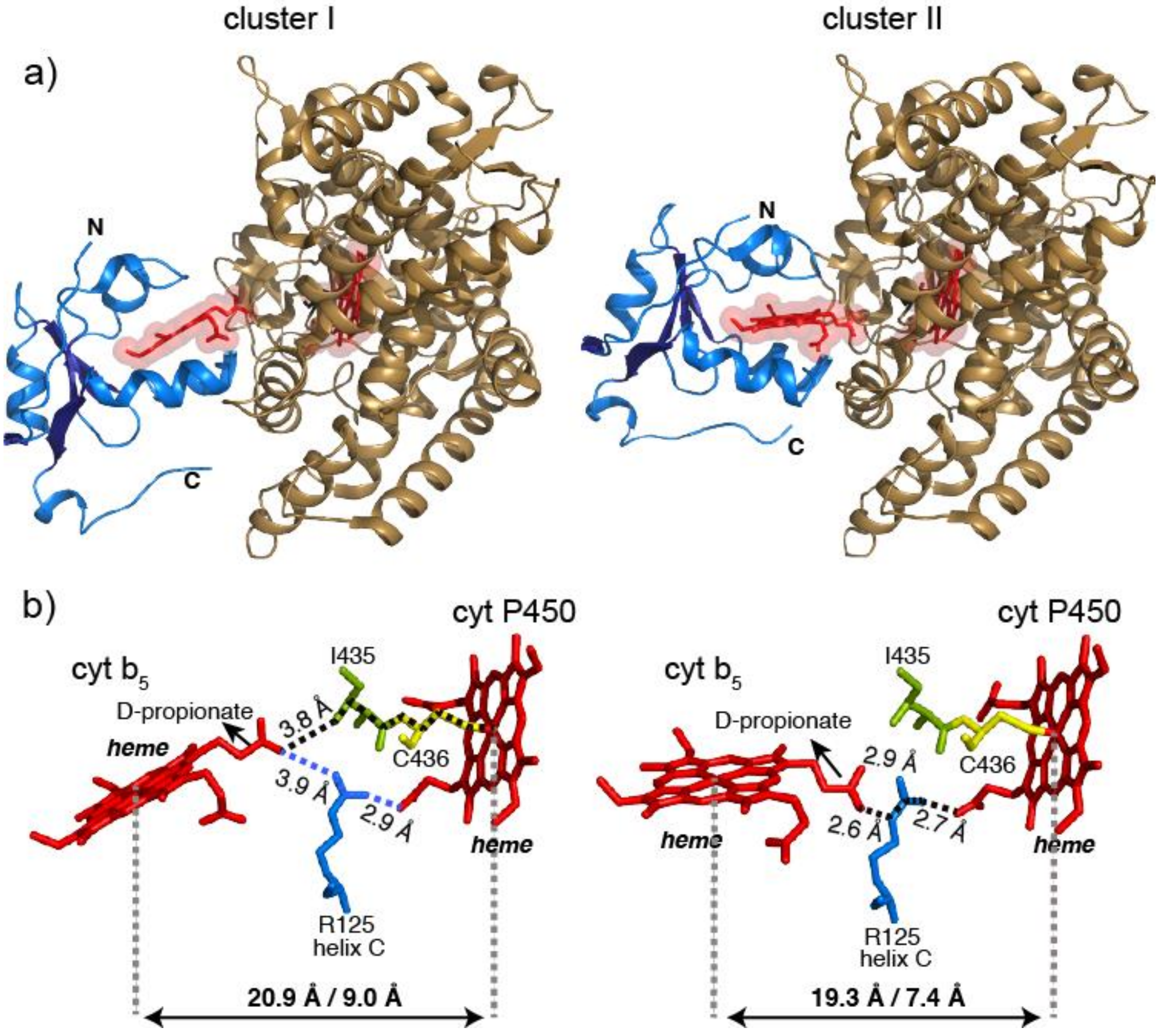
cluster I
cluster II
a)
N
C
N
C
b)
cyt b$_5$
cyt P450
I435
D-propionate
heme
3.8 Å
C436
3.9 Å
2.9 Å
heme
R125
helix C
20.9 Å / 9.0 Å
cyt b$_5$
cyt P450
I435
D-propionate
2.9 Å
C436
heme
2.6 Å
2.7 Å
heme
R125
helix C
19.3 Å / 7.4 Å

Figure 4.18 Structure of the full-length membrane-bound cyt b_5-cyt P450 complex and electron pathway prediction. (a) The two lowest energy clusters (I and II) of the complex between the catalytic, heme-binding domains of rabbit cyt b_5 (NMR structure; blue) and cyt P450 2B4 (PDB code 1SUO; gold) generated from HADDOCK driven by NMR and mutagenesis restraints. Heme molecules are presented in red. (b) Proposed electron transfer pathway between the redox centers of cyt b_5 and cyt P450 are presented as broken lines. The shortest electron transfer pathway predicted using HARLEM[77] is shown in the black dotted lines for cluster II. The shortest heme-edge to heme-edge distance is 7.4 Å and 9.0 Å in cluster II and I, respectively.

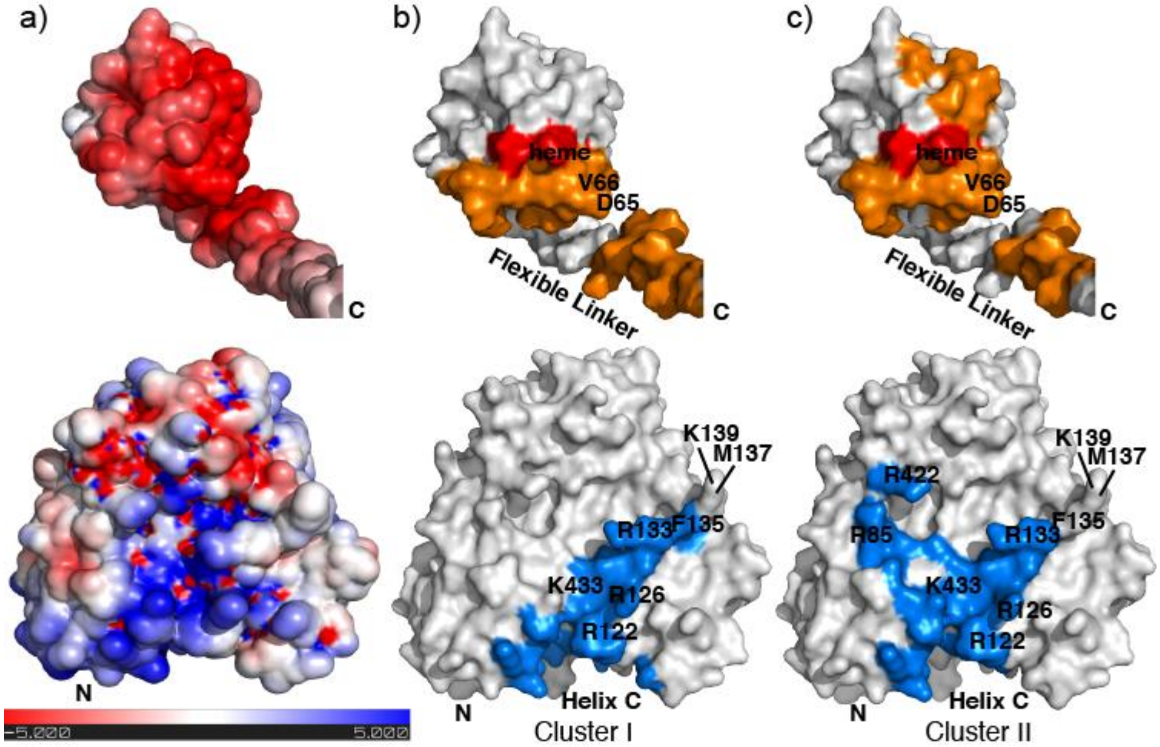
a)
C
N
-5.000
5.000
b)
heme
V66
D65
Flexible Linker
C
K139
M137
R133
F135
K433
R126
R122
Helix C
N
Cluster I
c)
heme
V66
D65
Flexible Linker
C
K139
M137
R422
R85
R133
F135
K433
R126
R122
Helix C
N
Cluster II

Figure 4.19 Interacting surfaces of cyt b_5 and cyt P450 2B4. (a) Electrostatic potential surfaces for the high-resolution NMR structure of rabbit cyt b_5 (top) and the X-ray crystal structures of the truncated heme-binding domain of rabbit cyt P450 2B4 (pdb code: 1SUO[55]; bottom) generated using APBS software[78] and pdb2pqr server[57,58] in combination with PyMOL (see Appendix B). The proximal surface of cyt P450 (facing the viewer) contains the binding pocket for its redox partners. In the case of cyt b_5, the electrostatic potential map shows a predominantly negatively charged surface (highlighted in red) that is expected to align with and bind to the positively charged surface on cyt P450 2B4 (highlighted in blue). (b) and (c) are surface representations of the proximal side of cyt b_5 (top) and cyt P450 (bottom) generated from HADDOCK for clusters I and II, respectively. Residues that form the interaction interface are colored orange for cyt b_5 and blue for cyt P450.

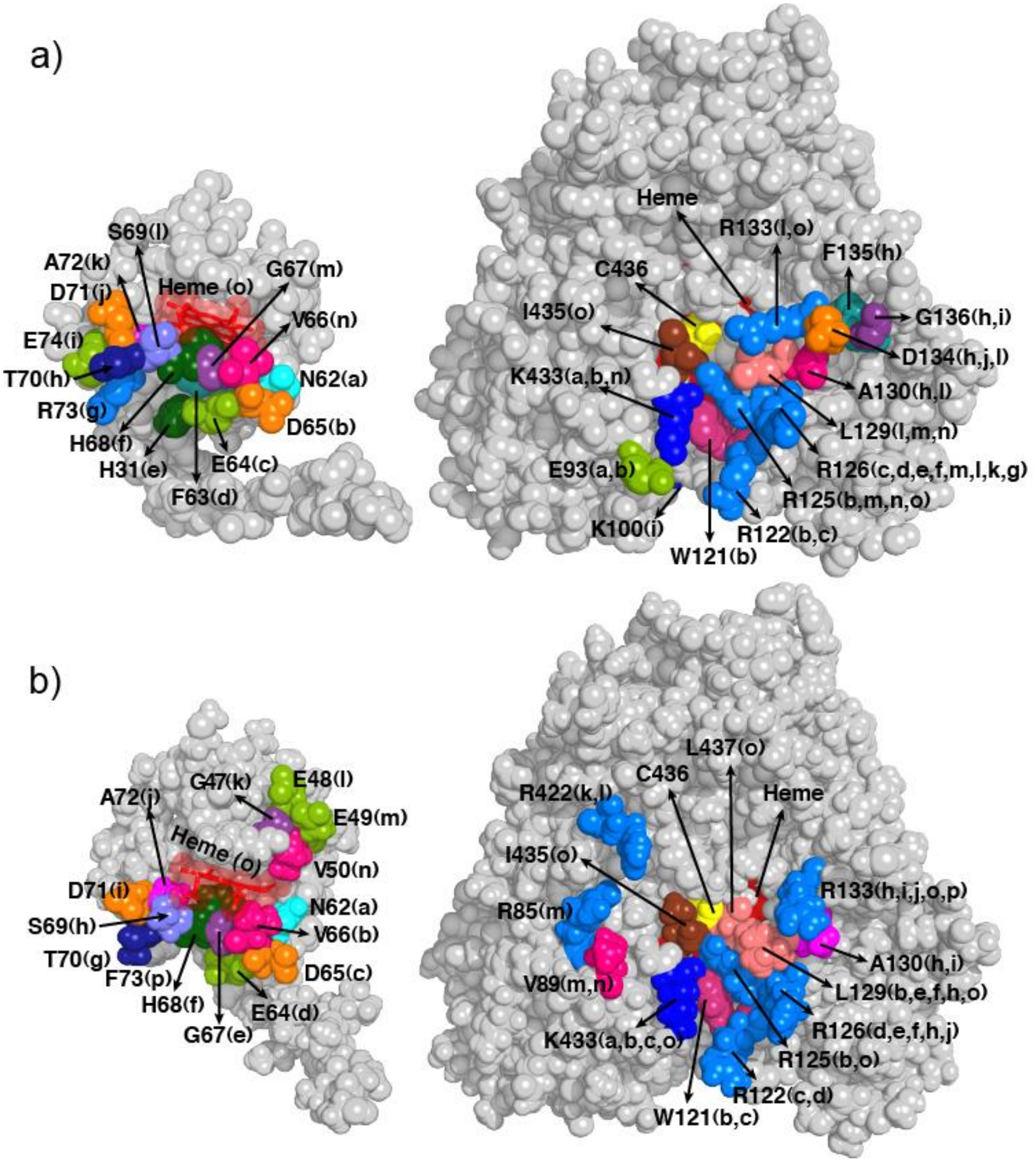
a)
S69(l)
A72(k)
D71(j)
Heme (o)
G67(m)
V66(n)
E74(i)
T70(h)
N62(a)
R73(g)
D65(b)
H68(f)
H31(e)
E64(c)
F63(d)
Heme
R133(l,o)
F135(h)
C436
I435(o)
G136(h,i)
D134(h,j,l)
K433(a,b,n)
A130(h,l)
L129(l,m,n)
R126(c,d,e,f,m,l,k,g)
E93(a,b)
R125(b,m,n,o)
K100(i)
R122(b,c)
W121(b)
b)
G47(k)
E48(l)
A72(j)
E49(m)
Heme (o)
V50(n)
D71(i)
N62(a)
S69(h)
V66(b)
T70(g)
D65(c)
F73(p)
H68(f)
E64(d)
G67(e)
L437(o)
C436
R422(k,l)
Heme
I435(o)
R133(h,i,j,o,p)
R85(m)
A130(h,i)
V89(m,n)
L129(b,e,f,h,o)
K433(a,b,c,o)
R126(d,e,f,h,j)
R125(b,o)
R122(c,d)
W121(b,c)

Figure 4.20 Residues at the binding interface of the membrane-bound cyt b_5-cyt P450 complex. The figure is presented by opening the complex like pages of a book with the interaction interface of cyt b_5 and cyt P450 facing the viewer. The space filling model of cyt b_5 (NMR structure) and cyt P450 (pdb code: 1SUO) is presented highlighting the interfacial residues involved in protein-protein contacts in the (a) cluster I and (b) cluster II complex structures. Residues on cyt b_5 that are in contact with residues on cyt P450 are denoted with matching letters in parenthesis. For example, D65 (orange) on cyt b_5 is H-bonding to R122 (blue) on cyt P450 in (a). R125 highlighted in blue is H-bonded to the heme-D-propionate in (b). An important point to note is that the residues on cyt b_5 and cyt P450, which form the interaction interface, are largely the same between the two clusters. The residues in the interface are in excellent agreement with our NMR data and site-directed mutagenesis presented here (Table 4.11, Table 4.12 and Table 4.13), as well as elsewhere.[13]

Table 4.28 Non-covalent interactions in HADDOCK-generated cluster I and II. Non-covalent interactions were calculated using CCP4[65] and PISA[63].

Cluster I	**cyt b_5**		**cyt P450**	
	residue	**atom**	**residue**	**atom**
hydrogen bonds	Asn62	HD22	Glu93	OE1
	Asn62	OD1	Lys433	HZ3
	Glu64	OD1	Arg126	HH11
	Asp65	OD1	Lys433	HZ1
	Asp65	OD2	Arg122	HH11
	His68	O	Arg126	HE
	His68	O	Arg126	HH21
	Ser69	OG	Leu129	O
	Asp71	N	Asp134	OD2
	Heme	O1A	Arg133	HH12
salt bridges	Glu64	OE1	Arg126	NH1
	Glu64	OE2	Arg126	NHE
	Glu64	OE2	Arg126	NH1
	Asp65	OD1	Lys433	NZ
	Asp65	OD2	Arg122	NH1
van der Waals	His31		Arg126	
	Phe63		Arg126	
	Val66		Lys433/Arg125	
	Gly67		Arg126	
	Thr70		Ala130/Asp134/Gly136	
	Ala72		Arg126	
	Arg73		Arg126	
	Glu74		Lys100	
	Heme		Arg125/Ile435	

Cluster II	**cyt b_5**		**cyt P450**	
	residue	**atom**	**residue**	**atom**
hydrogen bonds	Glu48	OE1	Arg422	HH12
	Glu48	OE2	Arg422	HH22
	Glu49	OE2	Arg85	HH12
	Glu64	OE1	Arg126	HH22
	Glu64	OE2	Arg126	HH12
	Asp65	OD1	Lys433	HZ2
	Asp65	OD2	Arg122	HH11
	His68	O	Arg126	HE
	Ser69	OG	Arg133	HH22
	Asp71	OD2	Arg133	HH21

Cluster II	cyt b_5		cyt P450	
	residue	**atom**	**residue**	**atom**
hydrogen bonds	Heme	O1A	Arg133	HH12
	Heme	O1D	Arg125	HE
	Heme	O2D	Arg125	HH21
salt bridges	Glu48	OE1	Arg422	NH2
	Glu48	OE1	Arg422	NH1
	Glu48	OE2	Arg422	NH2
	Glu48	OE2	Arg422	NH1
	Glu49	OE2	Arg85	NH1
	Glu49	OE2	Arg85	NH2
	Glu64	OE1	Arg126	NH1
	Glu64	OE1	Arg126	NH2
	Glu64	OE2	Arg126	NH1
	Glu64	OE2	Arg126	NH2
	Asp65	OD1	Lys433	NZ
	Asp65	OD2	Arg122	NH1
	Asp65	OD2	Arg122	NE
	Asp65	OD2	Lys433	NZ
	Asp71	OD2	Arg133	NH2
van der Waals	Gly47		Arg422	
	Val50		Val89	
	Asn62		Lys433	
	Phe63		Arg126	
	Val66		Arg125/Lys433	
	Gly67		Arg126	
	Thr70		Ala130	
	Arg73		Arg133	
	Heme		Leu129/Lys433	

4.5 Discussion

4.5.1 Identification of the binding epitope for cyt P450 2B4 on cyt b_5 by NMR

2D ^{1}H-^{15}N-TROSY-HSQC experiments were used to monitor the perturbations in amide-NH chemical shifts and intensities of isotopically labeled full-length cyt b_5 upon complex formation with unlabeled full-length cyt P450 2B4 in isotropic bicelles composed of DMPC and DHPC lipids (DMPC/DHPC *q* ratio of 0.25). The addition of cyt P450 to cyt b_5 in an equimolar ratio caused an overall reduction of cyt b_5 amide signal intensities, indicating complex formation between cyt P450 and cyt b_5, which increases the overall correlation time of cyt b_5 (Figure 4.6a, yellow color histogram). The average chemical shift perturbations observed for most of the backbone amides of cyt b_5, upon addition of cyt P450, are relatively small in magnitude, < 0.01 ppm, and include residues on both the proximal and distal surface of cyt b_5. As a result, no specific regions of cyt b_5 can be highlighted as being part of the interaction epitope based on chemical shift perturbations. This lack of widespread changes in chemical shifts across the ^{1}H-^{15}N-TROSY-HSQC spectrum indicates that there is no notable change in the overall tertiary fold of cyt b_5 upon interaction with cyt P450.

The reason for the small chemical shift perturbations could be two-fold: either fast-to-intermediate chemical exchange between the bound and the unbound forms of the complex or the formation of an ensemble of dynamic encounter complexes (see Section 1.4).[79–81] Firstly, complex formation between cyt b_5 and cyt P450 could be in the fast-to-intermediate (ns-µs) regime, on the NMR time scale, relative to the chemical exchange[22,81] where an overall broadening of the cyt b_5 resonances is observed. Secondly, small and widespread chemical shift perturbations could be a result of the formation of an ensemble of dynamic encounter complexes, as has been reported previously for other metalloprotein complexes[31,32], such as cyt b_5-metmyoglobin[33] (see Section 1.4). Encounter complexes are comprised of an equilibrium ensemble of protein orientations within the complex, which results in very small chemical shift perturbations as observed for the cyt b_5-cyt P450 complex.

A closer inspection of Figure 4.6a reveals differential line broadening of cyt b_5 resonances upon complex formation with substrate-free cyt P450 (yellow), which further suggests a dynamic interaction between these two proteins on a fast-to-intermediate (ns-μs) time scale with respect to NMR chemical exchange.[34,82] The line broadening could be a result of: a) exchange between the unobservable bound state of the cyt b_5-cyt P450 complex in isotropic bicelles (> 100 kDa) and the free observable cyt b_5 in isotropic bicelles or b) a change in the transverse relaxation rate of cyt b_5 resonances caused by a direct interaction with cyt P450.[34] The absence of significant chemical shift perturbations suggest that the differential line broadening observed is predominantly due to a direct interaction with cyt P450, enabling the characterization of the interaction interface between cyt b_5 and cyt P450. Cyt b_5 residues that exhibit significant differential line broadening (with a decrease in intensity > 20% as compared to free cyt b_5) were mapped onto the NMR structure of cyt b_5. These residues, which include E48, E49, D65, V66, and T70-S76, highlight a region of cyt b_5 around the solvent-exposed edge of the heme that potentially forms the interaction interface with cyt P450 (Figure 4.6b). Broadening of H68 and S69 resonances of cyt b_5 was also observed and may be due to the close proximity of the paramagnetic center in cyt P450 and/or due to steric interaction between H68 and S69 and residues on cyt P450 in the interface.

Interestingly, extensive line broadening and disappearance of most of the cyt b_5 amide resonances in the ^{1}H-^{15}N-TROSY-HSQC spectrum were observed upon addition of an equimolar amount of substrate-bound cyt P450. Two different compounds were tested: 3,5-di-*tert*-butyl-4-hydroxytoluene (BHT; type I substrate), and the heme iron-binding inhibitor, 1-(4-chlorophenyl) imidazole (1-CPI, type II substrate) (Figure 4.6c). The widespread broadening of the cyt b_5 resonances suggests that the interaction of cyt b_5 with the substrate-bound cyt P450 has shifted from a fast/intermediate (ns-μs) to an intermediate/slow time scale (μs-ms), which causes the disappearance of the majority of cyt b_5 resonances upon titration of substrate-bound cyt P450. This conjecture is further supported by the measurement of a sub-micromolar K_d for the cyt b_5-cyt P450 complex in the presence of the substrates, methoxyflurane ($K_d \approx 0.02$ μM, Table 4.13) and BHT ($K_d \approx 0.3$ μM). These sub-micromolar K_d values are consistent with an intermediate-to-slow exchange on the NMR time scale leading to extensive line broadening of cyt b_5 amide resonances. A previous kinetic study has reported a greater than 10-fold decrease in K_d of the cyt b_5-cyt P450 complex upon addition of a substrate benzphetamine (compared to the substrate-free complex).[83] Unfortunately, only this publication[83] has been able to measure the K_d between cyt b_5 and cyt P450 in the absence of a cyt P450 substrate; we were unable to perform such measurements because the type I spectral change caused by cyt b_5 alone was not substantial enough for a robust measurement. Due to extensive line broadening and disappearance of most of the resonances of the heme domain of cyt b_5 in the ^{1}H-^{15}N-TROSY-HSQC spectrum, relaxation NMR experiments could not be performed to validate the change in the time scale of interaction.

4.5.2 Mutagenesis identifies the “hot spots” of the cyt b_5-cyt P450 complex

To complement the NMR data collected on the cyt b_5-cyt P450 complex, we carried out site-directed mutagenesis of residues on both cyt b_5 and cyt P450 (Table 4.11, Table 4.12 and Table 4.13). Residues (E42, E43, P45, G46, E49, V50, E53, Q54, N62, D65, V66, D71 and L75) on the anionic surface surrounding the solvent-exposed heme of cyt b_5 were mutated to alanine to explore the role of atoms distal to the β-carbon of the wild-type amino acid in binding to cyt P450 2B4. Of the 13 different single mutations of cyt b_5, only two, D65A and V66A, exhibited both a significantly lower affinity (15- and 7-fold higher K_d, respectively) and decreased ability (85% and 43%, respectively) to stimulate cyt P450 2B4 catalysis (Table 4.11). These data indicate that D65 and V66 of cyt b_5 are important for both binding to cyt P450 and its function as an enhancer of cyt P450 catalysis. The P45A, G46A, E53A, Q54A, D71A and L75A mutants of cyt b_5 were found to be indistinguishable from wild-type (data not shown). Whereas E42A, E43A, E49A, V50A and N62A exhibited a modest decrease in binding affinity with cyt P450, these mutations did not decrease the ability of cyt b_5 to stimulate cyt P450 2B4 activity (Table 4.11); as a result, these residues were deemed to only play a minor role in the inter-protein interactions.

Previous mutagenesis studies on cyt P450 2B4 (Table 4.12 and elsewhere[13]) have shown that residues in the C-helix and C-D loop (R122, R126, R133, F135, M137 and K139) and K433 in the β-bulge near the axial C436 are important for binding to cyt b_5. The R133A mutant showed a drastic decrease in binding affinity to cyt b_5; in fact, the binding was too weak to obtain a robust K_d measurement. All other mutants, showed a decrease in binding affinity of at least 10-fold.

To determine the amino acids that are in contact at the interface between cyt b_5 and cyt P450, a double mutant cycle analysis[13,84] was then performed using mutants of both cyt b_5 and cyt P450 that are defective in binding to one another (Table 4.13). In such cycles the sum of the free energy change for the two single amino acid mutant proteins is compared to that of the double mutant protein complex. When the sum of the free energy change of the single mutants is not equal to that of the double mutant, the two residues are defined as interacting and not behaving independently. This assumes that the two residues are not interacting indirectly, e.g. through a structural perturbation. If the sum of the free energy changes of the two mutants is equal to that of the double mutant, i.e. their interaction energy is zero, then either there is no interaction between the two residues or the interaction energy is of the same magnitude as the free energy change of the double mutant, which is an infrequent occurrence.[69,84] A difference of greater than 1.0 kcal/mol was considered significant.[69,84] The free energy of binding, ΔG, of all possible pairs of wild-type and poorly binding alanine mutants of both cyt P450 2B4 (R122, R126, F135, M137, K139 and K433, Table 4.12) and cyt b_5 (D65 and V66, Table 4.11) was measured (Table 4.13). The results of the double mutant cycle analysis indicate that K433 of cyt P450 interacts with both D65 and V66 of cyt b_5 and that R122 of cyt P450 interacts with D65 of cyt b_5. Because of the 68-fold decreased affinity of the R133A-cyt P450 mutant for cyt b_5, a robust double mutant cycle analysis could not be performed. However, R133A-cyt P450's poor affinity for cyt b_5 indicates that R133 is critical to the inter-protein interaction.

4.5.3 Analysis of the cyt b_5-cyt P450 predicted interaction interface

A structural model of the cyt b_5-cyt P450 complex was generated using the data-driven docking program HADDOCK,[40,41] governed by unambiguous and ambiguous intermolecular restraints obtained from NMR and mutagenesis data (Table 4.9). The NMR structure of the membrane-bound rabbit cyt b_5 (Chapter 3) and a 1.9 Å resolution crystal structure of the heme-containing domain of cyt P450 2B4 (PDB code: 1SUO[55]) were used in HADDOCK calculations. Docking was performed in the absence of a membrane environment and therefore our structure of the complex reveals the interactions between the structured heme domains of cyt b_5 and cyt P450. However, it is important to note that all NMR and mutagenesis data were collected on membrane-bound full-length proteins and the enzymatic function of the complex under these conditions was confirmed by activity assays (Figure 4.5 and Table 4.15).

As described in the above section, the double mutant cycle analysis revealed that K433 of cyt P450 interacts with both D65 and V66 of cyt b_5 and that R122 of cyt P450 interacts with D65 of cyt b_5; these interactions were incorporated as unambiguous intermolecular restraints in HADDOCK. The ambiguous intermolecular restraints were generated using active and passive residues for cyt b_5 and cyt P450 (all > 40% solvent accessible). As active residues, eight cyt b_5 residues exhibiting significant differential line broadening upon complex formation with cyt P450, and seven cyt P450 residues deemed essential for binding to cyt b_5 based on site-directed mutagenesis were selected.

As passive residues, amino acids flanking the active residues were selected for cyt b_5, and for cyt P450 all residues on the proximal side where the heme is closest to the surface were selected (Table 4.9).

The docking simulations reveal not a single specific complex but rather an ensemble of two low-energy complex orientations (Table 4.27), where the acidic convex surface of cyt b_5 is sampling an extended surface area on the concave, basic proximal side of cyt P450 where the heme is closest to the surface. The two dominant subpopulations of low-energy complex structures (clusters I and II) include two unique but overlapping clusters of residues on cyt b_5 and cyt P450 2B4 (Figure 4.19, Figure 4.20 and Table 4.28). The residues of cyt b_5 that are common between the majority of the low-energy complex structures are found mostly on the lower edge of the protein cleft (i.e. below the heme, on the α4 and α5 helix). The cyt P450 and cyt b_5 hemes are nearly perpendicular to one another in both clusters, and the shortest distance between the two heme-edges is 9.0 and 7.4 Å respectively in clusters I and II, which is well within the 14.0 Å limit predicted for efficient electron transfer (Figure 4.18b).[72] The Fe-Fe distance is 20.9 and 19.3 Å in clusters I and II, respectively.

Complex formation between electron transfer proteins, like cyt P450 and cyt b_5, proceeds via the formation of dynamic encounter complexes driven by the oppositely charged surfaces (Figure 4.19a). In the encounter complexes, the different complex orientations are interchanging among themselves at a fast-to-intermediate time scale as shown by our NMR data. The encounter complexes then undergo local rearrangements upon binding of a substrate/ligand, resulting in one or more productive complex orientations capable of electron transfer. These productive complexes allow for efficient electron transfer and then rapidly dissociate to obtain another electron for the next reaction cycle. Electron transfer complexes are engineered to be robust and resistant to mutational changes and thermal fluctuations, and carry a redundancy of similarly charged residues neighboring each protein's hot spot.[81] The two lowest-energy complex orientations presented here (clusters I and II) likely represent productive cyt b_5-cyt P450 complex orientations since the heme-edge to heme-edge distances allow for efficient electron transfer.[72] Both complex structures are typical to other redox complexes in that, although there is a large interfacial area of contact (~937 $Å^2$ in cluster I and ~903 $Å^2$ in cluster II, Table 4.27), the bulk of the binding energy can be attributed to a small number of complementary residues.[24,85]

The cyt b_5-cyt P450 complex orientations reveal that the acidic convex surface of cyt b_5 docks, like a *ball in a socket*, into the entire concavity on the proximal surface of cyt P450 (Figure 4.16), with the C-helix residues contributing the vast majority of the binding energy as indicated by the mutagenesis data (Table 4.12). A closer look at the complex structures from clusters I and II (Figure 4.20 and Table 4.28) highlights that the interactions at the complex interface occur between 14 residues and the heme-D-propionate of cyt b_5 and 14 residues of cyt P450. Based on the double mutant cycle analysis (Table 4.13), we identified that the interactions contributing the most binding energy to the complex formation were between the cyt P450 C-helix residue R122 and K433 in the β-bulge (near the axial C436), and D65 and V66 at the C-terminus of helix α4 of cyt b_5 (Table 4.13). These interactions were shown to be critical for both complex formation and function. From the HADDOCK structures, we see that D65 of cyt b_5 is able to form hydrogen bonds and/or salt bridges with R122 and K433 of cyt P450, and that V66 of cyt b_5 is in van der Waals contact with K433 of cyt P450 (as well as R125). Residue R133 of cyt P450, which was found to be very important for binding to cyt b_5 in our studies, is hydrogen bonded with the heme propionate group on cyt b_5 in both clusters (additional interactions were also found for R133 in cluster II, Table 4.28). The predicted structures provide new insights into the function of cyt P450 2B4 residues previously mutated to alanine (Table 4.12 and elsewhere[13]). R126 of cyt P450 was found to form hydrogen bonds and salt bridges with E64 of cyt b_5 in both clusters and hydrogen bonds with H68 (Table 4.28). Surprisingly, C-D loop residues, M137 and K139, which mutagenesis data revealed were important for cyt b_5 binding (Table 4.12), were not found at the complex interface (Figure 4.20 and Table 4.28). We hypothesize that their mutation might induce a structural perturbation in the flexible C-helix, which in turn destabilizes the interaction with cyt b_5. The K139A mutation was previously shown to disrupt a hydrogen-bond network between the K139 amino group and P261 and N260 in the G-H loop,[55] suggesting an allosteric interaction between the C-helix and the G-H loop. Residue R443, which was shown to be important only for binding to CPR,[13] is not found in the interaction interface of the predicted complex structures (Figure 4.20).

On cyt b_5, both D65 and V66, which were shown to be in the binding site for cytochrome c,[18,86] are now shown to be in the binding site for cyt P450 2B4 both experimentally and in our HADDOCK complex structures. A double cyt b_5 mutant E48G and E49G mutant (which introduced a very flexible sequence of four glycine residues) has been shown to be deficient in its ability to stimulate the activity of cyt P450c17.[87] This observation is consistent with the presence of E48 and E49 in the interaction interface of cluster II and is in accordance with our NMR data where we observed considerable line broadening for E48 and E49 upon complex formation with cyt P450.

The HADDOCK structures of the cyt b_5-cyt P450 complex based on our NMR data and site-directed mutagenesis studies, as well as previous experiments,[13] demonstrate that cyt b_5 and CPR compete for a binding site on cyt P450, and rule out the possibility of separate, functional binding sites for cyt b_5 and CPR and the formation of a ternary complex between the three proteins.

4.5.4 Electron transfer pathway between cyt b_5 and cyt P450

The structure of the cyt b_5-cyt P450 complex generated from HADDOCK shows that the guanidinium group of R125 on the C-helix of cyt P450 forms a salt bridge between the heme-D-propionates of both cyt b_5 and cyt P450. This network was predicted, using HARLEM,[77] to serve as one of the shortest electron transfer pathways between the two proteins (Figure 4.18b). R125 is one of the most highly conserved cyt P450 residues and is homologous to R112 in cyt $P450_{cam}$, which has been shown to be essential for electron transfer.[88] The physiological significance of R125 was also highlighted when mutation of the R125 homolog in human cyt P450 24A1 resulted in a defect in vitamin D degradation.[89] We have also previously attempted to characterize the R125A mutant of cyt P450 2B4, and found that the mutation rendered the protein unstable.[13] The proposed network involving the heme propionates is consistent with previous studies that have demonstrated that the heme propionate groups of cyt b_5

interact with charged groups on cytochrome c[47,90] and cyt P450 isozymes[76], suggesting that other cyt P450 complexes might employ a similar interface. Figure 4.18b presents another possible electron transfer pathway between the heme-D-propionate of cyt b_5 and I435, the non-conserved amino acid preceding the axial ligand, C436, on cyt P450. However, our mutagenesis data have shown that the I435A mutant is as active as the wild-type cyt P450 (data not shown), suggesting that it does not play a critical role in electron transfer between the two proteins.

The extensive knowledge of the structure of the cyt b_5-cyt P450 complex provides insights into the principles governing interprotein interactions and will markedly facilitate our ability to unravel the molecular mechanism by which the rate of cyt P450 catalysis is regulated by its redox partners, cyt b_5 and cytochrome P450 reductase.

4.6 Conclusion

Here we report the structural and functional interaction interface between two full-length membrane-bound microsomal proteins, cyt b_5 and cyt P450 2B4, studied by NMR and site-directed mutagenesis. The two proteins form a dynamic complex mediated by both hydrophobic and electrostatic interactions (Figure 4.20 and Table 4.28). The electrostatic interactions between the oppositely charged residues, as well as the fact that the two proteins are anchored in the membrane, play important roles in orienting the two proteins prior to complex formation and help in considerably increasing the number of productive collisions that control and direct the flow of electrons from cyt b_5 to cyt P450. Addition of a small molecule substrate (BHT or 1-CPI) significantly increased the binding affinity between cyt b_5 and cyt P450, moving the dynamic interaction between the two proteins from a fast-to-intermediate regime to an intermediate-to-slow regime on the NMR time scale as indicated by the extensive line broadening of cyt b_5 amide NMR resonances upon complex formation with substrate-bound cyt P450. The structure of the cyt b_5-cyt P450 complex presented allows us to define the pathway of interprotein electron transfer from cyt b_5 to cyt P450 through the highly conserved R125 residue on cyt P450. Our study demonstrates how a combinatorial approach, including NMR and mutagenesis studies (particularly double mutant cycle experiments), can be exploited to obtain atomic-level structural, functional and dynamic information on intact, membrane-bound, large metalloprotein redox complexes in a near-native environment.

4.7 Contributions

Le Clair determined the histidine protonation states of cyt b_5 and cyt P450; ran, analyzed and prepared figures for all HADDOCK simulations apart from the one published; and wrote the bulk of the chapter as well as provided detailed editing of and conceptual feedback for the manuscript. Jahr did the NMR titration experiments and analysis of the cyt b_5-cyt P450 complex in the presence of BHT. Ahuja did the NMR experiment of the complex without substrate. Ahuja and Popovych established how to prepare all the files for HADDOCK and did the run and analysis of the simulation presented in the manuscript. Im and Bridges expressed all proteins and ran the single mutagenesis binding and activity assays, as well as the double mutant cycle experiments.

4.8 References

(1) Guengerich, F. P.; Wu, Z. L.; Bartleson, C. J. Function of human cytochrome P450s: characterization of the orphans. *Biochem. Biophys. Res. Commun.* **2005**, *338*, 465–469.

(2) Shen, A. L.; O'Leary, K. A.; Kasper, C. B. Association of multiple developmental defects and embryonic lethality with loss of microsomal NADPH-cytochrome P450 oxidoreductase. *J. Biol. Chem.* **2002**, *277*, 6536–6541.

(3) Nebert, D. W.; Russell, D. W. Clinical importance of the cytochromes P450. *Lancet* **2002**, *360*, 1155–1162.

(4) Im, S.-C.; Waskell, L. The interaction of microsomal cytochrome P450 2B4 with its redox partners, cytochrome P450 reductase and cytochrome b_5. *Arch. Biochem. Biophys.* **2011**, *507*, 144–153.

(5) Zhang, H.; Hamdane, D.; Im, S.-C.; Waskell, L. Cytochrome b_5 inhibits electron transfer from NADPH-cytochrome P450 reductase to ferric cytochrome P450 2B4. *J. Biol. Chem.* **2008**, *283*, 5217–5225.

(6) Gruenke, L. D.; Konopka, K.; Cadieu, M.; Waskell, L. The stoichiometry of the cytochrome P-450-catalyzed metabolism of methoxyflurane and benzphetamine in the presence and absence of cytochrome b_5. *J. Biol. Chem.* **1995**, *270*, 24707–24718.

(7) Finn, R. D.; McLaughlin, L. A.; Ronseaux, S.; Rosewell, I.; Houston, J. B.; Henderson, C. J.; Wolf, C. R. Defining the in vivo role for cytochrome b_5 in cytochrome P450 function through the conditional hepatic deletion of microsomal cytochrome b_5. *J. Biol. Chem.* **2008**, *283*, 31385–31393.

(8) Guengerich, F. P. Cytochrome P450s and other enzymes in drug metabolism and toxicity. *AAPS J.* **2006**, *8*, E101–E111.

(9) Shimada, T.; Mernaugh, R. L.; Guengerich, F. P. Interactions of mammalian cytochrome P450, NADPH-cytochrome P450 reductase, and cytochrome b_5 enzymes. *Arch. Biochem. Biophys.* **2005**, *435*, 207–216.

(10) Canova-Davis, E.; Chiang, J. Y. L.; Waskell, L. Obligatory role of cytochrome b_5 in the microsomal metabolism of methoxyflurane. *Biochem. Pharmacol.* **1985**, *34*, 1907–1912.

(11) Morgan, E. T.; Coon, M. J. Effects of cytochrome b_5 on cytochrome P-450-catalyzed reactions - Studies with manganese-substituted cytochrome b_5. *Drug Metab. Dispos.* **1984**, *12*, 358–364.

(12) Zhang, H.; Im, S.-C.; Waskell, L. Cytochrome b_5 increases the rate of product formation by cytochrome P450 2B4 and competes with cytochrome P450 reductase for a binding site on cytochrome P450 2B4. *J. Biol. Chem.* **2007**, *282*, 29766–29776.

(13) Bridges, A.; Gruenke, L.; Chang, Y. T.; Vakser, I. A.; Loew, G.; Waskell, L. Identification of the binding site on cytochrome P450 2B4 for cytochrome b_5 and cytochrome P450 reductase. *J. Biol. Chem.* **1998**, *273*, 17036–17049.

(14) Clarke, T. A.; Im, S.-C.; Bidwai, A.; Waskell, L. The role of the length and sequence of the linker domain of cytochrome b_5 in stimulating cytochrome P450 2B4 catalysis. *J. Biol. Chem.* **2004**, *279*, 36809–36818.

(15) Chudaev, M. V; Gilep, A. A.; Usanov, S. A. Site-directed mutagenesis of cytochrome b_5 for studies of its interaction with cytochrome P450. *Biochemistry (Mosc)* **2001**, *66*, 667–681.

(16) Halpert, J. R. Structure and function of cytochromes P450 2B: from mechanism-based inactivators to X-ray crystal structures and back. *Drug Metab. Dispos.* **2011**, *39*, 1113–1121.

(17) Scott, E. E.; He, Y. A.; Wester, M. R.; White, M. A.; Chin, C. C.; Halpert, J. R.; Johnson, E. F.; Stout, C. D. An open conformation of mammalian cytochrome P4502B4 at 1.6-angstrom resolution. *Proc. Natl. Acad. Sci. U.S.A.* **2003**, *100*, 13196–13201.

(18) Banci, L.; Bertini, I.; Rosato, A.; Scacchieri, S. Solution structure of oxidized microsomal rabbit cytochrome b_5. Factors determining the heterogeneous binding of the heme. *Eur. J. Biochem.* **2000**, *267*, 755–766.

(19) Nunez, M.; Guittet, E.; Pompon, D.; Van Heijenoort, C.; Truan, G. NMR structure note: oxidized microsomal human cytochrome b_5. *J. Biomol. NMR* **2010**, *47*, 289–295.

(20) Ghosh, D.; Griswold, J.; Erman, M.; Pangborn, W. Structural basis for androgen specificity and oestrogen synthesis in human aromatase. *Nature* **2009**, *457*, 219–223.

(21) Pellecchia, M. Solution nuclear magnetic resonance spectroscopy techniques for probing intermolecular interactions. *Chem. Biol.* **2005**, *12*, 961–971.

(22) Zuiderweg, E. R. P. Mapping protein-protein interactions in solution by NMR spectroscopy. *Biochemistry* **2002**, *41*, 1–7.

(23) Ofran, Y.; Rost, B. Protein-protein interaction hotspots carved into sequences. *PLoS Comput. Biol.* **2007**, *3*, e119.

(24) Bogan, A. A.; Thorn, K. S. Anatomy of hot spots in protein interfaces. *J. Mol. Biol.* **1998**, *280*, 1–9.

(25) Di Cera, E. Site-Specific Thermodynamics: Understanding cooperativity in molecular recognition. *Chem. Rev.* **1998**, *98*, 1563–1592.

(26) Horovitz, A. Double-mutant cycles: a powerful tool for analyzing protein structure and function. *Fold. Des.* **1996**, *1*, R121–R126.

(27) Wells, J. A. Additivity of mutational effects in proteins. *Biochemistry* **1990**, *29*, 8509–8517.

(28) Mildvan, A. S.; Weber, D. J.; Kuliopulos, A. Quantitative interpretations of double mutations of enzymes. *Arch. Biochem. Biophys.* **1992**, *294*, 327–340.

(29) LiCata, V. J.; Ackers, G. K. Long-range, small magnitude nonadditivity of mutational effects in proteins. *Biochemistry* **1995**, *34*, 3133–3139.

(30) Di Cera, E. *Thermodynamic Theory of Site-Specific Binding Processes in Biological Macromolecules*; Cambridge University Press: Cambridge, United Kingdom, 1995.

(31) Volkov, A. N.; Ferrari, D.; Worrall, J. A. R.; Bonvin, A. M. J. J.; Ubbink, M. The orientations of cytochrome c in the highly dynamic complex with cytochrome b_5 visualized by NMR and docking using HADDOCK. *Protein Sci.* **2005**, *14*, 799–811.

(32) Suh, J.-Y.; Tang, C.; Clore, G. M. Role of electrostatic interactions in transient encounter complexes in protein-protein association investigated by paramagnetic relaxation enhancement. *J. Am. Chem. Soc.* **2007**, *129*, 12954–12955.

(33) Worrall, J. A. R.; Liu, Y.; Crowley, P. B.; Nocek, J. M.; Hoffman, B. M.; Ubbink, M. Myoglobin and cytochrome b_5: a nuclear magnetic resonance study of a highly dynamic protein complex. *Biochemistry* **2002**, *41*, 11721–11730.

(34) Matsuo, H.; Walters, K. J.; Teruya, K.; Tanaka, T.; Gassner, G. T.; Lippard, S. J.; Kyogoku, Y.; Wagner, G. Identification by NMR spectroscopy of residues at contact surfaces in large, slowly exchanging macromolecular complexes. *J. Am. Chem. Soc.* **1999**, *121*, 9903–9904.

(35) Sette, M.; Van Tilborg, P.; Spurio, R.; Kaptein, R.; Paci, M.; Gualerzi, C. O.; Boelens, R. The structure of the translational initiation factor IF1 from E. coli contains an oligomer-binding motif. *EMBO J.* **1997**, *16*, 1436–1443.

(36) Ni, F.; Zhu, Y.; Scheraga, H. A. Thrombin-bound structures of designed analogs of human fibrinopeptide A determined by quantitative transferred NOE spectroscopy: a new structural basis for thrombin specificity. *J. Mol. Biol.* **1995**, *252*, 656–671.

(37) Smith, G. R.; Sternberg, M. J. E. Prediction of protein-protein interactions by docking methods. *Curr. Opin. Struct. Biol.* **2002**, *12*, 28–35.

(38) Bonvin, A. M. J. J. Flexible protein-protein docking. *Curr. Opin. Struct. Biol.* **2006**, *16*, 194–200.

(39) Gray, J. J. High-resolution protein-protein docking. *Curr. Opin. Struct. Biol.* **2006**, *16*, 183–193.

(40) De Vries, S. J.; Van Dijk, A. D.; Krzeminski, M.; Van Dijk, M.; Thureau, A.; Hsu, V.; Wassenaar, T.; Bonvin, A. M. HADDOCK versus HADDOCK: new features and performance of HADDOCK2.0 on the CAPRI targets. *Proteins* **2007**, *69*, 726–733.

(41) Dominguez, C.; Boelens, R.; Bonvin, A. M. HADDOCK: a protein-protein docking approach based on biochemical or biophysical information. *J. Am. Chem. Soc.* **2003**, *125*, 1731–1737.

(42) De Vries, S. J.; Van Dijk, M.; Bonvin, A. M. J. J. The HADDOCK web server for data-driven biomolecular docking. *Nat. Protoc.* **2010**, *5*, 883–897.

(43) Van Dijk, A. D. J.; Boelens, R.; Bonvin, A. M. J. J. Data-driven docking for the study of biomolecular complexes. *FEBS J.* **2005**, *272*, 293–312.

(44) Luna, R. E.; Arthanari, H.; Hiraishi, H.; Nanda, J.; Martin-Marcos, P.; Markus, M. a; Akabayov, B.; Milbradt, A. G.; Luna, L. E.; Seo, H.-C.; Hyberts, S. G.; Fahmy, A.; Reibarkh, M.; Miles, D.; Hagner, P. R.; O'Day, E. M.; Yi, T.; Marintchev, A.; Hinnebusch, A. G.; Lorsch, J. R.; Asano, K.; Wagner, G. The C-terminal domain of eukaryotic initiation factor 5 promotes start codon recognition by its dynamic interplay with eIF1 and eIF2β. *Cell Rep.* **2012**, *1*, 689–702.

(45) Jensen, G. A.; Andersen, O. M.; Bonvin, A. M. J. J.; Bjerrum-Bohr, I.; Etzerodt, M.; Thøgersen, H. C.; O'Shea, C.; Poulsen, F. M.; Kragelund, B. B. Binding site structure of one LRP-RAP complex: implications for a common ligand-receptor binding motif. *J. Mol. Biol.* **2006**, *362*, 700–716.

(46) Serniwka, S. A.; Shaw, G. S. The structure of the UbcH8-ubiquitin complex shows a unique ubiquitin interaction site. *Biochemistry* **2009**, *48*, 12169–12179.

(47) Deep, S.; Im, S.-C.; Zuiderweg, E. R.; Waskell, L. Characterization and calculation of a cytochrome c-cytochrome b_5 complex using NMR data. *Biochemistry* **2005**, *44*, 10654–10668.

(48) Bashir, Q.; Volkov, A. N.; Ullmann, G. M.; Ubbink, M. Visualization of the encounter ensemble of the transient electron transfer complex of cytochrome c and cytochrome c peroxidase. *J. Am. Chem. Soc.* **2010**, *132*, 241–247.

(49) Van Dijk, A. D. J.; Ciofi-Baffoni, S.; Banci, L.; Bertini, I.; Boelens, R.; Bonvin, A. M. J. J. Modeling protein-protein complexes involved in the cytochrome c oxidase copper-delivery pathway. *J. Proteome Res.* **2007**, *6*, 1530–1539.

(50) Saribas, A. S.; Gruenke, L.; Waskell, L. Overexpression and purification of the membrane-bound cytochrome P450 2B4. *Protein Expr. Purif.* **2001**, *21*, 303–309.

(51) Mulrooney, S. B.; Waskell, L. High-level expression in Escherichia coli and purification of the membrane-bound form of cytochrome b_5. *Protein Expr. Purif.* **2000**, *19*, 173–178.

(52) Omura, T.; Sato, R. [90] Isolation of cytochromes P-450 and P-420. *Methods Enzymol.* **1967**, *10*, 556–561.

(53) Goddard, T. D.; Kneller, D. G. SPARKY 3. University of California, San Francisco.

(54) Dürr, U. H.; Yamamoto, K.; Im, S.-C.; Waskell, L.; Ramamoorthy, A. Solid-state NMR reveals structural and dynamical properties of a membrane-anchored electron-carrier protein, cytochrome b_5. *J. Am. Chem. Soc.* **2007**, *129*, 6670–6671.

(55) Scott, E. E.; White, M. A.; He, Y. A.; Johnson, E. F.; Stout, C. D.; Halpert, J. R. Structure of mammalian cytochrome P450 2B4 complexed with 4-(4-chlorophenyl)imidazole at 1.9-A resolution: Insight into the range of P450 conformations and the coordination of redox partner binding. *J. Biol. Chem.* **2004**, *279*, 27294–27301.

(56) Schüttelkopf, A. W.; Van Aalten, D. M. F. PRODRG: a tool for high-throughput crystallography of protein-ligand complexes. *Acta Crystallogr. D Biol. Crystallogr.* **2004**, *60*, 1355–1363.

(57) Dolinsky, T. J.; Czodrowski, P.; Li, H.; Nielsen, J. E.; Jensen, J. H.; Klebe, G.; Baker, N. A. PDB2PQR: expanding and upgrading automated preparation of biomolecular structures for molecular simulations. *Nucleic Acids Res.* **2007**, *35*, W522–W525.

(58) Dolinsky, T. J.; Nielsen, J. E.; McCammon, J. A.; Baker, N. A. PDB2PQR: an automated pipeline for the setup of Poisson-Boltzmann electrostatics calculations. *Nucleic Acids Res.* **2004**, *32*, W665–W667.

(59) Accelrys Software Inc., Discovery Studio Modeling Environment, Release 3.5, San Diego: Accelrys Software Inc. (2012).

(60) Ahmad, S.; Gromiha, M.; Fawareh, H.; Sarai, A. ASAView: database and tool for solvent accessibility representation in proteins. *BMC Bioinf.* **2004**, *5*, 51.

(61) Ahuja, S.; Nicole, J.; Im, S.-C.; Vivekanandan, S.; Popovych, N.; Le Clair, S. V; Bridges, A.; Waskell, L.; Ramamoorthy, A. A dynamic structure of the membrane-bound cytochrome b_5-cytochrome P450 complex from NMR and mutagenesis data. *Submitted*.

(62) DeLano, W. L. The PyMOL Molecular Graphics System, Version 1.5.0.4 Schrödinger, LLC **2010**.

(63) Krissinel, E.; Henrick, K. Inference of macromolecular assemblies from crystalline state. *J. Mol. Biol.* **2007**, *372*, 774–797.

(64) Krissinel, E.; Henrick, K. Protein interfaces, surfaces and assemblies service PISA at European Bioinformatics Institute http://www.ebi.ac.uk/pdbe/prot_int/pistart.html.

(65) Potterton, E.; Briggs, P.; Turkenburg, M.; Dodson, E. A graphical user interface to the CCP4 program suite. *Acta Crystallogr. D Biol. Crystallogr.* **2003**, *59*, 1131–1137.

(66) Shimizu, T.; Tateishi, T.; Hatano, M.; Fujii-Kuriyama, Y. Probing the role of lysines and arginines in the catalytic function of cytochrome P450d by site-directed mutagenesis. Interaction with NADPH-cytochrome P450 reductase. *J. Biol. Chem.* **1991**, *266*, 3372–3375.

(67) Shen, S.; Strobel, H. W. Role of lysine and arginine residues of cytochrome P450 in the interaction between cytochrome P4502B1 and NADPH-cytochrome P450 reductase. *Arch. Biochem. Biophys.* **1993**, *304*, 257–265.

(68) Shen, S.; Strobel, H. W. The role of cytochrome P450 lysine residues in the interaction between cytochrome P450IA1 and NADPH-cytochrome P450 reductase. *Arch. Biochem. Biophys.* **1992**, *294*, 83–90.

(69) Harel, M.; Cohen, M.; Schreiber, G. On the dynamic nature of the transition state for protein-protein association as determined by double-mutant cycle analysis and simulation. *J. Mol. Biol.* **2007**, *371*, 180–196.

(70) Bayburt, T. H.; Sligar, S. G. Single-molecule height measurements on microsomal cytochrome P450 in nanometer-scale phospholipid bilayer disks. *Proc. Natl. Acad. Sci. U.S.A.* **2002**, *99*, 6725–6730.

(71) Zhao, Y.; White, M. A.; Muralidhara, B. K.; Sun, L.; Halpert, J. R.; Stout, C. D. Structure of microsomal cytochrome P450 2B4 complexed with the antifungal drug bifonazole: Insight into P450 conformational plasticity and membrane interaction. *J. Biol. Chem.* **2006**, *281*, 5973–5981.

(72) Page, C. C.; Moser, C. C.; Dutton, P. L. Mechanism for electron transfer within and between proteins. *Curr. Opin. Chem. Biol.* **2003**, *7*, 551–556.

(73) Moser, C. C.; Chobot, S. E.; Page, C. C.; Dutton, P. L. Distance metrics for heme protein electron tunneling. *Biochim. Biophys. Acta, Bioenerg.* **2008**, *1777*, 1032–1037.

(74) Lewis, D. F.; Lake, B. G. Molecular modelling of mammalian CYP2B isoforms and their interaction with substrates, inhibitors and redox partners. *Xenobiotica* **1997**, *27*, 443–478.

(75) Stayton, P. S.; Poulos, T. L.; Sligar, S. G. Putidaredoxin competitively inhibits cytochrome b_5-cytochrome P-450cam association: a proposed molecular model for a cytochrome P-450cam electron-transfer complex. *Biochemistry* **1989**, *28*, 8201–8205.

(76) Tamburini, P. P.; Schenkman, J. B. Mechanism of interaction between cytochromes P-450 RLM5 and b_5: evidence for an electrostatic mechanism involving cytochrome b5 heme propionate groups. *Arch. Biochem. Biophys.* **1986**, *245*, 512–522.

(77) Kurnikov, I. V. HARLEM Molecular Modeling Package. version 1.0, Department of Chemistry, University of Pittsburgh, Pittsburg, PA **2000**.

(78) Baker, N. A.; Sept, D.; Joseph, S.; Holst, M. J.; McCammon, J. A. Electrostatics of nanosystems: Application to microtubules and the ribosome. *Proc. Natl. Acad. Sci. U.S.A.* **2001**, *98*, 10037–10041.

(79) Tang, C.; Iwahara, J.; Clore, G. M. Visualization of transient encounter complexes in protein-protein association. *Nature* **2006**, *444*, 383–386.

(80) Volkov, A. N.; Ubbink, M.; Van Nuland, N. A. J. Mapping the encounter state of a transient protein complex by PRE NMR spectroscopy. *J. Biomol. NMR* **2010**, *48*, 225–236.

(81) Prudêncio, M.; Ubbink, M. Transient complexes of redox proteins: structural and dynamic details from NMR studies. *J. Mol. Recognit.* **2004**, *17*, 524–539.

(82) Zamoon, J.; Nitu, F.; Karim, C.; Thomas, D. D.; Veglia, G. Mapping the interaction surface of a membrane protein: unveiling the conformational switch of phospholamban in calcium pump regulation. *Proc. Natl. Acad. Sci. U.S.A.* **2005**, *102*, 4747–4752.

(83) Tamburini, P. P.; Gibson, G. G. Thermodynamic studies of the protein-protein interactions between cytochrome P-450 and cytochrome b_5. Evidence for a central role of the cytochrome P-450 spin state in the coupling of substrate and cytochrome b_5 binding to the terminal hemoprotein. *J. Biol. Chem.* **1983**, *258*, 13444–13452.

(84) Frisch, C.; Schreiber, G.; Johnson, C. M.; Fersht, A. R. Thermodynamics of the interaction of barnase and barstar: changes in free energy versus changes in enthalpy on mutation. *J. Mol. Biol.* **1997**, *267*, 696–706.

(85) Clackson, T.; Wells, J. A. A hot spot of binding energy in a hormone-receptor interface. *Science* **1995**, *267*, 383–386.

(86) Shao, W.; Im, S.-C.; Zuiderweg, E. R.; Waskell, L. Mapping the binding interface of the cytochrome b_5-cytochrome c complex by nuclear magnetic resonance. *Biochemistry* **2003**, *42*, 14774–14784.

(87) Naffin-Olivos, J. L.; Auchus, R. J. Human cytochrome b_5 requires residues E48 and E49 to stimulate the 17,20-lyase activity of cytochrome P450c17. *Biochemistry* **2006**, *45*, 755–762.

(88) Nakamura, K.; Horiuchi, T.; Yasukochi, T.; Sekimizu, K.; Hara, T.; Sagara, Y. Significant contribution of arginine-112 and its positive charge of Pseudomonas putida cytochrome P-450cam in the electron transport from putidaredoxin. *Biochim. Biophys. Acta* **1994**, *1207*, 40–48.

(89) Schlingmann, K. P.; Kaufmann, M.; Weber, S.; Irwin, A.; Goos, C.; John, U.; Misselwitz, J.; Klaus, G.; Kuwertz-bröking, E.; Fehrenbach, H.; Wingen, A. M.; Güran, T.; Hoenderop, J. G.; Bindels, R. J.; Prosser, D. E.; Jones, G.; Konrad, M. CYP24A1 ,utations in idiopathic infantile hypercalcemia. *N. Engl. J. Med.* **2011**, *365*, 1741–1743.

(90) Rodgers, K. K.; Pochapsky, T. C.; Sligar, S. G. Probing the mechanisms of macromolecular recognition: the cytochrome b_5-cytochrome c complex. *Science* **1988**, *240*, 1657–1659.

CHAPTER 5

Anatomy of the cytochrome b_5 interface in its stereospecific and encounter complexes with cytochrome P450

5.1 Summary

For redox protein complexes, data analysis can be complicated by the presence of two types of complexes: the electrostatic-driven encounter complexes and the stereospecific complex(es). In this chapter, we impart a simple NMR approach to identify residues involved in encounter and stereospecific complexes between redox partners. We successfully applied this approach, in which we monitored extensive line broadening as a concentration of NaCl, to the two full-length membrane-bound proteins cytochrome b_5 (cyt b_5) and cytochrome P450 (cyt P450). Encounter complex formation between the two proteins encompasses all sides of cyt b_5, and the prevalence and strength of non-covalent interactions in these complexes are highly dependent on the cyt b_5 surface charge density. Cyt b_5 residues V66, G67 and T70 were identified as being strongly involved in stereospecific complex formation with cyt P450. We propose an overall and residue-specific mode of interaction between cyt b_5 and cyt P450, which encompasses the involvement of charged, polar and hydrophobic residues. Upon

Adapted from the manuscript entitled “Anatomy of the cyt b_5 interface in its stereospecific and encounter complexes with cytochrome P450” by Le Clair S., Zhang M., Im S.-C., Waskell L. and Ramamoorthy A. This study was supported by NIH (GM084018 and GM095640 to A. R., and GM35533 and GM094209 to L. W.) Veterans Administration Merit Review Grant P/G 0006 to L. W.

addition of a cyt P450 type I substrate, a shift was seen in the interaction between cyt b_5 and cyt P450. We show that there is an increase in the encounter complex population and that substrate-bound cyt P450 has the ability to scan a larger surface area of cyt b_5, compared to substrate-free cyt P450. This lengthens the lifetime of the encounter complex, thereby leading to a higher frequency of stereospecific complex formation.

5.2 Introduction

Understanding protein-protein interactions is essential to unraveling the intricate networks that execute crucial biological functions, such as cellular respiration or xenobiotic metabolism. Although significant progress has been made,[1] studying the molecular mechanisms of electron transfer complexes, which are highly transient, is still challenging. Characteristics of these complexes differ from other protein complexes for two main reasons: redox proteins interact with numerous partners, and they need to associate and dissociate quickly with one another (for high turnover of electrons). The protein-protein interactions therefore need to strike a balance between being non-specific enough to allow for quick dissociation but specific enough to allow the two redox centers to be close enough (< 14 Å)[2] for electron transfer.[3]

Redox partners are hypothesized to interact via dynamic docking.[4,5] Like other molecules, redox partners diffuse through solution and membranes via Brownian motion, until they experience stochastic macrocollisions.[6] This probability of a macrocollision is usually enhanced by the two proteins being oppositely charged.[7] Following the macrocollision, the proteins interact non-specifically via long-range electrostatic interactions as they scan each other's surfaces through diffusional and rotational motions.[7–11] Encounter complexes are formed at this stage, and the proteins then either dissociate or find each other's "hot spots" and are able to form a stereospecific/productive complex in which electron transfer can occur. Since the rate of electron transfer falls off exponentially as the distance between the redox centers increases,[2] this productive/stereospecific complex formation needs to be driven by specific, short-range interactions such as hydrogen bonding, salt bridges, van der Waals and hydrophobic contacts.[3] It is also possible that there is fast exchange between the encounter complexes and the stereospecific complex since binding affinities of redox complexes can be quite low (K_d of 10^{-6}-10^{-3} M).[3]

While studying tight complexes is becoming more routine using NMR and X-ray crystallography,[12] investigating dynamic redox complexes is still a difficult task, due to the millisecond timescale of complex formation[2,3,13–15] and the sample heterogeneity from the presence of both stereospecific and encounter complexes. The encounter complexes' population can vary greatly, from 5% to 100%, depending on the redox partners, and can therefore have a significant impact on observable measurements.[3,7] Another level of complexity is added to the system if the electron transfer proteins are also membrane-bound. Although significant discoveries have been made in the field of transient complexes through the use of NMR Paramagnetic Relaxation Enhancement (PRE) techniques, PRE often requires mutation and/or addition of a prosthetic group to an amino acid.[16,17] For a small protein interacting with a large protein, the binding interface can also be studied via differential line broadening, which does not require any protein alterations.[18] Chapter 4 introduced this type of analysis to study complex formation between cytochrome b_5 and cytochrome P450 using solution NMR.

For the well-known oxidation of non-activated hydrocarbon molecules,[19] cytochrome P450 (cyt P450) requires two electrons from its redox partners: cytochrome P450 reductase (CPR) and cytochrome b_5 (cyt b_5). Cyt b_5 can only donate the second electron, while CPR can donate both the first and second electron.[20] Cyt b_5 has been shown to be an essential component of the cyt P450 catalytic system *in vivo*.[21,22] As redox partners, cyt b_5 and cyt P450 should follow the dynamic docking model of complex formation.[4,5] According to theory[23] and experiments[11,24], the addition of salt causes more significant dissociation of the encounter complexes of soluble proteins than the stereospecific complex(es). The hypothesis is that salt more easily interferes with the long-range, electrostatic-driven interactions present in the encounter complexes[7–11] than the short-range interactions present in the stereospecific complex[3,7].

In this chapter, we present a detailed look at the interactions between the two membrane-bound, full-length ferric proteins rabbit cyt P450 2B4 and rabbit cyt b_5 (from the cyt b_5 point of view). By utilizing a series of $^{1}H,^{15}N$-TROSY-HSQC spectra to monitor differential line broadening as a concentration of NaCl, we make a distinction between cyt b_5 residues involved in encounter complexes versus those implicated in the stereospecific complex. We show the extent of the cyt b_5 residues' involvement in encounter complex formation and identify cyt b_5 residues which are likely at the interface with cyt P450. We also compare the protein-protein interactions in the absence and presence of a type I substrate (BHT), showing the differences and similarities in the encounter and stereospecific complexes formed.

5.3 Materials and methods

5.3.1 Materials

Phosphate buffer components (potassium phosphate monobasic and dibasic), glycerol and 3,5-di-*tert*-butyl-4-hydroxytoluene (BHT) were purchased from Sigma-Aldrich. Sodium chloride was purchased from Fischer Scientific. 1,2-dihexanoyl-*sn*-glycero-3-phosphocholine (DHPC) and 1,2-dimyristoyl-*sn*-glycero-3-phosphocholine (DMPC) were purchased from Avanti Polar Lipids, Inc. (Alabaster, AL).

5.3.2 NMR sample preparation and experiments

^{15}N full-length cyt b_5 and unlabeled full-length cyt P450 were expressed and purified as detailed previously.[25,26] NMR experiments were performed at 298 K on a Bruker 900 MHz spectrometer equipped with a 5 mm triple-resonance TXI cryo-probe. All NMR samples were prepared in 100 mM potassium phosphate buffer, pH 7.4, with 5% (w/v) of glycerol. DMPC/DHPC isotropic bicelles, with a q ratio of 0.25 of [DMPC] to [DHPC], were prepared by co-solubilizing DMPC and DHPC in chloroform. The solvent was then evaporated with N_2 gas to form a thin film along the bottom of the test tube; any residual chloroform was removed by placing the test tube in a vacuum oven overnight. The lipid film was rehydrated prior to preparing the NMR sample.[27] The final concentration of bicelles in all NMR samples was 10% (w/v). Detailed instructions on the isotropic bicelle preparation can be found in Appendix D.

The NMR experiments on cyt b_5 alone were done on 0.2 mM of cyt b_5 incorporated in DMPC/DHPC isotropic bicelles. A series of ^{1}H,^{15}N-SOFAST-HMQC spectra of cyt b_5 were collected under the following four conditions: 0, 100, 250 and 400 mM NaCl. All NMR samples containing the cyt b_5-cyt P450 complexes were prepared to give a final concentration of 0.2 mM of each protein, with a 1:1 molar ratio of cyt b_5 to cyt P450. The complexes were preformed and then incorporated in DMPC/DHPC isotropic bicelles. The complex samples containing BHT had a molar ratio of 2:1 of BHT to cyt P450. NaCl titrations were performed on both the protein complex samples with and without BHT. For both types of cyt b_5-cyt P450 complexes, a series of ^{1}H,^{15}N-TROSY-HSQC spectra was collected for the following salt concentrations: 0, 100, 250 and 400 mM NaCl.

5.3.3 NMR data analysis

All spectra were processed in TopSpin 2.0. Peak assignments were made using Sparky, and chemical shifts and peak heights were obtained from Sparky.[28] The assignment of each ferric cyt b_5 resonance in the HSQC spectra can be found in Figure 3.3. In order to compare intensities of residues in the spectra at each NaCl concentration, the intensities of cyt b_5 were internally normalized by setting the intensity of D134 as 100% and all other intensities as a percentage of D134 (referred to as “relative intensities”). Residue D134 was chosen for the normalization because it is the highest intensity resonance in all spectra. It is also located at the end of the C-terminus of cyt b_5 and it does not appear to be affected by complex formation in any the experiments we have performed. Curves were generated in Excel using the relative intensities of each residue, at each salt NaCl concentration, and slopes were calculated according to the data points between 0-250 mM NaCl for cyt b_5 with substrate-free cyt P450, and 0-400 mM for cyt b_5 with BHT-bound cyt P450. For the residues that were absent from the spectrum at a specific salt concentration, the value was set at 0% for that point, and a maximum of one data point with 0% was used in any given slope calculation for a residue. For this reason, most slopes for the complex between cyt b_5 and BHT-bound cyt P450 only had 2-3 data points. The intensities of residues near the N-terminus (K7-V9) and in the linker fluctuated a lot upon addition of NaCl for free cyt b_5 in bicelles and were not considered when discussing slopes.

The following cyt b_5 residues are either unassigned or invisible in the ^1H-^{15}N-TROSY-HSQC spectra: M1-D6, S23, L30, K33, P45, G46, G47, P86, S90, K91, K94, P95 and I100. Additionally, the resonances of H32, H68 and S69 do not reliably appear in the spectra. The following residues have the lowest intensities in the free cyt b_5 ^1H-^{15}N-TROSY-HSQC spectrum and could not be discussed in our analysis since any small variation in intensity might cause their resonances to become undetectable: T26, H31, V34, L37, L51, G56, I81 and H85. It is interesting to note that three of these residues (T26, L37 and L51) are located in a cleft that has been hypothesized to become exposed during a molecular dynamics (MD) simulation of cyt b_5 (Figure 5.1).[29] For the cyt b_5-cyt P450 complex, four (S93, E97, T102 and D104) out of fifteen of the linker residues were identified and assigned conclusively in the cyt b_5-cyt P450 complex and only had a single conformer peak that could be easily monitored during experiments. Other residues for which incomplete information could only be obtained are listed in Table 5.1.

Table 5.1 Residues for which only incomplete (or no) intensity information could be obtained in the given experiments. The intensities of these residues were unreliable as they either overlapped with nearby peaks, their intensities fluctuated a lot during the salt titration of cyt b_5 alone, or they alternated between multiple conformers in either all or some of the spectra. These residues are colored light grey in their respective figures.

cyt b_5-cyt P450	cyt b_5-cyt P450 with BHT
T13, L14, I17, H20, S25, W27, L41, E42, E43, L75 and S76	I17, H20, S25, K24, I29, F40, E42, L84 and D88

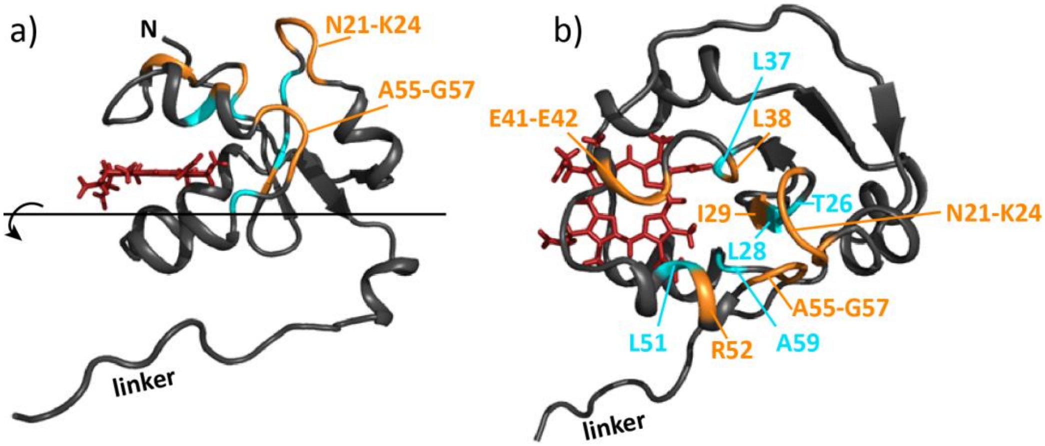

Figure 5.1. Cleft opening on the top of cyt b_5 as determined by MD simulations in Storch *et al.*[29] The left side of cyt b_5 is shown in a) with the axis and arrow demonstrating the 90° rotation performed to show the top portion of cyt b_5 in b). In blue are residues that become exposed during the cleft opening and orange residues are those that border the cleft.

5.3.4 Calculation of solvent accessibility of cyt b_5 residues

The cyt b_5 structure obtained from NMR in Chapter 3 was used for the generation of all figures. NACCESS,[30] with the default parameters, was used to calculate the solvent accessibility of cyt b_5 residues (see Appendix C) in our NMR structure of cyt b_5. Residues that were considered solvent accessible had a relative solvent accessibility

≥ 35% for either the main chain or side chain atoms, or all atoms. A threshold of 35% was used because a cyt P450 residue shown to be important for the cyt b_5-cyt P450 interaction, as determined from mutagenesis,[31] was calculated to have a main chain solvent accessibility of 35.8%. It should be noted that although Y35 was shown to be inaccessible with NACCESS, Y35 has been previously shown to be accessible to nitration;[32] this partial solvent accessibility might be caused by the opening of the cleft shown by MD simulations[29] (Figure 5.1).

5.3.5 Circular dichroism experiments of cyt P450 2B4

Circular dichroism experiments were performed on a Jasco J-715 spectrapolarimeter fitted with a 150-W xenon lamp at 25°C using a 1 mm cuvette. Bandwidth was set at 1.0 nm and the time constant was 1.0 sec. Spectra were recorded in the far UV region from 190 nm to 270 nm, with eight scans accumulated and averaged for each spectrum. A background (with everything present except cyt P450 2B4) was subtracted for all experiments. NaCl was titrated into a solution containing 1 µM cyt P450 2B4 and 2% (w/v) DMPC/DHPC bicelle (q = 0.25) in 100 mM potassium phosphate buffer, pH 7.4, containing 5% (w/v) glycerol. The following concentrations of NaCl were tested: 1 µM, 250 µM, 500 µM, 675 µM, 1 mM and 1.25 mM. These concentrations provide molar ratios of cyt P450 to lipids that are equivalent to those in the NMR samples.

5.4 Results

5.4.1 NaCl does not affect the structures of cyt b_5 and cyt P450 2B4

Cyt b_5 is a 15 kDa protein with a heme-containing soluble domain, a 15-residue linker and an α-helical transmembrane anchor (Section 1.1). The full assignment of the ^{1}H,^{15}N-TROSY-HSQC spectrum of the soluble domain of full-length cyt b_5 can be found in Figure 3.3. To assess whether the structure of cyt b_5, incorporated in 1,2-dimyristoyl-*sn*-glycero-3-phosphocholine (DMPC) and 1,2-dihexanoyl-*sn*-glycero-3-phosphocholine (DHPC) isotropic bicelles (q = 0.25), is affected upon addition of NaCl, a series of 2D ^{1}H,^{15}N-SOFAST-HMQC spectra of cyt b_5 were taken at the following salt concentrations: 0, 100, 250 and 400 mM NaCl. The spectra revealed that the structure of cyt b_5 does not change significantly under these salt conditions, with the overall HMQC pattern remaining identical (Figure 5.3). Although there were slight perturbations for some residues, the shifts were not significant enough to suggest structural changes, as they were within experimental error (average perturbation < 0.009 ppm). These small shifts are likely a result of the change in buffer conditions experienced by solvent-exposed residues. Through circular dichroism experiments of cyt P450 2B4 in DMPC/DHPC isotropic bicelles (q = 0.25), we also confirmed that the overall secondary structure content of cyt P450 2B4 does not change with addition of NaCl (Figure 5.2). This is in agreement with a previous study which showed no secondary structure changes in cyt P450 2B4 at different sodium phosphate and NaCl concentrations.[33]

In addition to the lack of structural changes, the intensities of cyt b_5 resonances were not affected by the addition of NaCl. The relative intensities (see Methods) of each residue fluctuated around a single value within a standard deviation of only 1.4% (which is an error range < 9%) over all NaCl concentrations. Addition of BHT to cyt b_5 also caused no spectral changes, neither in intensities nor chemical shifts (Figure 5.4). The changes in intensity described in the following sections can therefore be ascribed to modifications in the interaction between the heme domains of cyt b_5 and cyt P450.

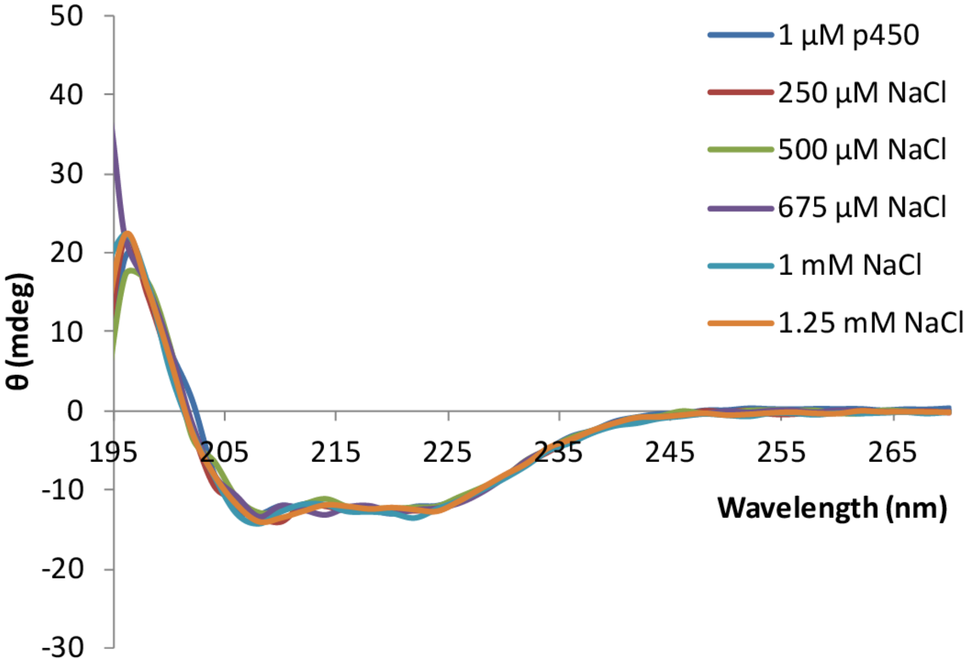

Figure 5.2. The secondary structure of cyt P450 is not affected upon addition of NaCl. Circular dichroism spectra of cyt P450 2B4, incorporated in 2% (w/v) DMPC/DHPC isotropic bicelles (*q* = 0.25), collected before and after titration of NaCl (molar ratios of cyt P450 to lipids are equivalent to those in the NMR samples).

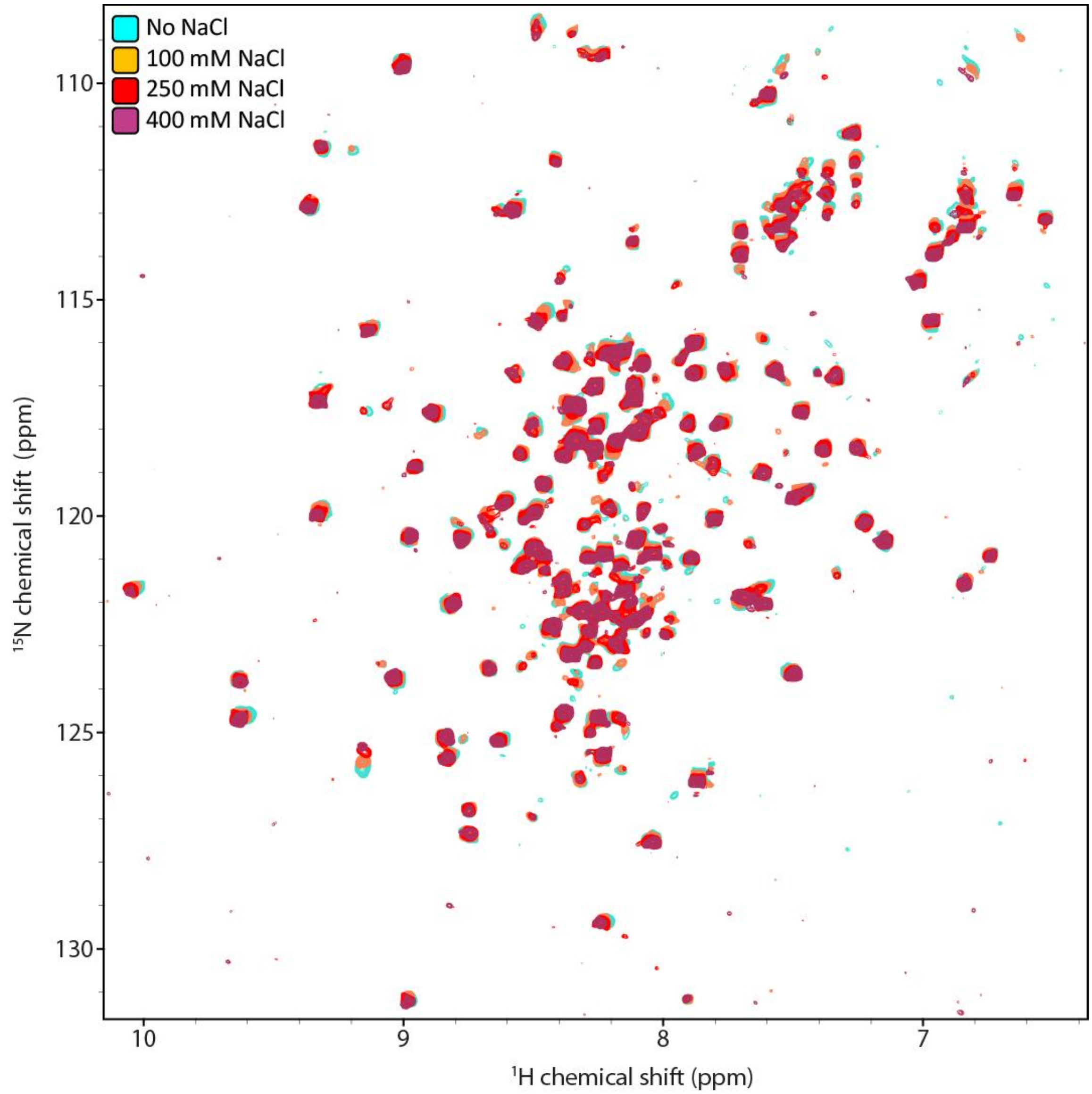

Figure 5.3. The overall structure of cyt b_5 is not affected by the presence of NaCl. ^{1}H,^{15}N-SOFAST-HMQC of cyt b_5, incorporated in DMPC/DHPC isotropic bicelles (*q* = 0.25), collected under the indicated salt conditions.

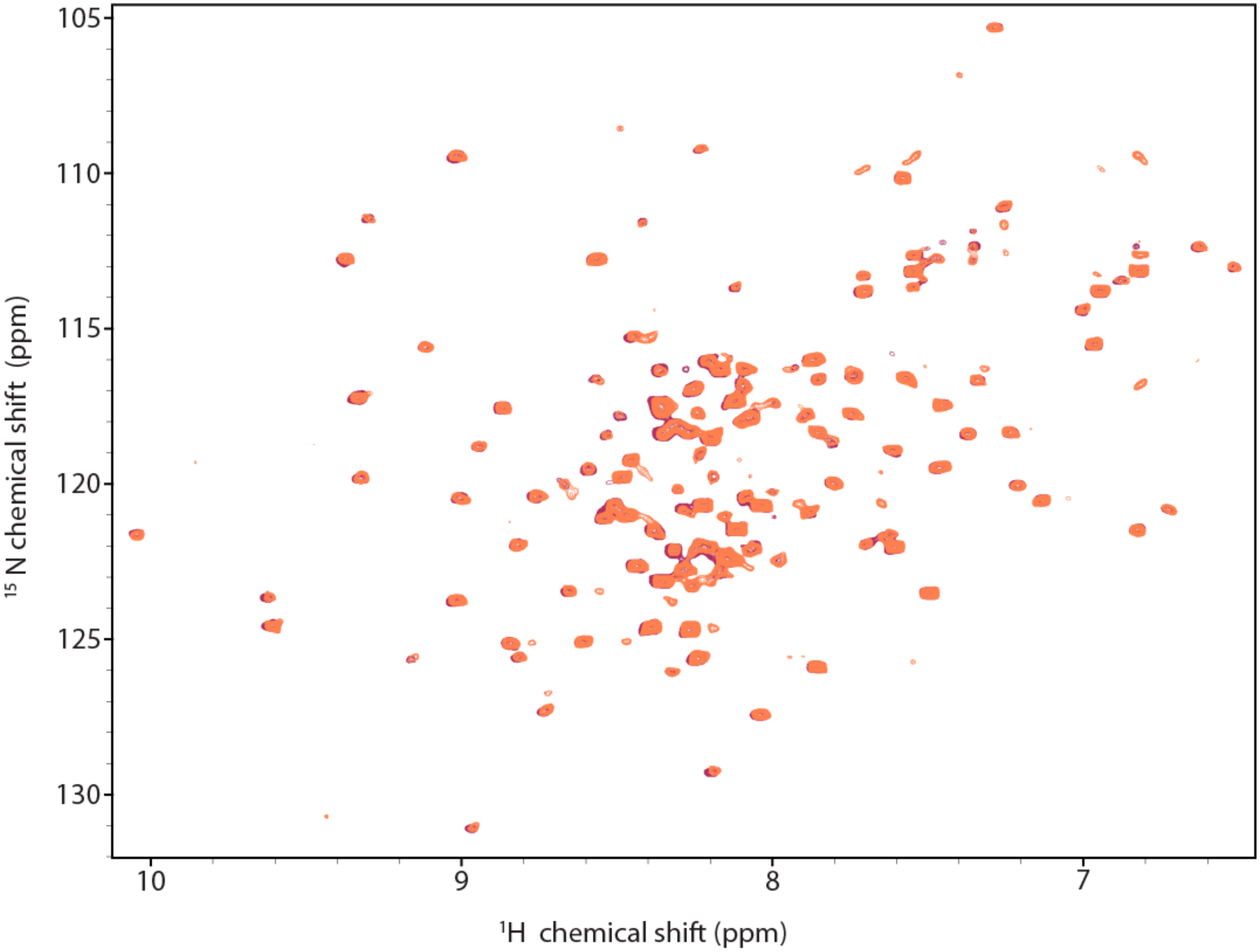

Figure 5.4. Addition of BHT affects neither intensities nor chemical shifts of cyt b_5 backbone NH nuclei. ^{1}H,^{15}N-SOFAST-HMQC spectrum of cyt b_5 in isotropic bicelles (maroon) and the spectrum obtained after addition of BHT in a 1:1 molar ratio (coral) superimposed above it.

5.4.2 Interaction between cyt b_5 and substrate-free cyt P450

To identify interfacial cyt b_5 residues, the full-length 1:1 cyt b_5-cyt P450 complex was studied incorporated in DMPC/DHPC isotropic bicelles (*q* ratio of 0.25). Upon addition of cyt P450, there was an overall drop in the intensities of cyt b_5 resonances in the ^{1}H-^{15}N-TROSY-HSQC spectrum but only a few cyt b_5 residues showed a drastic decrease in intensity or became undetectable (Table 5.2 and Figure 5.6a). The reappearance of cyt b_5 resonances in the ^{1}H-^{15}N-TROSY-HSQC spectrum and the concurrent increases in relative intensities (see Methods) of resonances were then monitored as a function of NaCl concentration (0 to 400 mM NaCl, Table 5.2 and Figure 5.5). Residues K7 and D8 were not affected by addition of cyt P450 and their intensities did not change upon addition of NaCl (M1-D6 are unobservable[34]). By the addition of 250 mM NaCl, the intensities of 88% of the residues, including those from the linker region, reached a plateau and experienced no further disruptions by NaCl (Figure 5.5); the residues that continued to be influenced by further increases in ionic strength are shown in Figure 5.6b. The intensities of the following residues were significantly influenced by the addition of NaCl (slope > 0.0391%/mM NaCl, see Methods and Discussion): E53, A55, N62, K77, T78* and F79* (*indicates solvent inaccessible, see Methods). At 400 mM NaCl, the intensities of cyt b_5 (in complex with cyt P450) were still only 78.5 ± 20.5% (on average) of the intensities of cyt b_5 alone in isotropic bicelles (free cyt b_5). In the complex at 400 mM NaCl, cyt b_5 residues I17, K24, A59, V66 and T70 had intensities significantly lower (< 58%) compared to the free cyt b_5 spectrum.

Table 5.2 Cyt b_5 residues that experience extensive line broadening in the presence of substrate-free cyt P450, at different ionic strengths.

[NaCl] (mM)	*Absent* or low intensity (< 2%) Solvent accessible	Solvent inaccessible
0	T38*, E64-G67*, *T70*, D71, *R73*	*Y35*, H44, *A59*, *T60*, *F63*, A72, L84
100	T70	none
250	none	none

In italics are residues that were absent from the spectrum.

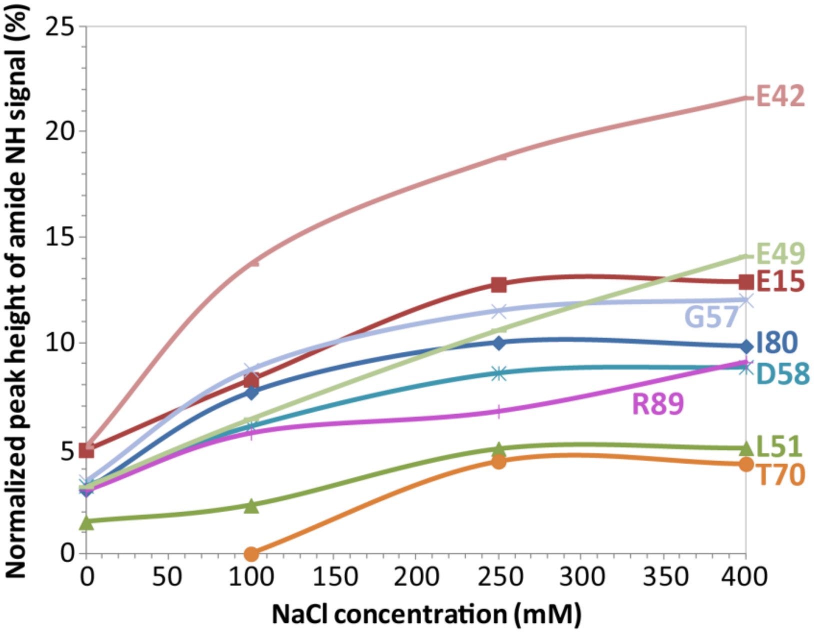

Figure 5.5 Effect of NaCl on the relative intensities of selected cyt b_5 residues in the presence of substrate-free cyt P450. All intensities were internally normalized (shown in %) to the intensity of D134 (see Methods). The relative intensities were monitored with additions of NaCl. Most residues reached a plateau by 250 mM NaCl in the presence of substrate-free cyt P450. The trend for R89 (shown), as well as T60 and D87, was different than for other residues since the increase in intensity from 100 to 250 mM was smaller than the increase from 250 to 400 mM NaCl.

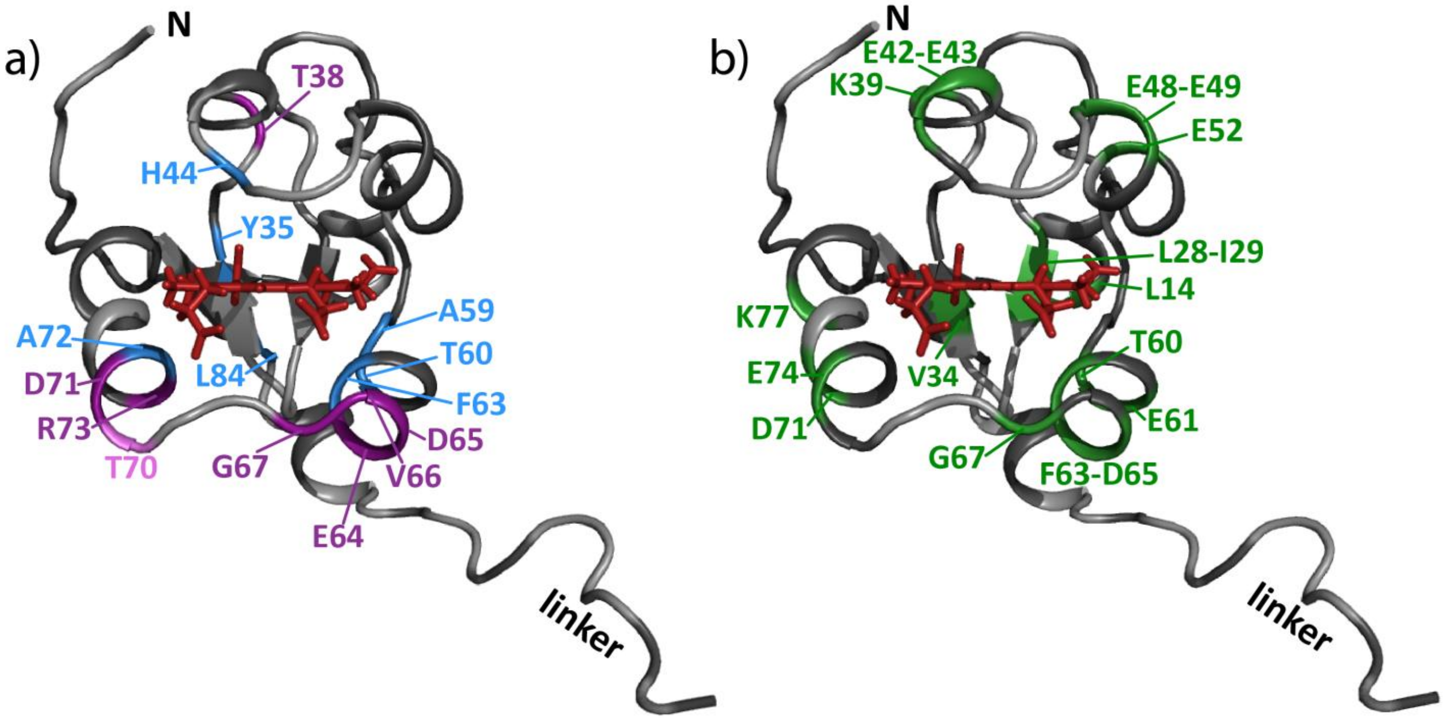

a)
N
T38
H44
Y35
A59
A72
T60
L84
D71
F63
R73
D65
T70
G67
V66
E64
linker
b)
N
E42-E43
K39
E48-E49
E52
L28-I29
L14
K77
T60
E74
V34
E61
D71
G67
F63-D65
linker

Figure 5.6 Residues playing a role in the formation of the stereospecific and encounter complexes between cyt b_5 and substrate-free cyt P450. a) Residues that broadened drastically upon complex formation with substrate-free cyt P450; purple highlights residues which are solvent accessible (≥ 35% based on NACCESS[30]) and blue those that are solvent inaccessible. The residue in pink (T70) was still absent from the spectrum even at 100 mM NaCl. b) Residues that continued to be affected by ionic strength even at 400 mM NaCl, and that are therefore prevalent interactions in the encounter complexes. Each of these residues had a slope > 0.006%/mM NaCl between 250 and 400 mM (those that plateaued had an average positive slope of ≤ 0.003%/mM NaCl). Only T28, I29 and T60 are solvent inaccessible.

5.4.3 Interaction between cyt b_5 and substrate-bound cyt P450

In Chapter 4, we showed that the interaction between cyt b_5 and cyt P450 is altered by the presence of a cyt P450 substrate.[34] To understand the cause of this change, we sought to study the effect of ionic strength on the complex between cyt b_5 and cyt P450 in the presence of the type I substrate 3,5-di-*tert*-butyl-4-hydroxytoluene (BHT). BHT is a synthetic additive that is commonly used as a preservative for foods, cosmetics and other products.[35] Mammalian cyt P450 2B enzymes convert BHT into reactive metabolites which have been linked to adverse effects such as lung tumor promotion[36]. Similarly to the previous section, the reappearance of cyt b_5 resonances and the concurrent increases in relative intensities (see Methods) were monitored as a function of NaCl concentration (0-400 mM NaCl) for the full-length cyt b_5-cyt P450 complex in the presence of BHT (1:2 cyt P450:BHT), incorporated in DMPC/DHPC isotropic bicelles (q = 0.25). In the absence of NaCl, nearly all cyt b_5 residues broadened beyond detection upon addition of substrate-bound cyt P450 (in agreement with the results in Chapter 4[34]). The only cyt b_5 resonances remaining in the spectrum originated solely from the N-terminus (K7-V9) and C-terminal end of the linker (E97, T102 and D104) (Table 5.3 and Figure 5.7). Peaks reappeared differentially in the spectrum with addition of 100 and 250 mM NaCl (Table 5.3, green in Figure 5.8a). Some residues continued to be absent even at 250 and 400 mM NaCl (Table 5.4 and Figure 5.10). None of the residues reached a plateau in intensity by the addition of 400 mM NaCl (Figure 5.9). The increases in the relative intensities were linear for all residues and a slope could be calculated for each residue with R^2 > 0.92 (see Methods and Figure 5.9). The average slope for all residues was 0.0204 ± 0.0106%/mM NaCl. Two residues were affected more significantly by NaCl (slope > 0.0310%/mM NaCl): Q54* and A55 (*not solvent accessible). The relative intensities of cyt b_5 residues in the complex spectrum at 400 mM NaCl were, on average, only 50.7 ± 20.1% of the intensities observed for free cyt b_5. In addition to V66, G67 and T70 still being absent in the spectrum, the following residues had significantly lower intensity (< 30.6%) compared to free cyt b_5: L14, K24, E48, D65, D71 and A72 (this percentage could not be calculated for F63 and T78).

Table 5.3 Cyt b_5 resonances present in the spectrum for the complex between cyt b_5 and substrate-bound cyt P450.

[NaCl]	Present (relative intensity > 1.6%)	
(mM)	Solvent accessible	Solvent inaccessible*
0	K7-V9, E97, T102, D104	
100	K10-Y11, E15-E16, N21-H22, S25, A55, G57, S93	
250	T13, K18-K19, T38-K39, L41-E43, E48-E49, R52-E53, D58, E61-N62, E74, K77, D87, R89	Y12, W27, D36, V50, T78-I80, E83

*While these residues were calculated to be solvent inaccessible by NACCESS, they are visible on the surface representation of cyt b_5 and are therefore listed here (these were also colored dark green in Figure 5.8a).

Table 5.4 Cyt b_5 residues that experience extensive line broadening in the presence of BHT-bound cyt P450, at different ionic strengths.

[NaCl]	*Absent* or low intensity (< 2%)	
(mM)	Solvent accessible	Solvent inaccessible
250	L14, E64, *D65*, *V66*, *T70*, D71, *R73*	Y35, *H44*, *A59*, *T60*, *F63*, A72, *S76*
400	V66, G67*, T70	

*The resonance of G67 did not reliably appear in the spectra during the salt titration and it was noise-level at 400 mM NaCl, suggesting strong participation in complex formation with cyt P450.

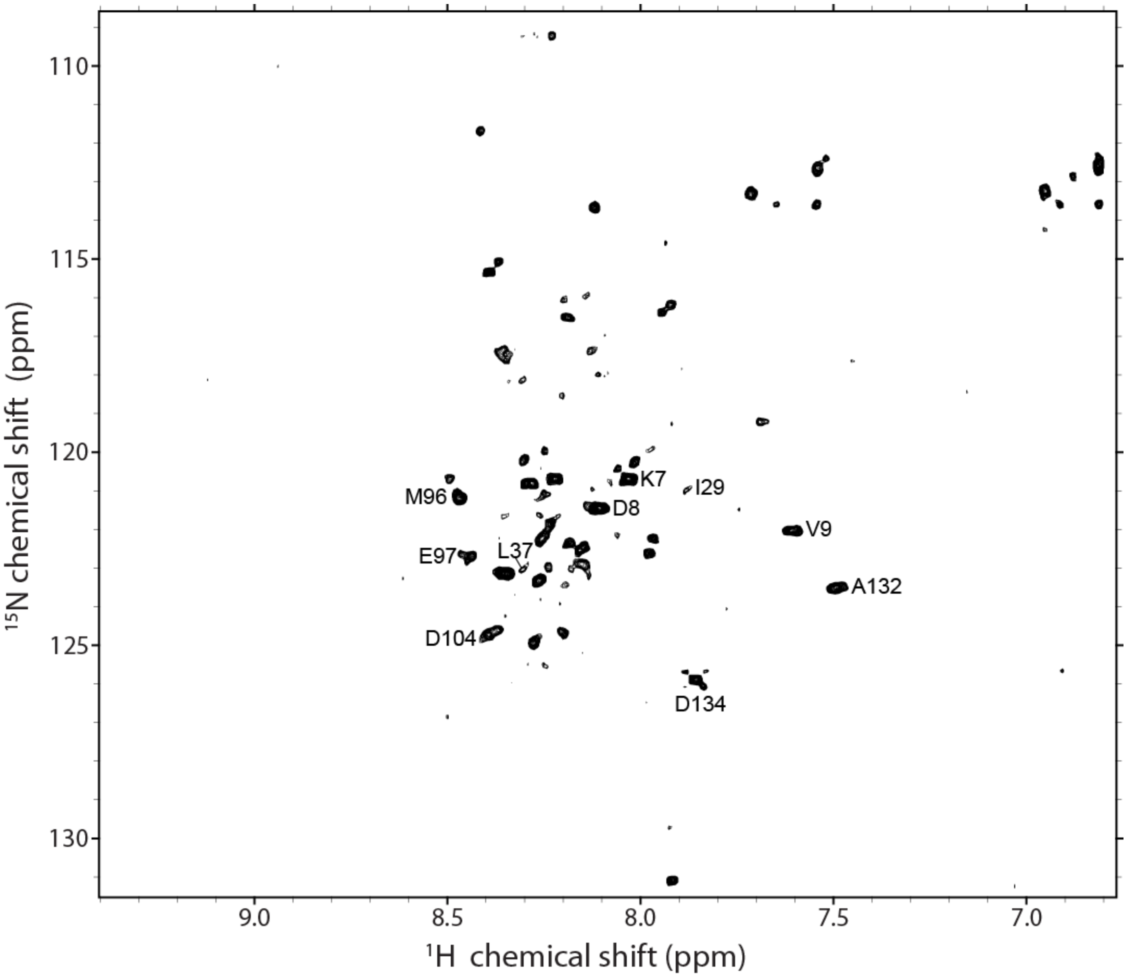

Figure 5.7. ^{1}H-^{15}N-TROSY-HSQC spectrum of cyt b_5 with substrate-bound cyt P450 (1:1) in isotropic bicelles. Only cyt b_5 residues at the N-terminus and in the linker region near the membrane anchor remain in the spectrum at 0 mM NaCl. I29 and L37 are labeled but have multiple peak centers and low intensities and were not considered in the analysis. Unlabeled resonances are either unassigned or originate from minor conformers of cyt b_5.

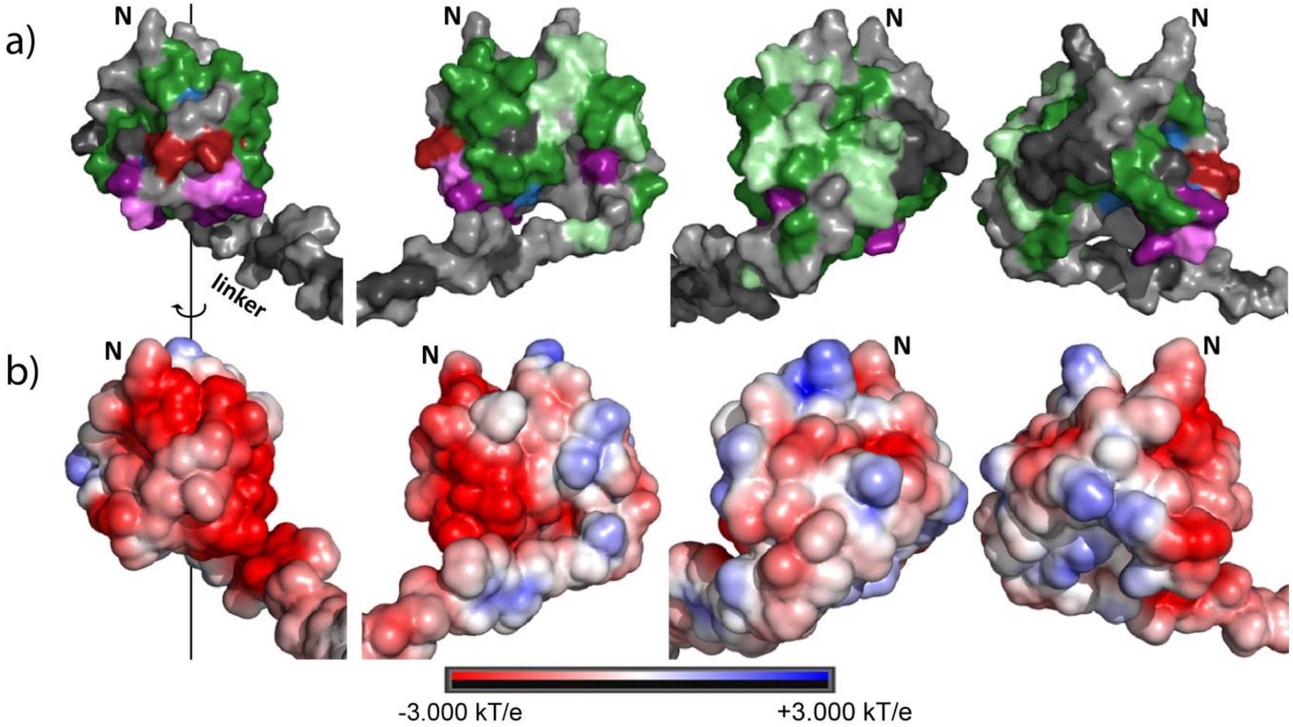

Figure 5.8 a) Residues on all sides of cyt b_5 are involved in encounter complexes between cyt b_5 and cyt P450. Surface representation of cyt b_5 with different shades of green indicating the residues that are very loosely involved in the encounter complexes' formation (light green, reappeared at 100 mM NaCl) and residues that interact more prevalently (dark green, reappeared at 250 mM NaCl). Dark purple and light violet indicate the residues that are involved in stereospecific complexes (see Figure 5.10). The residues in dark grey are involved in neither the encounter complexes nor the stereospecific complexes. Information could not be obtained for the residues in light grey. The leftmost figure shows the proximal side of cyt b_5 where the heme is solvent exposed and the figures to the right are successive 90° rotations around the axis shown. **b) The surface charge density of cyt b_5 dictates the level of interaction within the encounter complexes.** b) shows the electrostatic potential surface for rabbit cyt b_5 (NMR structure from Chapter 3) calculated using the PDB2PQR[37,38] server and PyMOL[39] with the APBS plugin 2.1[40] (see Appendix B). The surface of cyt b_5 is highly acidic on the proximal side of the soluble domain, as are parts of the linker region. The distal face and sides of cyt b_5 contain some negative charges, but their concentration is much lower than on the proximal side.

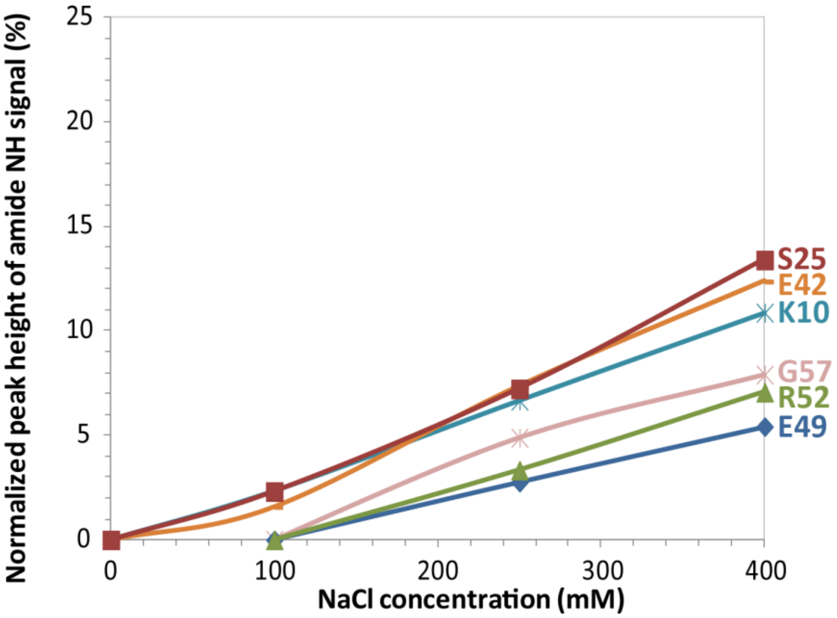

Figure 5.9 Effect of NaCl on the relative intensities of selected cyt b_5 residues in the presence of substrate-bound cyt P450. All intensities were internally normalized (shown in %) to the intensity of D134 (see Methods). The relative intensities were monitored with additions of NaCl.

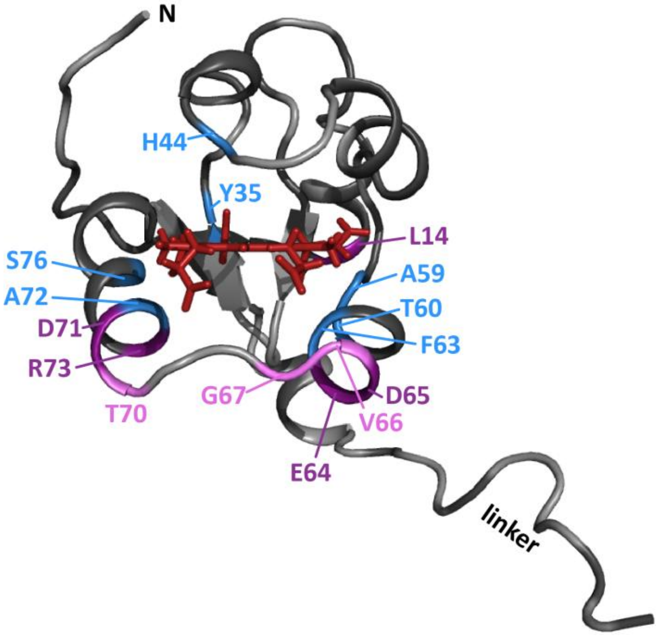

Figure 5.10 Residues playing a role in the stereospecific complex formation between cyt b_5 and substrate-bound cyt P450. Solvent accessible residues whose intensities were drastically affected in the presence of BHT-bound cyt P450 are shown in pink and purple, with solvent inaccessible residues in blue. Residues that were still absent or low in intensity at 250 mM NaCl but reappeared at 400 mM NaCl are shown in purple, and those still absent at 400 mM NaCl are shown in pink.

5.4.4 The effect of increasing ionic strength

By looking at the order of reappearance of cyt b_5 residues upon addition of NaCl, specifically in the complex between cyt b_5 and BHT-bound cyt P450, several conclusions can be reached about the effect of NaCl on complex dissociation. If it were simply the intensities of all cyt b_5 resonances increasing in the same manner with addition of NaCl, residues T26, H31, V34, L37, L51, G56, I81 and H85 should be the last to reappear in the complex spectrum, since these eight residues have the lowest intensities in the free cyt b_5 spectrum (Section 5.3.3). However, this is not the case: only I81 reappeared at 400 mM NaCl, and T26, V34, L51, G56 and H85 appeared at 250 mM NaCl and L37 reappeared at 100 mM NaCl (Table 5.3 and Table 5.4). Along the same lines, if the decrease in intensity upon complex formation was only due to the overall correlation time of cyt b_5 increasing, and if salt was breaking up complexes in an even fashion, we would expect the regions of cyt b_5 that are internally more flexible and dynamic to reappear first with addition of NaCl. Based on the higher mobility of certain regions of full-length cyt b_5 (judged by low heteronuclear ^{15}N-{^{1}H} steady-state nuclear overhauser effect values (Section 3.4.3[41]), residues E42-E43, R73 and L75 should be among the first peaks to reappear (after N-terminal and linker residues); this is not the case as they reappear only at 250 or 400 mM NaCl (Table 5.3 and Table 5.4). These two findings suggest that the broadening is not only due to a longer correlation time of cyt b_5 upon binding cyt P450 and that salt is not simply dissociating the complexes in a manner affecting all residues equally. Furthermore, salt is not simply breaking up all electrostatic interactions since some charged residues are still absent at 250 mM NaCl (Table 5.4).

5.5 Discussion

5.5.1 Characterizing the cyt b_5-cyt P450 2B4 complex

Interestingly, no significant chemical shift perturbations were observed (< 0.01 ppm), under any of the conditions studied here (and in Chapter 4), for the complex between cyt b_5 and cyt P450 2B4 in DMPC/DHPC isotropic bicelles (q = 0.25). The lack of chemical shift perturbations indicates that the complex formed between the two proteins is either highly dynamic[5,7,42] or that only free cyt b_5 is observable (because the complex is unobservable by solution NMR due to a size > 100 kDa). The intensities of cyt b_5 resonances were, however, affected by the presence of cyt P450. The broadening of cyt b_5 residues, caused by both substrate-free and BHT-bound cyt P450, can be attributed to cyt b_5 binding to cyt P450 for several reasons: NaCl and BHT caused no effect on the free cyt b_5 spectrum and the broadening observed for cyt b_5 in complex with cyt P450 was reversible upon addition of NaCl. Moreover, the data suggest that NaCl caused a differential reappearance of resonances based on the residues' interactions with cyt P450. The broadening can be hypothesized to originate from one or two different mechanisms: an enhancement of the relaxation rates of the nuclei upon complex formation (from direct interfacial contacts with cyt P450 and/or immobilization of cyt b_5 upon interaction with cyt P450), and/or intermediate-to-slow exchange between the bound and unbound forms of cyt b_5. Regardless, analysis of residues experiencing extensive broadening can aid in identifying the interfacial residues of the complex.[34,43] The interaction epitope was successfully determined for HPr and HPrK/P despite the lack of chemical shift perturbations and the absence of new cross-peaks after addition of the binding partner.[44]

5.5.2 The interface between cyt b_5 and substrate-free cyt P450 2B4

As mentioned in Section 5.4.2, upon addition of substrate-free cyt P450, only a few cyt b_5 residues experienced extensive line broadening (Table 5.2). By filtering these residues based on their solvent accessibility, the following cyt b_5 residues are likely to be found at the interaction interface with substrate-free cyt P450: E64, D65, V66, G67, T70, D71 and R73 (purple and pink in Figure 5.6a). These residues are all located on the lower cleft of the proximal side of cyt b_5 where the heme is exposed to the solvent. The placement of E64, D65 and D71 at the interface would agree with previous knowledge that cyt b_5 carboxyl groups are involved in charge-pairing interactions with cyt P450 2B4.[45,46] Mutagenesis and docking studies have shown V66[34] and D65[34,47,48] to be implicated in interactions with cyt P450. Here we show experimentally that the other residues E64, G67, T70, D71 and R73 are involved in the interaction of cyt b_5 with cyt P450 2B4. These residues agree with prior knowledge of cyt b_5 complexes and/or the general understanding of redox partner association. Earlier molecular modeling proposed the interaction of D65 and E64 with R122 and R126 on cyt P450 2B4, respectively,[49] and data-driven protein docking[34] showed non-covalent interactions between all five of these residues and cyt P450 2B4 residues. Experimentally-speaking, D71 was previously thought to only be relevant for interactions of cyt b_5 with electron donor proteins (e.g. cyt b_5 reductase[50,51]), but we show here that it is also pertinent for electron acceptor proteins. The presence of R73 at the interface would be consistent with the fact that arginines are frequently found at protein interfaces,[52] and that arginines are the only charged residues found at the core of redox partners' interfaces.[13] As for G67 (and V66), while hydrophobic residues are rarely found in ordinary protein interfaces,[52] they are common in the interfaces of redox protein complexes,[13] such as cyt b_5-cyt c[53] and others[54,55].

A number of buried cyt b_5 residues are affected upon complex formation with cyt P450 (Table 5.2). Residue Y35, which is on a β-sheet in the back of the heme pocket, is affected by addition of cyt P450 2B4; this agrees with a previous study showing that the nitration of Y35 was inhibited by the presence of cyt P450 2B4.[32] Residues Y35, T38, A59 and T60 are located in or adjacent to the cleft opening, on the top of cyt b_5, proposed by MD simulations (Figure 5.1);[29] upon complex formation with cyt P450, these residues might experience restricted motions (i.e. the cleft might not be able to open anymore) which would explain the drop in intensity observed. Residues A59, T60 and F63 are also indirectly affected, likely because they are located on the same helix as D65 and V66. Similar reasoning can be applied to A72 which is located on the α-helix where residues T70 and D71 reside.

Introduction of 100 mM NaCl into the sample caused reappearance of all residues except for T70. This suggests that T70 might be the most important cyt b_5 residue modulating complex formation with substrate-free cyt P450. Threonine residues have been found in the center of binding sites of other redox complexes,[13,56] and T70 was found to be within van der Waals contact at the cyt b_5-cyt P450 interface obtained from simulations[34]. Beyond 250 mM NaCl, only the intensities of a number of solvent accessible residues continued increasing with addition of 400 mM NaCl: L14, K39, E42-E43, E48-E49, R52, E61, F63-D65, G67, D71, E74 and K77 (Figure 5.6b). We hypothesize that these residues are involved in a larger number of encounter complexes and therefore continue to be affected by the addition of salt even at higher ionic strengths. These residues are all charged and five are on the upper cleft of cyt b_5. Some of these residues have been hypothesized to be at the interaction interface with other cyts P450: E42,[57] E48,[57–59] E49,[47,58,59] and R52[59]. While these residues are not tightly bound to cyt P450 (as judged by the absence of extensive broadening), they are present in a wide array of encounter complexes with cyt P450. The relaxation rates of residues L28, I29 and T60, which are in or around the cleft opening on the top of cyt b_5[29] (Figure 5.1), also continue to be affected by complex formation even at high ionic strength (400 mM NaCl). Complex formation is likely still occurring at 400 mM NaCl, as evidenced by the fact that numerous residues did not reach their original intensity (compared to the intensities for free cyt b_5) even though they had reached a plateau; these included I17*, A59*, V66 and T70 (*not solvent accessible). In complex formation with substrate-free cyt P450, the importance of V66 and T70 was therefore still apparent even at 400 mM NaCl.

5.5.3 Encounter complexes between cyt b_5 and substrate-bound cyt P450

In the presence of BHT-bound cyt P450, extensive line broadening was observed across the entire cyt b_5 spectrum (Figure 5.7). At lower concentrations of NaCl, broadening can be attributed to the presence of both encounter and stereospecific complexes. With addition of 100 and 250 mM NaCl, interactions between cyt b_5 and cyt

P450 should be screened based on their prevalence (i.e. the number of encounter/stereospecific complexes in which they are involved) and whether the interactions are short-range (stereospecific complexes) or loose (encounter complexes).[24] Certain regions of cyt b_5 were found to be less frequently involved in encounter complexes (light green, Figure 5.8a) and required minimal salt to reappear in the spectrum (100 mM NaCl, e.g. K10 and Y11), while other interactions were found to require higher ionic strength (250 mM, dark green in Figure 5.8a, e.g. Y12) to reappear. By looking at which residues reappeared in the spectrum by the addition of 250 mM NaCl, we can hypothesize that residues on all sides of cyt b_5 are involved in encounter complex formation (Figure 5.8a). Cyt b_5 is able to perform nearly a full 360° when sampling these complexes, with the distribution of negative charges on all sides of cyt b_5 facilitating this rotation (Figure 5.8b). The involvement of cyt b_5 residues in the encounter complexes is strongly correlated with the localization of surface charge density on cyt b_5. Regions that were found to be more prevalent (and required higher ionic strength to dissociate) in the encounter complexes have a higher density of negative charges (Figure 5.8); cyt b_5 must be adhering to cyt P450 slightly longer and more frequently in these regions. Similar cyt b_5 residues were found to be more frequently involved in encounter complexes in both the cyt P450 substrate-free case (those that did not reach a plateau by 250 mM NaCl) and in the cyt P450 BHT-bound case (reappeared at 250 mM NaCl): K39, E43, E48-E49, R52, E61, E74 and K77 (all are solvent accessible). There is therefore overlap in the populations of encounter complexes formed both when cyt P450 is BHT-bound and substrate-free.

By looking at the regions of cyt b_5 involved in encounter complexes, a number of other conclusions can be drawn. The N-terminal residues of cyt b_5 (K7, D8 and V9) do not broaden out beyond detection under any of the conditions; this reveals that the N-terminus is not at the cyt b_5-cyt P450 interface in any of the complexes formed. Beginning at K10, the residues in the remainder of the structured soluble domain are involved in at least one of the encounter complexes (green in Figure 5.8a). Y12 is only involved in encounter complex formation with cyt P450 and would therefore still be accessible and modifiable by nitration[32] since it is engaging in only loose, dynamic interactions. Moving down to the linker region of cyt b_5, when in the presence of BHT-bound cyt P450, the linker region residue S93 that is connected closely to the soluble domain was shown to be involved in some encounter complex formation (reappearing at 100 mM NaCl), whereas residues E97, T102 and D104, which are close to the membrane anchor, had no direct interactions with cyt P450.

5.5.4 Stereospecific complexes between cyt b_5 and substrate-bound cyt P450

As mentioned in Section 5.4.4, with the addition of NaCl, there was a differential increase in the intensities of cyt b_5 residues, suggesting that some complexes were preferentially dissociated compared to others. Based on the extent of broadening, by the addition of 250 mM NaCl it appears that the encounter complex population was sufficiently reduced and that the broadening originated predominantly from the stereospecific complex(es). At 250 mM NaCl, cyt b_5 residues L14, E64-G67, T70, D71 and R73 were identified as being involved in the interaction with BHT-bound cyt P450 (Figure 5.10), based on solvent accessibility and low intensity (Table 5.4). These residues are nearly identical to those that experienced broadening with substrate-free cyt P450 (Table 5.2). While it is unclear how L14 is involved, the remainder of the data indicates that cluster I of the simulated cyt b_5-cyt P450 complex structures,[34] in which only the lower cleft of cyt b_5 interacts with cyt P450 (Figure 5.11), is the predominant complex formed both in the presence and absence of a cyt P450 substrate. This is in agreement with previous results indicating that mutagenesis of E42, E43, P45-G46, E49-V50 and E53-N54 (on the upper cleft of cyt b_5) did not affect cyt b_5-cyt P450 2B4 binding and metabolism.[34] The only discrepancy is for D71, which was found to be unimportant by mutagenesis but is shown here to be important via NMR; however, it is not uncommon for interfacial residues to contribute insignificant free energy of binding.[60] The solvent inaccessible residues, whose intensities are affected by the presence of BHT-bound cyt P450, are similar to those observed with substrate-free cyt P450 (Table 5.2 and Table 5.4).

We can further home in on the essential cyt b_5 residues by looking at residues that are still absent from the spectrum at 400 mM NaCl. Although every other resonance is now visible in the spectrum at this ionic strength, the resonances of V66, G67 and T70 are still broadened beyond detection when in complex with BHT-bound cyt P450 (Table 5.4, pink in Figure 5.10); all three of these resonances are, however, very intense in the free cyt b_5 spectrum. This suggests that these three residues are involved either directly, or indirectly, in interactions within the stereospecific complex, since they are the hardest to dissociate with increasing NaCl concentration. V66 was previously

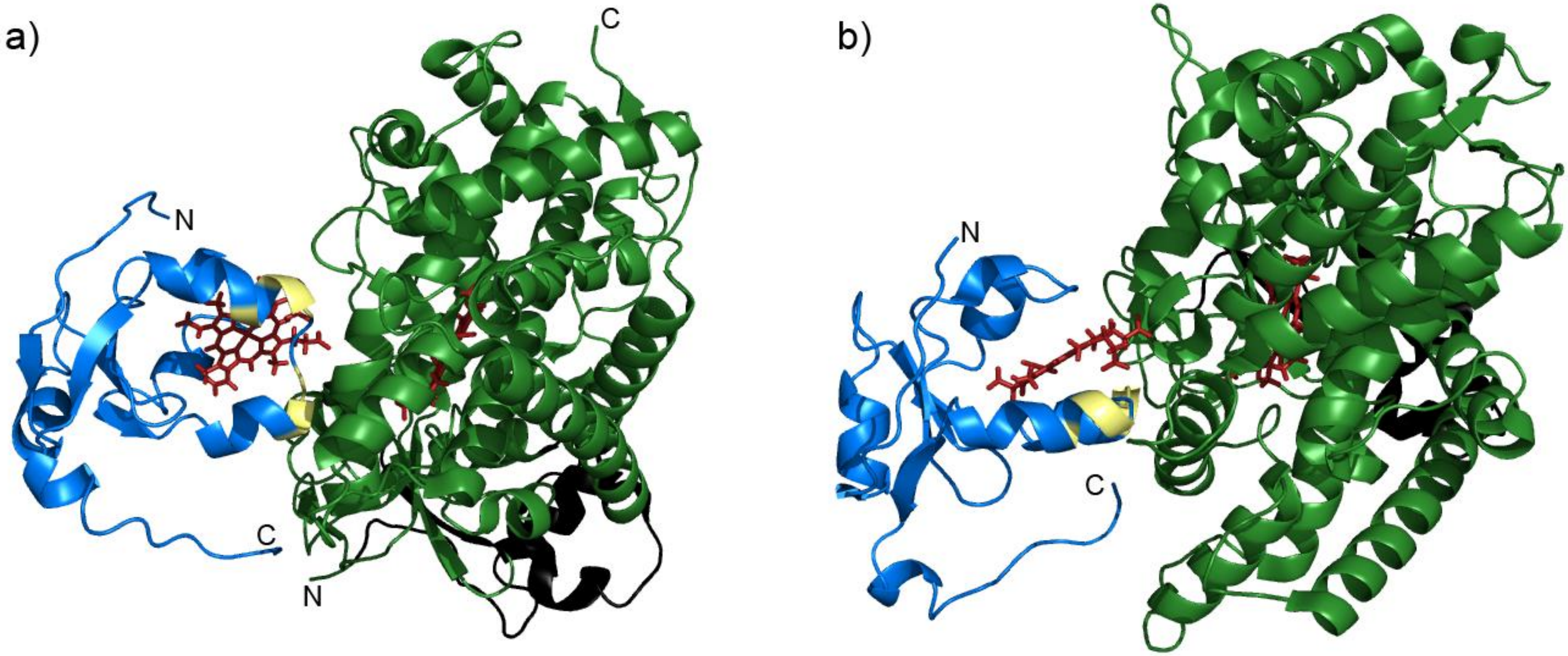

Figure 5.11 Cluster I of the data-driven simulated cyt b_5-cyt P450 structure (obtained in Chapter 4) is in agreement with the findings that only the lower cleft of cyt b_5 interacts with cyt P450 (from this Chapter). Cyt b_5 (NMR structure from Chapter 3) is in blue and cyt P450 (PDB code 1SUO[61]) is in green. Areas of cyt P450 in black are regions proposed to be buried in the membrane (Section 1.2.2). Residues in yellow are V66, G67 and T70. In a) cyt P450 is oriented in accordance with the membrane topology discussed in Section 1.2.2. In b) the complex is oriented such that it is evident that only the lower cleft of cyt b_5 is interacting with cyt P450.

shown by mutagenesis to contribute significantly to the free energy of binding of the cyt b_5-cyt P450 complex.[34] The work in this chapter suggests that cyt b_5 residues G67 and T70 might also be involved in similar strong interactions with cyt P450 2B4 (both in the presence and absence of substrate). This is the first report that T70 and G67 may play a significant role in this interaction; neither of these residues has been previously mutated. Residue V66 was previously found to interact with K433 by a double mutant cycle analysis, and V66, G67 and T70 were all proposed to be in van der Waals contacts at the interface of the simulated cyt b_5-cyt P450 2B4 complex (interacting with R125/K433, R126 and A130/D134/G136, respectively).[34] As mentioned, we also found that these three residues were involved in the interaction of cyt b_5 with substrate-free cyt P450, with T70 being the final residue to reappear with addition of NaCl (Table 5.2).

When in the presence of BHT-bound cyt P450, ionic strength continued to have an effect on the complex formation even at high concentrations of NaCl (Figure 5.9); this is dissimilar to what was obtained with substrate-free cyt P450 (Figure 5.5). Furthermore, at 400 mM NaCl, the intensities of cyt b_5 residues, in the presence of BHT-bound cyt P450, were still only 50% of the intensities in the free cyt b_5 spectrum. Accordingly, it can be concluded that there are still many complexes being formed at this high ionic strength; however, residues involved in tighter binding or more frequent interactions can still be identified since they experience considerably more broadening than other residues. A comparison of the intensities at 400 mM NaCl to the intensities in the free cyt b_5 spectrum revealed an additional residue, E48, which seems to be a key residue in encounter complex formation (but not involved in tight interactions that would result in extensive line broadening).

5.6 Conclusion

Using data presented in this chapter and the general understanding of complex formation between redox partners, it is possible to start piecing together the residue-specific mode of interaction between cyt b_5 and cyt P450 2B4. The dipole moments of cyt b_5 and cyt P450 cause the negatively charged cyt b_5 (Figure 5.8b) to be drawn to the positive surfaces on cyt P450 (Figure 5.12). Following the macrocollision between the two proteins, the proteins either dissociate or cyt b_5 is able to rotate a full 360° when sampling encounter complexes with cyt P450 2B4. This rotation is allowed by the 15-residue linker of cyt b_5, and the surface charge density dictates the level of interaction within the encounter complexes' population (Figure 5.8); it is important to note that a reduction in the length of the linker region by eight residues markedly inhibits the interaction between cyt b_5 and cyt P450 2B4.[62] Attachment to the membrane likely allows for a reduction in the dimensionality search prior to and during the encounter complex formation. The two proteins scan each other's surfaces until the side containing the largest area of condensed negative charges (on the proximal side of cyt b_5) is facing the proximal side of cyt P450 where the heme is closest to the surface (Figure 5.12). Upon experiencing more specific microcollisions, charged clusters on the proximal side of cyt b_5, located on each side of the lower cleft and on the upper cleft of cyt b_5, participate in orienting the cyt b_5 redox center relative to cyt P450 (Figure 5.13). The heme propionates also likely play a similar role.[47,63] This pre-orientation guides the residues of cyt b_5, T70, V66 and G67 (yellow, Figure 5.13), to form short-range interactions with residues on cyt P450, which should aid in placing the hemes within a 14 Å edge-to-edge distance from one another,[2,34] allowing for electron transfer to occur.

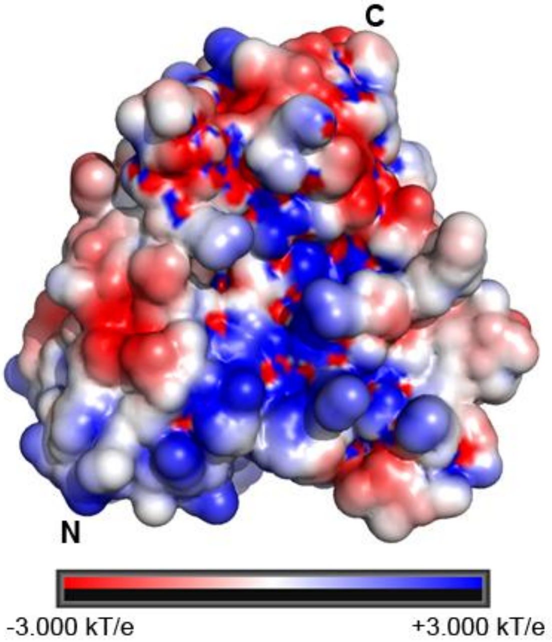

Figure 5.12. Electrostatic potential surface for the proximal side (where the heme is closest to the surface) of the soluble domain of cyt P450 2B4. This was calculated for the pdb structure 1SUO[61] using the PDB2PQR[37,38] server and PyMOL[39] with the APBS plugin 2.1[40] (see Appendix B) The proximal side of cyt P450 2B4 has a slight concave depression which is highly positively charged in the center (located near the buried heme); this is the location postulated to interact with cyt P450 redox partners.[31] This figure is not to scale when compared with the cyt b_5 figures.

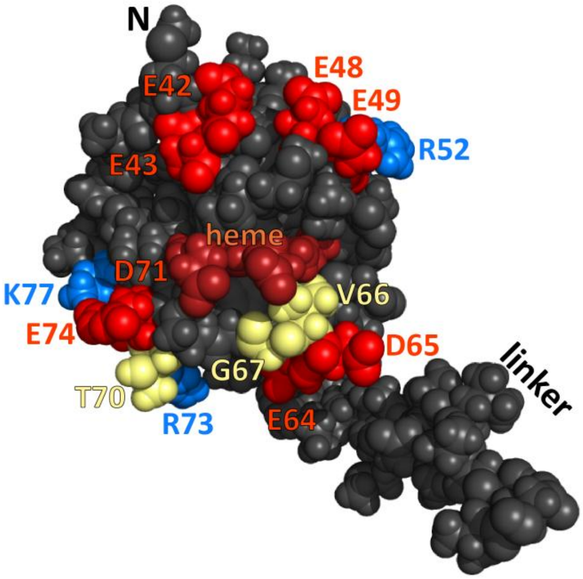

Figure 5.13 Summary of the residues involved in the association with cytP450 Residues in red and blue are the negatively and positively charged residues, respectively, which are involved in orienting the two redox centers during the microcollisions. In yellow are the residues that are central to the interactions between cyt b_5 and cyt P450 and likely serve as the close-range, specific contacts to get the redox centers close enough to allow for electron transfer.

Identical cyt b_5 residues appear to be involved in complex formation regardless of whether cyt P450 is bound to a substrate or not. Similar cyt b_5 residues are also involved in the encounter complexes with both BHT-bound and substrate-free cyt P450; however, the population of encounter complexes and the surface area of cyt b_5 scanned during the macrocollision are much higher when cyt P450 is BHT-bound. Even at 400 mM NaCl, broadening indicates that cyt b_5 is still involved in a large number of complexes with BHT-bound cyt P450; this differs from the substrate-free cyt P450 case for which the majority of complexes appear to have dissociated at this ionic strength. BHT-bound cyt P450 must adopt a conformation that enables it to encapsulate cyt b_5 and sample more encounter complexes with cyt b_5 (as shown by the extensive broadening observed for residues on all sides of cyt b_5). This increase in the population of encounter complexes leads to the two proteins finding more frequently favorable orientations that allow for interactions between residues of cyt b_5 and cyt P450, thereby permitting electron transfer.

We anticipate that the simple approach presented here should be applicable to similar dynamic systems in which only line broadening is observed. As shown in this study, this method provides very detailed information on the residues involved in protein complex formation and can separate contributions from the encounter and stereospecific complexes.

5.7 Contributions

Everything in this chapter was performed, analyzed and written by Le Clair, except for the CD experiments which Zhang performed. Proteins were expressed by Im.

5.8 References

(1) Mathews, F. S.; Mauk, A. G.; Moore, G. R. Protein-protein complexes formed by electron transfer proteins. In *Protein-Protein Recognition*; Kleanthous, C., Ed.; Oxford University Press: New York, 2000; pp. 60–101.

(2) Page, C. C.; Moser, C. C.; Dutton, P. L. Mechanism for electron transfer within and between proteins. *Curr. Opin. Chem. Biol.* **2003**, *7*, 551–556.

(3) Bashir, Q.; Scanu, S.; Ubbink, M. Dynamics in electron transfer protein complexes. *FEBS J.* **2011**, *278*, 1391–1400.

(4) Liang, Z.-X.; Nocek, J. M.; Huang, K.; Hayes, R. T.; Kurnikov, I. V; Beratan, D. N.; Hoffman, B. M. Dynamic docking and electron transfer between Zn-myoglobin and cytochrome b_5. *J. Am. Chem. Soc.* **2002**, *124*, 6849–6859.

(5) Worrall, J. A. R.; Liu, Y.; Crowley, P. B.; Nocek, J. M.; Hoffman, B. M.; Ubbink, M. Myoglobin and cytochrome b_5: a nuclear magnetic resonance study of a highly dynamic protein complex. *Biochemistry* **2002**, *41*, 11721–11730.

(6) Berg, O. G.; Von Hippel, P. H. Diffusion-controlled macromolecular interactions. *Annu. Rev. Biophys. Biophys. Chem.* **1985**, *14*, 131–160.

(7) Ubbink, M. The courtship of proteins: understanding the encounter complex. *FEBS Lett.* **2009**, *583*, 1060–1066.

(8) Volkov, A. N.; Ubbink, M.; Van Nuland, N. A. J. Mapping the encounter state of a transient protein complex by PRE NMR spectroscopy. *J. Biomol. NMR* **2010**, *48*, 225–236.

(9) Tang, C.; Iwahara, J.; Clore, G. M. Visualization of transient encounter complexes in protein-protein association. *Nature* **2006**, *444*, 383–386.

(10) Rosokha, S. V; Kochi, J. K. Fresh look at electron-transfer mechanisms via the donor/acceptor bindings in the critical encounter complex. *Acc. Chem. Res.* **2008**, *41*, 641–653.

(11) Schreiber, G.; Fersht, A. R. Rapid, electrostatically assisted association of proteins. *Nat. Struct. Biol.* **1996**, *3*, 427–431.

(12) Bernstein, F. C.; Koetzle, T. F.; Williams, G. J.; Meyer, E. F.; Brice, M. D.; Rodgers, J. R.; Kennard, O.; Shimanouchi, T.; Tasumi, M. The Protein Data Bank: a computer-based archival file for macromolecular structures. *J. Mol. Biol.* **1977**, *112*, 535–542.

(13) Crowley, P. B.; Carrondo, M. A. The architecture of the binding site in redox protein complexes: implications for fast dissociation. *Proteins Struct. Funct. Bioinf.* **2004**, *55*, 603–612.

(14) Page, C. C.; Moser, C. C.; Chen, X.; Dutton, P. L. Natural engineering principles of electron tunnelling in biological oxidation-reduction. *Nature* **1999**, *402*, 47–52.

(15) Crowley, P. B.; Ubbink, M. Close encounters of the transient kind: protein interactions in the photosynthetic redox chain investigated by NMR spectroscopy. *Acc. Chem. Res.* **2003**, *36*, 723–730.

(16) Keizers, P. H. J.; Ubbink, M. Paramagnetic tagging for protein structure and dynamics analysis. *Prog. Nucl. Magn. Reson. Spectrosc.* **2011**, *58*, 88–96.

(17) Xu, X.; Keizers, P. H. J.; Reinle, W.; Hannemann, F.; Bernhardt, R.; Ubbink, M. Intermolecular dynamics studied by paramagnetic tagging. *J. Biomol. NMR* **2009**, *43*, 247–254.

(18) Matsuo, H.; Walters, K. J.; Teruya, K.; Tanaka, T.; Gassner, G. T.; Lippard, S. J.; Kyogoku, Y.; Wagner, G. Identification by NMR spectroscopy of residues at contact surfaces in large, slowly exchanging macromolecular complexes. *J. Am. Chem. Soc.* **1999**, *121*, 9903–9904.

(19) Ortiz de Montellano, P. R. Hydrocarbon hydroxylation by cytochrome P450 enzymes. *Chem. Rev.* **2010**, *110*, 932–948.

(20) Im, S.-C.; Waskell, L. The interaction of microsomal cytochrome P450 2B4 with its redox partners, cytochrome P450 reductase and cytochrome b_5. *Arch. Biochem. Biophys.* **2011**, *507*, 144–153.

(21) Finn, R. D.; McLaughlin, L. A.; Ronseaux, S.; Rosewell, I.; Houston, J. B.; Henderson, C. J.; Wolf, C. R. Defining the in vivo role for cytochrome b_5 in cytochrome P450 function through the conditional hepatic deletion of microsomal cytochrome b_5. *J. Biol. Chem.* **2008**, *283*, 31385–31393.

(22) McLaughlin, L. A.; Ronseaux, S.; Finn, R. D.; Henderson, C. J.; Roland Wolf, C. Deletion of microsomal cytochrome b_5 profoundly affects hepatic and extrahepatic drug metabolism. *Mol. Pharmacol.* **2010**, *78*, 269–278.

(23) Northrup, S. H.; Boles, J. O.; Reynolds, J. C. Brownian dynamics of cytochrome c and cytochrome c peroxidase association. *Science* **1988**, *241*, 67–70.

(24) Suh, J.-Y.; Tang, C.; Clore, G. M. Role of electrostatic interactions in transient encounter complexes in protein-protein association investigated by paramagnetic relaxation enhancement. *J. Am. Chem. Soc.* **2007**, *129*, 12954–12955.

(25) Mulrooney, S. B.; Waskell, L. High-level expression in Escherichia coli and purification of the membrane-bound form of cytochrome b_5. *Protein Expr. Purif.* **2000**, *19*, 173–178.

(26) Saribas, A. S.; Gruenke, L.; Waskell, L. Overexpression and purification of the membrane-bound cytochrome P450 2B4. *Protein Expr. Purif.* **2001**, *21*, 303–309.

(27) Durr, U. H.; Yamamoto, K.; Im, S.-C.; Waskell, L.; Ramamoorthy, A. Solid-state NMR reveals structural and dynamical properties of a membrane-anchored electron-carrier protein, cytochrome b_5. *J. Am. Chem. Soc.* **2007**, *129*, 6670–6671.

(28) T. D. Goddard and D. G. Kneller, SPARKY 3, University of California, San Francisco.

(29) Storch, E. M.; Daggett, V. Molecular dynamics simulation of cytochrome b_5: implications for protein-protein recognition. *Biochemistry* **1995**, *34*, 9682–9693.

(30) Hubbard, S. J.; Thornton, J. M. NACCESS **1993**.

(31) Bridges, A.; Gruenke, L.; Chang, Y. T.; Vakser, I. A.; Loew, G.; Waskell, L. Identification of the binding site on cytochrome P450 2B4 for cytochrome b_5 and cytochrome P450 reductase. *J. Biol. Chem.* **1998**, *273*, 17036–17049.

(32) Hlavica, P.; Kellermann, J.; Golly, I.; Lehnerer, M. Chemical modification of Tyr34 and Tyr129 in rabbit liver microsomal cytochrome b_5 affects interaction with cytochrome P-450 2B4. *Eur. J. Biochem.* **1994**, *224*, 1039–1046.

(33) Voznesensky, A. I.; Schenkman, J. B. The cytochrome P450 2B4-NADPH cytochrome P450 reductase electron transfer complex is not formed by charge-pairing. *J. Biol. Chem.* **1992**, *267*, 14669–14676.

(34) Ahuja, S.; Nicole, J.; Im, S.-C.; Vivekanandan, S.; Popovych, N.; Le Clair, S. V; Nanga, R. P. R.; Bridges, A.; Waskell, L.; Ramamoorthy, A. A structural model of the membrane-bound cytochrome P450-cytochrome b_5 complex from NMR and mutagenesis data. *Unpublished*

(35) Lanigan, R. S.; Yamarik, T. A. Final report on the safety assessment of BHT. *Int. J. Toxicol.* **2002**, *21*, 19–94.

(36) Dwyer-Nield, L. D.; Thompson, J. A.; Peljak, G.; Squier, M. K.; Barker, T. D.; Parkinson, A.; Cohen, J. J.; Dinsdale, D.; Malkinson, A. M. Selective induction of apoptosis in mouse and human lung epithelial cell lines by the tert-butyl hydroxylated metabolite of butylated hydroxytoluene: a proposed role in tumor promotion. *Toxicology* **1998**, *130*, 115–127.

(37) Dolinsky, T. J.; Nielsen, J. E.; McCammon, J. A.; Baker, N. A. PDB2PQR: an automated pipeline for the setup of Poisson-Boltzmann electrostatics calculations. *Nucleic Acids Res.* **2004**, *32*, W665–W667.

(38) Dolinsky, T. J.; Czodrowski, P.; Li, H.; Nielsen, J. E.; Jensen, J. H.; Klebe, G.; Baker, N. A. PDB2PQR: expanding and upgrading automated preparation of biomolecular structures for molecular simulations. *Nucleic Acids Res.* **2007**, *35*, W522–W525.

(39) DeLano, W. L. The PyMOL Molecular Graphics System, Version 1.5.0.4 Schrödinger, LLC **2010**.

(40) Baker, N. A.; Sept, D.; Joseph, S.; Holst, M. J.; McCammon, J. A. Electrostatics of nanosystems: Application to microtubules and the ribosome. *Proc. Natl. Acad. Sci. U.S.A.* **2001**, *98*, 10037–10041.

(41) Ahuja, S.; Vivekanandan, S.; Popovych, N.; Le Clair, S. V; Huang, R.; Jahr, N.; Soong, R.; Xu, J.; Yamamoto, K.; Nanga, R. P. R.; Im, S.-C.; Waskell, L.; Ramamoorthy, A. NMR structure of full-length mammalian cytochrome b_5. *Unpublished*.

(42) Ubbink, M.; Bendall, D. S. Complex of plastocyanin and cytochrome c characterized by NMR chemical shift analysis. *Biochemistry* **1997**, *36*, 6326–6335.

(43) Matsuo, H.; Walters, K. J.; Teruya, K.; Tanaka, T.; Gassner, G. T.; Lippard, S. J.; Kyogoku, Y.; Wagner, G. Identification by NMR spectroscopy of residues at contact surfaces in large, slowly exchanging macromolecular complexes. *J. Am. Chem. Soc.* **1999**, *121*, 9903–9904.

(44) Maurer, T.; Meier, S.; Kachel, N.; Munte, C. E.; Hasenbein, S.; Koch, B.; Hengstenberg, W.; Kalbitzer, H. R. High-resolution structure of the histidine-containing phosphocarrier protein (HPr) from Staphylococcus aureus and characterization of its interaction with the bifunctional HPr kinase/phosphorylase. *J. Bacteriol.* **2004**, *186*, 5906–5918.

(45) Tamburini, P. P.; MacFarquhar, S.; Schenkman, J. B. Evidence of binary complex formations between cytochrome P-450, cytochrome b_5, and NADPH-cytochrome P-450 reductase of hepatic microsomes. *Biochem. Biophys. Res. Commun.* **1986**, *134*, 519–526.

(46) Tamburini, P. P.; White, R. E.; Schenkman, J. B. Chemical characterization of protein-protein interactions between cytochrome P-450 and cytochrome b_5. *J. Biol. Chem.* **1985**, *260*, 4007–4015.

(47) Stayton, P. S.; Poulos, T. L.; Sligar, S. G. Putidaredoxin competitively inhibits cytochrome b_5-cytochrome P-450cam association: a proposed molecular model for a cytochrome P-450cam electron-transfer complex. *Biochemistry* **1989**, *28*, 8201–8205.

(48) Peng, H.-M.; Auchus, R. J. The action of cytochrome b_5 on CYP2E1 and CYP2C19 activities requires anionic residues D58 and D65. *Biochemistry* **2012**.

(49) Lewis, D. F.; Lake, B. G.; Dickins, M.; Eddershaw, P. J.; Tarbit, M. H.; Goldfarb, P. S. Molecular modelling of CYP2B6, the human CYP2B isoform, by homology with the substrate-bound CYP102 crystal structure: evaluation of CYP2B6 substrate characteristics, the cytochrome b_5 binding site and comparisons with CYP2B1 and CYP2B4. *Xenobiotica* **1999**, *29*, 361–393.

(50) Nishida, H.; Miki, K. Electrostatic properties deduced from refined structures of NADH-cytochrome b_5 reductase and the other flavin-dependent reductases: pyridine nucleotide-binding and interaction with an electron-transfer partner. *Proteins* **1996**, *26*, 32–41.

(51) Kawano, M.; Shirabe, K.; Nagai, T.; Takeshita, M. Role of carboxyl residues surrounding heme of human cytochrome b_5 in the electrostatic interaction with NADH-cytochrome b_5 reductase. *Biochem. Biophys. Res. Commun.* **1998**, *245*, 666–669.

(52) Bogan, A. A.; Thorn, K. S. Anatomy of hot spots in protein interfaces. *J. Mol. Biol.* **1998**, *280*, 1–9.

(53) Ren, Y.; Wang, W.-H.; Wang, Y.-H.; Case, M.; Qian, W.; McLendon, G.; Huang, Z.-X. Mapping the electron transfer interface between cytochrome b_5 and cytochrome c. *Biochemistry* **2004**, *43*, 3527–3536.

(54) Ejdebäck, M.; Bergkvist, A.; Karlsson, B. G.; Ubbink, M. Side-chain interactions in the plastocyanin-cytochrome f complex. *Biochemistry* **2000**, *39*, 5022–5027.

(55) Senda, M.; Kishigami, S.; Kimura, S.; Fukuda, M.; Ishida, T.; Senda, T. Molecular mechanism of the redox-dependent interaction between NADH-dependent ferredoxin reductase and Rieske-type [2Fe-2S] ferredoxin. *J. Mol. Biol.* **2007**, *373*, 382–400.

(56) Müller, J. J.; Lapko, A.; Bourenkov, G.; Ruckpaul, K.; Heinemann, U. Adrenodoxin reductase-adrenodoxin complex structure suggests electron transfer path in steroid biosynthesis. *J. Biol. Chem.* **2001**, *276*, 2786–2789.

(57) Chudaev, M. V; Gilep, A. A.; Usanov, S. A. Site-directed mutagenesis of cytochrome b_5 for studies of its interaction with cytochrome P450. *Biochemistry (Mosc)* **2001**, *66*, 667–681.

(58) Gao, Q.; Doneanu, C. E.; Shaffer, S. A.; Adman, E. T.; Goodlett, D. R.; Nelson, S. D. Identification of the interactions between cytochrome P450 2E1 and cytochrome b_5 by mass spectrometry and site-directed mutagenesis. *J. Biol. Chem.* **2006**, *281*, 20404–20417.

(59) Naffin-Olivos, J. L.; Auchus, R. J. Human cytochrome b_5 requires residues E48 and E49 to stimulate the 17,20-lyase activity of cytochrome P450c17. *Biochemistry* **2006**, *45*, 755–762.

(60) Clackson, T.; Wells, J. A. A hot spot of binding energy in a hormone-receptor interface. *Science* **1995**, *267*, 383–386.

(61) Scott, E. E.; White, M. A.; He, Y. A.; Johnson, E. F.; Stout, C. D.; Halpert, J. R. Structure of mammalian cytochrome P450 2B4 complexed with 4-(4-chlorophenyl)imidazole at 1.9-A resolution: Insight into the range of P450 conformations and the coordination of redox partner binding. *J. Biol. Chem.* **2004**, *279*, 27294–27301.

(62) Clarke, T. A.; Im, S.-C.; Bidwai, A.; Waskell, L. The role of the length and sequence of the linker domain of cytochrome b_5 in stimulating cytochrome P450 2B4 catalysis. *J. Biol. Chem.* **2004**, *279*, 36809–36818.

(63) Tamburini, P. P.; Schenkman, J. B. Mechanism of interaction between cytochromes P-450 RLM5 and b_5: evidence for an electrostatic mechanism involving cytochrome b_5 heme propionate groups. *Arch. Biochem. Biophys.* **1986**, *245*, 512–522.

CHAPTER 6

The role of the cytochrome b_5 linker region in complex formation with cytochrome P450 2B4

6.1 Summary

In this chapter, we establish the structure, internal dynamics and diffusion tensor of a membrane-bound cytochrome b_5 mutant in which eight residues (E97-D104) are deleted from the linker region. This mutant (referred to as *m*-cyt b_5) was found to have a similar fold as wild-type cyt b_5 based on an analysis of the $^1H,^{15}N$-HSQC-NOESY spectrum. The internal dynamics of *m*-cyt b_5 were also shown to be similar to wild-type, with the N-terminus and linker residues being highly flexible, and certain residues in helices α2, α3 and α5 having large amplitude motions. The diffusion tensor, however, was found to be more asymmetrical for *m*-cyt b_5 than wild-type and its effective correlation time was longer by ~1 ns. Through the use of the NMR approach developed in Chapter 5, the complex formation between *m*-cyt b_5 and cyt P450 (both with and without substrate) was studied in isotropic bicelles. We found that *m*-cyt b_5 and substrate-free cyt P450 were not able to engage in stereospecific complex formation and only remained as a pure encounter complex, with all complexes being dissociated by the addition of 400 mM NaCl. By looking at the interaction between the two proteins in the presence of a cyt P450 substrate, it was shown that *m*-cyt b_5 is not able to sample

as many orientations within the encounter complex. Residues V66 and T70 were identified as being important in complex formation between *m*-cyt b_5 and substrate-bound cyt P450, indicating that the interactions with the lower cleft of cyt b_5 are essentially unaffected by the shortening of the linker. Truncation of the linker, however, renders the upper cleft of cyt b_5 unable to successfully interact with cyt P450 (even in encounter complex formation), and renders cyt b_5 unable to perform the full 360° rotation, within the concavity of substrate-bound cyt P450 (as was observed for wild-type cyt b_5 in Chapter 5). This study shows that the length of the linker modulates the number of encounter complexes (and the surface area sampled within them) that can form between cyt b_5 and cyt P450. Truncation of the linker therefore results in a lower probability of finding the stereospecific orientation during each macrocollision. We therefore show that the cyt b_5 15-residue linker is required to allow the adequate rotational/diffusional freedom in its interaction with cyt P450.

6.2 Introduction

The length, structure or sequence of linker regions connecting protein domains can prove to be essential in modulating the interaction between protein partners.[1–3] In the case of cytochrome b_5 (cyt b_5), only the length of the linker has been shown to be of importance for interaction with cytochrome P450.[1] Cyt b_5 can be thought of as three separate domains: a large cytosolic heme domain, a linker region and a membrane anchor. The two regions of cyt b_5 that have been shown to be insensitive to protease cleavage[4] are S5-D88 (the heme domain) and D104-Y127 (the membrane domain). Based on sequence alignment, the heme domain is believed to encompass residues M1-

R89 and the transmembrane domain has been predicted, using the MPEx program, to be D104-M131.[1] By deduction, the linker domain was therefore estimated to be from S90-D104.[1] Structural characterizations of the heme domain from NMR using truncated rabbit cyt b_5[5] and full-length cyt b_5 (Chapter 3) have determined the structured part of the heme domain to be from L14-R89 and K10-R89, respectively. The microsomal cyt b_5 sequence of the linker region is 60-80% conserved in vertebrates and its length is conserved at 15 amino acids.[1] Until our studies on the full-length protein, little was known about the structure of the linker region[6] though it was determined to be unstructured in truncated cyt b_5 proteins.[5–7] As discussed in Chapter 3, the linker region (S90-D104) of full-length cyt b_5, incorporated in dodecylphosphocholine micelles, is completely unstructured.

As discussed in Chapter 1, cyt b_5 interacts with many different electron acceptor and electron donor proteins.[8–18] Of particular interest in our lab (and this thesis) is the association of cyt b_5 with cyt P450 proteins.[8–13] As discussed in Chapters 1 and 3, cyt b_5 has been shown to be an important part of the cyt P450 metabolism cycle *in vivo*.[19,20] The role of the length and sequence of the linker region in the interaction between cyt b_5 and cyt P450 2B4 was the focus of a previous study done by Clarke *et al*.[1] In it, they observed that a deletion of six or less amino acids from the linker induced a minor (a maximum of 4-fold) increase in the spectral dissociation, K_s. With a deletion of eight residues, however, K_s increased drastically by 30-fold. The rate of metabolism of methoxyflurane, in the presence of the 8-deletion mutant of cyt b_5, was shown to be ~36% less than for wild-type cyt b_5. Deleting more than eight residues resulted in a K_s

> 100. Reversing the sequence, lengthening the linker, or altering one or two highly conserved residues, resulted in (comparatively) minor changes in the K_s.

In the studies presented in this chapter, the same 8-deletion mutant of cyt b_5 (referred to as mutant cyt b_5, or *m*-cyt b_5) was studied. The structure and internal dynamics of *m*-cyt b_5, which has residues E97-D104 deleted from its linker region,[1] was studied by solution NMR and compared to results obtained for wild-type cyt b_5. An analysis of the NMR relaxation measurements was also done with TENSOR2[21] to yield the diffusion tensor of the soluble domain of *m*-cyt b_5. The interaction between *m*-cyt b_5 and cyt P450 was then studied with the NMR approach developed in Chapter 5. Both the interactions of *m*-cyt b_5 with substrate-free cyt P450 and substrate-bound cyt P450 were examined and compared to the results obtained for wild-type cyt b_5 in Chapter 5. Through these studies, we shed light on the drastic decrease in activity and binding observed for *m*-cyt b_5.

6.3 Materials and methods

6.3.1 Materials

Uniformly ^{15}N-labeled 8-deletion mutant of cyt b_5, in which residues E97-D104 were truncated from the linker, was overexpressed and purified according to the procedures outlined in previous publications[1,22–24] and Chapter 3. The lipids 1,2-dihexanoyl-*sn*-glycero-3-phosphocholine (DHPC) and 1,2-dimyristoyl-*sn*-glycero-3-phosphocholine (DMPC) were purchased from Avanti Polar Lipids (Alabaster, AL). ^{2}H-dodecylphosphocholine (DPC) and D_2O were purchased from Cambridge Isotope Laboratories (Andover, MA). Phosphate buffer components (potassium phosphate monobasic and dibasic), glycerol and 3,5-di-*tert*-butyl-4-hydroxytoluene (BHT) were purchased from Sigma-Aldrich. Sodium chloride was purchased from Fischer Scientific.

6.3.2 Solution NMR

All solution NMR experiments were performed at 298 K on a Bruker 900 MHz NMR spectrometer equipped with a 5 mm triple-resonance TXI cryo-probe (at the Michigan State University facility). In all instances, the NMR buffer for each sample consisted of 100 mM potassium phosphate buffer, pH 7.4, with 5% (w/v) glycerol (referred to as NMR buffer). The protein concentration of ^{15}N-*m*-cyt b$_5$ was 0.2 mM for all complex samples (with 0.2 mM of cyt P450), 0.1 mM and 0.2 mM for the ^{1}H, ^{15}N-TROSY-HSQC spectra of *m*-cyt b$_5$ in micelles and bicelles, respectively, and 0.5 mM for the ^{15}N-HSQC-NOESY experiment. Proteins were incorporated in either DPC micelles or 10% (w/v) DMPC/DHPC isotropic bicelles with a *q* ratio (molar ratio of DMPC to DHPC) of 0.25. The isotropic bicelles were prepared as described in Chapter 5 and Appendix D, which was based on a previously published method.[25] All NMR data were processed using TopSpin 2.0 (Bruker) and analyzed with Sparky[26], except where indicated.

6.3.2.1 Structure determination of mutant cyt b$_5$

A ^{15}N-HSQC-NOESY spectrum was collected on uniformly ^{15}N-labeled *m*-cyt b$_5$ incorporated in ^{2}H-DPC micelles. For this spectrum, 2048 x 84 x 300 complex data points were recorded with 8 scans and 128 dummy scans, and a mixing time of 100 ms. The spectrum was recorded with spectral widths of 15290 Hz, 3650 Hz and 14006 Hz for ^{1}H, ^{15}N and aliphatic protons. NOE distance restraints (Table 6.3) were input into CYANA

2.1[27] for structure calculation. Thirty minimum energy conformers were selected from 100 structures calculated in 10,000 annealing steps.

6.3.2.2 Backbone ^{15}N relaxation measurements of mutant cyt b$_5$

The ^{15}N longitudinal relaxation rate (R_1), ^{15}N transverse relaxation rate (R_2) and ^{15}N-{^{1}H} steady-state nuclear overhauser effect (NOE) were measured on a sample containing 0.5 mM uniformly ^{15}N-labeled *m*-cyt b$_5$ in 100 mM phosphate buffer, pH 7.4 with 45 mM DPC and 5% (w/v) glycerol. The ^{15}N longitudinal and transverse relaxation time constants, T_1 and T_2, respectively, were determined by collecting a time series of ^{15}N-HSQC spectra with sensitivity enhancement. For T_1 measurements, the spectra were collected with relaxation delays of 5, 40, 80, 130, 210, 330, 470, 630, 800, 1000 and 1400 ms (duplicate points for 40 and 130 ms). T_2 measurements were achieved by Carr-Purcell-Meiboom-Gill (CPMG) spin echo experiments[28] with relaxation delays of 7.2, 14.4, 28.8, 43.2, 72, 100.8, 115.2 and 158.4 ms (with duplicate points for 14.4 and 43.2 ms). In the CPMG pulse train, the delays between the 180 degree pulses were set to 0.9 ms. For both T_1 and T_2 measurements, a recycle delay of 1 s was used and 2048 x 200 complex data points were collected with 24 scans and 16 dummy scans, and duplicate points for two relaxation delays were recorded for estimation of errors. 2D ^{15}N-{^{1}H} steady-state NOE experiments[29,30] with water flip-back pulse for water suppression[31] were recorded with and without pre-saturation of the amide protons; the proton saturation period and recycle delay were 3 s and 4 s, respectively, and 2048 x 512 complex data points were collected with 20 scans and 32 dummy scans. All the spectra were processed using NMRPipe[32] and peak heights were determined using Sparky[26]. T_1

and T_2 values were calculated by fitting the peak heights as a function of relaxation delays in Sparky[26]. The NOE values were calculated with NOE= $I_{saturated}/I_{unsaturated}$, where $I_{saturated}$ and $I_{unsaturated}$ are the peak heights for each residue with and without pre-saturation, respectively; the error was calculated in the same manner as Bailey *et al.*[33]

Relaxation data were analyzed using the Lipari-Szabo model-free analysis[34,35] in TENSOR2[21]. The chemical shift anisotropy tensor angle from the N-H bond vector was set at 18° according to the work done by Pandey *et al.* on full-length rabbit cyt b_5 in DPC micelles.[36] The value of τ_c (for the isotropic model) and diffusion tensor (for the anisotropic model) were calculated based on the relaxation parameters of residues within secondary structure elements[37] (based on the structure of wild-type cyt b_5) of the soluble domain (K10-R89), which had NOE > 0.65 and an R_2/R_1 value within 1.5 standard deviations from the mean.[38] The errors for the diffusion tensor components and the isotropic correlation time were obtained from 1000 Monte Carlo simulations.

6.3.2.3 NaCl titration on mutant cyt b_5-cyt P450 complex samples

For all *m*-cyt b_5-cyt P450 complex samples, ^{15}N-*m*-cyt b_5 and wild-type unlabeled cyt P450 were concentrated together (at a 1:1 molar ratio) in order to pre-form the complex. In the samples containing BHT, BHT was added in a 1:2 molar ratio of cyt P450:BHT after pre-forming the *m*-cyt b_5-cyt P450 complex. The protein complexes were carried on ice to the Michigan State University 900 MHz NMR facility. There, the bicelle film (which had remained in the vacuum oven overnight) was rehydrated in NMR buffer, and added in small aliquots to the protein complex. NaCl titrations were performed on the protein complex samples both with and without BHT. For each NaCl titration point

(0, 100, 250 and 400 mM NaCl), a $^{1}H,^{15}N$-TROSY-HSQC spectrum was collected. CO assays[39] were performed to confirm that the active form of cyt P450 was present at the end of the NMR experiments.

The peak heights for each residue, in all complex spectra, were calculated using Sparky.[40] In order to be able to compare the intensities obtained at each NaCl concentration, each $^{1}H,^{15}N$-TROSY-HSQC spectrum was internally normalized to the intensity of D134 (setting D134 as 100% and all other residues as a percentage of D134); these intensities are referred to as "relative intensities" in the text. As mentioned in Chapter 5, D134 was chosen because it is the highest intensity resonance in all spectra and is located at the C-terminus of cyt b_5 and therefore should not be affected by complex formation with cyt P450 (similar to wild-type cyt b_5 in Chapter 5, the intensity of D134 was not affected in any of the *m*-cyt b_5-cyt P450 spectra). The relative intensities for each *m*-cyt b_5 residue were plotted as a function of the concentration of NaCl in Excel. Slopes were calculated according to the data points between 0-400 mM NaCl for *m*-cyt b_5 with substrate-free cyt P450. In addition to the missing resonances listed in Section 6.4.1, for the *m*-cyt b_5-cyt P450 complex, only L92 and S93 (out of the seven residue linker) were identified and assigned conclusively in the *m*-cyt b_5-cyt P450 complex and only had a single conformer peak that could be easily monitored during experiments.

The cyt b_5 structure obtained from NMR in Chapter 3 was used for the generation of all figures, with the linker truncated at residue E97. NACCESS,[41] with the default parameters, was used to calculate the solvent accessibility of cyt b_5 residues (see

Appendix C) in our NMR structure of cyt b_5 (Chapter 3). Residues that were considered solvent accessible had a relative solvent accessibility ≥ 35% for either the main chain or side chain atoms, or all atoms. A threshold of 35% was used because a cyt P450 residue shown to be important for the cyt b_5-cyt P450 interaction, as determined from mutagenesis,[24] was calculated to have a main chain solvent accessibility of 35.8%.

6.4 Results

6.4.1 Sequence specific assignment of the soluble domain of full-length *m*-cyt b_5

The ^1H-^{15}N-TROSY-HSQC spectrum of *m*-cyt b_5 in DPC micelles at 25 ^oC was well-resolved and had dispersed NH correlations (Figure 6.6), indicating that *m*-cyt b_5 was well-folded and monomeric under the sample conditions. Because the spectrum was nearly identical to the one of wild-type cyt b_5 (Figures 6.1 and 6.2); the peak assignments were transferrable. For the peaks that shifted in the *m*-cyt b_5 spectrum (compared to wild-type cyt b_5), nearby peaks were assigned to the given residues. This initial assignment was confirmed by collecting and assigning a ^{15}N-HSQC-NOESY spectrum. The complete assignment of the ^1H-^{15}N-TROSY-HSQC spectrum of *m*-cyt b_5 can be found in Figures 6.6 and 6.7.

By comparing the ^1H,^{15}N-TROSY-HSQC spectra of *m*-cyt b_5 spectrum to the one for wild-type cyt b_5, both in DPC micelles and DMPC/DHPC isotropic bicelles, it can be seen that the majority of residues that differ in the spectrum of *m*-cyt b_5 (compared to wild-type cyt b_5) are the residues that were deleted in the mutant (E97, T98, L99, T102 and D104), and the other linker residues L92 and S93 which are adjacent to the residues that were deleted in the mutant. The other residues that differ in the spectrum are identical to residues that were identified as shifting among different cyt b_5 samples in Section 3.4.4.

Similar to wild-type cyt b_5 (Chapter 3), it can be seen in Figure 6.6 and Figure 6.7 that the minor isomer is also present in the *m*-cyt b_5 samples (labeled in grey with asterisks). As discussed in Chapter 3, this minor isomer differs from the more populated isomer with respect to the heme orientation (Section 3.4.1); more specifically, the heme plane is rotated by 180° about the α-γ *meso*-axis (Figure 3.1).[42,43] As discussed extensively in Section 3.4.1, these two isomeric species originate from the initial incorporation of the heme (type B) molecule into apo-cyt b_5 during expression. In all subsequent analyses in this chapter, including the experiments performed on the *m*-cyt b_5-cyt P450 complex, only the major isomer was considered.

The following resonances for *m*-cyt b_5 residues are either unassigned or invisible in the spectrum: M1-D6, S23, L30, K33, P45, G46, P86, S90, S90, K91, K94, P95 and I100. The following residues have the lowest intensities in the *m*-cyt b_5 ^{1}H-^{15}N-TROSY-HSQC spectrum and cannot be quantitatively discussed in the following sections, as any small changes in intensity might cause the resonances to become undetectable: T26, H31, H32, Y35, L37, G47, L51, H68, S69, I81 and H85.

6.4.2 Structure of the soluble domain of full-length *m*-cyt b_5

A detailed comparison of the NOE cross-peaks in the ^{15}N-HSQC-NOESY spectra of wild-type and mutant cyt b_5 was done to see if the soluble domain structure of *m*-cyt b_5 was the same as for wild-type cyt b_5. NOE cross-peaks within/to/from all α-helical segments (Figure 6.8 and Table 6.2), β-sheets (Figure 6.9 and Table 6.1) and unstructured regions were compared. As can be seen in Figure 6.8, the α-helical segments of *m*-cyt b_5, helix α4 and the 3_{10} helix have identical patterns for $d_{\alpha N}$ and d_{NN} (i,i+3 and above). Additionally, helices α1 and α5 have NOE cross-peak patterns that indicate identical structures for both mutant and wild-type cyt b_5. Helix α2 has identical NOE patterns for $d_{\alpha N}$ but has an additional cross-peak for d_{NN}(i,i+3) from residue 41 to 44 in the mutant cyt b_5 spectrum; this might indicate a slight difference at the terminal region of the helix. Compared to mutant cyt b_5, the wild-type helix α3 has one additional long-range NOE cross-peak for d_{NN}(i,i+4) from residue 50 to 54, and a few additional cross-peaks to/from residues in helix α3, including $d_{\alpha N}$(i,i+3) 48-51 and $d_{\alpha N}$(i,i+4) 51-55; this could indicate a slight difference in the positioning of helix α3. The β-sheet structures appear to be fairly similar for wild-type and mutant cyt b_5, with only a few scattered long-range NOEs differing for wild-type and mutant cyt b_5 (Table 6.1). The only key differences are the absence of two NOE cross-peaks to Y35-NH (35-82 and 35-80) and the cross-peak between residue L28-NH and D58-NH in the *m*-cyt b_5 spectrum.

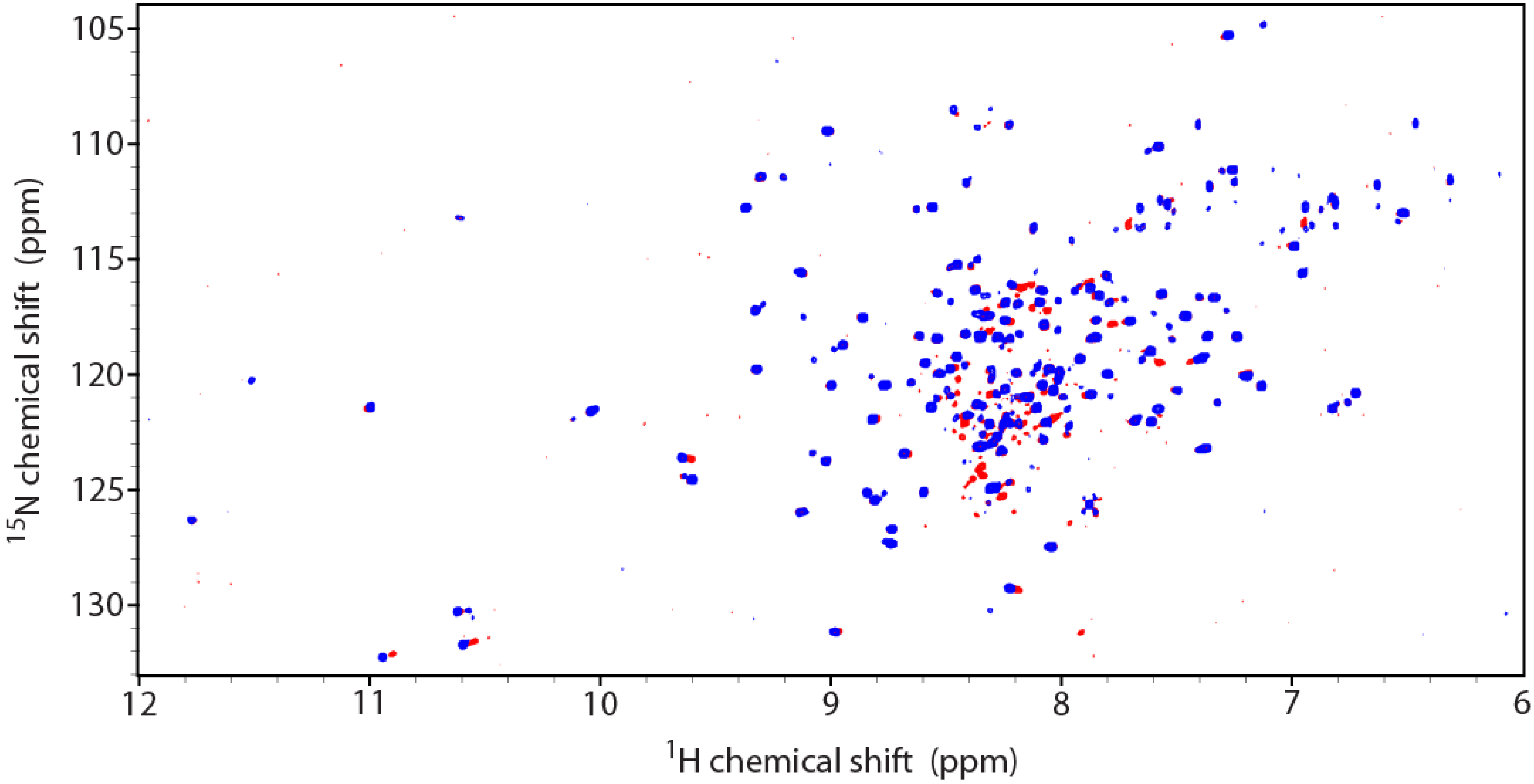

Figure 6.1 Comparison of ^{1}H-^{15}N-TROSY-HSQC spectra of wild-type cyt b_5 (red) and mutant cyt b_5 (blue), each incorporated in DPC micelles. Linker residues that are deleted in the mutant are labeled, as well as other residues that shifted in the mutant spectrum compared to wild-type.

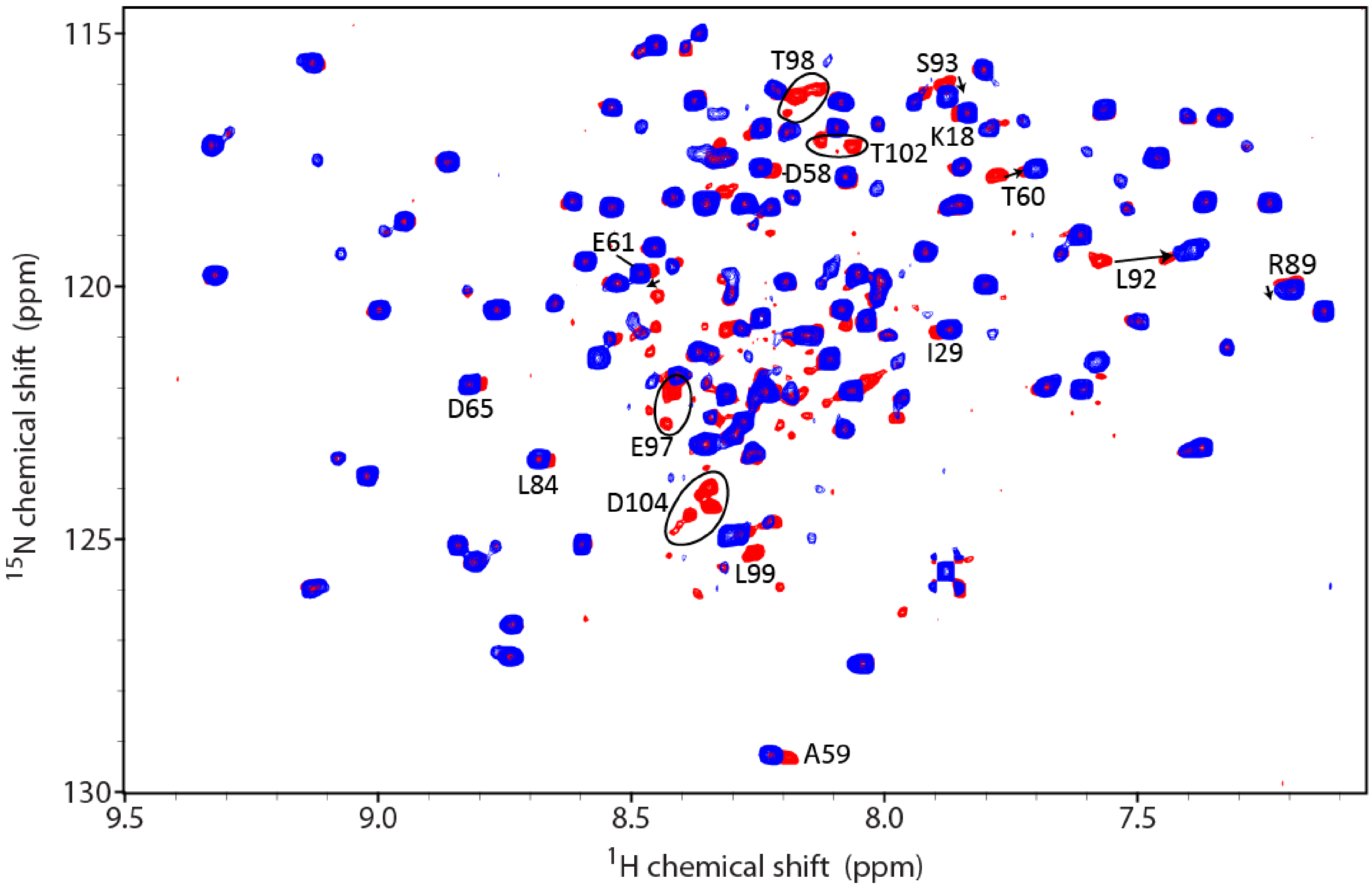

Figure 6.2 Comparison of the central region of the ^{1}H-^{15}N-TROSY-HSQC spectra of wild-type cyt b_5 (red) and mutant cyt b_5 (blue), each incorporated in DPC micelles. Linker region residues that are deleted in the mutant are labeled, as well as other residues that shifted for the mutant compared to wild-type.

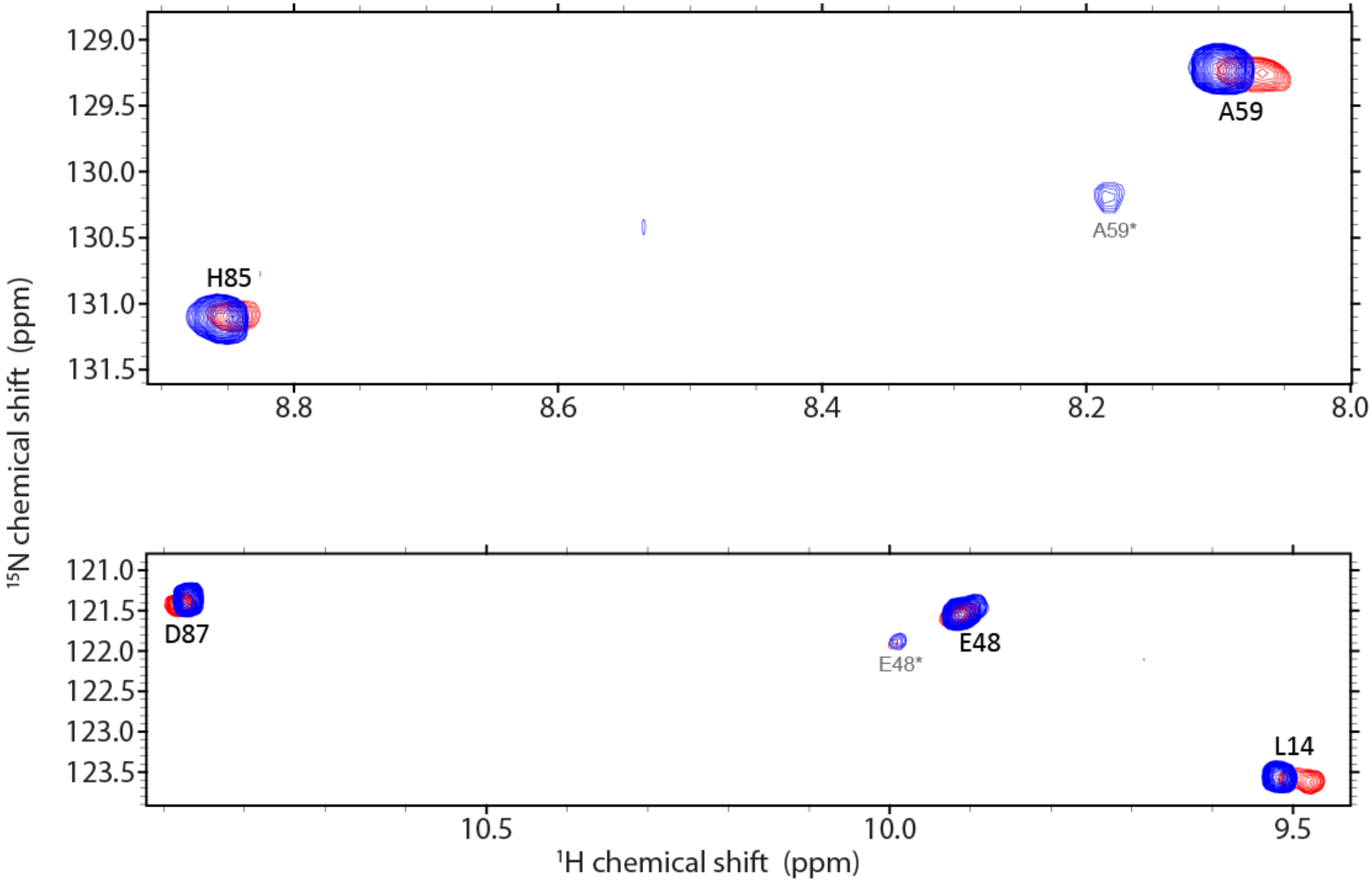

Figure 6.3 Comparison of sections of the ^{1}H-^{15}N-TROSY-HSQC spectra of wild-type cyt b_5 (red) and mutant cyt b_5 (blue). Residues that shifted for mutant cyt b_5 (compared to wild-type) are labeled.

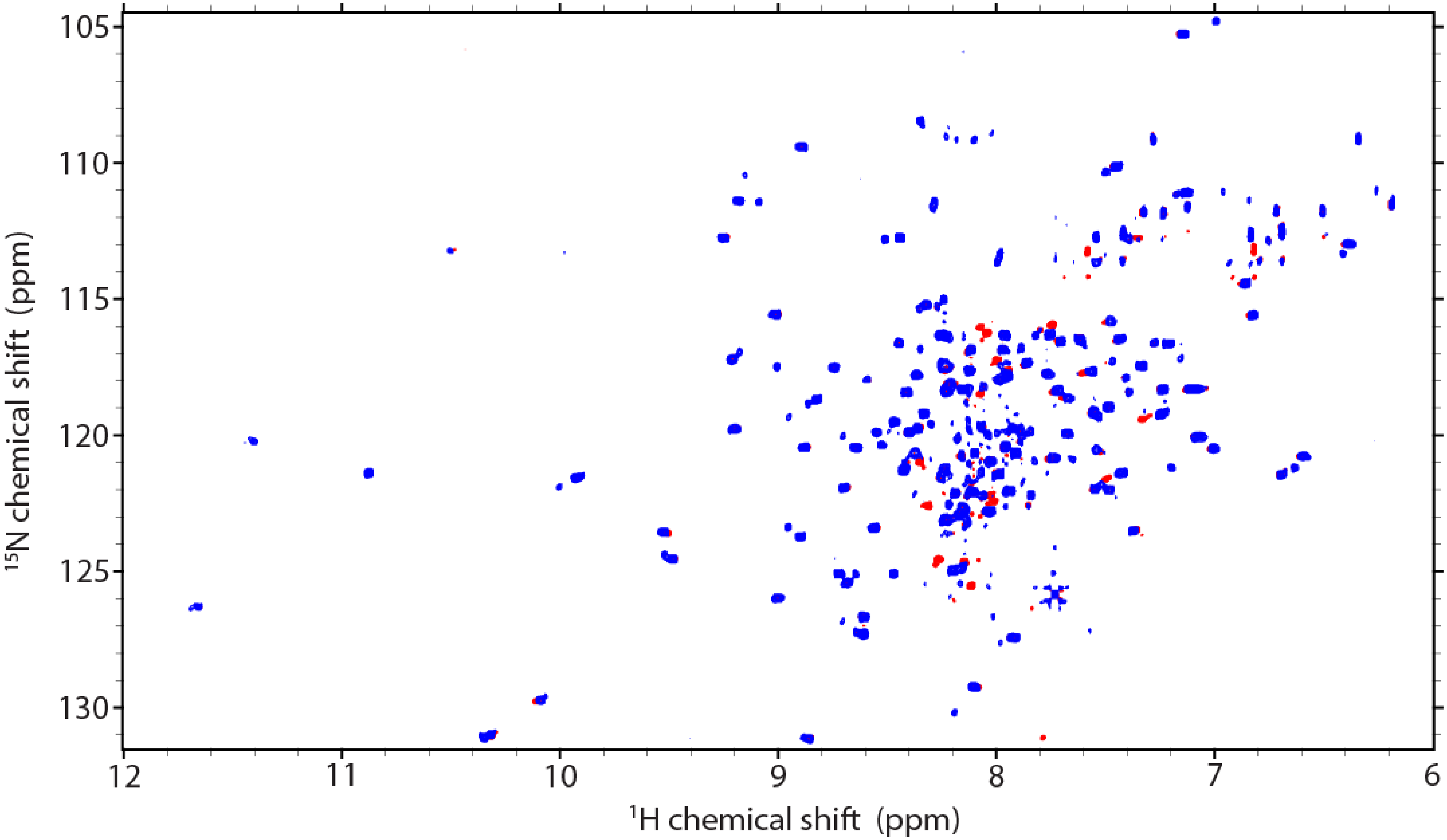

Figure 6.4 Comparison of ^{1}H-^{15}N-TROSY-HSQC spectra of wild-type cyt b_5 (red) and mutant cyt b_5 (blue), each incorporated in DMPC/DHPC isotropic bicelles (*q* ratio of 0.25). The overall spectrum is identical for *m*-cyt b_5 and wild-type cyt b_5, except for the deleted linker residues and the remaining linker residues, as well as T60 (see Figure 6.5).

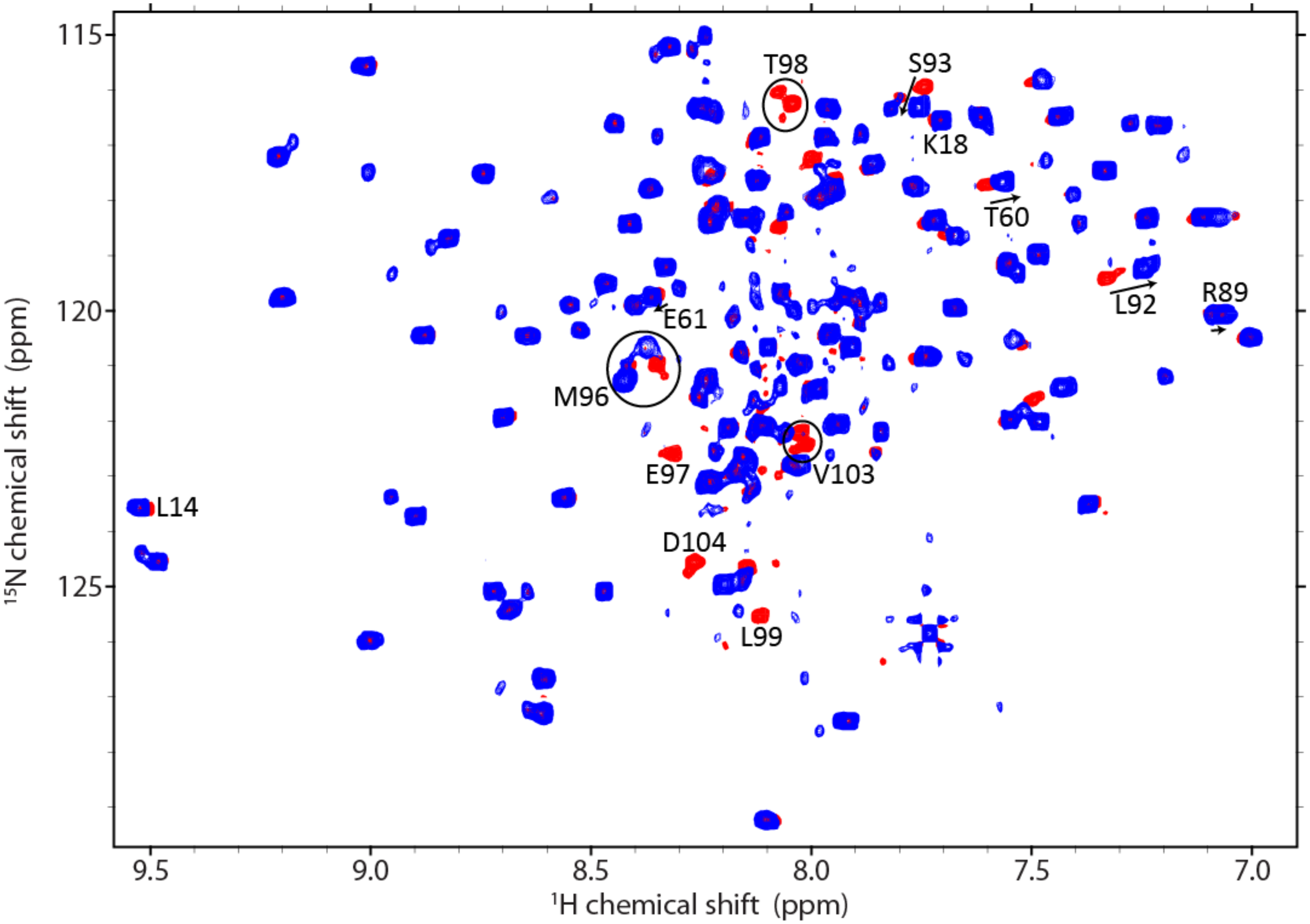

Figure 6.5 Comparison of the central region of the ^{1}H-^{15}N-TROSY-HSQC spectra of wild-type cyt b_5 (red) and mutant cyt b_5 (blue), each incorporated in DMPC/DHPC isotropic bicelles (*q* ratio of 0.25). Linker region residues that are deleted in the mutant are labeled, as well as other residues that shifted for the mutant compared to wild-type. Note that D87 overlaps perfectly between the two membrane mimetics (not shown).

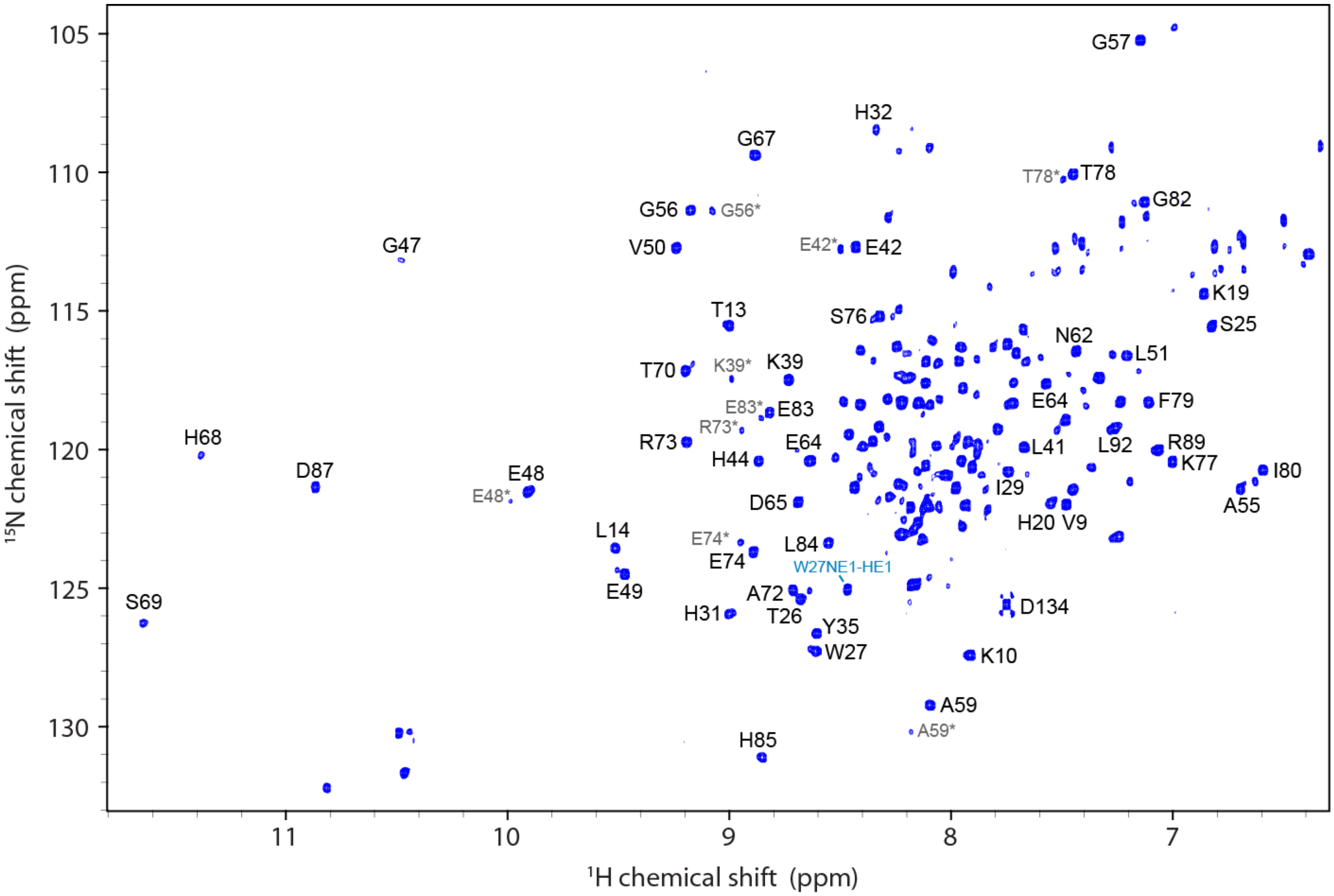

Figure 6.6 Labeled ^{1}H-^{15}N-TROSY-HSQC spectrum of *m*-cyt b$_5$ (E97-D104) in DPC micelles.

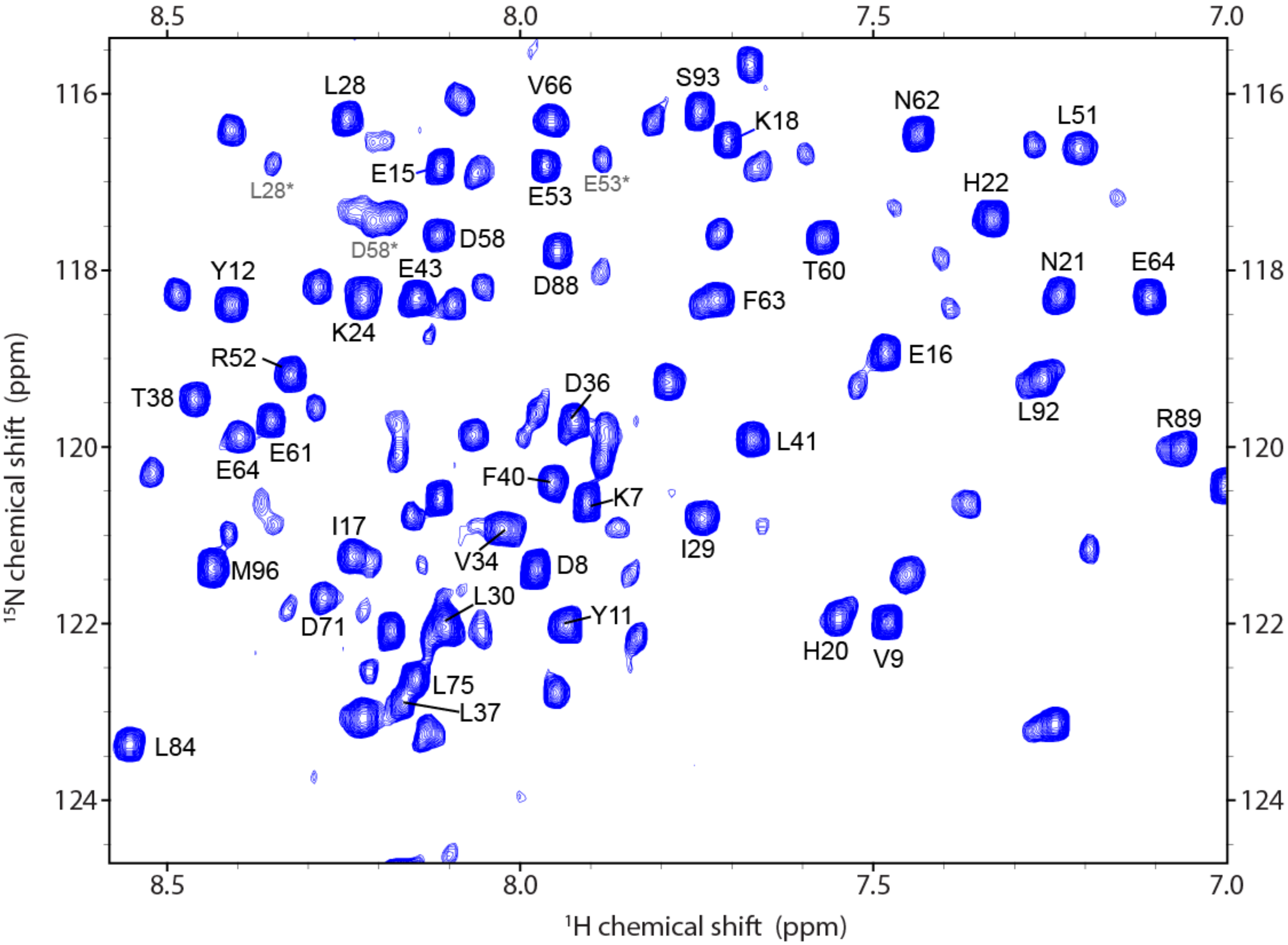

Figure 6.7 A closer look at the crowded region of the ^{1}H-^{15}N-TROSY-HSQC spectrum in Figure 6.6.

For residues in unstructured regions of cyt b_5, there are some weak NOEs in the wild-type spectrum which are missing in the *m*-cyt b_5 spectrum. A few of these long-range NOE connectivities are associated with the region N21-I29: d_{NN}(21-25, 27-21, 28-35, 29-89 and 35-29) and $d_{\alpha N}$(21-27, 21-56, 26-54 and 55-22). The following long-range NOE cross-peaks are also weak in the wild-type spectrum and missing in the mutant spectrum: 14NH-88NH, 17NH-56NH, 31NH-61NH, 37NH-39NH, 40HA-79NH, 48HA-L51NH, 50NH-42NH, 73HA-66NH, and 78HA-73NH. Compared to wild-type cyt b_5, the mutant ^{15}N-HSQC-NOESY spectrum has two additional, weak cross-peaks for 18NH-58NH and 48HA-E42NH. These might indicate small differences in the tertiary fold of *m*-cyt b_5 (compared to wild-type) but do not point to global changes for *m*-cyt b_5. Also, no record was kept for the concentration used for the wild-type NOESY spectrum and it is therefore possible that it was collected at a higher concentration and therefore had a better signal-to-noise ratio, which might explain why some of the cross-peaks are missing for *m*-cyt b_5.

NOE distance restraints (a total of 856, Table 6.3) were extracted from the ^{15}N-HSQC-NOESY spectrum and inputted into CYANA2.1[27], with chemical shift tolerances of 0.02, 0.3 and 0.45 ppm for ^{1}H, ^{13}C and ^{15}N, respectively. The CYANA-generated structure, with a backbone RMSD of 1.24 Å, is presented in Figure 6.12(a and b). It can be seen that the secondary structure (Figure 6.13) and tertiary fold (Figure 6.12) of *m*-cyt b_5 are poorly defined in the CYANA-generated structures. Compared to wild-type cyt b_5 (Figure 6.12c), the structure appears distorted and loosely held together. A direct comparison of the secondary structure elements of the CYANA structures of *m*-cyt b_5

and wild-type cyt b_5 (Figure 6.13) shows that *m*-cyt b_5 is lacking three β-strands and one α-helix, and the matching secondary structure segments are far smaller in the *m*-cyt b_5 CYANA structure. However, based on the manual NOE cross-peak analysis explained in the previous paragraph, we know that the secondary structure elements of *m*-cyt b_5 should be nearly identical to those of wild-type, with very minor differences if any. Similarly, we concluded from the manual analysis of long-range NOEs that the tertiary structure should be very similar if not identical. The differences in the CYANA structures definitely arise from the much smaller amounts of restraints used for *m*-cyt b_5 in the structure calculation. As mentioned, only 856 NOE restraints were used for the calculation of the *m*-cyt b_5 structure, while 1787 NOE restraints, 112 TALOS dihedral angle restraints and 39 hydrogen bonds were inputted for the calculation of wild-type cyt b_5 (Table 3.2 in Chapter 3). Therefore, despite the differences in the CYANA structures, it is safe to assume that the structure of *m*-cyt b_5 is the same as wild-type cyt b_5, based on the nearly identical ^{1}H,^{15}N-TROSY-HSQC spectra of wild-type cyt b_5 and *m*-cyt b_5 (both in micelles and bicelles, Figures 6.1 and 6.4) and the observation of similar NOE cross-peaks in the secondary structure elements and tertiary fold (discussed at the beginning of this section).

Parallel to what was observed for wild-type cyt b_5, the structure of *m*-cyt b_5 appears to be similar in DPC micelles and isotropic bicelles. The ^{1}H,^{15}N-TROSY HSQC spectra of *m*-cyt b_5 in DPC micelles and DMPC/DHPC isotropic bicelles overlap, with the exception of C-terminal and linker residues, as was observed for wild-type cyt b_5 (Section 3.4.4 and Figures 3.15 and 3.16).

Table 6.1 Differences in the cross-peaks observed in the ^{15}N-HSQC-NOESY spectrum of mutant cyt b_5 and wild-type cyt b_5 for β-sheet structures.

Helix	Additional NOEs observed for	d_{NN}	$d_{\alpha N}$
β1	wild-type	14-85^{vw}	13-83^{vw}
	mutant		
β2	wild-type	60-29^{w}	28-58 55-28^{vw}
	mutant		30-58^{w}
β3	wild-type	35-82^{w} 79-36^{vw}	11-85^{vw} 35-80
	mutant		

^{w} and ^{vw} denote weak and very weak NOE cross-peaks

Table 6.2 Differences in the cross-peaks observed in the ^{15}N-HSQC-NOESY spectrum of mutant cyt b_5 and wild-type cyt b_5 for α-helical structures.

Helix	Additional NOEs observed for	$d_{\alpha N}$			d_{NN}		
		(i,i+2)	(i,i+3)	(i,i+4)	(i,i+2)	(i,i+3)	(i,i+4)
α1	wild-type				13-15^{vw} 14-16^{w}	16-19^{vw}	
	mutant	16-18^{w}					
α2	wild-type						
	mutant					41-44^{vw}	
α3	wild-type		48-51^{vw}	51-55^{vw}	48-50^{vw}		50-54^{vw}
	mutant						
α4	wild-type						
	mutant	62-64^{vw}					
α5	wild-type		76-79^{u}				
	mutant						

^{w} and ^{vw} denote weak and very weak NOE cross-peaks; for ^{u}: in the mutant spectrum, there is a broad peak that overlaps the region of the assigned peak in the wild-type spectrum

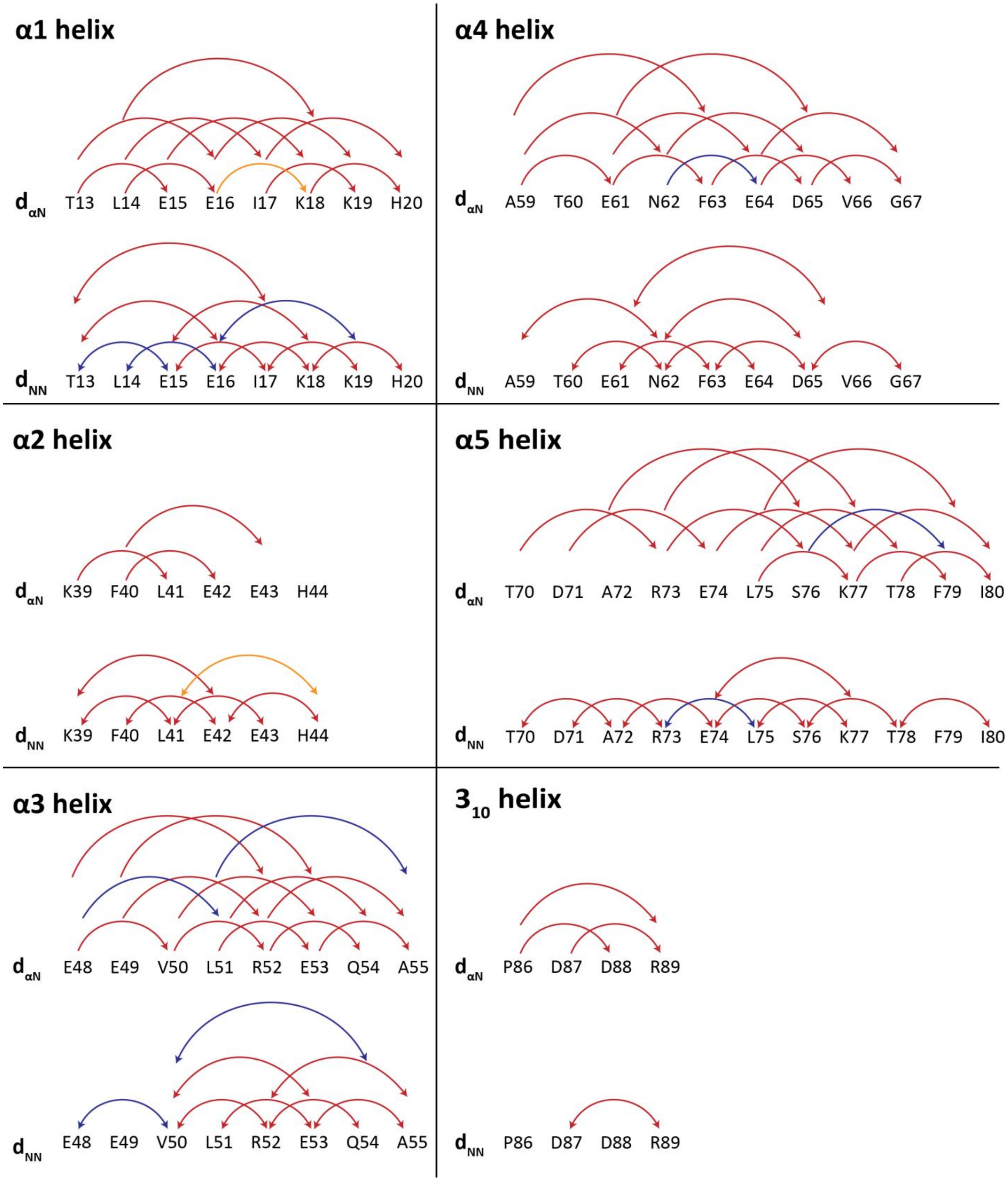
α1 helix
dαN T13 L14 E15 E16 I17 K18 K19 H20
dNN T13 L14 E15 E16 I17 K18 K19 H20
α4 helix
dαN A59 T60 E61 N62 F63 E64 D65 V66 G67
dNN A59 T60 E61 N62 F63 E64 D65 V66 G67
α2 helix
dαN K39 F40 L41 E42 E43 H44
dNN K39 F40 L41 E42 E43 H44
α5 helix
dαN T70 D71 A72 R73 E74 L75 S76 K77 T78 F79 I80
dNN T70 D71 A72 R73 E74 L75 S76 K77 T78 F79 I80
α3 helix
dαN E48 E49 V50 L51 R52 E53 Q54 A55
dNN E48 E49 V50 L51 R52 E53 Q54 A55
310 helix
dαN P86 D87 D88 R89
dNN P86 D87 D88 R89

Figure 6.8 Comparison of Hα-NH and NH-NHNOE connectivities for all helices (α1-α5 and 3_{10}) in mutant cyt b_5 and wild-type cyt b_5, based on ^{15}N-HSQC-NOESY. NOE connectivities observed for both proteins are in red, only in wild-type cyt b_5 are in blue, and only in mutant cyt b_5 are in orange.

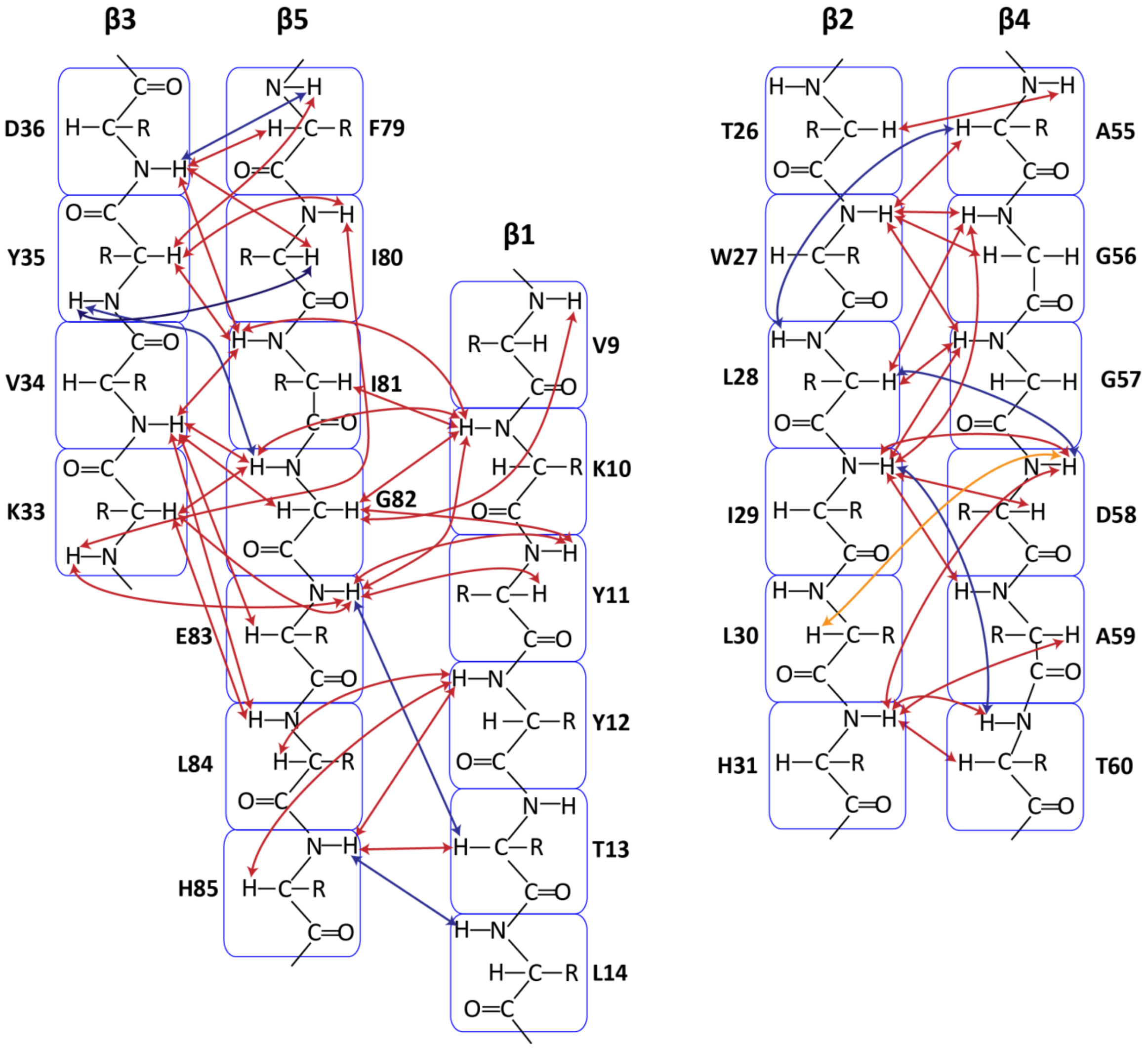
β3
β5
β1
β2
β4
D36
Y35
V34
K33
F79
I80
I81
G82
E83
L84
H85
V9
K10
Y11
Y12
T13
L14
T26
W27
L28
I29
L30
H31
A55
G56
G57
D58
A59
T60

Figure 6.9 NOE connectivities comparison, within the β-strands, between mutant cyt b_5 and wild-type cyt b_5 based on ^{15}N-HSQC-NOESY. NOE connectivities observed for both proteins are in red, only in wild-type cyt b_5 are in blue, and only in mutant cyt b_5 are in orange.

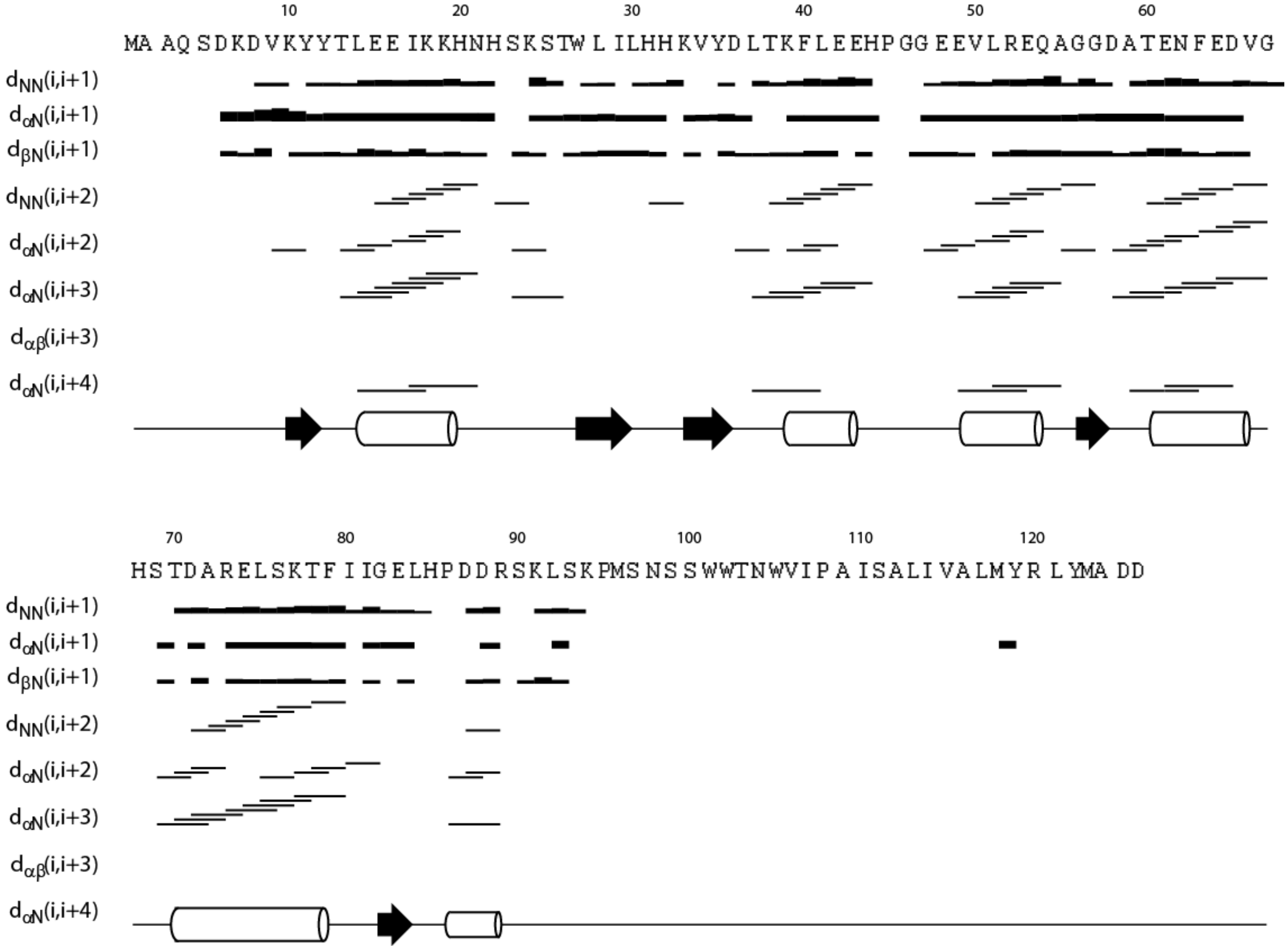

Figure 6.10 NOE connectivity plot for mutant cyt b_5 incorporated in DPC micelles. Thicker lines correspond to stronger NOE cross-peak intensities. The secondary structures are the ones obtained for wild-type cyt b_5 (helices as cylinders and β-strands as arrows).

Table 6.3 NMR structural statistics for mutant cyt b_5.

Total NOEs	856
Intra-residue	222
Short range/Sequential	337
Medium range	254
Long range	143
Dihedral angles ϕ and φ (°)	112
Ramachandran plot statistics (Figure 6.11)	
Residues in most favored regions (%)	69.10
Residues in additionally allowed regions (%)	30.00
Residues in generously allowed regions (%)	0.80
Residues in disallowed regions (%)	0.00
NOE violations > 0.5 Å	0
Angle violations	0
Average backbone RMSD (Å)	1.24 ± 0.39
Average heavy atoms RMSD (Å)	1.85 ± 0.34

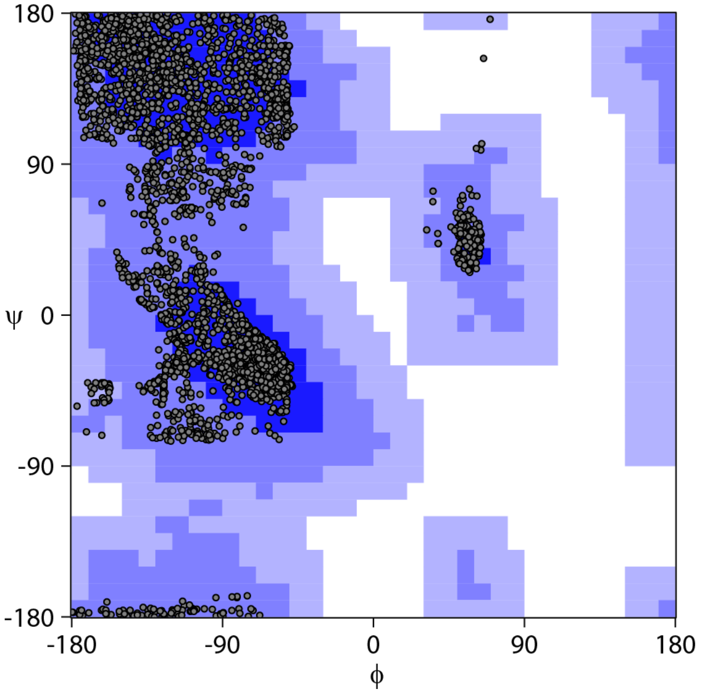

Figure 6.11 Ramachandran plot for the backbone structure of mutant cyt b_5. All 30 final structures (generated from NOESY and CYANA) are represented in this figure.

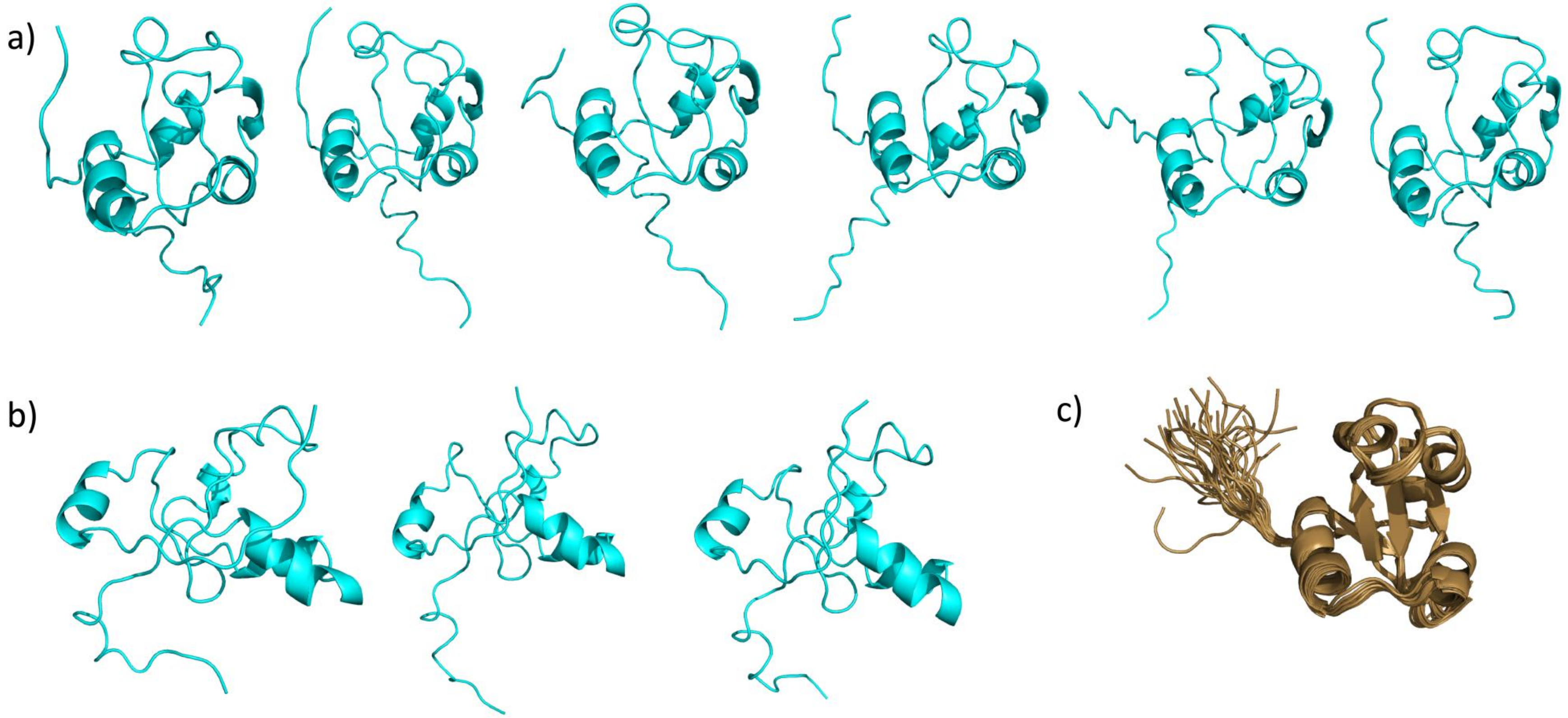

Figure 6.12 Low energy structures of *m*-cyt b_5 calculated by CYANA2.1 from 856 NOE restraints and 112 dihedral angles (Table 6.3). The NOE restraints were obtained from *m*-cyt b_5 incorporated in DPC micelles. a) Proximal sides of six low energy structures of *m*-cyt b_5 showing how unstructured, wide and distorted the tertiary structure is according to CYANA. b) Side-view of *m*-cyt b_5 showing how loosely held to each other the proximal and distal sides of *m*-cyt b_5 are. The lack of restraints inputted into CYANA2.1 is the cause of the poorly defined secondary and tertiary structures.

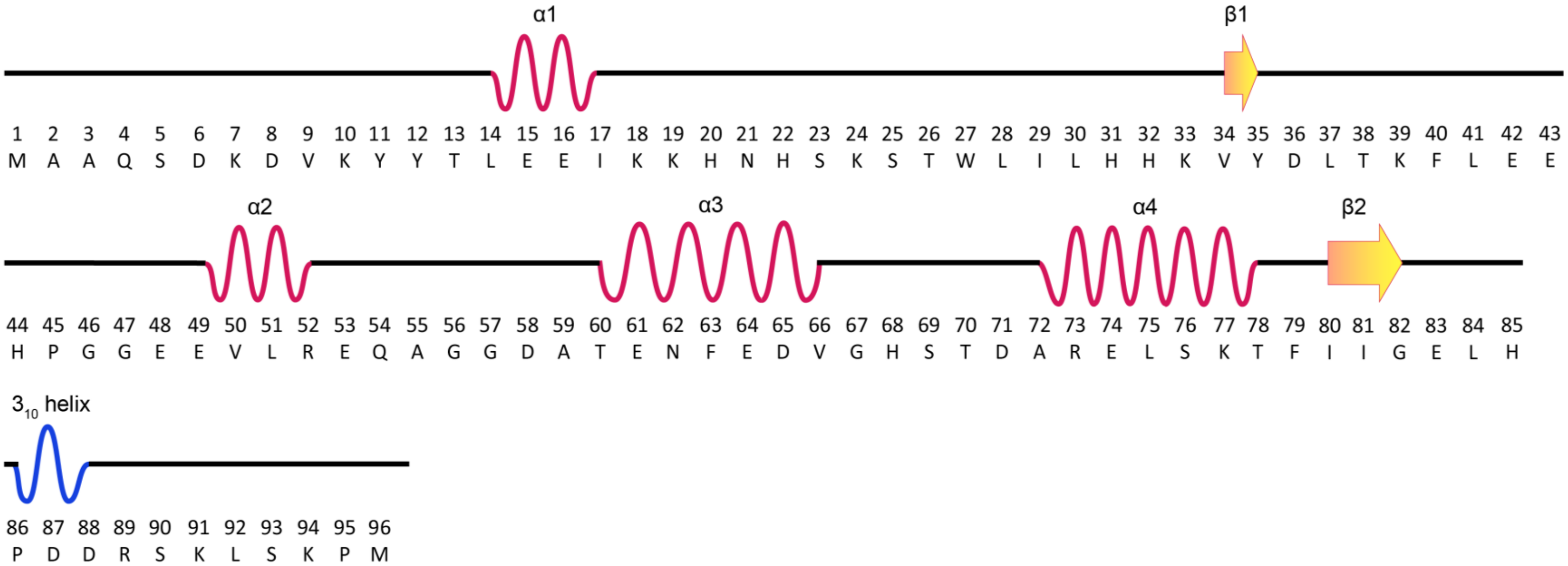
α1
β1
1 2 3 4 5 6 7 8 9 10 11 12 13 14 15 16 17 18 19 20 21 22 23 24 25 26 27 28 29 30 31 32 33 34 35 36 37 38 39 40 41 42 43
M A A Q S D K D V K Y Y T L E E I K K H N H S K S T W L I L H H K V Y D L T K F L E E
α2
α3
α4
β2
44 45 46 47 48 49 50 51 52 53 54 55 56 57 58 59 60 61 62 63 64 65 66 67 68 69 70 71 72 73 74 75 76 77 78 79 80 81 82 83 84 85
H P G G E E V L R E Q A G G D A T E N F E D V G H S T D A R E L S K T F I I G E L H
3₁₀ helix
86 87 88 89 90 91 92 93 94 95 96
P D D R S K L S K P M

Figure 6.13 Secondary structure and sequence of the soluble domain of *m*-cyt b_5 (E97-D104), incorporated in DPC micelles, generated from CYANA.

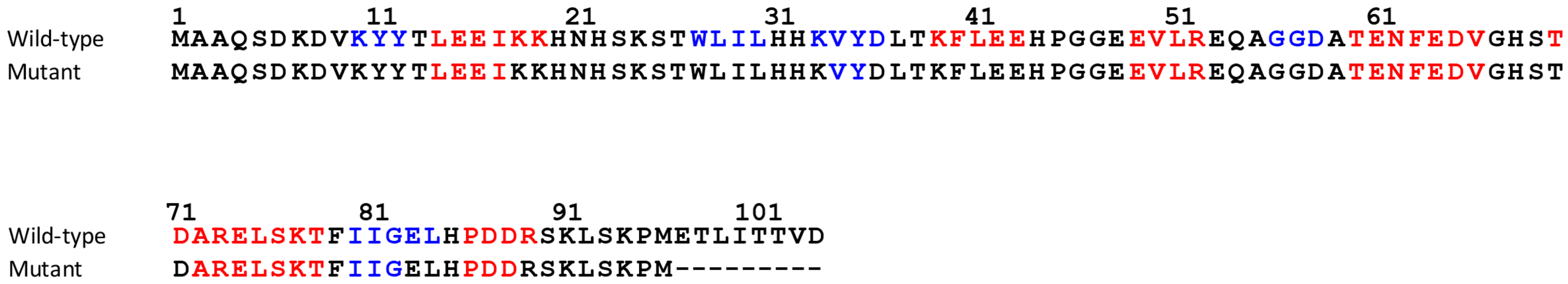

```
           1         11        21        31        41        51        61
Wild-type  MAAQSDKDVKYYTLEEIKKHNHSKSTWLILHHKVYDLTKFLEEHPGGEEVLREQAGGDATENFEDVGHST
Mutant     MAAQSDKDVKYYTLEEIKKHNHSKSTWLILHHKVYDLTKFLEEHPGGEEVLREQAGGDATENFEDVGHST

           71        81        91        101
Wild-type  DARELSKTFIIGELHPDDRSKLSKPMETLITTVD
Mutant     DARELSKTFIIGELHPDDRSKLSKPM---------
```

Figure 6.14 Comparison of secondary structure elements for wild-type cyt b_5 and mutant cyt b_5 (E97-D104) based on the CYANA-generated structures. The colors denote the different secondary structure elements, with blue for beta-sheet elements and red for alpha-helices and one 3_{10} helix (86-89 and 86-88 for wild-type and mutant protein

6.4.3 Backbone relaxation measurements of mutant cyt b_5 in DPC micelles

6.4.3.1 Statistical analysis of R_1, R_2 and R_2/R_1 and steady-state NOE parameters of mutant cyt b_5

The R_1, R_2 and ^{15}N-{^{1}H} NOE values were measured for ^{15}N-*m*-cyt b_5 in DPC micelles. In the following analyses, a deviation greater than one standard deviation from the mean (for the entire range of the measurement ± its respective fitting error) was deemed significant. Residues with a fitting error greater than 15% were omitted from all analyses. The effect of the paramagnetic Fe(III) was discussed in Section 3.4.3; assuming an identical structure for *m*-cyt b_5, only the S69 amide nitrogen is within 7 Å from Fe(III). Nothing could be said about the relaxation rates or NOE values for S69 for because all three parameters had very large errors. The average R_1 value for all observed *m*-cyt b_5 residues K7-M96 was 0.918 ± 0.236 s^{-1}. The N-terminus (K7-D8) and linker residues (L92, S93 and M96) had significantly higher R_1 values than the rest of *m*-cyt b_5: 1.885 ± 0.068 s^{-1} and 1.490 ± 0.092 s^{-1}, respectively. Considering only the *m*-cyt b_5 soluble domain (V9-R89), the average R_1 value was 0.868 ± 0.134 s^{-1}. Two residues, V9 and H22, were identified as having R_1 values significantly larger than other residues in the soluble domain (> 1.003 s^{-1} for their entire error range); V9 is located near the N-terminus and H22 is in the α1-β2 loop. Residues with R_1 values significantly lower than other residues within the soluble domain (< 0.734 s^{-1} for their entire error range) included E43 and R52, which are in secondary structure elements.

The average R_2 value for all observed *m*-cyt b_5 residues K7-M96 was 26.30 ± 4.95 s^{-1}. The lowest R_2 values were observed for the N-terminus residues K7-V9 (13.5 ± 0.9

s^{-1}) and the linker residues S93 and M96 (19.3 s^{-1}). The average R_2 value for the soluble domain (K10-L92) was 27.0 ± 4.2 s^{-1}. For *m*-cyt b_5, L92 was not observed to have a low R_2 value (25.2 s^{-1}), even when compared only to residues K10-L92. Residues, within the soluble domain, that had significantly low R_2 values (< 22.82 s^{-1}) included K10, L37, E42, Q54 and D65.

The average R_2/R_1 value was 30.29 ± 8.41 for all *m*-cyt b_5 residues (K7-M96). N-terminal residues K7-V9 and linker residues L92-M96 had R_2/R_1 values significantly lower than other residues (8.71 ± 2.56 and 14.41 ± 3.27, respectively), and none were significantly higher. Within the structured soluble domain (K10-R89), the average R_2/R_1 value was slightly higher at 31.85 ± 6.60. Within this subset, no residues varied significantly from the mean value.

The average NOE value for all *m*-cyt b_5 residues (K7-M96) was 0.80 ± 0.14. NOE values were significantly lower for N-terminus residues K7-K10 and all linker residues (L92, S93 and M96), with averages of 0.401 ± 0.091 and 0.492 ± 0.123, respectively. Within the soluble domain (defined here as Y11-R89), residues V34, F40, E42-E43, L51, R73 and I80 had significantly low NOE values (< 0.771 s^{-1} for their entire error range). Within the soluble domain (Y11-R89), residues T13, D36, D58, L84 and H85 had significantly higher NOE values (> 0.893 s^{-1} for their entire error range).

Upon analysis with TENSOR2[21], the anisotropic model (fully asymmetric) proved to be the best fit for *m*-cyt b_5 in DPC micelles ($\chi^2_{(5\%)}$ = 58.60 and χ^2_{exp} = 65.59). The principal components of the anisotropic rotational diffusion tensor were D_x = (1.340 ± 0.052) x 10^7 s^{-1}, D_y = (1.446 ± 0.047) x 10^7 s^{-1} and D_z = (1.528 ± 0.052) x 10^7 s^{-1}. The axes of this tensor were not defined in the same way as for wild-type (chosen by TENSOR2) and so the absolute values cannot be compared. The effective correlation time, $\tau_{c,eff}$, was then 11.59 ns (as calculated by the same formula as given in Eisenmann *et al.*[44]) As a reference, the isotropic model yielded a similar τ_c value of 11.57 ± 0.10 ns (χ^2_{exp} = 70.38 and $\chi^2_{(5\%)}$ = 65.61).

6.4.3.2 Comparison of the relaxation measurements of mutant and wild-type cyt b$_5$

Due to the differences in the labeling scheme, with wild-type cyt b$_5$ being deuterated and *m*-cyt b$_5$ being protonated, the absolute R_1 and R_2 values between the two proteins could not be compared, as deuteration is known to decrease both relaxation rates and affect each rate to a different extent.[45] If cyt b$_5$ and *m*-cyt b$_5$ had similar relaxation rates, the deuteration present in wild-type cyt b$_5$ should cause the rates to be smaller than for *m*-cyt b$_5$. However, the R_1 values for wild-type cyt b$_5$ are actually larger than *m*-cyt b$_5$ by an average factor of 1.10 ± 0.20, indicating that the longitudinal relaxation rates are much larger in wild-type cyt b$_5$ than *m*-cyt b$_5$. The R_2 rates are indeed smaller for wild-type cyt b$_5$, by a factor of 0.91. A comparison of the relaxation rate trends and residues that are significantly different (from the mean within their own dataset) between wild-type and mutant cyt b$_5$, can be found in Section 6.5.2.

6.4.4 NaCl titration experiments

6.4.4.1 Interaction between *m*-cyt b$_5$ and substrate-free cyt P450

To identify interfacial residues, *m*-cyt b$_5$ was studied in complex with cyt P450 2B4 in a 1:1 molar ratio, incorporated in DMPC/DHPC isotropic bicelles, *q* ratio of 0.25. The relative intensities (see Methods) of each *m*-cyt b$_5$ resonance in the ^{1}H-^{15}N-TROSY-HSQC

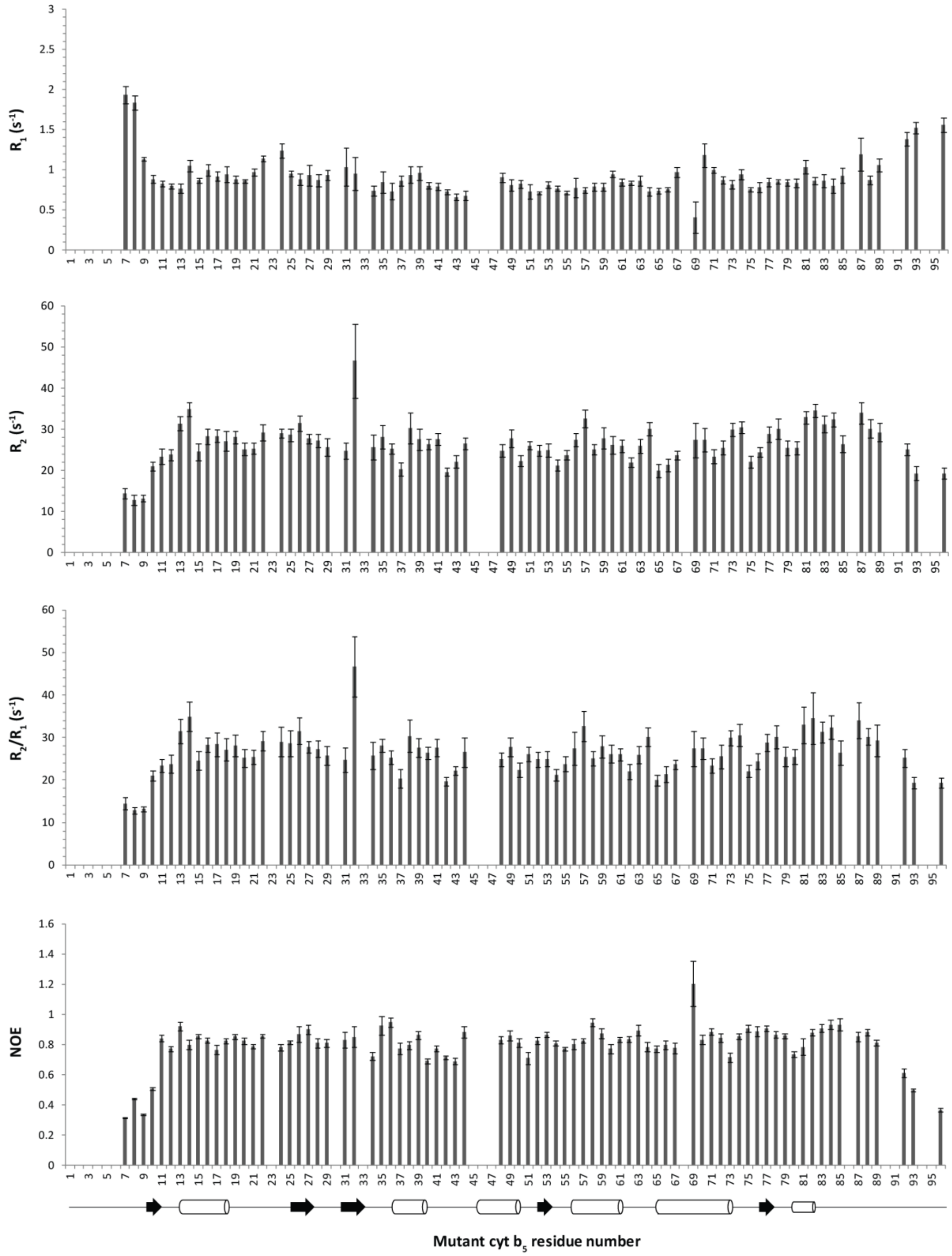

Figure 6.15 ^{15}N-R_1, -R_2 and ^{1}H{^{15}N}-NOE relaxation parameters obtained for mutant cyt b_5 at 900 MHz in DPC micelles. The observed relaxation data for the residues specific residues are plotted versus residue number for R_1 ($^{15}N_x$), R_2 ($^{15}N_{x,y}$), NOE and R_2/R_1 in 45 mM DPC micelles. The secondary structure at the bottom of the figure is the one obtained for wild-type cyt b_5.

spectrum were monitored upon titration of NaCl (0 to 400 mM NaCl). In the absence of substrate and NaCl, no *m*-cyt b_5 residues broadened beyond detection and only T70 had a low intensity (< 0.6%, see Methods). At 100 mM NaCl, all residues had an intensity > 1% and were very intense in the spectrum; only T70 had a relative intensity of 1.1% but should not be considered low intensity as its signal-to-noise ratio was 20. The increase in the relative intensities was plotted as a function of NaCl concentration for each residue. With addition of NaCl, the increase in intensity was linear for all residues, with an average slope of 0.0179 ± 0.0067 %/mM NaCl (see Methods) and an R^2 value > 0.93 (average R^2 of 0.98) (Figure 6.16). No plateau was reached by the addition of 400 mM NaCl, as shown in Figure 6.16. The following residues increased in intensity at a faster rate than others (slopes > 0.0246%/mM NaCl): K10, E43, E53, A55, N62, D65 and K77. The following had significantly lower slopes (slopes < 0.0112%/mM NaCl): L51, G56, F63, R73*, L84 and H85* (*are the residues which are solvent accessible, see Methods); however, these slopes were still high and all were above 0.009%/mM NaCl. A comparison of the relative intensities of each resonance in the ^{1}H,^{15}N-TROSY-HSQC spectrum of *m*-cyt b_5 in isotropic bicelles (free *m*-cyt b_5) revealed that the intensities in the complex spectrum at 400 mM were identical to those in free *m*-cyt b_5, indicating that all complexes had dissociated and we were only observing free *m*-cyt b_5. When the relative intensities of free *m*-cyt b_5 were compared to those of *m*-cyt b_5 residues in complex with substrate-free cyt P450 at 250 mM NaCl, the average intensity in the complex spectrum was 75.2 ± 13.9 % of the intensities in free *m*-cyt b_5. At this ionic strength (400 mM NaCl), five residues could be identified as having their relative intensities ≤ 61.3% of their respective intensities in *m*-cyt b_5 alone: E64, V66, T70, D71 and S76* (*solvent inaccessible).

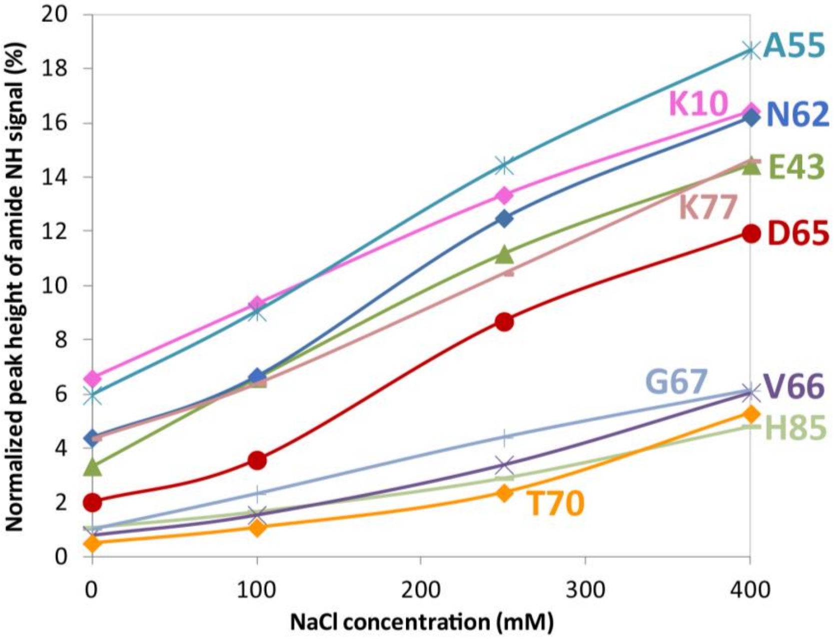

Figure 6.16 Effect of NaCl on the relative intensities of selected *m*-cyt b_5 residues in the presence of substrate-free cyt P450. All intensities were internally normalized (shown in %) to the intensity of D134 (see Methods). Most residues reached a plateau by 250 mM NaCl in the presence of substrate-free cyt P450.

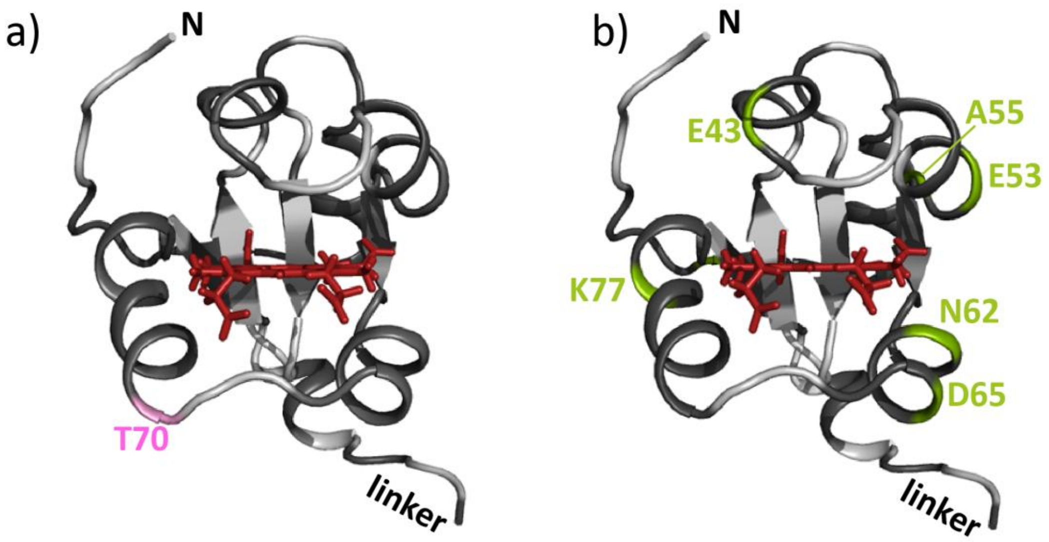

Figure 6.17 Residues playing a role in the complex formation between *m*-cyt b_5 and substrate-free cyt P450. (a) T70 (pink) broadened considerably upon complex formation with substrate-free cyt P450 and is solvent accessible (≥ 35% based on NACCESS[41]). (b) Residues that were significantly affected by ionic strength and should be involved in encounter complex formation.

Partial to no information on I17, K24, S25, D36, L37, E61, L75, I81, D88 and S93 could be obtained in these experiments because their intensities were not reliable as they either overlapped with nearby peaks, their intensities fluctuated a lot during the salt titration of cyt b_5 alone (Chapter 5), or they alternated between multiple conformers.

6.4.4.2 Interaction between *m*-cyt b_5 and substrate-bound cyt P450

The complex between *m*-cyt b_5 and cyt P450, in the presence of the cyt P450 substrate 3,5-di-*tert*-butyl-4-hydroxytoluene (BHT, 1:2 cyt P450:BHT) was also studied. Upon addition of substrate-bound cyt P450, several *m*-cyt b_5 resonances broadened beyond detection (Table 6.4); the remainder of the resonances were intense in the spectrum, see Figure 6.18. The relative intensities (see Methods) of each *m*-cyt b_5 resonance was then monitored with addition of NaCl (0 to 400 mM NaCl).

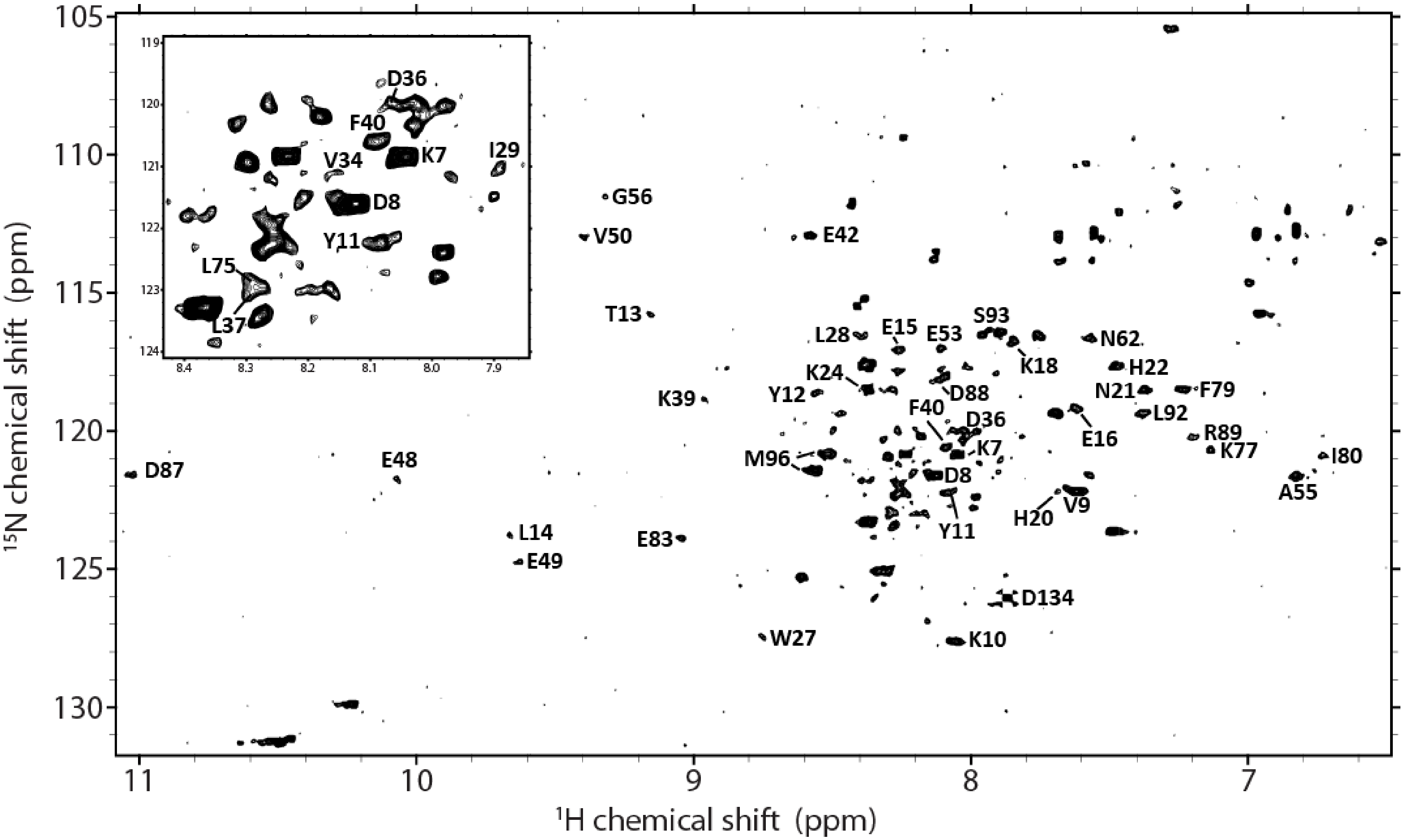

Figure 6.18 ^{1}H-^{15}N-TROSY-HSQC spectrum of *m*-cyt b$_5$ with substrate-bound cyt P450 (1:1) in bicelles. An inset of the crowded region is presented in the top left corner. Unlabeled resonances are either unassigned or originate from other conformers of *m*-cyt b$_5$.

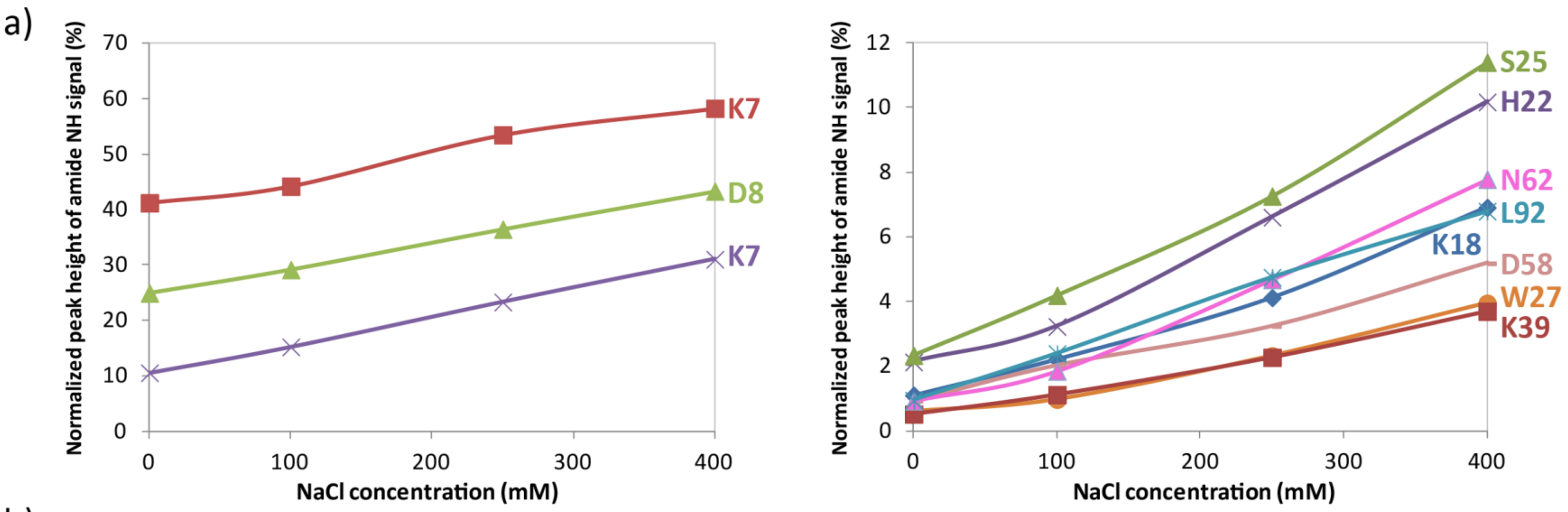

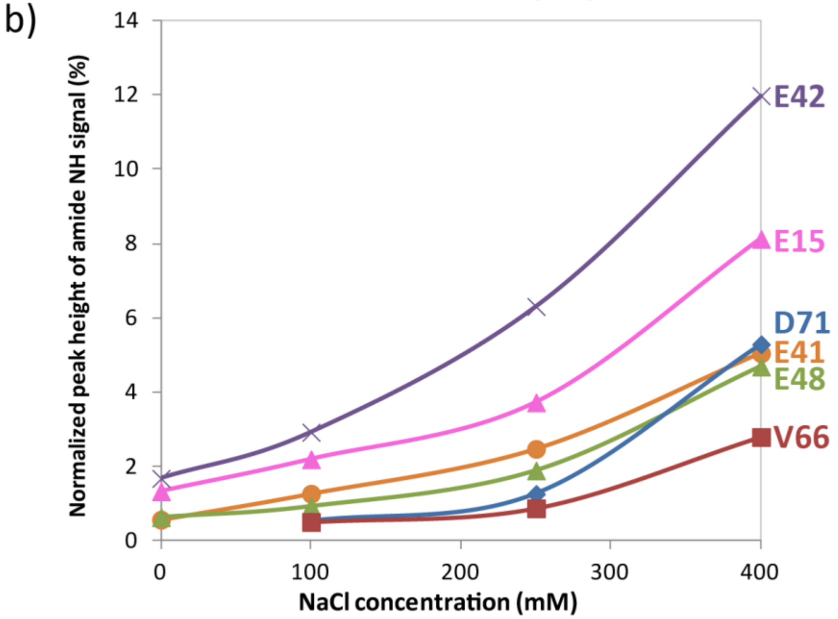

Figure 6.19 Effect of NaCl on the relative intensities of selected *m*-cyt b_5 residues in the presence of substrate-bound cyt P450. All intensities were internally normalized (shown in %) to the intensity of D134 (see Methods). a) Excerpt of some residues which experienced a linear increase in intensity as a function of NaCl concentration. b) Excerpt of residues which experienced an increase that was not as clearly linear.

At 100 mM NaCl, only solvent accessible residues on the lower cleft of *m*-cyt b_5 (and S76) were still absent or low in intensity (Table 6.4). The relative intensities of all residues' resonances increased with addition of NaCl (Figure 6.19), and at 400 mM NaCl, only T70 was still absent from the spectrum while all other resonances had a relative intensity > 2%. When plotted as a function of NaCl concentration, the trend for the intensity increase appeared linear in some cases (Figure 6.19a) and slightly exponential in other cases (Figure 6.19b). Because of the varying trends observed for different residues, a strict slope comparison could not be carried out (unlike what was done in Section 6.4.4.1 or Chapter 5).

Table 6.4 Mutant cyt b_5 residues that experienced extensive line broadening in complex with BHT-bound cyt P450 over the range of 0-100 mM NaCl.

[NaCl]	*Absent* or low intensity	
(mM)	Solvent accessible	Solvent inaccessible
0	T38^1, *E64*, *D65*, *V66*, *G67*, *T70*, *D71*, *R73*	*I17*, *H44*, *A59*, *T60*, A72^1, S76, L84^1
100	*E64*, D65^2, V66^2, G67^2, *T70*, D71^2, R73^2	A59^2, S76^2
250	E64^3, V66^3, *T70*	A59^3
400	*T70*	none

The relative intensities threshold for resonances considered having low intensities were ≤ 0.4%^{1}, ≤ 0.7%^{2} and ≤ 1.1%^{3}.

The intensities (in the ^{1}H,^{15}N-TROSY-HSQC spectrum) of *m*-cyt b_5 resonances in complex with substrate-bound cyt P450 at 400 mM NaCl were compared to those of free *m*-cyt b_5 in bicelles, the average of the resonances' intensities was 55.6 ± 17.3 % of the intensities in free *m*-cyt b_5 spectrum. At 400 mM NaCl, residues H44, E64 and D65 had resonances that were significantly broadened, with < 38% of the intensities found in the free *m*-cyt b_5 spectrum.

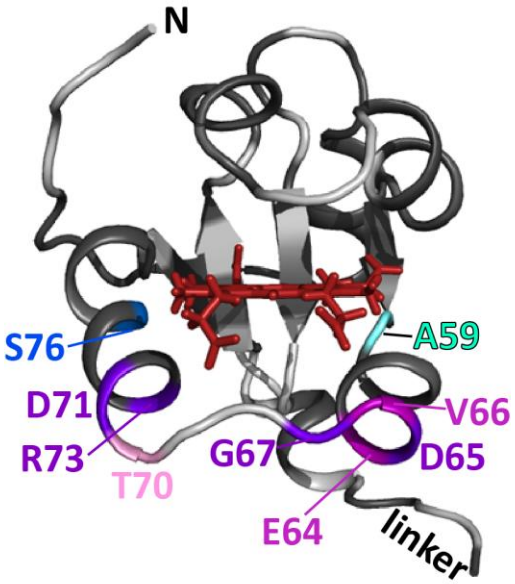

Figure 6.20 Residues playing a role in the complex formation between *m*-cyt b_5 and substrate-bound cyt P450. Solvent accessible (≥35% based on NACCESS[41]) residues that are low in intensity/undetectable at 100 mM NaCl (dark purple), 250 mM NaCl (light purple) and still at 400 mM NaCl (light pink). In blue are residues that are solvent inaccessible and low in intensity at 100 mM NaCl (dark blue) and still absent at 250 mM NaCl (light blue).

Partial to no information on Y11, Y12, L14, K24, T26, L28, I29, V34, Y35, D36, L37, T38, F40, G56, T60, E61, F63, L75, F79, I81, G82, H85 and D88 could be obtained in these experiments because their intensities were not reliable as they either overlapped with nearby peaks or alternated between multiple conformers.

The NMR sample was diluted and a CO assay was performed on it.[39] The assay revealed that only the active form (absorbance at 450 nm) of cyt P450 was present in the sample and that none of the protein had converted to the P420 form (Figure 6.21).

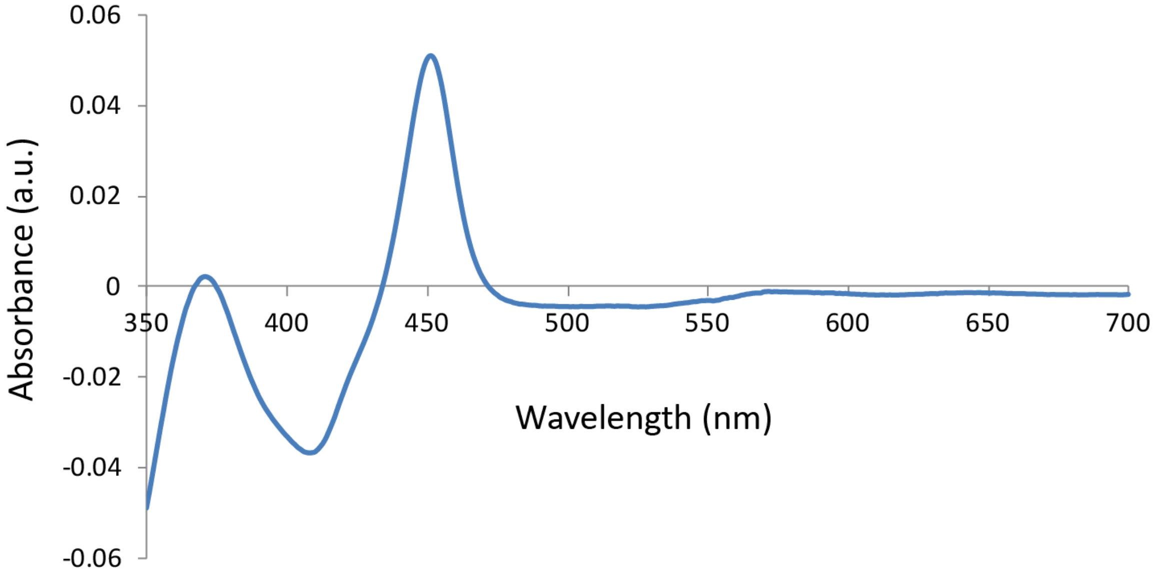

Figure 6.21 CO assay UV-Vis spectrum showing that cyt P450 is in its active conformation (blue) under the NMR conditions. This spectrum was obtained on a diluted aliquot of the following NMR sample: 0.2 mM *m*-cyt b_5 + 0.2 mM cyt P450 + 0.4 mM BHT + 400 mM NaCl + 10 w% of DMPC/DHPC isotropic bicelles (q=0.25) in NMR buffer. Note: the sample was stable for over two days

6.5 Discussion

6.5.1 The structure of mutant cyt b_5 is very similar to wild-type cyt b_5

Since only a ^{15}N-HSQC-NOESY spectrum was collected for *m*-cyt b_5, a mere total of 856 NOE restraints were obtained (Table 6.3). This number is less than half the number of restraints obtained for wild-type cyt b_5 (Table 3.2) for which we also collected a ^{13}C-HSQC-NOESY spectrum. Compared to wild-type cyt b_5, the thirty lowest energy CYANA-generated structures of *m*-cyt b_5 were not well-defined (Figures 6.13 and 6.14). When comparing the secondary structure content of these CYANA-generated structures (Figure 6.13) to those obtained for wild-type cyt b_5 (Figure 6.14), it is evident that the majority of β-sheets are missing from the *m*-cyt b_5 structures, with only 34-35 and 80-82 involved in β-sheets. When comparing the α-helices between the two proteins, it can also be seen that fewer and shorter α-helices were defined for *m*-cyt b_5. Because of these drastic changes in the secondary and tertiary structures of *m*-cyt b_5 according to the CYANA-generated structure, a qualitative comparison of the NOE cross-peaks present in mutant and wild-type cyt b_5 was pursued. Upon comparing the ^{15}N-HSQC-NOESY spectra, the secondary structures and overall tertiary fold of *m*-cyt b_5 appear to be very similar to wild-type cyt b_5 (Tables 6.1 and 6.2, and Figures 6.8 and 6.9); only a few NOE cross-peaks differ between the two proteins and their overall patterns indicate the same structure. Overall, the deletion of eight residues in the linker region of cyt b_5 does not appear to significantly affect the fold of the soluble domain of cyt b_5.

6.5.2 Shortening of the linker does not affect internal dynamics of cyt b_5 but causes the soluble domain to diffuse through solution differently

For both wild-type and mutant cyt b_5, the N-terminal and linker residues (for *m*-cyt b_5, this included only L92, S93 and M96) had increased mobility on a fast time scale compared to the remaining residues, with significantly high R_1 values, low R_2 (except for L92) and low steady-state NOE values. For *m*-cyt b_5, Fewer residues deviated from the R_1 average value, with only residue H22 (in the α1-β2 loop) experiencing fast time scale motions. Restricted motions were observed in both proteins for the following residues: E42 (low R_1 and R_2 in wild-type and low R_2 in mutant), E43 (low R_1 in both), R52 (low R_1 in both) and Q54 (low R_1 in wild-type and low R_2 in mutant). There were some differences with L84 and D87-D88 having high R_1 and high R_2 values, respectively, in wild-type cyt b_5 but average relaxation rates in *m*-cyt b_5 (D87 cannot be compared as it had large errors for both its R_1 and R_2 measurements). As mentioned in Section 3.5, for molecules of the size of cyt b_5 (17 kDa), ^{15}N-{^{1}H} steady-state NOE is more sensitive to internal dynamics than R_1 and R_2,[29] and additional residues could be highlighted as deviating from the mean value with a comparison of the NOE values. Residues in the α2-helix, α3-helix and α5-helix were seen as having large amplitude internal motions in both the wild-type and mutant proteins (at a slower time scale between T_2 and T_1); some of these residues agree with those shown to be dynamic in MD simulations.[46]

The diffusion tensor was markedly asymmetrical along each axis for *m*-cyt b_5, while wild-type cyt b_5 had similar D_x and D_y components indicating a prolate axially symmetric diffusion tensor (Chapter 3).[44] The effective correlation time, $\tau_{c,eff}$, also increased by ~1 ns upon shortening the linker. The length of the linker, as expected, affects the overall diffusion of the soluble domain through solution.

6.5.3 The effect of the length of the linker on the complex formation between cyt b_5 and cyt P450

Upon interaction with substrate-free cyt P450, no residues in the ^{1}H-^{15}N-TROSY-HSQC spectrum of *m*-cyt b_5 broadened beyond detection. This is in stark contrast to the complex formation of substrate-free cyt P450 with wild-type cyt b_5, in which case ten residues broadened beyond detection (Y35, A59, T60, F63-G67, T70 and R73). If we expand the list of *m*-cyt b_5 residues to those that have low intensities (< 0.6%), only T70 can be described as being key in the interaction of *m*-cyt b_5 with substrate-free cyt P450. When looking at the increase in relative intensities of *m*-cyt b_5 residues as a function of NaCl concentration, a congruent set of residues were found to experience a significantly steep increase in intensity with addition of NaCl for both wild-type and mutant cyt b_5 (Figure 6.17b). Interestingly, while 88% of residues' resonances reached a plateau by 400 mM NaCl in the wild-type cyt b_5 complex with substrate-free cyt P450, none of the residues reached a plateau in the complex between substrate-free cyt P450 and *m*-cyt b_5. However, at 400 mM NaCl, *m*-cyt b_5 residues' intensities reflected that we were only observing free *m*-cyt b_5, whereas for wild-type cyt b_5 complex formation was still occurring (intensities were on average only 79% of the intensities in free cyt b_5). This indicates that the *m*-cyt b_5-cyt P450 complex, in the absence of substrate, requires lower ionic strength to dissociate all stereospecific complexes (T70 is intense in the spectrum at 100 mM NaCl and only low in intensity - but not absent - at 0 mM NaCl). The complex between *m*-cyt b_5 and substrate-free cyt P450 appears to be a pure electrostatic-driven encounter complex,[47–49] with ionic strength completely dissociating all complexes by 400 mM NaCl. In the case of wild-type cyt b_5, stereospecific complexes are able to form, in addition to the encounter complexes, which explains why higher ionic strength is requires to break up some of the residue-specific interactions.

In the presence of BHT, the interaction between *m*-cyt b_5 and substrate-bound cyt P450 was nearly identical to the interaction observed between wild-type cyt b_5 and substrate-free cyt P450, with the solvent accessible residues T38, E64-G67, T70, D71 and R73 being undetectable or having low intensity (Table 6.4 and Table 5.2). Similar solvent inaccessible residues were also affected and included H44, A59, T60, A72 and L84. However, all residues were intense, except for T70, by the addition of 100 mM NaCl for wild-type cyt b_5's interaction with substrate-free cyt P450, whereas in the case of *m*-cyt

b_5 with BHT-bound cyt P450, an addition of 400 mM NaCl was required. In both complexes, however, T70 was found to be the most important hydrophobic residues in the protein-protein interaction. Residue V66 and E64 was also found to be affected upon interaction of substrate-bound cyt P450 and *m*-cyt b_5. The widespread broadening observed for wild-type cyt b_5 (in the presence of BHT-bound cyt P450) was attributed to a large population of non-specific encounter complexes since their broadening was heavily influenced by ionic strength. In the wild-type protein, it was shown that all sides of cyt b_5 were able to participate in encounter complex formation (Figure 5.9); the mutant, however, experiences restricted motions (as seen by the increase in the effective correlation time and a more anisotropic diffusion tensor) and is therefore unable to sample as many orientations in the encounter complexes. In fact, it appears that *m*-cyt b_5 might only capable of interacting with cyt P450 through its proximal side and only via its lower cleft, as none of the residues in the upper cleft, except for E43 and E53, were highlighted in any of the spectral analyses (Figure 6.17 and 6.20). Because *m*-cyt b_5 is only capable of interacting with substrate-bound cyt P450 through a limited surface area, the number of encounter complexes that *m*-cyt b_5 is able to form is much smaller than for wild-type cyt b_5. Because *m*-cyt b_5 is unable to perform a 360° rotation within the concavity of substrate-bound cyt P450, the two proteins need to collide in a specific orientation in order to yield a productive orientation; otherwise they just dissociate and there is no electron transfer. Out of all the macrocollisions, only a small percentage of the time will *m*-cyt b_5 and substrate-bound cyt P450 collide the correct orientation, which explains why *m*-cyt b_5 has a 60% decrease in its ability to stimulate cyt P450.

6.6 Conclusion

The structure and internal dynamics of *m*-cyt b_5 were found to be very similar to wild-type cyt b_5. Deletion of eight residues in the linker, however, did affect the correlation time of the soluble domain and its diffusion through solution. The NMR spectra reflect that the binding between *m*-cyt b_5 and cyt P450 was much less than wild-type cyt b_5, in agreement with previous binding and activity assays.[1] This was assessed by a drastic decrease in the number of *m*-cyt b_5 residues experiencing extensive line broadening (compared to wild-type cyt b_5), both when cyt P450 is substrate-free and substrate-bound, indicating very little stereospecific complex formation and a decrease in the encounter complex population. Even when cyt P450 was BHT-bound, the shortened linker did not allow *m*-cyt b_5 to sample as many encounter complexes as the wild-type protein and only very localized broadening was observed for *m*-cyt b_5 residues. We can hypothesize that *m*-cyt b_5 is not able to form as many stereospecific complexes because it is unable to sample as many encounter complex orientations. For wild-type cyt b_5, the increased surface area sampled and the higher population and lifetime of the encounter complexes, cyt b_5 and cyt P450 are able to find - more frequently - productive orientations that allow for electron transfer (compared to *m*-cyt b_5). Interestingly, we were able to identify that both wild-type cyt b_5 and *m*-cyt b_5 utilize the same key residues, V66 and T70, in specific complex formation with cyt P450.

6.7 References

(1) Clarke, T. A.; Im, S.-C.; Bidwai, A.; Waskell, L. The role of the length and sequence of the linker domain of cytochrome b5 in stimulating cytochrome P450 2B4 catalysis. *J. Biol. Chem.* **2004**, *279*, 36809–36818.

(2) Walsh, J. D.; Meier, K.; Ishima, R.; Gronenborn, A. M. NMR studies on domain diffusion and alignment in modular GB1 repeats. *Biophys. J.* **2010**, *99*, 2636–2646.

(3) Fujita, N.; Endo, S.; Ishihama, A. Structural requirements for the interdomain linker of α subunit of Escherichia coli RNA polymerase. *Biochemistry* **2000**, *39*, 6243–6249.

(4) Ozols, J. Structure of cytochrome-b_5 and its topology in the microsomal membrane. *Biochim. Biophys. Acta* **1989**, *997*, 121–130.

(5) Banci, L.; Bertini, I.; Rosato, A.; Scacchieri, S. Solution structure of oxidized microsomal rabbit cytochrome b_5. Factors determining the heterogeneous binding of the heme. *Eur. J. Biochem.* **2000**, *267*, 755–766.

(6) Nunez, M.; Guittet, E.; Pompon, D.; Van Heijenoort, C.; Truan, G. NMR structure note: oxidized microsomal human cytochrome b_5. *J. Biomol. NMR* **2010**, *47*, 289–295.

(7) Muskett, F. W.; Kelly, G. P.; Whitford, D. The solution structure of bovine ferricytochrome b5 determined using heteronuclear NMR methods. *J. Mol. Biol.* **1996**, *258*, 172–189.

(8) Schenkman, J. B.; Jansson, I. The many roles of cytochrome b5. *Pharmacol. Therapeutics* **2003**, *97*, 139–152.

(9) Vergères, G.; Waskell, L. Cytochrome b5, its functions, structure and membrane topology. *Biochimie* **1995**, *77*, 604–620.

(10) Hildebrandt, A.; Estabrook, R. W. Evidence for the participation of cytochrome b_5 in hepatic microsomal mixed-function oxidation reactions. *Arch. Biochem. Biophys.* **1971**, *143*, 66–79.

(11) Juvonen, R. O.; Iwasaki, M.; Negishi, M. Roles of residues 129 and 209 in the alteration by cytochrome b5 of hydroxylase activities in mouse 2A P450S. *Biochemistry* **1992**, *31*, 11519–11523.

(12) Yamazaki, H.; Nakano, M.; Imai, Y.; Ueng, Y. F.; Guengerich, F. P.; Shimada, T. Roles of cytochrome b5 in the oxidation of testosterone and nifedipine by recombinant cytochrome P450 3A4 and by human liver microsomes. *Arch. Biochem. Biophys.* **1996**, *325*, 174–182.

(13) Perret, A.; Pompon, D. Electron shuttle between membrane-bound cytochrome P450 3A4 and b(5) rules uncoupling mechanisms. *Biochemistry* **1998**, *37*, 11412–11424.

(14) Strittmatter, P.; Spatz, L.; Corcoran, D.; Rogers, M. J.; Setlow, B.; Redline, R. Purification and properties of rat liver microsomal stearyl coenzyme A desaturase. *Proc. Natl. Acad. Sci. U.S.A.* **1974**, *71*, 4565–4569.

(15) Dailey, H. A.; Strittmatter, P. Structural and functional properties of the membrane binding segment of cytochrome b_5. *J. Biol. Chem.* **1978**, *253*, 8203–8209.

(16) Dailey, H. A.; Strittmatter, P. Characterization of the interaction of amphipathic cytochrome b_5 with stearyl coenzyme A desaturase and NADPH:cytochrome P-450 reductase. *J. Biol. Chem.* **1980**, *255*, 5184–5189.

(17) Maghzal, G. J.; Thomas, S. R.; Hunt, N. H.; Stocker, R. Cytochrome b_5, not superoxide anion radical, is a major reductant of indoleamine 2,3-dioxygenase in human cells. *J. Biol. Chem.* **2008**, *283*, 12014–12025.

(18) Vottero, E.; Mitchell, D. A.; Page, M. J.; MacGillivray, R. T. A.; Sadowski, I. J.; Roberge, M.; Mauk, A. G. Cytochrome b_5 is a major reductant in vivo of human indoleamine 2,3-dioxygenase expressed in yeast. *FEBS Lett.* **2006**, *580*, 2265–2268.

(19) McLaughlin, L. A.; Ronseaux, S.; Finn, R. D.; Henderson, C. J.; Roland Wolf, C. Deletion of microsomal cytochrome b_5 profoundly affects hepatic and extrahepatic drug metabolism. *Mol. Pharmacol.* **2010**, *78*, 269–278.

(20) Finn, R. D.; McLaughlin, L. A.; Ronseaux, S.; Rosewell, I.; Houston, J. B.; Henderson, C. J.; Wolf, C. R. Defining the in vivo role for cytochrome b_5 in cytochrome P450 function through the conditional hepatic deletion of microsomal cytochrome b_5. *J. Biol. Chem.* **2008**, *283*, 31385–31393.

(21) Dosset, P.; Hus, J. C.; Blackledge, M.; Marion, D. Efficient analysis of macromolecular rotational diffusion from heteronuclear relaxation data. *J. Biomol. NMR* **2000**, *16*, 23–28.

(22) Mulrooney, S. B.; Waskell, L. High-level expression in Escherichia coli and purification of the membrane-bound form of cytochrome b_5. *Protein Expr. Purif.* **2000**, *19*, 173–178.

(23) Saribas, A. S.; Gruenke, L.; Waskell, L. Overexpression and purification of the membrane-bound cytochrome P450 2B4. *Protein Expr. Purif.* **2001**, *21*, 303–309.

(24) Bridges, A.; Gruenke, L.; Chang, Y. T.; Vakser, I. A.; Loew, G.; Waskell, L. Identification of the binding site on cytochrome P450 2B4 for cytochrome b_5 and cytochrome P450 reductase. *J. Biol. Chem.* **1998**, *273*, 17036–17049.

(25) Dürr, U. H.; Yamamoto, K.; Im, S.-C.; Waskell, L.; Ramamoorthy, A. Solid-state NMR reveals structural and dynamical properties of a membrane-anchored electron-carrier protein, cytochrome b_5. *J. Am. Chem. Soc.* **2007**, *129*, 6670–6671.

(26) T. D. Goddard and D. G. Kneller, SPARKY 3, University of California, San Francisco.

(27) Guntert, P. Automated NMR structure calculation with CYANA. *Methods Mol. Biol.* **2004**, *278*, 353–378.

(28) Palmer III, A. G.; Skelton, N. J.; Chazin, W. J.; Wright, P. E.; Rance, M. Suppression of the effects of cross-correlation between dipolar and anisotropic chemical shift relaxation mechanisms in the measurement of spin-spin relaxation rates. *Mol. Physics* **1992**, *75*, 699–711.

(29) Kay, L. E.; Torchia, D. a; Bax, A. Backbone dynamics of proteins as studied by 15N inverse detected heteronuclear NMR spectroscopy: application to staphylococcal nuclease. *Biochemistry* **1989**, *28*, 8972–8979.

(30) Farrow, N. A.; Zhang, O.; Forman-Kay, J. D.; Kay, L. E. Comparison of the backbone dynamics of a folded and an unfolded SH3 domain existing in equilibrium in aqueous buffer. *Biochemistry* **1995**, *34*, 868–878.

(31) Grzesiek, S.; Bax, A. The importance of not saturating water in protein NMR. Application to sensitivity enhancement and NOE measurements. *J. Am. Chem. Soc.* **1993**, *115*, 12593–12594.

(32) Delaglio, F.; Grzesiek, S.; Vuister, G. W.; Zhu, G.; Pfeifer, J.; Bax, A. NMRPipe - a multidimensional spectral processing system based on Unix pipes. *J. Biomol. NMR* **1995**, *6*, 277–293.

(33) Bailey, L. K.; Campbell, L. J.; Evetts, K. A.; Littlefield, K.; Rajendra, E.; Nietlispach, D.; Owen, D.; Mott, H. R. The structure of binder of Arl2 (BART) reveals a novel G protein binding domain: implications for function. *J. Biol. Chem.* **2009**, *284*, 992–999.

(34) Lipari, G.; Szabo, A. Model-free approach to the interpretation of nuclear magnetic resonance relaxation in macromolecules. 1. Theory and range of validity. *J. Am. Chem. Soc.* **1982**, *104*, 4546–4559.

(35) Lipari, G.; Szabo, A. Model-free approach to the interpretation of nuclear magnetic resonance relaxation in macromolecules. 2. Analysis of experimental results. *J. Am. Chem. Soc.* **1982**, *104*, 4559–4570.

(36) Pandey, M. K.; Vivekanandan, S.; Ahuja, S.; Pichumani, K.; Im, S.-C.; Waskell, L.; Ramamoorthy, A. Determination of (15)n chemical shift anisotropy from a membrane-bound protein by NMR spectroscopy. *J. Phys. Chem. B* **2012**, *116*, 7181–7189.

(37) Sibille, N.; Favier, A.; Azuaga, A. I.; Ganshaw, G.; Bott, R.; Bonvin, A. M. J. J.; Boelens, R.; Van Nuland, N. A. J. Comparative NMR study on the impact of point mutations on protein stability of Pseudomonas mendocina lipase. *Protein Sci.* **2006**, *15*, 1915–1927.

(38) Sharpe, T.; Jonsson, A. L.; Rutherford, T. J.; Daggett, V.; Fersht, A. R. The role of the turn in beta-hairpin formation during WW domain folding. *Protein Sci.* **2007**, *16*, 2233–2239.

(39) Omura, T.; Sato, R. [90] Isolation of Cytochromes P-450 and P-420. *Methods Enzymol.* **1967**, *10*, 556–561.

(40) Kneller, D. G.; Kuntz, I. D. Ucsf Sparky - an Nmr Display, Annotation and Assignment Tool. *J. Cell. Biochem.* **1993**, 254.

(41) Hubbard, S. J.; Thornton, J. M. NACCESS **1993**.

(42) La Mar, G. N.; Burns, P. D.; Jackson, J. T.; Smith, K. M.; Langry, K. C.; Strittmatter, P. Proton magnetic resonance determination of the relative heme orientations in disordered native and reconstituted ferricytochrome b_5. Assignment of heme resonances by deuterium labeling. *J. Biol. Chem.* **1981**, *256*, 6075–6079.

(43) Keller, R. M.; Wüthrich, K. Structural study of the heme crevice in cytochrome b_5 based on individual assignments of the 1H-NMR lines of the heme group and selected amino acid residues. *Biochim. Biophys. Acta* **1980**, *621*, 204–217.

(44) Eisenmann, A.; Schwarz, S.; Prasch, S.; Schweimer, K.; Rösch, P. The E. coli NusA carboxy-terminal domains are structurally similar and show specific RNAP- and lambdaN interaction. *Protein Sci.* **2005**, *14*, 2018–2029.

(45) Markus, M. A.; Dayie, K. T.; Matsudaira, P.; Wagner, G. Effect of deuteration on the amide proton relaxation rates in proteins. Heteronuclear NMR experiments on Villin 14T. *J. Magn. Res., Series B* **1994**, *105*, 192–195.

(46) Storch, E. M.; Daggett, V. Molecular dynamics simulation of cytochrome b_5: implications for protein-protein recognition. *Biochemistry* **1995**, *34*, 9682–9693.

(47) Xu, X.; Reinle, W.; Hannemann, F.; Konarev, P. V; Svergun, D. I.; Bernhardt, R.; Ubbink, M. Dynamics in a pure encounter complex of two proteins studied by solution scattering and paramagnetic NMR spectroscopy. *J. Am. Chem. Soc.* **2008**, *130*, 6395–6403.

(48) Worrall, J. a R.; Liu, Y.; Crowley, P. B.; Nocek, J. M.; Hoffman, B. M.; Ubbink, M. Myoglobin and cytochrome b_5: a nuclear magnetic resonance study of a highly dynamic protein complex. *Biochemistry* **2002**, *41*, 11721–11730.

(49) Bashir, Q.; Scanu, S.; Ubbink, M. Dynamics in electron transfer protein complexes. *FEBS J.* **2011**, *278*, 1391–1400.

CHAPTER 7

Conclusions and future directions

7.1 Conclusions

The preceding chapters of this dissertation have described various projects related to the characterization the full-length cyt b_5-cyt P450 complex in a membrane environment. The broad goals were 1) to determine the structure and dynamics of full-length cyt b_5, 2) to identify residue-specific interactions at the cyt b_5-cyt P450 interface and use this information to generate a model of the complex structure, 3) to classify residues involved in encounter and stereospecific complexes, 4) to understand how cyt P450 substrate modulates the interaction between the two proteins and 5) to address the role of the cyt b_5 linker in the complex formation.

The work in Chapter 3 established the structure and dynamics of full-length cyt b_5 in DPC micelles. Using solution NMR, only the soluble domain of full-length cyt b_5 was visible in the spectra. Sequence specific assignment of 88.5% of the cyt b_5 soluble domain's backbone and side chain atoms was achieved. The structure of the soluble domain was then successfully solved with a final backbone RMSD of 0.32 Å. Although there were similarities between our structure and the previously reported structure of truncated rabbit cyt b_5[1], we found the presence of two additional β-strands, six longer/shorter secondary structure elements, and only three identical structured segments. We also established that the linker region, connecting the soluble domain and transmembrane domain, was completely unstructured. Relaxation measurements pointed to the flexibility of the linker region, as well as the N-terminus. Overall, the rest of the soluble domain was fairly rigid, with only a few residues experiencing higher than average mobility (including just three loop residues). Using TENSOR2,[2] the diffusion tensor of the soluble domain of cyt b_5 was shown to have a prolate axial symmetry and en effective correlation time twice as large as those reported for previous truncated cyts b_5[3,4]. We also found that the structure of the soluble domain was essentially the same in both DPC micelles and DMPC/DHPC isotropic bicelles. Using static solid-state experiments, the transmembrane domain of full-length cyt b_5, in DMPC/DHPC bicelles, was found to be α-helical with an average tilt of ~15° (relative to the bilayer normal).

The focus in Chapter 4 was then shifted to studying the interaction between cyt b_5 and cyt P450. In collaboration with Lucy Waskell's lab, we obtained single site-directed mutagenesis analyses of both cyt b_5 and cyt P450 2B4. These mutagenesis results pointed to cyt b_5 residues V66 and D65 as being hot spots for cyt P450, and cyt P450 2B4 residues on the C-helix, C-D loop and K''' 3_{10} helix as being hot spots for cyt b_5. A double mutant cycle analysis was then done to identify exactly which cyt b_5 residues interacted with which cyt P450 2B4 residues. Solution NMR differential line broadening analysis identified many other cyt b_5 residues as being important for the interaction with cyt P450 2B4. A series of docking simulations with HADDOCK were then performed in which all experimental data was considered as restraints. Double mutant cycle data and NMR differential line broadening results were entered as unambiguous restraints and ambiguous restraints, respectively. We found that the complex structures did not converge, and were not physiologically relevant, when only NMR-derived ambiguous restraints were considered. The unambiguous restraints, which in this case were the double mutant cycle analysis data, therefore proved essential in driving the docking results. Two final models for the cyt b_5-cyt P450 complex structure were proposed and a detailed analysis of the interface was performed. Hydrogen bonds, van der Waals contacts and salt bridges were all shown to be present at the interaction interface. This structural model of the complex then allowed us to propose an inter-protein electron transfer pathway involving the highly conserved R125 on cyt P450 serving as a salt bridge between the heme propionates of cyt P450 and cyt b_5.

In Chapter 5, we introduced a new approach for studying the cyt b_5-cyt P450 interaction, using solution NMR, based on previous knowledge of redox complexes (see Section 1.4) and work showing the role of electrostatic interaction in the encounter complexes compared to the stereospecific complexes.[5–7] The approach, in which we observed the intensities of the residue's resonances as a function of NaCl concentration, allowed us to isolate the broadening originating from the encounter complexes and the stereospecific complexes. We saw that all sides of cyt b_5 are able to interact with cyt P450 during the encounter complex, and were able to identify which residues participate in more pervasive interactions in these encounter complexes. By progressively shielding the electrostatic interactions, we then observed the stereospecific complexes in solution and were able to identify additional hot spots to those discussed in Chapter 4. We saw that, in addition to V66, residues G67 and T70 played key roles in the hydrophobic interactions between the two proteins. From the conglomeration of data, we were able to propose a detailed mode of interaction between the two proteins (Section 5.6). In the presence of a cyt P450 substrate, we discovered that there was an increase in the encounter complex population and that cyt P450 was able to scan a larger surface area of cyt b_5. We concluded that addition of a substrate therefore lengthens the lifetime of the encounter complex and allows the two proteins to find a productive orientation (for electron transfer) more frequently.

In Chapter 6, we then turned our focus to understanding how the cyt b_5 linker region modulates the interaction between cyt b_5 and cyt P450. Based on previous data,[8] we selected a mutant in which the linker region was truncated by eight residues. This mutant, referred to as *m*-cyt b_5, was previously shown to have a drastic decreased affinity for cyt P450 2B4 and a reduction, by more than half, in its ability to stimulate cyt P450 methoxyflurane metabolism. Using solution NMR, we first set out to establish the validity of using this mutant to understand the role of the linker. We established that the soluble domain of *m*-cyt b_5 was essentially unchanged from wild-type cyt b_5. In addition, the internal dynamics of cyt b_5 were essentially identical to those of wild-type cyt b_5. The main differences between *m*-cyt b_5 and the wild-type protein lay in the diffusion tensor of *m*-cyt b_5 being much more anisotropic than wild-type cyt b_5 and *m*-cyt b_5 having a longer effective correlation time. The interface between *m*-cyt b_5 and cyt P450 was then characterized using the approach described in Chapter 5. In agreement with binding assays and activity assays,[8] we found that the extent of broadening of *m*-

cyt b_5 resonances, upon interaction with cyt P450, was much less than for wild-type cyt b_5. In both cases, however, the same hot spot residues, V66 and T70, were identified as being important for stereospecific complex formation. The key differences between *m*-cyt b_5 and the wild-type protein, in their interactions with cyt P450, lay in the absence of interaction between the upper cleft of cyt b_5 and cyt P450 (even in the encounter complex) and the fact that the *m*-cyt b_5 surface area that cyt P450 is able to scan, during the encounter complex, is much smaller and only encompasses the lower cleft of *m*-cyt b_5. The unstructured and dynamic linker region of wild-type cyt b_5 therefore allows cyt b_5 to be able to sample more encounter complex orientations, essentially lengthening the lifetime of the encounter complex, and increasing the probability of the two proteins finding a productive orientation (for electron transfer) within each macrocollision.

7.2 Future directions

In both Chapters 5 (wild-type cyt b_5) and 6 (mutant cyt b_5), the importance of T70 was made apparent both in the presence and absence of substrate; it was always the last residue to re-appear with salt titration. This NMR result could be cross-checked my mutating T70 to an alanine and seeing how this mutation affects both the binding to cyt P450 and the ability of cyt b_5 to stimulate methoxyflurane metabolism. While residue D71 and L75 were mutated and shown not to be important functionally, T70 has so far been omitted from mutational studies, even for other variants of cyt b_5 (see Table 1.2). From our NMR results, we would expect that cyt b_5 might not be able to interact with cyt P450 at all (i.e. no K_d measurements would be successful) or the binding and metabolism would be drastically reduced. Similarly, G67 (found to be important in Chapter 5) would be important to mutate (as long as it would not affect the H68 coordination to the heme).

We also would like to shift the focus to getting more details on cyt P450. For example, very little is known on the membrane interaction of cyt P450. As discussion in Section 1.2.2, the soluble domain (in addition to the transmembrane domain) of cyt P450 2B4 (as well as other cyts P450) are predicted to be buried in the membrane. We are currently studying how the secondary structure of cyt P450 (using circular dichroism) is affected by the presence of different membrane mimetics and by the presence of different lipid types. In the end, we hope to understand which types of lipids cyt P450 may be interacting with on the cytoplasmic side of the endoplasmic reticulum membrane[9] in order to make the model membrane more physiologically relevant than just DMPC/DHPC bicelles. In order to refine the models presented in Section 1.2.2, we also plan to study how deeply cyt P450 is incorporated into the lipids by observing the order parameter of each C-H bond in the lipid acyl chain, using a modified version (introduced by our lab)[10,11] of a solid-state NMR technique called Proton Detected Local Field.

It is also hoped that the NMR approach used in Chapters 5 and 6 will be applied to other redox protein complexes that experience line broadening upon complex formation. In this manner, we could start piecing together the mode of interaction of multiple redox partners (how these proteins form encounter and stereospecific complexes) and start visualizing how proteins interact with one another on the cell membrane.

7.3 References

(1) Banci, L.; Bertini, I.; Rosato, A.; Scacchieri, S. Solution structure of oxidized microsomal rabbit cytochrome b_5. Factors determining the heterogeneous binding of the heme. *Eur. J. Biochem.* **2000**, *267*, 755–766.

(2) Dosset, P.; Hus, J. C.; Blackledge, M.; Marion, D. Efficient analysis of macromolecular rotational diffusion from heteronuclear relaxation data. *J. Biomol. NMR* **2000**, *16*, 23–28.

(3) Banci, L.; Bertini, I.; Cavazza, C.; Felli, I. C.; Koulougliotis, D. Probing the backbone dynamics of oxidized and reduced rat microsomal cytochrome b_5 via ^{15}N rotating frame NMR relaxation measurements: biological implications. *Biochemistry* **1998**, *37*, 12320–12330.

(4) Kelly, G. P.; Muskett, F. W.; Whitford, D. Analysis of backbone dynamics in cytochrome b5 using 15N-NMR relaxation measurements. *European Journal of Biochemistry* **1997**, *245*, 349–354.

(5) Northrup, S. H.; Boles, J. O.; Reynolds, J. C. Brownian dynamics of cytochrome c and cytochrome c peroxidase association. *Science* **1988**, *241*, 67–70.

(6) Suh, J.-Y.; Tang, C.; Clore, G. M. Role of electrostatic interactions in transient encounter complexes in protein-protein association investigated by paramagnetic relaxation enhancement. *J. Am. Chem. Soc.* **2007**, *129*, 12954–12955.

(7) Schreiber, G.; Fersht, A. R. Rapid, electrostatically assisted association of proteins. *Nat. Struct. Biol.* **1996**, *3*, 427–431.

(8) Clarke, T. A.; Im, S.-C.; Bidwai, A.; Waskell, L. The role of the length and sequence of the linker domain of cytochrome b_5 in stimulating cytochrome P450 2B4 catalysis. *J. Biol. Chem.* **2004**, *279*, 36809–36818.

(9) Nilsson, O.; Dallner, G. Distribution of constitutive enzymes and phospholipids in microsomal membranes of rat liver. *FEBS Lett.* **1975**, *58*, 190–193.

(10) Dvinskikh, S.; Dürr, U.; Yamamoto, K.; Ramamoorthy, A. A high-resolution solid-state NMR approach for the structural studies of bicelles. *J. Am. Chem. Soc.* **2006**, *128*, 6326–6327.

(11) Dvinskikh, S. V; Dürr, U. H. N.; Yamamoto, K.; Ramamoorthy, A. High-resolution 2D NMR spectroscopy of bicelles to measure the membrane interaction of ligands. *J. Am. Chem. Soc.* **2007**, *129*, 794–802.

APPENDICES

Appendix A

Instructions for running HADDOCK on the cyt b_5-cyt P450 complex

new.html document – creates the run and all files needed for the run

Contains:

- Line 9: The path to the HADDOCK program
- Line 11 & 12: The path to the pdb of the proteins you are docking
- Line 13: The directory where the run will be saved
- Line 15 & 16: define the proteins as A, B, C, etc. based on the pdb number it had in Line 11 &12
- Line 17: Path to the table of unambiguous restraints
- prot = protein ; prot_segID = protein segment ID

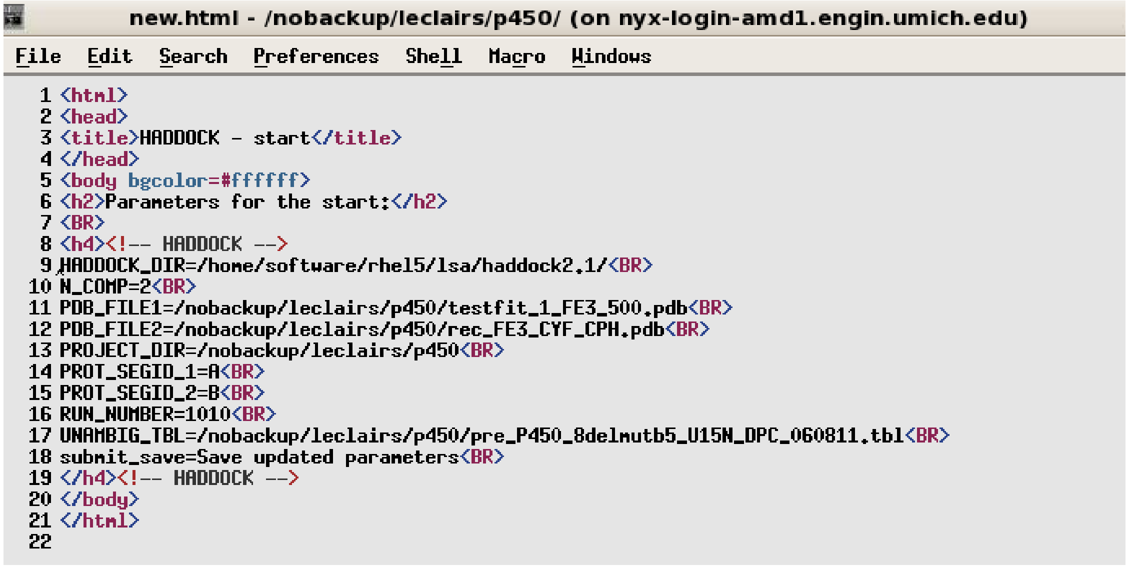
new.html - /nobackup/leclairs/p450/ (on nyx-login-amd1.engin.umich.edu)
File
Edit
Search
Preferences
Shell
Macro
Windows

```
 1 <html>
 2 <head>
 3 <title>HADDOCK - start</title>
 4 </head>
 5 <body bgcolor=#ffffff>
 6 <h2>Parameters for the start:</h2>
 7 <BR>
 8 <h4><!-- HADDOCK -->
 9 HADDOCK_DIR=/home/software/rhel5/lsa/haddock2.1/<BR>
10 N_COMP=2<BR>
11 PDB_FILE1=/nobackup/leclairs/p450/testfit_1_FE3_500.pdb<BR>
12 PDB_FILE2=/nobackup/leclairs/p450/rec_FE3_CYF_CPH.pdb<BR>
13 PROJECT_DIR=/nobackup/leclairs/p450<BR>
14 PROT_SEGID_1=A<BR>
15 PROT_SEGID_2=B<BR>
16 RUN_NUMBER=1010<BR>
17 UNAMBIG_TBL=/nobackup/leclairs/p450/pre_P450_8delmutb5_U15N_DPC_060811.tbl<BR>
18 submit_save=Save updated parameters<BR>
19 </h4><!-- HADDOCK -->
20 </body>
21 </html>
22
```

cd run__/begin – don’t need to worry about this; it only contains iterations.cns prior to submitting the simulation.

cd run__/data/

- **distances**: *ambig.tbl* and *unambig.tbl* (took the distance file that we referred to in the *new.html* and renamed it as *unambig.tbl*)
- **new.html** – copies the new.html in here, so that you can always go back and check which table you used for the restraints for the given run.
- **sequence** – stores the pdbs of the proteins in here that it took from the new.html file. File_A is cytb5 and File_B is cytP450 (see how these are defined in new.html).

cd run__/protocols

- These are all default files that HADDOCK creates to run the simulation. Some of these files need to be edited based on the system that we are using. Our protein is paramagnetic and has an iron and a heme, which are not included in the default files of HADDOCK.
- **numtrees.cns** – need to change the number of trees as 10, and not 1 (unsure what this does). Alex told use to change this. That's why we just copy this file from previous runs because it's already been modified.
- **covalions.cns** – defines covalent bonds to heteroatoms. In our case, the Fe3+ of cytP450 is covalently bound to CPH and the cysteine (CYF). **If do not have a ligand, need to remove all the information on the ligand here, here CPH.
    - Line 2: $pcount =2 because are defining two atoms covalently bound to one ion (the ligand and the cysteine). If only have the cysteine bound to the ion, then change
    - Line 3: defines the first atom as $id1 and make sure that the ion in your system is defined; in our case: Fe+3.
    - Line 3-4: defines all the ions that HADDOCK recognizes. If need to add more, will have to add topology and parameter files.
    - Line 18: defines the two atoms that are covalently bound to the ion
    - Line 20-26: List of atoms that can covalently bind to the ions listed. Add "resn CPH" so that HADDOCK looks for a heteroatom named CPH to bind to the iron (since 1SUO has CPH bound to the iron). Add the three letter code here so that it finds the atom that is covalently bound to Fe3+.
    - Line 28: picks the bond between $id1 and $id2.

- **generate_B.inp** (B stands for molecule B, which is cytP450). Need to add the Line 353 saying that the patch is HEB (pheb) reference residue 436 and the atom is S, and it is covalently bound to residue 500 (which is the heme) and the atom is Fe3+. This lines connects those two atoms together.

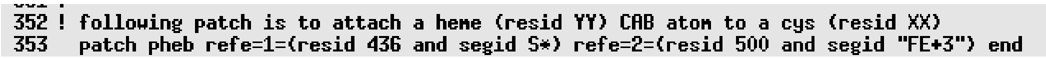

```
352 ! following patch is to attach a heme (resid YY) CAB atom to a cys (resid XX)
353   patch pheb refe=1=(resid 436 and segid S*) refe=2=(resid 500 and segid "FE+3") end
```

- **generate_B-water.inp** (same file as above, but this is used for the water refinement stage), so need to change the same line as the previous bullet point.
- The A, C, D, E, F denote the molecule for which the file was created. In our case, A is cytb5 and B is P450.

cd run__/toppar – Contains all the topology and parameter files for the proteins and ligands. For proteins, it has the topology of peptide bonds (how the atoms are linked together in space – the network in 3D – defines all the possible angles for every amino acid and links all the amino acids). The PDB file only contains coordinates of atoms.

- Need to change the heme files, because the default folder only has *heme.pdb* and *heme.psf*. These are for heme C. These do not contain the topology and parameter data, so they need to be included in *ligand.param*, *ligand.pep*, and *ligand.top*.
- Alex created *hemeB.pdb* and *hemeB.psf*. Need to add those two files to the toppar directory.
- Modify the following ligand files so that they include the topology and parameter files that you obtained from PRODRG2 for the ligand that you have in the crystal structure. These ligand files contain any small molecule that exists in your structure (e.g. cholesterol, BHT, 1CPI, hemeB, hemeC). The topology and parameter files contain information for heme B and heme C. If you don't have any other ligands, delete the ligand information from the following files, but always keep the heme in the ligand files. Never leave ligand information from a ligand that is not in the system you are submitting for the simulation or you will get errors.
    - *ligand.param* – need to add the ligand information from param.txt on pg. 2 above
        - The first part of the ligand file, starting at "evaluate" contains parameter information on the heme, which we obtained from Alex.
        - Copy the ligand information, which you obtained from PRODRG2 from "evaluate" to "set message on echo on end" below the information for the heme.
    - *ligand.top* – get the ligand information from top.txt from PRORDG2 (see pg. 2). Copy from "AUTOGENERATE" to
        - The heme topology is defined up until Line 618.
        - Line 575: refers to the patch that we added in *generate_B.inp* and *generate_B-water.inp*
        - The small ligand information starts at Line 620 with "AUTOGENERATE" until "END."

        - The script should end with “set echo=true end”
    - *ligand.pep* – this is an empty file for us because our ligand is not a peptide.

cd run__/run.cns

- *Never use the default run.cns*. Always copy from a previous run, since we have changed so many files compared to the default.
- Contains papers that you should cite when you use HADDOCK.
- Line 58: # of molecules you are docking, “ncomponents= “ (2 in our case because we have cytP450 and cytb5)
- Line 65: “fileroot=” uses this name for the generated complex structures and puts a number next to it.
- Line 69: Path of the current run (where it’s being conducted) for “run_dir=” When copy *run.cns* from previous runs, the path is already properly defined, you just need to change the run #.
- Line 71-81: define the pdb and psf files and labels molecule as A, for molecule A
    - The .psf file is just the pdb filename followed by .psf
- Line 83-93: define the pdb and psf files and labels molecule as B, for molecule B
- Line 95-141 defines pdf and psf files for molecules C-F if have them.
- Line 152-154: defines the path where the HADDOCK program is; this is automatically defined when you do *haddock* and create the run.
- Line 156-158: define the path for the log files. Make sure to change the run # so that it puts it in the folder of your current run (otherwise will overwrite other run’s data).
- All the following information has to be inputted based on our needs (this is why we just copy the *run.cns* file for each run).
- Line 161: Histidine patches – this has to do with defining the protonation state of your histidines based on the pH of your sample. Need to define the histidine protonation states based on pH and need to make sure that H44 and H68 are deprotonated.
    - Line 165: define how many histidines you are going to define in the list below.
    - Line 168-169: define the protonation state of the histidines HD1, which are coordinated to the heme. They do not have a HD1 proton attached to the nitrogen because they are coordinated to the heme.
- Line 297: definition of semi-flexible interface – the side-chains and backbone of the residues defined here will be allowed to move during the semi-flexible simulated annealing http://www.nmr.chem.uu.nl/haddock/docking.html#sa

    - Wanted the side-chains at the interface of the complex to move so that they could pack better, so they took the stretches of residues that they saw at the interface during the first few runs and defined them here so that the refinement could include packing of the side-chains and backbones.
    - Line 304: Defines the number of segments that you will keep as semi-flexibles in molecule A.
    - Line 309-328 defines all the segments of molecule A that are defined as semi-flexible (all the other segments of the proteins are assumed to be rigid). Here, they have the segments 40-42, 46-59, 60-66 and 70-79. If you put too many flexible regions, the simulation will crash.
        - Did not include His44 and His68 in these semi-flexible regions because their side-chains need to stay coordinated to the iron (if you keep them flexible, you can lose the coordination to the iron). We do not have these coordination bonds defined anywhere so have to keep these residues rigid to hold the heme in place.
        - They first ran the simulation keeping everything rigid, then looked at the complex structure and determined which regions of the protein would likely have side-chain interactions/packing at the interface. The residues defined here will affect the H-bonding and packing, but will not affect the overall complex structure too much.
    - Line 333: Defines the number of segments that you will keep as semi-flexibles in molecule B.
    - Line 337-356 defines the semi-flexible regions of cytP450.
        - Ran it rigid first and then figured out which regions of cytP450 came in contact with cytb5 in those complex structures. Defined those regions as semi-flexible so that HADDOCK could do side-chain packing refinement. The segments are 118-144 (which is Helix C), 339-346, 414-433, and 439-446.
        - Cys436 is kept rigid (and is not included in the semi-flexible segments) because don't want the heme to pop out. Want the cysteine to remain covalently bonded to the iron.
- Line 470: define the segments of the proteins that you will keep as fully-flexible during all of it1. If define too many segments as fully-flexible, the run would crash, or it did not make much of a difference.
    - Line 477: the number of fully-flexible segments for molecule A you will define below.
    - Line 482-491: the fully-flexible segments in molecule A.

    - Line 496: the number of fully-flexible segments for molecule B you will define below.
    - Line 498-509: the fully-flexible segments in molecule B.
    - Since we don't see the first 6 amino acids at the N-terminus of cytb$_5$, need to keep those residues as fully flexible. The percentage of the dominant versus minor complex structures change but end up with the same structures. The side-chains and backbones will be allowed to move throughout every stage of the simulation, including water refinement.
- NCS restraints (non-crystallographic symmetry restraints) (Line 586-629)
- Symmetry restraints (Line 630-800)
- Can ignore the distance restraints section because we have already defined them in a separate table and want to keep everything as default. (Line 801-884)
- DNA-RNA restraints (Line 885-891)
- Dihedrals (Line 892-903)
- Karplus coupling restraints (Line 904-959)
- Residual dipolar couplings (Line 960-1107)
- Relaxation data (Line 1108-1181) – can refine the complex structure further by including T_1 and T_2 data.
- Line 1182: topology and parameter files – just make sure this section is there
- Energy and interaction parameters (Line 1229-1266)
- Line 1267: Number of structures to dock (looked at HADDOCK papers and saw what people used for these numbers)
    - Line 1271: The number of structures for rigid body docking (it0): 2000
    - Line 1274: The number of structures for semi-flexible refinement (it1): 500 (the 500 lowest energy structures from it0 are selected for it1 refinement)
    - Line 1278: Number of low energy structures you want the program to pick up for final analysis. Have been using 50 for this.
- DOCKING protocol (Line 1295-1359) can be ignored – just use default
- Solvated rigid body docking (Line 1360-1407) can be ignored – just use default
- Line 1408: Final explicit solvent refinement
    - Line 1419: number of structures used for water refinement. Defined that as 150.
    - Should have at least 3-5 times more structures selected for this step compared to the amount of structures you will use for the final structure analysis (i.e. if select 50 lowest energy structures for the final analysis, need at least 150 structures here).
- Scoring (Line 1440-1498) – use default here because we did a manual analysis of all 50 structures instead of having a score for all structures.

- Did not change “analysis and clustering,” “Structure quality analysis,” and “final clean-up” (Line 1499-1533)
- Line 1534-1579: parallel jobs
  - Copy lines 1540-1578 from previous runs – defines the number of CPUs used on the LSA server. These were generated by Tony for efficient running of HADDOCK on the LSA server.

Appendix B

Histidine protonation states

The Henderson-Hasselbach equation can be re-written as:

$$10^{pH-pKa} = \frac{[A^-]}{[HA]} \qquad \textbf{Equation B.1}$$

From this equation, the probability of the residue/atom being protonated or de-protonated can be derived as:

$$\text{probability of being protonated} = \frac{[HA]}{[A]+[HA]} = \frac{10^{pKa-pH}}{1+10^{pKa-pH}} \qquad \textbf{Equation B.2}$$

The pKa values in Tables B.1 and B.2 were calculated from the PROPKA web interface.[1,2] The percent of histidines protonated versus de-protonated in the tables was calculated using Equation B.2.

To assign the protonation state (HD1, HE2, both or neither), the PQR file for the NMR structure of cyt b_5 (Chapter 3) was generated from the PDB2PQR server[3,4] with PROPKA[2] set at pH 7.4. By inspecting the output pqr file, it is possible to assign which nitrogens are protonated in the histidines of cyt b_5.

Instructions for generating the pqr files to assess protonation

Need to generate a pdb file that has all of the hydrogrens present. This step also calculates the charges on the surface of the protein.

- Go to: http://nbcr-222.ucsd.edu/pdb2pqr_1.8/ (moved from http://kryptonite.nbcr.net/pdb2pqr/)
- Either put in the pdb # or upload your pdb file
- Leave all the default options selected
- Make sure that the following are checked:
    - ✓ Ensure that new atoms are not rebuilt too close to existing atoms
    - ✓ Optimize the hydrogen bonding network
    - ✓ Use PROPKA to assign protonation states at pH _____ ← fill in pH
    - ✓ Create an APBS input file
- Click Submit
- Right-click and select “Save Link As…” for all the output files generated, as well as the runtime and debugging information files.

Table B.1 Protonation state of histidines in the pdb file of the NMR structure of rabbit cyt b_5.

Histidine residue #	pKa	% protonated at pH 7.4	% de-protonated at pH 7.4	de-protonated	HE2 present	HD1 present
20	7.03	29	71	Yes		x
22	7.17	37	63			x
31	7.23	40	60		x	
32	7.23	40	60		x	
44	4.04	bound to Fe^{3+}		Yes		x
68	6.27	bound to Fe^{3+}		Yes		x
85	7.16	37	63			x

Table B.2 Protonation state of histidines in the 1SUO pdb structure.

Histidine residue #	pKa	% protonated at pH 7.4	% de-protonated at pH 7.4	de-protonated	HE2 present	HD1 present
172	2.29	7.762 x 10^{-4}	~100	Yes	x	
231	6.22	6	94	Yes	x	
252	9.40	99	1	No	x	x
284	6.75	18	82	Yes		x
285	6.43	10	90	Yes		x
319	6.50	11	89	Yes	x	
335	6.43	10	90	Yes	x	
354	6.57	13	87	Yes		x
369	0.39	9.8 x 10^{-6}	~100	Yes		x
397	2.35	8.9 x 10^{-4}	~100	Yes		x
412	6.59	13	87	Yes	x	
492	6.36	8	92	Yes		x

Generating electrostatic potential surfaces

The generated pqr file can also be used for calculating the electrostatic potential surface of a protein (this was done for cyt b_5 and cyt P450 in Figures 1.2, 1.4, 5.9 and 5.12). Here are some brief instructions on how these structures were generated:

In PyMOL[5],

- Open the pdb file (if you open the pqr file instead, the heme will not be present)
- Go to Plugin → APBS Tools [this opens the APBS user interface]
- Main
    - Select “Use another pqr”
    - Click Choose Externally Generated PQR and find the pqr file you just generated

- Program Locations [should have the locations of the plug-ins]

- Temp File Location [this is where it puts the files it generates]
    - Put the full path for Temporary PQR file
    - Put the full path for Temporary PDB file

- Configuration
    - Click Set grid
    - Click Run APBS

- Visualization
    - Click Update
    - Under “Molecular Surface”
        - ✓ Solvent accessible surface
        - ✓ Use settings such as “Low -5” (negative) and “High 5” (positive); other settings commonly used are -1,1 or -10,10
- When you “Show: surface” – will show the electropotential map

References

(1) The PROPKA Web Interface http://propka.ki.ku.dk/.

(2) Li, H.; Robertson, A. D.; Jensen, J. H. Very Fast Empirical Prediction and Rationalization of Protein pKa Values. *Proteins: Structure, Function, and Bioinformatics* **2005**, 61, 704–721.

(3) Dolinsky, T. J.; Nielsen, J. E.; McCammon, J. A.; Baker, N. A. PDB2PQR: an automated pipeline for the setup of Poisson-Boltzmann electrostatics calculations. *Nucleic Acids Research* **2004**, 32, W665–W667.

(4) Dolinsky, T. J.; Czodrowski, P.; Li, H.; Nielsen, J. E.; Jensen, J. H.; Klebe, G.; Baker, N. A. PDB2PQR: expanding and upgrading automated preparation of biomolecular structures for molecular simulations. *Nucleic Acids Research* **2007**, 35, W522–W525.

(5) DeLano, W. L. The PyMOL Molecular Graphics System, Version 1.5.0.4 Schrödinger, LLC **2010**.

(6) Hubbard, S. J.; Thornton, J. M. NACCESS **1993**.

Appendix C

Solvent accessibility of cyt b_5 residues

The solvent accessibility of cyt b_5 residues in the NMR structure (Chapter 3) was assessed using NACCESS[6]. These solvent accessibility values were the ones used in Chapters 5 and 6.

For Table C.1 and Table C.2:

- **Relative % SA:** relative % solvent accessibility of the selected amino acids (see below)
- **All-atoms:** all atoms of the entire amino acid
- **Total-Side:** all atoms of the side chain of the amino acid. Alpha-carbons are considered as side chain atoms.
- **Main-Chain:** only backbone atoms of the amino acid
- **Non-polar atoms:** only non-polar atoms (all non-oxygens and non-nitrogens) of the side chain of the amino acid
- **All polar atoms:** only polar atoms (nitrogens and oxygens) of the side chain of the amino acid

Table C.1 Cytochrome b_5 (NMR structure) residues that *are* solvent accessible ($\geq$35.0% for side chain, all-atom, or backbone) based on NACCESS.

Amino acid type	Amino acid #	All-atoms, Relative % SA	Total-Side, Relative % SA	Main-Chain, Relative % SA	Non-polar atoms, Relative % SA	All polar atoms, Relative % SA
MET	1	97.3	102.3	76.4	104.4	66.5
ALA	2	43.4	48.3	34.6	50.2	30.1
ALA	3	98.9	100.3	96.5	102.4	92.1

Amino acid type	Amino acid #	All-atoms, Relative % SA	Total-Side, Relative % SA	Main-Chain, Relative % SA	Non-polar atoms, Relative % SA	All polar atoms, Relative % SA
GLN	4	59.8	70.3	20.4	70.6	55.4
SER	5	68.2	71.9	60.5	48.7	82
ASP	6	36.7	49.8	1.2	23.4	43.9
LYS	7	92.5	92.9	90.6	95.5	88.3
ASP	8	50.4	67.7	3.4	59.9	45.3
VAL	9	56.6	62.1	39.9	61.4	41.3
LYS	10	53.8	66.2	0	53.5	54.3
TYR	11	62.5	62.9	60.5	52.1	81.1
THR	13	45.3	62	0	53.7	35.3
LEU	14	31	37.4	6.6	37.1	6.9
GLU	15	61.8	77.3	6.1	102.2	40
GLU	16	42.2	53.9	0.3	35.5	45.9
LYS	18	51	59.7	13.1	41.8	63.7
LYS	19	65.3	75.7	20	67.3	62.5
HIS	20	28.3	35.2	0	39.2	15.9
ASN	21	41	36.4	54	15.2	53.2
HIS	22	82.6	80.3	91.8	78.4	87.4
SER	23	60.1	73.9	32	99.7	31.9
LYS	24	79.5	92.3	23.9	88.2	67.5
SER	25	27	40.3	0	16	34.9
HIS	31	52.1	55.9	36.5	59.5	43.7
LYS	33	31.8	39.1	0	32.4	31.1

Amino acid type	Amino acid #	All-atoms, Relative % SA	Total-Side, Relative % SA	Main-Chain, Relative % SA	Non-polar atoms, Relative % SA	All polar atoms, Relative % SA
THR	38	9.6	0	35.6	0	21.1
LYS	39	41.4	47.8	13.9	50.8	28.5
LEU	41	29.1	35	6.9	34.7	7.2
GLU	42	73	76.1	62	91.9	62.9
GLU	43	42.5	36.7	63.2	75.6	24.6
PRO	45	40.1	45.5	0.5	45.1	0.6
GLY	46	95.2	77.7	107	80.9	107.8
GLY	47	21.6	51.9	1	46	0
GLU	48	66.8	81.4	14.2	61.2	69.8
GLU	49	64.5	81.3	4.3	101.7	44.5
ARG	52	72	84.7	4.1	81.3 1	67.5
GLU	53	56.2	54.4	62.7	50.8	59.1
ALA	55	27.9	21.7	39.2	21.1	41.3
GLY	57	33.4	81.2	1.1	70.8	0.5
ASP	58	49.3	54.5	35.4	68.5	39
GLU	61	72.8	83.9	32.9	88.9	64.2
ASN	62	29.7	40.2	0	4	41.8
GLU	64	59.3	59.4	59	70	53.6
ASP	65	91.9	100.9	67.3	51.2 1	113.9
VAL	66	37.5	28.4	65.4	28.1	67.5
GLY	67	56.8	81.9	39.8	79.7	36.6
HIS	68	19.9	2	93.5	6.1	35.5

Amino acid type	Amino acid #	All-atoms, Relative % SA	Total-Side, Relative % SA	Main-Chain, Relative % SA	Non-polar atoms, Relative % SA	All polar atoms, Relative % SA
SER	69	38.7	53.6	8.5	81.6	8.1
THR	70	75.1	96.4	17.5	97.6	48.3
ASP	71	70.3	93.7	6.6	70.4	70.3
ARG	73	71.7	77.9	38.4	52.2 1	81.1
GLU	74	51.5	65.4	1.6	74.3	39.2
LEU	75	41.6	52.6	0	52.2	0
LYS	77	59.8	71.2	10.4	72.8	41.9
HIS	85	41.1	50.2	3.4	47.3	34
PRO	86	58.2	64.5	11.6	65	4.4
ASP	87	73.6	88.3	33.5	98.7	60
ARG	89	42.5	43.9	34.8	33.4	46.9
SER	90	82.5	88	71.4	99.2	70.6
LYS	91	64.4	68.4	47.1	58.7	72.4
LEU	92	61.1	64.4	48.3	64.2	48.6
SER	93	83.6	82.4	85.9	95.2	75.2
LYS	94	78.5	77.8	81.4	76.7	81
PRO	95	87.9	89.3	77.9	90.6	66.5
MET	96	94.6	98.3	79.1	98.2	78.6
GLU	97	62.9	63.6	60.4	69.7	59.2
THR	98	78.3	94.4	34.6	94.6	58.8
LEU	99	96.7	103.3	71.5	103	71.6
ILE	100	77.3	82.7	57.2	82.4	57.4

Amino acid type	Amino acid #	All-atoms, Relative % SA	Total-Side, Relative % SA	Main-Chain, Relative % SA	Non-polar atoms, Relative % SA	All polar atoms, Relative % SA
THR	101	92.7	113	37.9	111.8	70
THR	102	77.6	86.2	54.2	93.8	58.1
VAL	103	96.9	114.3	43.2	115.5	36.9
ASP	104	88.9	94.3	74.2	81.7	92.8

Table C.2 Cytochrome b_5 residues that solvent *in*accessible (< 35.0% for side chain, all-atom, or backbone) based on NACCESS.

Amino acid type	Amino acid #	All-atoms, Relative % SA	Total-Side, Relative % SA	Main-Chain, Relative % SA	Non-polar atoms, Relative % SA	All polar atoms, Relative % SA
TYR	12	26.9	32.3	0	25.6	29.2
ILE	17	2.4	3	0.4	3.1	0
THR	26	13.4	18.3	0	18.1	7.8
TRP	27	16	18.8	0.1	21	0
LEU	28	1.1	1.4	0	1.4	0
ILE	29	8.7	10.9	0.5	10.8	0.5
LEU	30	0.9	1.1	0	1.1	0
HIS	32	29.6	33.8	12.2	30.5	28.5
VAL	34	0	0	0	0	0
TYR	35	9.3	11.2	0	4.3	18.3
ASP	36	4.8	6.5	0	10.5	1.7
LEU	37	4.7	5.9	0	5.9	0
PHE	40	11.4	12.9	4	12.9	4.2

Amino acid type	Amino acid #	All-atoms, Relative % SA	Total-Side, Relative % SA	Main-Chain, Relative % SA	Non-polar atoms, Relative % SA	All polar atoms, Relative % SA
HIS	44	12.1	10.6	18.3	16.6	7.1
VAL	50	21.7	28.8	0	28.5	0
LEU	51	1.6	0.4	6.2	0.8	4.7
GLN	54	18.5	22.9	2	6.4	23.5
GLY	56	14.3	0.9	23.3	6.2	21.4
ALA	59	0	0	0	0	0
THR	60	23.7	32.1	1	42.1	1.8
PHE	63	11.7	13.8	1.8	13.7	1.9
ALA	72	1.1	0.4	2.4	0.3	2.5
SER	76	12.8	18.1	2.2	14.2	11.8
THR	78	23.6	29.1	8.6	32	13.5
PHE	79	10.5	12.8	0	12.7	0
ILE	80	20.7	26.3	0	26.1	0
ILE	81	10.8	11.8	7	11.7	7.2
GLY	82	0	0	0	0	0
GLU	83	11.3	14.5	0	19.4	7
LEU	84	0.5	0.5	0.3	0.5	0.3
ASP	88	16.9	23	0.4	22.9	13.7

Appendix D

Preparing isotropic bicelles

Here are the instructions that were followed for all isotropic bicelles prepared in this thesis:

- Take out lipids from freezer and let the containers equilibrate to room temperature before opening them (do not want moisture to come into the container when you open it).
- Wash Pasteur pipette connected to N_2 gas tube with ethanol (and wipe with kimwipe) and dry out the ethanol inside the pipette by blowing N_2 gas out of it.
- Wash medium-sized test tubes with ethanol and set upside down on clean kimwipe (want test tubes that are large enough to pipette into, but not too large). Dry test tubes with N_2 gas.
- Weigh out long-chain lipids (e.g. DMPC) into test tube. Always keep the lipid container closed when not actively using it.
- Cover the test tube with parafilm if weighing out lipids for another test tube (do not want lipids to be exposed to air; otherwise will get oxidized).
- Add DHPC (in solution) to test tube without touching the tip of the micropipette to the sides of the test tube (since have to add two different volumes), then wash walls with the lipid/detergent solution to remove powder from walls.
- Vortex test tube while covering the top of the tube to ensure that no solution comes out.
- Dry the lipid solution under a slow flow of N_2 gas (have the Pasteur pipette pointing straight down into the test tube; adjust the test tube up and down accordingly so that there is a gentle flow of air on the surface of the lipid/detergent solution).
- When ~half the volume has evaporated, hold the test tube sideways and rotate it as the rest of the volume evaporates – want to form a thin film onto the walls of the test tube (don’t want the film to go too high on the tube or it will be difficult to reconstitute it). To help speed up the process, can warm the bottom of the tube with your hand.
- Cover the test tubes with parafilm; then puncture holes through it using a syringe tip.

- Put in vacuum oven overnight (29 psi) at ~1.3 (37°C). At some point during this time, open up the vacuum chamber and then put the vacuum on again (to get rid of the evaporated chloroform). In the morning, all chloroform should be evaporated and you can rehydrate the dried lipid mixture with buffer to form isotropic bicelles.